

Proposal to the National Science Foundation

A
**LASER INTERFEROMETER
GRAVITATIONAL-WAVE
OBSERVATORY
(LIGO)**

LIGO-M890001-00-M

**VOLUME 1:
LIGO Science and Concepts**

December 1989

CALIFORNIA INSTITUTE OF TECHNOLOGY
MASSACHUSETTS INSTITUTE OF TECHNOLOGY

LIGO PROJECT

Proposal to the National Science Foundation

**THE CONSTRUCTION, OPERATION, AND
SUPPORTING RESEARCH AND DEVELOPMENT
OF A**

**LASER INTERFEROMETER
GRAVITATIONAL-WAVE
OBSERVATORY**

*Submitted by the
CALIFORNIA INSTITUTE OF TECHNOLOGY
Copyright © 1989*

Rochus E. Vogt
Principal Investigator and Project Director
California Institute of Technology

Ronald W. P. Drever
Co-Investigator
California Institute of Technology

Frederick J. Raab
Co-Investigator
California Institute of Technology

Kip S. Thorne
Co-Investigator
California Institute of Technology

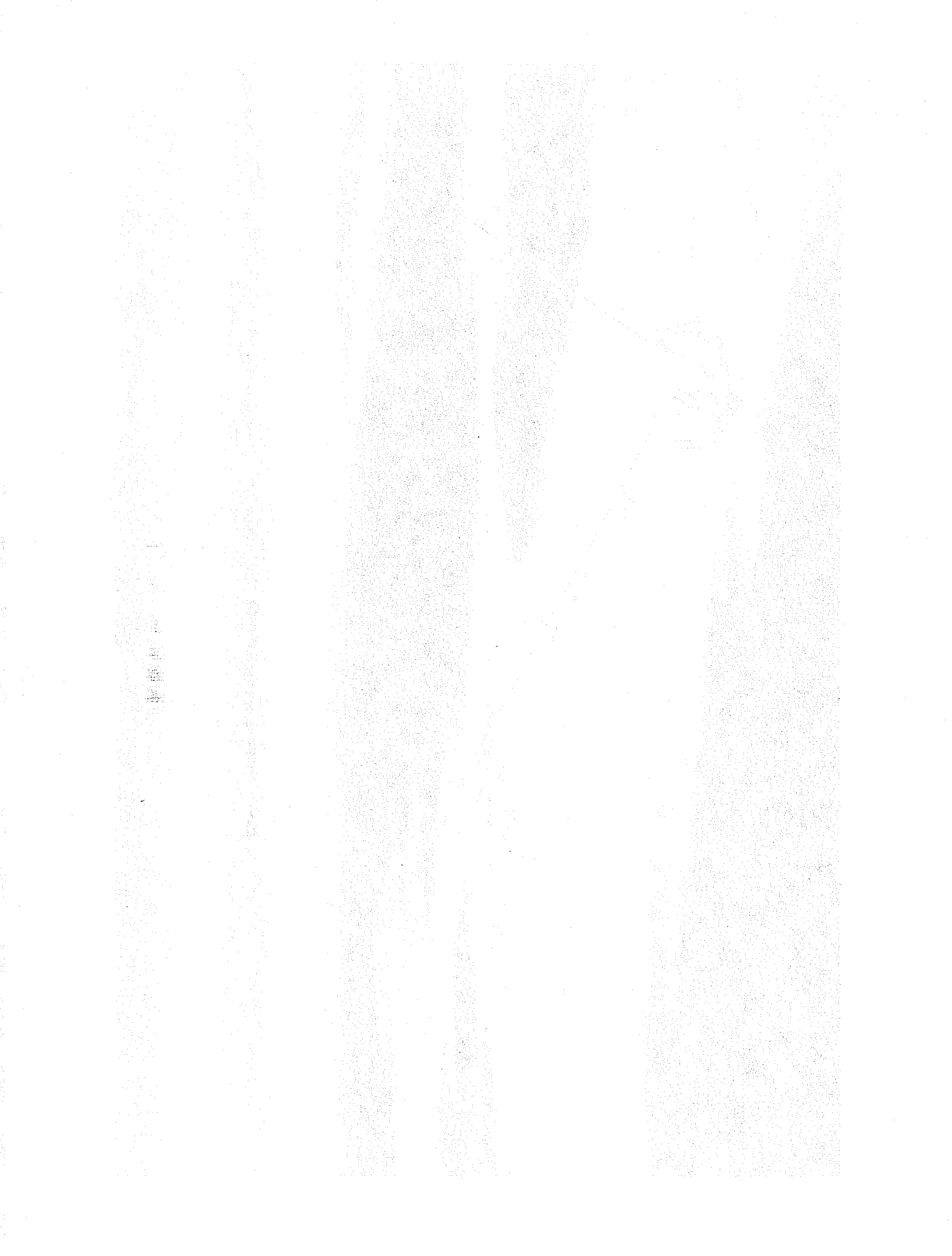
Rainer Weiss
Co-Investigator
Massachusetts Institute of Technology

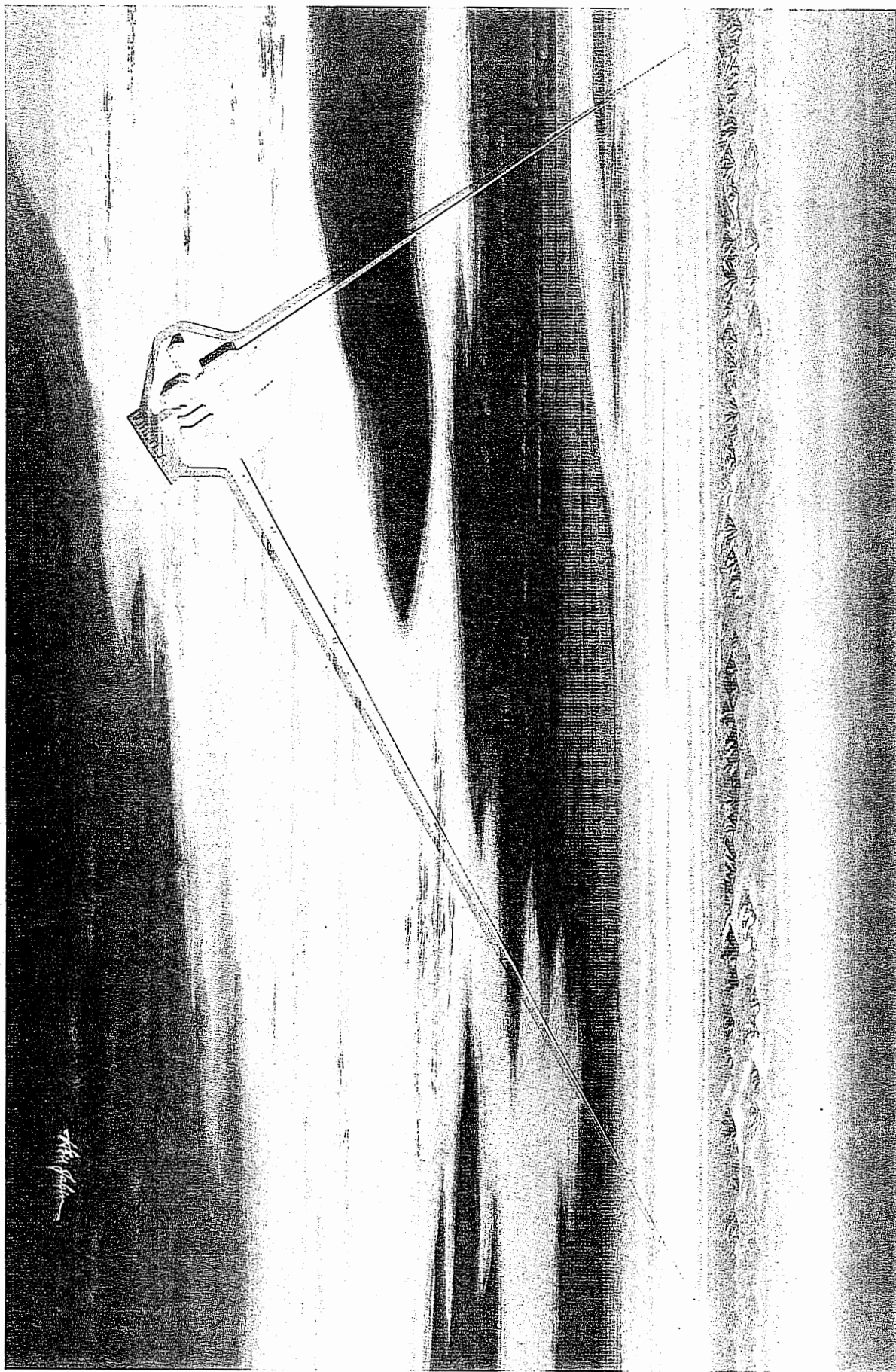
Table of Contents: Volume 1

PREFACE	i
SUMMARY	1
I. INTRODUCTION	3
II. PHYSICS OF GRAVITATIONAL WAVES, SOURCES, AND DETECTORS	5
III. LASER INTERFEROMETERS	13
A. General Characteristics and Noise Effects	13
B. 40-meter Prototype Interferometer	22
IV. LIGO CONCEPT	31
A. Requirements	31
B. Implementation	35
V. DESIGN AND SITING OF INTERFEROMETERS	43
A. Conceptual Design of the Initial LIGO Interferometers	43
B. Evolution of LIGO Interferometers	52
C. LIGO Sites: Scientific Aspects	58
VI. LIGO OPERATIONS	61
VII. STRATEGY FOR IDENTIFICATION OF GRAVITATIONAL WAVES	67
VIII. CAMPUS RESEARCH AND DEVELOPMENT IN SUPPORT OF LIGO	76
A. Results from Prior NSF Support	76
B. Future Activities	82
IX. ORGANIZATION AND MANAGEMENT	90
X. INTERNATIONAL AND DOMESTIC COLLABORATION	92
XI. REFERENCES	94
XII. SCHEDULE AND BUDGET	96
RESPONSE TO NSF NOTICE NO. 107	98
KEY PERSONNEL: VITAE	
KEY PERSONNEL: PUBLICATIONS	
APPENDICES:	
A. The Physics of Gravitational Waves, and Comparison of Source Strengths with Detector Sensitivities	
B. Interferometer Concepts and Noise	
C. Concepts for Advanced Interferometers	
D. Calculation of Vibration Isolation	
E. Power Spectral Density and Detector Sensitivity	
F. Scattering and Optical Properties of the Beam Tubes	
G. LIGO Project Gravitational-Wave Searches	
H. Report on Recent Progress	
J. History of the Project	
K. Memoranda of Understanding	

Outline of Contents: Volume 2

- I. Introduction**
 - II. Design Requirements, Specifications, and Goals**
 - III. Phased Implementation**
 - IV. Design Description**
 - A. Overview**
 - B. Initial Interferometer Design Description**
 - C. Vacuum System: Mechanical Design**
 - D. Vacuum System: Vacuum Design**
 - E. Enclosure Design**
 - F. Instrumentation, Control, and Data System**
 - G. Electrical Power**
 - V. Sites**
 - VI. Implementation Plan**
 - A. Work-Breakdown Structure**
 - B. Organization and Responsibilities**
 - C. Design and Construction Schedule**
 - D. Subcontracting Plan**
 - E. Interferometer Design and Fabrication**
 - VII. Cost Summary**
**(Including: Proposal Budget in NSF Format,
Current and Pending Support, and Residual Funds Statement)**
- Appendices:**
- A. Expansion to Phase-B and Phase-C Configurations**
 - B. Post-Construction Operations Cost**
 - C. Design and Construction Cost Detail**
 - D. Measured Outgassing Properties of Stainless Steel**





*"There is nothing more difficult to take in hand,
more perilous to conduct,
or more uncertain in its success,
than to take the lead
in the introduction of a new order of things."*

—MACHIAVELLI, *The Prince* (1513)

PREFACE

This proposal requests support for the design and construction of a novel scientific facility—a gravitational-wave observatory—that will open a new observational window on the universe.

The scale of this endeavor is indicated by the frontispiece illustration, which shows a perspective of one of the two proposed detector installations. Each installation includes two arms, and each arm is 4 km in length.

In view of the magnitude of the proposed project, and because reviewers will have varying degrees of familiarity with the subject matter, we have provided a substantial amount of tutorial material and scientific justification. While this should provide a comprehensive basis for forming a reasoned judgment, it also challenges the readers' fortitude and endurance in absorbing the material.

A reader who wishes to come quickly to the heart of the proposal may want to scan Section I, then read Section II, which introduces the characteristics and sources of gravitational waves and the principles of their detection, and then proceed to Section IV, which outlines our basic concept of a gravitational-wave observatory. The remaining sections of Volume 1 may be studied as the spirit—and the Table of Contents—moves the reader. Volume 2 presents the plans for construction and implementation of the concepts introduced in Volume 1.

1. *Introduction*
2. *Methodology*
3. *Results*
4. *Conclusion*

The first section, *Introduction*, provides an overview of the study, including its purpose, scope, and methodology. The second section, *Methodology*, details the research design and methods used to collect and analyze the data. The third section, *Results*, presents the findings of the study, including the main results and their implications. The fourth section, *Conclusion*, summarizes the key findings and concludes the study.

SUMMARY

This proposal requests support for a 4-year program to build and operate a Laser Interferometer Gravitational-Wave Observatory (LIGO) and to continue research and development of interferometric detectors of ever higher sensitivities. The proposed LIGO includes interferometer installations of 4-km arm length and support facilities; these installations would be located at two widely separated sites in the continental United States and operate in coincidence for the detection of gravitational waves. The LIGO project is a joint effort of scientists at the California Institute of Technology and the Massachusetts Institute of Technology and includes collaborative programs with scientists at other institutions. The observatory will be open for use by the national community, and will become part of a planned worldwide network of gravitational-wave observatories. The proposed LIGO is based on almost two decades of science research and development. The ultimate objectives of the LIGO program include (1) tests of Einstein's General Theory of Relativity—in particular, measurement of the graviton's rest mass and spin and studies of the domain of highly nonlinear, dynamic gravity, and (2) the opening of an observational window on the universe that differs fundamentally from that provided by electromagnetic or particle astronomy.

INTRODUCTION

The first part of this paper describes the development of a new technique for the determination of the concentration of a solution of a weak acid or base. This technique is based on the fact that the equilibrium constant of a weak acid or base can be determined from the ratio of the concentrations of the acid and base at the point of equivalence. The second part of this paper describes the use of this technique to determine the equilibrium constant of a weak acid or base. The third part of this paper describes the use of this technique to determine the equilibrium constant of a weak acid or base.

I. INTRODUCTION

Gravitational waves are traveling perturbations in the curvature of spacetime. They are predicted by Einstein's theory of general relativity and all other relativistic theories of gravity [I-1]. Gravitational waves should be emitted by coherent bulk motions of matter (e.g., collapsing stellar cores) and by coherent, nonlinear vibrations of spacetime curvature (e.g., colliding black holes).

Gravitational waves have not been directly detected as yet. Their observation will open a new window on the universe and may materially change our view of a cosmos based primarily upon the study of electromagnetic waves.

Research and development by members of the Laser Interferometer Gravitational-Wave Observatory (LIGO) Project team and others over almost two decades, largely supported by the National Science Foundation, have created technology and techniques that are likely to make possible the detection of gravitational waves and the successful pursuit of gravitational-wave astronomy. In particular, experience with prototype laser-interferometer gravitational-wave detectors has made it possible to design full-scale instruments with sensitivities in the range of anticipated astrophysical signals.

This proposal requests support for the construction of the LIGO and for its initial operations. The proposed 4-year program will be conducted by members of the LIGO Project, a joint undertaking of the California Institute of Technology (Caltech) and the Massachusetts Institute of Technology (MIT).¹

The LIGO will consist of two observatory facilities located far apart, but within the continental United States. These facilities will incorporate L-shaped vacuum systems with arms of 4-km length that house the laser interferometer detectors for gravitational waves. Comparison of data from interferometers at the two sites will give convincing identification of gravitational waves and will extract a significant portion of the information they carry. The LIGO concept incorporates capabilities for concurrent observation and detector development. LIGO facilities will support an extensive program of gravitational-wave astronomy open to participation by the broader scientific community. The LIGO will become part of a planned worldwide network of gravitational-wave detectors coordinated to extract the full information carried by gravitational waves.

This proposal consists of two volumes. Volume 1, **LIGO Science and Concepts**, presents the scientific justification, with Section II introducing the characteristics and sources of gravitational waves and the principles of their detection. Section IV outlines our basic concept of a gravitational-wave observatory. For greater depth, Section III.A provides a tutorial on the principles and capabilities of laser interferometer detectors, and Section III.B describes our working prototype interferometer. Sections V.A and V.B discuss the concept of the initial LIGO detectors and their

¹ For details on the history of the LIGO project, see Appendix J.

evolution. Section VI describes plans for initial observatory operations, and Section VII explains how we plan to produce credible results. Section V.C addresses how interferometer facilities need to be located in order to optimize astrophysical observations. Section VIII summarizes the key developments of the enabling research leading to the present proposal and outlines future research and development tasks. Sections IX and XII present a management, schedule, and budget overview.

Appendices provide in-depth discussion of scientific or technical issues or historical perspective. In particular, Appendix A presents a more comprehensive discussion of astrophysical sources of gravitational waves, and Appendix C provides a physical discussion of interferometer evolution and possibilities for enhanced measurement sensitivity.

Volume 2, Phase-A Design and Construction Implementation, addresses the requirements derived from Volume 1 and presents a conceptual design description, a construction implementation plan, and a cost analysis for LIGO.

The conceptual design of the LIGO detector is based on the design of the two existing detectors, the LIGO and Virgo detectors. The conceptual design is intended to be a detailed description of the detector's design, including the basic design philosophy, the major components, and the overall system architecture.

The conceptual design of the LIGO detector is based on the design of the two existing detectors, the LIGO and Virgo detectors. The conceptual design is intended to be a detailed description of the detector's design, including the basic design philosophy, the major components, and the overall system architecture.

The conceptual design of the LIGO detector is based on the design of the two existing detectors, the LIGO and Virgo detectors. The conceptual design is intended to be a detailed description of the detector's design, including the basic design philosophy, the major components, and the overall system architecture.

The conceptual design of the LIGO detector is based on the design of the two existing detectors, the LIGO and Virgo detectors. The conceptual design is intended to be a detailed description of the detector's design, including the basic design philosophy, the major components, and the overall system architecture.

The conceptual design of the LIGO detector is based on the design of the two existing detectors, the LIGO and Virgo detectors. The conceptual design is intended to be a detailed description of the detector's design, including the basic design philosophy, the major components, and the overall system architecture.

The conceptual design of the LIGO detector is based on the design of the two existing detectors, the LIGO and Virgo detectors. The conceptual design is intended to be a detailed description of the detector's design, including the basic design philosophy, the major components, and the overall system architecture.

II. PHYSICS OF GRAVITATIONAL WAVES, SOURCES, AND DETECTORS

This section presents, in brief, the scientific justification and goals of the LIGO Project. For greater detail and references to the literature, see Appendix A.

A. The Physics of Gravitational Waves and Interferometric Detectors

Gravitational waves are predicted by general relativity theory and by all other relativistic theories of gravity; all the theories agree—in rough order of magnitude—on the strengths of the waves to be expected from astrophysical sources. However, the theories disagree on a wave's propagation speed (from which one can infer the rest mass of the gravitons that carry the wave) and on its polarization properties (from which one can infer the gravitons' spin). In general relativity, the propagation speed is the same as that for light (the graviton has zero rest mass), and the wave's force field is transverse to its propagation direction and has quadrupolar symmetry (the graviton has spin two). The two polarization states of general relativity's wave are called + ("plus") and \times ("cross") and are characterized by two dimensionless fields h_+ and h_\times .

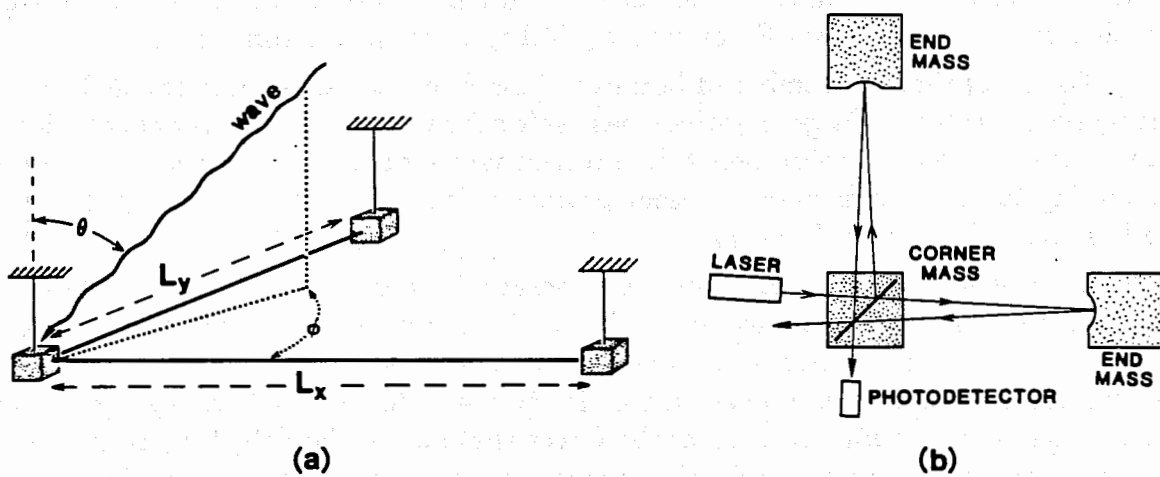


Figure II-1 Schematic diagrams of a laser interferometer gravitational wave detector, showing (a) the arrangement of three masses in an "L" configuration that responds to an incoming wave, and (b) interferometric determination of the motion of the test masses.

A *laser interferometer gravitational-wave detector*, in its simplest conceptual variant, consists of three masses hung by wires from overhead supports at the corner and ends of an "L" (Figure II-1a). A gravitational wave pushes the masses back and forth relative to each other, changing the difference $L_x - L_y$ in the length of the detector's two arms by an amount ΔL that is proportional to arm length, $L \simeq L_x \simeq L_y$, and to a linear combination of h_+ and h_\times :

$$\frac{\Delta L}{L} = [(1/2)(1 + \cos^2 \theta) \cos 2\phi] h_+ + [\cos \theta \sin 2\phi] h_x \equiv h \quad (\text{II.1})$$

Here (θ, ϕ) is the wave's propagation direction. By laser interferometry one directly reads out $\Delta L/L$ and from its time evolution, the combination (called h) of $h_+(t)$ and $h_x(t)$ in Equation (II.1). This h is sometimes called the *gravitational-wave strain* because it is the direct producer of the strain $\Delta L/L$ in the detector.

Laser interferometry—in its simplest theoretical variant—is performed as follows. Light from a laser shines on a beam-splitting mirror that rides on the corner mass (Figure II-1b). The beam splitter directs half the light toward each of the two end masses, and mirrors on those masses return beams to the splitter where they recombine. The gravity-wave-induced change in the arm-length difference ΔL produces a relative phase shift in the recombining beams, affecting the amounts of light received by the photodetector or returned to the laser. The photodetector output, therefore, varies in direct proportion to ΔL and thus proportionally to the combination of $h_+(t)$ and $h_x(t)$ appearing in Equation (II.1). In realistic variants of such a detector (Section III), the ΔL -induced phase shift is increased by placing mirrors on the corner mass as well as well as on the ends, and bouncing the light back and forth many times in each arm (“delay-line interferometer”) or operating each arm as a giant Fabry-Perot cavity (“Fabry-Perot interferometer”).

For an optimized number of bounces¹ (and because ΔL is proportional to L), longer arms result in larger relative phase shifts for the beams that propagate down the arms, and thus a more sensitive interferometric detector. That is why we are planning to upgrade from our present prototype interferometers with $L \leq 40$ m to a full-scale LIGO with $L = 4$ km.

By cross-correlating the outputs of several interferometers with different orientations and different locations on Earth, i.e., by using them as a detector network, one can read the full information carried by a gravitational wave: the direction (θ, ϕ) of its source and the time evolution of its two waveforms $h_+(t)$ and $h_x(t)$. One can also read the spatial pattern of the forces that act on the detector's masses and from it infer the wave's polarization properties and thence the graviton's spin. If the wave's source is, e.g., a supernova that is also seen with electromagnetic detectors (such as optical, radio, or X-ray telescopes) a measure of the delay between the electromagnetic and gravitational signals can be used to determine whether gravitons propagate at the same speed as photons; if they do, gravitons have zero rest mass.

The gravitational waveforms $h_+(t)$ and $h_x(t)$ carry detailed information about the waves' sources. Because the strongest sources in the LIGO's broad frequency band ($10 \text{ Hz} \lesssim f \lesssim 10^4 \text{ Hz}$) are likely to be neutron stars and black holes, the waveforms can bring us detailed information about the dynamical behaviors of

¹ See Appendix B.

these objects in such violent events as their births and collisions (cf. Figure A-3 in Appendix A). Detection of a stochastic background of gravitational waves from the big bang could bring us detailed information about the earliest moments of the universe; coalescing, compact binary stars could act as standard candles for measuring the large-scale structure of the universe in later epochs (see Appendix A for details).

Gravitational and electromagnetic waves differ greatly. Gravitational waves should be emitted by coherent bulk motions of matter (e.g., collapsing stellar cores) and coherent, nonlinear vibrations of spacetime curvature (e.g., collisions of black holes). By contrast, astronomical electromagnetic waves are usually incoherent superpositions of emission from individual atoms, molecules, and charged particles. Gravitational waves are emitted most strongly in regions of spacetime where gravity is relativistically strong, whereas electromagnetic waves come almost entirely from weak-gravity regions, since strong-gravity regions tend to be obscured by surrounding matter. Because of these differences, the information carried by gravitational waves is almost "orthogonal" to that carried by electromagnetic waves and our present electromagnetically based understanding of the universe is inadequate to predict with confidence the strengths of the gravitational waves bathing the Earth. Obversely, if gravitational waves are detected and studied, they may create a revolution in our view of the universe comparable to that wrought by radio astronomy.

B. Scientific Payoff from the LIGO Project

From the above discussion and the details in Appendix A, we select the following list of scientific payoffs that might come from the LIGO Project. The project is designed and managed, so far as possible, to maximize the likelihood that some or most of these payoffs will be achieved.

1. Possible payoffs for physics

- The direct verification of the existence of gravitational waves.
- Measurement of the propagation speed and polarization properties of the waves, and from them the rest mass and spin of the graviton: do they agree with general relativity's predictions, $m = 0$ and $s = 2$?
- Verification (by comparing theoretical and observed wave forms) that black holes exist and that their dynamics are as predicted by general relativity. By this, test general relativity for the first time in the domain of highly nonlinear, dynamic gravity.

2. Some possible payoffs for astronomy and astrophysics

- Open up a new window on the universe, one almost certain to bring surprises and that may bring a revolution comparable to that which came from the radio window in the 1950s and 60s.

- Study the behavior of neutron stars in highly dynamical situations. By this, extract information about the uncertain physics that governs neutron stars.
- Use the waves from the coalescence of black-hole and neutron-star binaries as “standard candles” for the determination of the Hubble expansion rate and deceleration parameter of the universe (see Appendix A).
- Detect primordial gravitational waves from the big bang and from them extract information about the initial conditions and earliest stages of evolution of the universe.

C. Estimates of the Strengths of the Waves at Earth and Comparison With Anticipated LIGO Sensitivities

When these payoffs can be achieved will depend on when detectors in the LIGO can reach the required sensitivities. Figure II-2 gives some indication of the prospects for this by comparing the wave strengths from various hypothesized burst sources with several benchmarks for detector sensitivity. (For the details underlying Figure II-2, and for similar figures for periodic and stochastic waves, see Appendix A.)

The most certain of the sources is coalescence of neutron-star binaries. Estimates based on pulsar statistics in our own galaxy suggest that to see three such events per year one should look out to 100^{+100}_{-40} Mpc distance. (See Appendix A for further details on this and all sources). For supernovae, the event rate is known to be roughly one each 40 years in our own galaxy (10 kpc distance) and several per year in the Virgo cluster (10 Mpc), but the amount of radiation emitted is very uncertain. For black-hole births, both the wave-emission efficiency and the distance to which one must look are highly uncertain.

The upper solid curve and stippled region in Figure II-2 indicate the best sensitivity achieved to date by our 40-meter prototype. The middle solid curve and stippling indicate the sensitivity of an early detector that might operate in the LIGO. The concept for this early detector is described in Section V.A. Once the early detector has been operated near the sensitivity of the middle curve, a succession of ever-improving detectors will evolve, continually pushing the sensitivity level down (to smaller h) and left (to lower frequencies, f). As a rough indication of where this might lead after a few years, we show (lower solid curve and stippling) the sensitivity of an “advanced detector” based on concepts given in Section V.B and Appendix C.

It is reasonable to expect, in later years of the LIGO, improvements beyond this advanced detector, as indicated by the arrows labeled “improved seismic isolation,” “improved thermal noise,” “improved recycling,” and “squeezed light” (see Appendix C). The only limit of principle on detector sensitivities in the LIGO is the “quantum limit” (solid line); with cleverness, ways of circumventing it might be developed.

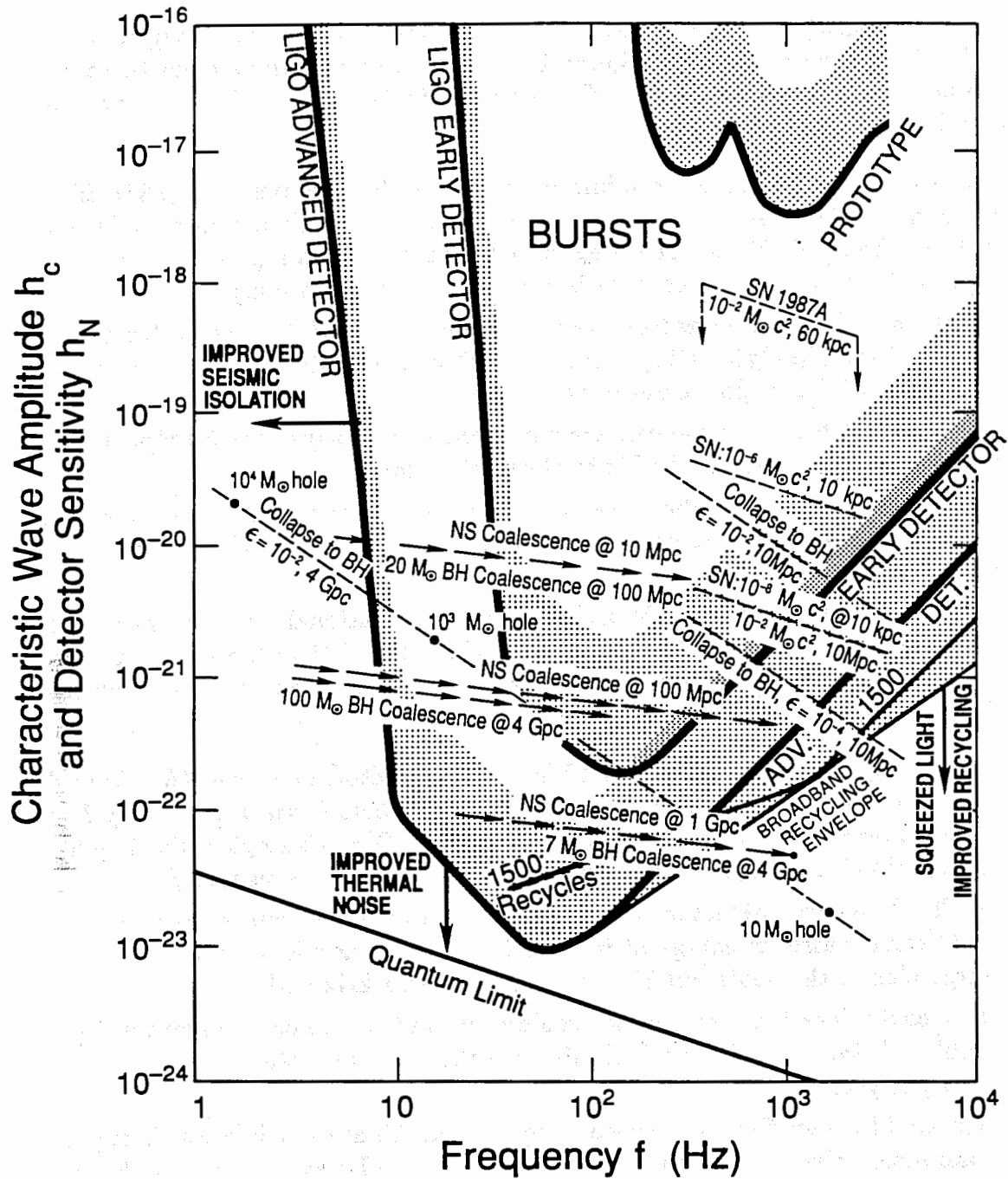


Figure II-2 A comparison of the strengths of gravitational waves (characteristic amplitude h_c and frequency f) for burst signals from various sources (dashed lines and arrows), and benchmark sensitivities h_N (solid curves and stippled strips atop them) for interferometric detectors today (*prototype*) and in the proposed LIGO (*early detector*, *advanced detector*). See the caption of Figure A-4a (a duplicate of this figure) and the associated discussion in Appendix A for more details.

By comparing the benchmark sensitivities with the source strengths in Figure II-2 (burst sources) and in Figures A-4b and c (periodic and stochastic sources) of Appendix A, one sees that *the first detector in the LIGO will have significant possibilities for detecting waves*:

- It could have detected the initial wave burst from Supernova 1987A if that burst carried $\sim 10^{-4}$ solar masses of energy or more. (This amount could easily have been the result if the collapsing stellar core were rotating rapidly enough to produce a 0.5 millisecond pulsar, as is suggested by observation.)
- It could detect the low-frequency radiation (< 300 Hz) in bursts from supernovae that have rapidly rotating cores and that fragment during the collapse—this at a distance of the Virgo cluster of galaxies.
- It could detect the coalescence of a neutron-star binary out to 30 Mpc distance (three times the distance of the Virgo cluster of galaxies).
- It could detect periodic waves from the Crab pulsar if the wave amplitude exceeds 1/10 of the current limit, which is based on the rate of spindown of the pulsar.
- It could detect a stochastic background of gravitational waves between 50 Hz and 150 Hz, if that background carries more than 2×10^{-7} of the energy required to close the universe. (This is close to the level expected from non-superconducting GUT cosmic strings, if they exist.)

If waves are not detected by the LIGO's first detector, *they probably will be detected by a subsequent detector with sensitivity somewhere between the "early detector" and "advanced detector" sensitivities of Figure II-2*. Examples that illustrate the *high probability* of detection at the "advanced detector" sensitivity are:

- The "advanced detector" could detect a supernova in our galaxy that puts out 10^{-8} solar masses of energy at frequencies of 1 kHz and less, or a supernova in the Virgo cluster that puts out 10^{-2} solar masses at 1 kHz and less.
- It could detect a neutron-star coalescence out to almost 1 gigaparsec (1/4 the Hubble distance)—within which distance there are expected to be many coalescences per year.
- It could detect the coalescence of equal-mass binary black holes throughout the observable universe, so long as the hole masses are between 10 and 1000 times the mass of the Sun.
- It could detect the Crab and Vela pulsars if they are as strong as the current (highly unreliable) best guess.
- It could detect a stochastic background between 30 Hz and 90 Hz if that background carries an energy exceeding 10^{-10} of the energy required to close the universe.

D. Other Methods of Detecting Gravitational Waves

The above discussion provides a basis for comparing the LIGO Project with other methods of detecting gravitational waves.

There is a rich potential for gravitational-wave astronomy at frequencies below the LIGO's 10-Hz cutoff, but such frequencies probably cannot be reached with Earth-based detectors. The best long-term promise in the band from 1 Hz to 10^{-5} Hz lies with interferometric detectors in space, which will rely in considerable measure on experience with the LIGO; and below 10^{-5} Hz the best promise lies with timing of pulsars and measurements of anisotropy of the cosmic microwave radiation.

In the LIGO's frequency band, Earth-based bar detectors have been under development since the early 1960s, a decade longer than interferometric detectors. Room-temperature bars achieved an h -sensitivity for bursts of 3×10^{-17} in the mid 1970s (before the Caltech and MIT prototypes were operational); by cooling to 4K, they (Stanford and Rome/CERN) are now at 1×10^{-18} . For the foreseeable future, bars will remain an important component of the world's gravitational-wave research effort and they may well improve into the vicinity of 10^{-20} , which is adequate for the detection of rare events in our own galaxy or the Magellanic clouds, but inadequate for extragalactic astronomy, the realm of large event rates.

Bar detectors cannot be lengthened to kilometer scales with an accompanying large sensitivity improvement (recall: $\Delta L \sim hL$), because they rely on sound waves (speed ~ 1 m/ms) rather than light (speed 300 km/ms) for coupling their two ends. As a result, it is unlikely they will reach the LIGO's projected sensitivity region of $\sim 10^{-21}$ to $\sim 10^{-23}$ (the realm of extragalactic astronomy) (cf. Figure II-2). Also, bar detectors have difficulty achieving large bandwidths, and correspondingly can extract only limited information from any waves they discover. At present, their bandwidths are $\Delta f/f \sim 0.01$ at $f \simeq 900$ Hz, and there is hope in the future of reaching $\Delta f/f \sim 0.2$. By contrast, the present prototype interferometers have $f_{\max}/f_{\min} \sim 10$, and the LIGO is projected to have $f_{\max}/f_{\min} \sim 1000$ (Figure II-2)—adequate for essentially full information extraction.

Some Observations on the Life of a Magpie

The magpie is a bird of great interest and beauty. It is a bird of the forest, and its song is a sweet melody. It is a bird of the wood, and its flight is graceful and elegant. It is a bird of the stream, and its voice is melodious and musical. It is a bird of the field, and its song is a sweet melody. It is a bird of the garden, and its voice is melodious and musical. It is a bird of the sky, and its song is a sweet melody. It is a bird of the earth, and its voice is melodious and musical.

The magpie is a bird of great interest and beauty. It is a bird of the forest, and its song is a sweet melody. It is a bird of the wood, and its flight is graceful and elegant. It is a bird of the stream, and its voice is melodious and musical. It is a bird of the field, and its song is a sweet melody. It is a bird of the garden, and its voice is melodious and musical. It is a bird of the sky, and its song is a sweet melody. It is a bird of the earth, and its voice is melodious and musical.

The magpie is a bird of great interest and beauty. It is a bird of the forest, and its song is a sweet melody. It is a bird of the wood, and its flight is graceful and elegant. It is a bird of the stream, and its voice is melodious and musical. It is a bird of the field, and its song is a sweet melody. It is a bird of the garden, and its voice is melodious and musical. It is a bird of the sky, and its song is a sweet melody. It is a bird of the earth, and its voice is melodious and musical.

III. LASER INTERFEROMETERS

A. General Characteristics and Noise Effects

This section presents a brief discussion of the general characteristics of laser interferometers and of limits to the interferometers' sensitivity. For details of calculations and references to the literature, see Appendix B.

1. Gravitational-wave detection using interferometers

The sensitivity of an interferometric gravitational-wave detector— $h = \Delta L/L$ (Section II.A, Equation (II.1))—can be increased by making its arms longer, up to one-fourth the wavelength of the signal. For example, a detector optimized for 100-Hz waves would be 750 km long. Although this is prohibitively long for Earth-based detectors, interferometers several kilometers in length are realizable.

Interferometric detectors have two arms. A single, long, resonant cavity consisting of two mirrors excited by a stable laser can be used to measure motion of the cavity mirrors, motion that might be caused by gravitational waves. However, such a single-arm detector does not distinguish between a gravitational wave and frequency fluctuations in the light. A second arm is necessary to eliminate the effect of fundamental frequency fluctuations associated with all practical light sources; the maximum sensitivity is achieved when the arms are orthogonal.

2. Fabry-Perot interferometers for gravitational-wave detection

The response of an interferometer to changes in arm length can be increased by folding the optical path, thereby increasing the time that light is stored between the mirrors, until a storage time of about one-half the gravitational-wave period is reached. We have chosen to store the light by making each arm a resonant Fabry-Perot cavity.¹ Each cavity is composed of two mirrors with low-loss reflective coatings. The input mirror has a small transmission, and the end mirror is coated for highest reflectivity. The light is stored between the mirrors for a time $\tau_s \approx 2L/cT_1$, where T_1 is the intensity transmission of the input mirror. The light-transit time from one mirror to the other is $\tau_t = L/c$; one can think of the beam going back and forth between mirrors $2/T_1$ times before it reemerges from the input mirror.

One arrangement of Fabry-Perot cavities for a gravitational-wave detector is shown in Figure III-1. In their quiescent state, the cavities are in resonance² with the laser light. The incident laser light is split evenly by the beam splitter (BS) and reflects from both cavities with a phase shift of 180 degrees before returning to the splitter. There the beams are again divided. The beam returning from

¹ The theory of the Fabry-Perot cavity as an optical storage element for gravitational-wave detectors is given in Appendix B.

² The cavity length L equals a half-integral multiple of the laser wavelength.

cavity 1 (top) is in part reflected back toward the laser and in part transmitted to the photodetector (D1) at the antisymmetric port of the beam splitter. The beam returning from cavity 2 (right) is in part transmitted back toward the laser and in part reflected (with an additional 180-degree phase shift) toward the photodetector at the antisymmetric port. The two beams incident on the photodetector interfere destructively; in other words, the interferometer operates on a minimum intensity “dark fringe.”

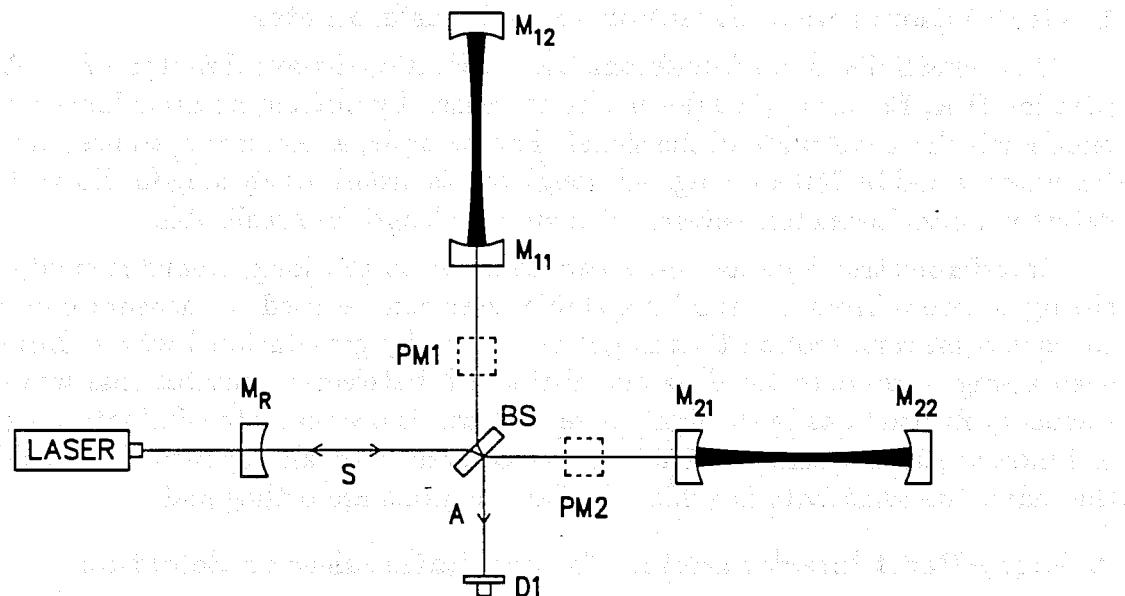


Figure III-1 Schematic of a recombined Fabry-Perot interferometer that includes a mirror, M_R , for broad-band recycling. Cavity 1 is formed by mirrors M_{11} and M_{12} , Cavity 2 by M_{21} and M_{22} . Other components include a beam splitter (BS), phase modulators (PM1 and PM2), and a photodetector (D1). The symmetric and antisymmetric ports are designated by “S” and “A”.

Assume that a gravitational wave is incident normal to the plane of the interferometer and has a polarization that stretches cavity 1 and shrinks cavity 2. When it travels through the detector, it disturbs the resonance by causing small phase shifts in the light reflected from the cavities. In the interaction with the gravitational wave, the reflected light from cavity 1 experiences, say, a positive phase shift, ϕ_1 , and the reflected light from cavity 2 has a negative phase shift, $\phi_2 = -\phi_1$. The destructive interference at the photodetector is no longer complete; a signal is developed that is proportional to the difference in phase between the two cavities, which in turn is proportional to ΔL and hence to the gravitational-wave strain, h .

The interference of the beams returning toward the laser at the symmetric port of the beam splitter is constructive (the “bright fringe”) and, if the optical losses in the interferometer are small, most of the incident light returns in this direction.

The returned light can be reused by placing a partially transmitting mirror, M_R , between the splitter and the laser. By selecting the transmission and controlling the location of this mirror, the interference is adjusted so that no light returns to the laser and the light in the cavities is enhanced.³ This technique is broad-band and has the same frequency response as the non-recycling interferometer; the only change is an increase in effective light power.

After processing, the signal from the photodetector is applied as a feedback force to cavity mirror M_{12} to hold the interferometer on the dark fringe. This use of feedback reduces sensitivity to laser amplitude noise and improves system linearity; it also makes recycling possible. The gravitational-wave signal appears at the output of the amplifier that is connected to the force transducer controlling M_{12} .

An interferometer which gives a large enhancement in sensitivity over a limited bandwidth around a chosen frequency can be obtained by arranging that the optical signal is magnified by resonance in a coupled-cavity system, in what is known as a resonant recycling interferometer. A related modification to broad-band recycling, known as dual recycling, has been proposed recently. This is a flexible optical configuration, which enables a single interferometer to be adjusted to operate over a range of modes all the way from broad-band recycling to narrow-band resonant recycling.⁴

The optical phase modulators PM1 and PM2 impress a small phase dither on the light at radio frequencies, translating the optical phase information from frequencies in the gravitational-wave band to signals at radio frequencies. This technique reduces the interferometer sensitivity to low frequency amplitude noise in the light and electronics. The optical phase modulators are also used to provide fast control of optical phase in order to stabilize the feedback loops that hold the optical fringes.

The optical components in the interferometer are suspended by wires, so above the resonance frequency of the suspensions (on the order of 1 Hz) they are effectively free in inertial space and responsive to the gravitational-wave strain. The suspensions also help isolate the optical components from seismic noise and provide a means for system alignment.

The foregoing description of a laser interferometric gravitational-wave detector gives only the basic concepts. Actual implementation of such a system involves many more components; more detailed descriptions are given in Sections III.B and V.A.

³ This "recycling" interferometer is, in effect, a resonant cavity in which the circulating power has been increased by approximately the reciprocal of the optical losses in the non-recycling interferometer.

⁴ These interferometer systems are discussed in more detail in Appendix C.

the detector's performance, particularly around the strain measurement frequency, will depend on the quality of the optical components and the mechanical design of the detector.

3. Noise sources and sensitivity

Sources of noise that can limit the sensitivity of an interferometric gravitational-wave detector are of three types. First, there are random processes *intrinsic* to the measurement. Examples are shot noise in the light, "quantum noise" associated with the uncertainty principle, and thermal fluctuations in masses, mirrors, suspension wires and other physical elements, that induce motions of the optical surfaces. These intrinsic noise sources give calculable theoretical limits to the detector performance.

A second source is noise induced by the *environment*; examples include the transmission of random seismic motions to the optical components, as well as random forces on the optical components due to fluctuating, Newtonian gravitational-field gradients. These influences can be reduced by good design and experiment strategy; nevertheless, they present a background that becomes increasingly important as the detector sensitivity is improved.

A third group of noise sources are *technical*. These are nonfundamental effects—those whose influence can be reduced by care and by advances in the technology. Examples are interferometer phase fluctuations resulting from instability of laser-beam geometry, phase fluctuations from residual gas along the transmission paths, and scattering of light by mirrors and tube walls.

Noise sources that have been identified, estimated, and in many cases measured in the laboratory, are listed in Table III-1. This table classifies the noise sources into two groups: those that influence the strain measurement (sensing noise), and those that impose random forces on the interferometer end points. In general, the influence of random forces is reduced linearly by increasing the interferometer arm length while the various types of sensing noise decrease as different powers of arm length.

TABLE III-1
IDENTIFIED AND ESTIMATED NOISE SOURCES

Noise terms influencing the strain measurement (various dependencies on L)

- Photon shot noise
- Laser amplitude noise
- Laser frequency fluctuations
- Scattering of light by
 - 1. Moving surfaces
 - 2. Stationary surfaces
- Laser beam fluctuations in position and angle
- Fluctuations in forward scattering of light that are caused by residual gas

Random forces on interferometer end points (all scale as $1/L$)

- Seismic noise
- Thermal noise in the suspension
- Thermal noise driving mirror modes
- Fluctuations in radiation pressure on the mirrors
- Fluctuating external gravitational gradients
- Fluctuating electric and magnetic fields⁵
- Cosmic-ray air showers⁶
- The quantum limit

⁵ Fluctuating magnetic and electric fields are not expected to be significant in the initial interferometers, but will have to be considered in the design of advanced interferometers operating below ~ 100 Hz. Electric field fluctuations ranging from 10^{-3} to 10^{-2} volts/cm arise from fluctuating charges on the surface of dielectrics and the "patch" effect (changes in the work function of conducting surfaces due to thermal migration of crystal faces or to fluctuations in the gas adsorbed on the surface). Magnetic field fluctuations ranging from 10^{-5} to 10^{-3} gauss may come from currents in wires driven by seismic noise, thermally driven polarization fluctuations in magnetic materials, or geomagnetic fluctuations, thunderstorms, magnetospheric phenomena, or transients in the power net. These fields can disturb the test masses through interaction with the much stronger electric or magnetic fields that might be used to control the position of the test masses. Shielding and careful design should bring these random forces below the level of other sources of noise.

⁶ The dominant source of noise will be the momentum transferred to test masses by secondary muons from energetic primary cosmic ray protons hitting the upper atmosphere. Individual muon events are not as significant as showers that could illuminate an entire building. The showers are not expected to give correlated events at two widely separated sites but could increase the singles rate. One scintillation detector per building will be used to monitor these events.

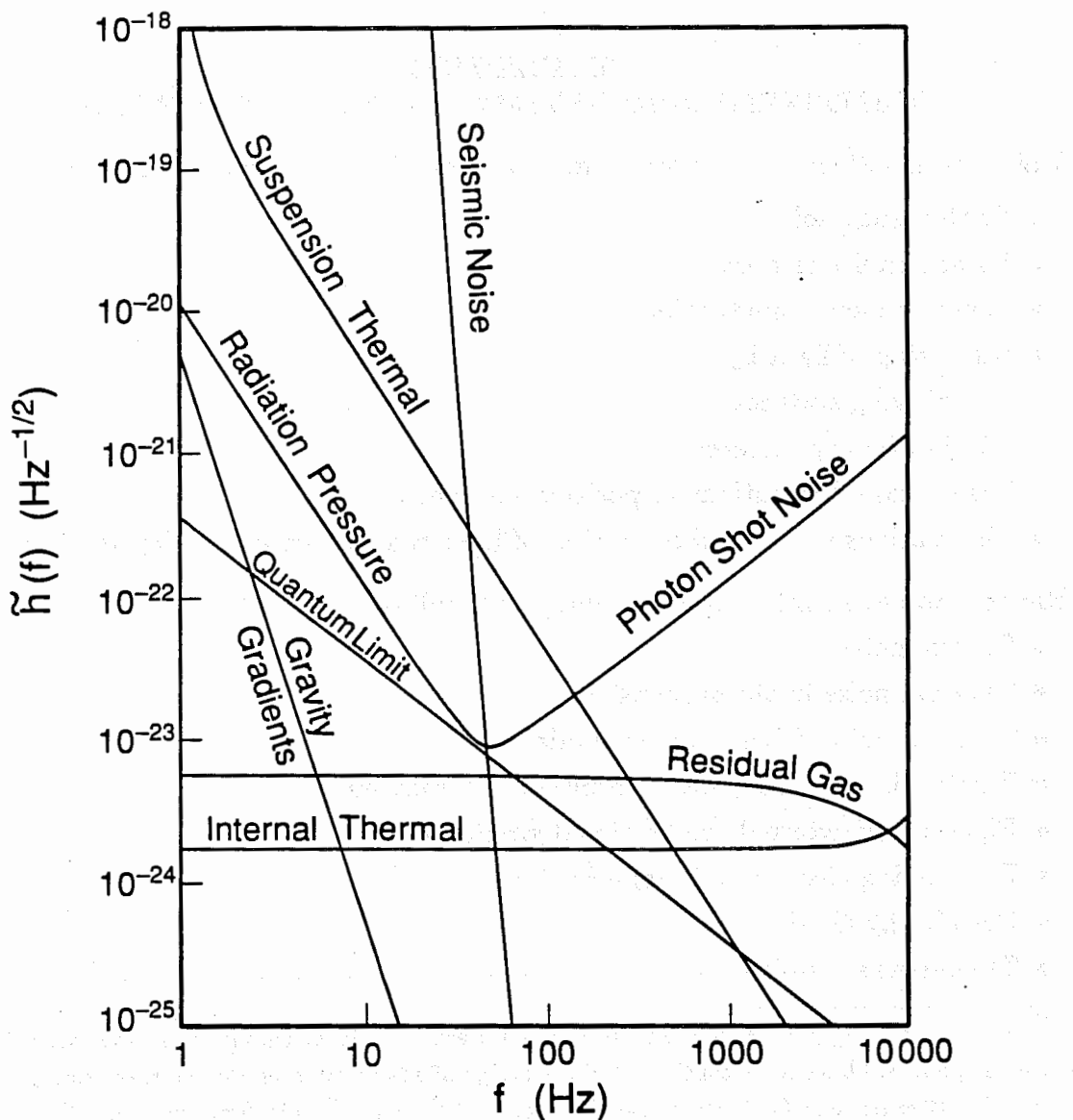


Figure III-2 Individual spectra for noise sources that can limit the performance of LIGO interferometers. They are plotted in terms of the equivalent amplitude spectral density of gravitational waves, $\tilde{h}(f)$, which has units of strain/ $\sqrt{\text{Hz}}$ and is defined in Appendix E. The expression $\tilde{h}(f)$ characterizes the instrument performance and corresponds to the rms noise amplitude normalized to an averaging time of order one second (1 Hz bandwidth). The comparison to the strength of signals depends on the signal waveform and the measurement duration (see Appendices A and E for details). The parameters used to illustrate the various noise sources are those of the initial interferometer described in Section V.A of this volume, and Section IV.B of Volume 2. The line for “photon shot noise” and “radiation pressure noise” is for a Fabry-Perot interferometer with a power buildup of 30 times (achieved with recycling), and 1 W of effective laser power (including inefficiencies). The sensitivity at the changeover from shot noise to radiation pressure noise is the quantum limit. See Appendix B for details on the other noise sources in the figure. At any frequency, the total noise level is approximately equal to the largest contributor at that frequency.

Figure III-2 shows illustrative spectra for the more important contributions to the interferometric gravitational-wave detector noise budget. In the remainder of this section we shall discuss the most important of these noise sources. Further details are given in Appendix B and references therein.

a. Photon shot noise. The ability to measure the optical phase difference at the output of the interferometer is limited by the quantum fluctuations of the light. The equivalent gravitational-wave strain noise that results from these phase fluctuations is proportional to $\sqrt{\lambda/P}$, where λ is the laser wavelength and P is the light power in the bright fringe. This photon-counting, or shot noise, depends on the gravitational-wave frequency f , and is expected to dominate the noise budget at high gravitational-wave frequencies. It also depends on the storage time τ_s ; the optimum storage time in a recycled system is $\tau_s = 1/4\pi f$. The shot noise in a broad-band recycling interferometer scales as $1/L^{1/2}$.

b. Frequency fluctuations of the laser. Laser frequency fluctuations produce phase noise if the two Fabry-Perot cavities have different storage times, τ_s . The resulting gravitational-wave strain noise spectrum is

$$\tilde{h}(f) \approx (\Delta\tau_s/\langle\tau_s\rangle)\nu(f)/\nu_0 \quad (\text{III.1})$$

where $\nu(f)$ is the spectrum of the laser frequency fluctuations and ν_0 is the laser frequency. The noise from this source is reduced by stabilizing the frequency of the laser, by balancing the two cavities, and by electronically subtracting the frequency noise common to the two arms.

Frequency noise can also enter the system through the phase fluctuations introduced by the interference between the principal beams and scattered beams that have taken different paths. The noise from stationary scatterers is reduced by using frequency stabilization. Frequency noise is not considered a major noise contributor to the initial LIGO interferometer and does not appear in Figure III-2.

c. Noise from residual gas. Residual gas in the vicinity of the test masses can produce noise by damping the suspensions (see the discussion of thermal noise, below) and by providing acoustic coupling to the outside world. These sources of noise are sufficiently reduced by operating at pressures less than 10^{-6} torr in the chambers enclosing the test masses.

A high vacuum in the long beam tubes is required to reduce the optical phase noise resulting from fluctuations in the number of residual gas molecules residing in the optical beam. The gravitational-wave strain noise spectrum is shown for an illustrative residual gas pressure (10^{-7} torr of H_2O) in Figure III-2. This noise depends on the molecular polarizability and the mass of the molecular species. Phase noise resulting from residual gas scales as $1/L^{3/4}$.

d. Thermal noise. The LIGO interferometers will operate at room temperature, and thermal excitation of mechanical elements may be a significant source

of noise. The spectrum of thermal motions depends on the frequency, mass, and the internal losses in the mechanical systems. Mechanical resonances are chosen to be outside of the gravitational-wave band. The pendulum suspensions for the optical components are designed to have resonances below the band, and the internal resonant modes of the optical components have resonances above the band.

The residual gas in the LIGO is specified to be low enough so that it does not contribute to the dissipation of the mechanical systems. The principal sources of thermal noise are expected to be dissipation in the flexure of the suspension-support elements and the internal dissipation of the normal modes of the cavity mirrors. Representative curves of the equivalent gravitational-wave strain noise, using modest-size masses and currently realized material dissipation, are shown in Figure III-2. Thermal noise is projected to be important in the noise budget of the initial interferometer at mid-frequencies; it scales as $1/L$.

e. Seismic noise. At low frequencies, an interferometer will be dominated by seismic noise transmitted through the suspension system. The amplitude of the seismic-noise spectrum varies from site to site, depends on wind conditions, and, in built-up areas, on the amount of human activity. A reasonable approximation of the noise spectrum (which we have measured at candidate sites) is given by

$$\tilde{x}(f) = 10^{-7} \left(\frac{\text{Hz}}{f} \right)^2 \text{ m}/\sqrt{\text{Hz}} \quad (\text{III.2})$$

for frequencies above 10 Hz, and as a constant $10^{-9} \text{ m}/\sqrt{\text{Hz}}$ for frequencies from 1 to 10 Hz. At frequencies above a few Hz, the seismic noise at points separated by 4 km is mostly uncorrelated; the equivalent gravitational-wave strain noise is $\tilde{h}(f) \approx 2\tilde{x}(f)/L$.

This noise level is reduced by many orders of magnitude by several cascaded spring-mass isolators, working multiplicatively with the isolation provided by the final suspension, for each test mass. Figure III-2 shows a representative noise spectrum of attenuated seismic noise⁷ for the type of multistage isolation system discussed in Appendix D. The contribution to the equivalent gravitational strain noise from seismic motions scales as $1/L$.

f. Fluctuating Newtonian gravitational gradients. Fluctuating gravitational-field gradients that arise because of moving masses in the neighborhood of the test masses may limit the performance at very low frequencies. Naturally occurring sources are the density variations in the Earth from seismic waves

⁷ This projection is not the best that can be done; seismic-noise isolation will continue to be an area in which cunning and elegance of new concepts will improve the performance of the interferometers at low frequencies. Examples of such techniques are active isolation systems and auxiliary interferometers (see Appendix C).

and in the atmosphere from sound waves. The fluctuating gravitational-field gradients are primarily uncorrelated at frequencies above a few Hertz, so the equivalent gravitational-wave strain noise from this source also scales as $1/L$. The calculated noise level is shown in Figure III-2.

g. Radiation-pressure noise and the standard quantum limit. Radiation pressure associated with the light trapped between the interferometer mirrors imparts a steady force on the mirrors, and fluctuation in the pressure driven by a fluctuating laser intensity is not expected to be a limiting factor in the LIGO performance. Additional intrinsic uncorrelated fluctuations in the radiation pressure on the cavity mirrors results from quantum fluctuations in the light.⁸ These are the source of the standard quantum limit for the interferometric gravitational detector and a macroscopic example of the application of the Heisenberg microscope. The fluctuations are uncorrelated between the cavities. Figure III-2 shows a representative estimate of the equivalent gravitational-wave strain noise from this radiation pressure source.

The radiation-pressure fluctuations are $\propto \sqrt{P}$, while the sensing shot noise is $\propto \sqrt{1/P}$. Consequently, there is an optimum circulating optical power in the interferometer that minimizes the total noise. When the interferometer operates at this power, the noise is at the standard quantum limit given by

$$h(f)_{\text{opt}} = \sqrt{4/\pi} \left(\frac{2\pi\hbar}{\eta^{1/2}m} \right)^{1/2} \frac{1}{2\pi fL} \quad (\text{III.3})$$

where $2\pi\hbar$ is Planck's constant, η the quantum efficiency of the photodetector, and m is the mass of the test mass. Figure III-2 shows the standard quantum limit for the representative system. The quantum limit is not a concern for the initial interferometers; however, it may be a fundamental limit to sensitivity and, like all other sources of random force, argues for a large detector length L .

⁸ A physically satisfying description was first given by Caves, who visualized the process by considering the fluctuating radiation pressure on the cavity mirrors as arising from the interference between the laser electric field and vacuum fluctuations entering the interferometer from the "output" (antisymmetric) port of the beam splitter.

B. 40-Meter Prototype Interferometer

The 40-meter prototype interferometer (Figure III-3), located on the Caltech campus, is the product of many years of effort in developing a laser interferometric gravitational-wave detector which uses Fabry-Perot cavities. The prototype interferometer demonstrates the feasibility and reliability of many of the proposed LIGO techniques (e.g., seismic isolation, positioning control, electro-optical servo systems), and has prepared the LIGO team to further enhance the technology. Its performance is comparable to the best existing gravitational-wave detectors. In the future, the prototype facilities⁹ will be used to identify and solve experimental problems that may arise in improving detector sensitivity, and will be used to develop and test the subsystems of full-scale LIGO interferometers.

Figure III-3 (facing page) The LIGO prototype interferometer, as of May 1989. The beam from the upper of the pair of argon-ion lasers in the foreground enters the vacuum system through a viewport on one end of a short section of vacuum tubing containing the input filter cavity. (The lower laser acts as a backup for interferometer operation, and is also used for other experiments.) The chamber in the center of the photograph houses electro-optical elements that modulate and control the phase of the beam. The beam is split in the chamber at the intersection of evacuated tubes that stretch 40 m to the ends of the corridors. (Photograph by A. Abramovici)

1. Description

The central part of the interferometer consists of two orthogonal Fabry-Perot cavities, 40 meters in length, with mirrors affixed to test masses. The chambers housing the test masses are linked by two sets of vacuum tubes: a lower pair of 20-cm-diameter tubes for the main interferometer beam, and an upper pair of 10-cm-diameter tubes for an auxiliary interferometer (under development) that will optically link the tops of the suspension wires of the test masses. Gate valves at the ends of the tubes allow the chambers to be individually vented to atmosphere without breaking vacuum in the tubes; a system of bellows compensates for atmospheric force. A cryopump maintains the vacuum at $2 \cdot 10^{-5}$ torr.

The control systems required to keep the masses precisely oriented and positioned, as well as the laser-stabilization and beam-conditioning systems, include approximately 20 separate servo loops that must function together. The interferometer has run for hour-long stretches completely unattended, even during the increased vibration levels of peak traffic, and has demonstrated the capability to operate around the clock with minimal intervention.

⁹ A second vacuum system for laser interferometers of 5-meter arm length has been constructed on the MIT campus and will be used by the LIGO team for development in parallel with the 40-meter system.

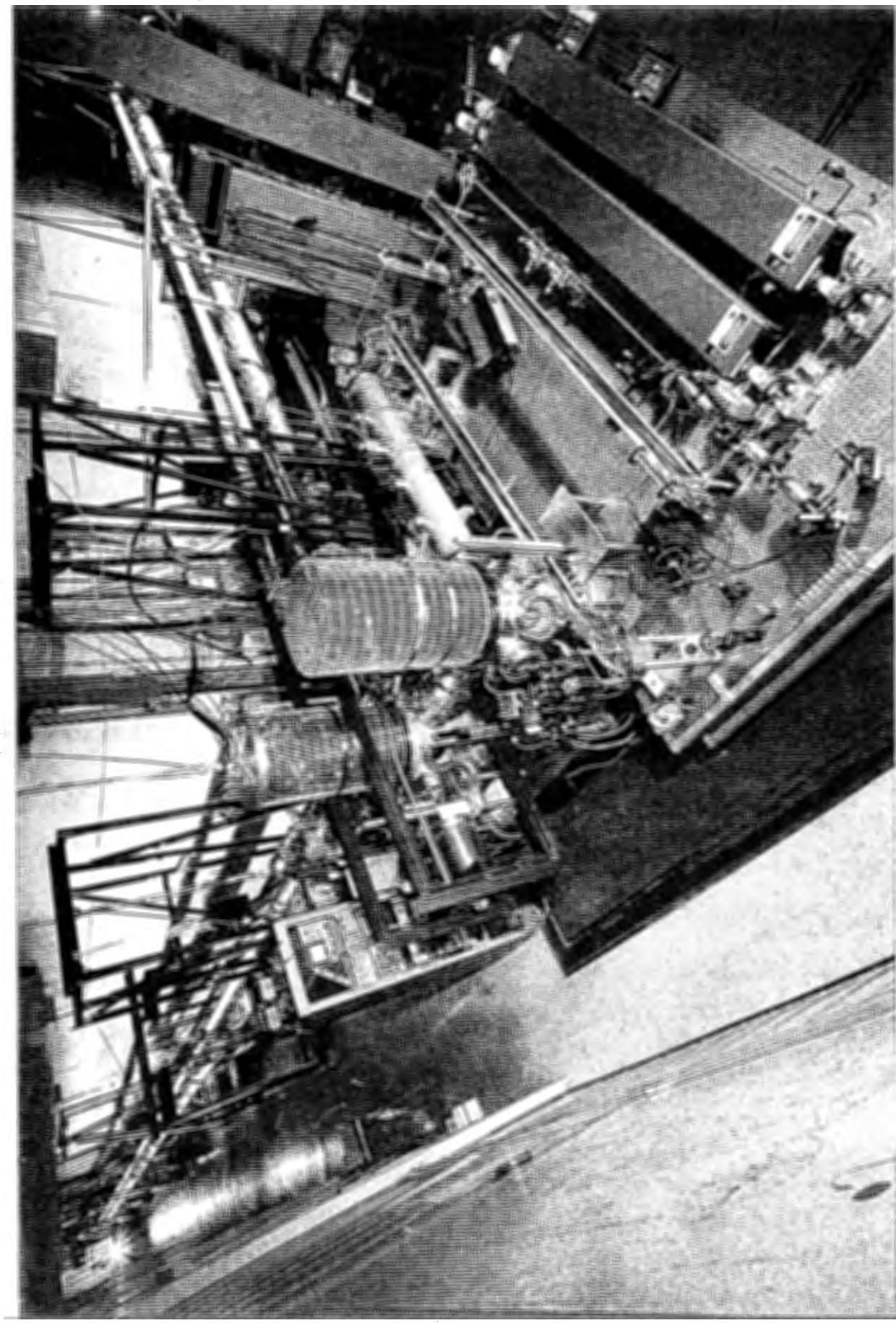




Figure III-4 shows the operational principles of the prototype interferometer, including the two-stage control of laser light frequency and phase. The optical path starts at a large-frame, argon-ion laser (Coherent I-100/20) capable of producing 5 W of single-frequency, single-transverse-mode green (514-nm) light. The beam enters an input Fabry-Perot cavity which is used as the reference for a first stage of laser frequency stabilization.¹⁰ This cavity also acts as a "mode cleaner" which filters out spatial fluctuations in the beam [III-1]. The Stage 1 frequency-control circuit causes the laser to track the mode cleaner's length, keeping the laser in resonance with the mode cleaner at all times.

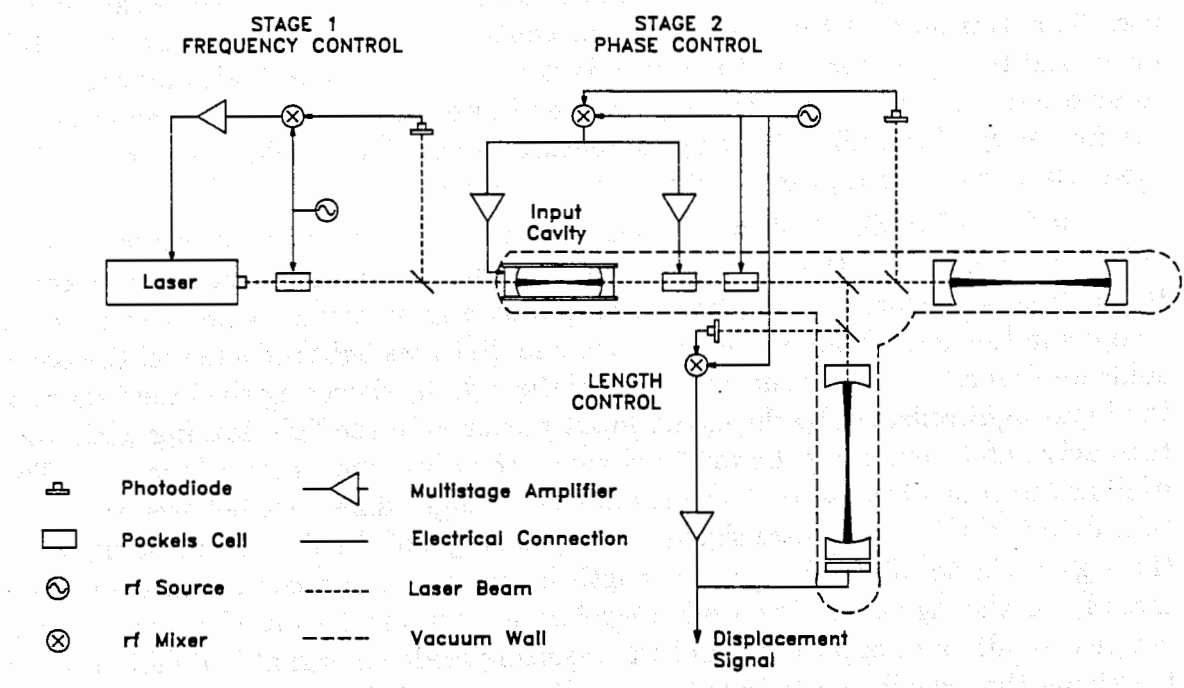


Figure III-4 The optical and electronic configuration of the 40-meter prototype interferometer, as of October 1989. Three servo loops operate to keep the input cavity and the interferometer arms on resonance. First (*Stage 1*), the laser wavelength is compared to the input cavity length by RF modulation of the optical phase via a Pockels cell. The correction signal is extracted from the reflected beam and fed back to the laser to control its frequency. Next (*Stage 2*), the light transmitted through the input cavity is stabilized to the upper interferometer arm with Pockels cells for modulation and for phase correction, and a piezo-electric transducer to adjust the length of the input cavity for frequency control. Finally (*Length Control*), the length of the other interferometer arm is controlled by pushing on the lower mass, keeping this arm in resonance with the stabilized light. The signal fed back to the mass is proportional to the length difference between the cavity arms, and hence contains the interferometer's response to gravitational waves.

¹⁰ We thank Dr. A. Brillet of the University of Paris-Sud, Orsay, France for providing the mechanical design of a fast piezoelectric controller for the laser frequency stabilization.

Most of the laser power passes through the input cavity to an auxiliary chamber containing Pockels cells for phase modulation and frequency stabilization. The beam is expanded by lenses to match the geometry defined by the 40-meter cavities, and directed to a beam splitter in the corner chamber.

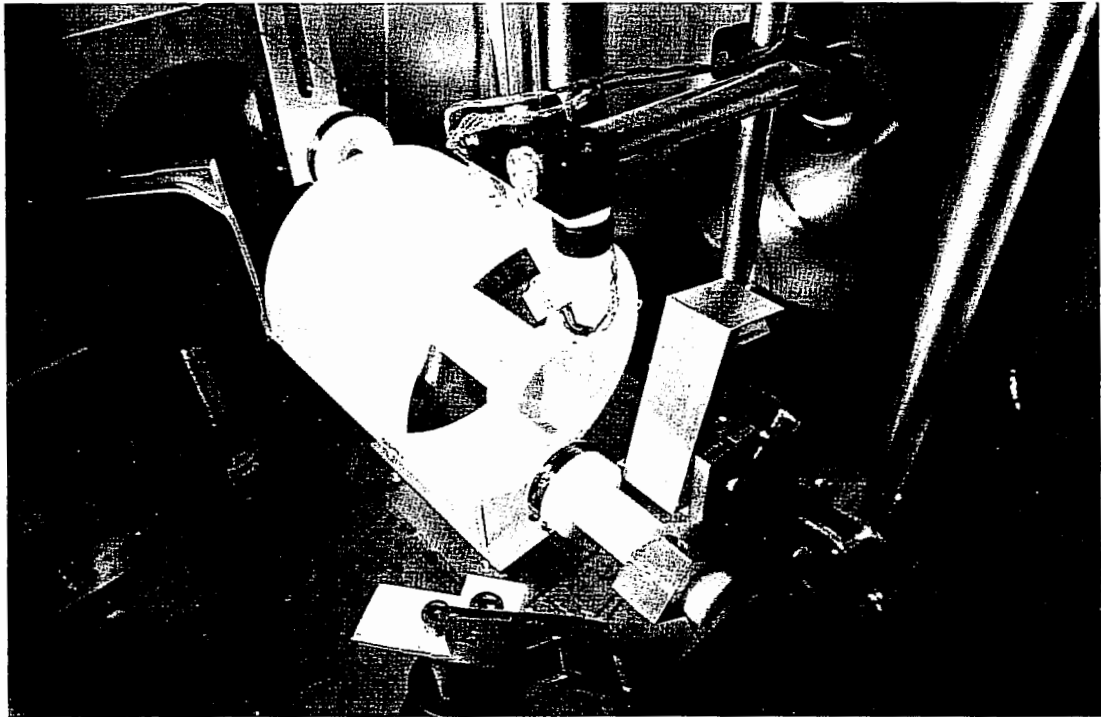
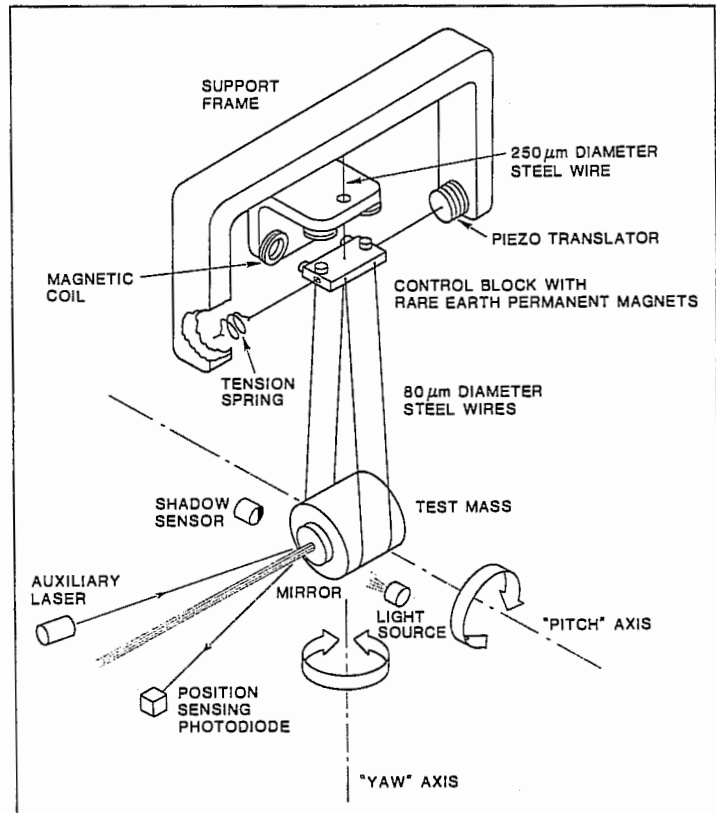
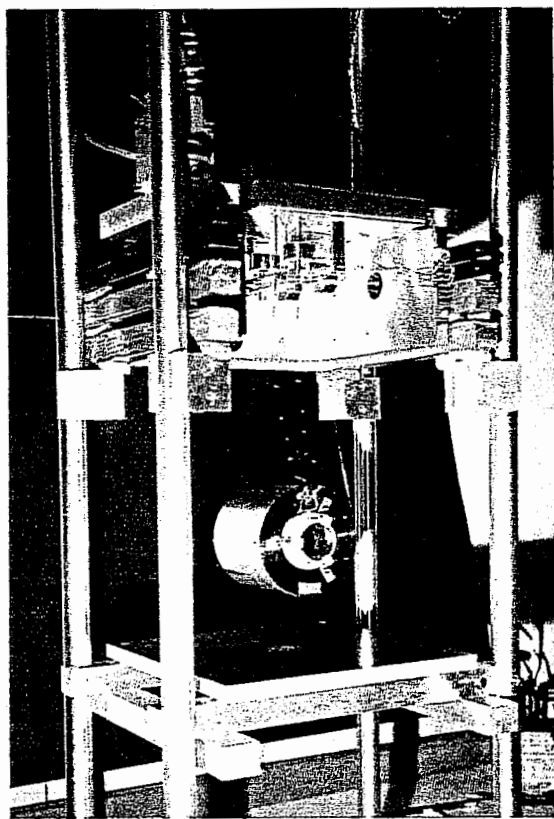
The beam splitter divides the light between the two 40-meter-long cavities, which are operated somewhat differently from the generalized configuration described in Section III-A. Instead of being recombined optically, the output light from each cavity is detected separately.

In Stage 2, noise from frequency fluctuations in the beam exiting the mode cleaner is reduced by stabilizing this beam to the *first* arm cavity—the cavity that uses light transmitted through the beam splitter. The interference between this beam and the light stored in the cavity is detected by a photodiode and converted to an electrical signal. After amplification and filtering, the signal is used to adjust the frequency of the input light by feedback to a length-controlling element on the mode cleaner and to a phase-correcting¹¹ Pockels cell.

The Stage 2 feedback of the first arm reduces frequency fluctuations to the shot noise level defined by the arm. At the same time, it transfers information about the motion of the masses, as might be caused by a gravitational wave, to frequency changes in the light. The *second* arm—the one that uses light reflected off the beam splitter—is made to follow the frequency of the light by detecting the interference of the input light reflected by the cavity input mirror with the light leaking back from the cavity, and then using the resulting signal to adjust the length of the arm. The feedback to control the second arm contains the length difference between the arms that is the gravitational-wave signal. Length changes of the first arm contribute to the signal via the light frequency; length changes of the second arm contribute directly to the signal. A vertically-traveling gravitational wave changes the arm lengths equally and oppositely, and the resulting feedback signal is double that of the signal that would result from motion of just one of the arms. The test masses and mirrors that comprise the cavities are sufficiently well isolated from external disturbances at kilohertz frequencies that noise-induced fluctuations in the lengths of the cavities are smaller than shot noise in the light.

¹¹ The phase correction provided by the Pockels cell complements the frequency control; the Pockels cell has a faster response, but less range than the piezoelectric transducers on the mode cleaner. The two acting together track the arm length and precisely maintain the resonance condition.

the first time, and the first time in the history of the world, that the
whole of the human race has been gathered together in a single
place, and that all the great nations have come to it to do what they
will with the dead body of their common master.



2. Test masses and mirrors

Four test masses with attached cavity mirrors are housed in three 45-cm-diameter chambers: two masses in the corner chamber, and one each in end chambers at the far ends of the laboratory. Figure III-5 shows test masses with attached cavity mirrors and associated controls. The masses are cylinders of fused silica, 10 cm in diameter by 9 cm long. Their lowest internal resonance is 28 kHz, with a mechanical quality factor Q of 9×10^4 . The masses are suspended from 30-cm-long, 80- μm -diameter steel wires, and move freely in the longitudinal direction of the interferometer beams in response to those forces which vary faster than the 1-s pendulum period. Shadow sensors, coupled with piezoelectric feedback to the suspension points of the wires, are used to damp the pendulum motion. The suspension wires serve as the final stage of seismic isolation; most of the isolation in the kHz-range occurs in three-layer stacks of lead and rubber between the top of the suspension wires and the supporting structure fixed to the vacuum chamber wall.

Figure III-5 (facing page) Details of prototype interferometer test mass and associated mirror, including wire suspension, orientation control, and seismic-isolation stacks.

Upper left: a previous-generation aluminum test mass (ca. 1986), the magnet coils used to control orientation, and a lead and rubber seismic-isolation stack, seen edge on. *Upper right:* a schematic drawing showing the optical lever used for sensing rotation ("yaw") and tilt ("pitch") of the mass, and the permanent magnets that interact with the coils. The beam from an auxiliary laser at the far end of the tube strikes the cavity mirror and returns to a two-axis position-sensing photodiode. The electrical signal is sent to magnet coils, which twist and tilt the control block to keep the mass aligned. (The separation between the coils and magnets is exaggerated for clarity; in practice the spacing is adjusted to keep the applied torques insensitive to ground motion). Also shown are the shadow sensor and piezo-electric translator that damp longitudinal pendulum motions. A modulated beam from a light emitting diode is partially obscured by the edge of the mass, producing a spot of light on the photodetector proportional in intensity to the displacement of the mass. This signal is filtered, amplified, and applied to a piezo-electric translator at the top, damping the pendulum without adding thermal noise associated with passive viscous damping. *Bottom:* a test mass with mirror joined by optical contacting. Coils front and rear apply balanced forces to permanent magnets affixed to the test mass for high-gain control of its longitudinal position.

Angular orientation of the test masses is sensed by 40-meter optical levers based on low-power, helium-neon lasers. Four beams directed from the region of the central test masses traverse the vacuum tubes and are reflected from the cavity mirrors at the far ends. Similarly, beams from the ends reflect off the central masses. The return beams are sensed by two-axis, position-sensitive photodetectors which feed signals back to the mass suspensions to adjust and stabilize their angular orientations.

The interferometer mirrors are made from fused-silica substrates, 3.8 cm in diameter by 1 cm thick, polished to sub-angstrom-average surface roughness and joined by optical contacting (molecular bonding) to the test masses. The beam split-

ter output rays pass through 2.5-cm-diameter holes in the corner masses, through the planar mirror substrates, and on to the multilayer dielectric reflective coating, manufactured to transmit 450 parts per million (ppm) of the incident intensity. The mirrors at the far ends are ground with a 62-meter radius of curvature, and are coated for maximum reflectivity. The fractional energy loss due to scattering from and absorption by the mirror surfaces is less than 100 ppm per mirror.

3. Details of interferometer operation

Selected details of the operation of the current 40-meter prototype interferometer are illustrated in Figure III-6.

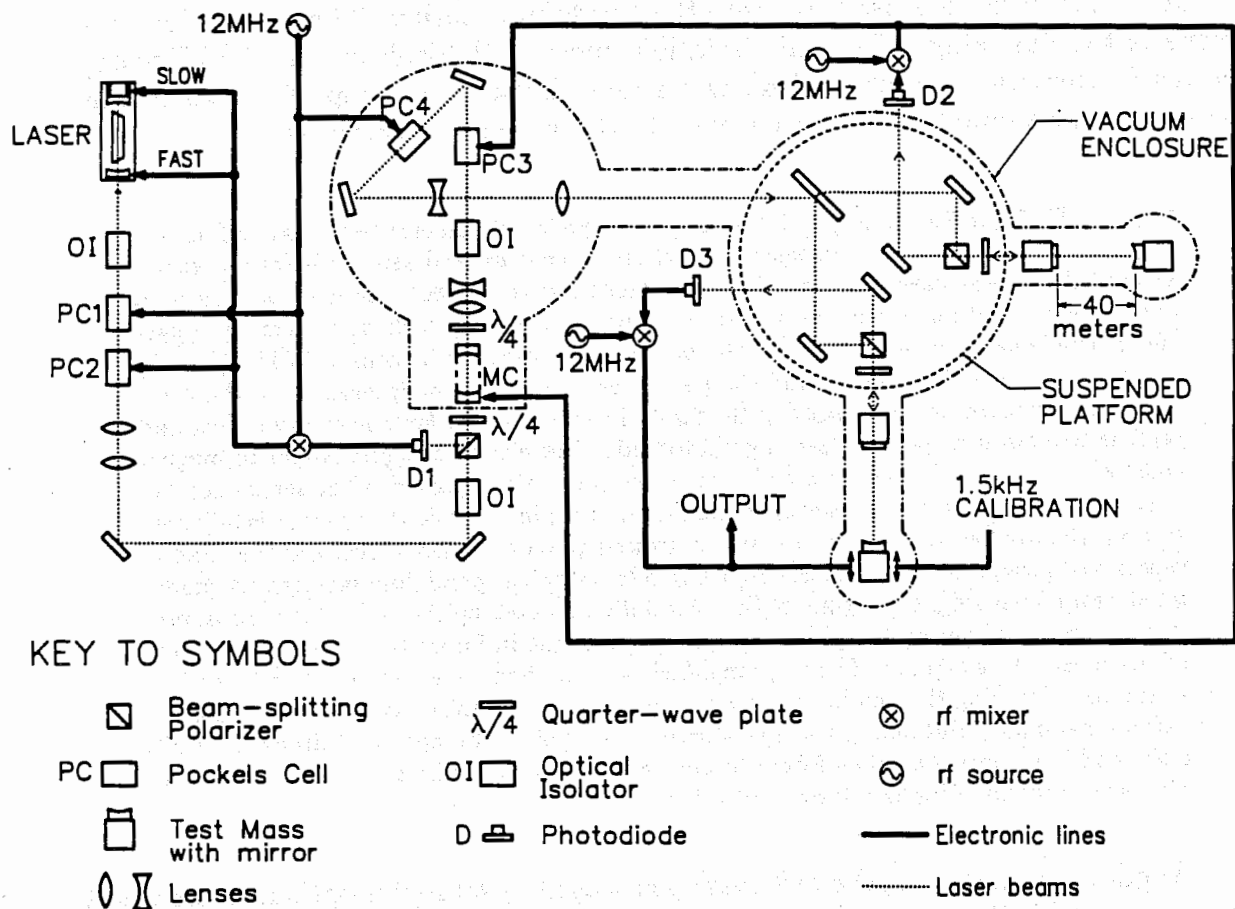


Figure III-6 Schematic of the 40-meter prototype interferometer, showing laser stabilization and cavity-locking servo loops. The input mode-cleaner cavity (MC) tracks the upper 40-meter arm, and the laser tracks the MC.

The first optical element in the vacuum system is the input mode-cleaner cavity (MC), made from a pair of mirrors with 50-cm-radius curvature. These mirrors are affixed to the ends of a 92-cm quartz spacer which is suspended by springs mounted on rubber-isolated blocks. Piezoelectric-transducer (PZT) elements between the

mirrors and the spacer are used to adjust the mirror separation. MC serves three purposes:

- (1) *Reduction of fluctuations in beam geometry.* The mirrors of the input cavity define a stable geometry that determines the direction and size of the output beam. Fluctuations in the beam pointing or wavefront which originate either in the laser or in the air path are suppressed by a factor of several hundred.
- (2) *Reduction of time-varying amplitude fluctuations.* The cavity acts as a passive low-pass filter against fluctuations in amplitude and wavelength that occur on timescales shorter than its storage time of 2.4×10^{-6} s.
- (3) *Frequency stabilization.* For fluctuations with timescales of about 1 ms, the cavity provides a length reference to stabilize the laser wavelength. The signal fed back to the laser reduces the fluctuations to $0.04 \text{ Hz}/\sqrt{\text{Hz}}$, compared to approximately $1000 \text{ Hz}/\sqrt{\text{Hz}}$ without active stabilization.

The modulation technique for laser frequency control [III-2] is also used on the 40-meter interferometer arms, and will be used on the LIGO. The Pockels cells PC1 and PC4 modulate the optical phase with an amplitude of approximately one radian at a frequency of 12 MHz. The phase modulation adds sidebands to the laser beam, spaced 12 MHz from the optical frequency (6×10^{14} Hz). The input cavity and 40-meter arms store the light energy for times, $\tau_s = 1/4\pi f_s$, corresponding to frequencies ($f_s = 70 \text{ kHz}$ and 1 kHz respectively) that are much lower than the modulation frequency. Consequently, the cavities reject the sidebands, and the light striking the photodiodes (D1 for the input cavity, D2 and D3 for the 40-meter arms) is the vector sum of two components: (1) the modulated beam reflected by the cavity input mirror; and (2) the unmodulated cavity output beam which passes back out through the input mirror. For an arm in resonance, the input and output beams have opposite phase, and the intensity on the photodiode is a minimum. If the mirror separation or the wavelength of the input beam moves slightly away from the resonance condition, the 12-MHz component of the photocurrent increases linearly. This error signal is coherently demodulated by an RF mixer which is referenced to the same oscillator that applies the phase modulation to the Pockels cell, PC4. The mixer signal from D2 is amplified, filtered, and fed back to the PZT elements and PC3 to keep the MC in resonance with the first arm. The signal from D3 is fed back to the end mass of the second arm to keep it in resonance with the light entering the beam splitter and is the output of the interferometer.

The light strikes the main beam splitter on the suspended platform after passing through two stages of stabilization. The frequency fluctuations at this point are reduced by the product of the gains in the MC loop and the first 40-meter arm loop (the upper arm in Figure III-6). This overall gain is adequate to reduce the frequency noise to the level defined by the shot noise on the light in the 40-meter arms.

4. Performance

The best gravitational-wave amplitude sensitivity achieved to date is shown in Figure III-7. Near 1.3 kHz, the sensitivity \tilde{h} is $8 \cdot 10^{-20} / \sqrt{\text{Hz}}$. The demonstrated performance corresponds to a sensitivity of position measurement of the test masses and mirrors of $3 \cdot 10^{-18} \text{ m} / \sqrt{\text{Hz}}$, corresponding to a displacement sensitivity of $\sim 10^{-16} \text{ m}$ for a 1 ms gravitational-wave burst. This sets upper limits to several sources of noise that might have been important, including thermal noise, seismic noise,¹² and noise from strain release in the suspension wires or in the masses themselves. Most of these potential sources of noise are below threshold at frequencies of $\approx 1 \text{ kHz}$ at this level of sensitivity. If the displacement sensitivity were maintained at this level in a 4-km system, the gravitational-wave sensitivity would be $8 \cdot 10^{-22} / \sqrt{\text{Hz}}$, or $4 \cdot 10^{-20}$ for a 1-ms gravitational-wave burst.

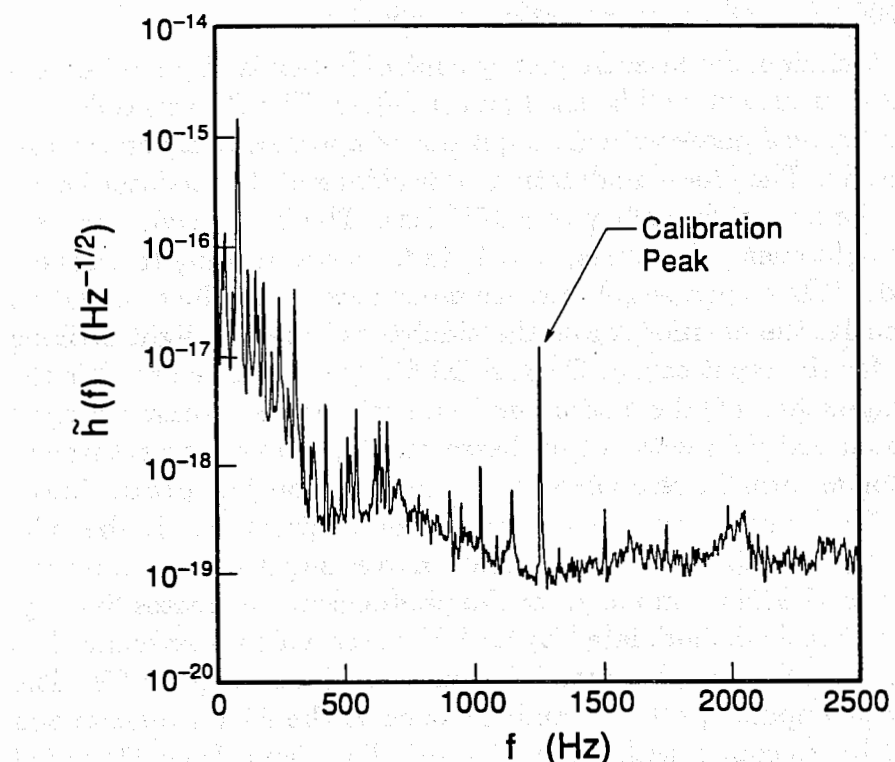


Figure III-7 Sensitivity of the 40-meter prototype interferometer. The “calibration” peak is the effect of a 10^{-15} -meter RMS sine wave motion on one of the test masses (given the 4.7-Hz bandwidth of this measurement, the calibration corresponds to 5×10^{-16} meter / $\sqrt{\text{Hz}}$). The collection of peaks below 500 Hz is in part from mechanical resonances in the beam-splitter support structure.

¹² Consistent with measurements of the isolation stacks that indicate seismic noise is at least a factor of 10 below the observed noise.

5. Future use

In addition to testing the fundamental limitations to sensitivity, the prototype apparatus is evolving to become more like the interferometers needed for LIGO operations. Many of the working units in the prototype, including much of the servo electronics, can be used in full-scale interferometers after some re-engineering. It has been demonstrated that the electronics used to stabilize laser frequency provide adequate gain, even for an interferometer with higher sensitivity than has been achieved with the prototype. Increasing the length by a factor of 100 should make possible a 100-fold decrease in equivalent gravitational strain noise from forces on the test masses, the likely dominant contributors at low frequency. Improvements now being tested show promise of higher sensitivity which can be exploited in early LIGO interferometers.

TABLE IV-1
LIGO SCIENCE CAPABILITIES

Facilities	Measurement Capability	Science Capability
I. 2 U.S. Sites	$(ah_+ + bh_x), \theta$	<p>1. <i>Physics:</i></p> <ul style="list-style-type: none"> • Confirmation of existence of gravitational waves • Propagation speed of gravitational waves (from periodic sources, or from burst sources if event also observed in electromagnetic band) • Graviton spin (from periodic sources) • Existence of Black Holes (if sufficient number of events) <p>2. <i>Astrophysics:</i></p> <ul style="list-style-type: none"> • Classification of signals • Statistics on types of sources (burst, periodic, semi-periodic...) • Distances and mass information for spiralling binaries • Source location on cone (from "time of flight") • Search for stochastic background
II. 2 U.S. + 1 abroad or 3 U.S.	h_+, h_x, θ, ϕ	<p>All of I, plus</p> <p>1. <i>Physics:</i></p> <ul style="list-style-type: none"> • Graviton spin (from polarization of waves) • Test of general relativity in strong-gravity, high-speed regime (via Black Hole waveforms) <p>2. <i>Astrophysics:</i></p> <ul style="list-style-type: none"> • Source location (θ, ϕ) • Waveforms give information on sources: e.g., core dynamics of supernovae, pulsar deformations, starquakes • Sky survey of sources
III. 2 U.S. + several abroad	h_+, h_x, θ, ϕ	All of II, but at higher sensitivity; more accurate source locations

IV. LIGO CONCEPT

A. Requirements

The Laser Interferometer Gravitational Wave Observatory (LIGO) will support a nationwide program in gravitational-wave astronomy over a period of decades. Resource constraints and other considerations prescribe a phased implementation of the project; we plan an orderly progression from startup of operations to the ultimate achievement of the LIGO capabilities.

The LIGO conceptual design has been guided by two goals: (1) maximizing the probability of detecting gravitational waves, and (2) extracting maximum information from the waves. The proposed design also provides the ability to maintain a continuous gravitational-wave monitoring program while allowing simultaneous development of enhanced-sensitivity and increased-bandwidth LIGO detectors. Specifically, the LIGO is designed to accommodate three primary objectives:

- *Observation* – the ability to monitor gravitational waves continuously (a “gravitational-wave watch”).
- *Development* – the capacity for final development and full functional testing of new and advanced interferometer-based detector concepts. Initial development of component parts will take place in campus R&D facilities.
- *Special Investigations* – the ability to accommodate specialized detectors to carry out scientific investigations of particular phenomena.

The LIGO design will allow the three primary missions to be conducted without mutual interference.

While the proposed LIGO, even in its initial phases, allows the unambiguous identification of gravitational waves and the pursuit of a number of physics and astrophysics objectives (see Table IV-1), one or more additional detectors at other sites are required to extract full waveform information ($h_+(t)$, $h_\times(t)$) and source location (θ, ϕ). Present planning assumes the construction of one or more laser interferometer facilities in Australia, Europe, Japan, or elsewhere (see Section X.A). In the very unlikely event that none of these should be constructed, it may be appropriate to build a third facility in the U.S.; the decision to do this is not required as a prerequisite for discovering gravitational waves.

The design goals dictate the following essential features of the LIGO:

- (1) Two widely separated sites under common management.
- (2) Vacuum systems to accommodate interferometer arm lengths of up to 4 km at each site.
- (3) The ability to operate several interferometric detectors at each site simultaneously and without mutual interference.
- (4) The ability to accommodate interferometers of two different arm lengths, at

least at one site.

- (5) A vacuum tube with a clear optical aperture of approximately 1 meter for the full length of the arms.
- (6) The ability to produce a vacuum of order 10^{-9} torr of hydrogen and 10^{-10} torr of other gases.
- (7) A minimum 20-year lifetime of the facilities.
- (8) Adequate support instrumentation.

Discussion of these essential features follows:

1. Two detectors at widely separated sites under common management

a. **Detector requirements.** At least two detectors located at widely separated sites are essential for unequivocal detection of gravitational-wave bursts. The only means to eliminate the large set of external noise sources which includes seismic and acoustic noise as well as internal phenomena such as laser fluctuations, sudden strain release in wire suspensions, and residual gas bursts is to operate two or more detectors with comparable sensitivities at separations sufficiently large so that the noise at the two locations is uncorrelated over the time resolution of the detector pair. Gravitational-wave signals, by contrast, would be correlated.¹ Also, the detectors should be sufficiently far apart to give source location information from time-of-flight measurements. Distances of the order of the continental size of the United States meet these requirements.

b. **Common management.** We consider it essential that the design, construction, and gravitational-wave searches of a two-site LIGO be conducted under a single management (as opposed to, for example, a multinational consortium). The LIGO technology is not "mature;" it is a first time effort. Design and development decisions embrace considerable latitude, and there must be a project director vested with the power to make decisions. Single management is needed during construction to: (1) optimize design tradeoffs, (2) assure a common completion schedule for both facilities, and (3) guarantee overlap of operating frequencies and sensitivity.² During operations, single management can effectively balance the conflicting requirements of maintaining maximum observatory "live-time," carrying

¹ Note that *periodic* source emissions, in principle, can be detected with a single-site detector, taking advantage of the frequency modulation given to the signal by the Doppler shift due to Earth's motion relative to the source. We believe it to be unwise, however, to initiate a search for gravitational waves with periodic sources as the only targets. Burst sources are likely to be stronger than periodic ones, in terms of signal-to-noise ratio; and the only source for which the strength estimates are fairly reliable is a burst source (coalescence of binary neutron stars). Moreover, there is value in having a second site, even in a periodic search, to help separate periodic signals of local origin from periodic gravitational waves.

² To the first order, the least sensitive detector sets the threshold for discrimination against spurious events and thus for successful detection.

out systematic investigations of the noise in the interferometers, and continuing development of the instruments.

2. Arm lengths of 4 kilometers

The choice of interferometer arm length is a complex tradeoff between achievable sensitivity and cost. A "first-order" version of the tradeoff is as follows (see Appendix B for details). In the frequency range $f \lesssim 100$ Hz, where the anticipated signal-to-noise ratios are expected to be the largest and the only fairly reliable source (coalescing binary neutron stars) resides, the dominant noise is likely to be random forces on the test masses (seismic, acoustic, thermal noise, and local gravity gradients). For distant sources, the gravitational-wave event rate (or probability of detection) scales with detector sensitivity as h_N^{-3} (h_N = equivalent detector-noise-strain amplitude). Because h_N scales with arm length as L^{-1} in this regime, the event rate scales $\propto L^3$. The coalescence of neutron-star binaries in distant galaxies is one of the most promising sources for detection, and an arm length of 4 km is required for sensitivity adequate to yield a good chance of seeing this source (see Section II, Figure II-2).

Practical considerations also favor arm lengths of about 4 km. For arm lengths $L \lesssim 4$ km, the fixed costs of the facilities (including buildings and vacuum facilities for optics) are much larger than the length-dependent costs (tubes); it is cost effective to maximize tube length for maximum sensitivity. Estimates of LIGO construction funding exclude placing the vacuum tubes in subterranean tunnels; more economical surface or open-ditch construction is mandated. Topographical data from a search for sites in the U.S. revealed a dramatic dropoff of possibilities at a range of 4 to 5 km. The choice of 4-km arms is a compromise between gravitational-wave-strain sensitivity, cost, and site availability.

3. Capability for several simultaneous interferometer systems at each site

The facilities will be designed to support three detector systems between the two sites, allowing the simultaneous pursuit of observations, detector development, and special investigations without mutual interference. The ability to support more than one detector system is required because (1) gravitational-wave bursts are believed to be relatively rare events, thus requiring continuous monitoring, and (2) the development and testing of interferometers that are new, more sensitive, or have different frequency ranges require unrestricted access to the LIGO facilities for periods of months or years.

4. Interferometers of different arm lengths

One of the two U.S. sites will be configured to accommodate interferometers with both 2 and 4-kilometer arm lengths acting together as a single detector system. The fact that gravitational-wave signals are proportional to arm length can be exploited to discriminate between them and local noise, which generally is not proportional to the interferometer length. In addition, the operation of any additional interferometer, whether full or partial length, will improve the rejection of accidental coincidences. Such rejection of spurious signals will be essential for unequivocal identification of gravitational-wave bursts (see Section VII).

The availability of a dedicated paired interferometer at the same site also will provide a useful diagnostic tool in interferometer development, particularly in rejecting noise sources not detected by the environmental, facility, and interferometer monitoring systems.

A gravitational-wave *detector* unit thus consists of one full-length (4 km) interferometer at each of the two sites and a half-length interferometer (2 km) at one site. Providing this additional capacity at only one site saves costs and at present appears adequate for initial operation.

5. Vacuum-tube clear aperture approximately 1 meter in diameter

The choice of beam-tube³ diameter is an irreversible decision once the facilities are constructed. The clear aperture must accommodate not only the initial goals, but also the plans for full-facility utilization including a wide range of interferometer designs and optical technologies that eventually may be required.

A clear aperture of 1-meter diameter has been chosen because it will accommodate up to six Fabry-Perot interferometers, using $0.5 \mu\text{m}$ light, without significant diffraction loss or scattering by the tube walls. This aperture includes room for auxiliary beams for orientation control of the test masses and for monitoring the seismic motion of their suspension points. The 1-meter aperture would also be filled by a single delay-line Michelson interferometer operating at $1 \mu\text{m}$.

6. Vacuum level of order 10^{-9} torr

The vacuum system will be designed so that fluctuations in the index of refraction of the residual gas in the interferometer arms (see Appendix B) will not become a limiting noise source. The ultimate sensitivity goals require residual gas pressures of less than about 10^{-9} torr for hydrogen and 10^{-10} torr for nitrogen or water. These pressures can be achieved through a combination of selection and preparation of materials, bakeout, and pumping strategy (see Volume 2, Section IV.D). The sensitivity of the first LIGO detector in broad-band operation (Figure V-3) may tolerate higher pressures, but the attainable vacuum cannot be allowed to limit sensitivities of this or of advanced interferometers in any mode of operation.

³ The "beam tube" provides the vacuum envelope for the 4-km interferometer arms.

7. Minimum 20-year lifetime of the facilities

The LIGO facilities are expected to support the evolution of gravitational-wave detectors with sensitivities that continually improve. Specialized interferometers will be developed with enhanced sensitivities for specific frequency bands or waveforms. As with other kinds of astronomical observatories, scientific productivity will be dependent in large measure on improvements in instrumentation over a period of many years.

The 20-year lifetime requirement is intended as a guide for design tradeoffs that balance capital costs against operating costs. The total life-cycle costs will be minimized. The facilities will maintain flexibility to deal with a variety of possible future situations (e.g., quick discovery of strong waves or a long span with no evidence of even weak waves).

The goals for the LIGO include not only the discovery of gravitational waves, but also opening of the field of gravitational-wave astronomy and a long-range program of scientific exploration.

8. Support instrumentation

The LIGO facilities will include instrumentation to monitor environmental disturbances (e.g., acoustic, seismic, electromagnetic interference, and cosmic rays) for possible correlation with interferometer signals.

B. Implementation

1. Phased construction

The LIGO is being designed to give a high probability of detecting gravitational-wave signals and thereby establish the field of gravitational-wave astronomy. A less ambitious goal would be incommensurate with the costs and scientific efforts expended. It is clearly not sufficient to plan the LIGO as only an extension of the technology development and demonstration now being carried out in prototype research.

Prototype design and development for laser interferometric gravitational-wave detectors has been underway for close to two decades. The next epoch of development requires arm lengths that cannot be accommodated on a university campus. Large facilities in remote areas are needed. There would be no significant cost savings in constructing intermediate sized facilities (e.g., interferometers of 1-km arm length); on the contrary, the long-range schedule delays and cost impacts of such a strategy would be negative. Stepping up to the ultimate, 4-km facility is, therefore, a prudent and logical initial course of action.

Similarly, the postponement of some costs by delaying construction of the second site would be far outweighed by the penalties of being unable to discriminate between noise and gravitational waves using correlations between widely separated sites. The initial construction of a two-site observatory, therefore, is both prudent and cost effective.

The only parameter that allows cost-saving compromises for the initial construction and startup periods, with tolerable impact upon subsequent capability to expand the system, is that of the number of interferometric detectors provided. The full LIGO system incorporates three detectors that allow concurrent observation, development, and special investigations. An optimal startup system would have two detectors, i.e., six interferometers distributed over two sites, four at Site 1 and two at Site 2. This would assure the most efficient progress towards the detection of gravitational waves by allowing the use of one detector in the dedicated observation mode while permitting the development of a next-generation, more-powerful system, in the second detector facility.⁴ Such a system, however, would exceed the funds expected to be available for the initial construction phase considered in this proposal.

We propose, therefore, an evolution of the LIGO in three phases.⁵

- *Phase A, The Exploration/Discovery Phase*, provides a *one-detector* facility that allows the conduct of observation *or* development. The facility has full capability for the discovery of gravitational waves and for early observatory operations, but progress will be limited by the competition between dedicated observations and advanced detector development. In particular, if the (yet unknown!) strength of gravitational-wave signals should fall below the sensitivity of the initial detector, the distribution of time between observation and development will present a serious judgmental challenge. However, at the very least, LIGO/Phase A will allow a full confirmation of the design performance of the LIGO system and will provide the basis for evaluation and decisions on future enhancements of the LIGO system.
- *Phase B, The Discovery/Observation Phase*, provides a *two-detector* facility⁶ that allows concurrent observation *and* development or specialized search.

Should gravitational waves have been discovered in Phase A, then Phase B, with its enhanced two-detector capability, will allow the continued collection of data via the dedicated observation detector while allowing the development of more advanced detectors with enhanced performance in strain sensitivity, gravitational-wave frequency coverage, and optimization for source types on the second LIGO detector.

Should the initial Phase-A detector demonstrate design performance but not have detected gravitational-wave signals, it might be prudent to introduce the enhanced capability of Phase B to accelerate the discovery of gravitational

⁴ While the campus laboratory facilities will allow some engineering development of more advanced interferometers, the LIGO facilities will be needed for full development.

⁵ Note that this proposal asks for approval of Phase A only. The Phase-A design accommodates subsequent implementation of Phases B and C, to be proposed at a future time.

⁶ It is possible, of course, to implement Phase B in steps, e.g., with the installation of the vacuum enclosures for one additional interferometer at a time. Described here is the end goal of Phase B.

waves.

- *Phase C, The Observatory Phase*, provides a three-detector facility that allows concurrent observation, development, special investigations, and optimal access for the scientific community at large. It completes the LIGO evolution to its presently conceived full-design capability.

SYMBOLS

- Test Mass
- Test Mass Chamber (Type1)
- Test Mass Chamber (Type2)
- ✓ Beam Splitter
- Beam Splitter Chamber
- Laser & Input Optics
- Output Optics
- Laser Beam

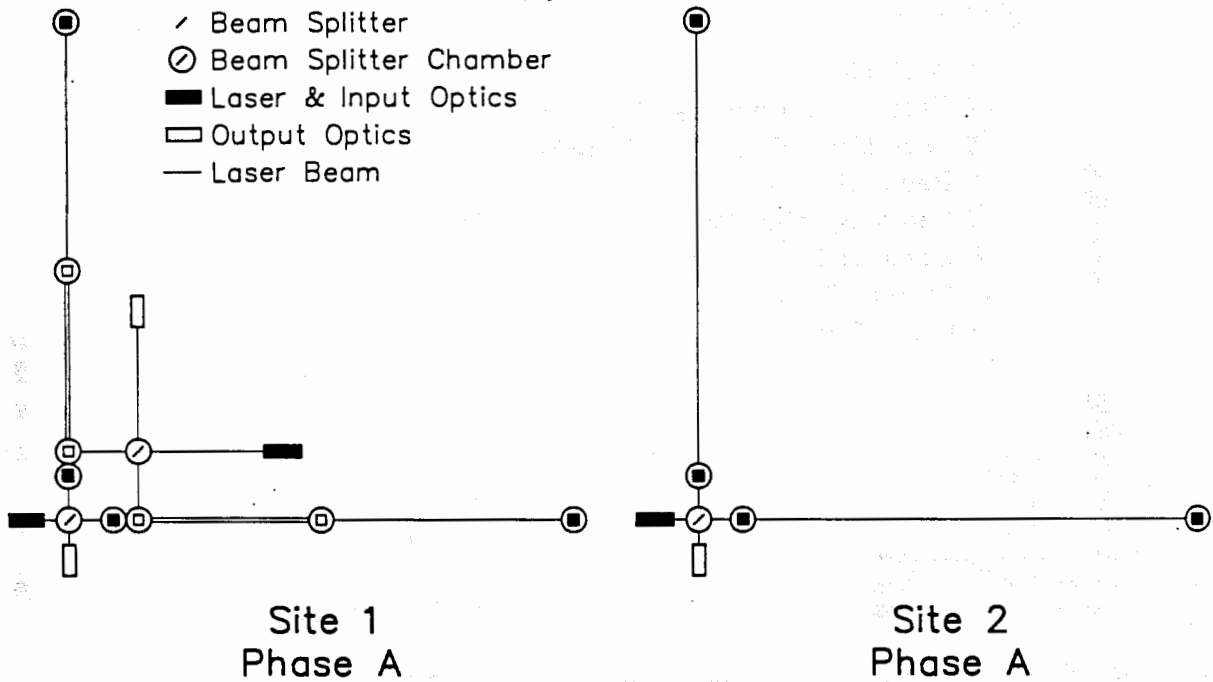


Figure IV-1 LIGO Phase A configuration at Sites 1 and 2. (See Volume 2, Section IV.C for descriptions of the two types of test mass chambers.)

a. **LIGO configuration in Phase A.** The LIGO Phase-A configuration is schematically illustrated in Figure IV-1. Phase A accommodates two Fabry-Perot interferometers at Site 1, of nominally a full-length and a half-length configuration;⁷ Site 2 accommodates one full-length interferometer. The three interferometers, the full- and half-length pair at Site 1 and the full-length version at Site 2, form a single detector. The facility is designed so that test masses, beam splitters, and all other in-vacuum components of the half-length interferometer at Site 1 can be introduced

⁷ It is possible to convert the half-length interferometer into a full-length version by transfer of its test mass from the mid length test- mass chamber to the end test mass chamber, but with some restrictions on the size of individual masses.

or removed from the vacuum system at will, without breaking the vacuum of the full-length interferometer or interrupting its operation, and vice versa.

Phase A thus has adequate facilities to support an initial observation and development program, and to conduct triple coincidence searches for gravitational waves to the ultimate sensitivity of the interferometers. The main limitation of this system is that full-scale LIGO detector development and testing is mutually exclusive with observation.

The Phase-A system is designed to allow expansion to Phase B without extensive interruption of operations.

SYMBOLS

- Test Mass
- Test Mass Chamber (Type1)
- Test Mass Chamber (Type2)
- ✓ Beam Splitter
- Beam Splitter Chamber
- Laser & Input Optics
- Output Optics
- Laser Beam

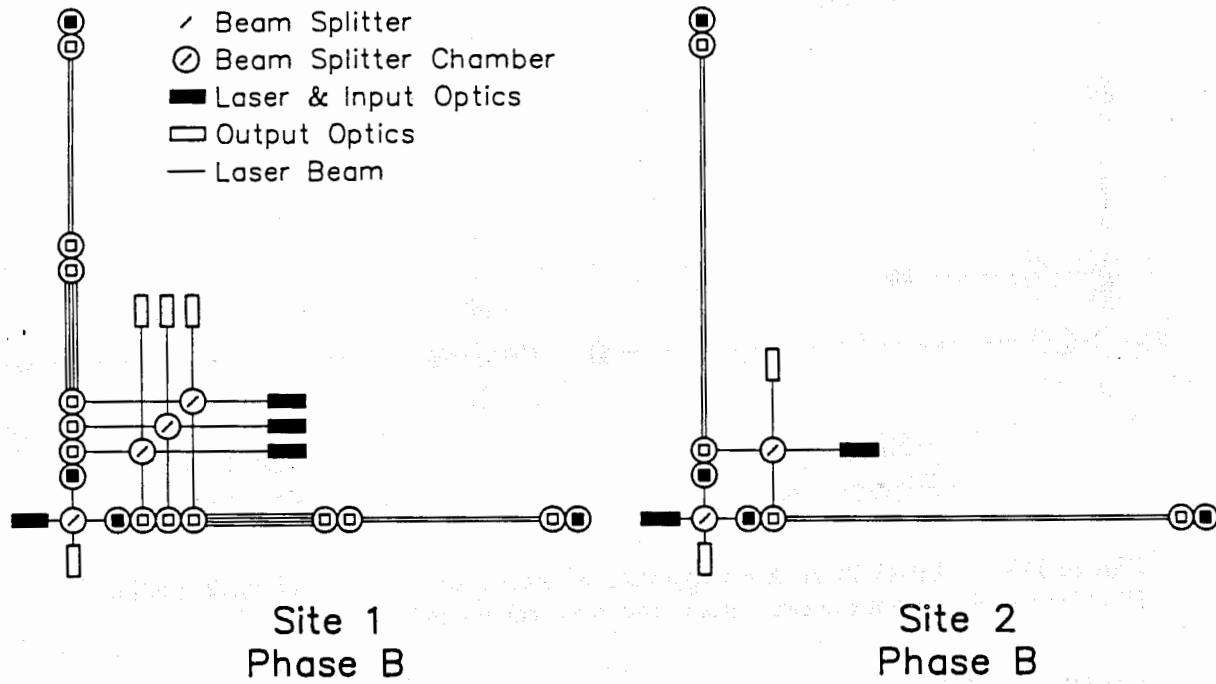


Figure IV-2 LIGO Phase B configuration at Sites 1 and 2.

b. **LIGO configuration in Phase B.** Phase B (Figure IV-2) doubles the capacities of Sites 1 and 2. It accommodates four Fabry-Perot interferometers at Site 1, that is, two full-length and two half-length configurations. Site 2 accommodates two full-length interferometers. This increased capacity allows the operation of two complete triple-coincidence detectors, each consisting of a full-length plus a half-length interferometer at Site 1 and a full-length interferometer at Site 2. The facility is designed so that the detectors (e.g., a development and an observation detector) can

be operated independently and without mutual interference. Test masses and optical components of any of the interferometers can be introduced or removed from the vacuum system without breaking vacuum and without interrupting operation of the others.

Phase B thus has adequate capacity to support, concurrently, observation and development or two independent observations, to the ultimate design limit of the facility.

SYMBOLS

- Test Mass
- Test Mass Chamber (Type1)
- Test Mass Chamber (Type2)
- ✓ Beam Splitter
- ✗ Beam Splitter Chamber
- Laser & Input Optics
- Output Optics
- Laser Beam

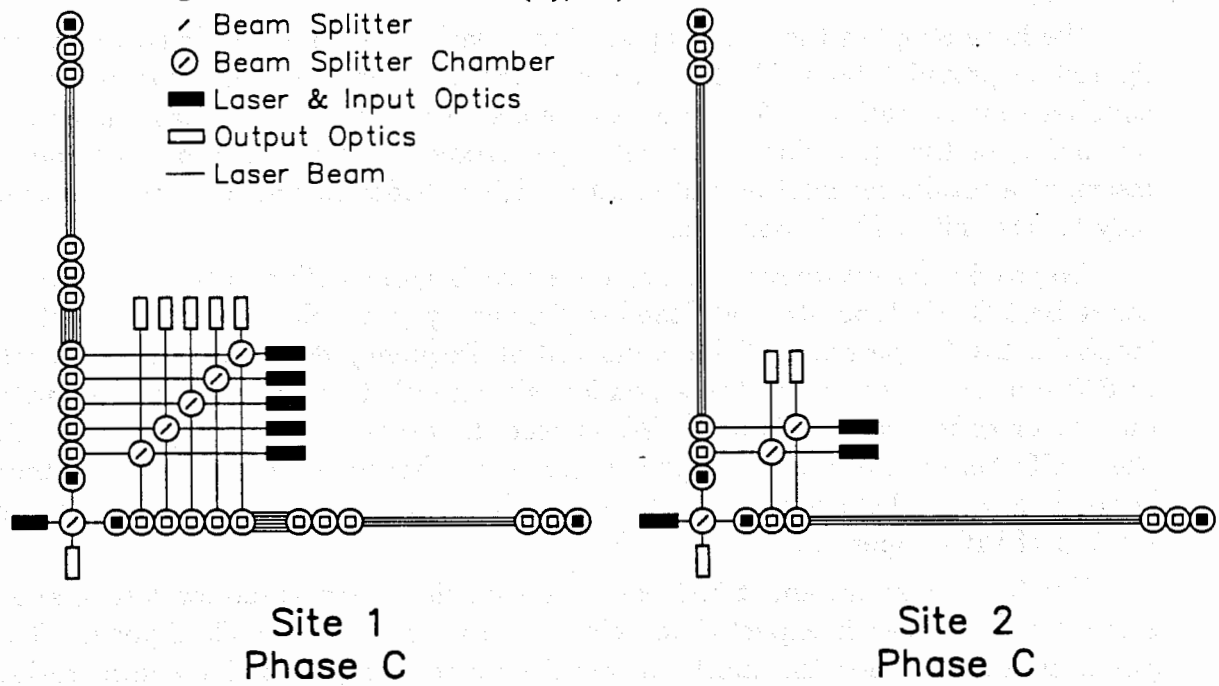


Figure IV-3 LIGO Phase C configuration at Sites 1 and 2.

c. **LIGO configuration in Phase C.** Phase C (Figure IV-3) will add a third interferometric detector port, providing for *special investigations* and opening up the facility for optimal access to the scientific community at large (see Section VI.B).

Phase C, as currently envisaged, is our present best concept for the evolution of the LIGO. In practice, the discoveries in Phases A and B will guide further development. Once gravitational waves have been observed, scientific needs will determine the best design for subsequent phases, as will considerations driven by the (then presumably existing) international network of gravitational-wave interferometric facilities.

2. Laser strategy

Gravitational-wave laser interferometers require extremely stable, single-mode, continuous-wave lasers. Our present prototypes use commercial large-frame argon-ion lasers operating at 514 nm wavelength. These lasers have been rebuilt in our laboratories for improved vibration isolation and have been further stabilized with high-gain control loops (see Section III.B). Their maximum light output is about 5 W single line. They consume about 55 kW of electrical power, plus about 25 kW for cooling.

The performance expected of the initial LIGO interferometers (Figure V-3) can be met with one such laser per interferometer. Higher power performance could be achieved by coherent addition of several argon-ion lasers, although at significant power costs.

We have adopted the following strategy: each LIGO installation will be configured to provide about 320 kW of power for all lasers on site. This allows the simultaneous operation of four interferometers with one argon-ion laser per interferometer, or the operation of a single interferometer with four coherently added lasers, at a total laser light output of 20 W. We consider this arrangement satisfactory for the initial LIGO operation.

To provide for future requirements, we have begun a collaboration with Professor Robert Byer's laboratory at Stanford University to develop solid-state Nd:YAG lasers for LIGO operations. The lasers will be frequency doubled to a wavelength of 530 nm, close enough to the argon-ion wavelength to allow replacement without major configuration changes. We expect these new lasers to be available for the LIGO before the need for higher power levels becomes serious. In fact, there is good reason to believe that these lasers will be available before or shortly after startup of LIGO operations.

Nd:YAG lasers are about 100 times more efficient than argon-ion lasers, and a single Nd:YAG laser is expected to deliver on the order of 100 W of power. This power is adequate for the most advanced detector designs under consideration; therefore, contingent on the success of the laser development program, the planned power capacity of the LIGO will accommodate the requirements of advanced interferometers.

3. Site strategy

Two sites are essential for the unambiguous detection of gravitational waves. Site selection and development depend on considerations discussed in the following paragraphs (for details, see Section V.C).

a. Scientific considerations.

i. *Interferometer alignment.* If the interferometers at the two sites are "co-aligned" (the alignment of the arms coincides when projected onto the bisecting plane), the instruments are optimally sensitive to the same polarization state, and the probability of wave detection in coincidence is maximized. If one of the interfe-

ometers, instead, is rotated 45 deg relative to co-alignment, the two are most sensitive to orthogonal polarizations and together extract the most information from the waves. We have chosen co-alignment to optimize the probability of discovery.

ii. *Distance between sites.* Optimization of the chance of discovery dictates that the sites be much farther apart than the correlation lengths of the various noise sources that can affect the interferometers; for this, 300 km is estimated to be adequate. Optimal determination of source directions, via time-of-flight between sites dictates a separation between sites as large as possible. If the site separation exceeds about 4500 km, then the overlap of the two beam patterns of interferometers at the two sites is significantly debilitated, and the detector's sensitivity is correspondingly reduced.

iii. *Direction between sites.* The probability of detection is not significantly sensitive to the geographic locations of two sites, but the accuracy of position determination via time-of-flight between sites will be direction sensitive when there is a network of three or more detectors. Optimal directionality requires a minimum of four detectors at the corners of a tetrahedron of maximum volume; failing that, there should be at least three detectors at the corners of a triangle of maximum area. The American sites will be chosen to contribute significantly to the area of an America-America-Europe triangle and to the volume of a global tetrahedron.

b. **Local specifications for U.S. sites.** The allowable tolerances on positioning an interferometer vacuum system at a site (such as tolerances on the 4-km nominal arm length and on the 90-deg angle between arms) have been chosen to optimize scientific returns but are constrained by construction costs. They are listed in Volume 2, Sections II and V.

An important consideration is the requirement that the LIGO arms be installed level within a few milliradians. This restriction is dictated by the fact that the "free" character of an interferometer's inertial test masses is generally brought about by a pendulum suspension. The isolation of pendulum suspensions from vibration and thermal noise is most effective when the optical axis of the interferometer is normal to the local gravity vector. The slope of the arm compromises this isolation. Note that the curvature of Earth over 4 km imposes an irreducible angle of 0.6 milliradians between the direction of the local gravity vectors at each end.

c. **Site selection.** Site accessibility, availability, topography, and geophysical nature are variables that may affect possible scientific return and construction costs.

We have undertaken a broad survey of potential sites in both the western and eastern United States. A smaller set of the more promising sites (Volume 2, Section V) has been further investigated for geotechnical and environmental features.

We propose to present to the National Science Foundation a short list of potential east- and west-coast sites, with detailed discussions of their properties. We hope to generate, together with NSF, a list of final candidates. Final selection will depend on the results of remaining geotechnical surveys (which can be conducted

only with permission of the land owners) and on our ability to negotiate satisfactory use permits with the owners.

Land acquisition is a critical element in the development of a new facility. It is important to have a clear understanding of the legal rights and responsibilities of all parties involved in the acquisition process. This includes the company's right to acquire land, the rights of the land owner, and the obligations of the company to the land owner. It is also important to understand the legal requirements for the acquisition of land, such as zoning laws, environmental regulations, and other legal requirements. It is important to have a clear understanding of the legal requirements for the acquisition of land, such as zoning laws, environmental regulations, and other legal requirements. It is important to have a clear understanding of the legal requirements for the acquisition of land, such as zoning laws, environmental regulations, and other legal requirements.

Land acquisition is a critical element in the development of a new facility. It is important to have a clear understanding of the legal rights and responsibilities of all parties involved in the acquisition process. This includes the company's right to acquire land, the rights of the land owner, and the obligations of the company to the land owner. It is also important to understand the legal requirements for the acquisition of land, such as zoning laws, environmental regulations, and other legal requirements. It is important to have a clear understanding of the legal requirements for the acquisition of land, such as zoning laws, environmental regulations, and other legal requirements. It is important to have a clear understanding of the legal requirements for the acquisition of land, such as zoning laws, environmental regulations, and other legal requirements.

Land acquisition is a critical element in the development of a new facility. It is important to have a clear understanding of the legal rights and responsibilities of all parties involved in the acquisition process. This includes the company's right to acquire land, the rights of the land owner, and the obligations of the company to the land owner. It is also important to understand the legal requirements for the acquisition of land, such as zoning laws, environmental regulations, and other legal requirements. It is important to have a clear understanding of the legal requirements for the acquisition of land, such as zoning laws, environmental regulations, and other legal requirements.

Land acquisition is a critical element in the development of a new facility. It is important to have a clear understanding of the legal rights and responsibilities of all parties involved in the acquisition process. This includes the company's right to acquire land, the rights of the land owner, and the obligations of the company to the land owner. It is also important to understand the legal requirements for the acquisition of land, such as zoning laws, environmental regulations, and other legal requirements. It is important to have a clear understanding of the legal requirements for the acquisition of land, such as zoning laws, environmental regulations, and other legal requirements.

V. DESIGN AND SITING OF INTERFEROMETERS

A. Conceptual Design of the Initial LIGO Interferometers

The general features of the initial LIGO interferometers are described in this section. Their detailed conceptual design will be initiated in the near future, and will reflect future research and development activities on the 5-meter and 40-meter interferometer prototypes. A design freeze for most subsystems of the initial interferometers will occur about 1 year after construction start, i.e., 2 years before completion of the first LIGO vacuum facility.

1. Comparison of prototype and initial LIGO interferometers

The initial LIGO interferometers will be based on the concepts being developed in the prototypes and on scaled-up versions of many of the prototype subsystems now in use. Table V-1 compares the parameters of the current prototype interferometer to those of the planned, fully evolved initial LIGO interferometer.

TABLE V-1
PARAMETERS OF PROTOTYPE AND LIGO INTERFEROMETERS

PARAMETER	PROTOTYPE	INITIAL LIGO
Optical Power:	Laser Output	5 W
	Bright Fringe	0.10 W
Main Cavities:	Configuration	Separately detected Fabry-Perot
	Length	40 m
	Beam waist w_0	0.2 cm
	Mirror Diameter	3.7 cm
	Storage time	1 msec
Auxiliary Cavities	Recycling factor	1 (no recycling)
		30
Input/Output Cavities:	Number	2
	Length	12 m
Filter and Reference Cavities:	Number	2
	Length	1 m
Test Masses:	Material	Fused Silica
	Mirror Interface	Optical Contact
	Mass	1.6 kg
Central Mass	Complex	Beam splitter only

Figure V-1 shows the conceptual design of the optical system to be used in an initial LIGO interferometer. The initial interferometer has several features in common with the 40-meter prototype, and the following differences:

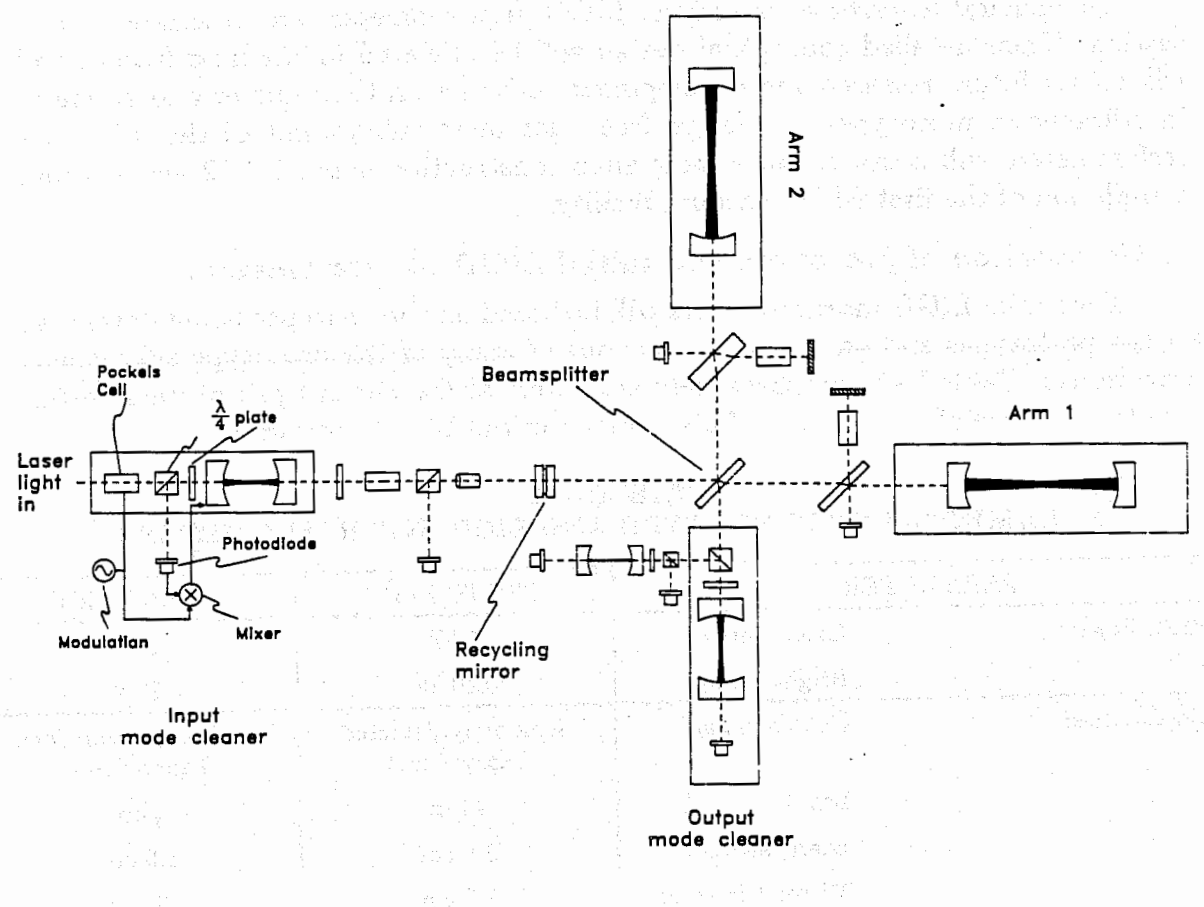


Figure V-1 Principal elements of the optical system planned for initial interferometers. The modules are: (1) *Input mode cleaner*, similar in purpose and operation to the prototype Reference Cavity described in Section III.B; (2) *Output mode cleaner*, to suppress the effects of scattered light; (3) *Arm 1* and *Arm 2*, the 4-km (2-km for half-length interferometers) optical cavities. The modulation and feedback, shown explicitly for the input mode cleaner, are implicitly associated with the other photodiodes. Key components include the main *Beam splitter*, which divides the light evenly between the interferometer arms, and the *Recycling mirror*, which in its simplest form has fixed transmission of a few percent. Also shown are plates downstream from the beam splitter oriented 45 deg to the arms; these are almost transparent (99% transmitting) pick-offs that reflect a small amount of light into side arms containing optical phase modulators. The modulators impress side bands onto the light for detection of (1) the cavity resonances, and (2) the gravitational wave output at the antisymmetric port of the beam splitter. The small cavity adjacent to the output mode cleaner extracts a signal to control the beam-splitter position. Several chambers and connecting tubes (see Volume 2, Section IV.C) comprise a contiguous vacuum system enclosing all the optical components shown. The recycling mirror and output mode cleaner might be omitted from the first operational interferometer.

- (1) The main optical cavities are 100 times longer. Consequently, the diffraction-limited beam diameter is 10 times larger, and the pointing precision required is also 10 times higher. The laboratory research program addresses these issues by the development of larger diameter optics, and of a hierarchical alignment system, using computer controlled automatic alignment in the final stage.
- (2) The design calls for constructing each mirror/test mass of a single monolithic piece of fused silica, rather than optically contacting a mirror to a larger block of fused silica as in the prototype. Research we have carried out shows that fused silica with sufficient optical homogeneity and low enough birefringence to meet the goals of the initial interferometer can be manufactured. The development and testing of techniques for polishing and coating monolithic mirrors are part of the proposed research program.
- (3) Low-loss optics will be used throughout, increasing the overall optical throughput and detection efficiency to 20% and making the total effective power available at the main photodetector (the "bright light fringe" power) 1 W.
- (4) The light beams will recombine at the splitter, so there is one principal optical output. (In the prototype, the arms are monitored by separate outputs.) Some methods for recombining the light in a Fabry-Perot interferometer involving monitoring beams at the input to the main cavities were suggested early [V-1]; and these and others have been demonstrated by Glasgow University, Scotland and University of Paris-Sud, Orsay, France [V-2]. Currently research is being carried out by the LIGO Project to recombine the interferometer with a technique using an optical subcarrier. The optical system is shown in Figure V-1. This operation is described below in Section V.A.2.
- (5) A recycling mirror, with associated modulation and servo systems, makes optimal use of low-loss mirrors and long arms by building up the power within the arms. Recycling of the light in an interferometer has been demonstrated at the Max Planck Institute for Quantum Optics (MPQ) [V-3], Garching, Germany and the University of Paris-Sud, Orsay [V-2]. The specific technique shown in Figure V-1 will be tested as part of the proposed LIGO laboratory research program.
- (6) An output "mode-cleaner" cavity suppresses the effects of scattered light on the output photodiode.
- (7) Several auxiliary subsystems, such as a filter cavity on the output to separate the signal used to control the beam splitter position, are added to the prototype design. The four auxiliary cavities listed in Table V-1 include a reference cavity, mode cleaners on the input and output, and a filter cavity.
- (8) Separately suspending the main mirrors and other components reduces noise in an interferometer and facilitates the alignment of the system [V-4]. The research plan for the 40-meter system includes separately suspending all critical optical components before completion of the final engineering design of the ini-

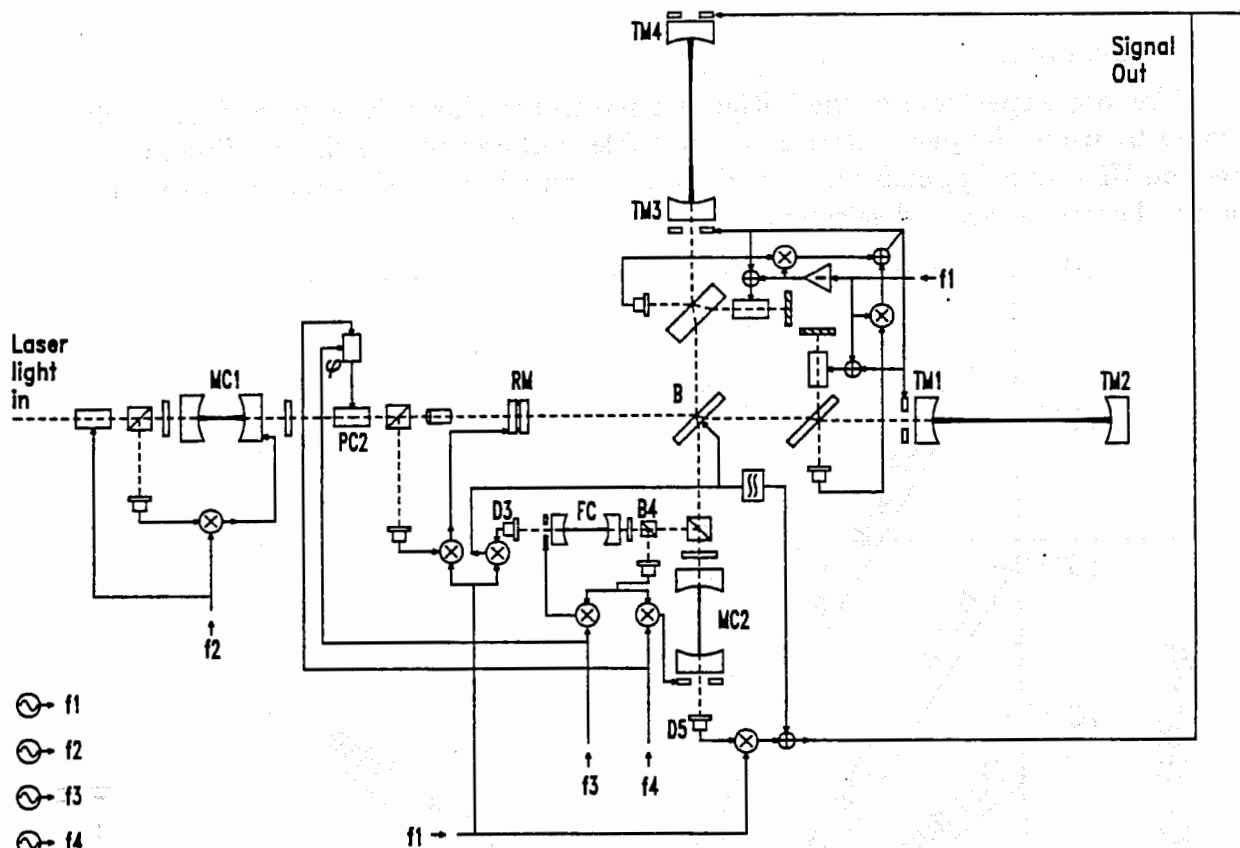
tial LIGO interferometer. The increased sensitivity demands for LIGO interferometers, together with the increased complexity of LIGO optical systems, require many more suspended optical components than have been used in the prototype to date. Modularized controllers that can be mass produced to suspend many similar components have been designed. Suspended components are discussed further in Volume 2, Section IV.B.

2. Details of interferometer operation

The initial LIGO interferometer will be developed according to the design shown in Figure V-2. This design uses eight separate radio-frequency modulated and stabilized cavity signals. Auxiliary components such as steering mirrors, isolators, and pick-offs—essential for a working implementation but not for a conceptual description—are not shown. Similarly, the optics and electronics necessary for alignment control and for a prestabilizing mode cleaner are omitted from the figure for clarity.

We describe here the main features of the design. The two optical cavities defined by the mirrors TM1, TM2 and TM3, TM4 lie along the 4-km-long arms. The light reflected by the cavities on resonance is recombined at the beam splitter, B. The light carrying the difference in phase of these two beams is incident on photodetector D5; the light carrying the sum of the phases is brought to the recycling mirror, RM. The transmission and position of the recycling mirror are adjusted so that the light emerging from the interferometer and the reflected laser light destructively interfere at the recycling mirror. This serves to match the laser light to the losses inside the interferometer and, thereby, maximizes the power circulating in the interferometer.

In addition to the primary parts of the interferometer, there is a set of auxiliary feedback systems. Light is picked off in front of the main cavities into side-arm cavities containing electro-optical phase shifters. These impress FM sidebands on the optical beams to accomplish several tasks: (1) to lock the two long Fabry-Perot cavities on resonance, (2) to hold the recycling mirror at the correct location, and (3) to maintain equal distance between the beam splitter and the input mirrors of the main cavities. External to the main interferometer are three resonant cavities and an additional electro-optical phase modulator. Cavity MC1, at the input to the system, is used to provide spatial and temporal filtering of the laser light and is a secondary frequency reference for the frequency stabilization of the input light. Electro-optical phase modulator PC2 impresses small amplitude subcarriers on the input light at frequencies (typically on the order of 500 MHz) chosen to be resonant with the recycling cavity composed of RM, TM1, and TM3, but out of the band accepted by the main cavities. The subcarriers and associated sidebands generated within the interferometer are used to control the position of the beam splitter. These subcarriers are stripped from the main beam by the filter cavity FC, and brought to photodetector D3. The final cavity, MC2, transmits the FM sidebands and the main beam to the antisymmetric detector D5. MC2 has a free spectral range equal



□	FARADAY ROTATOR	□	POLARIZING BEAMSPLITTER + QUARTER-WAVE PLATE	-	DOUBLE INTEGRATOR	+	SUMMING JUNCTION
■	MIRROR	PC	POCKELS CELL	-	ELECTRONIC PHASE MODULATOR	+	PHOTODIODE
RM	RECYCLING MIRROR			↔	INVERTER	+	RF SOURCE
B	BEAMSPLITTER		TEST MASS/CAVITY MIRROR			⊗	DEMODULATOR

Figure V-2 Optical and electronic design for the initial LIGO interferometer. Laser beams are represented by dashed lines; electrical connections are solid. Representative values for the four modulation frequencies f_1 through f_4 are 12, 14, 30, and 500 MHz, respectively. Details of electronic amplifiers and filters, and the orientation systems are omitted for clarity.

to f_1 (approximately 12 MHz). This cavity rejects light scattered by the optics and the 4-km beam tubes, and reflects the subcarriers to the filter cavity.

3. Performance

The noise spectrum of the initial interferometer, shown in Figure V-3, is estimated by using the parameters given in Table V-2 and by the theory discussed in Section III.A and Appendix B. The dominant contributions shown are photon shot noise, thermal noise, and seismic noise.

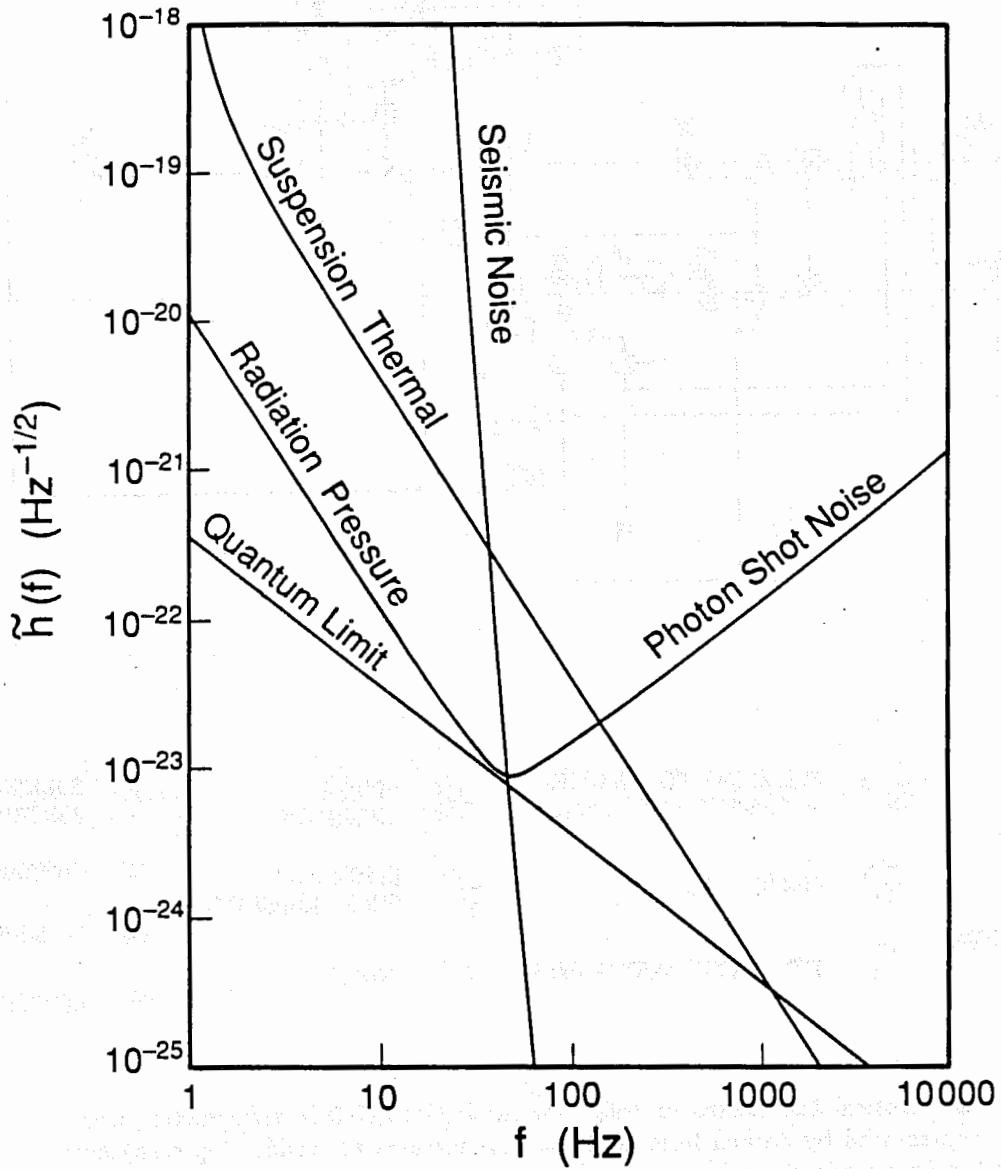


Figure V-3 Projected sensitivity of early LIGO interferometers in broad-band operation, in terms of strain amplitude spectral density, $\bar{h}(f)$. The sensitivity at a given frequency is determined by the noise source that dominates at that frequency.

a. Photon noise. Performance at high frequency is limited by photon shot noise. The dependence of shot noise on mirror parameters and laser power is indicated in Appendix B.4.a. In estimating the shot noise in initial interferometers, the laser system is assumed to produce 5 W of light at a wavelength of 514 nm, as may be achieved with lasers similar to those used in prototype work. Allowing for inefficiencies in transmitting the light into and out of the interferometer and in the process of photodetection, $P \approx 1$ W of effective laser power (including inefficiencies).

Sensitivity at high frequencies improves as $(Pb)^{\frac{1}{2}}$, where b is the recycling factor; the photon noise in Figure V-3 corresponds to $b = 30$ recycles. Mirrors are readily available that would, in principle, allow several hundred recycles before losses in the coatings and substrates limit performance; other inefficiencies, especially in matching the wavefronts from the arms, may limit the recycling factor achievable in early interferometers to $b \approx 30$. The recycling factor may be improved later by control of the figure of the pick-off plate between the beam splitter and TM3 in Figure V-2, which can perform the functions of a compensating plate. At low frequencies, the other form of photon noise—fluctuations in the radiation pressure on the test masses—dominates over shot noise. These fluctuations increase with the time that light is stored between the mirrors of the interferometer arms. In initial interferometers, radiation-pressure noise is not likely to be important, as thermal and seismic noise are substantially larger.

b. Thermal noise. The dominant thermal noise is expected to arise from mechanical losses in the simple pendulum mode of the suspended test masses. Because the restoring force in the pendulum comes mostly from gravity, losses sufficient to make a wire, by itself, a low Q oscillator have a much smaller effect in the complete pendulum.¹

The estimate of thermal noise shown in Figure V-3 assumes that the wire's bending loss is independent of frequency. Testing this assumption will be done as part of our research to develop improved configurations and materials (e.g., ribbon suspensions and lower loss materials) for pendulum suspensions.²

c. Seismic noise. The seismic noise is estimated by using the average of seismic displacement spectra measured at candidate sites (indicated in Table V-2), and multiplying by the isolation provided by a five-layer stack of encapsulated-elastomer springs and masses. The final stage of isolation is the wire suspension of the test masses.

The resonant frequency for horizontal motion of a single layer of the five-layer stack is 7 Hz. The vertical resonant frequency is higher—about 15 Hz. This anisotropy results in the vertical noise giving a bigger contribution than the hori-

¹ In initial interferometers, the ratio of the spring constant from the wires to the total spring constant of the pendulum will be smaller than 10^{-3} .

² Measurements of unstressed quartz fibers have shown $Q \approx 10^6$ in bending modes at 100 and 600 Hz.

zontal noise. In the high frequency limit, the vertical isolation of the stack in series with a 6-Hz vertical resonance in the pendulum is poorer than the horizontal isolation by a factor of about 3.6×10^4 . The interferometer's rejection of vertical test mass motion is, at best, equal to the angle of the optic axis with the horizontal.³ Thus, for the specified parameters, the vertical isolation sets the limit on the noise. A more sophisticated model of the isolator performance includes the imbalances that cause cross-coupling, making the amplitude of horizontal motion closer to that of vertical motion than this analysis suggests.

The seismic noise curve in Figure V-3 includes the effect of horizontal and vertical resonances in the suspension system; it is calculated by methods explained in Appendix D. The estimate represents the sum of direct horizontal motion and 1% of the vertical motion of the test masses, converted to horizontal motion by cross-coupling in the stacks.

The suspension system of the initial LIGO interferometer will be designed to accommodate additional auxiliary interferometers to monitor the suspension points of the main interferometer's mirrors (see Appendix C). These may be used later to reduce low-frequency seismic noise.

The seismic noise curve in Figure V-3 includes the effect of horizontal and vertical resonances in the suspension system; it is calculated by methods explained in Appendix D. The estimate represents the sum of direct horizontal motion and 1% of the vertical motion of the test masses, converted to horizontal motion by cross-coupling in the stacks.

The seismic noise curve in Figure V-3 includes the effect of horizontal and vertical resonances in the suspension system; it is calculated by methods explained in Appendix D. The estimate represents the sum of direct horizontal motion and 1% of the vertical motion of the test masses, converted to horizontal motion by cross-coupling in the stacks.

The seismic noise curve in Figure V-3 includes the effect of horizontal and vertical resonances in the suspension system; it is calculated by methods explained in Appendix D. The estimate represents the sum of direct horizontal motion and 1% of the vertical motion of the test masses, converted to horizontal motion by cross-coupling in the stacks.

The seismic noise curve in Figure V-3 includes the effect of horizontal and vertical resonances in the suspension system; it is calculated by methods explained in Appendix D. The estimate represents the sum of direct horizontal motion and 1% of the vertical motion of the test masses, converted to horizontal motion by cross-coupling in the stacks.

³ Because of the curvature of the earth, the minimum value for this angle is 3×10^{-4} .

TABLE V-2
PARAMETERS AFFECTING
INITIAL INTERFEROMETER SENSITIVITY

Parameter	Value	Notes
PHOTON SHOT NOISE		
Available Laser Power	5 W	Single argon ion laser
Cavity Mirror Coating Loss	50 ppm	$= 5 \cdot 10^{-5}$ power loss per reflection, achieved in prototype.
Optical Efficiency	0.2	40% efficiency in the optical chain; 50% modulation efficiency.
Recycling Factor	30	Limited by matching the arms, not by mirror coatings.
THERMAL NOISE		
Suspended Mass	10 kg	Fused silica monolithic mirror-masses.
Mechanical Q	10^7	Pendulum Q this high has been obtained [V-5].
SEISMIC NOISE		
Input Noise Spectrum	$10^{-7} m \left(\frac{1}{f} \right)^2 Hz^{-1/2}; (f > 10Hz)$	
Intra-vacuum Isolation ¹	$x: \left[\frac{f}{7Hz} \right]^{-2 \times 5} \times \left[\frac{f}{1Hz} \right]^{-2 \times 1}$ $y: \left[\frac{f}{15Hz} \right]^{-2 \times 5} \times \left[\frac{f}{6Hz} \right]^{-2 \times 1}$	

¹ The seismic noise intra-vacuum isolation is specified for horizontal (x) and vertical (y) motion of the test masses. Each of the five layers of the isolation stack, as well as the final pendulum suspension, provides multiplicative isolation proportional to f^{-2} (see Appendix D).

B. Evolution of LIGO Interferometers

To detect gravitational waves, the use of high performance detectors in extended observational runs is necessary. Development of better detectors that enhance our ability to make new discoveries is also vital. A continuing detector development program is planned to improve LIGO capabilities. The design of the first LIGO interferometer emphasizes simplicity, so that we may place a detector in service as rapidly as possible; succeeding generations of interferometers will more fully exploit the unique capabilities of the LIGO.

A conceptual outline of the development program is summarized in Table V-3. The effort will have three main themes: (1) to lower the photon shot noise, (2) to expand to lower frequencies the band in which measurements can be made at or near the shot noise level, and (3) to develop the techniques required to improve sensitivity for special classes of signals, such as narrow-band waves.

Detector evolution will be coordinated with the observational program. As a general rule, a detector in development will replace the previous operational detector as soon as it can provide a significant scientific advantage, even if further development could bring it closer to the performance limits of its design. Consequently, new detector development will sometimes involve pushing an earlier design closer to its performance limits, while at other times it will entail developing entirely new detector designs.

1. Joint observation and detector development in the initial facility

We are committed to perform gravitational-wave searches with the LIGO at the earliest possible time. The initial operations and the proposed strategy for installation and test of the initial interferometers in the LIGO are described in Section VI.

The initial Mark I detector, consisting of three interferometers (full-length and half-length at Site 1, and full-length at Site 2), will be brought on line as early as possible, conceivably with poorer sensitivity than the design level.

We will start a program of performance improvement, adjusting the development schedule to maximize observation time, as soon as the first detector becomes operational.

Development will proceed incrementally in carefully planned stages. Whenever the developmental interferometer is not disabled for testing or installing modifications, its data stream can provide data for observations. The development program will start with small modifications to the interferometer for diagnostic purposes, evolving into use as a test bed for the second-generation LIGO detector.

TABLE V-3
EVOLUTION OF DETECTOR CAPABILITIES

Performance Improvement	Scientific Benefit	Technical Developments
Better broad-band sensitivity in the original frequency band ($f \geq 200$ Hz), by reduction of shot noise	Deeper search for: <ul style="list-style-type: none"> • Supernovae • Late stages of binary neutron star coalescence • Low-mass black hole events • Millisecond pulsars 	<ul style="list-style-type: none"> • Higher power lasers • Improved broad-band or dual recycling • Operation of interferometer and optics at higher power • Use of "squeezed light" techniques • Reduction of other noise sources as they appear
Extend signal band to lower frequencies	Ability to see: <ul style="list-style-type: none"> • More massive black holes • Much larger fraction of pulsar population Better sensitivity to binary neutron star coalescence	<ul style="list-style-type: none"> • Improved seismic isolation (including active systems) • Lower thermal noise • Lower noise test mass damping and control systems • Reduction of other noise sources as they appear
Better sensitivity in narrow frequency range	<ul style="list-style-type: none"> • Allows deeper searches for particular periodic sources • Improved sensitivity to broad-band stochastic background 	<ul style="list-style-type: none"> • Implement resonant recycling or dual recycling • Reduction of other noise sources as they appear

2. Development of the second-generation LIGO detector

While the Mark I detector is going into operation, campus development of the second-generation LIGO detector, Mark II, will be proceeding. The Mark II design will include options not incorporated in Mark I and improvements based on the experience gained from operating Mark I. The advantages of new technology, made available after the Mark I design freeze, will be evaluated.

3. Development of advanced broad-band and narrow-band detectors with higher sensitivity

Development of advanced broad-band detectors will concentrate on two efforts: (1) reducing shot noise, which limits performance at higher frequencies; and (2) overcoming obstacles, such as vibration and thermal noise, which limit interferometer performance at low frequencies. Progress is expected to come both from research

in the LIGO campus facilities and from collaborative work with other groups.

a. Improved sensitivity above 200 Hz. Above 200 Hz the principal noise source in the interferometers is expected to be photon shot noise. Improving performance at these frequencies will require increasing the optical power in the interferometers.

Powerful and efficient solid-state lasers are expected to be incorporated, at the latest, into the second- or third-generation LIGO detectors. Currently, Prof. R. Byer of Stanford University is collaborating with the LIGO Project to develop Nd:YAG laser technology for use in gravitational-wave interferometers. This effort will concentrate on producing high power output with high efficiency and on stabilizing the light to LIGO specifications. The stabilization techniques will be similar to those already developed in prototype work with argon-ion lasers.

In addition to improving the light source, sensitivity can be increased by improving recycling efficiency. The number of times that light can be recycled in an interferometer is limited by absorption, scattering, depolarization, and distortion of the wavefronts by imperfections in the optics.⁴ Improved recycling efficiency may require the development of better optics. This effort will be supported and coordinated with industry through the campus Optics Test Facility (see Section VIII.B). It is likely that certain interferometer configurations in which light is exchanged between the main cavities will be relatively insensitive to optical deformations. Promising techniques for this are dual recycling and resonant recycling. Work in this area has been done at Glasgow University. We plan further work on new optical systems of these and other types.

Employing "squeezed light" [V-6, 7, 8] may make it possible to reduce the influence of shot noise at a given power level (see Appendix C). Eventually such techniques will be employed, if they prove suitable, but an R&D effort in this area is not currently being pursued.

b. Improved sensitivity below 200 Hz. The low-frequency limit to sensitivity is set by mechanical noise, principally seismic noise and thermal noise. Seismic isolation will be improved by the development of more sophisticated passive filters and by the implementation of schemes for active seismic isolation. Both of these approaches are being pursued by the LIGO team, as well as by scientists elsewhere.⁵

Passive isolation can be improved by increasing the number of resonant stages

⁴ Thermal distortion in mirrors made from conventional materials limits the maximum optical power usable in advanced interferometers. We will address this problem by a program to develop low-absorption coatings and substrate materials that can handle larger heat loads. We will also investigate interferometer geometries that are less susceptible to thermal distortion effects, as discussed in Appendix C. Still another strategy is to exploit the current development of optics and coatings in the near infrared where losses are substantially smaller than in the visible.

⁵ We have recently formed a collaboration on vibration-isolation systems with Professors P. Bender and J. Faller at the University of Colorado (see Section VI.B and Appendix K).

[V-9, 10, 11, 12] or by reducing the resonant frequency of each stage. The engineering challenges are substantial, as the springs need to be soft, roughly isotropic, compatible with high vacuum, and well damped. The isolation systems need to be designed and assembled to avoid cross-coupling of the different degrees of freedom.

Active systems use feedback to reduce the seismic noise transmission within the servo bandwidth. One such system, the suspension-point interferometer (see Appendix C), is an option in the initial LIGO interferometer design. Other active systems involve using the test mass as an inertial reference to which its own suspension point is locked [V-13, 14, 15, 16, 17].

Reduction of thermal noise associated with test-mass suspensions is accomplished by reducing the mechanical loss and by increasing the mass for a fixed level of loss (the LIGO test-mass chambers can accommodate up to 1-ton test masses and their associated isolation systems, although 10-kg masses will be used in the first interferometers). Thermal noise in low-loss pendulums has been analyzed theoretically, but no accurate measurements have yet been made. We have begun a research effort to learn more about the dissipation mechanisms, as well as to find what materials, processing methods, pendulum geometries, and clamping or welding procedures will yield the lowest level of noise.

c. **A candidate advanced broad-band interferometer.** The noise spectrum shown in Figure V-4 represents the possible performance of an advanced broad-band interferometer, after development is done as previously described. The high-frequency noise is shot noise from 60 W of green light, recycled 100 times. The thermal noise is that in a pendulum of 1-ton mass, with losses which correspond to a Q of 10^9 . The seismic noise is filtered through a passive five-layer isolation stack, with single-layer resonant frequencies of 2 Hz.

4. Specialized searches

A substantial part of our development effort will be directed toward techniques that allow detectors to be optimized for particular sources.

a. **Searches with narrow-band detectors.** In addition to improving sensitivity in broad-band detectors, searches can be conducted with interferometer configurations that enhance sensitivity in a narrow frequency band. Two methods of accomplishing this, resonant recycling and dual recycling, are described in Appendix C. These methods require modifications to the recycling optics in the beam-splitter chamber, although for dual recycling these may be fairly small. While the basic concepts for these techniques have been worked out for incorporation into the vacuum system design, prototype development will be required before such techniques are implemented.

The clearest advantage of using narrow-band detectors arises in searching for periodic sources. Figure A-4b of Appendix A shows the dramatic increase in search capability expected in a selected frequency band. If a periodic source is discovered in a broad-band search, a narrow-band detector would be quickly deployed for more

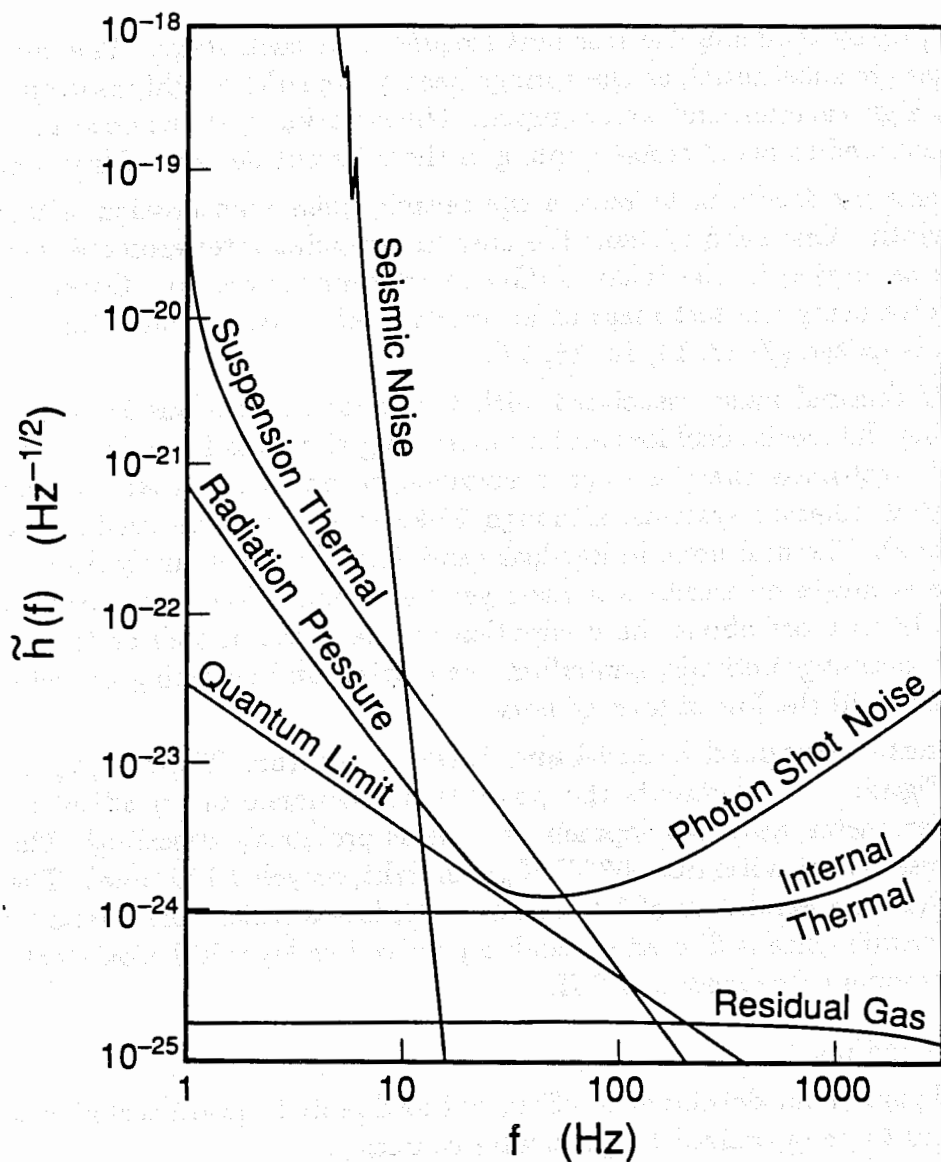


Figure V-4 Projected sensitivity of a possible advanced LIGO interferometer, in terms of strain amplitude spectral density, $\bar{h}(f)$. The parameters that set the level of the various sources of noise are as follows: 4-km arms, 1-ton test masses of fused silica with mechanical $Q = 10^6$, 60 W of bright-fringe power, broad-band recycling with 100 recycles, suspension $Q = 10^9$, residual gas = 10^{-9} torr hydrogen or 10^{-10} torr water.

detailed observations. At other times, the use of narrow-band detectors is planned to search for periodic sources too weak for detection with previously developed broad-band detectors. Such searches will be guided by whatever insights are provided by radio, optical, and X-ray observations.

Whenever information on the power spectrum of a specific type of burst source exists, either from data or theoretical prediction, the frequency and bandwidth of a

narrow-band detector can be suitably adjusted. Thus, narrow-band detectors can also be used advantageously to search for nonperiodic sources.

b. Stochastic-background searches. A search will be made for a stochastic background of gravitational waves by cross-correlating [V-18] the outputs of different interferometers. Data from the most suitable of the interferometers developed for other searches will be analyzed with cross-correlation algorithms.

The smallest spectral density signal of stochastic gravitational waves detectable by this technique is proportional to $h_N(f)/(\Delta f t_{int})^{1/4}$ where $h_N(f)$ is the equivalent gravitational strain noise in the interferometer due to noise sources other than the gravitational waves, Δf is the bandwidth over which the cross-correlation is done and t_{int} is the integration time of the observation. The strong dependence on the interferometer noise and the weak dependence on the bandwidth give advantages to narrow-band interferometers (resonant- or dual-recycled) in such a search.

Occasional searches for a stochastic background at low frequencies, in the outputs of two interferometers at different sites, will be carried out as a special project, as workforce and schedules permit. It may even be useful to set limits by cross-correlating the outputs of two interferometers at the same site if their noise spectra do not appear correlated.

Under development is a search for a stochastic background in the outputs of two different interferometers at different sites. This will be done by cross-correlating the outputs of the two interferometers over a range of frequencies and integration times. The results will be compared with theoretical predictions of the stochastic background. If the results are consistent with theory, it will be concluded that the background exists. If the results are inconsistent with theory, it will be concluded that the background does not exist. This search will be carried out as a special project, as workforce and schedules permit.

Under development is a search for a stochastic background in the outputs of two different interferometers at the same site. This will be done by cross-correlating the outputs of the two interferometers over a range of frequencies and integration times. The results will be compared with theoretical predictions of the stochastic background. If the results are consistent with theory, it will be concluded that the background exists. If the results are inconsistent with theory, it will be concluded that the background does not exist. This search will be carried out as a special project, as workforce and schedules permit.

Under development is a search for a stochastic background in the outputs of two different interferometers at the same site. This will be done by cross-correlating the outputs of the two interferometers over a range of frequencies and integration times. The results will be compared with theoretical predictions of the stochastic background. If the results are consistent with theory, it will be concluded that the background exists. If the results are inconsistent with theory, it will be concluded that the background does not exist. This search will be carried out as a special project, as workforce and schedules permit.

C. LIGO Sites: Scientific Aspects

LIGO Sites will be chosen to maximize the chance of discovering gravitational waves and to ensure the power of LIGO as an astrophysical observatory. The choice of sites also has an important bearing on the ability of the LIGO to form part of an effective international network for the extraction of scientific information from gravitational-wave signals.

1. Physical attributes of the sites

The environmental noise at a site affects the sensitivity of the interferometers and, thereby, both the depth and reliability of the search for gravitational-wave signals. Important considerations in a site choice are the levels of the local intrinsic and wind-driven seismic noise and the spectrum of man-made noise, including varying Newtonian gravitational gradients. The extent to which man-made noise is likely to increase over the lifetime of the LIGO due to local development is another consideration. Seismic noise is especially important for detectors designed to search for gravitational waves at low frequency, where noise levels are generally higher and isolation is more difficult.

Another criterion for site selection is that the plane defined by the interferometer arms should be level. Pendulum suspensions generally exhibit more noise for motion along the vertical than the horizontal. A site that is not level couples vertical noise to the sensitive optic axis of the interferometer. The Earth's curvature sets a limit to the orthogonality which can be achieved. This limit is 3 mrad for a separation of 4 km; all interferometer layouts with slope less than this are roughly equivalent.

2. Separation and relative orientation of sites

Separation of the two LIGO sites is important for the detection of gravitational waves and for the extraction of information from the signals. The LIGO strategy for the identification of gravitational waves is discussed in Section VII; here we concentrate on the influence of site separation in determining astrophysical information.

The discrimination of gravitational waves from environmental noise is satisfied by site separations of hundreds of kilometers or more. We choose to separate the sites by continental distances, thereby enhancing our ability to determine the position of sources in the sky. Because of the broad sensitivity pattern of an interferometer, we will use the difference in arrival time of the wave at different sites to learn the position of a source of gravitational waves. To get the most accurate position determination, the individual interferometers should be as far apart as possible, but limited to a distance such that the response patterns (discussed below) overlap sufficiently. This maximum desirable distance is approximately 4500 km because of the curvature of the Earth.

Several considerations enter into choosing the relative orientations of interferometers at separate sites. The response of a pair of interferometers operated in coincidence gives the highest probability of detection for an isotropic distribution of sources when the arms, projected into the plane that bisects the two detector planes, are aligned.⁶ We have chosen this "coincidence projection" alignment, at the cost of the loss of some information concerning the polarization of the waves.

Because a minimum of three sites must function together to extract complete wave information, LIGO site locations need to be planned with a view toward an international network. The quality of time-delay information from a three-site network is maximized by arranging the sites in a triangle of the largest possible area.⁷ Ratios of the signals at different interferometers will give both polarization states as a function of time. Gürsel and Tinto [V-20] have shown that three interferometers would suffice to uniquely determine all the wave properties, provided the signal-to-noise ratio is sufficiently high. Even an optimal three-site network, however, does not provide full sky coverage with good spatial resolution (see discussion below). Complete astronomy requires a fourth site. With four sites, the figure of merit is the volume of the enclosed tetrahedron. Thus not only the distance between the two LIGO sites will be considered, but also their arrangement with respect to the other possible sites in Europe and elsewhere.

3. Precision of source position determinations

An estimate of the precision obtainable in determining the position of a gravitational-wave burst is presented using a network of three sites.

For near-overhead sources, the uncertainty $\Delta\Theta$ in a burst source's position is approximately [V-21]

$$\Delta\Theta = \left[\frac{8}{\pi A \cos \theta} \right]^{1/2} \left[\frac{c}{2\pi f S/N} \right] = 10 \text{ arcmin} \frac{1}{\sqrt{\cos \theta}} \frac{10}{S/N} \left[\frac{0.22 R_{\text{Earth}}^2}{A} \right]^{1/2} \frac{1 \text{ kHz}}{f}. \quad (\text{V.1})$$

Here Θ is the angle between the source direction and the normal to the plane of the three sites, A is the area of the triangle defined by the three sites, f is the characteristic frequency of the signal, and S/N is the signal-to-noise ratio. R_{Earth} is the radius of the Earth, and $0.22 R_{\text{Earth}}^2$ is the value of the detector triangle's area A for a network with one detector in California, one in Germany, and one near the east coast of the United States.

⁶ In a two-site observatory, Schutz and Tinto [V-19] have analyzed the sensitivity of a coincidence search for burst sources in the Virgo cluster of galaxies and shown that there is a preferred relative orientation which differs from that for sources distributed isotropically over the sky. This "Virgo-optimized" alignment differs from the isotropic-optimized coincidence projection alignment by only 10 deg, and results in less than 5% change in sensitivity.

⁷ We have defined a figure of merit, the area factor, given by $A_M = \frac{|\vec{a} \times \vec{b}|}{R_{\oplus}^2}$ where \vec{a} and \vec{b} are vectors between the sites and R_{\oplus} is the Earth's radius.

This order of magnitude estimate has been confirmed by the detailed numerical simulations of Gürsel and Tinto [V-20]. Figure V-5 shows some results of these simulations for a one-cycle, circularly polarized signal with characteristic frequency 1 kHz, impinging on detectors in the Western and Eastern United States and Western Europe. The signal-to-noise ratio would have been 45 if the source had been overhead at a given detector but is less for sources not overhead. The two graphs in the figure are for different values of the angle θ between the source location and the normal to the plane formed by the three detectors. Each graph shows the magnitude $\Delta\Theta$ of the vectorial angular error in the algorithm's estimate of the source direction, for a sequence of simulations with varying azimuthal angle ϕ around the normal to the three-detector plane. Notice that when the source is nearly overhead [Figure V-5 (a), $\theta = 9^\circ$], the rms angular error is rather small: about 3 arcmin. When the source is near the three-detector plane [Figure V-5 (b), $\theta = 99^\circ$], the rms error is at least 1 deg.

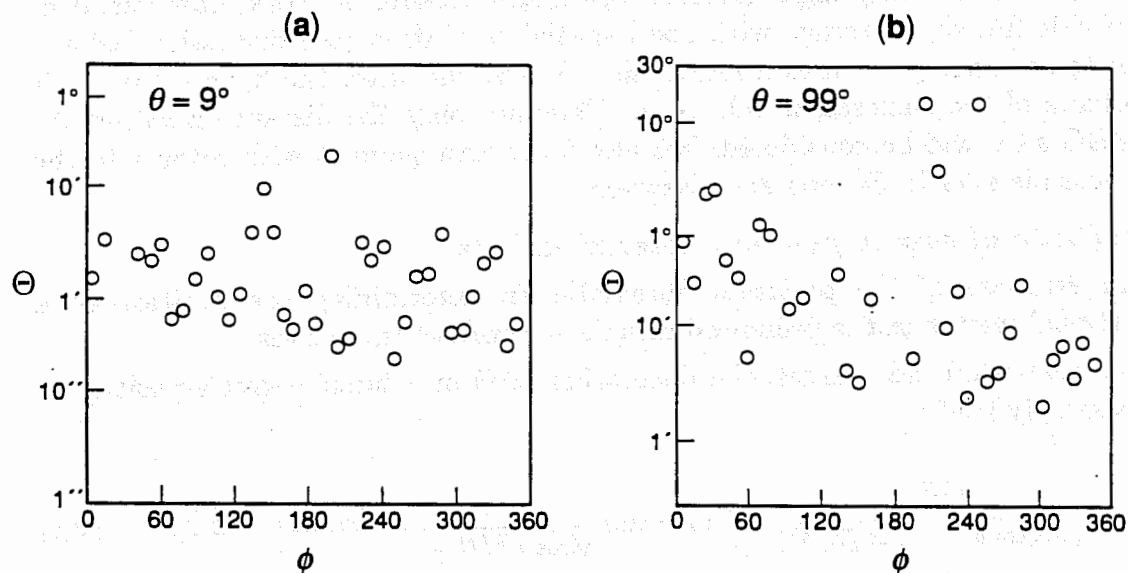


Figure V-5 The angular errors in the estimated source location as computed in simulation tests of a computer code [V-20] developed to extract the source direction and wave form from noisy data from a three-detector network. The plots give the angle, Θ , between the computed and known source locations as functions of azimuth, ϕ , for (a) sources nearly overhead relative to the three-detector plane, and (b) sources nearly in the three-detector plane. A signal-to-noise ratio of 45 (for sources directly overhead) is assumed.

The reduction in angular accuracy near the three-detector plane embodied in the $\cos\theta$ and S/N factors in Equation (V.1) and demonstrated in Figure V-5 shows the importance of having a network of four sites in order to get good full-sky coverage. The best coverage will result from a network whose four detectors are at the corners of a tetrahedron of maximum volume. Adding a detector in western Australia to the network formed by detectors in Europe and on the east and west coasts of the United States would provide an especially large tetrahedral volume.

VI. LIGO OPERATIONS

A. Evolution of Facilities

A successful initial science strategy for the LIGO must cope with uncertainty in the amplitudes, frequency spectra, and rates of the gravitational waves reaching Earth (see Section II). To deal with these uncertainties and to assure an orderly evolution, the LIGO concept includes a staged construction of facilities (Phase A, B, and C, see Section IV) with milestones for reviews and decision making.

Resource limitations dictate the start of operations with the one-detector Phase-A configuration instead of the preferred two-detector Phase-B system (which would allow concurrent observation and development). Although this will reduce the initial operating efficiency, it will not delay the discovery of gravitational waves if their strengths fall within the sensitivity range of the initial detector. The Phase-A design also permits upgrading to the ultimate sensitivity, although at a slower pace than the Phase-B design.

As discussed in Section IV, an important goal is the early expansion of the LIGO capabilities to the Phase-B configuration. This should be implemented as soon as LIGO Phase A has demonstrated satisfactory performance. A continuing program to develop detectors, working in parallel with uninterrupted observations (the "gravitational-wave watch"), is a necessity. Given the pioneering character of the operation, the detector-development program is needed whether or not the initial observations find gravitational waves. If no signals are observed with the first detectors, there will be an urgent need for new detector designs with increased sensitivity and spectral coverage. This development will be carried out in part in facilities on the Caltech and MIT campuses, and in part within the full-scale LIGO facilities themselves. The scaling from short to long baselines is an important factor in detector development, especially as some of the proposed methods to enhance the sensitivity in second-generation detectors cannot be adequately tested on small baselines. Therefore, we are designing the LIGO to enable both development and observation with a minimum of interference. We will plan smooth transitions from one observing detector system to the next iteration of an enhanced detector system that has been technically qualified in the LIGO.

If gravitational waves are detected in the initial observing program, the dual capability for observation and development is just as important. There will be multiple demands on the facilities as the field moves from a discovery phase to an investigative one. The success of the field will doubtless engender enough interest so that a much larger part of the scientific community, both observers and instrument developers, will want to join the new science. At this stage in the LIGO project it would be appropriate to upgrade the LIGO to its Phase-C configuration, enabling the use of the LIGO for many different and concurrent observing programs.

Once waves have been detected, we expect to be operating in concert with gravitational-wave observatories abroad in an international network (see Section V.C and Section X).

B. National Context

We envision the LIGO as an initial quasi-experimental project, focused upon the invention, development, verification, and first use of technologies for laser interferometer gravitational-wave astronomy, with a gradual transition to a mature facility. The early stages of evolution will be conducted primarily by the Caltech/MIT LIGO team, followed by a gradual transition to broader-based national and international participation.

Caltech and MIT, with the principal support of the National Science Foundation (NSF), have invested close to two decades of effort in developing a laser interferometer for gravitational-wave astronomy. The two institutions are committed to continuing a vigorous program leading to the establishment of the LIGO and gravitational-wave astronomy, and subsequently developing, operating, and maintaining LIGO under NSF sponsorship in the interest of the scientific community.

Completion of the LIGO, bringing it to operational readiness in the course of the early search for gravitational waves and, ultimately, conversion to a broadly accessible facility, will require the full commitment and expertise of the Caltech/MIT team. It is expected that once a firm NSF commitment towards construction and operation of the LIGO exists, a broader-based national scientific community will be interested in participation. Early indications of such efforts are an existing collaboration between Stanford University (Professor R. Byer) and the LIGO project in the development of Nd-YAG lasers for LIGO, and collaborative studies with the University of Colorado at Boulder (Professors P. Bender and J. Faller) towards the development of extremely low-frequency ($\lesssim 10$ -Hz) antivibration platforms for laser interferometers. With increasing maturity, the LIGO program will be able to evolve new modes of participation with the scientific community. It is to be expected that the Caltech/MIT LIGO team will continue to provide operations support and maintenance, and that it will conduct a basic gravitational-wave watch and development of advanced interferometers, either alone or in collaboration with others. There will also be outside users who will provide their own hardware and operate their own interferometer systems in the LIGO, as well as users who analyze data from the gravitational-wave watch program. It is proposed that the LIGO director will then work with a national advisory committee that will participate in experiment selection and planning.

C. Operations Plan

The operations phase starts upon completion of Site 1 construction when the facilities become available for installation and operation of interferometers. Although the details of early LIGO operations will depend on what is encountered after startup, there are certain principal lines of progress that will dominate the planning.

1. Phase A: early LIGO operations

The main goal of Phase A is to install and operate LIGO detectors at a sensitivity and duty cycle that will give a significant probability for the detection of gravitational waves. The scenario described below is likely to extend over a period of years (see also Figure XII-1):

- a. Task 1 (upon completion of vacuum facility at Site 1):**
 - i. Shakedown of Site 1 facilities.
 - ii. Installation and shakedown of full-length interferometer at Site 1.
 - iii. Installation and shakedown of half-length interferometer at Site 1.
- b. Task 2 (Site 2 vacuum system completed):**
 - i. Shakedown of Site 2 facilities.
 - ii. Installation and shakedown of full-length interferometer at Site 2.
- c. Task 3:**
 - i. Completion of control and data system for observatory operations: Sites 1 and 2 operating in triple coincidence mode.¹
 - ii. Tests of interferometers in coincidence between the two sites.
 - iii. Start of observatory operations. First detector (Mark I) committed to search for gravitational waves.²
 - iv. Startup of major effort in data analysis.
 - v. On-campus development of Mark II interferometer.
- d. Task 4:**
 - i. Alternating operation of Mark I detector in observation or development (sensitivity enhancements) modes.
 - ii. Qualification of LIGO performance for Phase B.

2. Phase B/C: regular LIGO operations

Regular LIGO operations will follow the implementation of the Phase-B or Phase-C capability enhancements as discussed in Section IV. In particular, these enhancements include the capability to conduct a gravitational-wave watch, detector development, and special investigations concurrently and without mutual interference.

¹ While we expect to conduct observations of burst sources in the multi-coincidence mode, single or paired interferometers may also be used to search for periodic sources or stochastic background as appropriate.

² The Mark I detector will be committed to the first gravitational-wave search as soon as it performs at a sensitivity of about an order of magnitude better than other preceding extended-time search detectors.

D. LIGO Staff

The organization of the fully operational LIGO is illustrated in Figure VI-1.

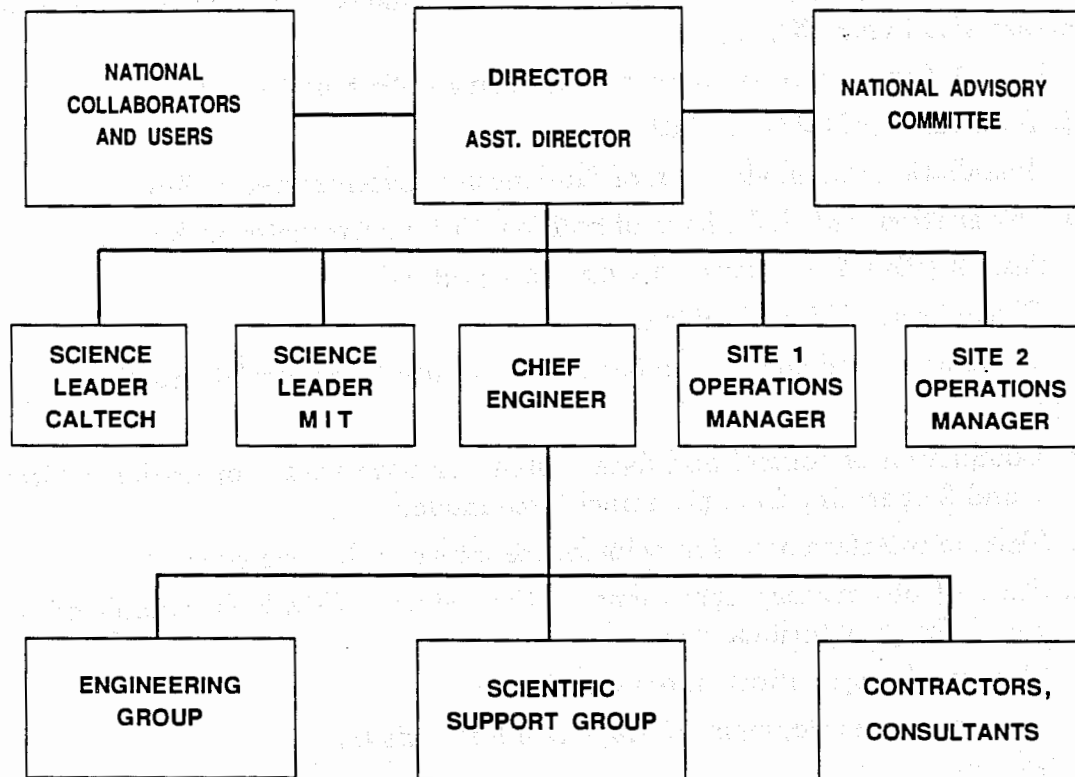


Figure VI-1 Organization of staff to support Phase-C operations.

1. Site operations staff

Each site will have a resident operations staff that is responsible for providing operations support, facilities maintenance and upgrade, and assistance to visiting scientists in their use of the facilities. The operations staff will consist typically of about a dozen persons per site: a resident scientist and site manager, secretary, operators (5), computer analyst, electronics technician, mechanical/vacuum technician, physical plant technician, and custodian.

Five operators will be required to staff the control room for round-the-clock operations (168-hour week). The other technical support staff will be assigned a day shift of 8 hours.

The resident technical staff will be augmented, as needed, by campus scientists and engineers on a detached-duty basis. In addition, visiting scientists will frequently be on site for the installation of new interferometers, trouble-shooting, and real-time data-taking operations.

2. Engineering staff

A core engineering group will be collocated with the director at Caltech. In addition to planning, designing, and implementing maintenance and changes to the LIGO facilities, this group will be instrumental in the development, construction, qualification, and installation of new, advanced interferometers. Meeting these responsibilities will require, typically, the services of the following staff: digital electronics engineer, analog electronics engineer, facilities/vacuum engineer, mechanical engineer, optics engineer, and software engineer. The engineering group activity will be led by a chief engineer who will be a de facto member of the director's office.

3. Scientific staff

At the conclusion of the construction phase, the LIGO science groups (expected to number about six professorial faculty, a dozen scientists, ten graduate students, a varying number of undergraduate students, plus technical and clerical support personnel) will be relieved of their construction support duties and will be able to concentrate fully on observation, data analysis, and detector research and development. The establishment of the LIGO will also create a fruitful environment for a number of postdoctoral research associates, additional graduate students, and additional junior professorial faculty.

E. Coordination of Campus and LIGO Site Activities

The distribution of work among campus and LIGO site facilities will be optimized in an integrated operation.

The LIGO installations will serve three principal objectives: (1) observation, (2) development, and (3) special investigations, in a continuous mode and without mutual interference (see Section IV). The sites will be equipped with all facilities necessary to support the installation, debugging, operation, and scientific diagnosis of gravitational-wave interferometers. These include small mechanical and electronic shops, laser maintenance clean rooms, environmental monitoring and diagnostic equipment, computers, and data-handling equipment.

Because the home university campuses cannot accommodate the testing and final development of the km-size interferometers, the LIGO systems themselves will have dedicated access ports for this purpose. However, the design and early development of interferometers, and the testing and qualification of complete interferometer subsystems, will take place on the home campuses. This approach takes advantage of the home locations of personnel, allows for the most intensive participation of students, and assures minimum interference with the field observing program.

VII. STRATEGY FOR IDENTIFICATION OF GRAVITATIONAL WAVES

We are designing the LIGO for the direct observation of gravitational radiation. Because the gravitational-wave sources have uncertain strengths, rates, and character, we must adopt a multifaceted strategy for the verification of their signals. An essential part of the LIGO concept, especially important early on, is high confidence that the signals observed are indeed gravitational waves and not instrumental or other terrestrial noise.

Should the signals be strong and of recognizable form, the wave shapes themselves can provide information to help identify them as gravitational waves. A good example is the chirp signal arising from the coalescence of a binary neutron star or black-hole system (Figure A-3 in Appendix A). Another example is the characteristic frequency and amplitude changes associated with a periodic source observed from the rotating and orbiting Earth.

Because we cannot count on these signatures, the LIGO design will include tests to assure that the signals are consistent with gravitational waves and inconsistent with spurious phenomena. The verification strategy includes the following elements:

- (1) *The operation of interferometers at widely separated locations.* Burst gravitational waves produce signals that are coincident in separated interferometers (except for a delay due to travel-time). If the interferometers are far enough apart, there is only a small probability of correlations from environmental and instrumental noise. Separated interferometers are also useful in identifying continuous gravitational-wave sources.
- (2) *The operation of an environmental and instrument monitoring system.* The signals that are due to gravitational waves must not correlate with measured perturbations in the environment or the instrument.
- (3) *The operation of interferometers of different length.* With two interferometers at the same site but of different lengths, the signals must be in the ratio of the lengths to qualify as gravitational waves.

All three elements of this strategy are required because no one by itself is sufficient to give the confidence needed for an unambiguous detection. Furthermore, each element contributes in other ways to the research program, as will be discussed below.

A. Statistical Characteristics of the Noise

The noise estimated in Sections III.A, V.A, and V.B is due to continuous random processes (shot noise, thermal noise, and the average seismic noise) and is a good predictor of the detector performance in a search for such continuous signals as periodic and stochastic-background gravitational-wave sources. The data used for a burst search have two components: (1) a Gaussian distribution of pulses

from continuous random processes and (2) a non-Gaussian distribution of pulses that occur infrequently but may have a large amplitude. An impulse given to a test mass from a sudden release of strain in a suspension wire is an example of a mechanism that can contribute to the non-Gaussian distribution. Experience with operating single interferometers in long-duration runs shows that the non-Gaussian noise can be described by a flat distribution of pulse amplitude versus the frequency of occurrence.

B. Noise Suppression and Signal Confirmation

We plan to use coincidence techniques between interferometers and veto information from the environmental and instrument monitoring systems to bring the sensitivity of a pulse search to the level of the Gaussian noise. The noise in widely separated interferometers is expected to have a low probability of correlation. Interferometers sharing the same site have a higher probability of correlated noise, but have the advantage that the gravitational-wave signal amplitudes will have well-defined ratios if the interferometers are of different length. We are proposing that the optimal broad-band LIGO detector will consist of three interferometers operating in coincidence: a full-length interferometer at Site 2, and a full-length/half-length pair of interferometers at Site 1.¹

1. Multiple interferometer coincidence detectors

In principle, it is possible to search for bursts using just two interferometers, one at each site, and operating the pair in coincidence. The simplest method would be to note whenever an event occurs (the interferometer output exceeds a preset threshold value) in either interferometer, and then look for coincidences between events from the two interferometers. If an event occurs at time t_0 in interferometer 1, then the double-coincidence criterion is true if an event occurs in interferometer 2 at time $t_0 \pm \tau_w/2$, where τ_w is the duration of the acceptance window. This two-fold coincidence method will work provided the rate of spurious double coincidences is sufficiently low.

For double-coincidence operation of two interferometers, the rate of spurious coincidences due to the noise is given by

$$R_{12} = \tau_w R_1 R_2 \quad (\text{VII.1})$$

where R_1 , R_2 are the singles rates (the rate of noise pulses) for interferometers 1 and 2, respectively. To allow detection of a pulse of duration τ_p , we set

$$\tau_w = \tau_p + 2l/c \quad (\text{VII.2})$$

¹ A full-length interferometer has test masses at each end of the 4-km vacuum tubes. A half-length interferometer has its central masses in the corner building and its end test masses in mid-station buildings located near the middle of each 4-km tube.

where l is the separation between the interferometers and c is the speed of light. The term $2l/c \approx 20$ ms $\cdot (l/3000\text{km})$ accounts for gravitational waves coming from all directions.

The rate of spurious coincidences can be greatly reduced by operating in triple-coincidence mode with a third interferometer at one of the two sites. In this case the spurious coincidence rate is given by

$$R_{123} = (\tau_P + 2l/c)\tau_P R_1 R_2 R_3 \quad (\text{VII.3})$$

where R_3 is the third interferometer's singles rate and l is the separation between the sites. Table VII-1 gives the allowable rate of noise events in each interferometer (assuming $R_1 = R_2 = R_3$) to achieve a spurious coincidence rate of 0.1 /yr if the noise is uncorrelated between the interferometers.

TABLE VII-1
CONSTRAINTS ON COINCIDENCE DETECTION¹

Number of Interferometers in Coincidence	Separation l	Tolerable Noise Event Rate/Interferometer	
		$\tau_P = 1\text{ms}$	$\tau_P = 10\text{ms}$
2	4000 km	1.2/hr	1.2/hr
2	0 km	6.4/hr	2.0/hr
3	$l_{12} = 0\text{ km}$ $l_{13} = 4000\text{ km}$	175/hr	74/hr

¹ Constraints on single interferometer noise event rates to achieve a spurious coincidence rate of 0.1/yr.

We see from Table VII-1 that triple-coincidence detection affords approximately two orders of magnitude better suppression of noise events than a double coincidence between two sites. This analysis assumes that the interferometer outputs are statistically independent. Some local correlation in the noise of the interferometers at Site 1 can be tolerated, depending on the singles rate R_2 at Site 2. Locally correlated noise increases the accidental triple-coincidence rate by

$$\Delta R_{123} = R_{c1} R_2 (\tau_P + 2l/c) \quad (\text{VII.4})$$

where R_{c1} is the rate of correlated noise events at Site 1. For example, in a search for millisecond bursts the accidental triple-coincidence rate increases by 0.1/yr for R_{c1} of order 1/day, assuming $R_2 = 20/\text{hr}$ (comparable to the observed unvetted singles rate in gravitational-wave searches using prototype interferometers). One can measure the degree of local correlation by comparing the coincidence rate between Site

1 interferometers with the prediction of Equation (VII.1). If locally correlated noise is a problem, it must be diagnosed and eliminated. One cannot test for globally correlated noise statistically, because a triple coincidence is itself a characteristic of a gravitational wave.

Past experience suggests that, at least during the early stages of LIGO operations, the singles rates will be high enough to require the simultaneous operation of three independent interferometers. If the singles rates can be adequately reduced, the option of using two interferometers for searches, and thereby freeing up the third interferometer for development, will become available.

2. Auxiliary diagnostic/veto monitors

Besides the interferometer output signal, there are many other other signals (such as laser power, pointing control, beam position, and mass damping controls) within the interferometer that will be monitored for correlations with the output signal. In addition, each LIGO site will have auxiliary instrumentation to monitor the physical environment of the interferometers. Representative phenomena to be monitored are given in Table VII-2. These monitors will be used to veto spurious pulses in burst searches,² reducing the singles rate of spurious pulses without affecting sensitivity.

3. Wave amplitude tests with collocated interferometers of different lengths

The ratio of the amplitudes of the signals developed in two interferometers of different length—specifically, one half the length of the other—at the same site is useful in discriminating gravitational waves from sources of noise. The basis of this discriminant is that gravitational-wave signals will be in the ratio of the interferometer lengths. This is the only element in the strategy that has the attribute of giving a positive signature for the gravitational waves from all classes of sources. A half-length interferometer also measures the effect of noise sources by a method qualitatively different from the environmental monitoring system. It provides discrimination against noise in general, independent of the generating mechanism. Thus, the combination of two interferometers can reject spurious events that bypass the auxiliary monitors. Moreover, it provides additional and qualitatively different diagnostic information on noise sources. This information can be especially useful when there is no correlation between the interferometer output and the auxiliary monitors.

There is a slight sensitivity penalty in configuring three interferometers as two full-length and one half-length, compared with using three full-length interferometers. The triple-coincidence sensitivity depends on the separation of the interferometers, their relative sensitivities, and the frequency band of the signals. For typical

² The monitors may also be useful in reducing noise in continuous wave searches, if the monitored quantities correlate with the interferometer output.

TABLE VII-2
ENVIRONMENTAL PARAMETERS TO BE MONITORED

PHENOMENON	MONITOR
Seismic Noise	Translation and rotation: $f < 10 \text{ Hz}$; 1 seismometer/building $f > 10 \text{ Hz}$; 3 accelerometers/test mass tank
Acoustic Noise	Microphones at test mass tanks and critical optical components
Magnetic Field Fluctuations	Low frequency: 1 magnetometer/building High frequency: 3 coils/test mass tank
Radio Frequency Interference (RFI)	Multilevel receiver to record rms noise in selected channels, one per building
Cosmic Rays	Shower detector, one per building
Electrical Power	Transient monitor, one per building
Fluctuations in Residual Gas Column Density in Beam Tubes ¹	UV absorption spectroscopy
Housekeeping Data From Facility Control	Temperatures, wind velocity, ion pump currents, etc.

¹ Although not planned for installation at the outset, a monitor for gas may be required based on experiences with the system. The standard vacuum measuring gauges are not sensitive enough to detect column density changes that would be interpreted as gravitational wave signals. A system using UV absorption spectroscopy on the gas column in the beam tubes has been devised which should have sufficient sensitivity to veto gas bursts at the level required to match the sensitivities of the advanced detectors being planned for the LIGO. The gas bursts, should they occur, will have a characteristic pulse signature that depends on the tube diameter and the pumping speed. There is no information that such gas bursts occur, however, the LIGO will be exploring a new measurement regime.

LIGO sites, and for the half-length interferometer operating with half the signal-to-noise ratio of the full-lengths, the sensitivity to kHz-band signals is reduced by at most 30%. This result applies to Gaussian noise, with the optimal setting for trigger thresholds of 4.9 and 6.5 times the rms Gaussian noise level in the full- and half-length interferometers, respectively.

C. Data Strategy

1. Requirements and essential features

We do not yet have a detailed design for data archiving and analysis; this will become a high-priority effort during the proposed grant period. We present here essential features of a design, based on our experience in gravitational-wave searches and on projected LIGO data recording and analysis requirements.

Appendix G describes five separate analyses from three data runs made between 1983 and 1987. The runs were conducted with prototype detectors at Caltech and MIT, at sensitivities insufficient to detect plausible astrophysical sources. The most recent (1987) data collection was a coincidence run complete with atomic standard time keeping at both sites. Conventional low-density recording techniques were used so data were taken for only a few days. Nevertheless, these searches provided useful experience in recording and analyzing data streams similar to what are expected from LIGO.

The data archiving and analysis strategy will be tailored to the following attributes of LIGO operations:

- Interferometers have a large bandwidth (10 Hz to 10 kHz, except for specialized narrow-band detectors) and nearly omnidirectional response to gravitational waves.
- Observations will use two or three interferometers operated in coincidence, along with auxiliary monitors.
- LIGO data will be used to search for and measure signals from a wide variety of sources in postdetection analysis, including burst waveforms, and periodic and stochastic-background signals.
- LIGO detectors will be used to conduct extended-duration searches with near 100% live time.

The total quantity of data accumulated will be large compared to most other physics experiments and astronomical observations, and high-density recording techniques are required. Even so, special techniques are needed to reduce the total amount of data recorded, especially from wide-bandwidth auxiliary measurement systems (see Volume 2, Section IV.F).

2. Types of signals and characteristic bandwidths

The signals to be recorded fall into three categories.

- a. **High-bandwidth, continuous.** The most critical signals, including the interferometer output and perhaps one or two monitor channels, will be recorded continuously and with full bandwidth—approximately $2 \cdot 10^4$ 2-byte samples/s, for a data rate of 40 kbytes/s/interferometer. These signals place the largest demands on the capacity of the recording and archiving system.

b. **High-bandwidth, sporadic.** Many auxiliary monitor signals—such as the intensity of laser beams at several parts in the optical chain, servo signals, and acoustic monitors—have inherently high bandwidth. Continuous archiving of these signals could overwhelm the data recording system; if necessary, they will be recorded on the basis of infrequent triggers, described below.

c. **Low-bandwidth, continuous.** A large number of low-bandwidth signals, including filtered forms of alignment servo signals, temperature monitors, and “alarm” signals that indicate out-of-range conditions for critical optical and electronic components, will be recorded. Continuous recording, at rates ranging from less than 1 to approximately 100 samples/s (depending on the signal), presents an aggregate load on the data system that is smaller than that of the high-bandwidth continuous signals.

The precise distribution, trigger rate, and bandwidth for these signals is yet to be determined. The overall average rate of recording, however, is constrained by the capacity of foreseen recording and archiving systems, and is expected to be approximately $5 \cdot 10^9$ bytes/day per interferometer. Even with 1989 technology, data at this rate can be stored by writing approximately two 8-mm video cassettes per day.

3. Archiving of data

a. **Shakedown/development phase.** During the diagnostic phase of interferometer installation and shakedown, all the signals will be useful. Our experience with the prototypes shows that the initial noise spectrum of a new interferometer is usually far from the theoretical limits. The process of reducing the instrument noise exploits the ancillary interferometer signals and other monitors to pinpoint the most performance-critical parts. Troubleshooting and development will rely on cross-correlating many pairs of available signals within one interferometer—such as the pointing servos against the interferometer output—and, when available, the outputs from different interferometers. Selected data from this phase of operations will be archived and made available for subsequent analysis in the improvement of the operating interferometer and to guide the development of advanced interferometers. The data from both sites will be sent to the university campuses for analysis.

b. **Searches with broad-band detectors.** The most important information is in the interferometer output that carries the gravitational-wave signal. These data will be filtered to whiten the spectrum and reduce the recording dynamic range requirements. Additional filtering will remove aliasing associated with the limited sampling rate. The archive will include time tags with a precision of $1 \cdot 10^{-6}$ s., UT.

A limited amount of real-time analysis will be performed on the interferometer output³ and on some of the monitor signals. One possible method is to pass the interferometer output through several specialized filters, arranged in parallel, each providing enhanced signal-to-noise ratio for a specified waveform. A flag will be raised whenever a candidate source is identified in the main output, or when a significant effect is reported by the auxiliary monitors. A time buffer will store auxiliary-monitor data that precede the identified event, so that bursts of data at full bandwidth may be recorded along with the interferometer output.

A simple set of processors—for example, bandpass filters covering several frequency bands—will reliably set flags on events that are large compared to the Gaussian noise level. More specific filters will potentially catch smaller events. Selection of the best filter function and threshold depends on the instrument's noise spectrum, which will be determined during instrument and facility shakedown. Because the gravitational-wave output from each interferometer in a search detector is continuously archived, it can be reanalyzed if developments in theoretical astrophysics predict new waveforms, or if new information about specific sources becomes available.

c. **Searches with narrow-band detectors.** The output of initial interferometers will be inherently broad-band, and bandwidth reduction to search for periodic or semiperiodic sources will be accomplished by specialized algorithms for off-line data analysis. Interferometers with resonant recycling, on the other hand, will have useful output over only narrow bands of frequencies; the required recording rate for these data will be reduced. Furthermore, several monitor signals from each interferometer can be recorded in narrow frequency bands around the search frequency and its subharmonics, without exceeding the capacity of the recording system. As with searches for bursts, the ultimate discrimination against false signals in periodic searches will be provided by a comparison of the outputs of separate interferometers.

4. Analysis of archived data

a. **A search for coincident burst events.** Candidate events can be processed by passing the flagged data through a set of specialized pulse-filter templates to improve the signal-to-noise ratio and then recording the pulses in a time-ordered list of events for each interferometer. The lists from each interferometer are next compared for coincidence. The pulses that fall into a coincidence window determined by the interferometer separations are studied one by one. An additional discriminant is provided by matching the pulse waveforms from each interferome-

³ Current planning for initial LIGO operations does not include real time links between sites for on-line analysis of coincident events. Once the field is established, and especially after a network (three or more) of gravitational-wave detectors is operating to give positional information, it will be advantageous to carry out on-line analysis of burst events in order to alert the astrophysical community to their occurrence. The communications technology for this service exists now and need not be developed.

ter.

b. A search for periodic sources. The continuous data stream from the interferometer output of any one interferometer can be analyzed for periodic sources. The techniques used initially are expected to be similar to those developed for searches made with the prototypes in which the optimal filter was a Fourier transform. The data for this analysis need not retain the full amplitude range of the original data stream but only enough (4 bits) to preserve information on the FM and AM components of the sources when averaged over periods of hours to months. Livas [VII-1] showed that a search for periodic signals over the complete bandwidth of the interferometer, optimized for a specific location in the sky, is within the capabilities of present supercomputers. A search for all frequencies, over the entire sky, would pose a formidable challenge and could require the development of dedicated hardware or new search algorithms.

One of the requirements for a search for periodic sources is separating spectral peaks originating in the environment or the instrument (e.g., low-amplitude oscillations of suspension wires) from those due to gravitational-wave sources. The principal discriminants available are the Doppler shift and the amplitude modulation of the signal from the motion of Earth relative to the wave. The LIGO offers an additional dimension in solving this observational problem through the operation of two sites. Cross-correlation of the analyzed power spectra will be a powerful tool in discriminating local mechanical oscillations (especially those that may wander in frequency) from astrophysical sources.

c. A search for a stochastic background. The signature of a stochastic background would be correlated broad-band noise in two interferometers, used in much the same manner as electromagnetic radiometers.⁴ The gravitational-wave stochastic background, if white over the interferometer response, grows against the uncorrelated noise as the quarter power of the product of the detector bandwidth and the correlator integration time; see Section V.B and Equation (A.20) of Appendix A. The computational requirements for this search are well within reach of present computers and do not require additional hardware development.

⁴ The techniques have already been used in an early search for gravitational-wave stochastic background with broad-band bar detectors. [V-18]

VIII. CAMPUS RESEARCH AND DEVELOPMENT IN SUPPORT OF LIGO

A. Results from Prior NSF Support

Almost two decades of research activity on laser interferometric gravitational-wave detectors form the supporting basis for this proposal. The highlights of this work are summarized here. Appendix H reports in greater detail progress during the most recent grant period.

1. Development of new concepts in gravitational-wave detection using laser interferometry

a. **New concepts for gravitational-wave detection.** Many of the key concepts and techniques of laser interferometer gravitational-wave detectors have been introduced and developed by members of the LIGO team.¹ LIGO team members were responsible for the invention and original development of two principal variants of interferometric detectors: the "optical delay line" (or "Michelson") variant [VIII-1, 2, 3] in which the laser beam makes many discrete passes in each arm of the interferometer, and the Fabry-Perot variant [VIII-4, 5], in which each arm is operated as a very long Fabry-Perot cavity.

In the Fabry-Perot system, the wavelength of the light from the laser source has to be controlled to very high precision, and a new technique for doing this was conceived and developed [III-2]. This involves modulating the phase of the laser light at a high radio frequency, and monitoring light reflected from the cavity input mirror. This laser stabilization method, now one of the most precise known, has subsequently been widely applied in laser physics and atomic spectroscopy laboratories.

Practical development of these techniques has proceeded over many years. Special techniques, such as use of feedback systems and modulation methods to shift gravitational-wave induced phase changes to higher frequencies where the laser light is quiet, are used to achieve interferometer performance at the level limited only by photon shot noise. New technical concepts and strategies have been introduced to overcome noise sources of various kinds as they were identified, and to gradually improve performance and sensitivity to the levels achieved to date. Advances in displacement sensitivity have exposed phenomena unobservable by other techniques. Examples are the broad-band, thermal noise vibration spectra of mechanical structures at room temperature, and subtle noise effects associated with various methods of bonding mirrors to test masses.

¹ Although all the work described was done by members of the LIGO team, some of it preceded or was done outside the NSF-supported groups at Caltech and MIT.

b. More advanced concepts to enhance interferometer sensitivity. Work with the 40-meter Fabry-Perot prototype interferometer led to the demonstration that mirrors made by techniques developed for laser gyroscopes were capable of storing light in a cavity for times longer than the periods of the gravitational waves being sought—and could give quality factors for cavity resonances of more than 10^{12} , hitherto unprecedented in optics. Consideration of what could be possible with large-scale systems of this type led to the invention of the techniques for enhancing efficiency and performance of interferometers now known as *broad-band recycling* and *resonant recycling* [V-1]. In the first of these the whole interferometer is turned into a large optical cavity, in which resonant build-up of the laser light can give a significantly improved shot-noise limit to sensitivity. In the second the optical signal from a gravitational wave builds up by resonance in a system of coupled cavities, which enhances further the sensitivity for periodic sources. These concepts are opening a new area in optical techniques for gravitational-wave research.

2. Technological developments

a. Experience acquired in construction and operation of prototype interferometers. Since 1972, members of the LIGO team have been engaged in construction and operation of gravitational-wave detectors of various types. This effort has involved experimental study of noise sources and development of experimental techniques. From this work experience has been gained in the following areas:

- The use of interferometer mirrors mounted to suspended test masses free at frequencies above the suspension resonance (approximately 1 Hz)—a departure from conventional interferometry, in which all components are rigidly mounted to a solid monolithic base.
- The development of systems to control the interferometer [VIII-6]. This includes the many servo systems for control of position and orientation of optical components and for optimization of cavity parameters relative to the input light beam.
- The development of simple but highly effective vibration-isolation stacks to suppress transmission of seismic noise into the interferometer [VIII-6].
- The use of spatial and temporal filters, such as optical fibers and mode-cleaning cavities, to reduce fluctuations in the frequency and spatial geometry of optical beams.
- The use of simple, high mechanical Q, test-mass structures employing optically contacted mirrors to reduce noise from thermal excitations.
- The use of optical cavities of very high finesse,² and multi-loop wide-band servo systems to lock lasers to them.
- The development of techniques to rebuild high-power lasers to operate with

² Finesse $F \approx \pi/(1 - \sqrt{R_1 R_2})$ where R_i is the intensity reflectivity of mirrors.

low levels of spatial and frequency fluctuations.

- The successful application to interferometry of advances in optical polishing and coatings which have provided low-loss components.
- The development of techniques to phase-modulate light with random noise and pseudo-random pulse sequences to control the effects of scattering in equal-path-length Michelson interferometers.

Based in part upon this experience with the prototypes, a Fabry-Perot design was adopted as the basis of the initial LIGO interferometer. The 40-meter prototype, described in Section III.B, began operation as a Fabry-Perot interferometer in 1983. Figure VIII-1 illustrates successive improvements in sensitivity in the working interferometer as various technical advances were introduced.

b. Implications for design of LIGO interferometers. Besides the demonstration of interferometric detection techniques, operation of the 40-meter prototype has led to the development of prototype designs for LIGO subsystems and has identified problems which require further research.

The 40-meter prototype is the longest interferometric gravitational-wave detector in existence. The high-precision mirror-alignment system developed for this baseline will guide the development of similar systems for LIGO. A 5-meter baseline vacuum system for a prototype interferometer with LIGO-scale test masses has also been constructed. The combination of the 5 and 40-meter prototypes will serve to investigate length-dependent effects for extrapolation to LIGO conditions.

The electro-optical technique for servo-locking lasers to optical cavities, described in Section III.B, can serve as a general purpose building block throughout the LIGO. This system has achieved suppression of laser frequency fluctuations by more than 2×10^8 over millisecond timescales, with more than an order of magnitude electronic gain in reserve. This technique is adaptable to various laser systems, including those operating at high power. This experience has uncovered no fundamental limitation in achieving the frequency control required for LIGO.

The 40-meter prototype has demonstrated that light can be stored in Fabry-Perot cavities for sufficiently long times to optimize LIGO interferometers for sensitive detection of gravitational waves at all frequencies above about 1 Hz. The heating of optical components by absorption of light has been identified as a problem associated with high input power and long storage times. Thermal distortion effects in Fabry-Perot cavities have been observed. Preliminary analysis suggests that the distortion is due to thermal lensing in the mirror substrates driven by optical power absorption in the mirror coatings. Based partly on these findings, an optical test facility is being established to develop and evaluate optical components that meet the high-power and large-aperture requirements of LIGO interferometers.

The best sensitivity achieved to date with the 40-meter prototype has established that our techniques for construction of test masses, suspension systems, and vibration-isolation systems are sufficient to achieve an equivalent displacement noise

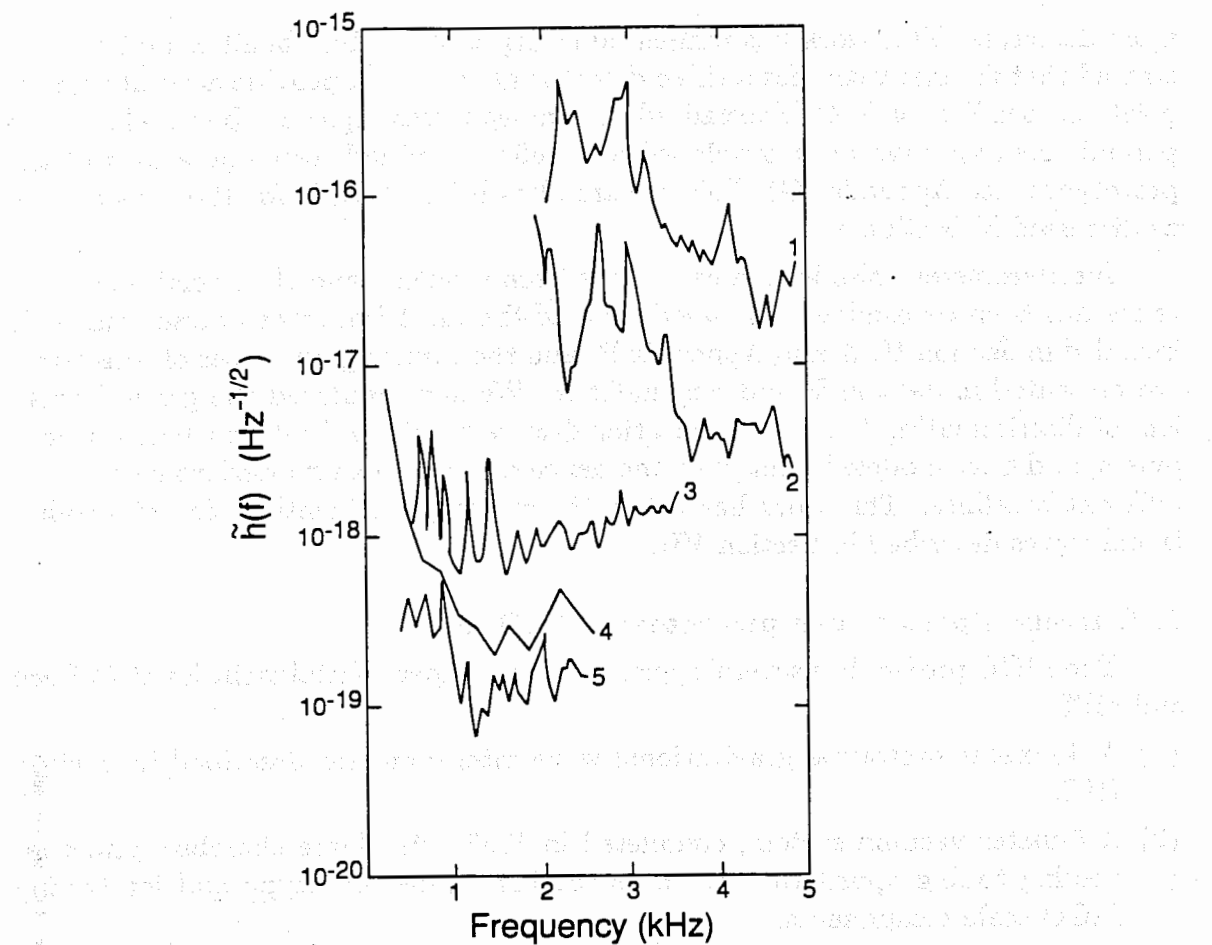


Figure VIII-1 Sensitivity improvements in the 40-meter prototype interferometer. The spectra show the increasing sensitivity from the time of first operation in May 1983 (1), to the best performance achieved to date (5). The improvements shown are attributable in part to the following changes: (1) to (2)—the installation of low-loss cavity mirrors for increased storage time; (2) to (3)—the replacement of complex test masses containing several optical components by simpler masses backing the cavity mirrors alone; (3) to (4)—the installation and rebuilding of a high-power argon-ion laser, and the refinement of electronic servos maintaining resonance in the interferometer; (4) to (5)—the installation of fused-silica test masses and an in-line mode cleaner.

of $\leq 3 \times 10^{-18} \text{ m}/\sqrt{\text{Hz}}$ at 1.5 kHz. A 4-km-baseline LIGO interferometer—if limited by mirror displacements of this magnitude—would exhibit a strain sensitivity of $\bar{h} \leq 8 \times 10^{-22}/\sqrt{\text{Hz}}$ at 1.5 kHz.

3. Analytical developments

Members of the LIGO team have carried out theoretical work to assess the likely strengths and event rates for various types of gravitational-wave sources [VIII-7]. Team members have also developed computer algorithms for extracting source direction (θ, ϕ) and waveforms ($h_+(t)$, $h_x(t)$) from the data of networks of three or

more detectors. This work has influenced siting of the LIGO facilities and demonstrated that for many sources a three detector network can provide accurate source positions; see Section V.C. Specialized data analysis strategies for burst, chirp, and periodic sources have been developed and refined through test operations of the prototypes (see Appendix G). This research has led to criteria for the data system as discussed in Section VII.

Interferometer noise mechanisms have been modeled and their relative importance has been determined. A description of the most important noise sources is included in Section III.A and Appendix B, and the resulting estimates of sensitivity are presented in Section V and Appendix A. We have analyzed the general problem of discriminating between gravitational-wave bursts and intermittent spurious pulses, and have modeled multiple coincidence detectors using interferometers with different baselines. This work has led to the strategy for identification of gravitational waves described in Section VII.

4. Current status of campus research facilities

The LIGO project has several special-purpose experimental facilities at Caltech and MIT:

- (1) A 40-meter prototype gravitational-wave interferometer described in Section III.B.
- (2) A 5-meter vacuum system, completed in 1988, with large chambers and connecting tubing appropriate for constructing a new prototype and for testing LIGO-scale components.
- (3) A vacuum facility to test suspensions and seismic isolation systems, including an electromagnetic shaker.
- (4) A facility to measure total losses in mirrors by determining the Q of optical cavities.
- (5) A facility to measure the angular distribution of light scattered by mirrors.
- (6) A vacuum test facility to measure the outgassing properties of vacuum enclosures and components.

5. Conceptual design

Based on the progress described above, as well as several dedicated studies made over the past 5 years, a conceptual design for the LIGO has been formulated. The basic LIGO concept and operations plan has been developed and is described in Sections IV and VI, respectively. We have decided to pursue a phased construction approach to deliver, at the earliest time, a system capable of directly detecting gravitational waves and exploiting the observations for physics and astrophysics. Later evolution of the facilities will enhance the scientific capabilities of LIGO and allow broad participation in this new field. We have identified a simultaneous search and development capability, with minimum interference between these

missions, as the optimum strategy to ensure successful LIGO operation. This has defined requirements for three distinct detector types (observation, development, and special investigation detectors), and a flexible modular vacuum system capable of supporting simultaneous operation of multiple interferometers.

The scientific functional requirements have been specified and documented for the LIGO facilities, including requirements on sites, vacuum systems, interferometer design, data and control systems, and support facilities. Preliminary designs for the facilities and hardware have been developed to meet these requirements, and the interaction between them to identify key driving parameters has been studied. The resulting design is described in Volume II.

Volume II contains the detailed design of the LIGO facilities. It includes the conceptual design of the facilities, the detailed design of the vacuum system, the design of the interferometers, the design of the data and control system, and the design of the support facilities. The design is presented in a series of chapters, each dealing with a specific aspect of the facility. The chapters are:

1. General Description of the Facility
2. Site Selection and Construction
3. Vacuum System Design
4. Interferometer Design
5. Data and Control System Design
6. Support Facilities Design

Volume III contains the detailed design of the LIGO detectors. It includes the conceptual design of the detectors, the detailed design of the optical components, the design of the mechanical structures, the design of the electrical systems, and the design of the software. The design is presented in a series of chapters, each dealing with a specific aspect of the detector. The chapters are:

B. Future Activities

Campus R&D activity during the period covered by this proposal will be divided into five areas:

- (1) The continuing development of the prototype interferometers to test techniques and designs that will be used in the initial LIGO system. This will guide the initial LIGO interferometer design toward improved sensitivity and reliability.
- (2) The development of subsystems for the prototypes—with application to the initial LIGO interferometer for automated operation and detailed investigations of noise sources.
- (3) The development and use of specialized facilities for R&D in optics and vibration-isolation systems to support both prototype and LIGO development.
- (4) Scientific planning and support of the LIGO engineering and construction, including the design, fabrication, and testing of the initial LIGO interferometer and the development of data analysis strategies and software.
- (5) A continuing basic research program to develop and test new interferometer concepts to enhance the sensitivity and frequency coverage of LIGO detectors.

1. Prototype development of techniques for Mark I interferometer

Conceptual design of the initial LIGO interferometer is in progress and will continue through the first two years of the proposal period. By early CY 1992, we expect to have a complete design, based partly on current concepts and partly on the results of the proposed research and development program. Specifying much of the design requires operating the prototypes at the very lowest noise levels we can achieve. This is necessary to uncover unanticipated problems with the conceptual design of the Mark I LIGO interferometers, and will lead to a higher performance in their final version. As described in Appendix H, we are currently reconfiguring our light-stabilization scheme and beam-splitting optics on the 40-meter prototype to develop the techniques to be used in the initial LIGO interferometers. Experimental parameters of the prototypes such as optical power, finesse, and modulation method will be chosen to simulate operating conditions in the LIGO.

a. **Development of techniques to recombine the beams in a Fabry-Perot interferometer.** In the full-scale LIGO interferometers, the light reflected by the two 4-km-long Fabry-Perot cavities will be recombined at the beam splitter. Recombination compares the signals from the two orthogonal arms optically rather than electronically, and should result in superior common-mode subtraction and better shot-noise-limited performance. It is also a prerequisite for recycling the light.

i. *Preliminary development of recombination techniques in a stationary interferometer.* We have constructed a stationary interferometer (Figure VIII-2) and are using it for the development of recombination and recycling techniques without the additional complications of suspended components. This initial development should be completed by the beginning of the proposed grant period. Coordinated recombination and recycling development will then be transferred to suspended-mass interferometers in the 5-meter baseline vacuum system and the 40-meter prototype, where it will continue through the design freeze for the Mark I LIGO detector.

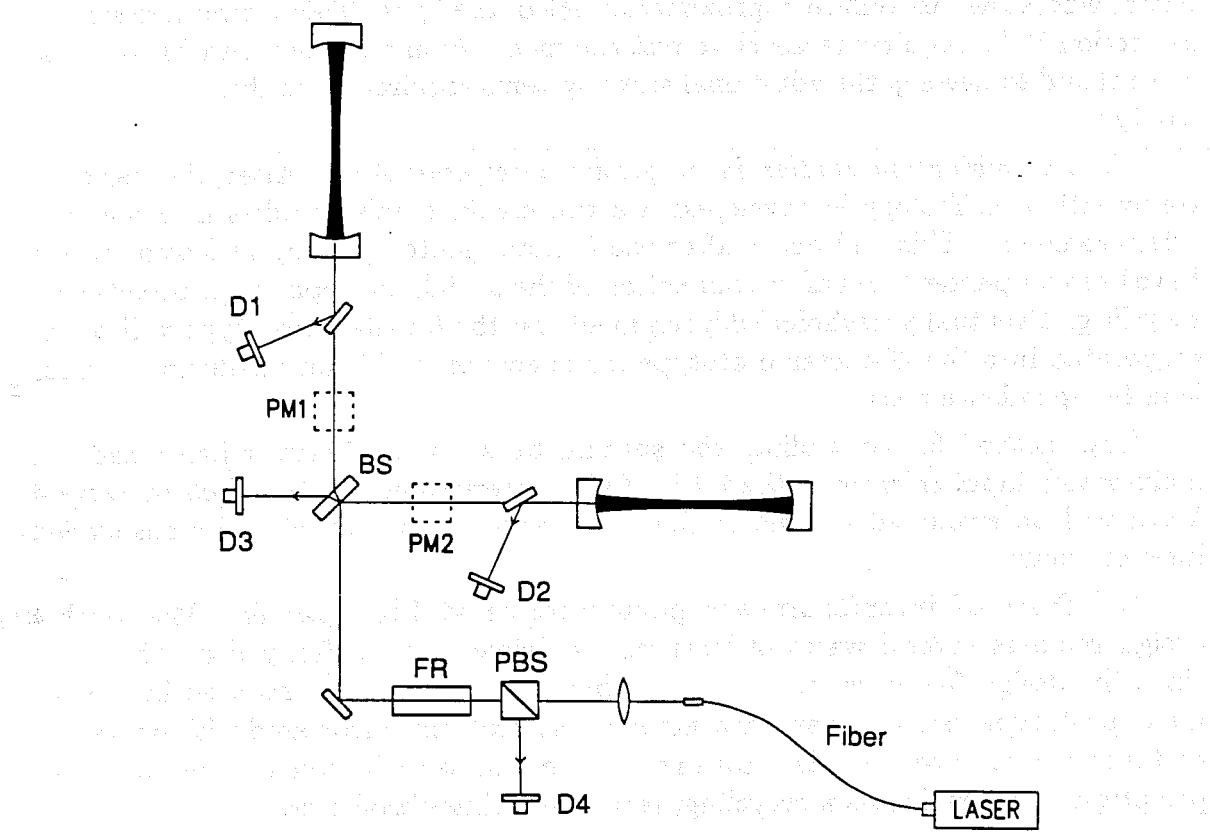


Figure VIII-2 Schematic diagram of stationary recombined interferometer. Photodetectors D1 and D2 monitor the Fabry-Perot cavities; D3 and D4 monitor the antisymmetric and symmetric outputs, respectively. PM1 and PM2 refer to modulation functions in the two arms of the interferometer. These functions are accomplished either by in-line Pockels cells, or by Pockels cells in a side-arm configuration. Other components include a beam splitter (BS), Faraday rotator (FR), polarizing beam splitter (PBS), and mode-matching optics.

The most straightforward recombination configuration entails placing electro-optic phase modulators in the main beams between the beam splitter and the cavity input mirrors. The modulators are used both to impress RF sidebands on the light

and for optical phase control to hold the dark fringe³ at the antisymmetric output. The Fabry Perot cavities are individually maintained on resonance by optical signals derived from pickoff plates and photodetectors in front of each cavity. This scheme is being tested in the stationary prototype as a preliminary step; its use in the initial LIGO interferometer with recycling would require development of higher power modulators because it places the electro-optic phase modulators in high-power beams.

We will next test the method proposed for the initial LIGO interferometer by placing the optical phase modulators in side arms outside of the main high-power beam, where they modulate approximately 1% of the light. This method, described in Section V.A., requires research to test the modulation efficiency and fringe phase control and to develop the additional servo systems required to control the side-arm cavity.

ii. Recombination studies in suspended interferometers. After the basic recombination technology is developed, we will conduct noise studies in suspended interferometers. This will occur after the 5-meter prototype's optical components have been suspended, and after completion of the initial development of broad-band recycling. Eventually, technical developments on the 5-meter prototype will be incorporated into the 40-meter prototype for operation at higher resolution and for length-dependence tests.

The method for controlling the spacing between the beam splitter and the main-cavity input mirrors in the initial LIGO interferometer, described in Section V.A., will be evaluated as part of the recombination studies with the suspended interferometer.

b. Tests of interferometer performance at high power. The Mark I design requires several watts of laser power delivered with fairly high efficiency. Until the design freeze, we will gradually increase the power levels used in the 40-meter prototype to uncover and characterize any problems associated with operation at these higher power levels. During this period, we will convert the 40-meter prototype to operation as a recycling, recombined interferometer.

The 40-meter prototype currently operates with much higher finesse than anticipated to be needed for the longer-baseline Mark I design. For some experimental tests, we intend to reduce the finesse of the 40-meter prototype to the value we will use in the Mark I interferometer. This will allow us to uncover problems that might be associated with high phase sensitivity, and are independent of displacement noise, or the effects of high circulating power in the cavities.

³ In LIGO designs, several electro-optic servo loops operate together to keep a large number of coupled and separate cavities in resonance. Throughout, sine-wave phase modulation is used to generate an error signal, and broad-band feedback is used to maintain the "dark-fringe" resonance—the condition where the detected signal at the modulation frequency is a minimum. The same type (and in some cases the identical unit) of electro-optic modulator serves both functions.

c. Development of broad-band recycling. Broad-band recycling is included in the Mark I design. We plan experimental work on recycling in the stationary interferometer this year. This effort will determine the number of recycles achievable in practice and how this limit is related to optical properties of materials inside the recycled interferometer. The electronics necessary to recycle a suspended interferometer will be developed on the 5-meter prototype and then transferred to the 40-meter prototype for final evaluation before the design freeze.

d. Development of the suspension-point interferometer. As mentioned in Section V.A., the Mark I design includes the option of a suspension-point interferometer to monitor and reduce the effect of vibrational perturbations (see Appendix C). We do not require this feature to function at the startup of operations, although it would be desirable. We intend to complete development work on the suspension-point interferometer at the 40-meter prototype before the design freeze.

2. Development of prototype subsystems for use in the LIGO

a. Development of position sensors and controllers. A substantial systems engineering task associated with the initial LIGO interferometer is the engineering design and fabrication of the optical position sensors and controllers that will be used on suspended optical components. The large number of these sensors and controllers required in LIGO interferometers sets requirements on the pumping capacity of the vacuum chambers, the number and type of vacuum feedthroughs, and the architecture of the data- and control-instrumentation system. Our effort will be directed toward small-scale mass production and the requirements of automated operation and control. During the proposal period, we will develop engineering specifications and a plan for the manufacture and testing of commercially produced position sensors, controllers, and associated electronics.

i. Sensors. The sensors used in damping and positioning servo loops in the initial interferometer need a position sensitivity of better than 10^{-9} cm/ $\sqrt{\text{Hz}}$ at frequencies between a fraction of a hertz and several hundred hertz, and a dynamic range of a few millimeters. The main-cavity mirrors impose the most stringent requirements on the sensors; requirements on other suspended components may be relaxed substantially.

Three types of sensors have been developed by LIGO scientists during the course of prototype research: a single-axis shadow detector, a reflective two-dimensional detector, and a fiber-optic interferometric detector. Each has properties particularly suited for a specific purpose.

ii. Controllers. Controllers apply forces to damp and position the suspended optical components. A magnetic controller,⁴ consisting of a permanent magnet mounted on the suspended object, and a stationary driving coil, is currently used in the 40-meter prototype. An electrostatic controller system is being developed for critical applications where the magnetic system might be a source of noise. Depending on its state of readiness at the time of the design freeze, the electrostatic controller may be used in the initial LIGO interferometer. It could be particularly useful in advanced detectors at lower frequencies.

b. Instrumentation system and automated operation. The prototypes have made use of computers for data acquisition and, in a more limited way, for interferometer control and monitoring. Both the 40-meter and 5-meter prototypes will be increasingly tied to computers, with the goal of developing single-console automated operation and data retrieval as planned for the initial LIGO interferometer. Instrumentation of the prototypes with state-of-the-art computers, instrumentation interfaces, and archival storage capability will become more important as the prototypes grow in complexity.

i. Control development. Although the plan for developing the control system is not yet well formulated, the steps required are clear. The early steps will be passive: monitoring, the display of instrument state, and archiving of operating parameters. Active computer control of interferometers will be introduced gradually. The low bandwidth control signals, such as the position and orientation of components in the optical train, the gain and filter properties of servo loops, and the compensation for drifts, will be automated. Procedures for fringe acquisition will be automated, and systems for automatic optimization of cavity mirror position and alignment will be introduced. The diagnostic tests and procedures used to optimize system performance, such as perturbations of beam position and angle and the introduction of AM and FM noise sidebands, will also come under computer control.

ii. Software development. Full utilization of the proposed monitoring and control system requires extensive software development. Basic software for data handling and communications can be purchased, whereas software to produce graphic representations of the instrument state must be custom designed. The software for analysis of instrument performance, such as cross-correlation studies of instrument parameters and transfer-function measurements, can be adapted from available, general computer "toolbox" programs for data analysis, statistics, and hypothesis testing.

3. Supporting R&D in special campus facilities

a. Optics research and development. The Optics Test Facility now being developed will be used throughout the proposed grant period to study special optics problems pertinent to the LIGO, but problems that do not require the full

⁴ A magnetic control system was developed first by the gravitational-wave research group at the MPQ, Garching, Germany, who kindly provided us with a sample of a coil and sensor of their system.

capabilities of a working prototype interferometer. This facility will support LIGO in several areas.

i. Research and development on mirrors and beam splitters. The initial LIGO interferometers will require mirrors and beam splitters of much larger aperture than those in the current prototypes. Early in the proposed grant period, we plan to acquire and test large-aperture optics for use in these interferometers. Our preliminary data on thermal distortion in fused-silica optics indicate that this material is suitable for LIGO interferometers operating with a few watts of injected power, i.e., at levels sufficient to perform significant gravitational-wave searches. In addition, fused-silica substrates and test masses of sufficient size can be produced with current technology.

Our current research effort in optics is focused on a systematic study of thermal distortion effects in Fabry-Perot cavities. As discussed in Appendix H, we have recently observed such effects in a variety of cavities and have developed a theoretical model consistent with preliminary observations. Our first goal is to refine this preliminary work. The thermal lensing model we are currently using has firm predictive power once the input data—thermal coefficient of refractive index, thermal expansion coefficient, thermal conductivity of substrate, and absorption coefficient of mirror coating and substrates—are known. These parameters are well known except those for absorption by the mirror coatings and substrates. We plan to measure the optical power absorbed by cavity mirrors and to correlate these data with the onset of thermal distortion effects.

Assuming the measurements confirm that the primary heating is due to absorption by the coatings, we plan to coordinate work with industry to produce mirror coatings that are less absorbing. A proven physical model will also help us to evaluate different substrate materials for advanced LIGO interferometers. Preliminary work indicates that high thermal conductivity and low thermal coefficients of expansion and refractive index change are achievable in improved substrates. Sapphire is one candidate material. We also intend to experiment with cavity geometries that are less susceptible to thermal distortion effects (see Appendix C). We expect that this work will continue throughout the period covered by this proposal.

ii. Preliminary investigations of interferometer noise mechanisms. The Optics Test Facility will be used to support investigations of noise mechanisms using the prototypes and for preliminary investigations of noise associated with optical parameters (e.g., phase noise induced by fluctuations in optical beam geometry). Methods to measure and reduce noise, including new monitors and electronic subsystems, will be developed in the test facility. These will then be added to the prototypes for further high-resolution studies.

iii. Evaluation and development of new lasers for LIGO. Development of new laser systems for LIGO will be done by outside groups in collaboration with LIGO personnel (see Section X). In addition to requiring high-power output and high efficiency, LIGO laser beams ideally are stable in amplitude, frequency and geometry.

The Optics Test Facility will provide the capability to measure intrinsic noise of new lasers and to develop any required stabilization techniques.

iv. Research and development related to scattering by optical components. The scattering of light by optical components degrades interferometer performance both by reducing the efficiency of light use, with a resulting poorer shot-noise limit per watt of input light, and by subsequent interference of the scattered light with the main optical beams. The Optics Test Facility will be used to evaluate scattering from optical components and to coordinate the development of low-scatter optics. In addition, we plan extensive theoretical simulation of noise contributed from scattered light in the LIGO, using test data as input.

v. Optical component testing and quality assurance. We will develop programs to test and evaluate the many optical components required for LIGO interferometers. A first task will be to set technical specifications and identify suppliers for the components of initial LIGO interferometers. We anticipate that most of the components will be stock items provided by the optics industry, but these must be certified to be reliable for long-term use under vacuum at LIGO power levels. For other components, in particular electro-optic modulators, Faraday isolators, and single-mode optical fibers, we may find it advantageous to support industrial development of components optimized for the LIGO. We will also establish routine quality assurance procedures for newly acquired optics and routine screening tests for components in use.

b. Vibration isolation and thermal noise studies. The Vibration and Thermal Noise Test Facility will be used throughout the proposed grant period for tests of vibration-isolation stacks and suspensions for optical components. We anticipate that initial characterization and modeling of key concepts for the isolation system design will be completed before the beginning of the proposed grant period. More detailed testing will be pursued during the detailed interferometer design. This will entail construction of a working model of the candidate vibration-isolation stack for measurements of transfer function, drift, and cross-coupling between different degrees of freedom.

We have begun studies of the intrinsic damping and low-loss clamping techniques for candidate materials used in the pendulum suspension of LIGO test masses. We plan to investigate fundamental dissipation mechanisms and to determine the materials, processing methods, and geometries that are likely to result in the lowest thermal noise. Basic research in this area should enhance future LIGO capabilities to observe gravitational-wave sources at low frequencies (see Section V.B.).

4. Science design and planning

A significant effort in science planning and design will continue throughout the proposed grant period. Major efforts will be devoted to:

- Analysis and modeling in support of the engineering design of facilities and

interferometers.

- Analytic studies of the scaling of the interferometer optical and servo systems from 40 m to 4 km.
- Scientific strategy and systems engineering for control of beam position and orientation and fringe acquisition.
- Development of data-analysis strategies.
- Support of LIGO interferometer fabrication and testing.
- Coordination of collaborative R&D programs with outside groups.

5. R&D activity after the initial interferometer design effort

During CYs 1993 and 1994, activity will shift toward interferometer fabrication, subsystem testing, and installation of an interferometer at Site 1. At the same time, we intend to maintain research activity on the campuses. Part of this effort will be devoted to solving unforeseen technical problems and developing and testing subsystems for the initial interferometers. Another part will be development of the more advanced interferometers. We will also maintain a core effort of basic research directed at laying the foundation for improvements in future interferometer systems. This effort will be crucial to the evolution of future LIGO detectors, discussed in Section V.B.

6. Improvements to campus facilities

The 40-meter prototype currently operates in its original (with slight modifications) vacuum system. As this system will not be adequate to support LIGO operations, the vacuum envelope will be rebuilt with larger vacuum chambers and beam tubes.

The recently completed 5-meter vacuum system has a sufficiently large envelope for LIGO support, and we plan no extensive renovation of this facility during the proposed grant period. We will install a new laser system to upgrade the 5-meter prototype to high-power operation.

We will upgrade the instrumentation of both campus facilities to improve their capability for LIGO support. The new instrumentation will enhance the efficiency of prototype operations and expand our capability to test LIGO components.

IX. ORGANIZATION AND MANAGEMENT

The LIGO project is an integrated, collaborative effort between scientists at the California Institute of Technology (Caltech) and the Massachusetts Institute of Technology (MIT). The proposed organization of the project throughout the construction phase of the LIGO is shown in Figure IX-1. It differs from the existing organization in the provision for an external design review board, which will be constituted upon NSF approval of this proposal, and in the designation of an Assistant Director, who will take on tasks and responsibilities as delegated by the Director.

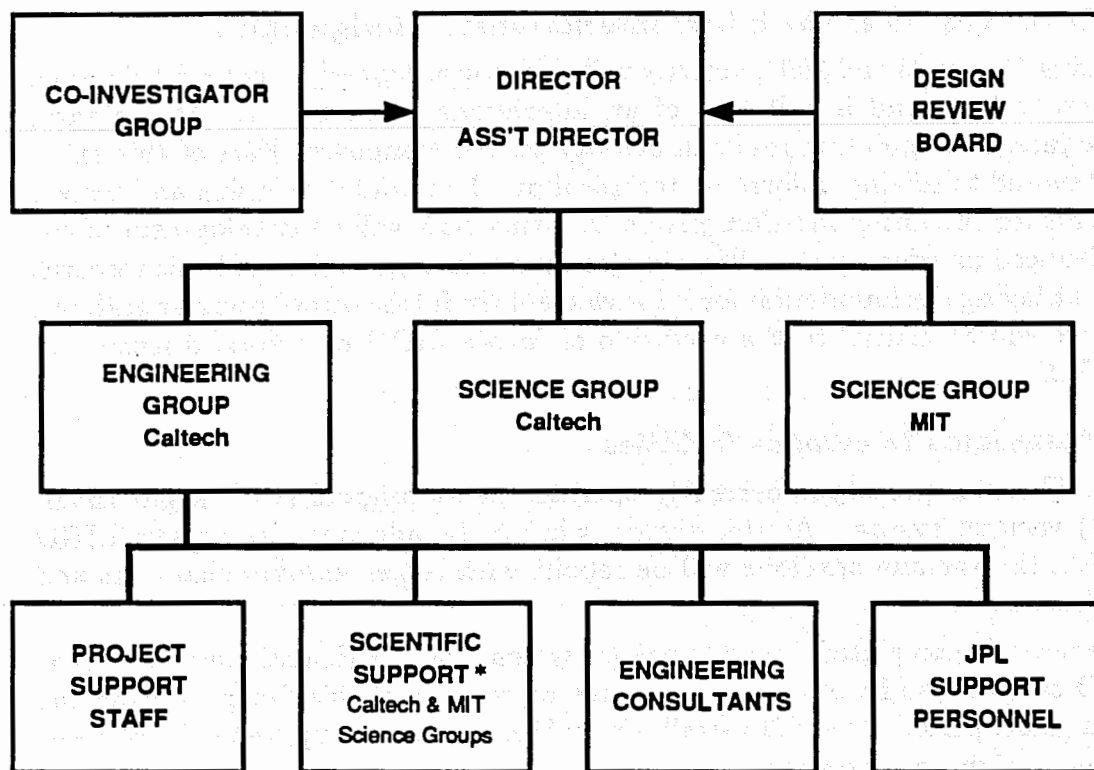


Figure IX-1 Organization and management of the LIGO project. (*Members of the science groups serve in two capacities: (1) the conduct of research and development, and (2) the support of engineering tasks.)

The Project Director and Principal Investigator has overall responsibility for all aspects of the LIGO Project. He reports administratively to the Provost of Caltech. His administrative contacts at MIT are the Chairman of the Department of Physics and the Director of the Center for Space Research.¹ Caltech serves as the prime contractor for the LIGO Project with the National Science Foundation

¹ See Appendix K, Memorandum of Understanding on the LIGO Project between Caltech and MIT.

(NSF); the activities of the MIT science group are supported under a subcontract from Caltech to MIT. The LIGO activities at MIT are coordinated by one of the Co-Investigators, Professor R. Weiss. The Project Director, Professor R. Vogt, and the other three Co-Investigators, Professors Drever, Raab, and Thorne, are resident at Caltech.

During the proposed construction phase, the science group will conduct interferometer research and development, provide science support to the engineering group, participate in the design, construction, installation, and operation of the LIGO interferometers, and conduct data analysis. The project's science staff includes, in addition to the Co-Investigators, eight scientists, six graduate students, and a varying number of undergraduates. We plan to strengthen the present science staff by about four physicists. We also expect to add another professorial faculty member (at MIT) in the near future. The number of graduate students on the project is expected to increase to about a dozen. The scientists will accomplish their work in task groups, whose leaders report to the director. Professor Thorne, a theoretical physicist/astrophysicist, and selected members of his research group² will provide analytical support to the project, as needed.

The engineering group is headed by a Chief Engineer, W. Althouse, who reports to the director. Its membership will increase from the current 12 to about 20 engineers, programmers, technicians, and programmatic support staff,³ counting personnel resident at both Caltech and MIT. During the construction phase, the engineering group, with close support from the science groups, will be responsible for overseeing the detailed engineering design and construction of the LIGO facilities. It also will implement the design and construction of interferometers and support equipment. The project will continue to take advantage, as needed, of engineering support from Caltech's Jet Propulsion Laboratory (JPL).

² The theoretical astrophysics activities are supported under separate grants.

³ Additional details on the engineering organization are provided in Volume 2, Section VI.B.

X. INTERNATIONAL AND DOMESTIC COLLABORATION

A. International

This proposal asks for construction in the United States of a two-site observatory, the minimum facility required for gravitational-wave event verification, diagnostics, and detector development (See Section VII). The LIGO, as proposed, cannot by itself extract the complete waveform information contained in a gravitational-wave burst. We will rely for full information upon an international network of observatories, to be established in a collaborative arrangement with scientists in Europe, Australia, and Japan.¹ At the present, there are serious proposals pending to establish two multi-kilometer-size observatory sites in Europe (British-German and French-Italian collaborations) and one in Australia. Participation of the United States LIGO in an international network will save the United States the construction costs for the third and fourth sites and assure an observing network with higher spatial resolution. Experience of radio astronomers with the VLBI (Very Long Baseline Interferometry) network has shown that such an undertaking can be executed successfully and at the same time provides information on how such a collaboration could be further improved.

A collaboration of the European and United States teams was officially initiated in Paris at a February 1989 meeting, convened by the NSF and attended by representatives of all European and United States gravitational-wave groups and their funding agencies. A number of working groups² has been established for efficient exchange of information on research topics of common interest.

B. Domestic

United States collaboration will be tightly focused and coordinated. Before and during the LIGO construction phase, collaborations will concentrate mainly upon the development of LIGO subsystems, such as lasers (Professor Byer, Stanford University; see Appendix K) and vibration isolation platforms (Professors Bender and Faller, University of Colorado at Boulder; see Appendix K). We expect that after the NSF makes a visible commitment to the construction of LIGO, other United States experimenters will want to establish collaborative arrangements with the

¹ As discussed in Sections II and V.C, the full information carried by a gravitational wave consists of the direction (θ, ϕ) to its source and its two waveforms $h_+(t)$ and $h_\times(t)$. For gravitational-wave bursts, extraction of their full information requires a minimum of three widely separated interferometers operating in coincidence. For better position resolution and waveform accuracy, especially for sources that lie in the plane defined by the three interferometers, it is important to have a minimum of four interferometers, distributed over the Earth so that they form a tetrahedron with large volume.

² Working group topics include Data Analysis, Data Acquisition, Lasers, Vibration Isolation, Mirrors, Vacuum, and Control Systems.

LIGO project on scientific and technical topics. We intend to maintain an effective interchange with the interested national community through publications, seminars, workshops, and visiting scientists; by the time LIGO becomes a fully operational facility, there will be considerable depth in the United States scientific community for participation in the observational and technical development program. During the LIGO operational phase, scientists from other than Caltech or MIT are expected to become users of LIGO both by (1) installing, cooperatively or independently, detector systems in the LIGO facilities and (2) engaging in the analysis of data derived from the Caltech/MIT "gravitational-wave watch" detectors.

We expect that a number of graduate students and postdoctoral fellows, who will be trained by the LIGO project, will enter the national scientific community to become LIGO outside users.

The LIGO project will provide opportunities for scientific collaboration between the scientific and engineering communities, and it is anticipated that the LIGO project will stimulate interest in gravitational wave research among the scientific community.

The LIGO project will provide opportunities for scientific collaboration between the scientific and engineering communities, and it is anticipated that the LIGO project will stimulate interest in gravitational wave research among the scientific community.

The LIGO project will provide opportunities for scientific collaboration between the scientific and engineering communities, and it is anticipated that the LIGO project will stimulate interest in gravitational wave research among the scientific community.

The LIGO project will provide opportunities for scientific collaboration between the scientific and engineering communities, and it is anticipated that the LIGO project will stimulate interest in gravitational wave research among the scientific community.

The LIGO project will provide opportunities for scientific collaboration between the scientific and engineering communities, and it is anticipated that the LIGO project will stimulate interest in gravitational wave research among the scientific community.

The LIGO project will provide opportunities for scientific collaboration between the scientific and engineering communities, and it is anticipated that the LIGO project will stimulate interest in gravitational wave research among the scientific community.

The LIGO project will provide opportunities for scientific collaboration between the scientific and engineering communities, and it is anticipated that the LIGO project will stimulate interest in gravitational wave research among the scientific community.

The LIGO project will provide opportunities for scientific collaboration between the scientific and engineering communities, and it is anticipated that the LIGO project will stimulate interest in gravitational wave research among the scientific community.

The LIGO project will provide opportunities for scientific collaboration between the scientific and engineering communities, and it is anticipated that the LIGO project will stimulate interest in gravitational wave research among the scientific community.

XI. REFERENCES

- I-1. C. M. Will, *Theory and Experiment in Gravitational Physics*, (Cambridge Univ. Press, Cambridge, 1981), chapt. 10.
- III-1. A. Rüdiger, R. Schilling, L. Schnupp, W. Winkler, H. Billing and K. Maischberger, *Optica Acta* **28**, 641, (1981).
- III-2. R.W.P. Drever, J. L. Hall, F. V. Kowalski, J. Hough, G. M. Ford, A. J. Munley, and H. Ward, *Appl. Phys.* **B31**, 97, (1983).
- V-1. R.W.P. Drever, "Interferometric Detectors for Gravitational Radiation," *Gravitational Radiation*, NATO Advanced Physics Institute, Les Houches, ed. N. Deruelle and T. Piran, (North Holland Publishing, 1983), 321.
- V-2. C. Man, A. Brillet, D. Shoemaker, "Ultra-high sensitivity interferometric techniques for the detection of gravitational waves," International Quantum Electronics Conference, Tokyo, July 1988.
- V-3. K. Maischberger, A. Rüdiger, R. Schilling, L. Schnupp, W. Winkler, and G. Leuchs, "Status of the Garching 30 meter prototype for a large gravitational wave detector," in *Experimental Gravitational Physics*, P. F. Michelson, H. En-ke, and G. Pizzella, eds., (World Scientific Publ., Singapore, 1988), p. 52.
- V-4. D. Shoemaker, R. Schilling, L. Schnupp, W. Winkler, K. Maischberger, *Phys. Rev.* **D38**, 423, (1988).
- V-5. W. Martin, "Experiments and Techniques for the Detection of Gravitational and Pulsed Electromagnetic Radiation from Astrophysical Sources," Ph.D. Thesis, University of Glasgow, 1978.
- V-6. C. M. Caves, *Phys. Rev.* **D23**, 1693, (1981).
- V-7. H. P. Yuen, *Phys. Rev.* **A13**, p. 2226, (1976).
- V-8. J. Gea-Banacloche, G. Leuchs, *J. Modern Opt.*, **34**, 793 (1987).
- V-9. C. A. Cantley, N. A. Robertson, and J. Hough, "A Suspension System for Use in a Laser Interferometric Gravitational Wave Detector," contributed talk, 12th Int. Conf. on Gen. Rel. and Grav., Boulder, (2-8 July 1989).
- V-10. R. Del Fabbro, A. di Virgilio, A. Giazotto, H. Kautzky, V. Montelatici, and D. Passuello, *Phys. Lett.* **A124**, 253, (1987).
- V-11. J. Kovalik, P. Saulson, M. Stephens, "The Performance of a Double Pendulum Vibration Isolation System," contributed talk, 12th Int. Conf. on Gen. Rel. and Grav., Boulder, (2-8 July 1989).
- V-12. R. Del Fabbro, A. di Virgilio, A. Giazotto, H. Kautzky, V. Montelatici, D. Passuello, *Phys. Lett.* **A132**, 237, (1988) and *Phys. Lett.* **A133**, 471, (1988).
- V-13. J. E. Faller, R. L. Rinker, *NBS Dimensions*, **63**, 25, (1979).
- V-14. N. A. Robertson, R.W.P. Drever, I. Kerr, and J. Hough, *J. Phys. E. Sci. Instr.* **15**, 1101, (1982).
- V-15. P. R. Saulson, *Rev. Sci. Instr.*, **55**, 1315, (1984).

- V-16. A. Giazotto, D. Passuello, A. Stefanini, *Rev. Sci. Inst.* **57**, 1145, (1986).
- V-17. R. T. Stebbins, P. L. Bender, J. E. Faller, D. B. Newell, and C. C. Speake, "A 1-to-10 Hz Prototype Isolation System for Gravitational Wave Interferometers and Thermal Noise Measurements," contributed talk, 12th Int. Conf. on Gen. Rel. and Grav., Boulder, (2-8 July 1989).
- V-18. J. Hough, J. R. Pugh, R. Bland, R.W.P. Drever, *Nature* **254**, 498, (1975).
- V-19. B. Schutz and M. Tinto, *Monthly Notices of the Royal Astronomical Society*, **224**, 131, (1987).
- V-20. Y. Gürsel and M. Tinto, "A Near Optimal Solution to the Inverse Problem for Gravitational Wave Bursts," *LIGO preprint 89-1*, accepted for publication in *Phys. Rev. D*.
- V-21. B. F. Schutz, "Sources of Gravitational Radiation," in *Gravitational Wave Data Analysis*, B. F. Schutz, ed., (Kluwer Academic, 1989), p. 3.
- VII-1. J. Livas, "Broadband Search Techniques for Periodic Sources of Gravitational Radiation," in *Gravitational Wave Data Analysis*, B. F. Schutz, ed., (Kluwer Academic, 1989), p. 217.
- VIII-1. R. Weiss, *Quartr. Progr. Rep. Res. Lab. Electr. MIT*, **105**, 54, (1972).
- VIII-2. J. Livas, R. Benford, D. Dewey, A. Jeffries, P. Lindsay, P. Saulson, D. Shoemaker, R. Weiss, "The M.I.T. Prototype Gravitational Wave Detector," in *Proc. Fourth Marcel Grossman Mtg. on Gen. Rel.*, R. Ruffini, ed. (Elsevier Science Publishers, 1986) p. 591, (1985).
- VIII-3. P. S. Lindsay, D. H. Shoemaker, *Rev. Sci. Instr.* **53**, 1014, (1982).
- VIII-4. R.W.P. Drever, G. M. Ford, J. Hough, I. M. Kerr, A. J. Munley, J. R. Pugh, N. A. Robertson, and H. Ward, "A Gravity-Wave Detector Using Optical Sensing," in *Proceedings of the Ninth International Conference on General Relativity and Gravitation* (Jena 1980), ed. E. Schmutz (VEB Deutscher Verlag der Wissenschaften, Berlin, 1983), 265.
- VIII-5. R.W.P. Drever, J. Hough, A. J. Munley, S.-A. Lee, R. Spero, S. E. Whitcomb, J. Pugh, G. Newton, B. Meers, E. Brooks III, Y. Gürsel, "Gravitational-Wave Detectors Using Laser-Interferometers and Optical Cavities," in *Quantum Optics, Experimental Gravity, and Measurement Theory* ed. P Meystere and M.O. Scully, (Plenum Publishing, 1983), 503.
- VIII-6. S. Whitcomb, D. Z. Anderson, R.W.P. Drever, Y. Gürsel, M. Hereld, R. Spero, "Laser-Interferometer Experiments at Caltech," in *Proc. Third Marcel Grossman Mtg. on Gen. Rel.*, Hu Ning, ed., (Science Press and North-Holland Publishing Co., 1983), p. 1399.
- VIII-7. K. S. Thorne, "Gravitational radiation," in *300 Years of Gravitation*, S. W. Hawking and W. Israel, eds., (Cambridge Univ. Press, Cambridge, 1987), p. 330.

XII. SCHEDULE AND BUDGET

This section presents an overview of the LIGO Project schedule and costs. Details may be found in Volume 2, Section VI and Section VII.

A summary project schedule is shown in Figure XII-1. The design and construction activities span the 4-year interval covered by this proposal. Engineering design of the LIGO facilities will proceed upon the availability of funds, estimated to be at the beginning of calendar year 1991. The engineering design is estimated to take 18 months. Procurement of some long-lead items will be initiated during this period. Construction at the first site, which may commence after completion of the first year of the design activity, is estimated to take about two years. Construction at the second site, also estimated to take about two years, starts one year after the start of construction at Site 1 to allow use of the same contractors at both sites and take maximum advantage of the experience gained at Site 1. At the end of the proposed 4-year period, construction at both sites will be completed, the first Mark I interferometer will be installed, and we should be ready to begin operations at Site 1. Operations at Site 2 will start 1 year later after completing checkout and acceptance testing of the Site 2 facilities and installation of a Mark I interferometer there.

LIGO PROJECT SCHEDULE

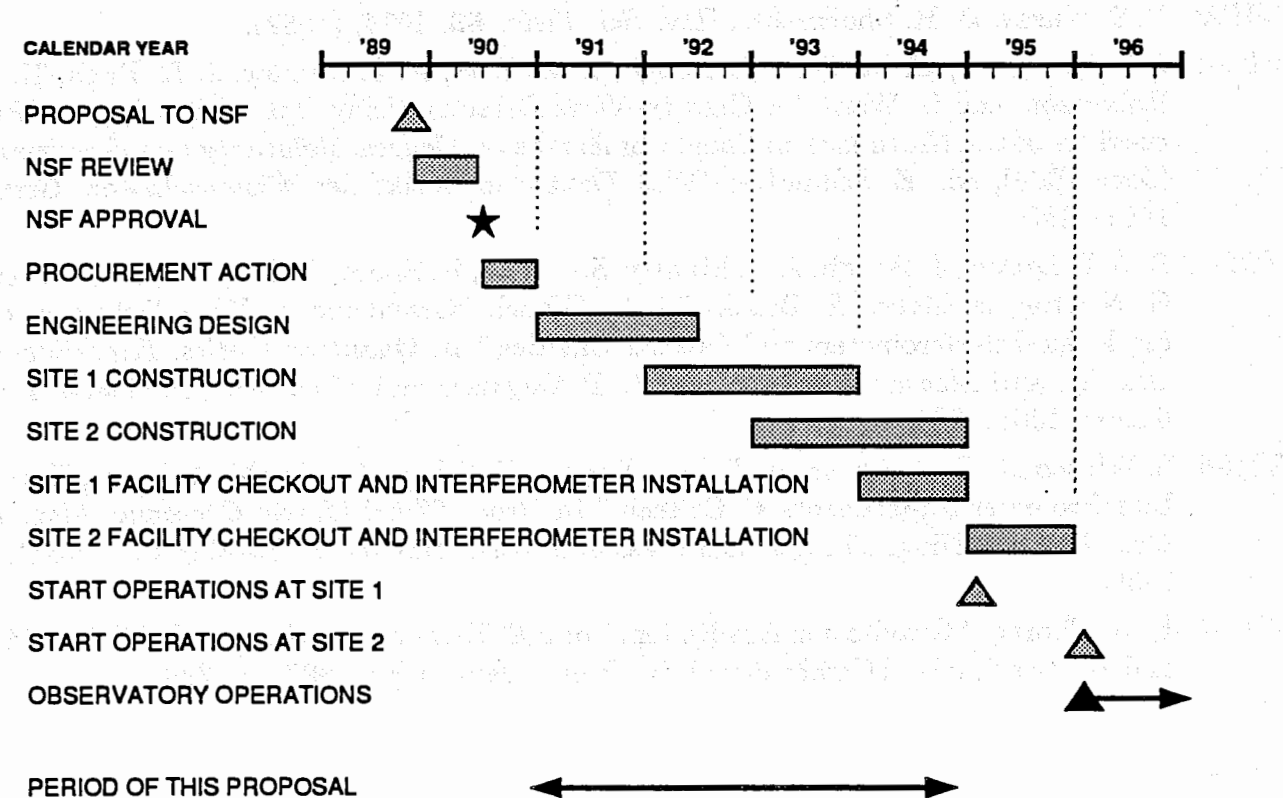


Figure XII-1 LIGO project schedule.

The total estimated cost of the LIGO Project during the construction phase is summarized in Table XII-1. The research and development item covers the estimated cost of LIGO team salaries, supplies, expenses, and equipment required to support the effort described in Section VIII.B. The amount for "LIGO Design and Construction" covers the total estimated cost of the LIGO facilities and initial interferometers, including in-house scientific, engineering, and management support of the construction project. "Remote Site Operations" covers the cost of on-site manpower, facility, and equipment maintenance, and utilities costs for the first site, the operation of which will commence in the fourth year of the proposed construction period. All costs are given in 1989 dollars. An inflation allowance, computed at a rate of 5% per year, is separately computed and added to the annual 1989 amounts shown. The total amount requested is \$193.8 million in FY'89 dollars.

**TABLE XII-1
LIGO PROJECT—TOTAL COST SUMMARY
FY89 \$M**

	1991	1992	1993	1994	TOTAL	Note:
Research and Development	3.0	3.0	3.0	3.0	12.0	1
LIGO Design and Construction	44.6	49.4	48.1	37.7	179.8	2
Remote Site Operations				2.0	2.0	3
TOTAL ESTIMATED COST, FY89 \$M	47.6	52.4	51.1	42.7	193.8	
Inflation allowance @ 5%/yr, FY89 base	4.9	8.3	11.0	11.8	36.0	
TOTAL ESTIMATED COST, ESCALATED \$M	52.5	60.7	62.1	54.5	229.8	

Note 1: Caltech/MIT on-campus research and development effort

Note 2: Total cost of remote LIGO installations including initial interferometers, excluding ~\$7.0M in local sales taxes pending decision on ownership of LIGO facilities (government or private)

Note 3: LIGO remote site operations cost for first year, Site 1

RESPONSE TO NSF NOTICE NO. 107

A. Education and Development of Human Resources

Interferometric gravitational-wave detection is a unique, developing discipline that does not yet fit the patterns of established research in physics and astrophysics. It provides training for scientists, primarily undergraduate and graduate students, in experimental skills associated with the design, construction and operation of sophisticated and precise electronic, optical, and mechanical systems. Scientists trained in this field acquire a deep understanding of experimental techniques that span several fields—an opportunity now rare in much of physics. These scientists often become consummate experimental physicists, employed by industry, government laboratories, and university research groups.

The *academic* career path for scientists in this discipline has been difficult and will continue to be so until the LIGO comes to fruition. The technically intensive nature of this work in its early stages does not match the criteria established for university hiring and promotions. Typically, physics faculties must gamble that gravitational-wave astronomy will become "scientifically" productive on a reasonable time scale. Other fields in physics, such as high-energy physics and space research, also have long-term technical phases, but these are established fields with virtually guaranteed scientific results. They also have a substantial network of laboratories and research centers that permit an academic researcher the mobility to remain in the field. The LIGO Project is obliged to recognize these facts in the recruitment and employment of tenure-track faculty and postdoctoral associates.

During the design and construction phase, research will be even more technically intensive than it is now. The major part of the effort will be focused on bringing the facilities and first interferometers into operation. This will require professional scientists, graduate students, and undergraduates working with engineers. The opportunities for training scientists in the LIGO Project will improve as the project proceeds. There will be a role for postdoctoral scientists willing to assume such technical research and development as interferometer subsystem development, analysis and testing, and development of software for data analysis. These efforts, however, will most likely not result in many scientific publications, and the project will employ the majority of additional scientists in longer-term staff positions.

Once the LIGO is operating, the opportunities for junior scientists will change dramatically. Many of the scientists who have worked through the design and construction phase then become the leaders of a new field. The expectation is that the initial observations will be scientifically important and publishable, even if only to set significant upper limits to the gravitational-wave flux. The data will be analyzed in many ways and in different types of independent investigations, limited only by the creativity of the individuals working with it. There will be continuing opportunities for students and junior scientists with technical interests

in the development of advanced interferometers. They will have the opportunity to work in a setting that is closer to "small science" than "big science."

In the observation phase, the LIGO will offer opportunities for training and development of junior experimental scientists in the disciplinary styles of physics (the development of sophisticated, fundamental measurement techniques and technologies) and astronomy (astrophysical observation, analysis, and modeling).¹

Once the LIGO exists, any investigation will break new ground in terms of astrophysical sensitivity. It is very likely that other universities will then become involved and the academic opportunities for young scientists in this field will expand. The style of gravitational-wave research will then resemble that of other productive areas in physics and astrophysics.

In summary, we foresee a gradual evolution in the training and development pattern of scientists as the LIGO progresses. During the construction phase, there will be opportunities for undergraduates to get their first exposure to research, or for graduate students to do thesis work. Junior scientists will have only limited opportunities to establish credentials; their careers will be better served by longer term scientific staff appointments than by short-term postdoctoral appointments. Beginning with the observation phase, opportunities for undergraduates, graduate students, and postdoctoral trainees will become abundant.

B. P. I.: Biography

(See Key Personnel: Vitae)

C. P. I.: List of (5) Publications Relevant to Proposed Research

None (P.I. took on duties of director of LIGO Project in Fall 1987).

D. P. I.: List of (5) Other Publications

"Electrons in the Primary Cosmic Radiation," (with P. Meyer), *Phys. Rev. Letters*, **6**, 193 (1961).

"The Isotopic Composition of Solar Flare Accelerated Neon," (with R. A. Mewaldt, J. D. Spalding, and E. C. Stone), *Ap. J. (Letters)*, **231**, L97 (1979).

"Voyager 1: Energetic Ions and Electrons in the Jovian Magnetosphere," (with W. R. Cook, A. C. Cummings, T. L. Garrard, N. Gehrels, E. C. Stone, J. H. Trainor, A. W. Schardt, T. Conlon, N. Lal, and F. B. McDonald), *Science*, **204**, 1003 (1979).

"Energetic Charged Particles in Saturn's Magnetosphere: Voyager 1 Results," (with D. L. Chenette, A. C. Cummings, T. L. Garrard, E. C. Stone, A. W. Schardt, J. H. Trainor, N. Lal, and F. B. McDonald), *Science*, **212**, 231 (1981).

¹ The LIGO will also offer, during both the development and operations phases, opportunities for applied research, including control systems and computation.

"Elemental Composition of Solar Energetic Particles," (with W. R. Cook and E. C. Stone), *Ap. J.*, **279**, 827 (1984).

E. P. I.: Names of Graduate Students and Postdoctoral Scholars Sponsored During Past Five Years

None (P.I. has held administrative and science management positions since 1975).

F. P. I.: Total Number of Graduate Students Advised and Postdoctoral Scholars Sponsored

Advisor or co-advisor to 21 Ph.D students

Sponsor or co-sponsor of ~ 12 postdoctoral scholars

G. P. I.: Collaborators or Associates During Past 48 Months

Members of LIGO team, including

Prof. R. Drever, Caltech

Prof. F. Raab, Caltech

Prof. K. Thorne, Caltech

Prof. R. Weiss, MIT

Collaborators:

Prof. P. Bender, JILA, Boulder

Prof. J. Faller, JILA, Boulder

Prof. R. Byer, Stanford University

H. P. I.: Graduate Advisors

Prof. P. Meyer, University of Chicago

Prof. J. Simpson, University of Chicago

KEY PERSONNEL: VITAE

Dr. John C. H. Smith, Ph.D., is a Research Professor at the University of Texas at Austin. He has been a member of the faculty at the University of Texas since 1965. Dr. Smith's research interests include the development of methods for the analysis of organic compounds by mass spectrometry, the use of mass spectrometry for the identification of organic compounds, and the use of mass spectrometry for the determination of the chemical structures of organic compounds. Dr. Smith has published numerous papers in the field of mass spectrometry and has given many lectures on the subject. He is a member of the American Society for Mass Spectrometry and the International Society for Mass Spectrometry.

Dr. John C. H. Smith, Ph.D., is a Research Professor at the University of Texas at Austin. He has been a member of the faculty at the University of Texas since 1965. Dr. Smith's research interests include the development of methods for the analysis of organic compounds by mass spectrometry, the use of mass spectrometry for the identification of organic compounds, and the use of mass spectrometry for the determination of the chemical structures of organic compounds. Dr. Smith has published numerous papers in the field of mass spectrometry and has given many lectures on the subject. He is a member of the American Society for Mass Spectrometry and the International Society for Mass Spectrometry.

KEY PERSONNEL: PUBLICATIONS

Key personnel publications are listed below. Publications are listed by author(s) and date of publication.

1. **1985**
- D. E. Lamb, "The LIGO Project: A Laser Interferometer Gravitational Wave Observatory," in *Laser Interferometers for Gravitational-Wave Detection*, ed. R. Drever et al., Plenum Press, New York, 1985, pp. 33-45.

- D. E. Lamb, "LIGO: A Laser Interferometer Gravitational-Wave Observatory," in *Gravitational-Wave Detectors*, ed. R. Drever et al., Plenum Press, New York, 1985, pp. 33-45.

This section contains a listing of publications by key LIGO personnel (see VITAE) (ordered alphabetically).

William E. Althouse

Publications

1. "A Solar and Galactic Cosmic Ray Satellite Experiment", (with E. C. Stone, R. E. Vogt, and T. H. Harrington), *IEEE Trans. on Nuclear Science*, NS-15, 229 (1968).
2. "A Cosmic Ray Isotope Spectrometer", (with A. C. Cummings, T. L. Garrard, R. A. Mewaldt, E. C. Stone, and R. E. Vogt), *IEEE Trans. on Geoscience Electronics*, GE-16, 204 (1978).
3. "The Voyager Cosmic Ray Experiment", (with D. E. Stilwell, W. D. Davis, R. M. Joyce, F. B. McDonald, J. H. Trainor, A. C. Cummings, T. L. Garrard, E. C. Stone, and R. E. Vogt), *IEEE Trans. on Nuclear Science*, NS-26, 513 (1979).
4. "A Balloon-Borne Imaging Gamma-Ray Telescope", (with W. R. Cook, A. C. Cummings, M. H. Finger, T. A. Prince, S. M. Schindler, C. H. Starr, and E. C. Stone), *Conf. Papers*, 19th International Cosmic Ray Conference, La Jolla, CA, 3, 299 (1985).
5. "Balloon-Borne Video Cassette Recorders for Digital Data Storage", (with W. R. Cook), *ibid*, 3, 395 (1985).
6. "First Flight of a New Balloon-Borne Gamma-Ray Imaging Telescope", (with W. R. Cook, A. C. Cummings, M. H. Finger, D. M. Palmer, T. A. Prince, S. M. Schindler, C. H. Starr, and E. C. Stone), *Conf. Papers*, 20th International Cosmic Ray Conference, Moscow, USSR, 1, 84 (1987).

Ronald W.P. Drever
Publications

1. "K-Capture in the Decay of Chlorine-36", (with A. Moljk), *Phil. Mag. (7th Series)*, **46**, 1336 (1955).
2. "Neutron Activation Applied to Potassium-Mineral Dating", (with A. Moljk and S. C. Curran), *Rev. Sci. Inst.*, **26**, 1034 (1955).
3. "Measurement of Tritium as Water Vapour", (with A. Moljk), *Rev. Sci. Inst.*, **27**, 650 (1956).
4. "Ratio of K-Capture to Positron Emission in Flourine-18", (with A. Moljk and S. C. Curran), *Nucl. Inst. and Meth.*, **1**, 41 (1957).
5. "L/K Capture Ratio of Germanium-71", (with A. Moljk), *Phil. Mag. (8th Series)*, **2**, 427 (1957).
6. "Proportional Counters for Demonstration Experiments", (with A. Moljk), *Amer. J. Phys.*, **25**, 165 (1957).
7. "The Background of Counters and Radiocarbon Dating", (with A. Moljk and S. C. Curran), *Proc. Roy. Soc.*, **A239**, 433 (1957).
8. "Studies of Orbital Electron Capture Using Proportional Counters", Ph.D. Thesis, University of Glasgow (1958).
9. "Proportional Counters for Low Activity Measurements", (with A. Moljk and S. C. Curran), (*Proceedings of the 1st UNESCO International Conference, Paris, 1957*), *Radioisotopes in Scientific Research*, **II**, 596 (1958).
10. "Upper Limit to Anisotropy of Inertial Mass", *Phil. Mag. (8th Series)*, **5**, 409 (1960).
11. "A Search for Anisotropy of Inertial Mass Using a Free Precession Technique", *Phil. Mag. (8th Series)*, **6**, 683 (1961).
12. "Effect of Hydrostatic Compression on the 14.4 keV Gamma Ray from Iron-57", (with R. V. Pound and G. B. Benedek), *Phys. Rev. Lett.*, **7**, 405 (1961).
13. "The L/K Capture Ratio of Argon-37", (with P. W. Dougan and K.W.D. Ledingham), *Phil. Mag. (8th Series)*, **7**, 475 (1962).
14. "The Decay of Chlorine-36 to Sulphur-36", (with P. W. Dougan and K.W.D. Ledingham), *Phil. Mag. (8th Series)*, **7**, 1223 (1962).
15. "The Ratio of K-Capture to Positron Emission in the Decay of Nitrogen-13", (with K.W.D. Ledingham and J. A. Payne), *Proceedings of the International Conference on Role of Atomic Electrons in Nuclear Transformations*, Warsaw, 1963, ed. D. Berenyi, **II**, 359 (1956).

16. "Search for High Energy Gamma-Rays from Pulsar CP 1133", (with W. N. Charman, J. V. Jelley, P. R. Orman and B. McBreen), *Nature*, **220**, 565 (1968).
17. "A Technique for Removing Pile-Up Distortion in High Precision Pulse Height Spectroscopy", (with M.D.C. Williams), *Proceedings of the International Symposium on Nuclear Electronics*, Versailles (1968).
18. "Further Search for High Energy Gamma-Rays from CP 1133", (with W. N. Charman), *Nature*, **224**, 567 (1969).
19. "A Search for Periodic High Energy Gamma-Rays from Pulsars", (with W. N. Charman and J. V. Jelley), *Proceedings of the 11th International Conference on Cosmic Rays*, Budapest, 1969; *Act Phys. Acad. Sci. Hungary*, **29**, Suppl. 1, 63 (1970).
20. "The Ratio of K-Capture to Positron Emission in the Decay of Carbon-11", (with J. L. Campbell, W. Leiper and K.W.D. Ledingham), *Nucl. Phys.*, **A96**, 279 (1967).
21. "Upper-Air Fluorescence as a Tool in X-Ray Astronomy and Searches for X-Rays from CP 0532 and Other Pulsars", (with W. N. Charman, J. H. Fruin and J. V. Jelley), in *Non Solar X- and Gamma-ray Astronomy*, ed. L. Gratton, Int. Astron. Union, (1970).
22. "Spaced Receiver Observations of Radio Pulses", (with W. N. Charman, J. H. Fruin, J. V. Jelley, E. R. Hodgson, P. F. Scott, J. R. Shakeshaft, G. A. Baird, T. Delaney, B. G. Lawless, W.P.S. Meikle, R. A. Porter and R. A. Spencer), *Nature*, **228**, 346 (1970).
23. "A Search for Isolated Radio Pulses from the Galactic Centre at 151.5 MHz.", (with W. N. Charman, J. H. Fruin, J. V. Jelley, R. F. Haynes, E. R. Hodgson, P. F. Scott, J. R. Shakeshaft, G. A. Baird, T. Delaney, B. G. Lawless and W.P.S. Meikle), *Nature*, **232**, 177 (1971).
24. "A Precision Sidereal Telescope Drive", (with J. H. Fruin and J. V. Jelley), *Observatory*, **91**, 203 (1971).
25. "K-Electron Capture to Positron Emission Ratio in the Decays of Oxygen-15 and Neon-19", (with W. Leiper), *Phys. Rev.*, **C6**, 1132 (1972).
26. "A Search for Isolated Radio Pulses from the Crab Nebula at 151.5 MHz.", (with W.P.S. Meikle, R. F. Haynes, J. R. Shakeshaft, W. N. Charman and J. V. Jelley), *Mon. Not. Astro. Soc.*, **160**, 50 (1972).
27. "Proportional Counters for the Localization of Ionizing Radiation", (with J. Hough), *Nucl. Instr. and Meth.*, **103**, 365 (1972).
28. "Contribution to Open Discussion on Gravitational Radiation Experiments", *Proceedings of the 6th Texas Symposium on Relativistic Astrophysics*, Ann. New York Acad. Sci., ed. J. H. Hegyi, **224**, 103 (1973).
29. "Weber's Waves", *Nature*, **243**, 553 (1973):

30. "Search for Short Bursts of Gravitational Radiation", (with J. Hough, R. Bland and G. W. Lessnoff), *Nature*, **246**, 340 (1973).
31. "An Experiment to Search for Prompt Emissions from Supernovae at Microwave Frequencies", (with J. V. Jelley, W.P.S. Meikle, G.G.C. Palumbo, F. Bonoli, H. Smith and T. Delaney), *Proceeding of the International Conference on Supernovae and Supernovae Remnants, Lecce, May, 1973*, ed. C.G. Cosmovici, **61**, (D. Reidel Publishing Co., 1974).
32. "Experiments and Observations with Wide Band Gravity-Wave Detectors", (with J. Hough, R. Bland, G. W. Lessnoff), *Colloque Internationaux du Centre National de la Recherche Scientifique (Ondes et Radiations Gravitationnelles, June, 1973): CNRS Report*, ed. Y. Choquet-Bruhat, **220**, 113 (Paris, 1974).
33. "Gravitational-Wave Experiments", *Proceedings of the 1973 School for Young High Energy Physicists, Rutherford Laboratory*, ed. H. Muirhead. Rutherford Lab. Report RL-74-038, VIII-1 (1974).
34. "Searches for Ionospheric Effects of X-Ray Bursts, and for Bursts of Radio Emission, Gravitational Radiation and Microwave Emission from Astronomical Sources", (with W.P.S. Meikle, J. Hough, R. Bland, G. W. Lessnoff; in association with J. V. Jelley, T. Delaney and G.G.C. Palumbo), *Proceedings of the Conference on Transient Cosmic Gamma and X-ray Sources, Los Alamos, September, 1978*, ed. I. Strong, LA-5505-C Conference Proceedings UC-34B (1974).
35. "A Search for Isolated Microwave Pulses from the Perseus Clusters of Galaxies", (with T. Delaney, G. A. Baird, H. Smith, J. V. Jelley, J. H. Fruin, W.P.W. Meikle, G. Morigi, G.G.C. Palumbo and R. G. Partridge), *Astronomy and Astrophysics*, **36**, 83 (1974).
36. "Contribution to Panel Discussion on Gravitational-Waves", *Proceedings of the 7th International Conference on General Relativity and Gravitation, Tel-Aviv, June 1974*, ed. G. Shaviv and J. Rosen, 243-298 (1975).
37. "A Search for VHF Radio Pulses in Coincidence with Celestial Gamma-Ray Bursts", (with G. A. Baird, T. Delaney, B. F. Lawless, D. J. Griffiths, J. R. Shakeshaft, W.P.S. Meikle, J. V. Jelley and W. N. Charman), *Astrophysics J. Lett.*, **196**, L11 (1975).
38. "Search for Continuous Gravitational Radiation", (with J. Hough, J. R. Pugh and R. Bland), *Nature*, **254**, 498 (1975).
39. "An Upper Limit to Microwave Pulse Emission at the Onset of a Supernova", (with W.P.S. Meikle, G. A. Baird, T. Delaney, J. V. Jelley, J. H. Fruin, G.G.C. Palumbo, G. Morigi and R. B. Partridge), *Astronomy and Astrophysics*, **46**, 477 (1976).
40. "Gravitational-Wave Astronomy", *Quarterly J. Roy. Astr. Soc.*, **18**, 9 (1977).
41. "Gravitational-Wave Detectors Using Optical Interferometry", (with J. Hough,

- W. Edelstein and W. Martin), *Gravitazione Sperimentale*, (Accademia Nazionale dei Lincei, Rome), ed. B. Bertotti, 365 (1977).
- 42. "Upper Limits for the Microwave Pulsed Emission from Supernova Explosions in Clusters of Galaxies", (with G.G.C. Palumbo, N. Mandolesi, G. Morigi, G. A. Baird, T. Delaney, W.P.S. Meikle, J. V. Jelley, J. H. Fruin and B. Partridge), *Astrophysics Space Science*, **54**, 355 (1978).
 - 43. "Gravity-Wave Detection: A Tough Challenge", (with J. Hough), *New Scientist*, **79**, 464 (1978).
 - 44. "Quantum Nondemolition Measurements of Harmonic Oscillators", (with K. S. Thorne, C. M. Caves, M. Zimmermann and V. D. Sandberg), *Phys. Rev. Lett.*, **40**, 667 (1978).
 - 45. "The Quantum Limit for Gravitational Wave Detectors and Methods of Circumventing It", (with K. S. Thorne, C. M. Caves, V. D. Sandberg and M. Zimmermann), *Sources of Gravitational Radiation*, ed. L. Smarr, 49 (1979).
 - 46. "On the Measurement of a Weak Classical Force Coupled to a Quantum Mechanical Oscillator", (with C. M. Caves, V. D. Sandberg, K. S. Thorne and M. Zimmermann), *Rev. Mod. Phys.*, **52** (2), 341 (1980).
 - 47. "Optical Cavity Laser-Interferometers for Gravitational Wave Detection", (with J. Hough, A. J. Munley, S.-A. Lee, R. Spero, S. E. Whitcomb, H. Ward, G. M. Ford, M. Hereld, N. A. Robertson, I. Kerr, J. Pugh, G. P. Newton, B. Meers, E. D. Brooks III and Y. Gürsel), *Proceedings of the 5th International Conference on Laser Spectroscopy (VICOLS)*, Jasper, Canada, **33**, (1981).
 - 48. "Interferometric Detectors for Gravitational Radiation", *Gravitational Radiation*, NATO Advanced Physics Institute, Les Houches, ed. N. Deruelle and T. Piran, 321-337, (1983).
 - 49. "Laser-Interferometer Gravitational Radiation Detectors", *Science Underground, American Institute of Physics*, Conference Proceedings No. 96, 336-346 (Los Alamos, 1982).
 - 50. "Passive and Active Isolation for Gravitational Radiation Detectors and Other Instruments", (with N. A. Robertson, I. Kerr and J. Hough), *Phys. E. Sci. Instr.*, **15**, 1101-1105 (1982).
 - 51. "The Search for Gravitational-Waves", *Engineering and Science*, 6-9; 24-26 (Caltech, 1983).
 - 52. "Gravitational-Wave Detectors Using Laser-Interferometers and Optical Cavities: 1. Ideas, Principles, and Prospects", (with J. Hough, A. J. Munley, S.-A. Lee, R. Spero, S. E. Whitcomb, J. Pugh, G. Newton, B. Meers, E. Brooks III and Y. Gürsel), in *Quantum Optics, Experimental Gravity, and Measurement Theory*, ed. Pierre Meystere and Marlan O. Scully, 503-514 (Plenum Publishing, 1983).
 - 53. "Gravitational-Wave Detectors Using Laser-Interferometers and Optical Cav-

- ities: 2. Some Practical Aspects and Results", (with J. Hough, A. J. Munley, S.-A. Lee, R. Spero, S. E. Whitcomb, J. Pugh, G. Newton, B. Meers, E. Brooks III and Y. Gürsel), in *Quantum Optics, Experimental Gravity, and Measurement Theory*, ed. Pierre Meystere and Marlan O. Scully, 515–524 (Plenum Publishing, 1983).
54. "Contribution on the Millisecond Pulsar", *Proceedings of the Meeting of the Royal Astronomical Society, (December, 1982)*, *The Observatory*, 103, 118 (June 1983).
 55. "Laser Phase and Frequency Stabilization Using an Optical Resonator", (with J. L. Hall, F. V. Kowalski, J. Hough, G. M. Ford, A. J. Munley and H. Ward), *Applied Physics*, B31, 97–103 (1983).
 56. "A Gravity-Wave Detector Using Optical Cavity Sensing", (with G. Ford, J. Hough, I. Kerr, A. J. Munley, J. Pugh, N. Robertson and H. Ward), *Proceedings of the 9th International Conference on General Relativity and Gravitation, 1981*, ed. E. Schmutzler, 265–267, (Veb Deutscher Verlag der Wissenschaften, DDR-1080, Berlin, 1983).
 57. "Direct Observational Upper Limit to Gravitational Radiation from Millisecond Pulsar PSR 1937 + 214", (with J. Hough, H. Ward, A. J. Munley, G. Newton, B. Meers, S. Hoggan and G. A. Kerr), *Nature*, 303, (5941), 216–217 (May, 1983).
 58. "Laser-Interferometer Experiments at Caltech", (with S. E. Whitcomb, D. Z. Anderson, Y. Gürsel, M. Hereld and R. Spero), *Proceedings of the Third Marcel Grossman Conference on General Relativity*, Shanghai, China 1982, ed. Hu Ning, 1399 (1983).
 59. "Developments in Laser-Interferometer Gravitational-Wave Detectors", (with S. Hoggan, J. Hough, B. J. Meers, A. J. Munley, G. P. Newton, H. Ward, D. Z. Anderson, Y. Gürsel, M. Hereld, R. Spero and S. E. Whitcomb), *Proceedings of the Third Marcel Grossman Conference on General Relativity*, Shanghai, China 1982, ed. Hu Ning, 739–753 (1983).
 60. "The Caltech Gravitational-Wave Detector", (with R. Spero, D. Z. Anderson, Y. Gürsel, G. Gutt, M. Hereld, K. Kaufman and S. E. Whitcomb), in *General Relativity and Gravitation, Proceedings of the 10th International Conference on General Relativity and Gravitation*, Padua, July 1983, eds. B. Bertotti, F. de Felice, and A. Pascolini, 930–932 (1984).
 61. "Development of Long Baseline Laser Interferometer Gravitational Radiation Detectors Using Resonant Optical Cavities", (with H. Ward, J. Hough, A. J. Munley, G. P. Newton, B. J. Meers, S. Hoggan and G. A. Kerr), in *General Relativity and Gravitation, Proceedings of the 10th International Conference on General Relativity and Gravitation*, Padua, July 1983, eds. B. Bertotti, F. de Felice, and A. Pascolini, 939–941 (1984).

Frederick J. Raab

Publications

1. "Improvements to a Home-Built Nitrogen Laser", (with M. Feldman, P. Lebow and H. Metcalf), *Appl. Opt.*, **17**, 774 (1978).
2. "Measurement of g-factors by Quantum Beats in the OH Free Radical", (with P. Lebow and H. Metcalf), *Phys. Rev. Lett.*, **42**, 85 (1979).
3. "Quantum Beat Spectroscopy of the A²Σ State of the OH Free Radical", (with T. Bergeman, D. Lieberman and H. Metcalf), *Opt. Lett.*, **5**, 427 (1980).
4. "Precision Study of the A²Σ State of the OH Radical", (with T. Bergeman, D. Lieberman and H. Metcalf), *Phys. Rev.*, **A24**, 3120 (1981).
5. "Search for a Permanent Electric Dipole Moment on the ¹²⁹Xe Atom", (with T. G. Vold, B. Heckel and E. N. Fortson), *Phys. Rev. Lett.*, **52**, 2229 (1984).
6. "Optically-Pumped Atoms: A Tool for Fundamental Physics", *Satellite Workshop on Atomic Tests of General Physical Principles, Ninth Int. Conf. Atomic Phys.*, (1984).
7. "Search for a Permanent EDM on Atoms and Molecules", in *Atomic Physics 9.*, R. S. Van Dyck and E. N. Fortson, eds., World Scientific, Singapore, (1984).
8. "Search for Electric Dipole Moments and Space Anisotropy", *Bull. Am. Phys.*, **30**, 715 (1985).
9. "Time Reversal Noninvariance and Electric Dipole Moments of Atoms", in *Advances in Laser Science I*, W. C. Stwalley and M. Lapp, eds., AIP Conf. Proc. No. 146, New York, (1986).
10. "Atomic Physics Tests of Gravity and the Equivalence Principle", *Bull. Am. Phys.*, **31**, 778 (1986).
11. "New Limits on Spatial Anisotropy Using Optically-Pumped Hg(201) and Hg(199)", (with S. K. Lamoreaux, J. P. Jacobs, B. R. Heckel and E. N. Fortson), *Phys. Rev. Lett.*, **57**, 3125 (1986).
12. "Search for an Intermediate Range Interaction", (with C. W. Stubbs, E. G. Adelberger, J. H. Gundlach, B. R. Heckel, K. D. McMurray, H. E. Swanson and R. Watanabe), *Phys. Rev. Lett.*, **58**, 1070 (1987).
13. "Search for Time Reversal Noninvariance in Atoms", in *Search for New and Exotic Phenomena*, J. Tran Thanh Van, ed., Proc. VIIth Moriond Workshop, Editions Frontieres, France, (1987).
14. "Search for an Intermediate Range Interaction: Results of the Eot.-Wash. I Experiment", in *Search for New and Exotic Phenomena*, J. Tran Thanh Van, ed., Proc. VIIth Moriond Workshop, Editions Frontieres, France, (1987).

15. "New Constraints on Composition-Dependent Interactions Weaker than Gravity", (with E. G. Adelberger, C. W. Stubbs, W. F. Rogers, B. R. Heckel, J. H. Gundlach, H. E. Swanson and R. Watanabe), *Phys. Rev. Lett.*, **59**, 849 (1987).
16. "New Constraints on Time-Reversal Asymmetry from a Search for a Permanent Electric Dipole Moment of ^{199}Hg ", (with S. K. Lamoreaux, J. P. Jacobs, B. R. Heckel and E. N. Fortson), *Phys. Rev. Lett.*, **59**, 2275 (1987).
17. "Limits on Composition-Dependent Interactions Using a Laboratory Source: Is There a "Fifth Force" Coupled to Isospin?", (with C. W. Stubbs, E. G. Adelberger, B. R. Heckel, W. F. Rogers, R. Watanabe and J. H. Gundlach), *Phys. Rev. Lett.*, **62**, 609 (1989).
18. "Optical Pumping Technique for Measuring Small Nuclear Quadrupole Shifts in 1S_0 Atoms and Testing Spatial Isotropy," (with S. K. Lamoreaux, J. P. Jacobs, B. R. Heckel, and E. N. Fortson), *Phys. Rev. A*, **39**, 1082 (1989).

Kip S. Thorne
Partial List of Publications

TECHNICAL BOOKS CO-AUTHORED

1. "Gravitation Theory and Gravitational Collapse," (with B. K. Harrison, M. Wakano, and J. A. Wheeler), *University of Chicago Press, Chicago, 1965*, 177 pp.
2. "High Energy Astrophysics, Vol. 3" (with A.G.W. Cameron), eds. C. DeWitt, E. Schatzman, P. Veron, *Gordon and Breach, New York, 1967*, 449 pp.
3. "Gravitation," (with C. W. Misner and J. A. Wheeler), *W. H. Freeman & Co., San Francisco, 1973*, 1279 pp.
4. "Black Holes: The Membrane Paradigm," (with R. H. Price and D. M. Macdonald), *Yale University Press, New Haven, Conn., 1986*, 367 pp.
5. "Gravitational Radiation: A New Window Onto the Universe," *Cambridge University Press, Cambridge, England, 1990*, in press.

SELECTED PUBLICATIONS ON GRAVITATIONAL RADIATION

6. "Gravitational Radiation Damping," *Physical Review Letters*, **21**, 320-323 (1968).
7. "Nonradial Pulsation of General Relativistic Stellar Models. III. Analytic and Numerical Results for Neutron Stars," *Astrophysical Journal*, **158**, 1-16 (1969).
8. "Gravitational-Wave Astronomy," (with W. H. Press), *Annual Review of Astronomy and Astrophysics*, **10**, 335-374 (1972).
9. "How to Test Gravitation Theories by Means of Gravitational-Wave Measurements," *Colloque Internationaux C.N.R.S. No. 220, "Ondes et Radiations Gravitationnelles," Institut Henri Poincaré, Paris*, 214-223 (1974).
10. "The Generation of Gravitational Waves. I. Weak-Field Sources," (with S. Kovacs), *Astrophysical Journal*, **200**, 245-262 (1975).
11. "Gravitational-Wave Bursts from the Nuclei of Distant Galaxies and Quasars: Proposal for Detection Using Doppler Tracking of Interplanetary Spacecraft," (with V. B. Braginsky), *Astrophysical Journal*, **204**, L1-L6 (1976).
12. "Recent JPL Work on Gravity Wave Detection and Solar System Relativity Experiments," (with H. D. Wahlquist, J. D. Anderson, and F. B. Estabrook), *Gravitàzione Sperimentale*, Proceedings of September 1976 Pavia Conference, ed. B. Bertotti (Rome: Accademia Nazionale dei Lincei), 335-350 (1977).
13. "The Generation of Gravitational Waves. IV. Bremsstrahlung," (with S. Kovacs) *Astrophysical Journal*, **222**, 62-85 (1978).

14. "The Generation of Gravitational Waves: A Review of Computational Techniques," *Topics in Theoretical and Experimental Gravitation Physics*, eds V. De Sabbata and J. Weber (Plenum Press, New York and London) 1-61 (1977).
15. "Quantum Nondemolition Measurements of Harmonic Oscillators," (with R.W.P. Drever, C. M. Caves, M. Zimmermann, and V. D. Sandberg), *Physical Review Letters*, **40**, 667-671 (1978).
16. "The Quantum Limit for Gravitational-Wave Detectors and Methods of Circumventing It," (with C. M. Caves, V. D. Sandberg, M. Zimmermann, and R.W.P. Drever), *Sources of Gravitational Radiation*, ed. L. Smarr (Cambridge: Cambridge University Press), 49-68 (1979).
17. "Quantum Non-demolition Measurements," (with V. D. Braginsky and Y. I. Vorontsov), *Science*, **209**, 547-557 (1980). Reprinted as Chapter VI.8 of "Quantum Theory and Measurement," ed. J. A. Wheeler and W. H. Zurek (Princeton University Press, Princeton, N.J.) 749-768 (1983).
18. "On the Measurement of a Weak Classical Force Coupled to a Quantum Mechanical Oscillator. I. Issues of Principle," (with C. M. Caves, R.W.P. Drever, V. D. Sandberg, and M. Zimmermann), *Reviews of Modern Physics*, **52**, 341-392 (1980).
19. "Multipole Expansion of Gravitational Radiation," *Reviews of Modern Physics*, **52**, 299-340 (1980).
20. "Gravitational-Wave Research: Current Status and Future Prospects," *Reviews of Modern Physics*, **52**, 285-298 (1980).
21. "The Gravitational Waves that Bathe the Earth: Upper Limits Based on Theorists' Cherished Beliefs," (with M. Zimmermann), *Essays in General Relativity. A Festschrift for Abraham Taub*, ed. F. Tipler (Academic Press, New York) 139-155 (1980).
22. "The Theory of Gravitational Radiation: An Introductory Review," *Gravitational Radiation*, eds. N. Dereulle and T. Piran (North Holland, Amsterdam), 1-57 (1983).
23. "Skyhook Gravitational Wave Detector," (with V. B. Braginsky), *Nature*, **316**, 610-612 (1985).
24. "Gravitational-Wave Bursts with Memory and Experimental Prospects," (with V. B. Braginsky), *Nature*, **327**, 123-125 (1987).
25. "Gravitational Radiation," *Three Hundred Years of Gravitation*, ed. S. W. Hawking and W. Israel (Cambridge: Cambridge University Press), 330-458 (1987).
26. "Light Scattering and Proposed Baffle Configuration for the LIGO," (1989); to be submitted to *Physical Review*.

Rochus E. Vogt

Publications in High Energy Astrophysics

1. "Electrons in the Primary Cosmic Radiation", (with P. Meyer), *Phys. Rev. Letters*, **6**, 193 (1961).
2. "The Primary Cosmic Ray Electron Flux during a Forbush-Type Decrease", (with P. Meyer), *J. Geophys. Res.*, **66**, 3950 (1961).
3. "Flux and Energy Spectra of Primary Cosmic Ray Protons from 70 to 400 MeV", *J. Phys. Soc. Japan*, **17**, SA-11, 436 (1962).
4. "Some Properties of Primary Cosmic Ray Electrons", (with P. Meyer), *J. Phys. Soc. Japan*, **17**, SA-III, 5 (1962).
5. "Primary Cosmic Ray and Solar Protons", *Phys. Rev.*, **125**, 366 (1962).
6. "High Energy Electrons of Solar Origin", (with P. Meyer), *Phys. Rev. Letters*, **8**, 387 (1962).
7. "Primary Cosmic Ray and Solar Protons II", (with P. Meyer), *Phys. Rev.*, **129**, 2275 (1963).
8. "Changes in the Primary Cosmic Ray Proton Spectrum in 1962 and 1963", (with P. Meyer), *Proc. 8th Int. Conf. on Cosmic Rays*, **3**, 49 (1963).
9. "A Solar and Galactic Cosmic Ray Satellite Experiment", (with W. E. Alt-house, T. H. Harrington, and E. C. Stone), *IEEE Trans.*, NS-15, 229 (1968).
10. "Long-Term Variations of the Primary Cosmic Ray Electron Component", (with J. L'Heureux, P. Meyer, and S. D. Verma), *Can. J. Phys.*, **46**, 896 (1968).
11. "Flux of Cosmic Ray Electrons between 17 and 63 MeV", (with M. H. Israel), *Phys. Rev. Letters*, **20**, 1053 (1968).
12. "Cosmic Ray Negatron and Positron Spectra between 12 and 220 MeV", (with K. P. Beuermann, C. J. Rice, and E. C. Stone), *Phys. Rev. Letters*, **22**, 412 (1969).
13. "Characteristics of the Diurnally Varying Electron Flux near the Polar Cap", (with M. H. Israel), *J. Geophys. Res.*, **74**, 4714 (1969).
14. "Cosmic Ray Negatron and Positron Spectra Observed near Fort Churchill in 1968", (with K. P. Beuermann, C. J. Rice, and E. C. Stone), *Acta Physica Academiae Scientiarum Hungaricae*, **29**, Suppl. 1, 173 (1970).
15. "Interplanetary Deceleration of Solar Cosmic Rays", (with S. S. Murray and E. C. Stone), *Phys. Rev. Letters*, **26**, 663 (1971).
16. "The Isotopes of H and He in Solar Cosmic Rays", (with T. L. Garrard and E. C. Stone), *High Energy Phenomena on the Sun Symposium Proceedings*, edited by R. Ramaty and R. G. Stone, GSFC Preprint X-693-73-193, 341 (1973).

17. "The Energy Spectrum of 0.16 to 3 MeV Electrons during Solar Quiet Times", (with G. J. Hurford, R. A. Mewaldt, and E. C. Stone) *Conf. Papers*, 13th Int. Cosmic Ray Conf., Denver, 1, 324 (1973).
18. "Observations of the Ratio of Low-Energy Cosmic Ray Positrons and Electrons during Solar Quiet Times", (with G. J. Hurford, R. A. Mewaldt, and E. C. Stone), *ibid*, 1, 330 (1973).
19. "Observations of Low Energy Hydrogen and Helium Isotopes during Solar Quiet Times", (with G. J. Hurford, R. A. Mewaldt, and E. C. Stone), *ibid*, 1, 93 (1973).
20. "Measurements of the Cosmic Ray Be/B Ratio and the Age of Cosmic Rays", (with J. W. Brown and E. C. Stone), *ibid*, 1, 484 (1973).
21. "The Elemental Abundance Ratios of Interstellar Secondary and Primary Cosmic Rays", (with J. W. Brown and E. C. Stone), *ibid*, 1, 556 (1973).
22. "Interstellar Electron Spectrum from the Galactic Non-Thermal Radio Emission", (with A. C. Cummings and E. C. Stone), *ibid*, 1, 335 (1973).
23. "Evidence for Primary Interstellar Cosmic Ray Electrons", (with A. C. Cummings and E. C. Stone), *ibid*, 1, 340 (1973).
24. "Interplanetary Diffusion Coefficients for Cosmic Rays", (with A. C. Cummings and E. C. Stone), *ibid*, 2, 772 (1973).
25. "Analytic Approximations in the Study of the Solar Modulation of Electrons", (with A. C. Cummings and E. C. Stone), *ibid*, 2, 765 (1973).
26. "Solar Modulation of Cosmic Ray Protons and He Nuclei", (with T. L. Garrard and E. C. Stone), *ibid*, 2, 732 (1973).
27. "Relation of the Radial Gradient of Cosmic Ray Protons to the Size of the Solar Modulation Region", (with T. L. Garrard and E. C. Stone), *ibid*, 2, 1336 (1973).
28. "Measurements of the Flux of Low-Energy Solar-Flare Positrons", (with G. J. Hurford, R. A. Mewaldt, and E. C. Stone), *ibid*, 2, 1613 (1973).
29. "The Energy Spectrum of 0.16 to 2 MeV Electrons During Solar Quiet Times", (with G. J. Hurford, R. A. Mewaldt, and E. C. Stone), *Ap. J.*, 192, 541 (1974).
30. "Particles and Fields in the Outer Solar System", (with G. L. Siscoe), *Icarus*, 24, 333 (1975).
31. "The Isotopic Composition of Hydrogen and Helium in Low Energy Cosmic Rays", (with R. A. Mewaldt and E. C. Stone), 14th International Cosmic Ray Conf., Munich, Germany, *Conf. Papers*, 1, 306 (1975).
32. "Isotopic Composition of the Anomalous Low Energy Cosmic Ray Nitrogen and Oxygen", (with R. A. Mewaldt, E. C. Stone, and S. B. Vidor), *ibid*, 1, 349 (1975).

33. "The Elemental Composition of 4–30 MeV/nuc Cosmic Ray Nuclei with $1 \leq Z \leq 8$ ", (with R. A. Mewaldt, E. C. Stone, and S. B. Vidor), *ibid*, **2**, 798 (1975).
34. "Implications of Time Variations for the Origin of Low Energy Cosmic Ray Nitrogen and Oxygen Nuclei", (with R. A. Mewaldt and E. C. Stone), *ibid*, **2**, 804 (1975).
35. "Observations of Hydrogen and Helium Isotopes in Solar Cosmic Rays", (with G. J. Hurford and E. C. Stone), *ibid*, **5**, 1624 (1975).
36. "A Search for Solar Flare Positrons", (with R. A. Mewaldt and E. C. Stone), *ibid*, **5**, 1668 (1975).
37. "Observations of Low Energy Interplanetary Electrons", (with R. A. Mewaldt and E. C. Stone), *ibid*, **2**, 758 (1975).
38. "The Quiet Time Flux of 0.16–1.6 MeV Cosmic Ray Positrons", (with R. A. Mewaldt and E. C. Stone), *ibid*, **1**, 401 (1975).
39. "The Quiet Time Spectra of Low Energy Hydrogen and Helium Nuclei", (with R. A. Mewaldt and E. C. Stone), *ibid*, **2**, 774 (1975).
40. "Enrichment of Heavy Nuclei in ^3He Rich Flares", (with G. J. Hurford, R. A. Mewaldt, and E. C. Stone), *Ap. J.*, **201**, L95 (1975).
41. "Splash Albedo Protons Between 4 and 315 MeV at High and Low Geomagnetic Latitudes", (with K. P. Wenzel and E. C. Stone), *J. Geophys. Res.*, **80**, 3580 (1975).
42. "The Isotopic Composition of Hydrogen and Helium in Low Energy Cosmic Rays", (with R. A. Mewaldt, and E. C. Stone), *Ap. J.*, **206**, 616 (1976).
43. "Observations of Jovian Electrons at 1 AU", (with R. A. Mewaldt and E. C. Stone), *J. Geophys. Res.*, **81**, 2397 (1976).
44. "Isotopic and Elemental Composition of the Anomalous Low Energy Cosmic Ray Fluxes", (with R. A. Mewaldt, E. C. Stone, and S. B. Vidor), *Ap. J.*, **205**, 931 (1976).
45. "Neutral Particle Background in Cosmic Ray Telescopes Composed of Silicon Solid State Detectors", (with R. A. Mewaldt and E. C. Stone), *Space Science Instrumentation*, **3**, 231 (1977).
46. "Cosmic Ray Investigation for the Voyager Missions; Energetic Particle Studies in the Outer Heliosphere—and Beyond", (with E. C. Stone, F. B. McDonald, B. J. Teegarden, J. H. Trainor, J. R. Jokipii, and W. R. Webber), *Space Science Review*, **21**, 355 (1977).
47. "Simultaneous Observations of Cosmic Ray Particles in Corotating Interplanetary Structures at Different Solar Distances between 0.3 and 1.0 AU from HE-LIOS 1 and 2 and IMP 7 and 8", (with H. Kunow, G. Wibberenz, G. Green, R. Müller-Mellin, R. Witte, E. Hemp, E. C. Stone, and R. Mewaldt), 15th International Cosmic Ray Conference, Plovdiv, Bulgaria, *Conf. Papers*, **3**, 227,

(1977).

48. "A Cosmic Ray Isotope Spectrometer", (with W. E. Althouse, A. C. Cummings, T. L. Garrard, R. A. Mewaldt, and E. C. Stone), *IEEE Trans. on Geoscience Electronics*, **GE-16**, 204 (1978).
49. "The Radial Diffusion Coefficient of 1.3–2.3 MeV Protons in Recurrent Proton Streams", (with R. A. Mewaldt and E. C. Stone), *Geophys. Res. Ltrs.*, **5**, 965 (1978).
50. "Characteristics of the Spectra of Protons and Alpha Particles in Recurrent Events at 1 AU", (with R. A. Mewaldt and E. C. Stone), *Geophys. Res. Ltrs.*, **6**, 589 (1979).
51. "The Isotopic Composition of Solar Flare Accelerated Neon", (with R. A. Mewaldt, J. D. Spalding, and E. C. Stone), *Ap. J. (Letters)*, **231**, L97 (1979).
52. "The Voyager Cosmic Ray Experiment", (with D. E. Stilwell, W. D. Davis, R. M. Joyce, F. B. McDonald, J. H. Trainor, W. E. Althouse, A. C. Cummings, T. L. Garrard, and E. C. Stone), *IEEE Trans. on Nuclear Science*, **NS-26**, 513 (1979).
53. "Voyager 1: Energetic Ions and Electrons in the Jovian Magnetosphere", (with W. R. Cook, A. C. Cummings, T. L. Garrard, N. Gehrels, E. C. Stone, J. H. Trainor, A. W. Schardt, T. Conlon, N. Lal, and F. B. McDonald), *Science*, **204**, 1003 (1979).
54. "Voyager 2: Energetic Ions and Electrons in the Jovian Magnetosphere", (with A. C. Cummings, T. L. Garrard, N. Gehrels, E. C. Stone, J. H. Trainor, A. W. Schardt, T. F. Conlon, and F. B. McDonald), *Science*, **206**, 984 (1979).
55. "Satellite Measurements of the Isotopic Composition of Galactic Cosmic Rays", (with R. A. Mewaldt, J. D. Spalding, and E. C. Stone), 16th International Cosmic Ray Conference, Kyoto, Japan, *Conf. Papers*, **12**, 86 (1979).
56. "The Elemental Composition of Quiet Time Low Energy Cosmic Rays Measured on the Voyager Spacecraft", (with W. R. Webber and E. C. Stone), *ibid*, **5**, 357 (1979).
57. "Elemental Composition of Solar Energetic Particles in 1977 and 1978", (with W. R. Cook, E. C. Stone, J. H. Trainor, and W. R. Webber), *ibid*, **12**, 265 (1979).
58. "High Resolution Measurements of Galactic Cosmic Ray Neon, Magnesium and Silicon Isotopes", (with R. A. Mewaldt, J. D. Spalding, and E. C. Stone), *Ap. J. (Letters)*, **235**, L95 (1980).
59. "The Isotopic Composition of Galactic Cosmic Ray Iron Nuclei", (with R. A. Mewaldt, J. D. Spalding, and E. C. Stone), *Ap. J. (Letters)*, **236**, L121 (1980).
60. "Elemental Composition of Solar Energetic Nuclei", (with W. R. Cook and E. C. Stone), *Ap. J. (Letters)*, **238**, L97 (1980).

61. "The Isotopic Composition of Solar Flare Accelerated Magnesium", (with R. A. Mewaldt, J. D. Spalding, and E. C. Stone), *Ap. J. (Letters)*, **243**, L163 (1981).
62. "Energetic Charged Particles in Saturn's Magnetosphere: Voyager 1 Results", (with D. L. Chenette, A. C. Cummings, T. L. Garrard, E. C. Stone, A. W. Schardt, J. H. Trainor, N. Lal, and F. B. McDonald), *Science*, **212**, 231 (1981).
63. "High Resolution Measurements of Solar Flare Isotopes", (with R. A. Mewaldt, J. D. Spalding, and E. C. Stone), 17th International Cosmic Ray Conference, Paris, France, *Conf. Papers*, **3**, 131 (1981).
64. "The Isotopic Composition of Low Energy Cosmic Rays", (with R. A. Mewaldt, J. D. Spalding, and E. C. Stone), *ibid*, **2**, 68 (1981). Erratum, *ibid*, **11**, 431 (1981).
65. "The Isotopic Composition of Cosmic Ray B, C, N, and O Nuclei", (with R. A. Mewaldt, J. D. Spalding, and E. C. Stone), *Ap. J. (Letters)*, **251**, L27 (1981).
66. "Energetic Charged Particles in Saturn's Magnetosphere: Voyager 2 Results", (with D. L. Chenette, A. C. Cummings, T. L. Garrard, E. C. Stone, A. W. Schardt, J. H. Trainor, N. Lal, and F. B. McDonald), *Science*, **215**, 577 (1982).
67. "Elemental Composition of Solar Energetic Particles" (with W. R. Cook and E. C. Stone), *Ap. J.*, **279**, 827 (1984).

Rainer Weiss
Publications

1. "Magnetic Moments and Hyperfine Structure Anomalies of Cs₁₃₃, Cs₁₃₅, and Cs₁₃₇", (with H. H. Stroke, V. Jaccarino, and D. S. Edmonds), *Physical Review*, **105**, 590 (1957).
2. "Molecular Beam Electron Bombardment Detector," *Review of Scientific Instruments*, **32**, 397 (1961).
3. "A Search for a Frequency Shift of 14.4 KeV Photons on Traversing Radiation Fields," (with L. Grodzins), *Physics Letters*, **1**, 342 (1962).
4. "Stark Effect and Hyperfine Structure of Hydrogen Fluoride", *Physical Review*, **131**, 659 (1963).
5. "The Cesium Fountain Experiment: The Paucity of Slow Atoms", Festschrift, for J. R. Zacharias (1965).
6. "A Gravimeter to Monitor the ₀S₀ Dilational Mode of the Earth", (with B. Block), *J. Geophy., Res.*, **70**, 5615 (1966).
7. "Experimental Test of the Freundlich Red-Shift Hypothesis, (with G. Blum), *Physical Review*, **155**, 1412 (1967).
8. "Electric and Magnetic Field Probes," *Journal of Applied Physics*, **35**, 1047 (1967).
9. "Laser-induced Fluorescence in a Molecular Beam of Iodine", (with S. Ezekiel), *Physical Review Letters*, **20**, 91 (1968).
10. "A Measurement of the Isotropic Background Radiation in the Far Infrared", (with D. Muehlner), *Physical Review Letters*, **24**, 742 (1970).
11. "Electromagnetically Coupled Broadband Gravitational Antenna", *Quarterly Progress Report*, Research Lab. of Electronics, MIT, **105**, 54 (1972).
12. "Balloon Measurements of the Far Infrared Background Radiation", (with D. Muehlner), *Physical Review D*, **7**, 326 (1973).
13. "Further Measurements of the Submillimeter Background at Balloon Altitude", (with D. Muehlner), *Physical Review Letters*, **30**, 757 (1973).
14. "Measurements of the Phase Fluctuations in a He-Ne Zeeman Laser", (with D. K. Ownes), *Review of Scientific Instruments*, **45**, 1060 (1974).
15. "The Oldest Fossil", *Technology Review*, **78**, 56 (1975).
16. "A Large Beam Sky Survey at Millimeter and Submillimeter Wavelengths Made from Balloon Altitudes", (with D. Owens and D. Muehlner) *Astrophysical Journal*, **231**, 702 (1979).
17. "Gravitational Radiation—The Status of the Experiments and Prospects for the Future," in *Sources of Gravitational Radiation*, Cambridge University Press, Cambridge, England (1979).

18. "Measurements of the Cosmic Background Radiation", *Annual Review of Astronomy and Astrophysics*, **18**, 489 (1980).
19. "The COBE Project", *Physica Scripta*, **21**, 670 (1980).
20. "Monolithic Silicon Bolometers", (with P. M. Downey, F. J. Bachner, J. P. Donnelly, W. T. Lindley, R. W. Mountain and D. J. Silversmith), *Journal of Infrared and Millimeter Waves*, **1** (1980).
21. "Monolithic Silicon Bolometers", (with P. M. Downey, A. D. Jeffries, S. S. Meyer, F. J. Bachner, J. P. Donnelly, W. R. Lindley, R. W. Mountain, and D. J. Silversmith), *Applied Optics*, **23**, 910 (1983).
22. "A Search for the Sunyaev-Zel'dovich Effect at Millimeter Wavelengths", (with S. S. Meyer and A. D. Jeffries), *The Astrophysical Journal Letters*, **271**, L1 (1983).
23. "Measurements of the Anisotropy of the Cosmic Background Radiation and Diffuse Galactic Emission at Millimeter and Submillimeter Wavelengths", (with M. Halpern, R. Benford, S. Meyer, D. Muehlner), *The Astrophysical Journal*, **332**, 596 (1988).

Conference Reports

24. "The MIT Prototype Gravitational Wave Detector", (with J. Livas, R. Benford, A. Jeffries, P. Lindsay, P. Saulson, D. Shoemaker), in *Proceedings of the Fourth Marcel Grossman Meeting on General Relativity*, ed. R. Ruffini, 591 (1985).
25. "Interferometric Gravitational Wave Detection at MIT", (with R. Benford, M. Burka, N. Christensen, M. Eisgruber, P. Fritschel, A. Jeffries, J. Kovalik, P. Lindsay, J. Livas, and P. Saulson), *13th Texas Symposium on Relativistic Astrophysics*, ed. M. Ulmer, Singapore: World Scientific, 15 (1986).
26. "Progress on the MIT 5-Meter Interferometer", (with R. Benford, M. Burka, N. Christensen, M. Eisgruber, P. Fritschel, A. Jeffries, J. Kovalik, P. Lindsay, J. Livas, and P. Saulson) *International Symposium on Experimental Gravitational Physics*, Guangzhou, China, ed. P. Michelson, Singapore: World Scientific, 312 (1987).

Reports

27. "Report of the Sub-Panel on Relativity and Gravitation", (with P. Bender, C. Misner, and R. V. Pound), Management and Operations Working Group for Shuttle Astronomy, NASA Headquarters, (Sept., 1976).
28. "Study Report for the Cosmic Background Explorer", (with S. Gulkis, M. Hauser, J. Mather, G. Smoot, and D. Wilkinson), Goddard Space Flight Center, (Feb. 1977).
29. "Report of the Detector Study Panel NASA", (with P. Richards, Chairman) (1979).

30. "A Study of a Long Baseline Gravitational Wave Antenna System", (with P. Lindsay and P. Saulson) (1983).
31. "Task Group on Fundamental Physics and Chemistry", (with P. Bender, A. Berlad, R. Donnelly, F. Dyson, W. Fairbank, G. Homsy, J. Langer, J. Nau-gle, R. Pellat, J. Reynolds, R. Ruffini, D. Saville, and R. Schrieffer), National Academy of Sciences Report on Gravitational Physics, (1987).

APPENDIX A

THE PHYSICS OF GRAVITATIONAL WAVES, AND COMPARISON OF SOURCE STRENGTHS WITH DETECTOR SENSITIVITIES

This appendix presents a detailed discussion of the issues raised in Sections II.A, II.B, and II.C of the proposal (for still greater detail see Reference [A-1]).

1. The Physics of Gravitational Waves

Gravitational waves are predicted by general relativity theory and by all other relativistic theories of gravity, and all the theories agree, in rough order of magnitude, on the strengths of the waves to be expected from astrophysical sources. Although gravitational waves have not yet been observed directly, the effect of the back-action of gravitational-wave emission on one source (the orbital decay of the binary pulsar PSR 1913+15) has been measured and agrees with general relativity's predictions to within the experimental error of several percent [A-2]. The primary goals of the LIGO Project are to detect gravitational waves directly, and use them to test the fundamental laws of physics and to open a new window onto the astrophysical universe.

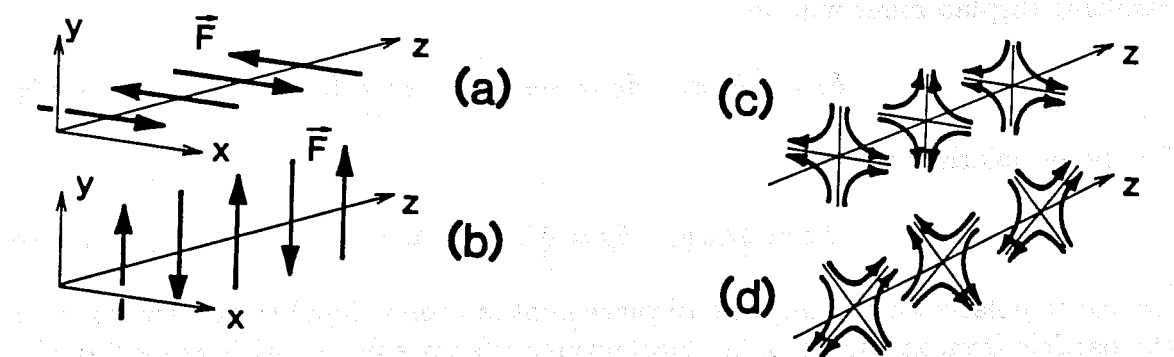


Figure A-1 Left half: The forces produced on charged particles by an electromagnetic wave propagating in the z direction: (a) for x -polarization, and (b) for y -polarization. Right half: The forces on massive particles produced by a gravitational wave propagating in the z direction: (c) for $+$ polarization, and (d) for x polarization.

a. The forces produced by gravitational waves. Just as an electromagnetic wave pushes a charged particle that initially is at rest back and forth in a direction transverse to the wave's propagation (Figure A-1 (a) and (b)), so also a gravitational wave pushes a massive particle, initially at rest, back and forth transversely (Figure A-1 (c) and (d)). The figures show the lines of force as measured in a local "proper reference frame", whose time coordinate t is equal to the proper time ticked by physical clocks and whose orthogonal spatial coordinates (x, y, z) measure proper (physical) distance. For a gravitational wave the force on a particle

of mass m at location (x, y, z) is the sum of contributions from two polarizations: the + ("plus") polarization (Figure A-1 (c)) with force

$$\vec{F} = \frac{1}{2}m\ddot{h}_+(x\vec{e}_x - y\vec{e}_y) \quad (\text{A.1a})$$

and the \times ("cross") polarization (Figure A-1 (d)) with force

$$\vec{F} = \frac{1}{2}m\ddot{h}_\times(y\vec{e}_x + x\vec{e}_y). \quad (\text{A.1b})$$

Here dots denote time derivatives, \vec{e}_x and \vec{e}_y are unit basis vectors in the x and y directions, and h_+ and h_\times are dimensionless *gravitational-wave fields*, which propagate in the z -direction at the speed of light

$$h_+ = h_+(t - z/c), \quad h_\times = h_\times(t - z/c). \quad (\text{A.2})$$

Notice that the gravitational force fields (Equations (A.1a,b)) are quadrupolar and are transverse to the waves' propagation direction.

If a test particle at (x, y, z) is unconstrained by other forces, then it will accelerate by an amount $\delta\ddot{x} = \vec{F}/m$ in response to the gravitational wave, and its resulting displacement will be

$$\delta x = \frac{1}{2}h_+x, \quad \delta y = -\frac{1}{2}h_+y, \quad \delta z = 0 \quad (\text{A.3a})$$

for the + polarization and

$$\delta x = \frac{1}{2}h_\times y, \quad \delta y = \frac{1}{2}h_\times x, \quad \delta z = 0 \quad (\text{A.3b})$$

for the \times polarization. Since the displacement is proportional to the separation of the particle from the origin of the local proper reference frame, with proportionality factor h_+ or h_\times , one can regard h_+ and h_\times as dimensionless "strains of space."

b. Effect of the wave on an interferometric detector. Figure A-2 is a simplified schematic diagram of an interferometric detector of the type to be operated in the LIGO. Three masses hang by wires from overhead supports at the corner and ends of an "L". We shall denote by $L \equiv (L_x + L_y)/2 \simeq L_x \simeq L_y$ the mean length of the (nearly equal) arms of the "L" and shall place the origin of a proper reference frame at the corner mass as shown. If a gravitational wave propagates vertically (z -direction), and has its + polarization axes parallel to the detector's arms, and has a frequency f high compared to the 1-Hz pendulum frequency of the masses, then the wave will move the end masses back and forth relative to the corner mass in just the same manner as if the end masses were free (the pendulum restoring force does not have time to act). The resulting wave-induced changes in the x -arm and y -arm lengths (Equation (A.3a)) will be $\delta L_x = \frac{1}{2}h_+L$ and $\delta L_y = -\frac{1}{2}h_+L$; i.e., they will be equal and opposite. These changes are monitored by

laser interferometry: laser beams, sent from the center mass down the two arms and reflected off mirrors on the end masses, will return to the corner with a relative phase change $\Delta\Phi$ that is proportional to the difference in arm lengths,

$$\Delta\Phi = 2\pi\Delta L/\lambda_l, \text{ where } \Delta L \equiv \delta L_x - \delta L_y = h_+(t)L. \quad (\text{A.4})$$

Here λ_l is the light's wavelength. By interfering the beams one can monitor this phase change and thence monitor the gravitational-wave field $h_+(t)$.¹

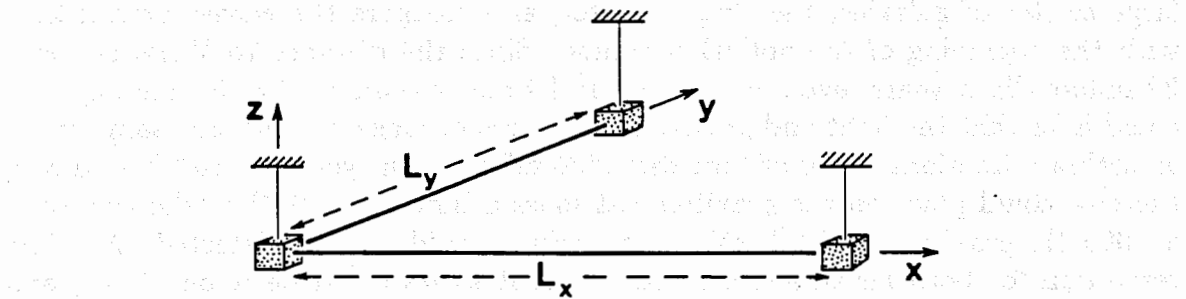


Figure A-2 Schematic diagram of a laser interferometer gravitational wave detector.

If the wave, instead of coming in vertically, comes in from a direction with polar angles (θ, ϕ) relative to the Cartesian coordinates of Figure A-2 (cf. Figure II-1 in Section II.A), and if we take one of the + state's polarization axes to be horizontal, then straightforward algebra shows that the forces (Equations (A.1a) and (A.1b)) produce the relative arm-length change

$$\Delta L/L = F_+(\theta, \phi)h_+(t) + F_x(\theta, \phi)h_x(t), \quad (\text{A.5a})$$

where F_+ and F_x are the detector's quadrupolar beam pattern functions

$$F_+ = \frac{1}{2}(1 + \cos^2 \theta) \cos 2\phi, \quad F_x = \cos \theta \sin 2\phi. \quad (\text{A.5b})$$

Note that the beam patterns are very broad. This means that the relative responses of different detectors, with different orientations, will give rather poorer information about source directions than the time-of-flight between widely separated detectors (cf. Appendix B and Section V.C).

¹ One might worry that the gravitational wave will interact with the laser beams and, thereby, alter the standard phase-change relation $\Delta\Phi = 2\pi\Delta L/\lambda_l$. Not so if one uses, as we have, a rigid, Cartesian coordinate system whose coordinate lengths are unaffected by the wave. Only if one uses "rubbery coordinates" (e.g., the "transverse-traceless coordinates" introduced in many textbooks) need one worry about interaction of the gravitational wave with the light. (This approach was taken in Appendix B to derive the frequency (and angular) response of a Fabry-Perot gravitational-wave interferometer.)

c. Measurement of the graviton's rest mass and spin. Quantum field theory tells us that classical waves are carried by quanta (photons for electromagnetic waves and gravitons for gravitational waves), and that the rest masses and spins of the quanta can be inferred from the propagation speeds and polarization properties of their waves.

The propagation speed will be precisely the speed of light if and only if the quanta have zero rest mass; otherwise it will be slower. Thus, one goal of the LIGO Project is to detect gravitational waves from a supernova outburst in the nearest large cluster of galaxies, the Virgo Cluster, and compare the waves' arrival time with the beginning of the optical outburst. Since the distance to Virgo is about 30 million light years, even with an optical time resolution of only one day, one could infer that the light and gravitational waves propagated with the same speed to within a fractional error of $(\text{one day})/(30 \text{ million light years}) \sim 10^{-10}$, and one, thereby, could place on the graviton rest mass a limit of $\sim 10^{-5} \times (\text{the energy of a } 1000 \text{ Hz graviton}) \sim 10^{-16} \text{ eV}$. If neutrinos could also be detected, the time resolution for both neutrinos and gravitational waves could be about 1 ms; and if their onsets were that close together, one would infer equal speeds to within $\sim 10^{-18}$ and corresponding rest mass limits of $\sim 10^{-20} \text{ eV}$ for the graviton, and $\sim 10^{-2} \text{ eV}$ for the neutrino. (This limit for the graviton is about the same as one obtains from the validity of the inverse square law for the sun's gravity as manifest in planetary orbits. Therefore, if gravitational waves were found to propagate at a different speed from light and neutrinos, we would infer that the gravitons which carry the waves are different from the gravitons which mediate the solar system's gravity—an unlikely but not impossible outcome. An alternative explanation could be that gravitons, like photons, have zero rest mass, but they propagate on the light curves of a different metric from that which governs photons [A-3].)

The spin S of the quantum that carries a classical wave determines the "return angle" of the wave's force field: rotate the force field (Figure A-1) about the wave's propagation direction. The minimum angle of rotation that brings the field back to its original orientation is its return angle θ_{ret} and is equal to $(360 \text{ deg})/S$. For the electromagnetic wave of Figure A-1 (a) and (b), θ_{ret} is 360 deg, so the photon must have spin one; for the gravitational wave of Figure A-1 (c) and (d), θ_{ret} is 180 deg, so the graviton must have spin two. Correspondingly, one goal of the LIGO project is to determine the return angle for gravitational waves by simultaneous measurements with several different detectors (in a worldwide network) that have several different orientations. Since most other relativistic theories of gravity predict a mixture of spin-two, spin-one, and/or spin-zero gravitons [A-3], such a measurement would be a powerful test of whether general relativity is correct.

d. The strengths of cosmic gravitational waves. Energy conservation dictates that the wave fields h_+ and h_x die out as $1/(\text{distance to the source}) = 1/r$. Just as an electromagnetic wave is produced by oscillating multipole moments of a charge distribution, so also a gravitational wave is produced by oscillating multipole moments of a mass distribution. In the electromagnetic case the monopole moment cannot oscillate because it is the source's total charge and charge is conserved; and, consequently, the radiation is typically dipolar. Similarly, in the gravitational case the monopole moment cannot oscillate because it is the source's total mass and mass is conserved; moreover, the mass dipole moment cannot oscillate because its time derivative is the source's total momentum and momentum is conserved; and, consequently, gravitational radiation is typically quadrupolar. Dimensional considerations then dictate that $h_+ \sim h_x \sim (G/c^4)\ddot{Q}/r$ where G is Newton's gravitation constant, c is the speed of light, Q is the quadrupole moment, and dots denote time derivatives. Because the quadrupole moment is of order the mass of the source times the square of its size, \ddot{Q} is of order the mass times the square of the source's internal velocities, i.e., of order the source's internal kinetic energy—or, more precisely, that part of the kinetic energy associated with oscillatory, nonspherical motions, $E_{\text{kin}}^{\text{ns}}$:

$$h_+ \sim h_x \sim \frac{G}{c^4} \frac{E_{\text{kin}}^{\text{ns}}}{r} \sim 10^{-20} \left[\frac{E_{\text{kin}}^{\text{ns}}}{M_\odot c^2} \right] \left[\frac{10 \text{ Mpc}}{r} \right]. \quad (\text{A.6})$$

Here M_\odot is the mass of the sun and $10 \text{ Mpc} \equiv (10 \text{ megaparsecs}) = (30 \text{ M light years})$ is the distance to the Virgo Cluster of galaxies. Equation (A.6) is a correct order-of-magnitude estimate not only for general relativity, but also for other theories of gravity; and it suggests that the strongest extragalactic waves bathing the Earth are not likely to exceed $h \sim 10^{-20}$.

e. Characteristics of the strongest sources. The strongest sources are those for which the nonspherical, internal kinetic energy is largest, which means those with large masses and large internal velocities. Since the internal velocities are generated by internal gravity, large internal velocities mean large internal gravity, which means compact size. Thus it is that the strongest sources are likely to be black holes and neutron stars—e.g., the violent births of black holes and neutron stars in stellar implosions, the inspiral and coalescence of binary neutron stars and black holes in distant galaxies, and the rotation of nonaxisymmetric neutron stars (pulsars) in our own galaxy.

f. The frequencies of cosmic gravitational waves. The characteristic frequencies of vibration and rotation for neutron stars are less than or of order a few kilohertz; and those for a black hole of mass M are

$$f \sim \frac{10 \text{ kHz}}{M/2M_\odot} \quad (\text{A.7})$$

(where $2M_\odot$ is the smallest possible mass for a black hole that forms by stellar collapse). Thus, the strongest waves are likely to lie at frequencies of 10 kHz and

below. The LIGO is designed to work from 10 kHz down to the lowest frequencies at which one can isolate the detectors from earth vibrations, \sim 10 Hz—a range in which a rich variety of sources should exist. At yet lower frequencies, where there should also be interesting sources, one must use space-based detectors—the most promising of which will be LIGO-type detectors that might fly in space in the early 21st century [A-4]. The LIGO Project will provide an important base of technology and experience for those future detectors.

g. Penetrating power of gravitational waves. Because the strongest sources of gravitational waves are compact concentrations of highly dynamical mass, they typically will lie in regions obscured by surrounding matter (e.g., in the core of a supernova explosion or at the center of a galaxy or in the big-bang origin of the universe). Fortunately, gravitational waves are highly penetrating. For example, whereas neutrinos scatter many times in emerging from the center of a supernova and photons cannot get out at all, gravitational waves should emerge nearly unscathed; the total loss to scattering and absorption should be many orders of magnitude below unity. Similarly, whereas photons from the big bang (the cosmic microwave radiation) last scattered off matter when the universe was about one million years old and neutrinos last scattered when it was a few seconds old, primordial gravitational waves should have last scattered near the Planck time, $\sqrt{G\hbar/c^5} \sim 10^{-43}$ seconds, when the initial conditions of the universe were being set by the (little understood) laws of quantum gravity [A-5].

h. Electromagnetic information as a poor predictor of cosmic gravitational waves. Electromagnetic waves studied by astronomers are almost always incoherent superpositions of the emissions from a large number of molecules, atoms, or charged particles. In contrast, cosmic gravitational waves are produced by the coherent, bulk motions of mass-energy (either in the form of matter as in neutron stars, or in the form of vibrating, nonlinear spacetime curvature as in colliding black holes). This difference of emission mechanism, together with the fact that the strongest gravitational-wave sources are probably opaque to photons, serves as a warning that our present photon-based knowledge of the universe may be a rather poor guide as to what gravitational-wave astronomy will bring. On one hand, we cannot estimate with confidence how sensitive a LIGO detector must be in order to discover waves. On the other hand, when waves are discovered, they are likely to bring surprises. Indeed, it seems likely that gravitational radiation will produce a revolution in our understanding of the universe comparable to that which came from radio waves in the 1950s and 1960s [A-6].

i. Astrophysical information carried by gravitational waves. Gravitational waves carry substantial information about their sources. The total information carried to earth is embodied in the celestial coordinates (α, δ) of the source, plus the two “gravitational waveforms” $h_+(t)$ and $h_\times(t)$ evaluated at the location of a detector. The LIGO detectors are broad-band instruments, designed to measure the waveforms in the time domain with a high-frequency cutoff around 10 kHz

and a seismic-noise-induced low-frequency cutoff, which in present prototypes is around 400 Hz and will be pushed continually downward toward 10 Hz over the coming years. A goal of the LIGO Project, in cooperation with other detectors in a worldwide network, is to extract the full information, α , δ , $h_+(t)$, and $h_x(t)$ from the waves (cf., Section V.C); and, where possible, to cross-correlate that information with data from other kinds of radiation.

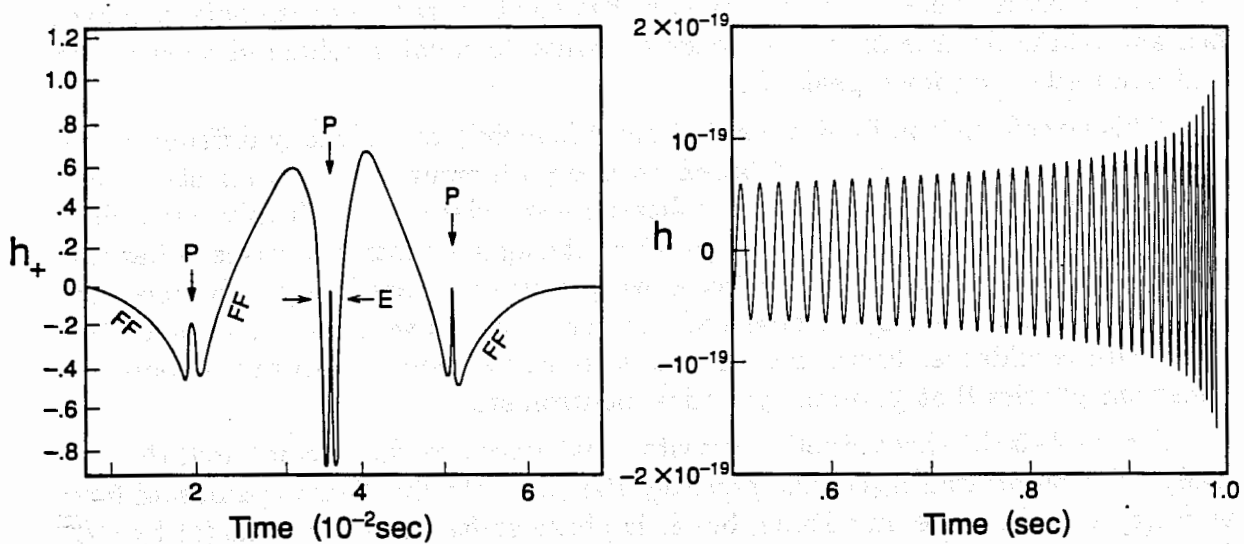


Figure A-3 Part (a): The gravitational waveform produced by one scenario for the collapse of a star to form a neutron core, as computed in a numerical simulation by Richard A. Saenz and Stuart L. Shapiro [A-7]. Part (b): The waveform produced by the inspiral, toward coalescence, of a binary system made of two $10 M_\odot$ black holes. The waveforms for black-hole and neutron-star coalescences are much the same when the objects are far apart (toward the left of the chirp) but differ substantially at the end points.

j. Extraction of information from a waveform. Figure A-3 (a) shows a waveform $h_+(t)$ computed several years ago by numerical simulation of a specific kind of source [A-7]. The associated $h_x(t)$ is identical to this $h_+(t)$ except for an overall multiplicative factor. If these $h_+(t)$ and $h_x(t)$ were measured by gravitational-wave detectors, one could infer the following from them: Because $h_x(t) = \text{const} \times h_+(t)$, the source must be axisymmetric. Because the shortest time scales present in the waveform are ~ 0.5 ms, the source must be either a neutron star or a several-solar-mass black hole. Assuming, as usually will be the case, that the radiation is predominantly quadrupolar, one can double-time-integrate the waveform to get the time evolution of the source's quadrupole moment. One then notices that the segments of the waveform marked FF have the shapes $h_+ \propto (t - \text{const})^{-2/3}$ that one expects from nonspherical, free-fall motion; and the sharply reversed peaks marked P are what one expects from a sharp acceleration in the direction opposite to the free fall. The natural and correct interpretation is that these waves are from

a stellar collapse that formed a neutron core which bounced three times. The fact that the three sharp peaks are all in the same direction (up, not down) indicates that the sharp bounces were all along the same axis. Surely the other axis or axes should have bounced as well, or at least stopped their collapse; so there should be at least one sharp peak in the down direction. Indeed there is; it is superposed on the central up peak (region labeled E). The natural and correct interpretation is that the collapsing star was centrifugally flattened by rotation; its pole collapsed fast and bounced three times (up peaks P) while its equator collapsed more slowly and bounced once (down peak E).

This waveform is not a firm prediction; it is merely one of many different waveforms that have been computed based on many different scenarios for stellar collapse. Neutron-star physics is so complicated—especially in the highly dynamical, shock-wave-endowed situations that produce strong gravitational waves—that theorists in the early years of gravitational wave astronomy are likely to be relegated to the task of interpreting the observed waveforms, as above, rather than predicting them with confidence. From those interpretations we should learn much about the uncertain physics that governs dynamical neutron stars.

Figure A-3 (b) shows another gravitational waveform $h_+(t)$ computed theoretically. The associated $h_x(t)$ has precisely the same slowly-changing-sinusoid form as $h_+(t)$ and the same amplitude, but it is phase shifted relative to $h_+(t)$ by $\pi/2$. From this same amplitude and the relative phase shift, and the fact that the amplitude varies with time as $(\text{const} - t)^{-1/4}$ and the frequency varies as $(\text{const} - t)^{-3/8}$, we infer that the source is a binary system which is spiraling inward, under the influence of gravitational radiation reaction, toward coalescence; and that we on Earth see the binary face on. From the actual amplitude at fixed frequency and the rate of change of frequency, we infer (see below) that the distance to the source is 100 Mpc and the reduced mass μ and total mass M of the system satisfy $\mu^{3/5}M^{2/5} = 9M_\odot$, which means that at least one of the objects in the binary is a black hole. By combining this with the frequency at which the inspiral terminates, we infer that both objects are black holes, with masses $M_1 = M_2 = 10M_\odot$.

k. Waveform tests of black-hole physics. Because black holes are made of pure vacuum gravity, their dynamics can be computed with far greater confidence (if one believes in general relativity) than the dynamics of neutron stars. In particular, numerical relativity experts expect [A-8], in the early 1990s, to compute in detail the waveforms produced in the final stages of coalescence of a binary black hole, as the two holes' horizons get deformed gravitationally, then touch and merge, and the resulting single hole vibrates nonlinearly. This final, coalescence waveform will terminate the inspiral waveform shown in Figure A-3 (b). A detailed agreement between the computed and observed waveforms would simultaneously confirm the existence of black holes in the real universe and test general relativity's predictions for the behavior of gravity in highly nonlinear, dynamical situations.

I. The signal-to-noise ratio required for waveform studies. One might worry that the LIGO detectors will never have good enough signal-to-noise ratio to see the details of the waveforms. On the contrary, if the LIGO is sensitive enough to make detections at all, it will be sensitive enough for waveform studies. This is because to detect so rare an event as a stellar collapse or binary coalescence in the midst of the detector's Gaussian noise will require an amplitude signal-to-noise ratio of 5 or more at both sites; and if the signal-to-noise is high enough to be confident the event was real, that full ≥ 5 signal-to-noise can be used for waveform extraction.

m. The use of waves to probe the large-scale structure of the universe. As we shall see, the coalescence of neutron-star and black-hole binaries is a promising source for detectors of the second or third generation in the LIGO. For such coalescences the waveform signatures (a sinusoid with frequency sweep from low to high) are so clean and the wave strength is so firmly predictable that they could act as a "standard candle" with which to measure the large-scale structure of the universe (the Hubble expansion rate and deceleration parameter) [A-9].²

2. Scientific Payoff from the LIGO Project

From the above discussion we can cull a list of scientific payoffs that might come from the LIGO Project. That list was presented in Section II; and we reproduce it here for ease of reading. The LIGO Project is being designed and managed, so far as possible, in such a way as to maximize the likelihood that some or most of these payoffs will be achieved.

Possible Payoffs for Physics

- The observational discovery of gravitational waves.
- Measurement of the propagation speed and polarization properties of the waves, and from them, the rest mass m and spin S of the graviton which carries the waves: do they agree with general relativity's predictions, $m = 0$ and $S = 2$?
- Verification (by comparing theoretical and observed wave forms) that black holes exist and that their dynamics are as predicted by general relativity. Thereby test general relativity for the first time in the domain of highly nonlinear, dynamic gravity.

Some Possible Payoffs for Astronomy and Astrophysics

- Open up a new window onto the universe, a window that is almost certain to bring surprises and that may bring a revolution comparable to that which came from opening the radio window in the 1950s and 60s.
- Study the behaviors of neutron stars in highly dynamical situations. Thereby extract information about the uncertain physics that governs neutron stars.
- Use the waves from binary coalescences as "standard candles" for the determination of the Hubble expansion rate and deceleration parameter of the universe.

² cf., the paragraph preceding Equation (A.10).

- Detect primordial gravitational waves from the big bang, and from them extract information about the initial conditions and earliest stages of evolution of the universe.

3. Estimates of the Strengths of the Waves at Earth and Comparison with Anticipated LIGO Sensitivities

When we achieve these payoffs will depend, primarily, on when detectors in the LIGO can reach the required sensitivities. The best estimates of the required sensitivities come from astrophysical source-strength calculations. Unfortunately, those calculations, being based on our electromagnetic understanding of the universe, are very uncertain. With the single exception of binary-neutron-star coalescences (see below), for each type of source either (1) the strength of the source's waves for a given distance from earth is uncertain by several orders of magnitude, or (2) the rate of occurrence of that type of source, and thus the distance to the nearest one, is uncertain by several orders, or (3) the very existence of that type of source is uncertain.

The source strength calculations are summarized by the thin curves and lines in Figures A-4a (short bursts), A-4b (periodic waves), and A-4c (stochastic waves). For full details of the assumptions and calculations that underlie these figures and for extensive references to the literature, see Reference [A-1, Section 9.4]. Here we shall give only a brief overview.

a. **Gravitational-wave bursts (Figure A-4a).** Gravitational wave bursts that have been modeled by theorists last for no more than a few thousand cycles, and usually no more than five cycles. We shall describe such a burst by a characteristic frequency f (horizontal axis of Figure A-4a) and by a characteristic dimensionless amplitude h_c which is approximately equal to the amplitude of the waveform oscillations $h_+(t)$ and/or $h_\times(t)$ multiplied by the square root of the number n of cycles that the burst spends near frequency f . (The factor \sqrt{n} accounts for the ability of the detector to amplify the signal by integrating up the cycles.)³

i. *Coalescing neutron-star binaries.* Our one moderately (but not highly) certain source is the coalescence of a neutron-star binary system. That coalescence should produce, during the inspiral phase, a "chirp", with characteristic frequency sweeping upward through the LIGO's band from a few tens of Hertz to 1000 Hz in a time of a few minutes. The characteristic amplitude of the inspiral waves for a binary at a given distance is predicted with confidence and accuracy by general

³ h_c is defined more precisely in Reference [A-1], Equation (31) in terms of optimal signal processing of a gravitational-wave detector's output and an average over source locations.

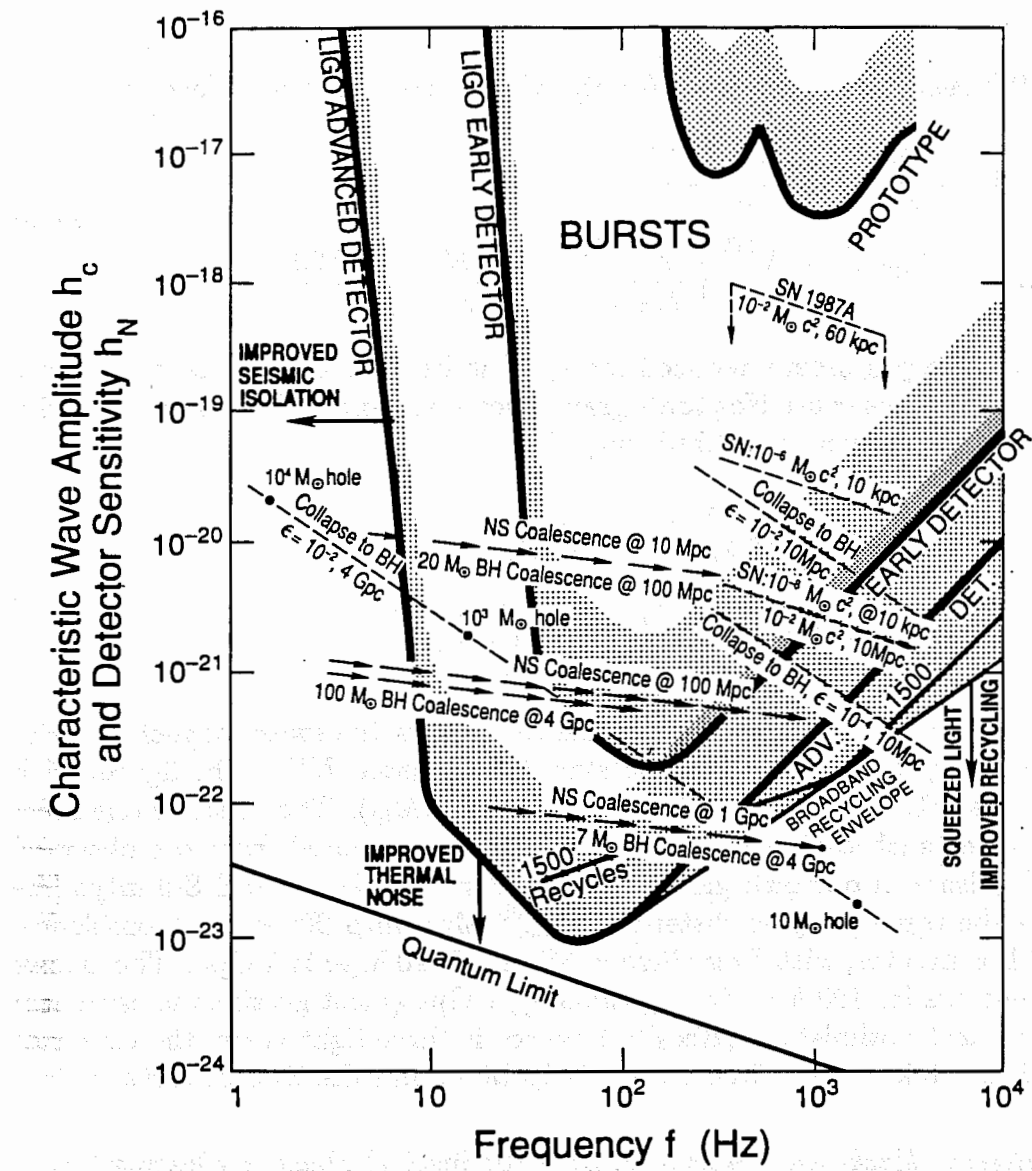


Figure A-4a The estimated characteristic amplitude $h_c \approx h\sqrt{n}$ and frequency f for gravitational-wave bursts from various sources (dashed lines and arrows); and benchmark sensitivities $h_N \approx \bar{h}(f)\sqrt{f}$ (solid curves and stippled strips atop them), for interferometric detectors today and in the proposed LIGO. n is the number of cycles in the burst for which the amplitude is near h and the frequency is near f (see text) and $\bar{h}(f)$ is the square root of the spectral density of the interferometer's noise; (see Equations (A.18), (A.19) and Appendix E). For each detector the solid curve corresponds to the characteristic amplitude of a gravitational wave burst which would be detected with unity signal-to-noise ratio, for optimal polarization and arrival direction. The top of the stippled strip corresponds to the characteristic amplitude of gravitational waves which would give significant detection of bursts occurring as infrequently as three times per year, with random polarizations and arrival directions, in detectors which are free from spurious non-Gaussian noise bursts. Stated more precisely, it corresponds to a confidence level of 90% that the signals are not false alarms caused by statistical fluctuations in Gaussian noise, in a cross-correlation experiment between two detectors at separate sites. The lowest solid line (Quantum Limit) is the limit to the sensitivity curve for the advanced detector set by the quantum limit for the test masses. "Envelope" defines the range of broad-band recycling improvements to the sensitivity, for detectors optimized for each frequency in the range shown. Abbreviations: *SN*—supernova; *NS*—neutron star; *BH*—black hole; $M_\odot c^2$ —one solar rest mass (units for energy carried by waves); ϵ —the fraction of the mass of a black hole emitted in the waves. The assumed distances to the sources include 10 kpc—10 kiloparsecs (center of our galaxy); 50 kpc (Large Magellanic Cloud); 10 Mpc—10 megaparsecs (Virgo cluster of galaxies); 4 Gpc—4 gigaparsecs (the edge of the observable universe).

relativity (Reference [A-1, Equation (46b)], with correction of a $\sqrt{2}$ error):

$$h_c = 0.34 \frac{G(\mu M)^{1/2}}{c^2 r} \left(\frac{\pi GMf}{c^3} \right)^{-1/6} \\ = 5.8 \times 10^{-22} \left(\frac{\mu}{M_\odot} \right)^{1/2} \left(\frac{M}{M_\odot} \right)^{1/3} \left(\frac{100 \text{ Mpc}}{r} \right) \left(\frac{100 \text{ Hz}}{f} \right)^{1/6}. \quad (\text{A.8})$$

Here μ is the binary system's reduced mass, M is its total mass, r is its distance from Earth, and G and c are Newton's gravitation constant and the speed of light. The number of cycles spent near frequency f is

$$n \equiv \frac{f^2}{\dot{f}} = \frac{5}{96\pi} \frac{M}{\mu} \left(\frac{c^3}{\pi GMf} \right)^{5/3} \\ = 3200 \frac{M/4}{\mu} \left(\frac{M_\odot}{M} \right)^{5/3} \left(\frac{100 \text{ Hz}}{f} \right)^{5/3}. \quad (\text{A.9})$$

The arrows at $h_c \sim 10^{-20}$ to 10^{-23} in Figure A-4a show the sweep of such binaries from low frequency to high, for neutron stars (abbreviated *NS* in the figure) with individual masses $1.4M_\odot$ (so $M = 2.8M_\odot$ and $\mu = 0.7M_\odot$). The distance one must look to see three such coalescences per year can be estimated from the observed statistics of pulsars in our own galaxy: Clark, Van den Heuvel and Sutantyo [A-10] compute the three per year distance 100_{-40}^{+100} Mpc with 90 percent confidence. Schutz [A-11] computes, with "very high confidence", 10 Mpc to 1 Gpc. The arrows in Figure A-4a are for 100 Mpc (best estimate), 1 Gpc (most pessimistic estimate) and 10 Mpc (most optimistic). (Recall: 1 parsec is three light years; the center of our galaxy is at 10 kpc, the Virgo cluster is 10 Mpc, and the Hubble distance is 4 Gpc.)

ii. Coalescing black-hole binaries. During the inspiral phase, coalescing black-hole binaries can be described by the same Equations (A.8) and (A.9) as neutron stars; see Figure A-3 (b). However, their final gravitational-wave burst, as their horizons coalesce and the combined hole then vibrates, will be very different. It is this final burst that will be computed with confidence using supercomputers in the next few years and that, by comparison of theory and experiment, should constitute both a firm proof of the existence of black holes and a powerful test of general relativity. Coalescing black-hole binaries should be more rare than coalescing neutron-star binaries. Most likely their event rate is somewhat larger than one per year out to the Hubble distance of ~ 4 Gpc; but they might not exist at all, and they might be as common as several per year at 100 Mpc. The characteristic amplitudes during the inspiral phase are shown in Figure A-4a for distances of 4 Gpc and 100 Mpc and for several masses.

iii. Coalescing binaries as standard candles. Notice that during the inspiral phase of any compact binary the number of cycles spent near a given frequency

(Equation (A.9)) and the characteristic amplitude (Equation (A.8)) depend on the same combination of masses, $\mu^{3/5} M^{2/5}$. Correspondingly, as Schutz [A-9] has pointed out, one can solve directly from the observational data for the distance r to the source. If one can also identify the galaxy or cluster of galaxies in which the source lies and get a redshift from its electromagnetic radiation, one therefrom can determine the Hubble expansion rate of the universe and perhaps get a handle on its deceleration parameter.

iv. Supernovae and other stellar collapses that form neutron stars. The rate of occurrence of supernovae is fairly well determined (about one every 30 years per galaxy as large as our own; several per year in the Virgo cluster). Stellar collapses that produce no bright optical display could be up to ten times more numerous, or might not occur at all. Unfortunately, the strengths of the waves from a stellar collapse at a given distance are highly uncertain. If the collapse is spherical, no waves are produced at all; if it is highly nonspherical, as much as 1 percent of the rest mass of the collapsing stellar core could come off in gravitational waves. Even the characteristic frequency of the waves is uncertain; various plausible models have given frequencies anywhere from a few hundred Hertz to 10 kHz. The characteristic amplitude h_c , as a function of the characteristic frequency f , the total energy ΔE_{GW} carried off in gravitational waves, and the distance r to the source is (Equation (37) of Reference [A-1]):

$$h_c \simeq \left(\frac{3}{2\pi^2} \frac{G\Delta E_{GW}/f}{c^3 r^2} \right)^{1/2} = 2.7 \times 10^{-20} \left(\frac{\Delta E_{GW}}{M_\odot c^2} \right)^{1/2} \left(\frac{1 \text{ kHz}}{f} \right)^{1/2} \left(\frac{10 \text{ Mpc}}{r} \right). \quad (\text{A.10})$$

Figure A-4a shows this characteristic amplitude for collapses that produce neutron stars (labeled "SN") with gravitational-wave outputs of 10^{-2} to 10^{-8} solar masses and distances of our galactic center (10 kpc), the Large Magellanic Cloud (50 kpc), and the Virgo Cluster (10 Mpc). Supernova 1987A in the Large Magellanic Cloud should have produced

$$h \simeq 5 \times 10^{-18} \left(\frac{\Delta E_{GW}}{M_\odot c^2} \right)^{1/2} \left(\frac{1 \text{ kHz}}{f} \right)^{1/2}. \quad (\text{A.11})$$

If the remnant of SN1987A is really a 1/2 ms pulsar as optical observations suggest, then the supernova's collapsing core must have been rotating very rapidly and thus have been highly nonspherical; and correspondingly, ΔE_{GW} was probably $\gtrsim 10^{-3} M_\odot$.

v. Stellar collapses that form black holes. Stellar collapses that form black holes produce short wave bursts with characteristic amplitude given by Equation (A.10) and with characteristic frequency $f \sim c^3/5\pi GM \simeq (1.3 \text{ kHz})(10M_\odot/M)$. The energy carried off can vary from $\Delta E_{GW} \sim 0.1 M c^2$ down to zero, depending on the degree of nonsphericity of the collapse. The wave strengths and frequencies

shown in Figure A-4a are for efficiencies $\epsilon \equiv \Delta E_{\text{GW}}/Mc^2$ of 10^{-2} and 10^{-4} and distances of 10 Mpc (Virgo) and 4 Gpc (Hubble).

b. Periodic gravitational waves (Figure A-4b). Periodic gravitational waves are characterized by the amplitude h of the waveforms' sinusoidal oscillations (vertical axis) and their frequency (horizontal axis). The sources shown in Figure A-4b are all *nonaxisymmetric, rotating neutron stars* in our own galaxy. The number of neutron stars in our galaxy is $\gtrsim 10^8$; but most may rotate so slowly and/or may be so axisymmetric as to be poor gravitational-wave sources. The dependence of the gravitational-wave amplitude on the neutron star's moment of inertia $I_{\bar{z}\bar{z}}$ about the rotation axis, its distance r from earth, its frequency f , and its ellipticity in the equatorial plane $\epsilon = (Q_{\bar{z}\bar{z}} - Q_{\bar{y}\bar{y}})/I_{\bar{z}\bar{z}}$ (where $Q_{j\bar{k}}$ is a component of its quadrupole moment) is (Equation (55) of Reference [A-1])

$$h = 8\pi^2 \sqrt{2/15} \frac{\epsilon I_{\bar{z}\bar{z}} f^2}{r} = 7.7 \times 10^{-20} \epsilon \left(\frac{I_{\bar{z}\bar{z}}}{10^{45} \text{ g cm}^2} \right) \left(\frac{f}{1 \text{ kHz}} \right)^2 \left(\frac{10 \text{ kpc}}{r} \right). \quad (\text{A.12})$$

This amplitude is shown (NS Rot'n) in Figure A-4b for a distance of 10 kpc (the center of our galaxy), a moment of inertia of 10^{45} (all neutron stars should be within a factor ~ 3 of this), and a range of plausible ellipticities, $\epsilon \leq 10^{-5}$. This amplitude is the relevant one for waves emitted at a frequency $f = 2f_{\text{rot}}$ where f_{rot} is the star's rotation frequency. For most neutron stars this frequency should dominate the gravitational-wave spectrum, but there may also be detectable waves at $f = f_{\text{rot}} + f_{\text{prec}}$ where f_{prec} is the star's free precession frequency, and at other frequencies. From the observed spectrum and its changes with time (e.g. in starquakes) one may be able to learn much about the physics of neutron stars.

i. Known pulsars. The large dots in Figure A-4b are known pulsars, for which the amplitudes are uncertain by ~ 5 orders of magnitude because we do not know the stars' ellipticities. For each pulsar are shown (1) a best (but highly unreliable) guess of h based on all present knowledge; and (2) an upper limit, based on the observed slow-down rate of the star's rotation and the (somewhat unlikely) assumption that the slow down is due to gravitational wave emission rather than electromagnetic emission.⁴ Present knowledge permits $h < 10^{-29}$ (off the bottom of the figure).

ii. Gravitational-spindown neutron stars. Each horizontal line (dashed) in Figure A-4b shows the h of the brightest member of a hypothesized population of rotating neutron stars that are spinning down because of gravitational radiation reaction rather than electromagnetic emission [A-12]. Each line is for a fixed mean time τ_B between births of those neutron stars; and the frequency-independent amplitude is ([A-1, Equation (57)])

$$h \simeq \left[\frac{4}{3} \frac{G I_{\bar{z}\bar{z}}}{c^3 R_G^2 \tau_B} \right]^{1/2} \sim 1 \times 10^{-25} \left(\frac{10^4 \text{ years}}{\tau_B} \right)^{1/2}. \quad (\text{A.13})$$

⁴ See Section 9.4.2b of Reference [A-1].

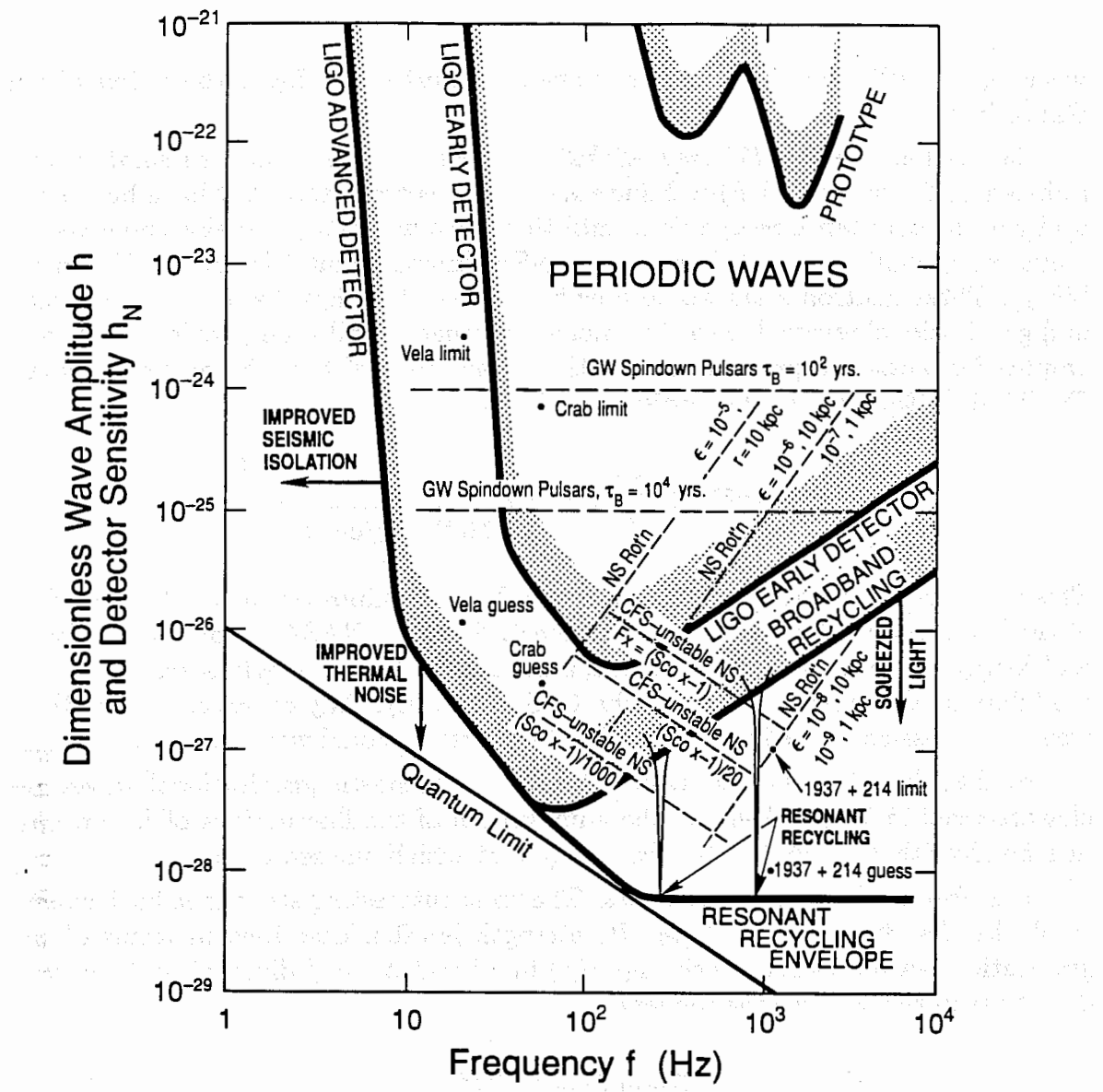


Figure A-4b The estimated dimensionless amplitude h for periodic gravitational waves from various sources (dashed lines and dots); and benchmark sensitivities (solid curves and stippled strips atop them) for interferometric detectors today and in the proposed LIGO. For each detector the solid curve corresponds to the dimensionless amplitude of a periodic gravitational wave, of previously known frequency, which would be detected at unity signal-to-noise ratio after integration for $\hat{\tau} = 10^7$ seconds, for optimal polarization and arrival direction. This amplitude, h_N , is related to the square root of the interferometer's spectral density of strain noise, $\bar{h}(f)$, by $h_N = \bar{h}(f)/\sqrt{\hat{\tau}}$ (see Equations (A.18), (A.19) and Appendix E). The top of the stippled strip corresponds to the dimensionless amplitude of a periodic gravitational wave of previously known frequency, with random polarization and arrival direction, which would give significant detection in 10^7 seconds. Stated more precisely, it corresponds to a confidence level of 90% that the signal is not a false alarm caused by a statistical fluctuation in Gaussian noise.

The lower right-hand part of the advanced detector curve indicates the envelope of peak responses of a resonant recycling detector when it is tuned for optimal operation at each frequency in the range shown. The slanting part of the advanced detector curve above this indicates the response of a broad-band recycling detector. The solid line near the bottom of the figure indicates limits to the advanced detector sensitivity curves set by the quantum limit for the test masses.

where $I_{zz} \sim 10^{45} \text{ g cm}^2$ is the star's moment of inertia and R_G is the radius of our Galaxy's disk.

iii. *Chandrasekhar-Friedman-Schutz instability.* The rightward slanted lines (labeled CFS—unstable NS) in Figure A-4b are neutron stars that have been spun up by accretion from a companion, until they became unstable against nonaxisymmetric perturbations (the “Chandrasekhar-Friedmann-Schutz” [A-13] or CFS instability). These neutron stars would now be sources of X-rays due to their accretion and gravitational waves due to their nonaxisymmetry, and their gravitational-wave amplitudes would be proportional to the square root of their X-ray luminosities, F_X ([A-14]; Equation (53) of Reference [A-1]):

$$h \simeq 2 \times 10^{-27} \left(\frac{300 \text{ Hz}}{f} \right)^{1/2} \left(\frac{F_X}{10^{-8} \text{ erg/cm}^2 \text{s}} \right)^{1/2}. \quad (\text{A.14})$$

This amplitude is shown in Figure A-4b for X-ray luminosities as fractions of that of the brightest candidate for such an object, *Sco X-1*. NASA is considering flying an “X-Ray Large Array” [A-15] which, among other things, would search for X-ray modulations that might be due to the CFS instability. Any observed modulations would be cross-correlated with the outputs of gravitational wave detectors.

c. **Stochastic waves (Figure A-4c).** Stochastic gravitational waves are characterized in Figure A-4c by the amplitude h of the fluctuations of h_+ and h_\times in a bandwidth Δf equal to the frequency f at which one searches.⁵

i. *Primordial gravitational waves.* The most interesting stochastic background would be that from the *big bang*. Its strength is often described in terms of the gravitational-wave energy density $\rho_{\text{GW}}(f)$ in a band $\Delta f = f$ divided by the energy density required to close the universe,

$$\Omega_{\text{GW}}(f) \equiv \frac{\rho_{\text{GW}}(f)}{\rho_{\text{closure}}}, \quad (\text{A.15})$$

which is related to h by (Equation (65) of Reference [A-1])

$$\begin{aligned} h &= \left[\frac{4G}{\pi f^2 c^2} \Omega_{\text{GW}}(f) \rho_{\text{closure}} \right]^{1/2} \\ &= 1.3 \times 10^{-18} \left(\frac{\rho_{\text{closure}}}{1.7 \times 10^{-8} \text{ erg cm}^{-3}} \right)^{1/2} \left(\frac{1 \text{ Hz}}{f} \right) [\Omega_{\text{GW}}(f)]^{1/2}. \end{aligned} \quad (\text{A.16})$$

Lines of constant Ω_{GW} are shown in Figure A-4c. Current speculations about gravitational waves from the very early universe would place Ω_{GW} for the LIGO frequency band in the range 10^{-4} on downward. These waves almost certainly

⁵ cf., Section 9.4.3a of Reference [A-1].

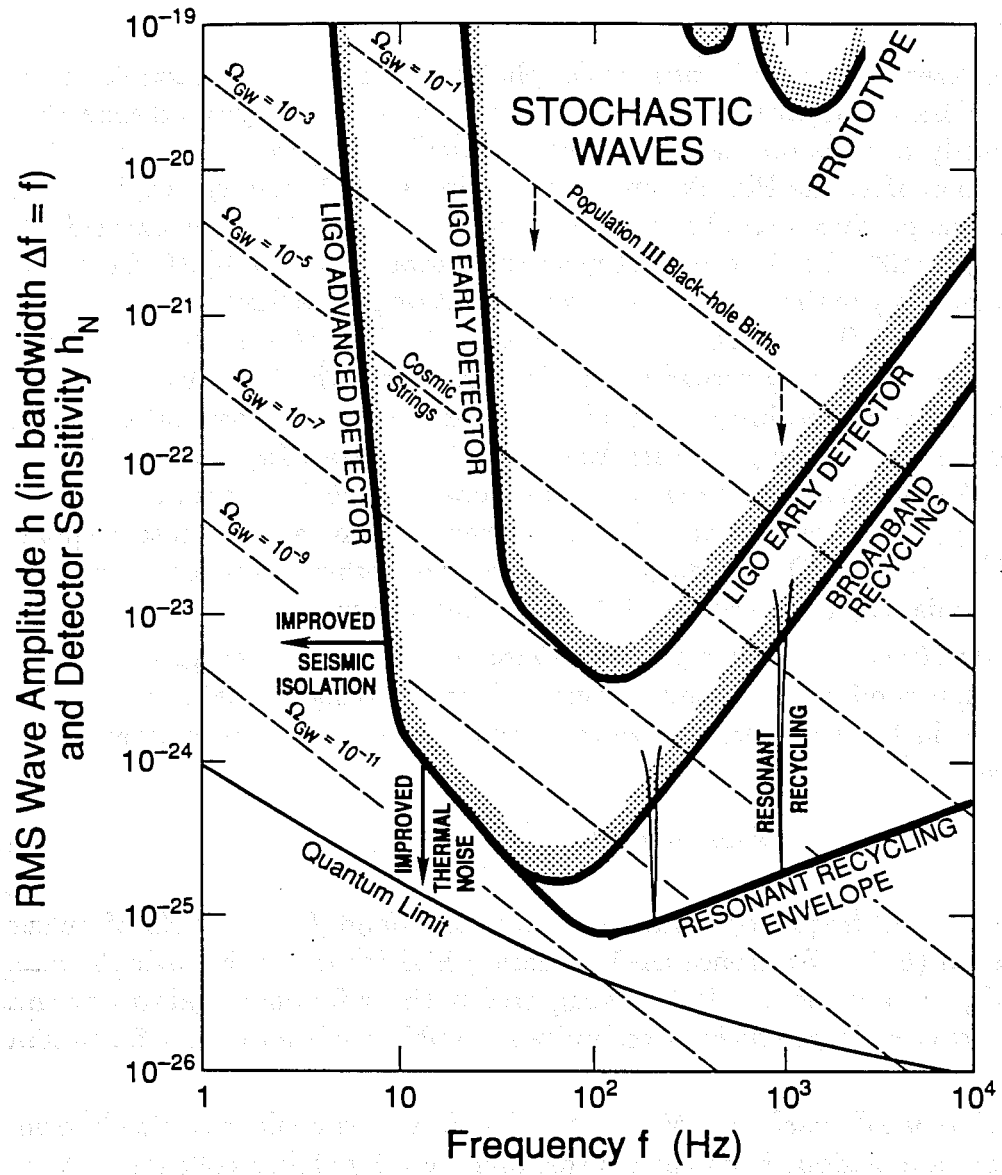


Figure A-4c The estimated rms amplitude h in a bandwidth $\Delta f = f$ for stochastic backgrounds of gravitational waves from various sources (dashed lines); and benchmark sensitivities $h_N \simeq \sqrt{5}h(f)[2f/\tau]^{1/4}[1 + fD/c]^{1/2}$ (see Equation (A.20)) (solid curves and stippled strips atop them) for interferometric detectors today and in the proposed LIGO. For each detector the solid curve corresponds to the rms amplitude in a bandwidth equal to the frequency for a stochastic background which would be detected at unity signal-to-noise ratio in a cross-correlation experiment between two interferometers at different LIGO sites, after integration for $\tau = 10^7$ seconds. The top of the stippled strip corresponds to the rms amplitude in a bandwidth equal to the frequency of a stochastic background which would give significant detection in 10^7 seconds. Stated more precisely, it corresponds to a confidence level of 90% that the signal is not a false alarm due to a statistical fluctuation in Gaussian noise. The lower right-hand part of the advanced detector curve indicates the envelope of peak responses of a resonant recycling detector system when tuned for optimal operation at each frequency in the range shown. Each of the resonance curves above this indicates response of a particular resonant recycling system. The solid line near the bottom of the figure indicates the limit to the advanced detector sensitivity curves set by the quantum limit for the test masses.

are not thermalized at $\sim 3\text{K}$ like primordial photons because they decoupled from matter at the Planck time, and because their interaction with background spacetime curvature is likely to have produced significant nonadiabatic, frequency-dependent amplification soon after the Planck time (e.g., during an inflationary era).⁶ Pulsar timing [A-16] has produced an observational limit $\Omega_{\text{GW}} \lesssim 10^{-6}$ at the exceedingly low frequency $f \sim 10^{-8} \text{ Hz}$, 10 orders of magnitude away from the LIGO frequency band; and the isotropy of the cosmic microwave radiation places limits $\Omega_{\text{GW}} \lesssim 10^{-12}$ at $f \sim 10^{-16} \text{ Hz}$ and $\Omega_{\text{GW}} \lesssim 10^{-8}$ at $f \sim 3 \times 10^{-18} \text{ Hz}$ ([A-17]; Section 9.5.5c of Reference [A-1]). A newly recognized limit comes from the time delay between different paths forming the image of a quasar deflected by the gravitational lens formed by a galaxy intervening between Earth and the quasar; $\Omega_{\text{GW}} < 10^{-8}$ at $f < 3 \times 10^{-18} \text{ Hz}$ [A-18]. Standard versions of inflationary cosmology predict a unique spectrum for $\Omega_{\text{GW}}(f)$ — one which, when combined with the above limits, requires $\Omega_{\text{GW}} \lesssim 10^{-12}$ in the LIGO frequency band. However, other cosmological models permit a primordial Ω_{GW} as large as 10^{-4} in the LIGO band.

ii. Cosmic strings. Another possible source of stochastic background is the decay of nonsuperconducting, cosmic strings. If such strings, created in a GUT phase transition in the very early universe, actually exist, they are estimated [A-19] to produce

$$\Omega_{\text{GW}} \sim 10^{-7} \left(\frac{\mu}{10^{-6}} \right)^{1/2} \quad (\text{A.17})$$

throughout the LIGO frequency band and also in the band $f \sim 10^{-8} \text{ Hz}$ of pulsar timing (Equation (68) of Reference [A-1]). Here μ is G/c^2 times the string's mass per unit length, and a value $\mu \sim 10^{-6}$ is suggested both by fundamental theory and by that value's success in producing from strings possible seeds for galaxy formation [A-19].

iii. Population III black-hole births. Stochastic waves could also result from a superposition of emissions from the deaths, long ago, by stellar collapse to form black holes, of a pre-galactic population of massive stars (“Population III stars”) [A-20]. Such a population has been hypothesized to help explain the observed abundances of the elements in very old stars. Figure A-4c shows an upper limit of $\Omega_{\text{GW}} \lesssim 0.1$ [A-20] in the LIGO band for the plausible strengths of such Population III waves—which, of course, might not exist at all.

d. Sensitivities of detectors in the LIGO

i. Characterization of detector sensitivities. Internal noise in an interferometric detector (discussed in more detail in Section III.A and Appendix B) causes the fractional arm length difference, $\Delta L/L$, as inferred from the detector's readout, to fluctuate stochastically in time. Those fluctuations are characterized statistically by their spectral density $S_{\Delta L/L}(f)$ (see Appendix E) as a function of frequency f .

⁶ See Section 9.4.3d of Reference [A-1] for details and references.

It is conventional in this field to denote the square root of that spectral density by

$$\tilde{h}(f) \equiv \sqrt{S_{\Delta L/L}(f)}, \quad (\text{A.18})$$

and call it the detector's *strain noise per root hertz*. The root-mean-square fluctuations of $\Delta L/L$ at frequency f and in a bandwidth Δf are

$$(\Delta L/L)_{\text{rms}} = \tilde{h}(f)\sqrt{\Delta f}. \quad (\text{A.19})$$

It is these rms fluctuations that compete with the gravitational wave (Equation (A.5a)) in the output data.

When searching for gravitational-wave bursts the relevant bandwidth is $\Delta f \sim f$; and, correspondingly, we plot the "noise amplitude" $h_N \equiv \tilde{h}(f)\sqrt{f}$ in Figure A-4a (solid curves) as a measure of detector sensitivity. A source with characteristic amplitude h_c equal to this noise amplitude and with optimal direction and polarization would produce unity signal to noise in the detector. As a second measure of the sensitivity we plot, as the top of the stippled strips, the quantity $11\tilde{h}(f)\sqrt{f}$. The factor 11 gives a 90% confidence level that wave bursts with random polarization and direction, observed three times per year, are not false alarms because of fluctuations in Gaussian noise (Equation (111) of Reference [A-1]).

When searching for periodic sources, the relevant bandwidth is $\Delta f \simeq 1/\hat{\tau}$, where $\hat{\tau}$ is the integration time; and correspondingly, we plot the noise amplitude $h_N \equiv \tilde{h}(f)\sqrt{1/\hat{\tau}}$ in Figure A-4b (solid curves) as our measure of detector sensitivity, with $\hat{\tau}$ set equal to 10^7 seconds. This corresponds to unity signal to noise for a source with optimal direction and polarization. The top of the stippled strips is $3.8\tilde{h}(f)\sqrt{1/\hat{\tau}}$. The factor 3.8 guarantees 90 percent confidence of detecting a periodic source, with previously known frequency, and with a random direction (Equation (112) of Reference [A-1]). If the period is not known in advance, the sensitivity is reduced by an additional factor 4 using conventional data processing. Computational techniques have been developed [A-21] to regain this factor if the position of the source is known. The analysis problem for sources with both unknown period and unknown position has been formulated but poses a substantial computational challenge.

When searching for a stochastic background one cross-correlates two detectors and, thereby, if one cross-correlates over a band Δf , one achieves an effective bandwidth of about $f/\sqrt{\frac{1}{2}\hat{\tau}\Delta f}$. Assuming that the background is isotropic and polarization independent (as we shall), one must use a direction-averaged sensitivity to describe the detector; this means reducing the sensitivity by a factor $\sqrt{5}$ relative to that for an optimal direction and polarization [A-1]. At low frequencies, waves from all directions excite the two detectors coherently, but at frequencies much above $c/D \simeq 75$ Hz (where $D \simeq 4000$ km is the separation of the LIGO detectors) only waves from a fraction $\simeq c/fD$ of the sky excite them coherently. The result is a

reduction in the amplitude sensitivity by a factor $\simeq \sqrt{1 + fD/c}$. By combining all these effects, we see that an isotropic background, whose rms amplitude in a bandwidth equal to frequency is h , will produce a unity signal-to-noise ratio in the cross correlation of the detectors if $h = h_N$, where

$$h_N \equiv \sqrt{5} \tilde{h}(f) \left[f / \sqrt{\frac{1}{2} \hat{\tau} \Delta f} \right]^{\frac{1}{2}} [1 + fD/c]^{\frac{1}{2}} \quad (\text{A.20})$$

Correspondingly, we plot this quantity in Figure A-4c (solid lines), with $\hat{\tau} = 10^7$ seconds and with cross-correlation bandwidth $\Delta f = f$, except in the case of resonant recycling (see below). The top of the stippled strips is 1.7 times larger than that given by Equation (A.20), corresponding to 90 percent confidence of detection of the isotropic background.

To a great extent, the choice of bandwidth and the details of the search are fixed in the data analysis. Thus, general purpose data can be collected and then analyzed in a variety of ways for a variety of sources. However, this is not entirely true: some special choices of the interferometric optics, e.g., resonant recycling, produce in the "hardware" special narrow-banding of the output, with significant gains of sensitivity at the price of a loss of frequency coverage. These issues are discussed in Appendix C and in greater detail in Section 9.5.3e of Reference [A-1] (especially Figure 9.13).

In Figures A-4 three detector sensitivity curves are shown:

(a) Prototype detector. The upper solid curve is the best sensitivity, as defined above, that has been achieved so far by our prototype detector with 40-meter arms (cf., Section III.B).

(b) LIGO early detector. The middle solid curve in each figure is the sensitivity of a possible detector that might operate soon after the LIGO is completed. The concepts for this detector are described in Section V.A and its estimated noise spectrum $\tilde{h}(f)$ is given in Figure V-3.

(c) LIGO advanced detector. Once the first detector has been operated successfully in the LIGO at something like the sensitivities of Figures A-4a, b, and c, there will follow a succession of generations of ever improving detectors, with the sensitivity levels being pushed continually downward (to smaller h) and leftward (to lower frequencies f). As a rough measure of where this might lead after a few years, we show a sensitivity curve which corresponds to an "advanced detector" whose concept is discussed in Section V.B and whose estimated noise spectrum $\tilde{h}(f)$ is given in Figure V-4.

(d) Further improvements beyond advanced detector. The LIGO "advanced detector" does not represent an ultimate limit on detector sensitivities in the LIGO. Further improvements are likely to occur in several different directions: (1) Improvements in antiseismic isolation are likely to push downward the detectors' low-frequency cutoff (left-pointing arrows in Figures A-4]. (2) Improvements in thermal

noise are likely to produce sensitivity improvements in the frequency band between 10 Hz and 50 Hz (down-pointing arrows in Figures A-4). (3) The “LIGO advanced detector” entails 100 broad-band recyclings of the light in the interferometer (cf., Section V.B and Appendix C). By increasing the number of recyclings, the broad-band sensitivity can be improved at frequencies above 100 Hz (Section 9.5.3(e) of Reference [A-1]); see, for example the sensitivity curve labeled “1500 recycles” in Figure A-4a and the curve labeled “broadband recycling envelope”, which represents the lower envelope of the sensitivities of detectors identical to the “LIGO advanced detector” except for having more recyclings. (4) The envelope can be pushed downward by improvements in mirror reflectivities, together with increases in the number of recyclings. (5) The \sqrt{N} photon shot noise, which is responsible for the limitations on sensitivity above 100 Hz, is actually produced by a superposition of laser light and quantum electrodynamical vacuum fluctuations [A-22]. The vacuum fluctuations enter the interferometer through the beam splitter from the direction of the photodetector (Figure II-1). By injecting, in place of vacuum fluctuations, “squeezed vacuum light” that is phase coherent with the laser, one can reduce the detector’s photon shot noise below the standard, Poissonian, \sqrt{N} level, and thereby improve the broad-band sensitivity in the region $f \gtrsim 100$ Hz [A-22], see Appendix C. (6) When searching for periodic sources or stochastic background one can use “resonant recycling” or “dual recycling” (see Appendix C) to improve the sensitivity over a narrow frequency band (see narrow solid curves in Figures A-4b and A-4c and lines marked “resonant recycling envelope”, which show the envelope of the achievable sensitivities with resonant recycling if one uses 100 W of laser power and mirrors whose losses are 10^{-4} per bounce.)

Quantum mechanics places an ultimate limit on the detector noise level achievable by any of the above techniques (Section 9.5.3(f) of [A-1]):

$$\bar{h}(f) = \left[\frac{2}{\pi^2} \frac{\hbar}{m L^2 f^2} \right]^{1/2} = 4 \times 10^{-26} \left(\frac{1000 \text{ kg}}{m} \right) \left(\frac{1000 \text{ Hz}}{f} \right)^{1/2} \text{ for bursts. (A.21)}$$

This *standard quantum limit* is enforced by the fluctuations in the pressure of laser light on the detector’s masses (analog of “Heisenberg-microscope” enforcement of uncertainty principle). Figures A-4a,b,c show this limit, translated into the form of detector sensitivity (unity signal-to-noise ratio for a source of optimal polarization and direction in Figures A4-a and A4-b, and for an isotropic stochastic background in Figure A4-c). In principle this limit can be circumvented; see [A-23]. However, it might never be circumvented in practice.

e. **Conclusions.** By comparing the source strengths and benchmark sensitivities in Figures A-4, one sees that *the first detector in the LIGO has significant possibilities for detecting waves*:

- It could have detected the initial wave burst from Supernova 1987A if that burst carried more than $\sim 10^{-4}$ solar masses of energy (an amount that would easily be produced if the collapsing stellar core was rotating rapidly enough to produce a 0.5 ms pulsar, as is suggested by observation).
- It could detect the low frequency radiation (<300 Hz) in bursts from supernovae that have rapidly rotating cores and fragment during the collapse at a distance of the Virgo cluster of galaxies.
- It could detect the coalescence of a neutron-star binary out to 30 Mpc distance (three times the distance of the Virgo cluster of galaxies).
- It could detect periodic waves from the Crab pulsar if the wave amplitude exceeds 1/10 of the current limit, which is based on the rate of spindown of the pulsar.
- It could detect a stochastic background of gravitational waves between 50 Hz and 150 Hz, if that background carries more than 2×10^{-7} of the energy required to close the universe. (This is close to the level expected from non-superconducting GUT cosmic strings, if they exist.)

If waves are not detected by the LIGO's first detector, then they probably will be detected by a subsequent detector with sensitivity somewhere between the "early detector" and "advanced detector" sensitivities of Figures A-4. Examples that illustrate the high probability of detection at the "advanced detector" sensitivity are:

- The "advanced detector" could detect a supernova in our galaxy that puts out 10^{-8} solar masses of energy at frequencies of 1 kHz and less, or a supernova in the Virgo cluster that puts out 10^{-2} solar masses at 1 kHz and less.
- It could detect a neutron-star coalescence out to almost 1 Gpc (1/4 the Hubble distance)—within which distance there are expected to be many coalescences per year.
- It could detect the coalescence of equal-mass binary black holes throughout the observable universe, so long as the hole masses lie between 10 and 1000 times the mass of the sun.
- It could detect the Crab and Vela pulsars if they are as strong as the current (highly unreliable) best guess.
- It could detect a stochastic background between 30 Hz and 90 Hz if that background carries an energy exceeding 10^{-10} of the energy required to close the universe.

References

- A-1. Thorne, K. S., "Gravitational Radiation," *900 Years of Gravitation*, S. W. Hawking and W. Israel (eds.), Cambridge University Press, Cambridge, England, pp. 330-458, 1987.
- A-2. Taylor, J. H., and J. M. Weisberg, *Astrophysical Journal*, Vol. 253, pp. 908-920, 1982; J. H. Taylor, *General Relativity and Gravitation*, M.A.H. MacCallum (ed.), Cambridge University Press, Cambridge, England, p. 209, 1987.
- A-3. Eardley, D. M., D. L. Lee, and A. P. Lightman, *Physical Review D*, Vol. 8, p. 3308, 1983; Will, C. M., *Theory and Experiment in Gravitational Physics*, Cambridge University Press, Cambridge, England, 1981.
- A-4. Faller, J. E., P. L. Bender, J. L. Hall, D. Hils, and M. A. Vincent, "Kilometric Optical Arrays in Space," *Proceedings of the Colloquium*, Cargese, Corsica, ESA SP-226, October 23-25 1984.
- A-5. See, e.g., Section 7.2 of Yakov B. Zel'dovich and Igor D. Novikov, "Relativistic Astrophysics, Vol. 2," *The Structure and Evolution of the Universe*, University of Chicago Press, Chicago, 1983.
- A-6. See, e.g., *Serendipitous Discoveries in Radio Astronomy*, K. I. Kellerman and B. Sheets (eds.), National Radio Astronomy Observatory, Green Bank, West Virginia, 1983.
- A-7. Saenz, R. A., and S. L. Shapiro, *Astrophysical Journal*, Vol. 221, p. 286, 1978.
- A-8. See, e.g., Nakamura, T., *Gravitational Collapse and Relativity*, H. Sato and T. Nakamura (eds.), World Scientific, Singapore, p. 295, 1987; also see the discussion and references in Section 9.3.3(e) of Reference 1.
- A-9. Schutz, B. F., *Nature*, Vol. 323, p. 310, 1986.
- A-10. Clark, J.P.A., E.P.J. van den Heuvel, and W. Sutantyo, *Astronomy and Astrophysics*, Vol. 72, p. 120, 1979.
- A-11. Schutz, B. F., "Sources of Gravitational Radiation," *Gravitational Wave Data Analysis*, B. F. Schutz (ed.), Kluwer Academic, Dordrecht, 1989.
- A-12. Blandford, R. D., unpublished work reviewed in equation (57) of Reference [A-1], and associated discussion.
- A-13. Chandrasekhar, S., *Physical Review Letters*, Vol. 24, p. 611, 1970; Friedman, J. L., and B. F. Schutz, *Astrophysical Journal*, Vol. 222, p. 281, 1978.
- A-14. Wagoner, R. V., *Astrophysical Journal*, Vol. 278, p. 345, 1984.
- A-15. Wood, K. S., P. F. Michelson, P. Boynton, M.R. Yearian, H. Gursky, H. Friedman, and J. Dieter, *A Proposal to NASA for an X-Ray Large Array (XLA) for the NASA Space Station*, Stanford, Palo Alto, CA, 1986.
- A-16. Taylor, J. H., *General Relativity and Gravitation*, M.A.H. MacCallum (ed.), Cambridge University Press, Cambridge, England, p. 209, 1987.

- A-17. Grishchuk, L. P., *General Relativity and Gravitation*, M.A.H. MacCallum (ed.), Cambridge University Press, Cambridge, England, p. 86, 1987.
- A-18. Allen, B., *Physical Review Letters*, **63**, 2017, 1989.
- A-19. Vilenkin, A., *300 Years of Gravitation*, S. W. Hawking and W. Israel (eds.), Cambridge University Press, Cambridge, England, p. 499, 1987.
- A-20. Bond, J. R., and B. J. Carr, *Monthly Notices of the Royal Astronomical Society*, Vol. 207, p. 505, 1984.
- A-21. Livas, J., "Broadband Search Techniques for Periodic Sources of Gravitational Radiation," *Gravitational Wave Data Analysis*, B. F. Schutz (ed.), Kluwer Academic, 1989.
- A-22. Caves, C. M., *Physical Review Letters*, **23**, 1693, 1981.
- A-23. Unruh, W. G., unpublished (1982); Caves, C. M., *Quantum Measurement and Chaos*, E. R. Pike (ed.), Plenum, New York, 1987.

APPENDIX B INTERFEROMETER CONCEPTS AND NOISE

This appendix provides some analytic basis and further explanations for the concepts introduced in Section III. The subjects discussed are

1. The theory of the Fabry-Perot Cavity
2. The transfer function of an interferometric gravitational wave detector
3. Basic optical concepts including the RF phase modulation of the optical beams
4. The physical basis of some of the noise terms

There is an extensive published literature on some of these issues [B-1]. We include a discussion of them in the same format and notation as other parts of the proposal for the convenience of the reader.

1. The Theory of the Fabry-Perot Cavity.

In a gravitational wave interferometer each arm's Fabry-Perot cavity is a light storage element. The input mirror, in the interferometer corner station, is partially transmitting with an intensity transmission coefficient of $T_1 = (1 - R_1 - A_1)$. Here A_1 is the mirror's optical absorption and R_1 is its intensity reflection coefficient. The rear mirror, which is in one of the interferometer's end stations a distance L from the input mirror, is coated for high reflectivity, $R_2 = (1 - A_2) \approx 1$, i.e. for negligible transmission. The electric field reflection and transmission coefficients of each mirror, r_1, r_2, t_1, t_2 are equal to the square root of the intensity coefficients; the reflection coefficients have opposite sign depending on whether the incident beam approaches the reflecting surface from the substrate side or from the vacuum.

When an optical electric field pulse of unit amplitude is incident on the cavity input mirror, a set of pulses is returned from the cavity. Figure B-1(a) shows the time series of these pulses. The first pulse, reflected by the input mirror, returns immediately and has an amplitude of r_1 . The second pulse, reflected once by the rear mirror where it is inverted in sign, arrives a time $2L/c$ later and is reduced in amplitude to $r_2 t_1 r_1$ as a result of two transmissions through the input mirror and one reflection off the end mirror. Subsequent pulses undergo reflections from both mirrors and are delayed in time by $n2L/c$ where n is the number of round trips in the cavity. The pulses become progressively smaller and have amplitudes $t_1 t_1 r_2 (r_1 r_2)^n$. The sum of all these pulses is the cavity's "reflected electric field impulse response" (Green's function), and is given algebraically by

$$h_r(t) = \frac{E_r(t)}{E_0} = r_1 \delta(t) - t_1 t_1 r_2 \sum_{n=0}^{\infty} (r_1 r_2)^n \delta\left(\frac{t - 2L(n+1)}{c}\right). \quad (\text{B.1})$$

The response of the cavity for an arbitrary incident electric field is the convolution

of the impulse response with the incident field.

$$E_r(t) = \int_{-\infty}^t h_r(\tau) E_{\text{inc}}(t - \tau) d\tau. \quad (\text{B.1a})$$

If the input light has a sinusoidal dependence, $E_{\text{inc}}(t - \tau) = E_0 e^{i\omega(t-\tau)}$, the convolution gives the cavity's reflection transfer function:

$$\frac{E_r(t)}{E_0} = e^{i\omega t} \left[r_1 - t_1 t_1 r_2 e^{-i2\omega L/c} \sum_{n=0}^{\infty} (r_1 r_2)^n e^{-i2\omega nL/c} \right]. \quad (\text{B.2})$$

Since $|r_1 r_2| < 1$ the series can be summed:

$$\begin{aligned} \frac{E_r(t)}{E_0} &= e^{i\omega t} \left[r_1 - \frac{t_1 t_1 r_2 e^{-i2\omega L/c}}{1 - r_1 r_2 e^{-i2\omega L/c}} \right] \\ &= e^{i\omega t} \left[\frac{r_1 - r_2(r_1^2 + t_1^2) e^{-i2\omega L/c}}{1 - r_1 r_2 e^{-i2\omega L/c}} \right]. \end{aligned} \quad (\text{B.3})$$

Figure B-1(b), a phasor diagram, shows how the convolution produces the reflection transfer function of the cavity. The resultant field is made up from the superposition of the individual waves from the multiple reflections described in Figure B-1(a). The net reflected electric field is the distance from the origin, the center of the circle, to the end point of a trajectory indicated by a progression of dots. The phase of the net reflected field is the azimuthal angle around the circle with zero degrees being to the right. Each trajectory, associated with a specific value of $x = (2\omega L/c) - (2\omega_0 L_0/c)$, begins at the point marked by * which represents the first term in the series: the initial reflection from the input mirror. Along any one trajectory the distance between dots is proportional to the magnitude of the individual reflected components. The angle of each line segment between dots, relative to the horizontal, is the phase of the individual reflected wave. The trajectory labeled $x = 0$ is the resonance case, with cavity length equal to a half-integral multiple of the laser wavelength. Going to the left one sees the individual reflections adding up coherently with the resultant field being almost equal to the incident field but shifted in phase by 180 degrees providing the cavity losses are small. In a low-loss cavity, the component of the field emerging from the cavity is almost twice the incident field. As the cavity is moved away from resonance, $x \neq 0$, by a change in length, the phase of the net reflected wave changes; this phase shift is proportional to an incident gravitational wave. The change in net phase produced by a unit change in cavity length is a maximum at resonance. At large values of x , far from resonance, the phase of the successive individual waves changes rapidly and the phase of the resultant reflected field changes little with a change in x . The entire cavity then behaves just like the input mirror without a cavity behind it.

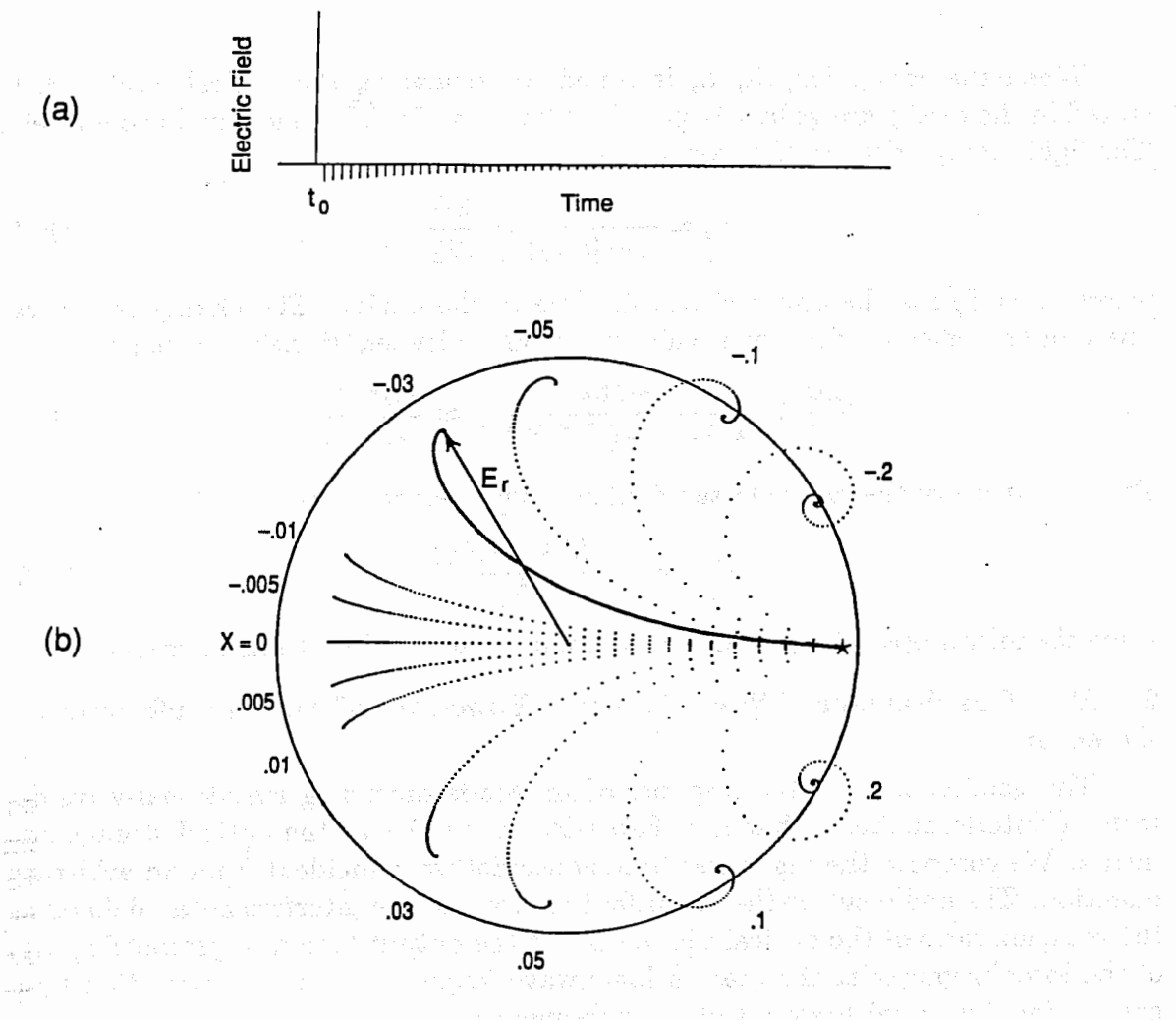


Figure B-1 (a) Time evolution of the optical response of a Fabry-Perot cavity to an input pulse. The figure is drawn for a cavity with an input mirror transmission $T = 0.1$, end mirror reflectivity $R = 1$, and 0.01 loss per pass in the cavity mirrors. The direct reflection from the input mirror occurs at time t_0 . The delayed pulses (with opposite phase from the initial one) correspond to light which enters the cavity, and reflects many times between the mirrors; a small amount of this light is transmitted upon each encounter with the input mirror. (b) Phasor diagram for light reflected from a Fabry-Perot cavity with the same properties, under continuous illumination. The radius of the circle is equal to the amplitude of the input light beam. The direct reflection from the input mirror is the vector (not drawn) from the center of the circle to the star. Each series of dots, originating at the star, represents the superposition of waves which have made different numbers of passes through the cavity, calculated for a given value of detuning between the input light and the cavity's resonance frequency. The length and direction of each line segment connecting adjacent dots corresponds to the amplitude and phase, respectively, of one of these waves. The vector from the origin to the end of the series (E_r) gives the net electric field reflected from the cavity. The vector from the star to the end of the series (not drawn) is the leakage field from the cavity.

When the cavity length, L , is tuned to resonance, the optical electric field stored in the cavity grows by resonant buildup to $\approx 2/\sqrt{T_1}$ times the incident field. The light storage time of the cavity is then

$$\tau_s = \frac{\tau_t}{1 - |r_1 r_2|} \approx \frac{2L}{cT_1} \quad (\text{B.4})$$

where $\tau_t = L/c$ is the one-way transit time in the cavity. The change in optical phase of the reflected field for a unit change in cavity length near resonance is

$$\frac{\Delta\varphi}{\Delta L} \approx \frac{-16\pi}{\lambda_o T_1 [1 - (\frac{A_1 + A_2}{T_1})^2]} \approx \frac{-8\pi}{\lambda_o} \frac{\tau_s}{\tau_t}. \quad (\text{B.5})$$

The amplitude of the net reflected field at cavity resonance is

$$\frac{E_r}{E_0} = 1 - \frac{2(A_1 + A_2)}{T_1} \quad (\text{B.6})$$

when the mirror optical losses are much smaller than the input mirror transmission.

2. The Gravitational Wave Transfer Function of the Interferometric Detector.

This section outlines the response of an interferometric gravitational-wave detector ("interferometer") that uses Fabry-Perot cavities as the optical storage elements. We compute the responses to a sinusoidal wave incident from an arbitrary direction. The end result is the "transfer function" of the interferometer, defined as the complex ratio of the optical phase shift at the output (the antisymmetric port) of the interferometer at the gravitational wave frequency, f , to an excitation by a gravitational wave with amplitude h at frequency f .

In our calculation the interferometer masses are idealized as free (a good idealization above the resonant frequencies of the mass suspensions). The masses then travel along geodesics of the spacetime, which are distorted by the gravitational wave. We perform the calculation in "transverse traceless (TT) coordinates" [B-2]. In these coordinates the masses are forever at rest (x, y, z are constant on their geodesic world lines), and their coordinate separations are forever constant. However, the gravitational wave perturbs the metric of spacetime, thereby altering the masses' physical separations.

One interferometer mass is located at the origin and the other two are situated a distance L on the the x and y axes. The metric tensor is

$$g_{ij} = \eta_{ij} + h_{ij}(t, \vec{r}) \quad (\text{B.7})$$

where η_{ij} is the flat spacetime Minkowski metric and $h_{ij}(t, \vec{r})$ is the metric perturbation produced by the gravitational wave. In TT coordinates h_{ij} is purely spatial ($h_{tt} = 0$), and the components that are relevant to our calculation are [B-2]

$$h_{xx} = h G_{xx} e^{(i\vec{k} \cdot \vec{r} - i\omega t)}, \quad h_{yy} = h G_{yy} e^{(i\vec{k} \cdot \vec{r} - i\omega t)} \quad (\text{B.8})$$

where

$$\begin{aligned} G_{xx} &\equiv \cos 2\Omega (\cos^2 \phi - \sin^2 \phi \cos^2 \theta) - \sin 2\Omega \sin 2\phi \cos \theta \\ G_{yy} &\equiv \cos 2\Omega (\sin^2 \phi - \cos^2 \phi \cos^2 \theta) + \sin 2\Omega \sin 2\phi \cos \theta. \end{aligned} \quad (B.9)$$

Here h is the gravitational wave strain in the plane perpendicular to the propagation direction and \vec{k} is the wave vector,

$$\vec{k} = \frac{\omega}{c} (\sin \theta \sin \phi \vec{x} - \sin \theta \cos \phi \vec{y} + \cos \theta \vec{z}). \quad (B.10)$$

The polarization of the wave is specified by the angle Ω . We can think of $\Omega = 0$ as being the + polarization state and $\Omega = \pi/4$ as being the x state.

Now consider a photon traveling between the central mass and the mass located at $x = L$. The equation $ds^2 = g_{ij}dx^i dx^j = 0$, which expresses the fact that the photon travels at the speed of light, takes the following form, accurate to first order in the wave amplitude h :

$$c \frac{dt}{dx} = \pm (1 + \frac{1}{2} h_{xx}). \quad (B.11)$$

By integrating this equation along the photon's world line as it travels from the central mass at time t_0 to the end mass and back, we obtain for the time t of its return to the central mass

$$t = t_0 + 2\tau_t + \frac{\tau_t h G_{xx}}{2} H(\omega, k_x) e^{-i\omega(t_0 + \tau_t)}. \quad (B.12)$$

Here $\tau_t = L/c$,

$$H(\omega, k_x) = \text{sinc} \frac{1}{2}(k_x L - \omega \tau_t) e^{i \frac{1}{2}(k_x L + \omega \tau_t)} + \text{sinc} \frac{1}{2}(k_x L + \omega \tau_t) e^{i \frac{1}{2}(k_x L - \omega \tau_t)}, \quad (B.13)$$

and $\text{sinc } z = \sin z / z$.

A similar calculation is carried out for the light leaving the central mass at time t_0 that travels back and forth along the y direction. The difference in transit time for the two paths is given by

$$\Delta t = \frac{h \tau_t}{2} [G_{xx} H(\omega, k_x) - G_{yy} H(\omega, k_y)] e^{-i\omega(t_0 + \tau_t)}. \quad (B.14)$$

Because the gravitational wave has $h_{tt} = 0$ and the central mass remains always at rest in the coordinate system, this Δt is equal to the proper time difference as measured by a physical clock riding on the central mass. The optical phase shift at the antisymmetric port of the interferometer due to this time difference is

$$\Delta\phi^{(1)} = \omega \Delta t = \frac{2\pi c \Delta t}{\lambda} \quad (B.15)$$

where λ is the optical wavelength.

For the Fabry-Perot cavity the procedure is applied iteratively to the terms that transit the cavity multiple times. When the cavity is on resonance the unperturbed phase shift for each transit is a multiple of 2π . The perturbed phase shifts are small enough so that $e^{i\Delta\phi^{(1)}}$ is well approximated by $1 + i\Delta\phi^{(1)}$ and can be summed over the infinite series of transits.

After some algebraic manipulation, the transfer function of the recombined Fabry-Perot interferometer is found to be given by

$$\frac{\phi(f)}{h(f)} = \frac{4\pi c\tau_t^2}{\lambda\tau_s} [G_{xx}H(\omega, k_x) - G_{yy}H(\omega, k_y)] \times \left(\frac{e^{i\omega\tau_t}}{1 - 2(1 - \tau_t/\tau_s)e^{i\omega\tau_t} \cos(\omega\tau_t) + (1 - \tau_t/\tau_s)^2 e^{i2\omega\tau_t}} \right) \quad (\text{B.16})$$

The transfer function simplifies at low gravitational wave frequencies, $f < 1/4\pi\tau_t$, and for optimal source direction ($\theta = \phi = 0$) and polarization ($\Omega = 0$). For this case it is

$$\frac{\phi}{h}(f) \approx \left(\frac{8\pi c\tau_s}{\lambda} \right) \frac{1}{(1 + (2\omega\tau_s)^2)^{1/2}} \quad (\text{B.17})$$

At other angles of incidence the angular dependence of the interferometer is primarily determined by $G_{xx} - G_{yy}$.

Figure B-2 shows the amplitude response of an interferometric gravitational-wave detector as a function of the propagation direction of the wave relative to the plane of the detector. The response has been averaged over the wave polarization angle (Ω).

3. Basic Optical Concepts and RF Phase Modulation.

In this section a rudimentary description of the basic optical concepts of an interferometer, such as that shown in Section III, Figure III-1, is given. The analysis makes many simplifying assumptions, the most important being that only a single mode and polarization of the light are considered. The Fabry-Perot cavities are assumed to be close enough to resonance that their phase response can be linearized, and the RF modulation has small enough amplitude that it too can be linearized.

The analysis is intended to show the steps involved in the propagation of the optical wave field from the beam splitter, through the RF phase modulators, reflection from the Fabry-Perot cavities, to recombination at the second encounter with the beam splitter, and finally to the photodiode at the antisymmetric port of the interferometer, which monitors the output signal of the system.

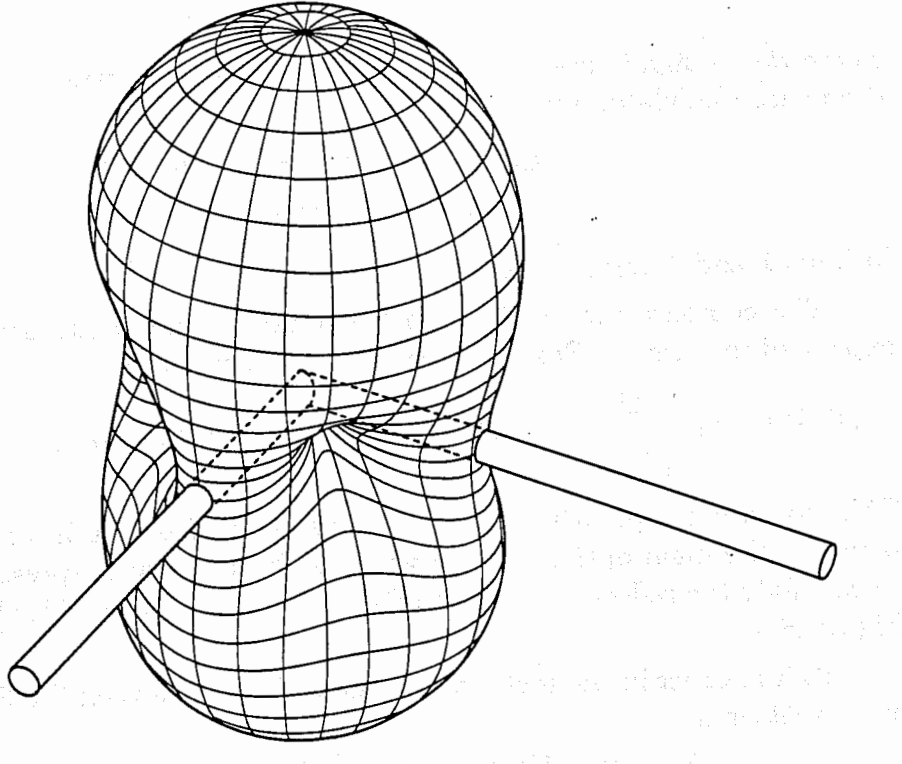


Figure B-2 The angular response pattern of an interferometer with orthogonal arms to unpolarized gravitational radiation. The tubes penetrating the response pattern surface represent the interferometer arms.

The time dependence of the input light at the beam splitter is given by

$$E = E_0 e^{-i\omega t}. \quad (\text{B.18})$$

The two waves leaving the beam splitter are

$$\begin{aligned} E_{10} &= r_s E && \text{the wave launched into arm 1,} \\ E_{20} &= t_s E && \text{the wave launched into arm 2,} \end{aligned} \quad (\text{B.19})$$

where t_s and r_s are the transmission and reflection coefficients of the beam splitter. The two waves next pass through optical phase modulators which are crystals with the property that their optical index of refraction is linearly proportional to an applied modulating field (Pockels effect). The modulating field is chosen to be at a radio frequency (RF), ω_m , sufficiently high that the laser amplitude noise and the noise in the photodetection circuitry at this frequency are close to fundamental limits. The phase modulation adds a time dependent phase to the optical beams given by

$$\phi(t) = \pm \Gamma \sin(\omega_m t), \quad (\text{B.20})$$

where the + sign is used in arm 1 and the - sign in arm 2. The wave fields after the phase modulator are

$$\begin{aligned} E_{11} &= E_0 r_s e^{i(\Gamma \sin(\omega_m t))} e^{-i(\omega t - \delta_{11})} \\ E_{21} &= E_0 t_s e^{-i(\Gamma \sin(\omega_m t))} e^{-i(\omega t - \delta_{21})} \end{aligned} \quad (\text{B.21})$$

in arms 1 and 2, respectively.

The complex exponentials with sinusoidal arguments are most conveniently expanded in terms of Bessel functions of the first kind

$$e^{i\Gamma \sin(\omega_m t)} = \sum_{n=-\infty}^{\infty} J_n(\Gamma) e^{in\omega_m t} \approx J_0(\Gamma) + J_1(\Gamma) (e^{i\omega_m t} - e^{-i\omega_m t}) + \dots \quad (\text{B.22})$$

This expansion explicitly expresses the phase modulation in terms of a set of sidebands of the main optical carrier wave. This is a useful representation with which to calculate the reflection from the Fabry-Perot cavities and is shown graphically in Figure B-3.

To first order in the modulation, the waves incident on the Fabry-Perot cavities are rewritten as

$$\begin{aligned} E_{12} &= E_0 r_s [J_0(\Gamma) + J_1(\Gamma) (e^{i\omega_m t} - e^{-i\omega_m t})] e^{-i(\omega t - \delta_{12})} \\ E_{22} &= E_0 t_s [J_0(\Gamma) - J_1(\Gamma) (e^{i\omega_m t} - e^{-i\omega_m t})] e^{-i(\omega t - \delta_{22})}, \end{aligned} \quad (\text{B.23})$$

in arms 1 and 2, respectively.

The reflection coefficients of the cavities given by Equation (B.3) are rewritten in terms of an amplitude and phase

$$r_j = A_j(\omega_j, \omega_l) e^{i\phi_j(\omega_j, \omega_l)} \quad (\text{B.24})$$

The index j takes on the value 1 or 2 indicating the cavity, ω_j is the resonance frequency of the cavity and ω_l is the frequency of the light. The gravitational wave affects the phases ϕ_j .

The waves after reflection from the cavities become

$$\begin{aligned} E_{13} &= E_0 r_s [J_0(\Gamma) A_1(\omega_1, \omega) e^{i\phi_1(\omega_1, \omega)} + J_1(\Gamma) \\ &\quad \times (A_1(\omega_1, \omega + \omega_m) e^{i\phi_1(\omega_1, \omega + \omega_m)} e^{i(\omega_m t + \delta_{1+})} \\ &\quad - A_1(\omega_1, \omega - \omega_m) e^{i\phi_1(\omega_1, \omega - \omega_m)} e^{-i(\omega_m t - \delta_{1-})})] e^{-i(\omega t - \delta_{13})} \end{aligned} \quad (\text{B.25})$$

in arm 1 and

$$\begin{aligned} E_{23} &= E_0 t_s [J_0(\Gamma) A_2(\omega_2, \omega) e^{i\phi_2(\omega_2, \omega)} - J_1(\Gamma) \\ &\quad \times (A_2(\omega_2, \omega + \omega_m) e^{i\phi_2(\omega_2, \omega + \omega_m)} e^{i(\omega_m t + \delta_{2+})} \\ &\quad - A_2(\omega_2, \omega - \omega_m) e^{i\phi_2(\omega_2, \omega - \omega_m)} e^{-i(\omega_m t - \delta_{2-})})] e^{-i(\omega t - \delta_{23})} \end{aligned} \quad (\text{B.26})$$

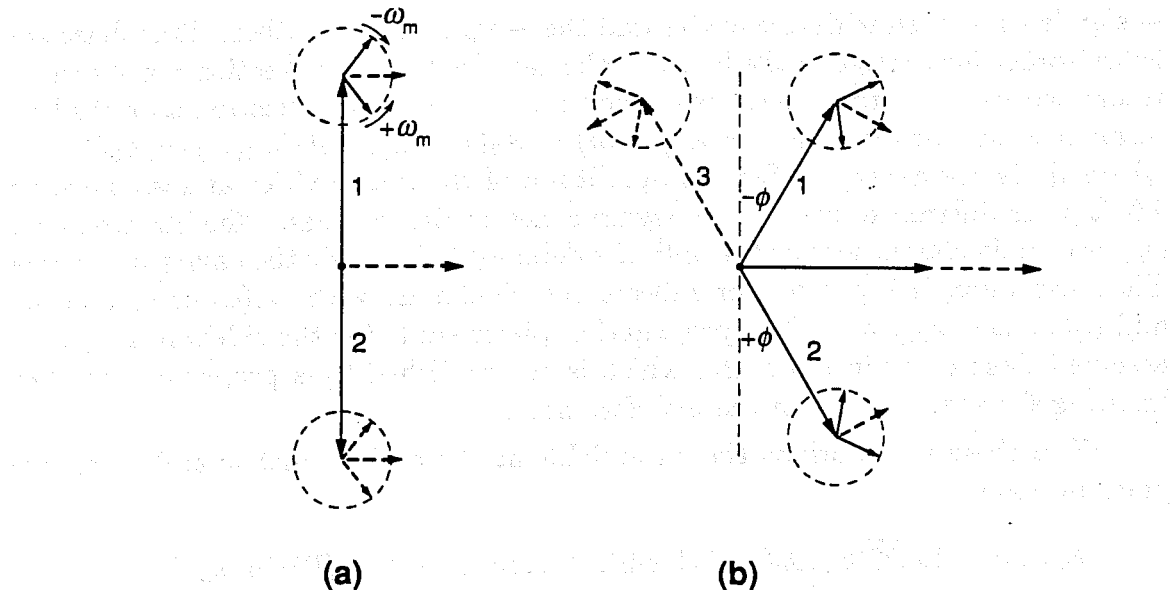


Figure B-3 Phasor diagrams for the optical fields returned by the two cavities of a Fabry-Perot interferometer, drawn in a reference system rotating at the average optical frequency, ω . The labels 1, 2, and 3 each denote a field complex composed of a stationary component (the long vectors), corresponding to a main optical field, and components rotating at $\pm\omega_m$ (the short vectors), which correspond to phase modulation sidebands. In (a) the field at the antisymmetric port is shown when cavities 1 and 2 are on resonance. The resultant field (sum of 1 and 2) is a small oscillating field due to the modulation (the dashed line). The intensity in this case has a small average value and a component at $2\omega_m$ but no component at ω_m . In (b), the interaction with a gravitational wave, produces opposing phase shifts in the two arms of the interferometer, each with magnitude ϕ . The resultant of the fields 1 and 2 is the total field at the antisymmetric output, which has both an average value (the solid line) and an oscillating component (the dashed line). The intensity now includes a term proportional to ϕ at ω_m . An additional set of vectors, labelled 3, depicts the field from arm 2 that appears at the symmetric port. The resultant of 1 and 3 is the total field at the symmetric port. When $\phi \approx 0$, the resultant field is approximately equal to the input field without modulation. This is the field that gets recycled.

in arm 2. Here δ_{1+}, δ_{1-} (or δ_{2+}, δ_{2-}) are small phase shifts that depend on the sum and difference modulation frequencies, respectively, for cavity 1 (or cavity 2).

After reflection from the cavities the waves are recombined at the beam splitter. The wave leaving the antisymmetric port of the splitter, given by $E_{\text{anti}} = t_s E_{13} - r_s E_{23}$ is detected on the output photodetector. The wave leaving the symmetric port of the splitter, given by $E_{\text{sym}} = r_s E_{13} + t_s E_{23}$ returns to the recycling mirror or laser depending on the interferometer configuration.

When the Fabry-Perot cavities are operated close to resonance, $\omega \approx \omega_j$, the reflected wave at the main optical carrier of frequency ω suffers a phase shift of $\pi \pm \phi$ (refer to Figure B-1). Here ϕ is the phase shift due to the gravitational wave; the

+ sign is associated with one cavity and the - sign with the other. The phase shift is first-order insensitive to the losses in the cavities but the reflection amplitudes at resonance are first-order sensitive to the cavity losses. The reflection amplitudes at resonance may be expressed as $A_1(\omega_1, \omega) = A_0(1 + \Delta)$, $A_2(\omega_2, \omega) = A_0(1 - \Delta)$, where A_0 is the average reflection amplitude of the two cavities at resonance and 2Δ is their difference due to any asymmetries in the cavities. The RF frequency, ω_m , is usually chosen so that the optical sidebands fall outside the cavity resonances. Then the cavity's input mirror reflects the sidebands with $A_j(\omega_j, \omega \pm \omega_m) \approx 1$ and $\phi_j(\omega_j, \omega \pm \omega_m) \ll 1$. The propagation phase shifts for the sidebands, $\delta_{k\pm}$, are assumed close to multiples of 2π , which is accomplished by a proper choice of ω_m knowing the path lengths in the interferometer.

With these assumptions the wave fields at the antisymmetric and symmetric ports become

$$\begin{aligned} E_{\text{anti}} &= -2\sqrt{RTE}E_0 \left[J_0(\Gamma)A_0(i \sin \phi + \Delta \cos \phi) - 2iJ_1(\Gamma) \sin \omega_m t \right] \\ E_{\text{sym}} &= -E_0 \left[J_0(\Gamma)A_0(\cos \phi((R+T) + \Delta(R-T)) \right. \\ &\quad \left. + i \sin \phi((R-T) + \Delta(R+T))) \right. \\ &\quad \left. - 2iJ_1(\Gamma)(R-T) \sin \omega_m t \right] \end{aligned} \quad (\text{B.27})$$

where $R = r_s^2$ and $T = t_s^2$ are the intensity reflection and transmission of the beam splitter. These fields are shown in Figure B-3. Terms that oscillate at the modulation frequency are shown with dashed lines.

The intensity is proportional to the envelope of the field given by $I = |E|^2$. The intensity at the output photodetector (antisymmetric port) becomes

$$\begin{aligned} I_{\text{anti}}(t) &= 4RTE_0^2 \left[J_0^2(\Gamma)A_0^2(\sin^2 \phi + \Delta^2 \cos^2 \phi) + 2J_1^2(\Gamma) \right. \\ &\quad \left. + \text{higher order time independent terms} \right] \\ &\quad - 4RTE_0^2 \left[4J_0(\Gamma)J_1(\Gamma)A_0 \sin \phi \sin \omega_m t - 2J_1^2(\Gamma) \cos 2\omega_m t \right. \\ &\quad \left. + \text{higher order time dependent terms} \right] \end{aligned} \quad (\text{B.28})$$

The interferometer output signal is the term associated with $\sin \omega_m t$, which after synchronous demodulation and for $\phi < 1$ is linearly proportional to ϕ , the gravitational wave induced phase shift. The time independent terms make up the background light on the photodetector. They are important in estimating the interferometer's photon shot noise limit. In a completely balanced interferometer with perfect contrast, $\Delta = 0$, the average background intensity becomes $2A_0^2 RTE_0^2(1 - J_0(2\Gamma))$ when $\phi = 0$. The small average intensity remaining in the dark fringe is then entirely due to the modulation: for $\Gamma \ll 1$, it is¹ $2A_0^2 RTE_0^2 \Gamma^2$.

¹ For small values of Γ the first two Bessel functions of the first kind are $J_0(\Gamma) \approx 1 - \Gamma^2/4$ and $J_1(\Gamma) \approx \Gamma/2$.

The intensity leaving the symmetric port becomes

$$\begin{aligned}
 I_{\text{sym}} = & E_0^2 \left[J_0^2(\Gamma) A_0^2 \left(\cos^2 \phi ((R+T) + \Delta(R-T))^2 \right. \right. \\
 & + \sin^2 \phi ((R-T) + \Delta(R+T))^2 \left. \right) \\
 & + J_1^2(\Gamma) (R-T)^2 \\
 & - 4J_0(\Gamma) J_1(\Gamma) A_0 \sin \phi (R-T) ((R-T) + \Delta(R+T)) \sin \omega_m t \\
 & - 2J_1^2(\Gamma) (R-T)^2 \sin 2\omega_m t \\
 & \left. + \text{higher order terms} \right] \quad (\text{B.29})
 \end{aligned}$$

To first order in Γ in the limit where the interferometer is symmetric, ($R = T = 0.5$, $\Delta = 0$, $\phi = 0$), the intensity leaving the symmetric port is $E_0^2 J_0^2(\Gamma) A_0^2$. This is just the input intensity degraded by the cavity loss and a small loss due to the modulation. This intensity is first-order insensitive to the modulation frequency and the gravitational-wave-induced phase shift ϕ . Figure B-3 shows this geometrically.

4. The Physical Basis of Some of the Noise Terms.

In this section we discuss the photon shot noise, the effect of laser frequency noise, the fluctuations in the forward scattering of the residual gas, the thermal noise, and the optical radiation pressure fluctuations that enforce the standard quantum limit. Seismic noise is discussed separately in Appendix D and fluctuating Newtonian gravitational field gradients are calculated in Reference [B-6].

a. Photon shot noise. Photon shot noise, which can be thought of as due to the counting statistics of the photons, dominates the estimated noise budget at high frequencies. The uncertainty in the optical phase and the uncertainty in the number of photons in a specific state of the radiation field are related by the electromagnetic uncertainty relation $\Delta\phi\Delta n > 1$. In the coherent state of single-mode laser light, the photons have a Poisson distribution: $\Delta n = \sqrt{\langle n \rangle}$. The amplitude spectral density of the photon "current" at frequency f is given by

$$\frac{dn}{dt}(f) = \left(2 \left\langle \frac{\delta n}{\delta t} \right\rangle \right)^{1/2} \quad (\text{B.30})$$

The resultant phase fluctuations, expressed as an optical phase amplitude density at the antisymmetric output of the interferometer, is given by

$$\tilde{\phi}_n(f) = \left(\frac{2hc}{\lambda\eta\epsilon P(1-L_{\text{opt}})G_R} \right) \quad (\text{B.31})$$

Here η =detector quantum efficiency, ϵ =optical efficiency of the entire optical train, P =laser optical power, L_{opt} =total optical loss $\geq 4A\tau_s/L$, A =average loss per

mirror, G_R =broad-band recycling power gain $\leq 1/L_{\text{opt}}$ ($G_R = 1$ for no recycling), λ =optical wavelength, h =Planck's constant.

The interferometer's shot noise limited sensitivity expressed as an equivalent gravitational wave strain amplitude, is given from Equations (B.17) and (B.31) by

$$\tilde{h}(f) = \tilde{\phi}_n(f) \left[\frac{\phi}{h}(f) \right]^{-1} \quad (\text{B.32})$$

For a Fabry-Perot interferometer without recycling this becomes

$$\tilde{h}(f) = f_0 \left(\frac{h\lambda}{\eta\epsilon P(1 - L_{\text{opt}})c} \right)^{1/2} [1 + (f/f_0)^2]^{1/2}. \quad (\text{B.33})$$

where $f_0 = 1/4\pi\tau_s$, and τ_s is the light's energy-storage time for each arm's cavity. This result includes a factor of 2 for recovery of the phase information from the RF modulation techniques used in a practical interferometer. The shot noise contribution becomes independent of the storage time at gravitational wave frequencies greater than f_0 , so there is no penalty in using large storage times.

For broad-band recycling, under the optimum assumption that all the optical loss in the system is due to the loss in the cavity mirrors, the shot noise limit is

$$\tilde{h}(f) = f_0^{1/2} \left(\frac{cA}{\pi L} \right)^{1/2} \left(\frac{h\lambda}{\eta\epsilon P(1 - L_{\text{opt}})c} \right)^{1/2} [1 + (f/f_0)^2]^{1/2}. \quad (\text{B.34})$$

In a broad-band recycled system the sensitivity is optimized at a frequency f by choosing the storage time so that $\tau_s = 1/4\pi f$, i.e. so that $f = f_0$.

b. Frequency fluctuations of the laser. Fluctuations in the frequency of the laser can contribute to the interferometer's phase noise in two ways: (i) Frequency fluctuations can couple to a difference in the storage times of the two Fabry-Perot cavities to produce a gravitational-strain noise $\tilde{h}(f) = \tilde{\nu}(f)\Delta\tau/\nu\tau$, where $\tilde{\nu}(f)$ = amplitude spectrum of frequency fluctuations, ν = laser frequency, $\Delta\tau/\tau$ = fractional storage-time unbalance of the two cavities. This noise can be reduced by electronically differencing the cavity locking signals and the antisymmetric output, since frequency noise is common to them. (ii) Frequency noise can introduce relative phase fluctuations between the main beam in a cavity and scattered-light beams, thereby enhancing scattered-light noise. Methods for controlling this are discussed in Appendix F.

c. Noise from the residual gas. The residual gas can produce mechanical noise in the interferometer by damping the suspensions (see below) and by producing acoustic coupling to the outside world. This mechanical noise will be reduced to a negligible level in the LIGO by operating at pressures less than 10^{-6} torr. More serious are fluctuations in forward scattering of light by residual gas in the beam

tubes. The gravitational wave noise due to fluctuations in scattering is calculated by determining the overlap of the forward scattered fields of each molecule in the beam with the main field mode at the photodetector. The scattered field of the individual molecules appears as pulses with different amplitudes and pulse lengths depending on the molecule's position and velocity transverse to the main beam axis. The power spectrum of these pulses, when averaged over all the molecules residing in the beam with a Maxwell distribution of molecular speeds, gives a gravitational-phase noise of

$$\tilde{h}_{\text{total}}(f) = \frac{2^{5/2} \pi^{5/4} \alpha (\omega_{\text{opt}}) \rho_{\#}^{1/2}}{b^{1/2} v_0^{1/2} \lambda^{1/4} L^{3/4}} e^{-\sqrt{2\pi} f(\lambda L)^{1/2}/v_0}. \quad (\text{B.35})$$

This expression assumes that the optical beam radius is the minimum allowed by the length L of an interferometer arm. In this expression α is the polarizability of the residual gas molecule at the optical frequency ω_{opt} , $\rho_{\#}$ is the average number of molecules per unit volume, v_0 is the average thermal velocity of the molecule, λ is the wavelength of the light and b is the number of light beams (for a Fabry-Perot interferometer, $b = 1$). Figure B-4 shows the numerical results for various gas species.

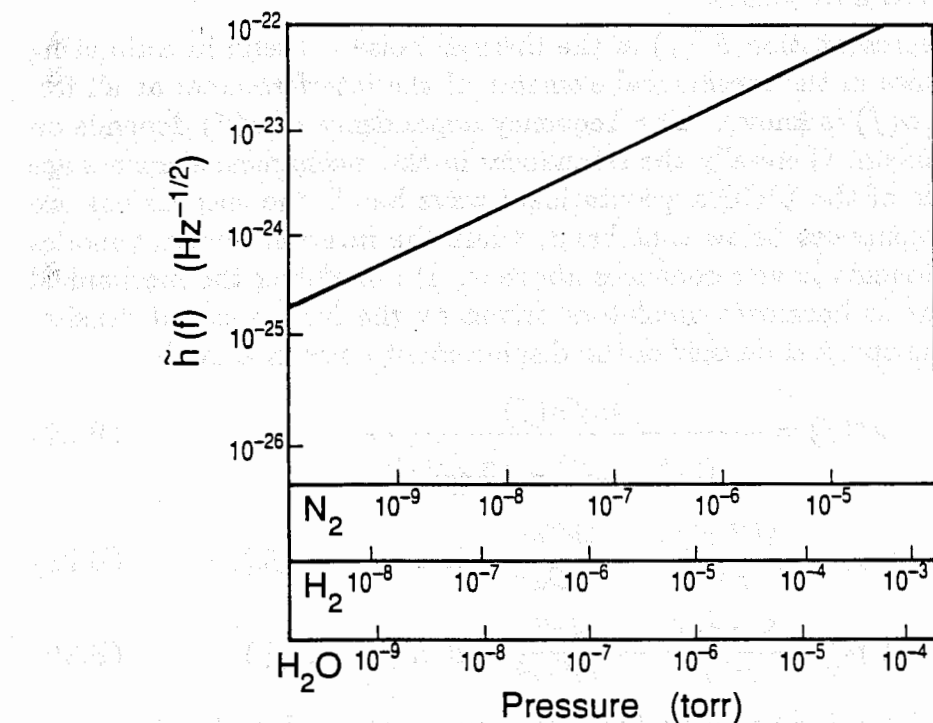


Figure B-4 Noise due to statistical fluctuations in the index of refraction of the residual gas in the LIGO beam tubes, expressed as an equivalent gravitational-wave strain amplitude spectral density $\tilde{h}(f)$. This noise is nearly independent of frequency over the LIGO's frequency band. The contribution to $\tilde{h}(f)$ is plotted as a function of partial pressure for various gas species.

d. Thermal noise. The fluctuation-dissipation theorem of statistical mechanics [B-3] asserts that the damping mechanism in a physical system produces thermally-driven random fluctuations in the system's modes of motion. The theorem is easy to understand in the case of the damping of a mechanical system by residual gas. The damping mechanism is the coherent transfer of momentum from the moving object to the residual gas particles (Doppler friction), while the fluctuations are imparted to the object by the random impacts of the residual gas particles, which are thermalized at temperature T.

The residual gas in the LIGO is specified to be low enough so that it does not contribute to the dissipation of the LIGO's mechanical elements (mirrors, masses, beam splitters, ...). The principal sources of thermal noise are expected to be dissipation in the flexure of the suspension support elements and the internal dissipation of the normal modes of the cavity mirrors.

Thermal noise in a mechanical system can be expressed as

$$F^2(f) = 4kT\alpha(f) \quad \text{dynes}^2/\text{Hz.} \quad (\text{B.36})$$

Here $\alpha(f)$ is the coherent damping coefficient (dynes sec/cm) of the mechanical system when driven at a frequency f .

The spectral representation $F^2(f)$ of the thermal noise is useful in estimating the displacement noise in the mechanical elements of the interferometer at all frequencies, providing $\alpha(f)$ is known. The frequency dependence of $\alpha(f)$ depends on the damping mechanism. Generally the resonances in the mechanical elements are chosen to be outside of the LIGO's gravitational wave band: the suspensions are designed to have resonances below that band, while the internal resonant modes of the optical components have resonances above it. By modeling the mechanical modes of an element as harmonic oscillators driven by the force spectral density, one computes for the spectral density of the displacement noise in a mode

$$x^2(f) = \frac{4kT\alpha(f)}{m^2((\omega_0^2 - \omega^2)^2 + (\frac{\alpha(f)\omega}{m})^2)}, \quad (\text{B.37})$$

$$x^2(f \gg f_0) \approx \frac{4kT\alpha(f)}{m^2\omega^4} \rightarrow \frac{4kT\omega_0}{mQ\omega^4} \quad \text{if } \alpha(f) = \alpha(f_0), \quad (\text{B.38})$$

$$x^2(f \ll f_0) \approx \frac{4kT\alpha(f)}{m^2\omega_0^4} \rightarrow \frac{4kT}{mQ\omega^3} \quad \text{if } \alpha(f) = \alpha(f_0), \quad (\text{B.39})$$

where $Q = m\omega_0/\alpha(f_0)$ = oscillator quality factor, m = the mode's effective mass, $\omega_0 = 2\pi f_0$ = the mode's resonance frequency.

In estimating the equivalent gravitational-strain noise due to the thermal noise from several elements, assumed uncorrelated, the noise power is summed

$$h^2(f) = \frac{\sum_{n=1}^m x^2(f)}{L^2} \quad (\text{B.40})$$

Several subtleties arise in estimating the thermal noise: (i) As indicated, the damping can be frequency dependent so that a simple measurement of the Q of an oscillator is not sufficient to predict the thermal noise off resonance. (ii) In an oscillator under the influence of several restoring mechanisms, such as in a pendulum where both gravity and the elasticity of the suspension fibers apply restoring forces, the Q of the entire mechanical system can be much larger than the intrinsic Q of the suspension fiber material. The Q of the pendulum is larger than the Q of the suspension material by the ratio of the energy stored in the gravitational field to that stored in the elastic deformation of the fiber. (iii) Estimates of the equivalent gravitational-wave strain due to thermal excitation of the normal modes of the test masses and mirrors depend on the overlap integral of the optical mode shape with the mechanical mode of the mass. The test masses and mirrors in the gravitational wave interferometer will usually be cylinders. The modal frequencies and shapes for cylinders with radii comparable to their height have been studied extensively [B-4]. The most perturbative modes are those that cause a net phase shift over a large part of the optical wavefront and are at the lowest frequencies. The lower order flexural modes tend to increase in frequency with cylinder height, while the longitudinal-mode frequencies decrease. Cylinders with ratio of height to radius between 1 to 2 give the best compromise. The modal frequencies are given by $f = \Lambda v_s/a$ where Λ is usually an eigenvalue between 1 and 5, v_s is the shear speed of sound in the material, and a is the radius.

e. Radiation-pressure noise and the standard quantum limit. The laser light, through the momentum it carries, imparts forces to the optical components of the interferometer. Fluctuations in the laser intensity introduce random forces on the cavity mirrors. The intensity fluctuations are symmetric between the two arms of the interferometer so that the resulting noise, which affects the gravitational-wave measurement, cancels except for the mechanical and optical unbalance of the two interferometer arms. The noise due to this source is not expected to be a major factor in the initial LIGO interferometer but will have to be considered in the advanced interferometers in which it may be necessary to amplitude stabilize the laser light by feedback techniques in the gravitational-wave band.

In addition to these symmetric radiation pressure fluctuations, there are pressure fluctuations antisymmetric between the two arms. These are produced by a superposition of the main beam's electromagnetic field and quantum-electrodynamical vacuum fluctuations that enter the interferometer through the dark side of the beam splitter [B-5]. These pressure fluctuations are one source of the "standard quantum" limit for the interferometric gravitational-wave detector and are a macroscopic example of the "Heisenberg microscope." Because the fluctuating radiation pressure is proportional to the correlated product of the vacuum field and the laser field, it varies as the square root of the laser power and fluctuates on time scales of the cavity storage time, a characteristic time for the vacuum electric-field fluctuations to change phase by π relative to the laser field.

Following this model, the rms fluctuating differential force on the pair of mirrors in one cavity is

$$\Delta F = \sqrt{< N >} \left[\frac{h\nu}{L} \right] \quad (\text{B.41})$$

where $< N >$ is the average number of quanta stored in the cavity mode and L is the cavity length. The spectral density of the fluctuating force is determined from

$$(\Delta F)^2 = \int_0^{1/2\tau} F^2(f) df,$$

where

$$F^2(f) = 2\tau(\Delta F)^2 = 2\tau < N > \left(\frac{h\nu}{L} \right)^2,$$

$$\text{and the mean time interval between successive fluctuations is } \tau \approx \frac{2L}{cT},$$

$$\text{the spectral density of the fluctuating force is given by} \quad F^2(f) = \frac{4 < N > (h\nu)^2}{cTL}, \quad (\text{B.42})$$

and we assume negligible losses in the cavity's central mirror, $A \ll T$. Assuming that the mirror masses, m , can be considered free, the force produces a differential motion $x(f) \approx F(f)/m\omega^2$. The average number of quanta in the mode and the laser power are related by

$$< N > = \frac{2LP_{\text{in}}}{cTh\nu}, \quad (\text{B.43})$$

$$P_{\text{in}} = \frac{\epsilon_{\text{opt}} P_{\text{laser}}}{2}, \quad (\text{B.44})$$

where it is assumed that the beam splitter divides the input power evenly between the two cavities. Finally, the equivalent gravitational-strain noise induced in both cavities is

$$\begin{aligned} \tilde{h}(f)_{\text{pressure}} &= \frac{\sqrt{2x(f)}}{L} \\ &= \frac{4(\epsilon_{\text{opt}} P_{\text{laser}} h\nu)^{1/2}}{cTLm\omega^2} \end{aligned} \quad (\text{B.45})$$

The sensing noise (shot noise) in the detection of the interferometer fringe at low frequencies is

$$\tilde{h}(f)_{\text{sense}} = \frac{T}{8\pi L} \left(\frac{h\lambda c}{\eta \epsilon_{\text{opt}} P_{\text{laser}}} \right)^{1/2}. \quad (\text{B.46})$$

The total noise of the interferometer if only due to optical field fluctuations is the incoherent sum

$$h^2(f) = h_{\text{pressure}}^2(f) + h_{\text{sense}}^2(f). \quad (\text{B.47})$$

Since the radiation pressure noise power varies directly as the laser power, while the sensing noise varies inversely as the laser power, there is a minimum in the total noise at a specific, optimum laser power given by

$$\begin{aligned} P_{\text{opt}} &= \frac{T^2 \lambda m c \omega^2}{32\pi \epsilon_{\text{opt}} \eta^{1/2}} \\ &= \frac{L^2 \lambda m \omega^4}{2\pi \epsilon_{\text{opt}} c \eta^{1/2}}. \end{aligned} \quad (\text{B.48})$$

The lower equation reexpresses the optimum input power in terms of the optimum cavity input mirror transmission for a gravitational wave frequency at $\omega = 2\pi f$. This is given by $T_{\text{opt}} = 4L\omega/c$. One contribution to the standard quantum limit for an interferometric detector at a gravitational-wave frequency f is the net pressure and sensing noise at the optimized power with photodetector efficiency $\eta = 1$. The quantum limit is actually $\sqrt{2}$ larger than that net noise, because of a contribution from the uncertainty principle associated with the center-of-mass motion of the mirrors [B-5]:

$$\tilde{h}(f)_{\text{QL}} = \sqrt{4/\pi} \left(\frac{h}{m} \right)^{1/2} \frac{1}{2\pi f L} \quad (\text{B.49})$$

This noise is shown in Section V, Figure V-3 for the initial LIGO interferometer and Figure V-4 for an advanced detector. The quantum noise is not a factor in the initial interferometers but it does set a fundamental limit to the technique and is one of the reasons along with all other sources of random forces that argues for a large arm length L .

There are methods, in principle, for circumventing the standard quantum limit in interferometers but it is not at all clear whether these methods can be realized in practice.

References

- B-1. See, e.g., J.-Y. Vinet, B. Meers, C. N. Man, and A. Brillet, *Physical Review D* **38**, 433 (1988), and references cited therein.
- B-2. See, e.g., L. D. Landau and E. M. Lifschitz, *The Classical Theory of Fields* (Pergamon Press, Oxford, 1962); or C. W. Misner, K. S. Thorne, and J. A. Wheeler, *Gravitation* (W.H. Freeman, San Francisco, 1973).
- B-3. F. Reif, *Fundamentals of Statistical and Thermal Physics* (McGraw-Hill, New York, 1965).
- B-4. J. Hutchinson, *Journal of Applied Mechanics* **47**, 901, (1980); G. McMahon, *Journal of the Acoustical Society of America* **36**, 85, (1964).
- B-5. C. M. Caves, *Physical Review D*, **23**, 1693 (1981).
- B-6. P. R. Saulson, *Physical Review D*, **30**, 643 (1984).

APPENDIX C

CONCEPTS FOR ADVANCED INTERFEROMETERS

1. Introduction

In Section V.B., "Evolution of LIGO Interferometers," we discussed a set of long-range scientific objectives for the LIGO that are based on our current view of the directions in which gravitational-wave physics and astrophysics may develop from LIGO's initial stages. In this appendix we present some of the technical concepts that have been proposed to attain these long-range objectives. The specific plan and emphasis of the research towards these objectives will be strongly influenced by the scientific results and technical experience gained with the initial LIGO interferometer and the prototypes; and also by new interferometer concepts, as they emerge.

2. Review of the Initial LIGO Interferometers

To help clarify the concepts underlying the developing sequence of interferometer designs, we first review the operation of the initial interferometers and then discuss some proposed developments. The initial interferometers will be broadband, Fabry-Perot interferometers [C-1] designed for operation with recycling of light. Initial testing will be done during installation, with the recycling mirror temporarily moved out of the optical train. We begin by reviewing operation in this non-recycling mode.

a. **The basic interferometer: non-recycling mode of operation.** A simplified diagram of the initial interferometer in the non-recycling mode is given in Figure C-1. The laser frequency is stabilized to a separate reference cavity (not shown) and is in resonance with the main 4-km cavities. Monochromatic light from the laser passes, via a 50% beam splitter, through two phase modulators, PM1 and PM2, which are driven in antiphase by a radio-frequency source, to the main cavities. The distant end mirrors of the two cavities have the highest possible reflectivity (about 99.995%). The input mirrors have lower reflectivity, to give a transmission that makes the storage time of light within each cavity comparable to the period of the gravitational waves to be studied. A typical transmission could be about 1%, with scattering and absorption losses much smaller (total loss on the order of 0.005%). When the cavity length is an integral multiple of a half-wavelength of the light there is a large resonant buildup of light intensity within each cavity.

If losses are negligible, the cavity light (labeled C1 and C2) passing back out through the input mirror of each arm has an equilibrium amplitude equal to twice the amplitude of the light coming to the cavity from the laser. It has opposite phase to that of the light (labeled F1 and F2) externally reflected by the front mirror, so interference between the C and F light types leaving each front mirror would give a resultant reflected beam equal in intensity to that of the incident beam.

However, the light within the cavity has traveled back and forth many times (about 100 times, if the transmission is 1%) so any change in cavity length gives a change in optical path, and thence in phase, for the light emerging from the front mirror that is increased (by about 100 times). A gravitational wave that causes the length of one cavity to increase and that of the other to decrease will give phase changes of opposite sign in the light emerging from the two cavities; this difference is detected by the photodiode, D1, after the beams have been brought into interference with one another by the beam splitter [C-2].

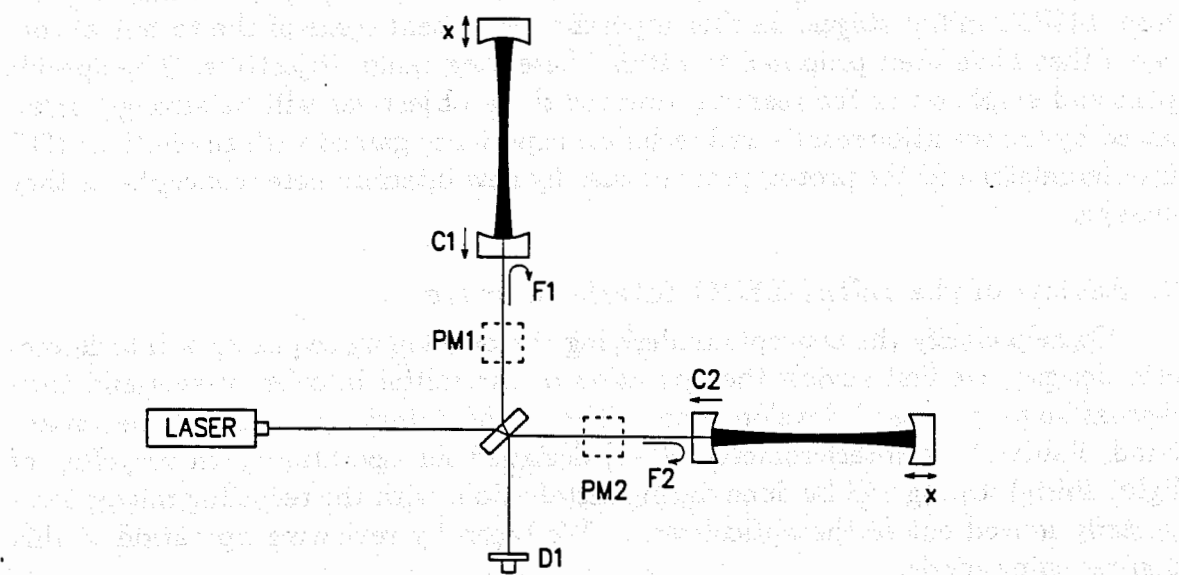


Figure C-1 Schematic diagram of a Fabry-Perot interferometer without recycling. PM1 and PM2 refer to modulation functions that are accomplished either by in-line Pockels cells or Pockels cells in side arms. F1 and F2 denote the wave components arising from direct reflection from the cavity input mirrors. C1 and C2 denote the wave components which arise from leakage of stored light from inside the cavities.

In operation, the distances between the input cavity mirrors and the beam splitter are controlled so that in the absence of a gravitational wave (or of any phase modulation), the light components from the two cavities will destructively interfere with the beam traveling to the photodiode. (The photodiode is at a "dark fringe" that is perhaps at 0.1 percent of the intensity of the input beam). A radio-frequency-modulation technique is used to enhance the sensitivity and linearity of the final phase-difference measurement. Two optical-phase modulators, labeled PM1 and PM2, are driven in antiphase at a frequency near 12 MHz. Any small additional phase deviation between the beams C1 and C2 modifies the symmetry of the intensity waveform at the photodiode, resulting in a signal that is proportional to the phase deviation and has the same frequency as the modulation. The signal is detected by coherent demodulation of the photodiode output. This technique enables the critical optical-phase measurement to be made at a frequency where

laser intensity noise is low and makes it possible to measure optical phase with a sensitivity close to the photon shot noise limit. Servo systems apply differential feedback forces to the test masses in each cavity to hold the interferometer precisely at an intensity minimum, and the feedback forces required to do this are recorded. This provides a measure of the gravitational-wave-induced forces on the test masses.

The phase modulators, PM1 and PM2, could be Pockels cells (electro-optic modulators) as used in some prototype experiments. In the LIGO interferometers, however, we will perform phase modulation at the location of PM1 and PM2 in the optical train by using a nearly transparent beam splitter to reflect a small fraction of the light into and out of an auxiliary side arm (not shown here), where the small modulation is applied by a low-power Pockels cell. This reduces losses in a critical region of the interferometer and avoids the need for Pockels cells that can accommodate the large diameter of the main beam at that point.

To give some idea of the sensitivity of this basic interferometer in non-recycling operation, we note that, for a burst search, the photon-shot-noise limit to strain sensitivity at a mean frequency f , over a bandwidth equal to f , and for optimal source direction and polarization and unity signal-to-noise ratio is given by (see Appendix B, Equation (B.33))

$$h_N = \tilde{h}(f)\sqrt{f} = \left[\frac{\pi \lambda \hbar f^3}{P \eta c} \right]^{\frac{1}{2}} \quad (\text{C.1})$$

Here, $\tilde{h}(f)$ is gravitational-wave strain sensitivity per root hertz at frequency f ; λ is the wavelength of light used; \hbar is Planck's constant/2π; P is the input-light power; η is the quantum efficiency of the photodiode; and c is the velocity of light. If we take the values $f = 1$ kHz, $P = 10$ watts, $\lambda = 514$ nm, and $\eta = 1$, this gives a burst sensitivity of approximately $h_N \simeq 8 \times 10^{-21}$.

In the arrangement just outlined, the photodiode has to monitor only a very small fraction of the total light entering the system. Most of the input light emerges from the other side of the main beam splitter, where constructive interference occurs, and passes back toward the laser. Recycling [C-2] takes advantage of this otherwise wasted light.

b. The basic interferometer: recycling mode of operation. Broad-band recycling is achieved by introducing an additional mirror to return light to the interferometer, and servo controls to maintain correct phase of the recycled light. A schematic diagram of the arrangement is shown in Figure C-2.

In effect, the recycling mirror forms a large Fabry-Perot cavity with the two main cavities and the beam splitter and is arranged so that a resonant buildup of light occurs in this whole system. The technique used to maintain resonance is similar to that employed to lock the laser to a stabilizing resonant cavity [C-3] (as described in detail in Section III-B). The phase difference between light reflected back

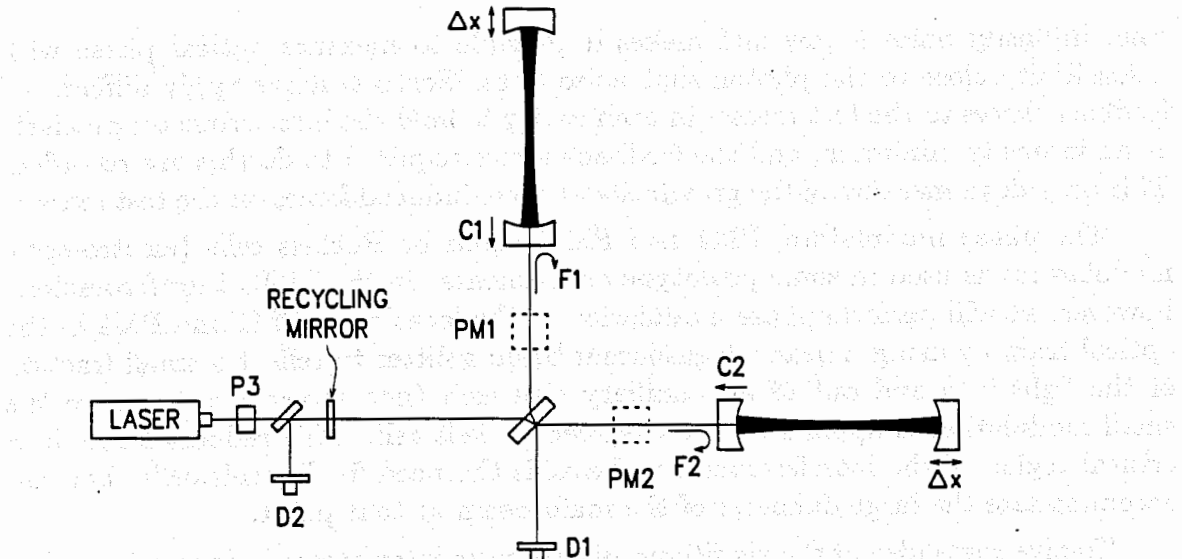


Figure C-2 Schematic diagram of a Fabry-Perot interferometer with broad-band recycling. This change is accomplished by addition of the recycling mirror and the standard modulation and detection optics used for reflection-locking the light to a cavity. Photodiode D_2 is used to monitor and correct the position of the recycling mirror.

toward the laser from the recycling mirror and light transmitted through the mirror from inside the interferometer is monitored by phase-modulating the laser light and detecting interference between the two components with a photodiode, D_2 . On resonance, the phase difference is exactly 180 degrees; this gives a minimum of intensity in the light reflected by the cavity and maximum acceptance of light by the interferometer. If the system is slightly off resonance, a signal at the modulation frequency (the frequency is in the range of 10 to 20 MHz) appears at the photodiode, and measurement of the amplitude of the photocurrent with a phase-sensitive detector gives a correction signal that moves the recycling mirror to the resonance position.

The optimum transmission of the recycling mirror is approximately equal to the total optical loss in the system. We propose to use a variable-reflectivity mirror formed from two closely spaced mirrors with adjustable separation to give partial destructive interference of the reflected light. This will aid the transition from a non-recycling mode of operation to a recycling one, as well as enable the light buildup to be measured.

The phase modulator, P_3 , used for controlling the recycling mirror can be a simple Pockels cell, because losses are less important here; lenses can be used to bring the laser beam to a convenient diameter.

The overall effect of light recycling in this interferometer is to increase the power in the interferometer and thereby improve the photon-shot noise without altering

the wide bandwidth of the system. An additional benefit is that the recycling cavity formed by the whole system will act as a narrow-band, 4-km filter and mode-cleaning cavity for the input laser light.

An estimate of the sensitivity of this type of recycling interferometer may be obtained by assuming the light storage time to be determined by the losses associated with the cavity's end mirrors (of reflectivity R). In this approximation, the burst sensitivity set by photon shot noise is given by Appendix B, Equation (B.34).

$$h_N = \tilde{h}(f)\sqrt{f} = \left[\frac{\hbar\lambda f^2(1-R)}{P\eta L} \right]^{\frac{1}{2}} \quad (\text{C.2})$$

with the same notation as used earlier. Here L is the arm length of the gravitational-wave detector. For a burst search at 1 kHz, an input power of 10 W, an output-mirror reflectivity of 0.99995, and an armlength of 4 km, the sensitivity over a 1-kHz bandwidth, at unity signal-to-noise ratio, becomes $h_N = 3 \times 10^{-22}$.

The number of recycles, and thus the potential sensitivity improvement, can be affected in practice by many factors. These include light losses in the mirrors and beam splitters, and any residual mismatch in the light wavefronts from the two cavities when the wavefronts are combined at the beam splitter. These effects have been taken into account in predicting sensitivities for this type of interferometer in Section V.

c. A resonant recycling interferometer. Another optical technique, "resonant recycling" [C-4], has been devised to obtain high shot-noise sensitivity over a narrow bandwidth. This technique has good prospects of bringing periodic signals from sources such as pulsars within range of the LIGO. It also gives optimum sensitivity in searches for a stochastic background of gravitational waves.

A simplified diagram of a version of the first proposed type of resonantly recycled interferometer is shown in Figure C-3.

The Fabry-Perot cavities are configured as in the broad-band interferometer of Figure C-1. In this system, however, the two cavities are coupled to one another by the mirror M2, which directly reflects light emerging from one cavity into the other cavity. Light from a stabilized laser passes through a 50 percent beam splitter M1 and is directed to the mirror M2 by the two paths shown. The transmission of mirror M2 is chosen to maximize buildup of light within the system formed by the two main cavities.

Mirror M2 couples the two main cavities to one another much more strongly than they are coupled to the input system. If there is a single axial-resonance mode of the same order in each cavity, then the coupling between the cavities has the effect of giving the combined system two modes of oscillation, a symmetrical one in which the light is in-phase in the two cavities, and an antisymmetrical one in which it is out of phase. The degree of coupling between the two cavities is determined by the transmission of their input mirrors, M3 and M3', and also by interference effects

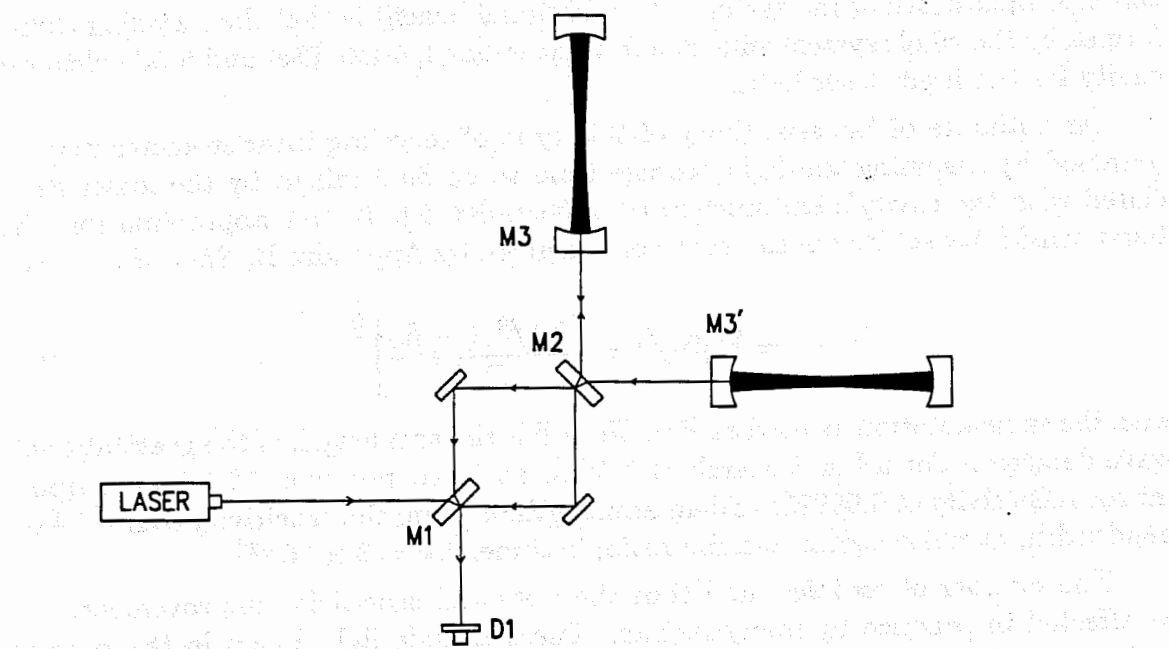


Figure C-3 A Fabry-Perot interferometer incorporating resonant recycling. The input light is divided into two beams at the beam splitter, M1, and directed into the two Fabry-Perot cavities. Light returned from the upper cavity, upon striking the recycling mirror, M2, is mostly deflected into the cavity on the right, and vice-versa. Eventually the stored light leaks out through M2, is recombined at the beam splitter and detected at photodiode D1. The modulation functions are not shown.

in the optical path between these two mirrors. In fact, the space between M3 and M3' acts as a third, shorter, optical cavity. To tune the interferometer to a known gravitational-wave frequency, the transmissions of M3 and M3', and the mirrors' spacing, are chosen so that the frequency splitting between the main symmetrical and antisymmetrical modes of the long cavities is equal to the frequency of the gravitational wave. The system is then adjusted so that the light from the laser is in resonance with the symmetrical mode of the long cavities, and a large buildup of intensity in that mode occurs.

A periodic gravitational wave incident on the system will move the cavity end mirrors and frequency modulate the cavities in such a way that some of the stored laser light is pumped into sidebands that are spaced from the laser frequency by the frequency of the gravitational wave. If one of these sideband frequencies matches an antisymmetrical resonance mode of the coupled-cavity system, there will be a buildup of this sideband component. There is thus both a resonant buildup of the laser light inside the system and also of the signal produced by the periodic gravitational wave.

In a perfectly balanced system, light at the laser frequency, traveling downward from the beam splitter, M1, should undergo complete destructive interference, so

only light from the cavities' antisymmetrical mode should emerge from that direction. That light is the interferometer's output; it is detected by photodiode D1.

This system of coupled cavities can be considered as a mechanical parametric amplifier of the laser light and as driven by the mirror motions induced by the gravitational wave. The total light-storage time in the system can approach one second, so that the buildup can extend over many cycles of the gravitational wave, and a large enhancement of sensitivity can be obtained. The photon-shot-noise-limited sensitivity is improved over that of a non-recycling interferometer by a factor approximately equal to the number of gravitational-wave periods in the light-storage time of the system. More specifically, the light-storage time in the system is determined by the maximum reflectivity, R , of the mirrors at the far ends of the cavities, the photon-shot-noise limit to sensitivity in the case of a search that extends over a measuring time $\hat{\tau}$ and is given for a periodic gravitational wave of known frequency by [C-4]

$$h_N = \left[\frac{\hbar \lambda c (1 - R)^2}{\pi P \eta L^2 \hat{\tau}} \right]^{\frac{1}{2}} \quad (C.3)$$

Here h_N is the amplitude of the periodic wave for unity signal-to-noise ratio and optimal source direction and polarization; the other symbols are as defined earlier. If we take a measuring time of 10^7 seconds, a light power of 10 W, and a mirror reflectivity of 0.99995, this gives a limit to sensitivity at unity signal-to-noise ratio of $h_N \simeq 1 \times 10^{-28}$. This sensitivity is achieved over a bandwidth equal to the reciprocal of the light storage time $\Delta f \simeq (1 - R)C/2\pi L \simeq 0.6$ Hz.

This is an impressive limit to sensitivity; it should be emphasized, however, that there is an assumption that the gravitational-wave frequency is accurately known and that Doppler shift variations in this frequency that are the result of the rotation of the Earth and the motion of the Earth in its orbit are allowed for. The technique is also useful for searches for signals of unknown frequency, over a bandwidth determined by the overall interferometer storage time.

d. A dual recycling interferometer. The two resonances required for a resonant recycling interferometer could also be obtained by adding a second recycling mirror to the output of a broad-band recycling interferometer [C-5]. One possible configuration for such a "dual-recycling" system is shown in Figure C-4. A periodic gravitational wave acting on the system will generate antiphase sidebands in the two Fabry-Perot cavities, which will give an output coming downward from the beam splitter. The second recycling mirror, M4, is arranged to reflect much of this output light back in such a way that a gravitational-wave-induced sideband of the laser light resonates within the effective cavity formed by mirror M4 and the two Fabry-Perot cavities. This gives a buildup of light at both the laser frequency and a gravitational-wave sideband frequency, just as in the earlier resonant recycling system shown in Figure C-3.

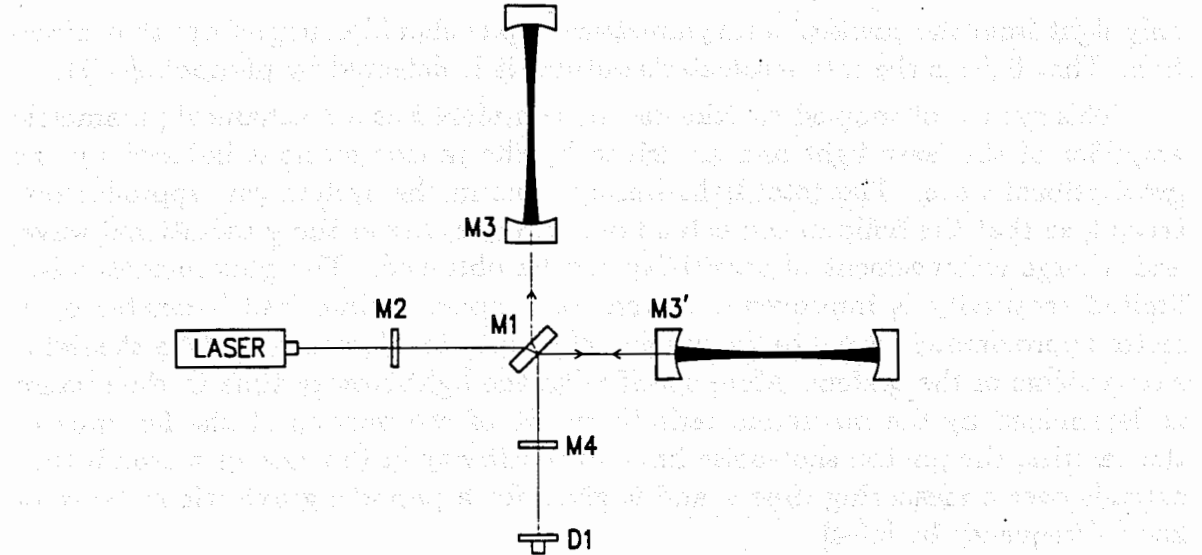


Figure C-4 A Fabry-Perot interferometer incorporating dual recycling. This configuration is identical to the broad-band recycling interferometer of Figure C-2, except for the addition of the output recycling mirror, M4.

In narrow-band operation, the maximum sensitivity of this dual-recycling system is similar to that of the standard resonant recycling configuration. The five mirrors, M1, M2, M3, M3', and M4, in Figure C-4, however, provide more flexibility in adjustment of overall response and a potentially wider bandwidth for a given sensitivity than the three corresponding mirrors, M2, M3, and M3', in Figure C-3; but the losses in the substrates may be higher.

Resonant recycling interferometers, and particularly the dual recycling configuration, are likely to have application more general than investigation of periodic signals. When adjusted for relatively broad-band response, these interferometers can be competitive with broad-band recycling systems for pulse searches, and for some pulse waveforms they can be more sensitive. Also, since reduced shot noise over a narrow bandwidth is obtainable in a resonant system, the system can give higher overall sensitivity in searches for a stochastic background of gravitational radiation (see Section V.B). Furthermore, these dual-recycling techniques are likely to be rather tolerant of optical distortions and figure errors because the exchange of light between the two interferometer arms in resonant recycling systems tends to average out some imperfections.

3. Concepts to Improve the High-frequency Sensitivity of Interferometers by Reducing Photon Shot Noise

a. **Interferometer configurations for high-power operation.** The mirror heating effects described in Section VIII are particularly important in advanced interferometers, which use high-power lasers and recycling to build up the power

within the main cavities to hundreds of kilowatts. The thermal distortions resulting from such high power levels may be reduced by developing low-absorption mirror coatings or by using substrate materials with higher thermal conductivity or with smaller temperature coefficients of expansion or of refractive index. It is also possible to design different optical systems that are less affected by a given heat input. We discuss such optical systems here.

i. *Reduction of thermal effects in optical cavities.* The relative importance of thermal expansion in the substrate and thermal lensing that results from a change of refractive index depends on the material and on the optical configuration. For a typical Fabry-Perot cavity with mirrors on fused quartz substrates and the input light passing through one of the mirrors, the lensing effect dominates over thermal expansion distortion by a factor of approximately 10. One way to avoid thermal lensing in the substrate is to arrange that no light passes through the substrate. The substrate material may then be chosen for high thermal conductivity and low expansion rather than for good optical properties, thereby further reducing thermal effects.

One way to build a cavity with nontransmitting mirrors is by use of a tilted transparent plate within the cavity as a coupling device (see Figure C-5). Light can be fed into or out of the cavity by reflection at one or both surfaces of the plate. The plate can be a thin wedge inclined to the stored beam in such a way that one surface is at Brewster's angle for (in principle) zero reflection while the other surface is at an angle chosen to give the required degree of coupling. In this arrangement, the coupling plate is free of coatings, and thermal effects in it arise only through its intrinsic absorption. The absorption may be reduced by making the plate as thin as is consistent with thermal noise arising from bending modes of vibration. Motion of the coupling plate can introduce phase noise in the output light from the cavity, although the noise amplitude is smaller than that from an equal motion of the main cavity mirrors by a factor close to the cavity finesse.

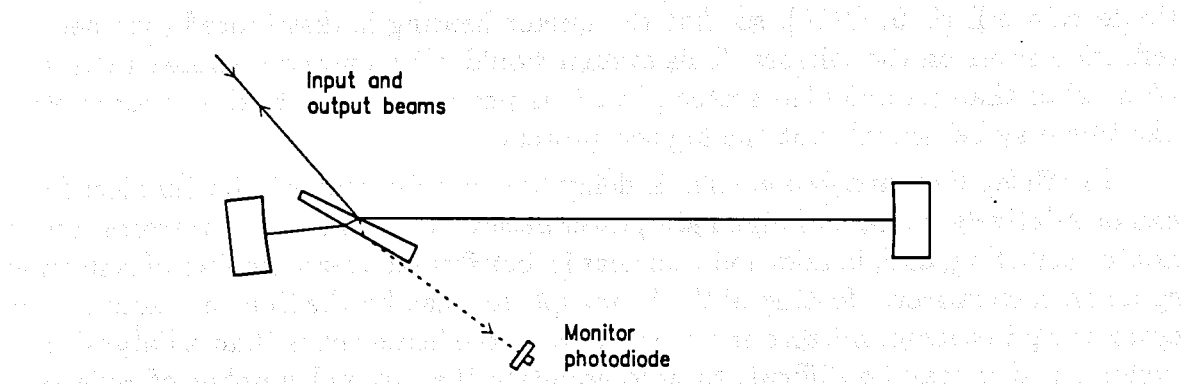


Figure C-5 Schematic of Fabry-Perot cavity with Brewster plate coupling, to avoid transmission of the input and output beams through the mirror substrates. When the cavity is resonant with the input light, a "dark fringe" appears at the photodiode and the output beam is reflected back along the input beam.

The optical action of this coupling system is slightly different from that of a partially transmitting input mirror. With the tilted plate coupler, the plate appears transparent to the input beam when the cavity is off resonance. When precisely on resonance, the plate reflects maximum light back toward the input and there is a minimum of transmitted light leaving the other side of the plate.

ii. Other heating effects in a Fabry-Perot interferometer. If cavity-heating effects are sufficiently reduced by use of tilted-plate couplers or by other means, then heating in the main beam splitter of the interferometer may become a factor limiting operating power. In a conventional symmetric beam splitter, heat absorption in the coating may give lensing and distortion effects similar to those in a cavity mirror.

One way to reduce the absorption is to make a symmetrical beam splitter by using two prisms coupled by the evanescent wave from a beam undergoing internal reflection. The distance between the coupling surfaces is of order one-tenth of the wavelength of the light and can be adjusted by piezoelectric transducers thereby varying the transmission. Beam splitters of this type have been tested by members of the LIGO team and used in interferometers by others [C-6]. By choosing the angles of the prisms so that all the light beams enter and leave the system at Brewster's angle it is possible to avoid requiring any optical coating. Heating then results only from intrinsic losses in the material. In this case, it is difficult to make the light-path length in the material as short as that in a cavity pick-off plate. However, this may not be important since the power at the beam splitter is less than that in the main cavities.

A Fabry-Perot interferometer using these techniques could operate at significantly higher power than is planned for initial LIGO interferometers and may be adequate to handle the power levels anticipated for advanced interferometers. However, if further power-handling capacity is required, enhancements are possible. For example, the cavity in each arm can be folded back and forth between large mirrors, using a configuration like that of a Herriott delay line [C-7, C-8], or of a White multireflection cell [C-9, C-10], so that the mirror heating is distributed over several reflection spots on the mirrors. This system would consume more space in the vacuum tubes than an unfolded system, but it is possible that hybrid interferometers like this may be desirable at the highest powers.

iii. Delay line interferometers. A delay-line interferometer in its simplest form can be relatively tolerant of high light power because the main cavity mirrors can be nontransmitting, and, in addition, the heat is distributed over a number of reflection spots on each mirror. Heating of the beam splitter may be the limiting factor. This system requires larger mirrors and more space in the beam tubes than a Fabry-Perot system, and it may be difficult to accommodate the optimal number of reflection spots. Use of dual recycling may make the system more compact, although this will increase the light power in the beam splitter to a level higher than that in an equivalent single-recycling delay-line or Fabry-Perot interferometer. Like the folded Fabry-Perot, this dual-recycling, delay-line system is a hybrid, incorporating

elements of both Fabry-Perot and delay-line interferometers. Both of these hybrid systems are compromises between power-handling capacity and usage of beam-tube space. If the power levels are so high that they cannot be accommodated by an unfolded Fabry-Perot, then it is likely that each of these hybrid systems could handle approximately equal light power for the same space usage, with a possible slight advantage to the Fabry-Perot that results from the less stringent demands on the beam splitter.

b. Concepts and techniques to increase the laser power

i. *Coherent addition of argon-ion lasers.* Coherent addition of several lasers can be used both to increase the power injected into an interferometer and to increase system reliability. In coherent addition, the primary laser is locked to a frequency-reference cavity. Any number of secondary lasers may be combined with the primary beam by adjusting their phases to match at combining beam splitters. This is accomplished by using the signal generated by the interference between the primary and secondary beams at a photodetector to control the frequency and phase of the secondary laser. The phase of the secondary laser is adjusted for destructive interference at one port while the beam emerging from the other port of the combining beam splitter constructively interferes. This combined beam has the frequency stability of the primary laser but a power equal to the sum of the two lasers. The scheme has been tested by members of the LIGO team and more extensively developed at University of Glasgow [C-11].

ii. *Use of frequency-doubled Nd:YAG lasers.* Frequency-doubled Nd:YAG and other solid-state lasers appear promising as future light sources for operation of LIGO interferometers. They have the potential advantage over argon-ion lasers of higher power efficiency, higher output power, and more stable operation (see Section V-B).

c. *The application of "squeezed states" of light.* Analyses of quantum limits in optical measurements [C-12] have shown that the statistical properties of light can be modified so as to reduce photon shot noise in an interferometer below its usual $\Delta N = \sqrt{N}$ level. The statistical fluctuations in the output of a Michelson interferometer can be regarded as arising from vacuum fluctuations that can enter the system through the normally unused path to the beam splitter. These fluctuations can be modified by injecting squeezed-vacuum light from the unused direction, in place of ordinary vacuum. (The squeezed vacuum is produced by parametrically modulating the ordinary vacuum with a nonlinear medium that is pumped by light phase-coherent with the interferometer's laser light.) In the interferometer the squeezed vacuum superposes on the laser light in such a way as to decrease the photon shot noise in the interferometer's output, while increasing the difference in light-pressure fluctuations in the two arms. Thus, this squeezed vacuum technique has the same effect on noise as increasing the power of the input laser.

Squeezed-light techniques show promise, but also have some limitations. Any

optical losses in the interferometer arms and in other key areas can introduce statistical fluctuations that are not reduced by the squeezing procedure and which may, in some situations, outweigh the potential gains. In particular, when narrow-band resonant and dual-recycling techniques are pushed to the limit where mirror losses prior to detection are dominant, squeezing techniques are unlikely to give any advantage. However, squeezing techniques are complimentary to broad-band recycling: in principle, the two operating together can reduce an interferometer's noise over broad bands to that of the resonant recycling envelope in Figure A-4b.

We do not plan near-term development of squeezed-light techniques in the LIGO program because the major advantages seem likely to be further in the future than do those from some of the other interferometer developments outlined above. However, expertise in squeezed-light experimental techniques exists at Caltech and MIT (H. J. Kimble and H. Haus groups); so when it becomes appropriate to develop squeezed-light interferometers for the LIGO, the team will be well positioned to do so.

4. Concepts to Improve the Low-frequency Performance

The initial LIGO interferometer will use relatively simple, passive-isolation systems effective above a few tens of Hz. Current astrophysical estimates suggest that the gravitational-wave signals that are strongest in terms of LIGO signal-to-noise ratios, are likely to occur toward the lower frequencies (see Figure A-4). The extension of operation downward in frequency is thus a major goal for the evolution of the LIGO and has had a substantial influence in the conceptual design of the facilities. We discuss here two concepts that will improve the sensitivity at lower frequencies.

a. **The seismic-monitor interferometer and its developments.** We plan to enhance performance at lower frequencies by adding an auxiliary interferometer [C-2] to monitor relative motions of the pendulum suspension points and, by feedback, to cause one of the points to track the longitudinal motion of the other. This arrangement is shown schematically in Figure C-6. Two unequal-arm Michelson interferometers sense relative motions of the suspension points of the test masses at the two ends of each 4-km arm. At frequencies above the 1-Hz pendulum resonance, the suspension point moves more than the suspended test mass. Therefore, even a single-bounce interferometer with relatively low-sensitivity can provide useful suspension-point signals. The signals from this interferometer will be monitored and will provide feedback to magnetic transducers driving the suspension points for the test masses that are remote from the corner station. This will reduce vibration-induced motions of the suspension points by a factor of 100 or more in the LIGO frequency range. Because of the isolating effect of the wire suspensions, reduction of this seismic noise does not affect the gravitational-wave signal as measured by the test masses.

Although the seismic interferometers shown are single-pass Michelson inter-

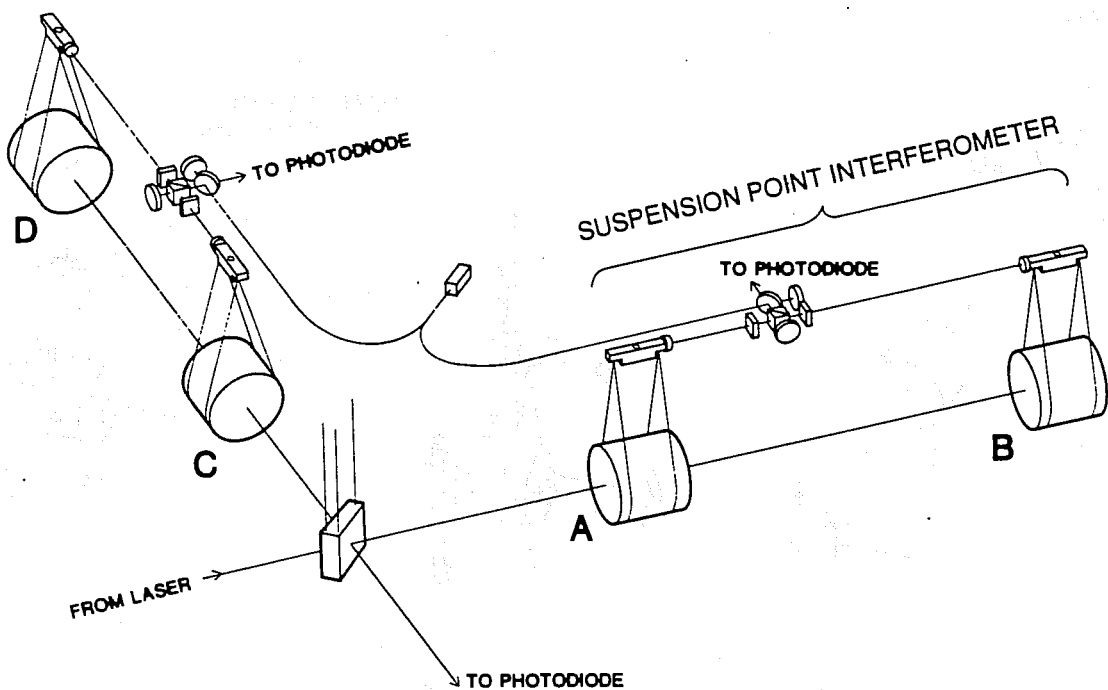


Figure C-6 Schematic representation of a suspension-point interferometer. A stabilized low-power laser excites two unequal-arm Michelson interferometers—one for each Fabry-Perot cavity. Each interferometer senses changes in the separation of the suspension points for the test masses in the associated cavity. The suspended test masses and beam splitter of the main interferometer are shown for context.

ferometers, the optical performance of the system can be improved by forming Fabry-Perot cavities between the suspension points. In either configuration, a lens, omitted from the diagram for simplicity, is used to form a cats-eye retroreflector with each small suspension-point mirror, making the system insensitive to small misalignment of the mirrors.

b. **An active seismic-isolation system.** A significant improvement in seismic isolation can be achieved by adding active control to a good passive-isolation system. Several concepts that use a well-isolated mass as an inertial reference in a feedback system to control the motion of a point of support have been proposed by gravitational-wave research groups [C-2, C-13, C-14, C-15]. A specific concept is shown schematically in Figure C-7.

Two basic ideas are used in this concept to achieve a good approximation to an inertial mass. The first is that the well isolated suspended test masses are the primary inertial reference for the feedback system. The second is that the feedback is arranged to null the motion of the point of support relative to the test mass by application of forces to the *point of support*. By this process the motion of the test mass relative to inertial space is reduced since the feedback forces on the point of support will tend to cancel the external disturbing forces. This “bootstrapping”

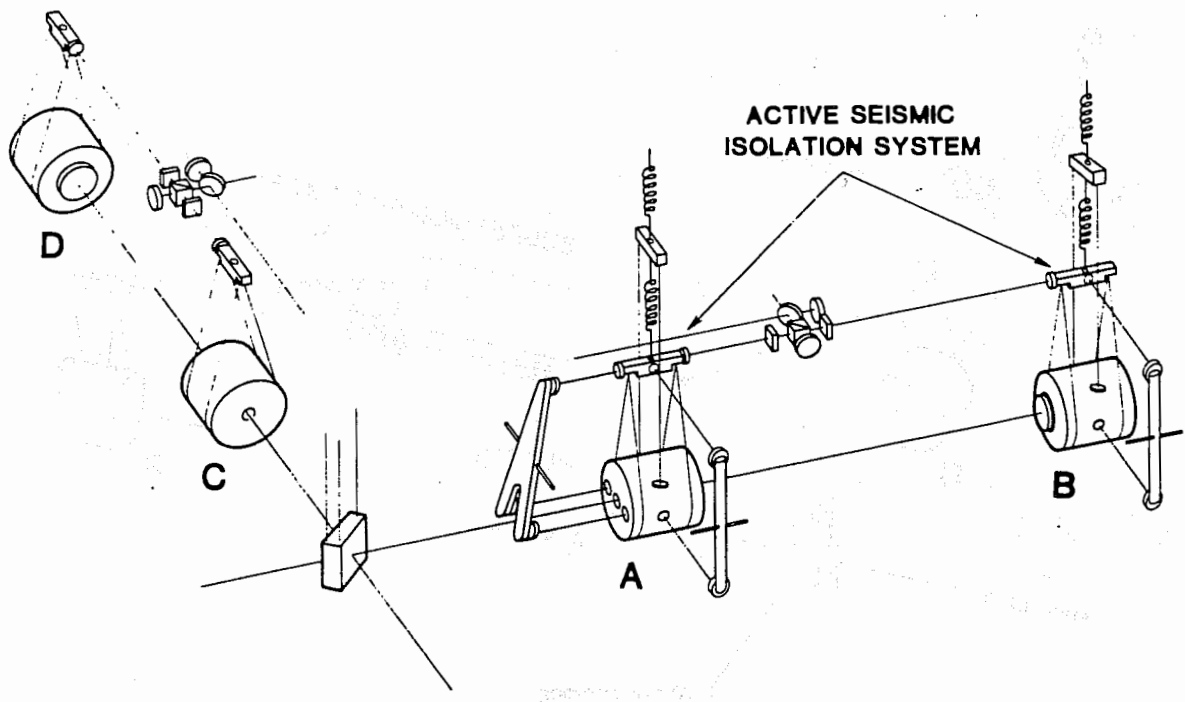


Figure C-7 Sketch of test mass suspension concept for extending interferometer operation to low frequency. An active anti-vibration guard system is shown for test masses A and B. The suspension block of the master test mass A is driven to track the longitudinal and sideways motions of the mass, using monitoring signals from auxiliary interferometers. The upper support piece, from which the main suspension block hangs by a spring, is driven to track the vertical motions of the test mass [C-16], using vertical-monitoring laser beams. Control of sideways and vertical motions of the effective suspension points of slave mass B is similar, but the longitudinal position of mass B is driven to track that of master mass A by the suspension point interferometer. The guard systems for test masses C and D are similar to those for A and B, respectively, but are not shown in the figure.

procedure is referred to as an active guard system. It realizes an inertial mass to a good, but finite, precision.

A third concept is now introduced, to further improve precision. The suspension points for the four test masses in the interferometer are tied together optically, so that if any residual disturbance does leak through the guard system, it will affect all the masses in the same way and cancel out motions in the directions of the optic axes. This is done by treating the test mass motions along and transverse to the optic axis by different techniques. The motions of the point of support relative to the test mass in the *transverse* directions are measured by two auxiliary interferometers which refer the motion of the point of support and the test mass to a well isolated reference arm. The reference arm is mounted on a long period torsional support so that it is isolated from rotational disturbances. The difference in the separations measured by the two interferometers thereby becomes proportional to the relative motion of the test mass and its point of support. The feedback to the

point of support is derived from this signal and applied locally to each test mass suspension.

Motions along the optic axis are dealt with globally. Test mass A is regarded as the "master" which defines an inertial frame for motions of all masses along the optic axis. The suspension points of the other masses are slaved to the "master" using signals provided by the main and seismic interferometers. Relevant degrees of freedom of each test-mass suspension are controlled as follows:

i. *Mass A: the master mass.* Translational motion in longitudinal, horizontal, and vertical directions is free, aided by the active guard system shown in Figure C-7. (Rotational degrees of freedom for this and the other masses are separately controlled by an automatic alignment system.)

ii. *Mass B: a slave mass.* Mass B has longitudinal motion of the suspension block forced to track the motion of the suspension block of mass A using the seismic-monitor interferometer. Transverse motions of the mass in horizontal and vertical directions are made free by the active guard system.

iii. *Mass C: the "secondary master" mass.* Mass C acts similarly to mass A, but very-low-frequency components (0 to 1 Hz, approximately) of horizontal and vertical transverse mass position are forced to track the position of the main interferometer beam by using signals from additional monitors.

iv. *Mass D: a slave mass.* This mass features suspension-block control similar to that of slave mass B, with longitudinal position slaved to mass C by the seismic-monitor interferometer. Additional high-precision control of the longitudinal position of the mass makes the main interferometer arms very closely equal (plus or minus an integral number of half-wavelengths).

The overall effect is to simulate a rigid, inertial, optical table, 4 km on a side, from which the masses are suspended.

Reliable prediction of the performance of an isolation system of this type is difficult since, at the large attenuation factors involved, leakage of seismic noise is likely to be determined by complex nonlinear coupling mechanisms and by limitations of servo-loop gain set by mechanical resonances. Active-isolation systems are expected to be an essential concept in bringing the performance of advanced LIGO interferometers within reach of the fundamental limits imposed by natural gravity-gradient fluctuations present near the surface of the Earth and by the quantum limit for the test masses.

References

- C-1. R.W.P. Drever, G. M. Ford, J. Hough, I. M. Kerr, A.J . Munley, J. R. Pugh, N. A. Robertson, and H. Ward, "A Gravity-Wave Detector Using Optical Sensing," *Proceedings of the Ninth International Conference on General Relativity and Gravitation* (Jena 1980), ed. E. Schmutzler (VEB Deutscher Verlag der Wissenschaften, Berlin, 1983), 265.

- C-2. R.W.P. Drever, J. Hough, A. J. Munley, S.-A. Lee, R. Spero, S. E. Whitcomb, J. Pugh, G. Newton, B. Meers, E. Brooks III, Y. Gürsel, "Gravitational-Wave Detectors Using Laser-Interferometers and Optical Cavities," *Quantum Optics, Experimental Gravity, and Measurement Theory* ed. P Meystere and M.O. Scully, (Plenum Publishing, 1983), 503.
- C-3. R.W.P. Drever, J. L. Hall, F. V. Kowalski, J. Hough, G. M. Ford, A. J. Munley, and H. Ward, *Appl. Phys. B31*, 97, (1983).
- C-4. R.W.P. Drever, "Interferometric Detectors for Gravitational Radiation," *Gravitational Radiation*, NATO Advanced Physics Institute, Les Houches, ed. N. Deruelle and T. Piran, (North Holland Publishing, 1983), 321.
- C-5. B. J. Meers, *Phys. Rev. D38*, 2317 (1988).
- C-6. M. Daehler and P. A. Ade, *Journal of the Optical Society of America*, **65**, 124 (1975).
- C-7. D. R. Herriott and H. J. Schulte, *Appl. Optics* **4**, 883 (1972).
- C-8. R. Weiss, *Quarterly Progress Report of the Research Laboratory of Electronics*, MIT, **105**, 54 (1972).
- C-9. J. U. White, *J. Opt. Soc. Am.* **32**, 285 (1942).
- C-10. N. A. Robertson, "Experiments Relating to the Detection of Gravitational Radiation and to the Suppression of Seismic Noise in Sensitive Measurements," Ph.D. Thesis, University of Glasgow, 1981.
- C-11. G. A. Kerr and J. Hough, *Appl. Phys. B* (in press 1989).
- C-12. C. M. Caves, *Phys. Rev. D23*, 1693, (1981).
- C-13. N. A. Robertson, R.W.P. Drever, I. Kerr, and J. Hough, *J. Phys. E. Sci. Instr.* **15**, 1101, (1982).
- C-14. A. Giazotto, D. Passuello, and A. Stefanini, *Rev. Sci. Inst.* **57**, 1145 (1986).
- C-15. P. R. Saulson, *Review of Scientific Instruments*, **55**, 1315 (1984).
- C-16. J. E. Faller, R. L. Rinker, *NBS Dimensions*, **63**, 25 (1979).

APPENDIX D CALCULATION OF VIBRATION ISOLATION

The test masses in a gravitational-wave interferometer must be held in place against the earth's gravitational field without disturbance by the substantial seismic motion of the earth's surface. At the same time, they must be free to respond to gravitational waves. The vibration-isolation and test-mass suspension systems of the LIGO are designed to meet these requirements.

The forces applied to balance gravity connect the test masses to the noisy outside world. If the connection is made through a compliant element such as a spring or a pendulum, then at frequencies large compared to the element's resonant frequency the mass is almost free in inertial space. This follows from the one-dimensional equation of motion for a mass on a spring: $m\ddot{x} = -k(x - x_g)$, where m is the mass and k is the spring constant of the support for the mass, x is the coordinate of the mass in inertial space and x_g is the coordinate describing the ground motion relative to inertial space. A frequency-domain solution to this equation, representing the response of the mass to a steady excitation of the form $x_g = X_g e^{i\omega t}$, yields the transfer function $T(\omega) = X/X_g$, which represents the response of the system. Assuming a sinusoidal response of the form $x = X e^{i\omega t}$,

$$T(\omega) = \frac{X}{X_g} = \frac{\omega_0^2}{\omega_0^2 - \omega^2}. \quad (\text{D.1})$$

(Here $\omega_0 = \sqrt{k/m}$, and $\omega = 2\pi f$.) This transfer function shows that at high frequencies, the influence of ground motion x_g on the motion of the mass x is small.

In gravitational wave detectors the amount of isolation given by a single spring is insufficient. The design adopted for the LIGO test mass isolation system includes the cascade of several vibration isolators, each consisting of a mass and a spring in series. Five sets of alternating layers of springs and masses make up the vibration-isolating stack. The test mass is suspended by a pendulum from the final layer of the stack. To a good approximation, the *high* frequency performance of such a multi-stage vibration isolator is given by the product of the transfer functions of the individual stages.

In practice, several complications arise. (1) Damping alters the transfer function; (2) the *low* frequency transfer function depends on the coupling between stages, the system must be considered in three dimensions to account for cross-coupling between different degrees of freedom; and (3) there is degradation of high frequency isolation due to the non-negligible mass of the springs and compliance in the masses. This third factor causes a sharp departure from the $1/\omega^2$ isolation at frequencies where the resonances of the internal modes of the individual suspension elements are excited. In the suspension systems proposed for the LIGO, these resonances are not expected to be a factor in the overall noise budget of the initial interferometer.

In the remainder of this appendix, we illustrate the method by which we have predicted the seismic noise that penetrates the isolation system planned for the LIGO.

A schematic diagram of a vibration isolation stack is shown in Figure D-1. It shows a model of a stack consisting of three layers of equal mass m and moment of inertia I , separated by springs. (A simpler system than the full LIGO suspension is described here merely to make the algebra less lengthy—the method of analysis is the same.)

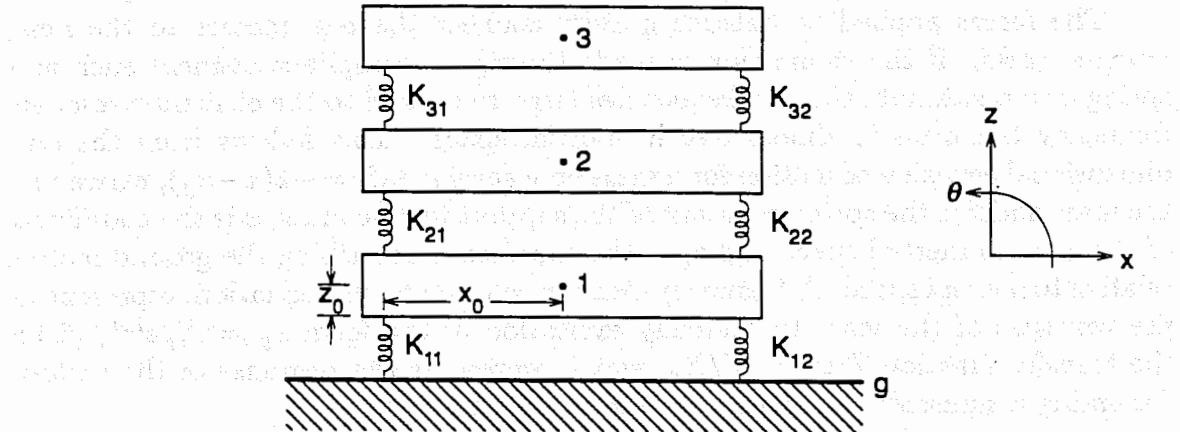


Figure D-1 Schematic diagram of a three-stage spring/mass isolation stack. Seismic noise enters at level g , and is attenuated by successive stages. The three masses (1, 2, 3) are separated by pairs of springs (k_{ij}). The vector from the attachment point of the springs to the center of mass for each layer has coordinates $(\pm x_0, 0, \pm y_0)$. The pitch angle of layer i is θ_i .

We treat each of the masses as a rigid body, and each of the springs as massless. The springs are not necessarily isotropic—they may have different spring constants for displacements in different directions. In general, we would need to keep track of six degrees of freedom for each mass, but if we align the principal axes of the springs with the symmetry axes of the system, then we need only follow three coordinates of a rigid body confined to a plane: the horizontal direction x parallel to the optic axis, the vertical z , and the angle θ about the third coordinate axis (the pitch angle).

Assuming that all of the springs and all of the masses are identical, the Lagrangian is

$$\begin{aligned} L = T - V = & \frac{1}{2}m(\dot{x}_1^2 + \dot{z}_1^2 + \dot{x}_2^2 + \dot{z}_2^2 + \dot{x}_3^2 + \dot{z}_3^2) + \frac{1}{2}I(\dot{\theta}_1^2 + \dot{\theta}_2^2 + \dot{\theta}_3^2) \\ & - \frac{1}{2}k_x(\Delta x_{11}^2 + \Delta x_{12}^2 + \Delta x_{21}^2 + \Delta x_{22}^2 + \Delta x_{31}^2 + \Delta x_{32}^2) \\ & - \frac{1}{2}k_z(\Delta z_{11}^2 + \Delta z_{12}^2 + \Delta z_{21}^2 + \Delta z_{22}^2 + \Delta z_{31}^2 + \Delta z_{32}^2) \\ & - mg(z_1 + z_2 + z_3). \end{aligned} \quad (D.2)$$

Here the coordinates with single subscripts refer to the motions of the masses, while those with double subscripts represent the length changes of the springs, which can be expressed in terms of the x_i, z_i, θ_i , and the ground motion x_g, z_g, θ_g .

In the limit of small displacements, the resulting equations of motion are

$$\begin{aligned}
m\ddot{x}_1 &= 4k_x x_1 - 4k_x z_0 \theta_1 + 2k_x x_2 + 2k_x z_0 \theta_2 + 2k_x x_g, \\
I\ddot{\theta}_1 &= 4k_x z_0 x_1 - 4(k_x z_0^2 + k_z x_0^2) \theta_1 + 2k_x z_0 x_2 + 2(k_x z_0^2 + k_z x_0^2) \theta_2 \\
&\quad + 2k_x z_0 x_g + 2(k_x z_0^2 + k_z x_0^2) \theta_g, \\
m\ddot{z}_1 &= -4k_z z_1 + 2k_z z_2 - 2k_z z_0 - mg + 2k_z z_g, \\
m\ddot{x}_2 &= 2k_x x_1 + 2k_x z_0 \theta_1 - 4k_x x_2 - 4k_x z_0 \theta_2 + 2k_x z_0 \theta_3, \\
I\ddot{\theta}_2 &= 2k_x z_0 x_1 + 2(k_x z_0^2 + k_z x_0^2) \theta_1 - 4k_x z_0 x_2 - 4(k_x z_0^2 + k_z x_0^2) \theta_2, \quad (\text{D.3}) \\
&\quad + 2k_x z_0 x_3 + 2(k_x z_0^2 + k_z x_0^2) \theta_3, \\
m\ddot{z}_2 &= 2k_z z_1 - 4k_z z_2 + 2k_z z_3 + 2k_z l + 4k_z z_0 - mg, \\
m\ddot{x}_3 &= 2k_x x_2 + 2k_x z_0 \theta_2 - 2k_x x_3 - 2k_x z_0 \theta_3, \\
I\ddot{\theta}_3 &= 2k_x z_0 x_2 + 2(k_x z_0^2 + k_z x_0^2) \theta_2 - 2k_x z_0 x_3 - 2(k_x z_0^2 + k_z x_0^2) \theta_3, \\
m\ddot{z}_3 &= 2k_z z_2 - 2k_z z_3 + 2k_z l + 4k_z z_0 - mg.
\end{aligned}$$

The position of the attachment points of the springs with respect to the centers of mass of the masses are given by the parameters x_0 and z_0 . The springs have equilibrium length l .

These equations of motion do not include damping. For velocity damping, a term proportional to the time derivative of length is added to each spring term. Another method of modeling damping, called structural damping [D-1], is to multiply each spring constant by $1 + i\gamma$, where $\gamma \ll 1$. We have chosen to model the LIGO isolation system with structural damping of $\gamma = 0.03$, in accord with our laboratory measurements of the behavior of rubber springs.

The transfer function from the input noise spectrum, $x_g(f)$, to the motion of the top mass, here $x_3(f)$, is obtained using matrix methods [D-2].

Stacks such as those in the 40-meter prototype interferometer incorporate rubber springs that have good damping properties but are anisotropic: they are typically stiffer in the vertical direction than in the horizontal direction. Further, the rubber springs are in the form of blocks placed between thick masses, giving a non-zero value of the parameter z_0 , the difference in height between a spring end and the center of mass of a mass layer to which it is attached. Under these circumstances, horizontal displacements cause torques on the masses, so the horizontal isolation depends in part on response of the springs to the vertical displacements of the rotating ends of the masses.

Interferometer sensitivity as limited by seismic noise is calculated from the isolation transfer function (including the isolation provided by any extra-vacuum

isolation, the stacks, and the final suspension) as

$$\tilde{h}_{\text{seismic}}(\omega) = \frac{2T(\omega)X_g(\omega)}{L} \quad (\text{D.4})$$

where L is the interferometer arm length and $X_g(\omega)$ is the input seismic noise, as approximated in Section V.A. If vertical noise dominates because of cross-coupling and poorer vertical isolation, then the transfer function for vertical noise, multiplied by the vertical-to-horizontal coupling coefficient—is used.

The seismic noise estimate for initial interferometers (“SEISMIC” line in Figure V-3) is based on the isolation system described in Volume 2, Section IV.B, including a 1-Hz final suspension, and the conservative factor of 10^{-2} for the coupling of vertical to horizontal motion. In the limit of ideal seismic isolation, sensitivity at low frequencies ($< 10\text{Hz}$) may be limited by fluctuating gravitational gradients resulting from seismic waves [D-3].

Mechanical cross-coupling is reduced by careful design. Optical cross-coupling resulting from a slope of the interferometer arms (or at flat sites from the curvature of the earth) may set the ultimate limit to seismic noise. The effective noise is then the sum of the horizontal noise and the vertical noise weighted by the sine of the angle between the optic axis and the horizontal. To generate the seismic noise curve shown in Figure D-2 we assumed that the coupling can be reduced to the level that causes horizontal motion to dominate. The horizontal resonances in the isolation stacks are taken to be 2 Hz and an additional stage of extra-vacuum isolation, provided by commercial air springs, has been included.

References

- D-1. Meirovitch, L., *Elements of Vibration Analysis*, McGraw-Hill, New York, (1986).
- D-2. Friedland, B., *Control System Design: An Introduction to State-Space Methods*, McGraw-Hill, New York, (1985).
- D-3. Saulson, P. R., *Physical Review D*30, 643, (1984).

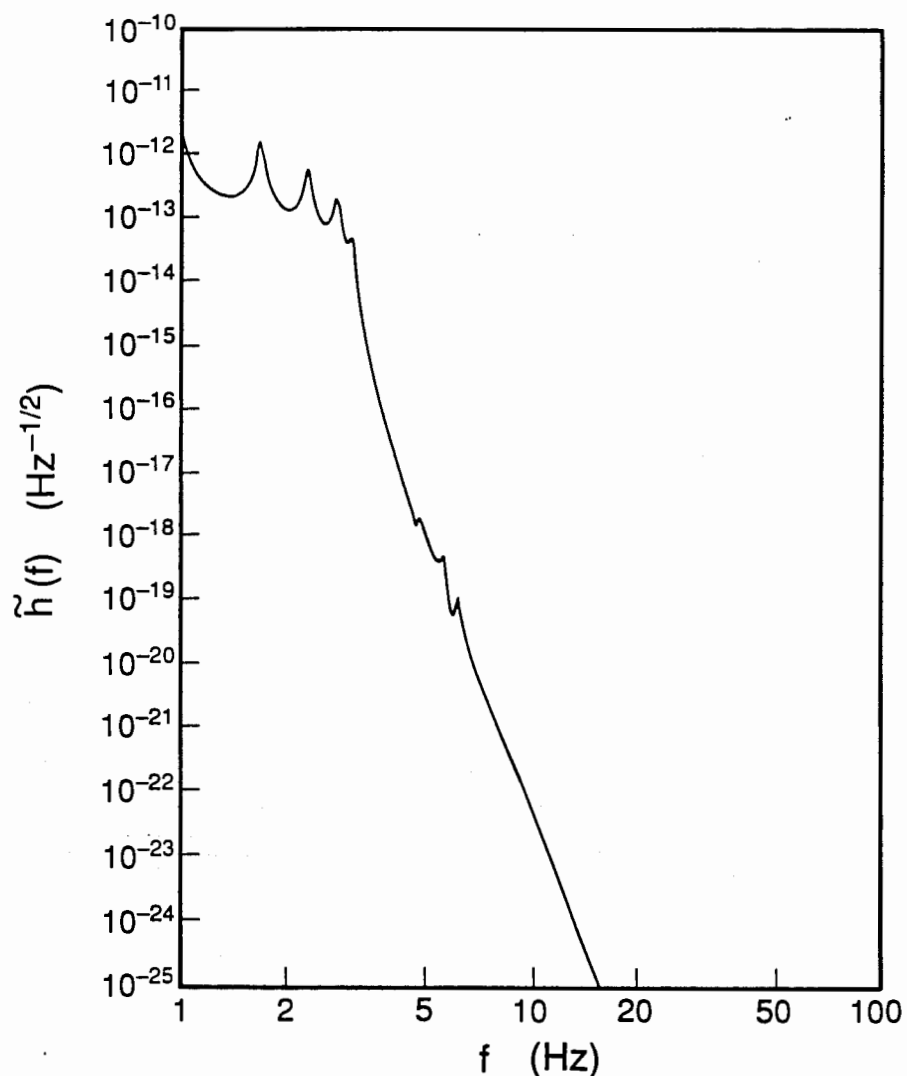
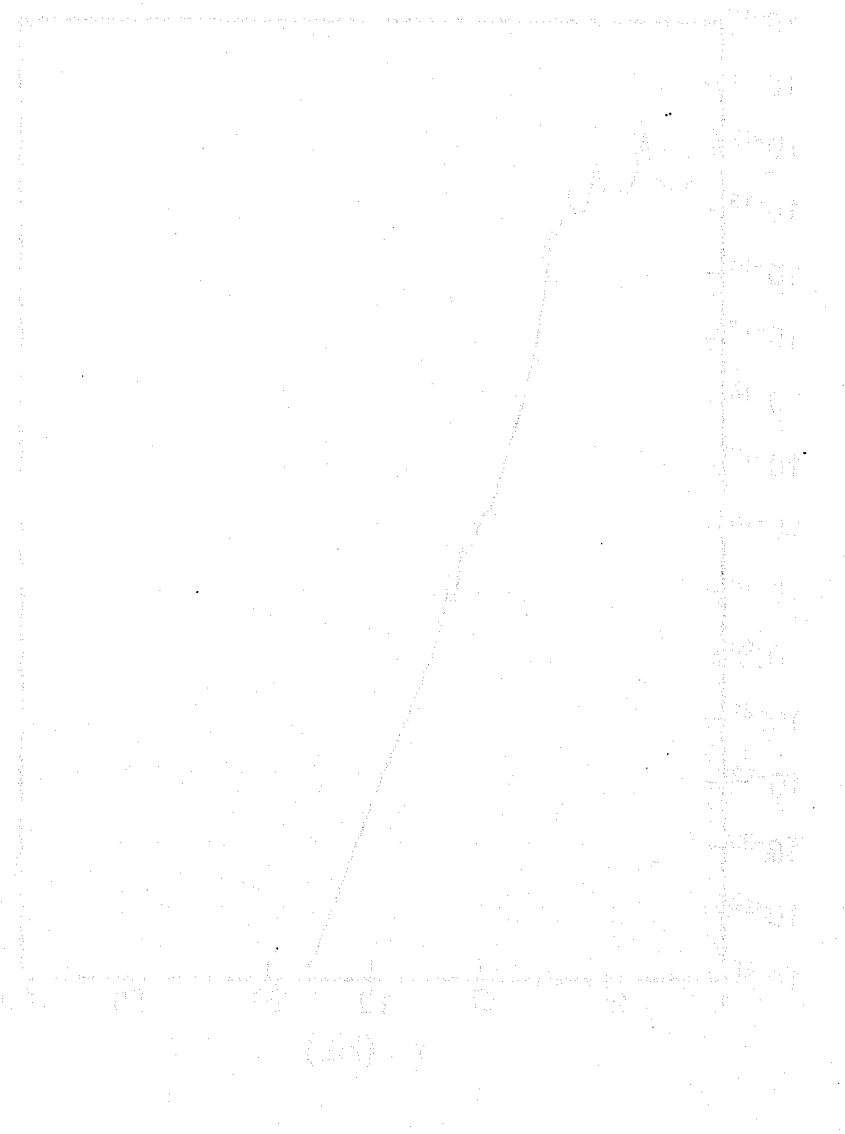


Figure D-2 The seismic noise in a LIGO interferometer of the “more advanced” design. The peaks in the spectrum are due to the pendulum suspension resonance ($f = 1$ Hz), and resonances in the isolation stack, ($f > 2$ Hz). The seismic excitation used in the model is the “standard” spectrum given in Table V-2.



Map of the United States showing state boundaries and major rivers. A dashed line indicates the location of the section of the Missouri River between the mouth of the Arkansas River and the confluence of the Platte and Missouri Rivers.

APPENDIX E

POWER SPECTRAL DENSITY AND DETECTOR SENSITIVITY

The sensitivity of gravitational-wave detectors is defined as the minimum detectable signal in the presence of background noise generated within the instrument or by the terrestrial environment. The noise is random in nature, and can be reduced relative to signals by averaging over time T = (duration of the signal or the measurement interval, whichever is shorter). The average value of random fluctuations diminishes as $1/\sqrt{T}$. Noise is most conveniently measured and estimated in the frequency domain. There, the measurement bandwidth is $\Delta f = 1/T$, and a long-duration (for high-sensitivity) measurement corresponds to narrow bandwidth. To characterize the sensitivity of a detector independently of the bandwidth, the noise is conventionally normalized to a bandwidth of 1 Hz and expressed in units of $(\text{noise}/\sqrt{\text{Hz}})$.

The noise spectrum, or noise level as a function of frequency, for a device that measures a quantity h is characterized by its power spectral density $S_h(f)$. This S_h is defined in terms of the noise level observed in the time domain, $h_N(t)$:

$$S_h(f) = \lim_{T \rightarrow \infty} \frac{2}{T} \left| \int_{-T/2}^{T/2} h_N(t) e^{-2\pi i f t} dt \right|^2. \quad (\text{E.1})$$

$S_h(f)$ is the noise power per unit frequency measured at frequency f . For gravitational-wave detectors, $h_N(t)$ is the noise of the detector expressed in equivalent dimensionless gravitational-wave strain amplitude, and $S_h(f)$ has the units of $[\text{strain}]^2/\text{Hz}$, or simply Hz^{-1} . The *amplitude* spectral density is defined by $\tilde{h}(f) = \sqrt{S_h(f)}$, and has units $\text{Hz}^{-1/2}$.

To compare the instrument noise to its signal, define the Fourier transform

$$H(f) = \int_{-\infty}^{\infty} h(t) e^{-2\pi i f t} dt \quad (\text{E.2})$$

where $h(t)$ (Section II, Equation (II.1)) is the signal output of the apparatus in the absence of noise. The exact value of the signal-to-noise-ratio (SNR) depends on the details of how the signal is filtered; the maximum SNR is achieved with optimal filtering¹ of the detector output:

$$\text{SNR} = \left[\int_0^{\infty} \frac{2 | H(f) |^2}{S_h(f)} df \right]^{1/2}. \quad (\text{E.3})$$

¹ The optimal linear filter, as defined by the Wiener-Hopf relations, minimizes the least square error between the output signal corrupted by noise and the noise-free input signal, once the signal waveform and the power spectral density of the noise are known. See Wiener, N., *The Extrapolation, Interpolation and Smoothing of Stationary Time Series with Engineering Applications*, John Wiley (1949).

(If there is no prior information available on the expected waveform—as in a general search for burst events—the filtering will not in general be optimal and the SNR will be reduced, though only slightly.)

Typically the signal has a maximum value $H_m(f_c)$ at characteristic frequency f_c , and S_h is approximately constant near f_c ; then:

$$\text{SNR} \approx \left[\frac{\int_0^\infty 2 |H(f)|^2 df}{S_h(f_c)} \right]^{1/2} \approx \sqrt{\frac{2H_m^2 \Delta f}{S_h(f_c)}}, \quad (\text{E.4})$$

where the signal bandwidth Δf is

$$\Delta f \equiv \frac{\int_0^\infty |H(f)|^2 df}{|H_m|^2}. \quad (\text{E.5})$$

The two components in the signal-to-noise ratio expressed in comparable units of equivalent gravitational wave strain are

$$\begin{aligned} h_{\text{sig}} &\equiv \sqrt{2} H_m \Delta f && \text{(signal)} \\ h_{\text{rms}} &\equiv \sqrt{S_h(f_c) \Delta f} = \tilde{h}(f_c) \sqrt{\Delta f} && \text{(noise),} \end{aligned} \quad (\text{E.6})$$

so $\text{SNR} = h_{\text{sig}}/h_{\text{rms}}$. Astrophysical models are used to predict expected values for H_m . $\tilde{h}(f)$ is the quadrature sum of uncorrelated noise sources, such as residual gas effects and photon shot noise.

As one application of these results, consider a search for periodic waves. In this case the bandwidth is $\Delta f = 1/\hat{\tau}$, where $\hat{\tau}$ is the observation time (10^7 s for a long-duration search), and h_{sig} as defined above is $1/\sqrt{2}$ times the amplitude of oscillation of $h(t)$. The unity signal-to-noise strength for a periodic source with optimal direction and polarization is then $h_{\text{sig}} = h_{\text{rms}} = \tilde{h}(f_c) \sqrt{1/\hat{\tau}}$. In Appendix A, periodic sources are described by a characteristic amplitude that is equal to h_{sig} : $h_c = h_{\text{sig}}$; and detectors are described by a noise amplitude that is equal to this h_{rms} : $h_N = h_{\text{rms}}$. As a second application, a gravitational wave burst that lasts for n cycles of oscillation, has bandwidth $\Delta f \approx f_c/n$. Correspondingly, the signal h_{sig} is approximately the amplitude of oscillation of $h(t)$ during the waves n cycles, and the rms noise level, assuming optimum direction and polarization, is thus $h_{\text{rms}} \approx \tilde{h}(f_c) \sqrt{f_c/n}$. The signal-to-noise ratio is then $h_{\text{sig}}/h_{\text{rms}} \simeq h_{\text{sig}} \sqrt{n}/\tilde{h}(f_c) \sqrt{f_c}$. In Appendix A and Section II the wave is described by a characteristic amplitude $h_c = h_{\text{sig}} \sqrt{n}$ and the detector by a sensitivity $h_N = \tilde{h}(f_c) \sqrt{f_c}$; i.e., the factor \sqrt{n} is absorbed in the source's amplitude rather than in the detector's noise.

This brief discussion ignores the reduction in the signal-to-noise ratio that results from the non-optimal direction and polarization of realistic sources of gravitational waves, and also ignores the issue of how large the SNR must be for, say, 90% confidence that an observed signal is real. These issues are discussed quantitatively in Appendix A.

APPENDIX F

SCATTERING AND OPTICAL PROPERTIES OF THE BEAM TUBES

A substantial effort was made during the conceptual design to understand the influence of scattered light on the noise in the interferometer and to develop a scheme to reduce the noise due to scattering [F-1]. The scattered light originates in both the optical components and the residual gas and arrives at the photodetector by various mechanisms involving both single and multiple scatterings.

The basic mechanism by which scattered light can disturb the gravitational-wave measurement is by adding optical fields of random phase and amplitude to the small main field in the "dark fringe" at the antisymmetric port of the interferometer. The fluctuations in the phase of the total field (scattered light added to the main field) are the critical parameter; the additional photon shot noise from the scattered light is far less important. The analysis of the scattering effects takes into account that: (1) that the main and scattered fields will usually have different spatial distributions at the photodetector, (2) the main field and the scattered fields may have taken different times to traverse the interferometer, and (3) the scatterers may be moving and the scattered light may reflect or diffract from moving elements, such as the inside wall of the vacuum tube.

1. Spatial Distribution

The main field defines a mode of the radiation field; the disturbing phase fluctuations are proportional to the fraction of the scattered field that projects onto this mode. The main field can be thought of as a spatial filter for the scattered field. This leads to both a substantial reduction in the effects of scattered light and a simplification in the analysis due to the orthogonality of the modes defined by the main beam geometry. The orthogonality, however, is not maintained if the spatial response of the photodetector is nonuniform. The photodetector and the main beam then define a new set of orthogonal modes different from those of the cavities. We have considered this in the analysis and have estimated the noise both for a bare photodetector and the case when a mode filter is placed before the photodetector. The design goal is that the estimated scattering noise in an interferometer be less than 1/10 of the noise due to the standard quantum limit for a one-ton test mass. We have adopted this conservative goal to allow for a reasonable safety margin, given the difficulty of the calculations.

2. Noise Due to Different Travel Times

We will attempt to make the travel times of the main light beams close to equal in the two interferometer arms, so as to reduce the sensitivity to laser frequency and amplitude fluctuations at the antisymmetric output. Scattered light will traverse a different path through the system and thereby degrade this symmetry. The noise is proportional to the amplitude of the scattered light, the difference in travel time

between the main beam and the scattered light and the spectrum of the laser amplitude and frequency fluctuations. With proper design of the interferometer and laser stabilization systems, we do not believe that this noise will be significant.

3. Noise From Moving Objects in the Scattered Light Paths

The dominant contributions to the scattering noise arise from the motion of the scatterers and other objects that reflect or diffract the scattered light. A successful strategy to suppress scattering noise seeks to eliminate the sources of single scatterings and to arrange that the individual amplitudes in multiple scatterings and diffraction processes are small. One important single-scattering process is the fluctuation in the forward scattering of the moving residual gas molecules. This is controlled by evacuating the optical path. Another important mechanism, in the absence of baffles, proceeds through the following steps: light from the main beam scatters from one of the main cavity mirrors, then reflects from the *moving* tube wall one or more times and then recombines with the main beam mode (either by scattering or diffraction at another optical component or through the nonuniformity of the photodetector). This process and considerations related to the angular fluctuations of the main mode (beam wiggle) have imposed the requirement for baffles in the LIGO beam tubes, and for baffles, blackening and possibly mode filtering in the paths following the antisymmetric port of the interferometer.

4. Concept for Specifying Baffles and the Optical Properties of the Tubes

The classical strategy for baffling in optical instruments is to arrange that no scattering path from an optical component in the main beam will arrive at the exit pupil due to specular or diffuse reflection from enclosures or other surfaces. We adopt the same strategy in the LIGO beam tubes (described in Volume 2, Section IV.C). This sets a relation between the baffle spacing, the baffle height and the clear aperture.

Scattered light that reflects from the tube walls at large grazing angles is strongly attenuated because: (1) the ratio of R/L (where R is the clear aperture radius and L is the beam-tube length) is extremely small, causing a large number of reflections, and (2) the tube walls are poor reflectors, except at grazing incidence. For example, the attenuation of scattered rays is greater than 80 dB at grazing angles of 0.1 radians for smooth stainless steel, .05 radians for the finishes being specified for the straight wall beam tubes, and .003 radians for standard corrugated tubing [F-2]. Because of this large attenuation the baffle design is particularly simple and exploits the principle of converting shallow grazing rays into paths with larger grazing angles that are strongly attenuated.¹

¹ The small grazing angle rays must be stopped by the baffles both because they suffer little attenuation in the tubes and because the differential scattering and recombining function of the mirrors grows as $1/\theta^n$ where θ is the grazing angle and n lies between 1.5 and 2, depending on the spatial spectrum of long-wavelength mirror distortions [F-3].

With the proposed baffle design a mechanism remains in which a scattered ray from a mirror is diffracted toward the wall by a baffle and continues to propagate down the tube by multiple reflections at small grazing angles until it is diffracted a second time toward the other mirror or the photodetector and recombines with the main field. Analysis of this mechanism predicts that, without an output mode filter, the scattering noise due to seismically induced motion of the tube walls becomes larger than 1/10 the standard quantum limit at frequencies above 30 Hz. With an output mode filter the design goal is met with a safety margin of several hundred.

Another mechanism considered in the analysis is backscatter from the seismically driven baffles. This results in specifications on the closest distance of baffles to the cavity mirrors and on the surface finish of these close baffles.

An extremely useful and non-obvious result of the analysis is that noise due to the coherent superposition of the scattered light is easily eliminated by simple measures that randomize the phases from multiple scattering, reflection and diffraction. The typical misalignment of the tubes during assembly as well as the standard manufacturing tolerances on tube roundness are sufficient to destroy the coherence. As an additional precaution we have designed the baffles with serrated edges, as has been done in coronagraphs, to average over several Fresnel zones [F-4].

The scattering analysis suggests that the LIGO will be able to meet the design goal providing that the tube walls and baffles move no more than the naturally occurring seismic ground motion. The tube enclosure should reduce acoustic and wind driven motions of the tubes sufficiently to maintain the scattering at acceptable limits.

A recommendation of the initial analytic study of the scattering [F-1] is to carry out computer modeling with available scattering codes, both to test the analytic model and to be sure that all important scattering mechanisms have been accounted for. A directed Monte Carlo technique such as the APART [F-5] code is appropriate for the calculation and this will be done during the engineering design.

References

- F-1. Thorne, K. S., "Light Scattering and Proposed Baffle Configuration for the LIGO," Preprint GRP-200, California Institute of Technology, Pasadena, CA 91125.
- F-2. Beckmann, P., A. Spizzichino, "The Scattering of Electromagnetic Waves from Rough Surfaces," Pergamon Press, 1967.
- F-3. Elson, J. M., H. E. Bennett, J. M. Bennett, "Scattering from Optical Surfaces," *Applied Optics and Optical Engineering*, Vol. III, Academic Press Inc., 1979.
- F-4. Newkirk, G. Jr., and D. Bohlin, "Reduction of Scattered Light in the Coronagraph," *Applied Optics*, Vol. 2, p. 131, 1963.
- F-5. APART, Breault Research Organization, Inc., Tucson Arizona.

que desempenha. A liberdade é um direito fundamental que deve ser garantido a todos os cidadãos. No entanto, é importante lembrar que a liberdade deve ser exercida dentro de limites e respeitando os direitos dos outros. É preciso encontrar um equilíbrio entre a liberdade individual e a segurança coletiva. A liberdade é um valor fundamental, mas também é necessário garantir a segurança e o bem-estar de todos os cidadãos. É importante que as autoridades respeitem os direitos humanos e promovam a igualdade social. A liberdade é um direito fundamental, mas também é necessário garantir a segurança e o bem-estar de todos os cidadãos. A liberdade é um direito fundamental, mas também é necessário garantir a segurança e o bem-estar de todos os cidadãos. A liberdade é um direito fundamental, mas também é necessário garantir a segurança e o bem-estar de todos os cidadãos.

APPENDIX G

LIGO PROJECT GRAVITATIONAL-WAVE SEARCHES

Several data runs and subsequent analyses have been performed using the LIGO Project prototype interferometers. Although such searches with the prototypes lack sufficient sensitivity to discover gravitational waves, they provide useful experience with data collection and analysis procedures. A brief description of previous gravitational-wave searches is given below.

1. Periodic Source of Known Period and Known Position

(M. Hereld, Ph.D. thesis, Caltech 1983).

A search was done for sinusoidal strain signals at 642 and 1284 Hz from PSR 1937+214 using the observed radio period to simplify the data recording and enhance the sensitivity. The data were analyzed for both gravitational-wave polarizations h_+ and h_\times by correcting for the Doppler shift due to the Earth's motion in the barycentric coordinate system. The noise exhibited the anticipated Rayleigh distribution associated with the noise of the instrument.

2. Burst Search Using Generic Templates

(D. Dewey, Ph.D. thesis, MIT 1986)

A search was done for gravitational wave bursts in the 800 to 5500 Hz band using a set of 22 generic, digital, three-state (-1,0,1) filter templates modeled on theoretical wave forms. The noise distribution of the filtered data exhibited Gaussian statistics appropriate to the instrument noise after correction for large amplitude but low-rate, non-Gaussian events; which were identified as instrument related.

3. Periodic Search for Sources of Unknown Period at Both Known and Unknown Positions

(J. Livas, Ph.D. thesis, MIT 1987)

A search was done for periodic sources in the 2 to 5 kHz band using a sinusoidal source model and two different methods. The first method involved an all-sky survey using a large Fourier transform ($2 \cdot 10^7$ points); a Cray 2 computer was utilized to search for peaks in the spectrum that exhibit characteristic FM and AM modulations due to the motion of the Earth. With the second method, a search for periodic sources in the galactic-center region was performed by applying Doppler corrections to the data in the time domain, so as to concentrate the Doppler FM sidebands into a single resolution bin of the Fourier transformation. The distribution of spectral peaks obeyed a Rayleigh distribution as expected, except for some large peaks associated with instrument resonances.

4. Search for Coalescing Binary Chirps

(S. Smith, Ph.D. thesis, Caltech 1988)

A search was done for the characteristic chirp of the radiative decay of a coalescing black-hole or neutron star binary (Appendix A, Equations (A.8) and (A.9); Figure A-3). The waveform for such a chirp is characterized (aside from overall amplitude and start time) by a single parameter $\mu^{2/5} M^{3/5}$, where μ is the binary's reduced mass and M is the total mass. This parameter was varied to make an optimized search for all possible masses. The algorithm that was developed distorts the time series so as to concentrate all the energy into one frequency before Fourier transformation of the data.

5. Search for Periodic Signals Following SN 1987A

(M. Zucker, Ph.D. thesis, Caltech 1989)

A search was done for periodic gravitational waves from Supernova 1987A in the band between 300 Hz and 5 kHz. The search was started ten days after the supernova explosion which occurred in the Large Magellanic Cloud in February 1987. Five samples, each lasting 105 seconds ($2 \cdot 10^6$ points), were Fourier analyzed after apodization. No signals other than apparatus resonances were detected.

Periodic signals from the supernova were sought in the band between 300 Hz and 5 kHz. The data were taken with the LIGO detector at Hanford, Washington, during the month of February 1987. The search was started ten days after the supernova explosion. Five samples, each lasting 105 seconds ($2 \cdot 10^6$ points), were Fourier analyzed after apodization. No signals other than apparatus resonances were detected.

Periodic signals from the supernova were sought in the band between 300 Hz and 5 kHz. The data were taken with the LIGO detector at Hanford, Washington, during the month of February 1987. The search was started ten days after the supernova explosion. Five samples, each lasting 105 seconds ($2 \cdot 10^6$ points), were Fourier analyzed after apodization. No signals other than apparatus resonances were detected.

APPENDIX H

REPORT ON RECENT PROGRESS¹

and the LIGO engineering team at Caltech. This proposal will be submitted to the National Science Foundation and will include the results of the work done since the last continuation proposal, and will also include a detailed description of the proposed construction of the detector, including a detailed description of the detector's performance.

CONTINUATION PROPOSAL NSF GRANT NO. PHY-8803557

CONTINUED PROTOTYPE RESEARCH & DEVELOPMENT AND PLANNING FOR THE CALTECH/MIT LASER GRAVITATIONAL WAVE DETECTOR

(PHYSICS)

Rochus E. Vogt, Principal Investigator
and Project Director

Ronald W. Drever, Co-Investigator

Kip S. Thorne, Co-Investigator

Rainer Weiss, Co-Investigator

October 1989

This section covers progress since the last continuation proposal (October 1988) on prototype research and development and on planning for a Laser Interferometer Gravitational Wave Observatory (LIGO) by the Caltech and MIT science groups and the LIGO engineering team located at Caltech.

Areas of highest priority included: (1) conceptual design of LIGO, (2) interferometer prototypes, (3) preparation of the LIGO construction proposal.

Conceptual design of LIGO has been completed. The conceptual design report was submitted to the National Science Foundation in October 1988. The report includes a detailed description of the detector, its performance, and its cost. The report also includes a detailed description of the engineering team, the science group, and the funding sources. The report also includes a detailed description of the detector's performance, and its cost.

¹ This summary of progress from October 1988 to October 1989 is excerpted from our Continuation Proposal to the National Science Foundation, October 1989. It is printed here in the same format as submitted.

A. LIGO Development

Work continued on the planning and conceptual design for the Caltech/MIT Laser Interferometer Gravitational Wave Observatory (LIGO).

1. Sites

Louisiana State University (LSU) delivered a report on a preliminary seismic survey of a potential LIGO site in Louisiana. This work was carried out under the direction of Drs. Warren Johnson of the Department of Physics and Astronomy and Don Stevenson of the Louisiana Geological Survey. The report revealed that an oil pipeline crossing the property is a source of low-frequency (< 10 Hz) seismic noise; this may restrict alignments of the LIGO at this site. A site plan with two possible alignments has been prepared.

A preliminary soil and geotechnical exploration of the LIGO site at Edwards Air Force Base, California, was carried out in October 1988, and the report of these studies was completed. A review of this preliminary survey yielded the conclusion that, because of the instability of the lake bed soils in the area, it would be necessary to support the LIGO installation on piles driven to a depth varying between 60 and 120 feet. The cost impact of these piles partially offsets the very low earthwork costs at this site, but Edwards remains a relatively low-cost potential site for the LIGO.

A hydrology study and a biological survey of the Edwards site were completed in January 1989. The biological survey of one of the potential LIGO sites there was submitted to, and accepted by the Air Force. A preliminary archeological/paleontological survey (Phase 1) was submitted to and accepted by the California State Historical Preservation Office. This survey brings together existing records and surveys, and recommends additional survey work in several regions of "cultural significance," as defined by the National Historic Preservation Act of 1966.

At the request of the NSF, the LIGO Project explored the feasibility of building a 4-km LIGO installation at the National Radio Astronomy Observatory (NRAO) site near Green Bank, West Virginia. We visited the site, collected and evaluated available data, and identified two possible LIGO alignments. We concluded that it is technically feasible to build a LIGO at Green Bank, although the site is topographically more complex than other sites we have studied. A series of reports containing details and conclusions were submitted to the NSF.

We have initiated a preliminary inquiry into the feasibility of a 4-km LIGO at the site of the Owens Valley Radio Observatory (OVRO). The 1983 Stone & Webster survey concluded that there was insufficient space for a 5-km LIGO, but more recent analysis shows that a 4-km installation will fit. The site possesses many attributes of a good LIGO site: a well-developed infrastructure, very flat topography, stable soil conditions, and a single landowner with whom Caltech has historically excellent relations.

2. Materials Testing

We have constructed a Vacuum Test Facility (VTF) and used the facility to evaluate outgassing properties of steel samples that are candidate materials for construction of the

LIGO vacuum system. Data from the VTF have been used in conjunction with theoretical modelling to design the vacuum pumping strategy for LIGO. The VTF measurements were required because there was no adequate data base on the outgassing properties of steel subject to very-long-term vacuum exposure. VTF results indicate that at least one supplier can deliver 304L stainless steel with sufficiently low hydrogen content to achieve the requisite hydrogen outgassing rate without high-temperature bakeout. We have also identified adequate cleaning and other procedures (including low-temperature bakeout techniques for water vapor) to reduce all other contaminants to sufficiently low outgassing rates.

3. Conceptual Design

During the past year we have conducted an extensive conceptual design process for the LIGO facilities. The purpose of this effort was to translate the scientific requirements for the facilities into technical solutions and provide the basis for costing the construction of the facilities. In this process we studied the interactions between solutions to various technical problems and clarified certain design criteria which were previously ill-defined.

a. Identification of scientific functional requirements:

A major effort was conducted during the past year to specify and document the scientific functional requirements for the LIGO. This process required unification and rationalization of previous work done by the Caltech and MIT teams as well as formulation of requirements for many specifications which were not yet well defined. Over one hundred internal working papers and reviews were written covering the following broad topics:

- Site requirements.
- Vacuum studies.
- Noise source analysis.
- Interferometer design requirements.
- Environmental requirements.
- Auxiliary physical measurements.
- Data and control system requirements.
- Scientific requirements for operations.

b. Formulation of operations scenario:

In addition to scientific specifications, the scenario for how the LIGO will operate plays an important role in defining the facilities to be built. We have defined such a strategy and analyzed its implications for the design of the LIGO. We have decided to pursue a phased construction approach to deliver at the earliest date a system capable of discovering gravity waves and exploiting the initial discovery. The later phases of construction will enhance the scientific capabilities of LIGO and allow broader participation by others in the new field of gravity wave astronomy. We have identified the need for a simultaneous search and development capability, with minimum interference between these missions, as the optimum strategy to ensure successful LIGO operation. This has defined the need for three distinct detector units (observation, development, and special investigation detectors), and a flexible modular vacuum system capable of supporting simultaneous operation of multiple interferometers. Finally we have developed a plan for early use and later evolution of the LIGO facilities.

c. Development of vacuum system concept:

i. Beam tubes:

A concept for the LIGO beam tubes which specifies physical characteristics, environmental requirements, and construction implementation was developed. Two possible construction implementations for the tube have been evaluated: smooth wall tubing with periodic reinforcement, and corrugated tubing. Construction and maintenance scenarios have been formulated.

ii. Vacuum chambers:

The LIGO concept requires a flexible vacuum system. We have conceptually defined four vacuum chamber types: test mass chambers types 1 and 2, diagonal chambers (which house the beamsplitter optics), and horizontal axis modules (for conditioning optics).

a) Test mass chambers:

The LIGO concept places strong demands on the test mass chambers (TMCs). These chambers house the critical test mass assemblies and Fabry-Perot cavity mirrors. These elements must receive the highest level of vibration isolation. The chambers need to accommodate different sizes of test masses and possible different configurations of test masses while allowing optical beams from other simultaneously operating interferometers to pass through the chambers unperturbed. Most importantly, some of the chambers (TMC, Type 1) must accommodate removal and installation of entire test mass assemblies for a given interferometer with minimal disturbance to the vacuum system and other interferometers. We have developed a solution which employs an airlock chamber design.

For those chambers located at the ends which may be opened without disturbing the remaining vacuum system and operating interferometers, a simpler and less expensive configuration, TMC Type 2, has been designed.

b) Diagonal chambers:

The diagonal chambers house the beamsplitter optics for the interferometers. While the diagonal chambers must accommodate vibration isolation systems similar to those employed in test mass chambers, a given diagonal chamber interfaces to only one detector. These chambers, therefore, do not require the complication of an airlock design.

c) Horizontal axis modules:

The conditioning optics chains at each interferometer input and output do not require the same degree of vibration isolation as test masses and beamsplitter optics. However, these optical chains have a high degree of complexity and will change more than other interferometer parts over the course of LIGO evolution. The corresponding vacuum chambers require the greatest degree of modularity, flexibility, and ease of access. We have developed a simple concept for these chambers in terms of modules which can be

connected or stacked together in open-ended fashion. Removable endcaps on both sides of each chamber will allow convenient access to all internal components.

iii. Pumping and leak testing strategies:

We have developed strategies for pumping and leak testing the LIGO vacuum system. The pumping strategy involves specifying type, placement, and capacity of pumping stations, based on estimates of interferometer gas loads and vacuum system outgassing properties. The leak testing strategy for the beam tubes is based on pulsed exposure to He gas with recovery and compression in the pumping stations.

d. Interferometer conceptual design:

We have worked to develop a conceptual design for LIGO interferometers in general, to establish boundaries on the facilities which would be compatible with future evolution, and in particular have developed a more specific conceptual design for the initial LIGO interferometers. We have developed a vibration-isolation strategy which is based on stacks of metal spaced by encapsulated rubber springs, and which takes account of the level of isolation required for different classes of interferometer components. The design has an open-ended feature in that the primary isolation stacks rest on platforms which can be further isolated, if required, due to care taken in the design of the various vacuum chambers.

During the conceptual design of the input and output conditioning optics chains for the interferometers, we discovered that the level of complexity of this part of the facilities had been seriously underestimated in all previous planning for interferometric gravity wave detectors. In fact the requirements for conditioning optics drive key aspects of the facilities design and have significant impact on how the remote and campus facilities will be used in LIGO. The outcome of this work led to the requirement of a flexible modular envelope for the conditioning optics chains, using the horizontal axis modules described above.

e. Supporting equipment and facilities:

i. Laser power, cooling and electrical capacity:

We have developed a plan for allotting electrical power for the lasers, pumps, electronics and building functions. We have chosen to allot sufficient electrical capacity to operate one large-frame argon ion laser per interferometer in the facility. This power level will be sufficient to allow initial interferometers to be shot-noise limited at sensitivity levels adequate to conduct viable gravity wave searches. For advanced interferometers we anticipate the use of more powerful and efficient systems such as Nd:YAG lasers which are currently under development. Because such lasers should be more efficient by orders of magnitude than current ion lasers, the initial laser power capacity will be sufficient for operation of advanced interferometers. Power for lasers represents approximately half of the

planned electrical capacity. The rest will be used for lighting, pumps, electronics and other building functions.

ii. Environmental specifications and auxiliary parameter monitors:

We have developed specifications for the laboratory environment required for LIGO and plans for implementation. This includes items such as power conditioning, temperature and air flow constraints, allowable mechanical noise, and drift and creep in structures. A significant problem which was identified is the cleanliness level of the lab environment. Measures were planned to ameliorate contamination of the optics and vacuum chambers. We have also formulated a plan for monitoring auxiliary physical parameters for the interferometers such as magnetic fields and line voltage, which will help to rule out spurious candidate gravity wave events.

iii. Interferometer/facility interfaces:

We have enumerated the mechanical, optical, and electrical interfaces between the interferometers and the facilities, and between separate site buildings. This work includes, for example, specifying the number and type of analog and digital signal lines which penetrate vacuum chambers, number and type of feedthroughs required, and possible levels of multiplexing.

iv. Data and control systems:

We have outlined the requirements for automated acquisition and logging of housekeeping data for the facilities, computer-assisted operation of control loops, and acquisition and logging of actual interferometer data. This includes enumeration of functions to be provided and estimation of signal bandwidths required.

v. Auxiliary and campus facilities:

We have identified auxiliary facilities to be provided at the LIGO sites and the campus facilities required to support LIGO operations. This has been done by developing scenarios for accomplishing various tasks associated with LIGO operations. For example, we have established procedures by which equipment is delivered to the sites, undergoes final assembly and testing, and is installed into the facility. From such scenarios we have identified what shop and storage facilities are required on site, and how quality and cleanliness controls are instituted. Similarly we have developed a concept of what type of tests, construction, etc., will be conducted at the LIGO sites, and which functions will be carried out on the campuses.

f. LIGO buildings and enclosures:

We have developed a conceptual design for buildings which will house the LIGO facilities and for an enclosure for the beam tubes. The building design seeks to provide an appropriate environment for LIGO activities while providing sufficient floor space and generality to accommodate future LIGO evolution. This need is especially

important in the corner buildings at each site. The tube enclosure is required to reduce wind-induced motion of the beam tubes, thus making noise induced by scattered light inside the tubes a tractable problem. Simultaneously it provides a more temperature-stable environment and affords some protection from vandalism.

B. Prototype Activities

The best displacement sensitivity in the 40-meter prototype so far has been measured at 3×10^{-18} m/ $\sqrt{\text{Hz}}$. Assuming this sensitivity is primarily limited by displacement noise (random motion of test masses) and that LIGO interferometers would be dominated by the same noise source, a 4km baseline LIGO would exhibit a strain sensitivity of 8×10^{-22} / $\sqrt{\text{Hz}}$, and would have a reasonable chance to discover gravity waves. However, this configuration of the 40-meter prototype could not be directly scaled up to an operating LIGO system. For instance, the frequency stabilization scheme was well suited for operation at low optical power levels but not at levels needed for the LIGO interferometers. Furthermore, the LIGO will require significant changes in the orientation and position control systems. During the current grant period we have emphasized the development of techniques which should not only lead to improved sensitivity in prototypes, but which can be directly scaled up to operating LIGO interferometers.

1. Development of a laser stabilization scheme consistent with LIGO power levels:

The Innova 100-20 large frame argon ion lasers at the 40-meter prototype have been tested at 7 watt single-mode output at 514 nm. The original stabilization scheme used an intracavity Pockels cell which required operation of the laser below 2 watt output power. In addition, an optical fiber used to inject light into the interferometer cavities, while providing reduction of fluctuations in laser beam geometry, severely limited the optical power that could be coupled into the interferometer.

We have constructed a new configuration for injecting light into the 40-meter interferometer. We have implemented a new two-stage frequency stabilization scheme. In the first stage, the laser is locked to a fixed length mode cleaning cavity. In the second stage, the phase of the light transmitted by this cavity is matched to one of the 40-meter cavities using a Pockels cell. We have extended the prototype's vacuum envelope to contain more of the conditioning optics, starting with the input mirror of the mode cleaner. This eliminates the optical fiber and any beam geometry perturbations caused by motion of the air path after the mode cleaner.

2. Development of the 5-meter facility:

Work began on the design of a 5-meter facility in 1986 and construction was completed near the beginning of the present grant period. The facility has 4 vacuum tanks. Three of the tanks are designed to house the 5-meter prototype. The fourth tank is configured to test suspensions. This tank is instrumented with an electromagnetic shaker to test vibration isolation of sample suspensions under vacuum.

At present, the central tank is dedicated to research on optical concepts in a stationary interferometer and the suspension tank is being used to carry out tests of a prototype

suspension. The facility is adequate in scale to develop and test selected LIGO optical and suspension subsystems during the next 4 years.

3. Development of recombination techniques in a stationary interferometer:

Work was begun on a stationary (not suspended) interferometer to test an interferometer configuration in which the beams reflected by the Fabry-Perot cavities are recombined. Beam recombination is required in any LIGO interferometer using high optical power or recycling. Because the components of the stationary interferometer are held in standard mounts on an optical table, seismic, acoustic and thermal noise are not attenuated; consequently the interferometer can approach theoretical shot-noise limits only at frequencies $\gtrsim 10$ kHz. This frequency range is useful for testing optical concepts and for developing the servo systems and electronics. The interferometer is assembled on an optical table inside the central tank of the 5-meter facility.

The system is being used to study different servo-control concepts of holding the interferometer in lock and to test two different techniques of applying RF modulation to the light. The stationary interferometer will also be used to develop a recombination system in which the phase modulators are placed in sidearms to reduce the optical power in the Pockels cells, much as is planned for the initial LIGO interferometer. Finally, the system will be used to test broad-band recycling by adding a recycling mirror and associated phase control servos.

4. Development of orientation and position control systems suitable for very long baseline interferometers:

The position and orientation of many optical components must be controlled precisely for interferometer operation. The elements requiring the most critical control and adjustment are the test masses that bear the main interferometer mirrors. During the current grant period we have designed, constructed, and tested new control subsystems which are suitable for LIGO scale applications:

a. Prototype work on a more sensitive orientation and position control system:

We have designed and tested a new position and orientation control system, suitable for controlling test masses and other suspended components. This compact self-contained system uses shadow sensing and electromagnetic feedback local to the suspended component being controlled. The design allows for simultaneous control of up to six degrees of freedom per component.

b. Development of a new diagnostic tool for detecting errors in coupling light into cavities:

A new device, called a phase camera, has been developed to diagnose errors in mode matching an input laser beam to a Fabry-Perot cavity. The device produces three-dimensional images of the phase difference between the input beam and the cavity. It can be installed in front of any of the cavities in the system.

5. Optics research and development:

a. Investigation of heating effects in mirrors:

Advanced LIGO interferometers will have very high light levels in the Fabry-Perot cavities. During the current grant period we have investigated the power handling capability of fused silica supermirrors coated by Litton Guidance and Control Division. We have measured the throughput of high-finesse-transmission Fabry-Perot cavities of different length, mirror spot size, and ratio of length to mirror radius. In these preliminary studies we found that most of the cavities exhibited a saturation phenomenon when the power stored in the cavity exceeded approximately 1 kW. In the saturation regime, the throughput efficiency decreased and the output mode distorted. We have developed a model which attributes these effects to thermal lensing in the input mirror substrate. This model predicts that these thermal distortion effects will persist even in very long baseline cavities as are planned for LIGO.

We plan to institute a systematic research program to characterize the thermal distortion effects in cavities and to develop better mirrors in a cooperative effort with industry.

b. Developments toward improving optics test and characterization capabilities:

We are currently planning to expand our capabilities to test and analyze optical components. Recent activities include:

i. Investigation of radiometric mapping to determine temperature profiles of mirrors:

An infrared camera was used to make a radiometric image (using 10μ radiation) of the heating of a mirror coating by the absorption of laser light. The test showed that surface temperature increments as small as 0.1°K could be measured by this technique. This method promises to be useful for experimental studies of thermal distortion in optical components.

ii. Preliminary tests of homogeneity and birefringence on large, fused-silica substrates:

The LIGO mirrors will require a high degree of optical homogeneity and low birefringence in blanks which are much larger than those currently in prototype use. We have obtained slow-annealed fused silica blanks comparable in size to LIGO mirrors. These were ground flat to $\lambda/50$ and tested under our supervision at Zyglo Corp. We collaborated on a modification to Zyglo's phase mapping interferometer which allowed us to measure both homogeneity and birefringence of these thick substrates over a large aperture. The Zyglo measurements are now being analyzed in part to determine the expected performance of thick substrates in a recycled interferometer.

iii. Development of improved experimental and analytical tools for scattering characterization:

The scattering angular distribution function for small angles is a key variable in estimating the noise due to scattered light in the LIGO. We have developed an apparatus which uses an optical fiber to map the scattered field in the region around the focal point of the mirror.

A substantial amount of analytic work was done to evaluate the effect of scattering in the LIGO beam tubes. The results of this analysis now form the basis for the design and placement of baffles.

6. Studies of vibration isolation and thermal noise:

a. Vibration isolation studies:

Research has continued on the development of a double suspension system in which the mirror is suspended from another object, the guard mass, which in turn is also suspended. This system should provide improved seismic isolation at frequencies below a few hundred Hz.

b. Thermal noise characterization:

Thermal noise in suspensions could limit the performance of high sensitivity interferometric gravitational wave detectors in the region of about 100 Hz. A new effort was begun to measure the internal dissipation of candidate suspension fiber materials in flexure at frequencies between a few hertz to several hundred hertz. The experiment in progress measures the Q, in vacuum, of the flexural resonances of suspension fibers clamped at one end. Once a short catalog of material Q has been established, the experiment will be used to measure the scaling of the loss with fiber dimensions.

C. Construction Proposal

Most of the work described in the preceding pages for this grant period was done in preparation for the LIGO construction proposal. This work has led to a design concept that serves as basis for an engineering design and cost estimate. A major effort on preparation of the construction proposal was started in May 1989.

Although a significant reduction in scope of the LIGO configuration occurred in July as a result of discussions with the NSF, most of the proposal has now (September 1989) been written and reflects the new configuration. Staged construction of the LIGO will be proposed. The construction proposal, to be submitted in the fourth quarter of 1989, will request funds for the first of these stages.

D. Other Progress

In November we began a series of monthly Project Status Review meetings. The purpose of these meetings was to convene members of the LIGO Project Office, the engineering group, and both science groups to review the current status and plans for developing the contents of the construction proposal.

A Sun 4/260 and 4/110 distributed computer system was installed and brought on line at MIT. The system is the same as that previously installed at Caltech and enhances as well as unifies the computing environment across the LIGO project. The system now has common software for engineering and scientific analysis at both locations.

Computer analysis of simulated gravity-wave signals continued, concentrating on extracting source location and polarization information from coincident detection of bursts in three or more detectors. Results obtained with the San Diego supercomputer facility indicate that the information from three detectors, each recording bursts with signal-to-noise ratios on the order of 5, spans approximately 80% of the sky.

An NSF/LIGO meeting was held at Caltech on April 10 and 11, 1989. LIGO design concepts, preliminary cost estimates, and management aspects were discussed.

E. International Cooperation

R. Vogt participated in a February 14, 1989 meeting in Paris, France, which had been convened upon initiative of and chaired by the NSF. Representatives of all major European gravity-interferometer research groups and their funding agencies attended. A principal focus of the discussion was the exploration of possibilities for international collaboration in the development of gravity wave interferometry, and several technical and scientific working groups were established.

As agreed at the Paris workshop, LIGO personnel have taken on the coordination of two international working groups: vacuum systems and control systems. The LIGO team also has assigned members to all other working groups coordinated by European scientists.

Full engineering and science briefings on the LIGO project were given, over the period of several days, to Drs. Hough and Leuchs, the respective leaders of the British and German gravity wave research groups. Similar courtesies were extended to Dr. Blair, who is organizing a new laser interferometer program in Australia.

Information on engineering advances also is being provided to Britain's Rutherford Laboratory on a continuing basis.

RECENT PUBLICATIONS AND CONFERENCE PAPERS

1. "Measuring High Mechanical Quality Factors of Bodies Made of Bare Insulating Materials," A. Čadež and A. Abramovici, *J. Phys. E: Scientific Instruments*, **21**, 453, 1988.
2. "Development of a Multi-dimensional Optimization Servo for Gravity Wave Detector Mirror Alignment," B. Lemoff, *Senior Thesis*, Caltech, May 1989.
3. "A Near Optimal Solution to the Inverse Problem for Gravitational Wave Bursts," Y. Gürsel and M. Tinto, LIGO Preprint 89-1, *submitted to Physical Review D*, June 1989.
4. "Frequency Fluctuations of a Diode-pumped Nd:YAG Ring Laser," P. Fritschel, A. Jeffries, T. Kane, *Optics Letters*, accepted for publication, 1989.

5. Conference Papers, 12th International Conference on General Relativity and Gravitation, Boulder, Colorado, 1989.
- i. "Tests of Recombination Schemes in a Fixed Arm Fabry-Perot Laser Interferometer," N. Christensen, P. Fritschel, J. Giaime.
 - ii. "Developments in Interferometric Gravity Wave Detectors for Large Scale Operation," R.W.P. Drever.
 - iii. "The Performance of a Double Pendulum Vibration Isolation System," J. Kovalik, P. Saulson, M. Stephens.
 - iv. "Observation and Analysis of a Mirror Heating Threshold in Fabry-Perot Cavities," F. J. Raab.
 - v. "Thermal Noise in Suspensions for Interferometric Gravitational Wave Antennas," P. Saulson.

vi. "Status Report on the Caltech 40-meter Fabry-Perot Prototype Gravitational Wave Detector," R. Spero.

vii. "The LIGO Project—A Progress Report," R. Vogt.

viii. "Laser Interferometer Detectors," R. Weiss.

ix. "The Status of the LISA Project," R. Weiss.

x. "The Status of the LISA Project," R. Weiss.

xi. "The Status of the LISA Project," R. Weiss.

xii. "The Status of the LISA Project," R. Weiss.

xiii. "The Status of the LISA Project," R. Weiss.

xiv. "The Status of the LISA Project," R. Weiss.

xv. "The Status of the LISA Project," R. Weiss.

xvi. "The Status of the LISA Project," R. Weiss.

xvii. "The Status of the LISA Project," R. Weiss.

APPENDIX J

HISTORY OF THE PROJECT

The LIGO project is based upon a large body of research and technical development over a period of almost 30 years.

After Joseph Weber's pioneering work on bar detectors for gravitational waves in the 1960s [J-1], other groups began to develop gravitational-wave detectors. In the late 60s, the idea of interferometric detectors was conceived independently by Weber, Weiss, and others. The basic design for a delay-line variant of an interferometric detector was described and the dominant noise sources quantified in 1972 by Weiss [J-2]. The first operation of an interferometric detector was conducted by Moss, Miller, and Forward in 1971-72 [J-3].

In the early 1970s, many groups, including Drever at Glasgow and others at Stanford, LSU, IBM, Bell Labs, Rochester, Munich, Rome, and Moscow began research with bar detectors. Several of these groups have continued a strong program of research with successive detectors. A switch from bar detectors to interferometers was made by the Munich group under Billing in 1975 and the Glasgow group under Drever in 1977. A year later, Drever at Glasgow introduced the concept of the Fabry-Perot variant of an interferometric detector [J-4].

In 1979 Drever started experimental gravitational-wave research at Caltech. In the same year, the National Science Foundation convened the Deslattes Committee which recommended strong funding of the gravitational-wave field, including new interferometer projects at Caltech (Drever) and MIT (Weiss). Weiss pursued a delay-line interferometer, while Drever continued development of Fabry-Perot interferometers.

In 1981, Weiss at MIT, with the firms of Stone & Webster and A. D. Little, began a detailed study of the design and costs of a large-scale Laser Interferometer Gravitational-Wave Observatory, or LIGO [J-5]. A presentation by Drever, Thorne, and Weiss in 1983 to the NSF Advisory Committee for Physics led to its strong endorsement of the LIGO concept. In 1984, Caltech and MIT formally joined in a project for the design, construction, and operation of the LIGO facility, with Drever, Thorne, and Weiss as a steering committee. In the same year the National Science Board approved project planning and feasibility studies. Further studies of design and cost were undertaken with the Caltech's Jet Propulsion Laboratory in this period.

In 1986, the NAS Physics Survey strongly endorsed the LIGO for ground-based research in gravity [J-6]. Concurrently, the International Society of General Relativity and Gravitation strongly endorsed the LIGO.

In November 1986 an NSF-sponsored Workshop was convened at Cambridge, Massachusetts to review the state of developments in the field with particular attention to plans for the LIGO Project. The Workshop was attended by 55 interna-

tional participants, and a report of the meeting was prepared by an eight-member panel from disciplines other than experimental gravity. The report was supportive of the program and endorsed a vigorous pursuit of its goals. The Summary of this January 1987 report to the NSF by the Panel on Interferometric Observatories for Gravitational Waves is included at the end of this Appendix. Two recommendations of the Panel have been implemented: management of the project was transferred in Fall 1987 from the steering committee to a Project Director, and a choice has been made of the type of interferometer (Fabry-Perot) to be used in the initial operations with the LIGO.

More recent reviews of the LIGO Project occurred in February 1988 (NSF Site Visit Committee, consisting of Drs. R. Byer, J. Faller, H. Grunder, A. Sessler, S. Teukolsky, D. Wilkinson, and R. Wilson) and in September 1988 (presentation by R. Vogt to the NSF Advisory Committee on Physics).

References

- J-1. J. Weber, *Physical Review D* **22** (1969), 1302.
- J-2. R. Weiss, *Quart. Progr. Rep. Res. Lab. Elect. MIT* **105** (1972), 54.
- J-3. G. E. Moss, L. R. Miller, and R. L. Forward, *Applied Optics* **10** (1971), 2495.
- J-4. R. W. P. Drever, G. M. Ford, J. Hough, I. M. Kerr, A. J. Munley, J. R. Pugh, N. A. Robertson, and H. Ward, "A Gravity-Wave Detector Using Optical Sensing," *Proceedings of the Ninth International Conference on General Relativity and Gravitation* (Jena 1980), ed. E. Schmutz (VEB Deutscher Verlag der Wissenschaften, Berlin, 1983), 265.
- J-5. P. Lindsay, P. Saulson, R. Weiss, "A Study of a Long Baseline Gravitational Wave Antenna System", Report to the National Science Foundation (1983).
- J-6. "Physics Through the 1990's—Gravitation, Cosmology, and Cosmic Ray Physics", National Research Council, National Academy Press, Washington, D. C., 1986.

SUMMARY OF NOVEMBER 1986 NSF REVIEW

The following is a copy of the title page and Summary from "Report to the National Science Foundation by the Panel on Interferometric Observatories for Gravitational Waves," which was submitted to NSF in January 1987 after a one-week (November 1986) review of the LIGO Project.

This document is a copy of the title page and Summary from "Report to the National Science Foundation by the Panel on Interferometric Observatories for Gravitational Waves," which was submitted to NSF in January 1987 after a one-week (November 1986) review of the LIGO Project.

This document is a copy of the title page and Summary from "Report to the National Science Foundation by the Panel on Interferometric Observatories for Gravitational Waves," which was submitted to NSF in January 1987 after a one-week (November 1986) review of the LIGO Project.

This document is a copy of the title page and Summary from "Report to the National Science Foundation by the Panel on Interferometric Observatories for Gravitational Waves," which was submitted to NSF in January 1987 after a one-week (November 1986) review of the LIGO Project.

Report to the National Science Foundation

by the

Panel on Interferometric Observatories for Gravitational Waves

This document is a copy of the title page and Summary from "Report to the National Science Foundation by the Panel on Interferometric Observatories for Gravitational Waves," which was submitted to NSF in January 1987 after a one-week (November 1986) review of the LIGO Project.

This document is a copy of the title page and Summary from "Report to the National Science Foundation by the Panel on Interferometric Observatories for Gravitational Waves," which was submitted to NSF in January 1987 after a one-week (November 1986) review of the LIGO Project.

This document is a copy of the title page and Summary from "Report to the National Science Foundation by the Panel on Interferometric Observatories for Gravitational Waves," which was submitted to NSF in January 1987 after a one-week (November 1986) review of the LIGO Project.

January 1987

5. SUMMARY

- A) A strong case has been made for the scientific value of the goals of the project.
- B) Though there are large uncertainties associated with the strengths of the many different kinds of astrophysical sources and the ultimate capability of interferometric detectors, there is a high probability that this facility will ultimately provide for a giant leap in our understanding of the gravitational force, one of the most fundamental forces of nature, as well as our knowledge of astrophysical phenomena.
- C) It is anticipated that this facility would uniquely provide the most sensitive and certain prospect for detecting astrophysical events and identifying their nature. Essential to this capability is the twin nature of the two interferometers. Though companion efforts in other countries are highly desirable, a common management of the two LIGO detectors is important both for the coordination of the observational program and for the analysis and identification of observed events. This facility would provide for a continued and thriving development of the field.
- D) It is important to proceed directly to the construction of a long baseline interferometer in a timely manner since many aspects of the detector development program cannot otherwise be tested.
- E) The rate of detectable extragalactic events increases as the cube of the interferometer sensitivity, thus putting a high premium on the long baseline. Though a multistage, or phased authorization to the final configuration was carefully considered, the panel does not recommend this approach. We recommend full authorization with phased construction and appropriate milestones.
- F) The plans as described in the presentations and in the various documents provided appear to be well conceived. The procedure which has been employed in drawing up the existing designs and in making the cost estimates appears reasonable and adequate for proceeding to the final design for submission. Effort should continue to examine design alternatives which may decrease costs, particularly in the area of the vacuum system and enclosure. We do not recommend that the project be delayed by this process of re-examination. It is important to make the choice between Fabry-Perot and Michelson interferometer type detectors before submission of the final design. However, it remains important to develop advanced detectors and therefore research should continue to this end.
- G) Because of the magnitude and dual nature of the facility, with laboratory sites widely separated, it is especially important that the construction and operation be well managed. The panel feels that the project requires a single scientific project leader of high stature to direct the activities. Efforts should immediately be directed to providing such leadership.
- H) In looking forward to the utilization of the facilities it should be recognized that in addition to a budget for its operation, adequate funds will be required to support both the needs of experimental groups and further detector development.

I) In conclusion, the panel enthusiastically supports this development effort and urges that the plans for the project be refined along the lines indicated and that the design be completed. We recommend, then, that the construction project be brought to the National Science Foundation Board for consideration and (hopefully) for funding.

Panel Members:

Daniel B. DeBra
Val L. Fitch
Richard L. Garwin
John L. Hall

Boyce D. McDaniel
Andrew M. Sessler
Saul A. Teukolsky
Alvin A. Tollestrup

APPENDIX K

MEMORANDA OF UNDERSTANDING

The LIGO Project has been working closely with a number of other organizations and individuals in the development of the LIGO detector. This appendix contains three memoranda of understanding which describe some of the relationships between the LIGO Project and these organizations.

These documents are intended to give a general overview of the relationships between the LIGO Project and these organizations. They do not contain all the details of the agreements, but they do provide a general overview of the nature of the relationships.

Included here are copies of three signed memoranda of understanding (MOU).

(1) MOU between Caltech and MIT on the LIGO Project.

(2) MOU between the LIGO Project and the Byer research group at Stanford University.

(3) MOU between the LIGO Project and the Low Frequency Isolation Project at the University of Colorado.

These documents are intended to give a general overview of the relationships between the LIGO Project and these organizations. They do not contain all the details of the agreements, but they do provide a general overview of the nature of the relationships.

These documents are intended to give a general overview of the relationships between the LIGO Project and these organizations. They do not contain all the details of the agreements, but they do provide a general overview of the nature of the relationships.

These documents are intended to give a general overview of the relationships between the LIGO Project and these organizations. They do not contain all the details of the agreements, but they do provide a general overview of the nature of the relationships.

These documents are intended to give a general overview of the relationships between the LIGO Project and these organizations. They do not contain all the details of the agreements, but they do provide a general overview of the nature of the relationships.

* MEMORANDUM OF UNDERSTANDING
BETWEEN THE
CALIFORNIA INSTITUTE OF TECHNOLOGY (CALTECH)
AND THE
MASSACHUSETTS INSTITUTE OF TECHNOLOGY (MIT)
ON THE
LIGO PROJECT

- 1) The LIGO project is an integrated and collaborative effort by Caltech and MIT scientists to design, build and operate an observatory to measure gravitational waves from astrophysical sources by laser interferometry.
- 2) Caltech serves as the prime contractor for the LIGO project with the National Science Foundation, and the activities of the MIT science team are supported under a subcontract from Caltech.
- 3) The project director is the Principal Investigator for the LIGO and has overall responsibility for the design, construction and operation of the LIGO.
 - a) The director reports to the Caltech provost and is appointed by Caltech in consultation with MIT.
 - b) The director's administrative contacts at MIT are the chairman of the department of physics and the director of the Center for Space Research.
- 4) Caltech and MIT Co-investigators have equal rights within the project, have access to the technical resources of the project and share in the responsibilities to make the project a success.
- 5) The functions carried out by Caltech and MIT scientists include the following:
 - a) Support the design, construction, and operation of the LIGO.
 - b) Carry out research and development of the initial and advanced interferometers.
 - c) Take responsibility for the development and testing of LIGO interferometer subsystems as appropriate.
 - d) Develop data analysis and diagnostic procedures for the LIGO.

Paul C. Jennings

P. C. Jennings, Provost
Caltech

R. E. Vogt

R. E. Vogt, Director
LIGO Project

G. M. Brown

G. M. Brown, Dean of the
School of Science, MIT

11-13-89

10 November 1989

Memorandum of Understanding
between
The LIGO PROJECT (Caltech/MIT)
and
The Byer research group at Stanford University

This memorandum of understanding describes technical and scientific exchanges that have occurred during the proposal preparation period, the proposal review period and those that are planned for the period during which the laser source will be under investigation by the Byer group at Stanford University for eventual application to the Laser Interferometer that is the key technical element of the Laser Interferometer Gravity Wave Observatory (LIGO).

Proposal Preparation Period

The Stanford group was in communication with the LIGO group during the preparation of the Stanford NSF proposal to study solid state lasers that will meet the requirements for the LIGO project. LIGO researchers provided invaluable information to the Stanford Group on the laser source requirements. In addition, during the preparation of the Stanford proposal, Professor Byer visited Cal Tech and MIT to learn first hand about the laser interferometer experiments and about the laser requirements. Both Professor R. Vogt and Professor R. Weiss visited the Stanford campus during the proposal preparation period to learn first hand of the solid state laser technology that was being proposed to meet the LIGO laser requirements.

Technical Discussions following the submission of the Proposal to the NSF

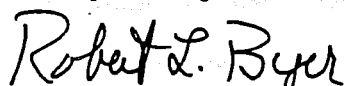
Since the submission of the Stanford Proposal to the National Science Foundation in June 1988, the contacts between the Stanford and the LIGO group have increased both in frequency and in the depth of the technical discussion. Stanford researchers have visited Caltech twice and LIGO researchers have visited Stanford once. During the first Stanford group visit, M. Zucker and A. Abramovici gave useful advice to T. Day and to E. Gustafson on control circuits for Pound-Drever locking and gave technical information on frequency stability measurements. In addition, Y. Gursel provided useful information on vibration isolation. The LIGO group offered assistance in the construction of a high finesse Fabry Perot interferometer. On a second visit to Caltech, Y. Gursel assisted T. Day in the construction of a 25 cm long, 600MHz free spectral range, high finesse interferometer to act as a reference cavity for laser stability measurements.

On August 16 and 17, A. Abramovici visited Stanford, presented a talk to the Byer Group on the laser requirements for the LIGO system and engaged in detailed technical discussions about the solid state laser sources being researched for the LIGO project.

Future Scientific and Technical Exchanges

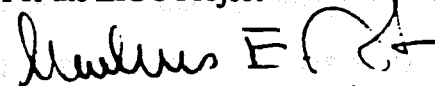
Biannual technical reviews of the Byer group diode pumped solid state laser research program are planned to insure that the work on the laser sources is consistent with the requirements of the LIGO project. These reviews will take place alternatively at the Caltech and at the Stanford locations. The Byer group will work to transfer the knowledge gained in the laser sources in a timely manner to the LIGO project. Work on laser amplitude and phase noise, spatial mode characteristics, temporal and spatial mode clean up, and on high power optics will be areas of continued discussion. To insure that the technical and scientific discussions occur in a timely manner, the Byer Group assigns liason responsibilities to Dr. E. Gustafson. The technical liason responsibilities for the LIGO project are assigned to Dr. F. J. Raab.

For the Byer Group



Robert L. Byer, Date 9/14/89

For the LIGO Project



Rochus E. Vogt, Date 9/18/89

MEMORANDUM OF UNDERSTANDING

on

LOW FREQUENCY ISOLATION RESEARCH

between the

Laser Interferometer Gravitational Wave Observatory Project

(California Institute of Technology and Massachusetts Institute of Technology)

and the

Low Frequency Isolation Project

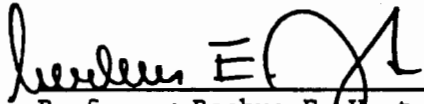
(University of Colorado)

The University of Colorado is proposing to develop a prototype two-stage

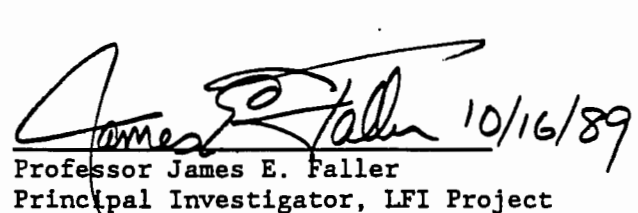
vibration isolation system capable of achieving a factor 10^4 isolation in all 6 degrees of freedom over the frequency band from 1 to 10 Hz. The goal for the internal noise level of the prototype system is $10^{-11} \times (1 \text{ Hz}/f)^2 \text{ cm/sec}^2/\text{Hz}^{0.5}$ or less for horizontal displacements. The time scale for carrying out this work is about four years.

After the prototype system is successful, the objective of the University of Colorado group is to join with the Laser Interferometer Gravitational Wave Observatory (LIGO) Project to design and build a 4 km low-frequency gravitational wave detector, probably covering the frequency range 1 to 30 Hz, to operate in the LIGO vacuum systems. It is recognized that the LIGO Project cannot commit itself at this time to participating in such a future program. However, collaboration between the Low Frequency Isolation (LFI) Project and the LIGO Project on the prototype isolation system and on tests of thermal noise using the prototype system is necessary in order to make the results as useful as possible to the LIGO Project and to achieve as rapid progress as possible by the LFI Project. To achieve these objectives, the LIGO Project and the LFI Project approve the following agreement.

1. The LFI Project will provide preliminary design information on the first stage of the isolation system to the LIGO Project, and utilize suggestions from the LIGO Project in the final design. It will keep the LIGO Project informed of progress on building and testing the first stage, and present the results to the LIGO Project for discussion before proceeding with construction of the second stage. Finally, the LIGO Project will be kept informed of all significant results from testing of the second stage and from tests of thermal noise in pendulums hung from the second stage.
2. The LIGO Project will provide information and advice to the LFI Project, in particular on desirable characteristics for the prototype low-frequency isolation system, and will make suggestions concerning the design and testing of the system. Finally, after measurements on the prototype low-frequency isolation system have been made, the LIGO Project will take part in discussions of whether to proceed further toward the design of a low-frequency gravitational detector, either as a supplement to the main LIGO program or as part of a future LIGO users program.
3. Annual joint meetings of the LFI Project and the LIGO Project will be held in order to achieve a necessary level of interaction between the two Projects.


Rochus E. Vogt
Professor
Director, LIGO Project

10/17/89


James E. Faller
Professor
Principal Investigator, LFI Project

10/16/89

Proposal to the National Science Foundation

A
**LASER INTERFEROMETER
GRAVITATIONAL-WAVE
OBSERVATORY
(LIGO)**

LIGO-M890001-00-M

VOLUME 2:
Phase-A Design and Construction Implementation

December 1989

CALIFORNIA INSTITUTE OF TECHNOLOGY
MASSACHUSETTS INSTITUTE OF TECHNOLOGY

LIGO PROJECT

Proposal to the National Science Foundation

**THE CONSTRUCTION, OPERATION, AND
SUPPORTING RESEARCH AND DEVELOPMENT
OF A**

**LASER INTERFEROMETER
GRAVITATIONAL-WAVE
OBSERVATORY**

Submitted by the
CALIFORNIA INSTITUTE OF TECHNOLOGY
Copyright © 1989

Rochus E. Vogt
Principal Investigator and Project Director
California Institute of Technology

Ronald W. P. Drever
Co-Investigator
California Institute of Technology

Frederick J. Raab
Co-Investigator
California Institute of Technology

Kip S. Thorne
Co-Investigator
California Institute of Technology

Rainer Weiss
Co-Investigator
Massachusetts Institute of Technology

Table of Contents: Volume 2

I. INTRODUCTION	1
II. DESIGN REQUIREMENTS, SPECIFICATIONS, AND GOALS	2
III. PHASED IMPLEMENTATION	9
IV. DESIGN DESCRIPTION	10
A. Overview	10
B. Initial Interferometer Design Description	13
C. Vacuum System: Mechanical Design	25
D. Vacuum System: Vacuum Design	49
E. Enclosure Design	60
F. Instrumentation, Control, and Data System	68
G. Electrical Power	72
V. SITES	74
VI. IMPLEMENTATION PLAN	78
A. Work-Breakdown Structure	78
B. Organization and Responsibilities	80
C. Design and Construction Schedule	82
D. Subcontracting Plan	84
E. Interferometer Design and Fabrication	85
VII. COST SUMMARY	87
Residual Funds Statement	90
Proposal Budget in NSF Format	91
Current and Pending Support	107

APPENDICES:

- A. Expansion to Phase-B and Phase-C Configurations
- B. Post-Construction Operations Cost
- C. Design and Construction Cost Detail
- D. Measured Outgassing Properties of Stainless Steel

Outline of Contents: Volume 1

Preface

Summary

I. Introduction

II. Physics of Gravitational Waves, Sources, and Detectors

III. Laser Interferometers

A. General Characteristics and Noise Effects

B. 40-meter Prototype Interferometer

IV. LIGO Concept

A. Requirements

B. Implementation

V. Design and Siting of Interferometers

A. Conceptual Design of the Initial LIGO Interferometers

B. Evolution of LIGO Interferometers

C. LIGO Sites: Scientific Aspects

VI. LIGO Operations

VII. Strategy for Identification of Gravitational Waves

VIII. Campus Research and Development in Support of LIGO

A. Results from Prior NSF Support

B. Future Activities

IX. Organization and Management

X. International and Domestic Collaboration

XI. References

XII. Schedule and Budget

Response to NSF Notice No. 107

Key Personnel: Vitae

Key Personnel: Publications

Appendices:

A. The Physics of Gravitational Waves, and Comparison of Source Strengths with Detector Sensitivities

B. Interferometer Concepts and Noise

C. Concepts for Advanced Interferometers

D. Calculation of Vibration Isolation

E. Power Spectral Density and Detector Sensitivity

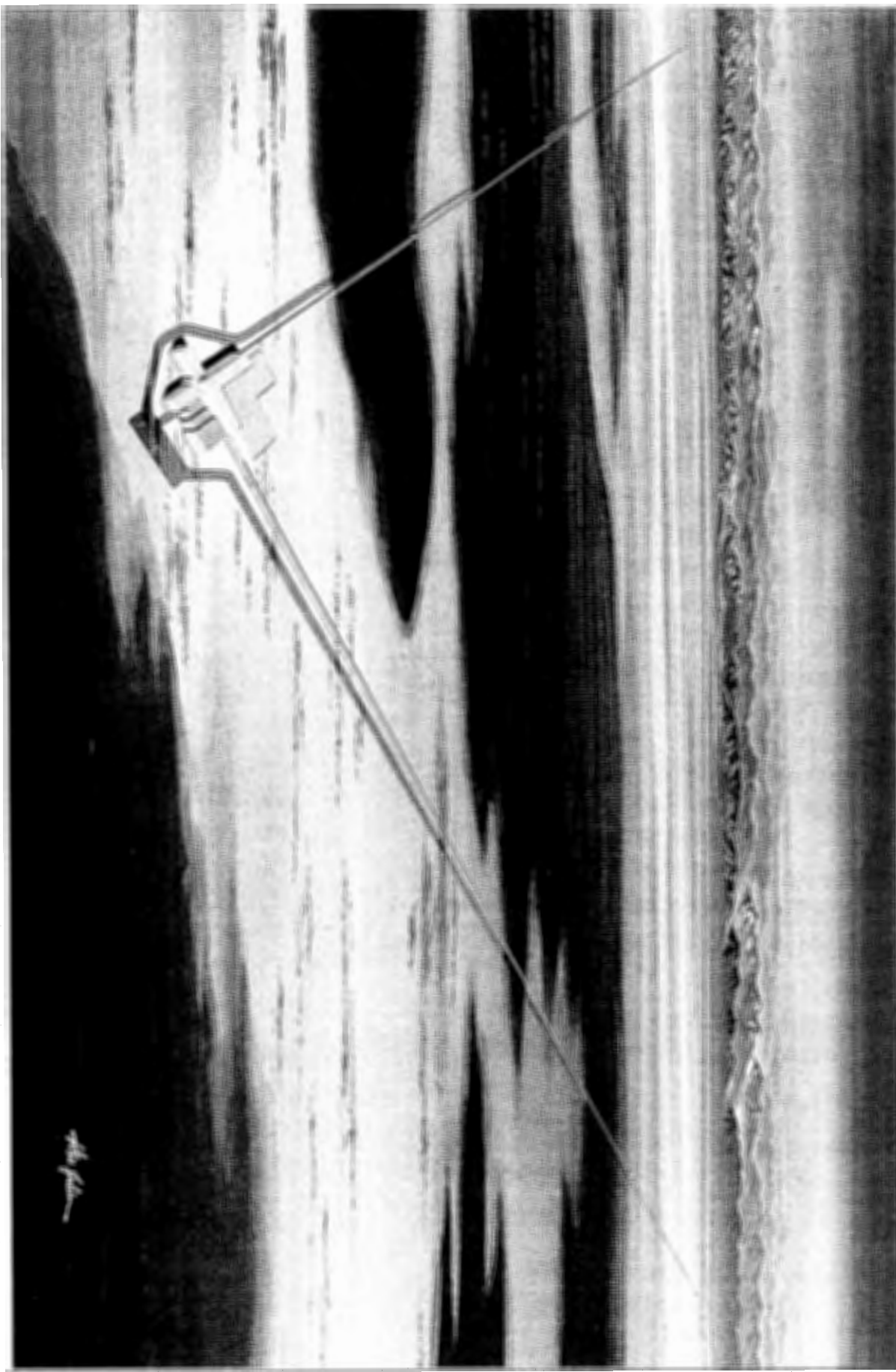
F. Scattering and Optical Properties of the Beam Tubes

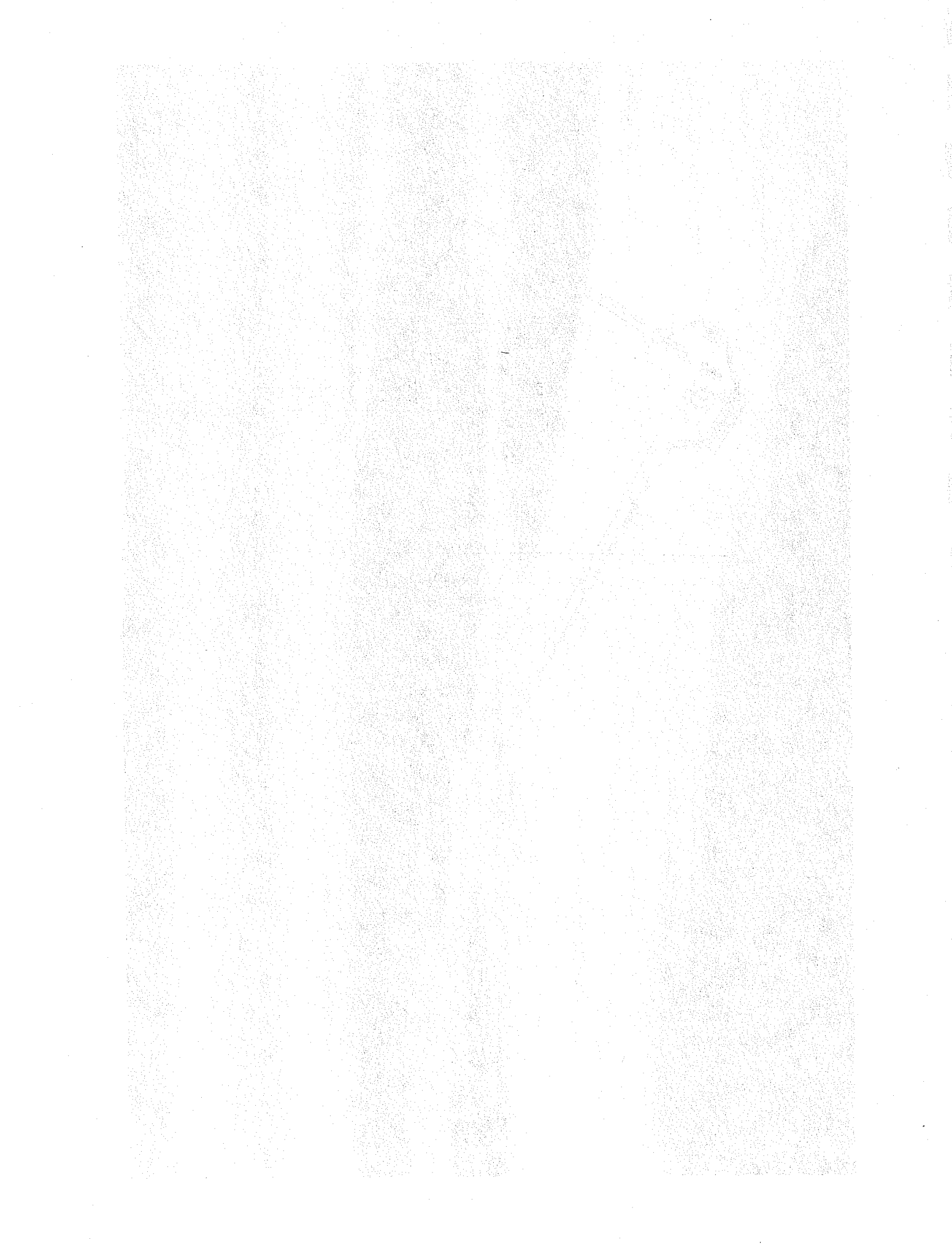
G. LIGO Project Gravitational-Wave Searches

H. Report on Recent Progress

J. History of the Project

K. Memoranda of Understanding





I. INTRODUCTION

This is the second of two volumes of a proposal to construct a Laser Interferometer Gravitational-Wave Observatory (LIGO). An artist's sketch of the facility at one of the sites is presented on the facing page. Volume 1, **LIGO Science and Concepts**, gives the scientific justification for the proposed LIGO, concepts for gravitational-wave detection, a general discussion of the conceptual design, and an overview of the LIGO project organization, budget, and schedule.

Volume 2, **Phase-A Design and Construction Implementation**, addresses the requirements derived from Volume 1 and presents a conceptual design description, a construction implementation plan, and a cost estimate. The LIGO requirements, specifications, and goals are given in Section II, the influence of phased construction on the design is discussed in Section III, and the detailed conceptual design is presented in Section IV. Site considerations are discussed in Section V, a project implementation plan is provided in Section VI, and project costs are presented in Section VII.

The present phase of the LIGO design process has sought to establish a sound basis for estimating the cost of implementation. It was not possible to scale the cost from an existing design because no similar facility has been built before. Therefore, selected design features were investigated at a fairly detailed level. Design priorities were derived primarily from a priori perceptions of cost and cost risk. The resulting design description in Section IV shows differing levels of detail, providing for a balanced cost analysis in Section VII.

II. LIGO REQUIREMENTS AND CONCEPTUAL DESIGN

Volume 1 gave a broad-based description of the LIGO facility and its scientific aims and concepts. This volume provides a more detailed description of the LIGO facility and its scientific aims and concepts. The LIGO facility will consist of two detectors, one located in each of two different countries. The detectors will be located in separate buildings, and each building will contain a large vacuum chamber. The vacuum chamber will be used to detect gravitational waves by observing the motion of a laser beam reflected off a mirror. The mirror will be suspended from a fixed point, and the motion of the mirror will be detected by a photodetector. The photodetector will be connected to a computer, which will analyze the data and determine if a gravitational wave has been detected. The computer will also control the laser beam and the mirror. The LIGO facility will be located in a remote area, away from sources of interference, such as power lines and other electronic equipment. The facility will be designed to withstand seismic activity and other natural disasters. The facility will be operated by a team of scientists and engineers, who will monitor the data and make adjustments as needed. The facility will be open to the public, and visitors will be able to see the equipment and learn about the science of gravitational waves.

II. DESIGN REQUIREMENTS, SPECIFICATIONS, AND GOALS

The LIGO Concept described in Volume 1, Section IV defines key features of the proposed facilities. We outline below the most important design considerations derived from this concept.

The LIGO will consist of two laser interferometer facilities located far apart within the continental United States. Each facility will include a vacuum system, laid out in the form of an "L", that is made up of 4-km tubes for the laser beams that define the interferometer arms and of chambers that house the interferometer components. The tubes will be approximately 1.2 m in diameter and will accommodate up to six primary-interferometer beams. The facilities will also include buildings to protect the vacuum chambers, protective enclosures for the beam tubes, and provisions for isolating sensitive interferometer components from vibration, acoustic noise, dust, and other disturbances.

A. 4-km Arm Length

Specifications associated with the arm length are summarized in Table II-1.

TABLE II-1
LIGO ARM LENGTH SPECIFICATIONS

Parameter	Value
Arm length (nominal)	4 km
Arm length match between sites	0.2 km
Arm length match at each site	2 cm

B. Several Interferometers at Each Site

An essential feature of the LIGO is the capability to operate concurrently several interferometers at each site¹ with minimum interference between the interferometers at a site (Volume 1, Section IV.A.3). Instead of separate vacuum systems for each interferometer, a more economical system has been designed that permits access to the components of any one interferometer while preserving the vacuum environment for the laser beams and components of the other interferometers.

This design is illustrated for the case of two interferometers in Figure II-1. Interferometer 1 has its test masses and optical components at the corner and extreme ends of the vacuum-system arms. Interferometer 2 shares most of this vacuum system, except that its beam splitter and associated optics are contained

¹ The Phase-C configuration of the LIGO will have 6 interferometers at Site 1 and 3 interferometers at Site 2. (See Appendix A for a discussion of a possible future expansion of the LIGO.)

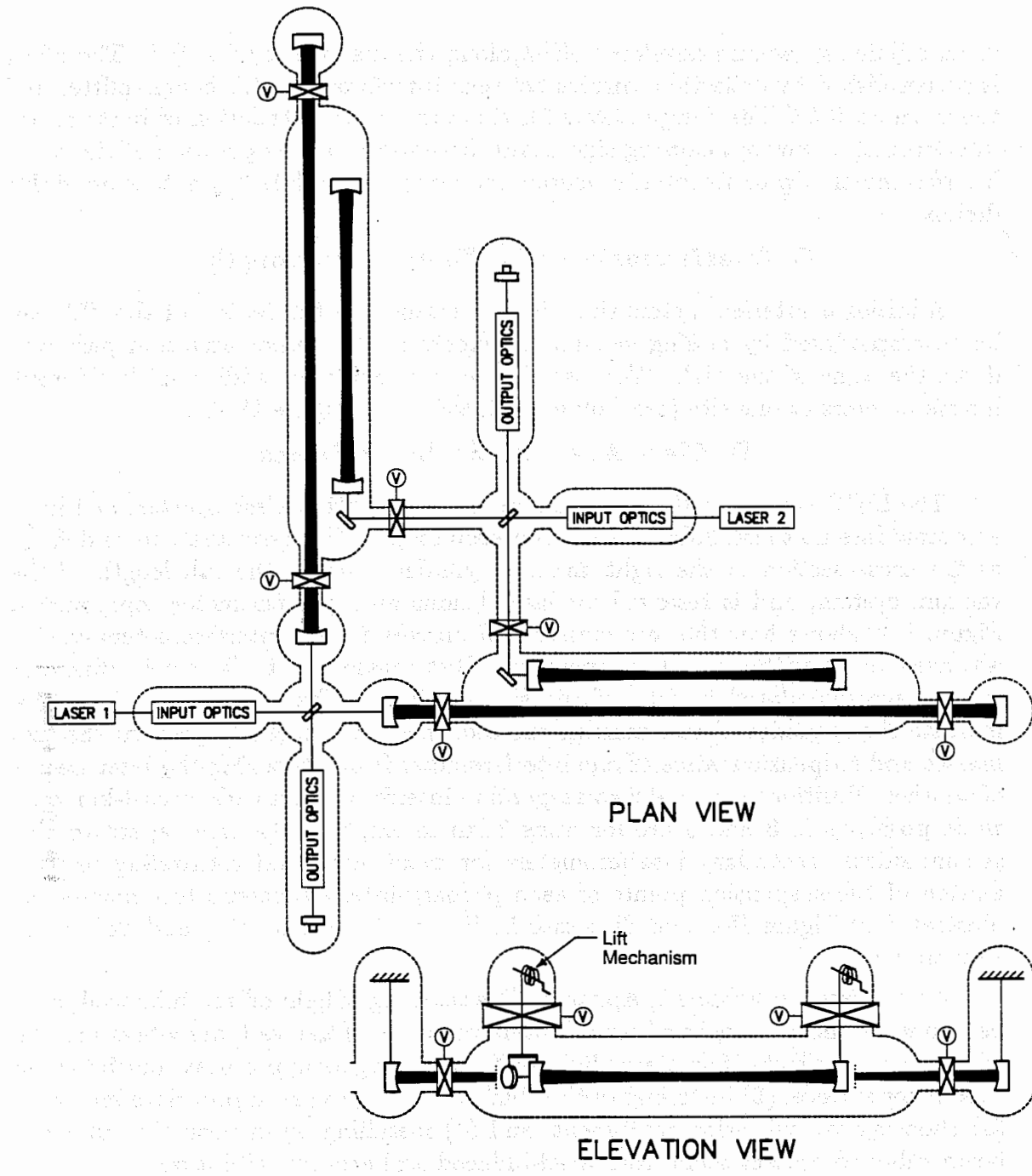


Figure II-1 Schematic illustration of two interferometers sharing the same vacuum system with minimum interference. One interferometer has its beam splitter and associated input and output optics at the intersection of the two arms. The second interferometer shares the vacuum envelope for the arms, but has an adjoining vacuum envelope for its beam splitter and associated optics, situated along the bisector of the arms. Deflection mirrors steer light between the beam splitter and the main cavities. The gate valves ("V") shown in the plan view allow most parts of either interferometer to be isolated for access while the other is operating. The remaining parts (deflection mirrors and main cavity mirrors of the second interferometer) are serviced by lifting them from the vacuum system arms (see elevation view) and closing horizontal gate valves.

in an adjoining vacuum envelope, offset along the diagonal of the "L". The offset is accomplished by deflection mirrors between Interferometer 2's beam splitter and the main cavities. The design allows for the removal or installation of parts of one interferometer, without causing significant disruption to the operation of the other interferometer. Up to six interferometers can be accommodated by extension of this design.

C. Interferometers of Different Arm Lengths

Additional interferometers that do not extend the full length of the "L" can be accommodated by adding vacuum chambers in the corner area and part way down the arms of the "L". We have chosen to provide for additional half-length interferometers at one site (see Volume 1, Section IV, Figure IV-1).

D. Clear Aperture for Laser Beams

The LIGO concept calls for a vacuum enclosure with a *clear aperture* of 1 m to accommodate up to six Fabry-Perot interferometers.² The clear aperture is defined as the cross section of the right circular cylinder running the full length of the vacuum system, and is reserved for laser beams and interferometer components. Figure II-2 shows how the test masses and mirrors for six interferometers can be arranged to fit within the 1 m aperture. Test masses up to 50 cm in diameter can be accommodated in four of the six positions. The numbers in the figure indicate the sequence of test masses; the sequence was chosen to prevent the test masses and suspension wires of one interferometer from obscuring the laser beams of another. Positions 1, 4, and 6 correspond to interferometers with arms 4-km long, while positions 2, 3 and 5 are for arms 2-km in length. The clear aperture also accommodates secondary interferometers for monitoring and controlling relative motion of the suspension points of each primary-interferometer's test masses, as illustrated in Figure II-2 and discussed in Volume 1, Section V.A and Volume 1, Appendix C.

As discussed in Volume 1, Appendix F, scattering of light off the tube walls may be a source of noise in more advanced interferometers, if the walls are vibrating. We will reduce the effects of scattered light by (1) choosing an appropriate finish for the tube inner surface, (2) installing optical baffles in the tube at appropriate intervals, (3) choosing low-vibration equipment, and (4) installing an enclosure around the beam tubes to protect them from wind-induced and acoustic vibration.

E. Vacuum System Properties

Statistical fluctuations in the index of refraction of the residual gas can limit interferometer sensitivity, as discussed in Volume 1, Section III.A.3. The effect varies with gas species and is cumulative along the gas column in the optical path. The LIGO pressure specifications are summarized in Table II-2.

² This aperture permits flexibility in interferometer design by accommodating both delay-line or mixed Fabry-Perot/delay-line interferometers, possibly operating at near-infrared wavelengths.

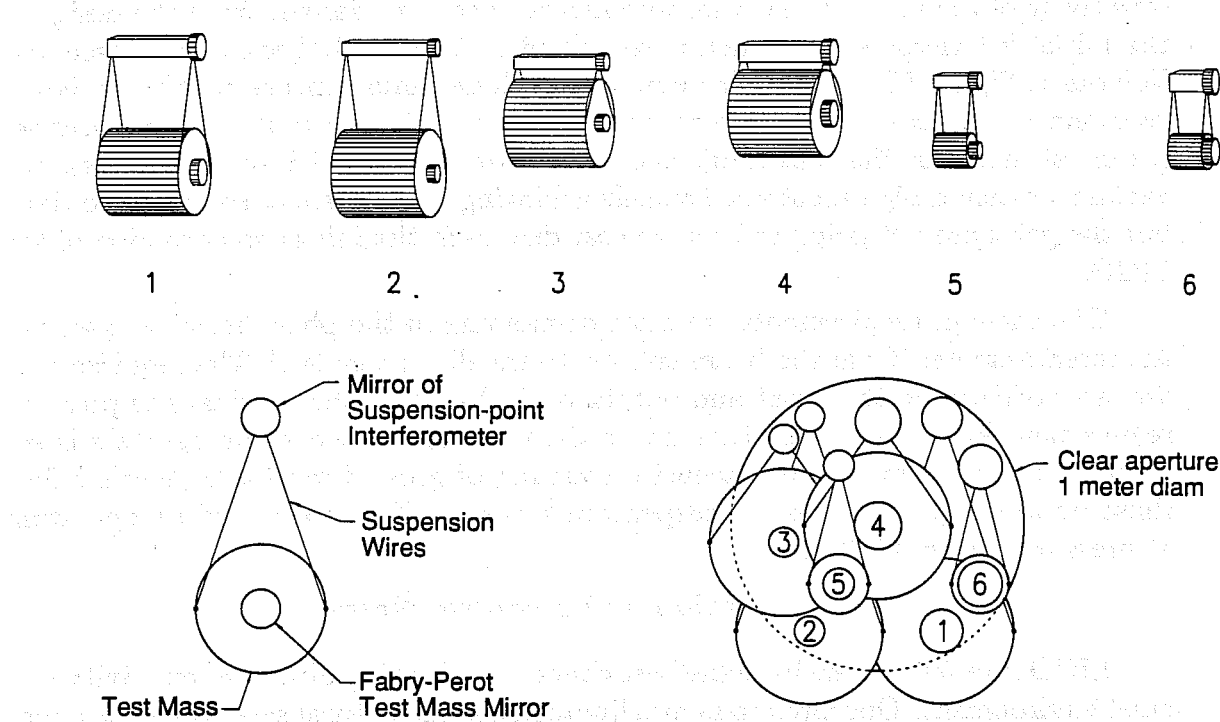


Figure II-2 Arrangement of test masses with attached interferometer cavity mirrors. *Upper:* Arrangement of individual test masses in the corner station that permits most efficient use of the clear aperture. The corresponding end masses at the end or mid stations are in the reverse order. *Lower left:* End-view of a suspended test mass. *Lower right:* A view of the corner station masses as seen from one of the beam tubes, showing the relation to the 1 meter clear aperture.

TABLE II-2
AVERAGE BEAM-TUBE PARTIAL PRESSURES¹
INITIAL REQUIREMENTS AND GOALS

GAS SPECIES	INITIAL REQUIREMENT	GOAL
(torr @ 300 K)		
H ₂	1×10^{-6}	1×10^{-9}
H ₂ O	1×10^{-7}	1×10^{-10}
N ₂	6×10^{-8}	6×10^{-11}
CO	5×10^{-8}	5×10^{-11}
CO ₂	2×10^{-8}	2×10^{-11}

¹Maximum pressure in chambers = 1×10^{-6} torr.

The initial pressure requirements are set so that residual gas will not limit the

sensitivity of the initial LIGO interferometers. They are derived from the design of the initial interferometers, which is described in Volume 1, Section V.A (see also Volume 1, Figure III-2). The vacuum system design must ensure that these *initial requirements* are met with some margin.³ The *goals* in the table are similarly set (from estimates of the sensitivity achievable with advanced interferometers); the vacuum system design must not *preclude* achieving these goals at some future time, but the goals are not going to become cost drivers in the initial construction of the LIGO.

The vacuum requirements are most demanding in the phase-sensitive paths of the interferometer (from the beam splitter to the distant ends).⁴ The requirements are less stringent in the input and output optical paths. The residual gas pressure requirement in the chambers that house the test masses and beam splitters is set to keep the gas damping and acoustic coupling of ground motion at levels below those imposed by the test-mass suspension systems. This is satisfied by operating at pressures below 10^{-6} torr.

F. Vibration and Acoustic Noise

LIGO interferometers have the best chance of achieving ultimate sensitivity in a quiet environment. One environmental limitation is the natural seismic background. Figure II-3 shows the vibration amplitude spectral density of typical ground motion at several representative locations. The dashed line represents the adopted LIGO design environment; the LIGO facilities will be designed to have vibrational motion at the support interfaces for the interferometer vibration-isolation stacks that is lower than this level.

Acoustic noise at the vacuum enclosure and lasers will be limited to a pressure amplitude spectral density of 10^{-4} Pa/ $\sqrt{\text{Hz}}$ and 45 dBA rms (about the level of a quiet office).

G. Cleanliness and Dust Control

Some of the optical components of LIGO interferometers are sensitive to dust, and are usually handled in clean room environments. Dust, volatile contaminants, and hydrocarbons can also collect on exposed vacuum-system surfaces during internal-access operations, limiting vacuum-system performance and, perhaps more

³ The current vacuum-system design, described in Section IV, can meet these initial requirements even without the bakeout that is planned as part of the installation.

⁴ Another consideration is the temporal stability of the gas column density. Although rapid fluctuations in the column density have not been observed in accelerator vacuum systems nor in the prototype interferometers, the LIGO will be many orders of magnitude more sensitive than prior systems, and the short-term stability of the column density merits attention. The optical phase change that results from a pulse of gas in the phase-sensitive part of an interferometer might simulate a gravitational-wave burst. The half-length interferometer should enable discrimination between pulses of gas and valid gravitational-wave signals (see Volume 1, Section VII).

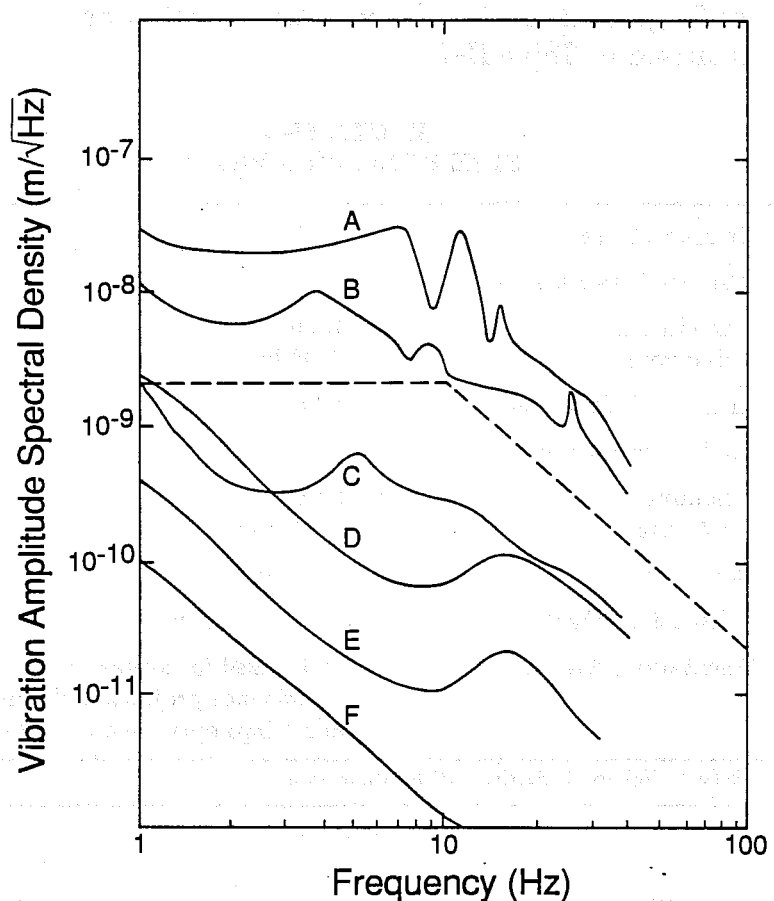


Figure II-3 Vibration amplitude spectral density data for typical motion of the ground at several locations: (A) MIT laboratory; (B) Caltech laboratory; (C and D) potential LIGO sites; (E) Lajitas, Texas (seismically quietest known location in the United States), with 3–10 mph wind conditions; (F) Lajitas, with no wind. The dashed line is the adopted LIGO specification for vibration measured at the instrument mounting structures.

seriously, exposing the contained optics to sources of contamination during vacuum operation.

The contamination problem is addressed by a hierarchical strategy for limiting dust contamination, beginning with control of building material and pressurization of buildings, and ending with dust filtration and local air curtains in the chambers and critical work areas.

H. Site Requirements

The scientific goals of the LIGO constrain the selection of sites; site specifications are summarized in Table II-3.

**TABLE II-3
SITE SPECIFICATIONS**

Number of sites	2
Distance between sites	
minimum	2500 km
maximum	4500 km
Arm length (nominal)	4 km
Angle between arms	
nominal	90 deg
tolerance	± 15 deg
Slope of arms	< 0.2 deg
Orientation, absolute	No requirement
Orientation, relative	Optimized for average of coincidence projection alignment and Virgo-optimized alignment ¹

¹Refer to Volume 1, Section V.C for discussion.

The site specifications are satisfied most economically by locations that can accommodate level interferometer arms with a minimum of earthwork. Sites should be sufficiently far from urban development to ensure that they are seismically and acoustically quiet, but near enough for convenient housing of resident and visiting staff. Electrical power and road (or rail) access should be sufficiently close to allow economical construction. Soils and drainage characteristics must be suitable for LIGO construction, and environmental-impact concerns must be addressable.

I. Laser Power

Installed electrical power and cooling capacity limit the optical power available from lasers. The total electrical power allocated to lasers will be 320 kW at a site (see Volume 1, Section IV.B.2). This is sufficient for a total of 20 W of argon-ion laser output, or 3 kW of output from Nd:YAG lasers.

III. PHASED IMPLEMENTATION

In this section, we describe how plans to expand the LIGO facilities beyond the Phase-A period (covered by this proposal) influence the design of the initial facilities. As described in Volume 1, Section IV, we anticipate three phases in the life span of the facilities:

- (1) *Phase A, The Exploration/Discovery Phase*, will provide a *one-detector*¹ facility for observation *or* development.
- (2) *Phase B, The Discovery/Observation Phase*, will provide a *two-detector* facility and allow concurrent observation *and* development.
- (3) *Phase C, The Observatory Phase*, will provide a *three-detector* facility and allow concurrent observation, development, and special investigations. It completes the LIGO evolution to its full capability as presently conceived.

The beam-tube length and diameter are fixed at the outset, and are determined by the needs of the Phase-A configuration. The basis for choosing the beam-tube length is discussed in Volume 1, Section IV. The beam-tube diameter is determined from the requirement for a "clear aperture" for laser beams (see Section II.D) and the need to provide space for baffles and a safety margin for alignment errors and drift.

The principal impact of the phased-implementation approach on the Phase-A design is that the initial vacuum system and enclosures must be configured so as not to preclude increasing the number of interferometers that share the beam tube.

The chambers that house interferometer components are modular; adding interferometers involves building and installing chambers of types already designed for Phase A. The initial vacuum system is designed with removable sections and appropriately placed valves to permit installation of hardware for future phases with a minimum of disruption to operations (see Section IV.C). The vacuum-chamber configurations for Phases B and C are described in detail in Appendix A.

The Phase-A buildings that house the vacuum chambers are designed from the outset to accommodate the full Phase-C vacuum-system configuration. This choice is partly motivated by the consideration that future expansion of an initially smaller building would cost far more than any relatively modest savings realized up front. However, our primary concern is to minimize the disruption that accompanies expansion.

¹ A *detector* is nominally defined as three laser interferometers, two at Site 1 and one at Site 2.

IV. DESIGN DESCRIPTION

A. Overview

The LIGO will incorporate L-shaped interferometric detectors with arms of 4-km length, located at two widely separated sites. This section of the proposal describes the concepts for design of the LIGO detectors and supporting facilities.

The major elements of each LIGO installation are:

- (1) The interferometers.
- (2) A vacuum system, which provides the operating environment for the interferometers.
- (3) Enclosures, which provide a controlled environment for the vacuum system and for personnel.
- (4) Additional supporting equipment and facilities.

The LIGO installation at Site 1 will consist of five *stations* connected by *beam-tube modules* (each 2 km in length); it will be laid out as shown in Figure IV-A-1. The *corner station*, two *end stations* (one each at the end of the right and left arms), and two *mid stations* (one on each arm) will provide access to the vacuum system and contain interferometer components, vacuum equipment, and instruments. The sole function of the beam tubes will be to provide an evacuated path for transmitting light between stations. Because these tubes will be passive, access to their interior will not be required. *Full-length* interferometers will be made up of components installed in the corner stations and end stations; *half-length* interferometer components will be installed at corner stations and mid stations. The Site 2 installation will be identical to that shown in Figure IV-A-1 for Site 1, except that Site 2 will have no half-length interferometers and no mid stations.

The remainder of this section is organized as follows:

- B. Initial Interferometer Design Description.
- C. Vacuum System: Mechanical Design.
- D. Vacuum System: Vacuum Design.
- E. Enclosure Design.
- F. Instrumentation, Control, and Data System.
- G. Electrical Power.

The reader may wish to review Volume 1, Section IV, which presents the rationale for the design features. Also, a quick survey of the remainder of this section may be achieved by scanning the figures and captions; much of the design information is contained in these illustrations.

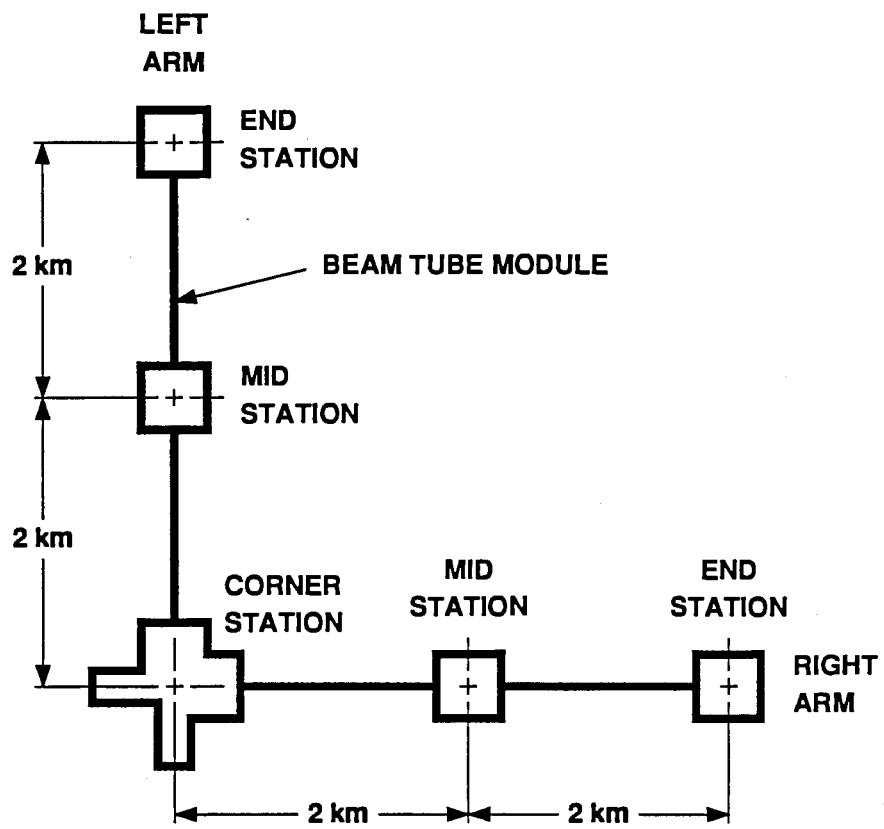


Figure IV-A-1 Layout of LIGO Site 1 facility showing the relationship of corner station, end stations and mid stations connected by beam-tube modules 2-km long (a reduced version of this figure appears in many other figures to help orient the reader). The Site 2 facility has no mid stations.

ஏன் கூடும் என்று பல வகையில் கீழே கொடுக்கப்படுகின்றது.

B. Initial Interferometer Design Description

The goal of the initial interferometer (see Volume 1, Section V.A) is to achieve the highest sensitivity consistent with simple and reliable operation, using a 5-W argon-ion laser and, to the maximum extent possible, using components and techniques proven in the prototypes. The design description presented in this section is in preliminary form; it represents the simplest implementation consistent with minimizing risks in the extension from prototype scales to 4-km arm lengths. LIGO interferometers will contain a number of modular subsystems, each as independent as practicable. The interferometers will be sufficiently flexible to allow switching between different modes of operation, from non-recycling mode in the first tests, to various recycling modes. The principal features for each subsystem in the initial interferometers are described and sample parameters are given.

1. Lasers and extra-vacuum optics

Each interferometer will have its own laser and associated prestabilization system on optical benches that are separate from the main vacuum chambers. Some of the parameters for this subsystem are listed in Table IV-B-1. These parameters are based on the assumption that commercial lasers will be modified by us for improved stability, using techniques developed during prototype research. The modification isolates the laser mirrors from vibrations (resulting from the turbulent flow of cooling water), and adds piezoelectric translators to control the laser frequency. The reference cavity is a length standard defined by a stable spacer between mirrors housed in a small vacuum chamber near the laser. A small fraction of the laser output will be sampled for frequency stabilization of the main beam.

TABLE IV-B-1
PARAMETERS FOR LASER AND EXTRA-VACUUM OPTICS

Parameter	Value	Notes
Laser type	Argon ion	
Wavelength	514 nm	
Power output	5 W	Single longitudinal mode
Reference cavity		
Length	≈ 1 m	
Power	≈ 0.1 W	
Finesse ¹	≈ 1000	

¹See Section IV.B.2.a

2. Input/output optics

Many of the components within the corner-station vacuum chambers are for conditioning and filtering the interferometer input and output beams. Figure IV-B-1 illustrates how the light is processed.

Figure IV-B-1 (facing page) The path of laser beams (arrows) through the functional units (boxes) in the initial interferometer. Many of the units are replicated several times with only minor modifications (see text). The functional units are grouped into subsystems denoted by dotted borders. The electrical connections are not shown in this figure.

a. Mode-cleaner and filter cavities. There will be one or two¹ (the pair arranged in series) mode-cleaner cavities (see Volume 1, Section III.B.3) at the input, and one at the output. The cavity mirrors for the mode cleaners will be separately suspended and controlled, with alignment controls similar to those for the main cavity mirrors (see below). As indicated in Table IV-B-2, the input mode cleaners must be capable of handling the full power available from the laser, and the output mode cleaner will be exposed to much less power. The optical phase modulation is simplified by choosing the length of the output mode cleaner so that the modulation sidebands and the laser frequency are transmitted by different resonance modes of the cavity. The finesse F ($F \simeq \pi/(1 - \sqrt{R_1 R_2})$, where R_i is the intensity reflectivity of mirror i) of the input and output mode cleaners is chosen to obtain the best filtering action without significant transmission loss.

A circulator² before the output mode cleaner diverts the light reflected from this mode cleaner into the subcarrier filter system, which contains the output filter cavity. This system separates optical signals with different carrier and modulation frequencies. These signals are used for interferometer control. The optical and mechanical specifications for the filter cavity are less demanding than those for a mode cleaner. The filter cavity may be made from separately suspended components, or from mirrors on the ends of a fixed spacer.

b. Functional units. Six distinct functional units are replicated throughout the input and output conditioning-optics chains:

i. Mode-matching telescope. This unit consists of lenses that match a beam to the TEM_{00} mode of a cavity or reduce the diameter of light beams exiting a cavity and passing through small-aperture components such as Faraday isolators and Pockels cells. Larger components may be used as they become available, especially if their use can reduce the number of mode-matching telescopes.

¹ The prefiltering mode cleaner may not be required for the initial interferometers. This will be determined from results of prototype experiments.

² A circulator (typically made from a polarizing beam splitter and a quarter-wave retardation plate) diverts reflected light from a cavity away from the incident beam axis.

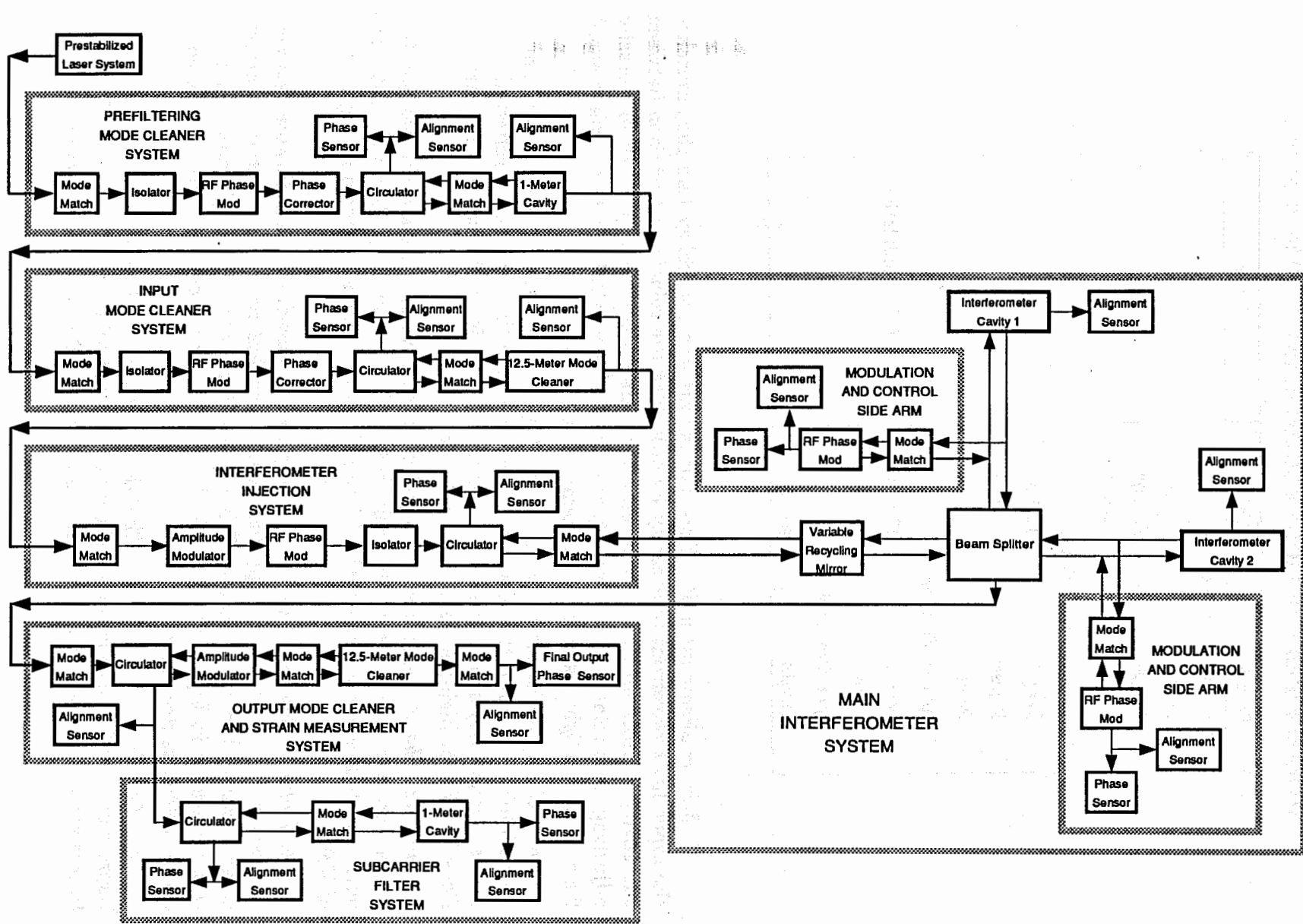


TABLE IV-B-2
PARAMETERS FOR MODE-CLEANER AND FILTER CAVITIES

Parameter	Value	Notes
Prefiltering mode cleaner		
Length	1 m	
Finesse	≈ 1000	
Power	5 W	
Main input mode cleaner		
Length	12.5 m	
Finesse	≈ 1000	
Power	5 W	
Output mode cleaner		
Length	12.5 m	For 12-MHz modulation
Power	$\lesssim 1$ W	
Output filter cavity		
Length	≈ 1 m	

ii. Mirror alignment unit. This unit is part of a control system that matches the input light wavefront to a cavity by adjusting the relative orientation between the cavity mirrors and the beam, and also centers the beam on the mirrors by adjusting their relative positions. It uses a pickoff beam splitter to sample a small fraction of the light reflected or transmitted by a mirror.

iii. Cavity stabilization unit. This typically consists of a circulator and a photodetector to sense the phase difference between the input light reflected from the cavity and the light stored in the cavity. The cavity stabilization unit may use Pockels cells for high-frequency phase correction.

iv. RF Phase modulator. Several of these devices generate the various RF subcarriers and sidebands on the main beams that are used to obtain the interferometer output and control signals. The modulation scheme is shown in Figure V-2 of Volume 1.

v. Isolator. Several of these units (typically a Faraday optical rotator between two polarizers) are used to suppress parasitic optical resonances between various components in the optical chain. The key isolators, which decouple adjacent cavities, are shown in Figure IV-B-1. Additional isolators between other components can be added as necessary.

vi. Amplitude modulator. This device is used in the input optics chain to impress amplitude modulation on the light for diagnostic tests, or as part of a servo to remove amplitude fluctuations. It is also employed in the output optics chain as

a variable attenuator during initial alignment, and as a shutter to prevent exposure of the photodiode to excessive light power.

3. Main interferometer system

a. **Mirrors and beam splitter.** The design radius of curvature for the interferometer-cavity mirrors is 3 km. The resulting spot sizes on the mirrors are within a few percent of the minimum possible (confocal geometry) size. The beam diameter is a minimum in the center of the cavity, where it is approximately 60% of the spot size on the cavity mirrors.

The diameter of the mirrors defining the 4-km Fabry-Perot cavities is set so that the diffraction of light does not limit the storage time or the number of recycles. Mirrors of 14 cm diameter are adequate to keep diffraction losses smaller³ than losses caused by imperfections in the coatings; allowing for a degradation in mirror quality near the edges, the design diameter for cavity mirrors is 20 cm (see Table IV-B-3 for the cavity parameters for full-length and half-length interferometers).

Storage time and loss parameters for the mirror coatings are discussed in Volume 1, Section V.A. The coating-uniformity and substrate-figure requirements listed in Table IV-B-3 follow from the initial interferometer specifications for shot noise, which determines the required storage time and number of recycles. The figure requirement corresponds to $\lambda/30$ ($\lambda = 633$ nm) rms variation from perfectly spherical mirror surfaces.

The diameter of the beam splitter (and associated beam-steering mirrors) will be larger than the interferometer cavity mirrors by a factor of approximately 1.4, to accommodate beams at 45-deg angles. Mechanical properties of the beam splitter are less critical than those of the cavity mirrors.

b. **Modulation and control side arms.** A compensation/pickoff plate between the beam splitter and each interferometer-cavity input mirror diverts a small fraction of the light inside the interferometer into a side arm. Each side arm is used for locking the adjacent main cavity and for applying phase modulation to the light.⁴ Each side arm terminates in an end mirror that sends the light back to the compensation/pickoff plate for reinjection into the interferometer.

4. Seismic isolation stacks

A conceptual design for five-layer isolation stacks for the test masses and beam splitter is shown in Figure IV-B-2, and the parameters are shown in Table IV-B-4. Each pair of layers is separated by four compliant encapsulated-elastomer modules.

³ The diffraction loss for a near-confocal, 4-km cavity with 14-cm-diam mirrors is approximately 10^{-6} per reflection. Relaxing the requirement to 10^{-4} per reflection, as needed for initial interferometers, would reduce the required diameter by only ~ 1 cm.

⁴ These phase modulations are used in obtaining the gravitational-wave signal and in controlling the separation between the beam splitter and each cavity input mirror, as shown in Figure V-2 of Volume 1.

TABLE IV-B-3
PARAMETERS FOR MAIN OPTICAL CAVITIES

Parameter	Value	Notes ¹
Mirror Coatings		
Cavity storage time	2 msec	for flat light amplitude
Scattering + absorption	$\lesssim 50$ ppm	of amplitude of 10% transmission
Surface microroughness	< 3 Å rms	for 10% transmission
Coating uniformity	$\lesssim 1.5\%$	rms variation of transmission coefficient over central 8 cm
Cavity length L	4.0 km	(2.0 km)
Mirror curvature R	3.0 km	(1.5 km)
Figure error	200 Å	rms over central 8 cm
Cavity stability parameter	$g = 1 - \frac{L}{R}$	ratio of cavity length to radius of curvature (-0.33)
Spot radius at mirror	w_1	at 10% transmission
	2.6 cm	(1.8 cm)
Spot diameter at mirror		at 10% transmission
for 10^{-6} loss	14.1 cm	(10.0 cm)

¹Parenthetical entries refer to half-length interferometers.

The "less critical" components will use three-layer stacks. The 300 kg capacity for the isolation stacks accommodates the optical benches in the beam-splitter and other chambers. See Volume 1, Appendix D, for an estimate of the achievable performance of this type of seismic isolation.

TABLE IV-B-4
PARAMETERS FOR ISOLATION STACKS

Parameter	Value	Notes
Test-mass and beam-splitter isolation		7-Hz horizontal resonance 15-Hz vertical resonance
Passive stages	5	total surface vibration displacement
Capacity	300 kg	maximum mass capacity
Isolation for less critical components		
Passive stages	3	total surface vibration displacement
Capacity	300 kg	maximum mass capacity

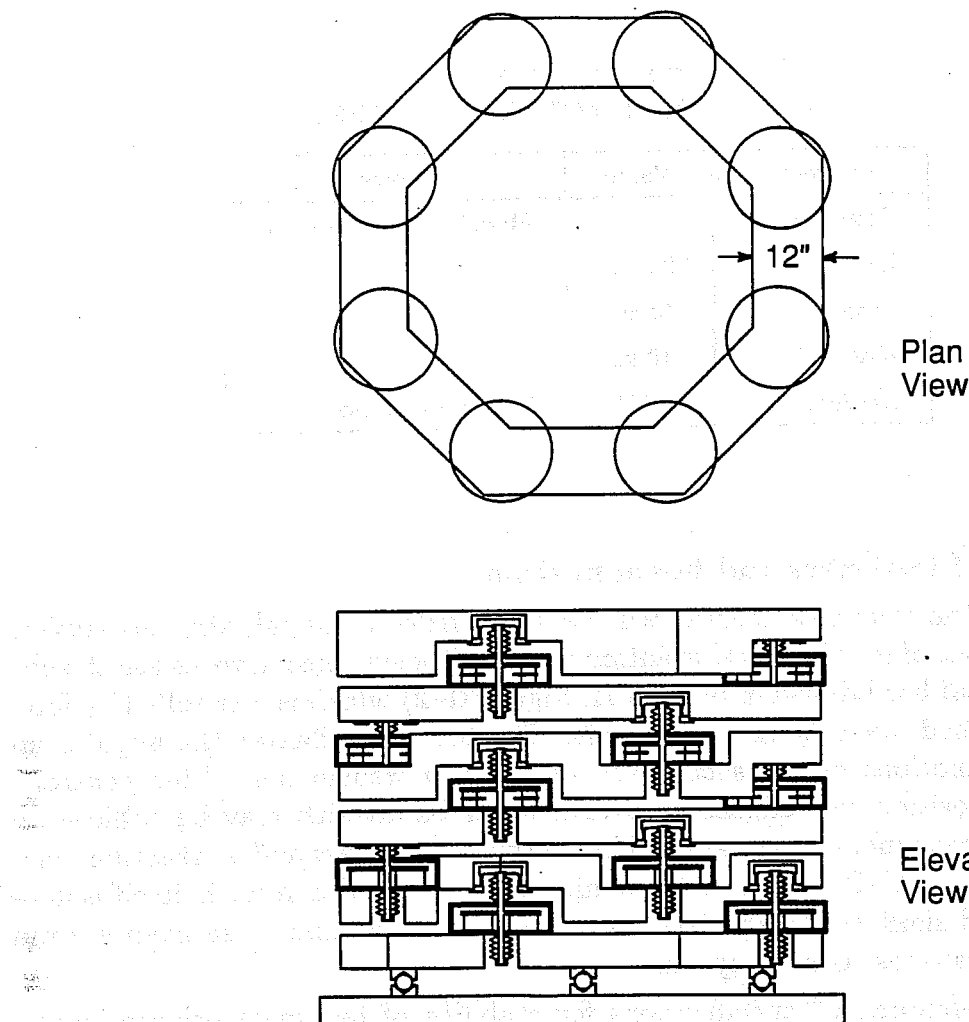


Figure IV-B-2 Five-stage isolation stack for test masses. Isolation between steel layers is provided by cylindrical modules consisting of elastomer elements encapsulated in vacuum-tight canisters with compliant bellows. *Upper:* Plan view of stack, with octagonal steel layers and cylindrical modules. *Lower:* Elevation view, showing offsets of modules and steel layers. The elastomer elements are represented by the rectangles under the horizontal plate in each canister. (The vertical rod, connected to this plate and to the bellows, is not connected to the canister.) The double bellows arrangement on each module provides compensation for forces when the gas pressure changes during pumping or venting.

5. Test masses

The parameters for the initial interferometer test masses are listed in Table IV-B-5. The optimum shape, as discussed in Volume 1, Appendix B, is that which minimizes the internal thermal noise of the mass.⁵ The design uses fused-silica test masses (the material used in prototype mirrors and masses), with the cavity mirrors

⁵ The table lists the lowest longitudinal mode resonance, at 16 kHz. A lower resonance, at

coated directly onto the masses.

TABLE IV-B-5
PARAMETERS FOR TEST MASSES

Parameter	Value	Notes
Composition		Monolithic, fused silica
Diameter	20 cm	
Length	14 cm	
Mass	10 kg	
Resonance	16 kHz	Longitudinal mode

6. Control of test-mass and beam position

Each of the four test masses will be hung from identical wire suspensions, connected to one of four identical isolation stacks. The suspension wires are attached to a small metal bar (shown in Section II, Figure II-2) which is controlled by forces between attached magnets and fixed coils. The test mass follows the angular and translational motions of the suspension bar at low frequencies. Fine control of longitudinal position and alignment over a wider bandwidth may be achieved by electrostatic or magnetic forces applied between the test mass and a "reaction mass" (visible in Figure IV-C-7) suspended behind it. The reaction mass is itself isolated and suspended similarly to the test mass, to prevent seismic noise from entering through the test-mass control system.

The "low-frequency" specifications for stability of test-mass orientation and input beam direction and position in Table IV-B-6 refer to slow drifts associated with thermal coefficients of the isolation stacks and position sensors. The upper limit specification stated for angular fluctuations in the signal band ($f \approx 1$ kHz) is determined by predicted first-order effects of beam motion on the interferometer cavity's optical length; higher-order effects may dominate, but the use of mode cleaners is likely to result in smaller fluctuation than this upper limit specification. The stability at intermediate frequencies (≈ 10 Hz) is likely to be intermediate between the values for thermal drift and the specification for motion in the signal band. Local position sensors and feedback transducers, as well as optical levers to determine the angular orientation of the mirrors, provide signals and control for interferometer alignment. When the interferometer is operating, the positions of the test masses and beam splitter are controlled to maintain the proper spacing.

12 kHz, has a smaller effect. Its contribution to the noise vanishes if the cavity beam center is coincident with the center of this mechanical mode.

TABLE IV-B-6
STABILITY OF CAVITY BEAMS AND TEST MASSES

Parameter	Value	Notes
Pendulum frequency	1 Hz	Nominal; for 30-cm wire suspension
Local position sensors		
Noise	$\lesssim 1 \cdot 10^{-11} \text{ m}/\sqrt{\text{Hz}}$	$f \lesssim 100 \text{ Hz}$
Dynamic range	3 mm	
Test-mass stability		
Angular stability	$< 4 \cdot 10^{-7} \text{ rad}$	Peak motion at low frequency
Position stability	$\lesssim 0.7 \text{ mm}$	Peak motion at low frequency
Beam stability		
Angular fluctuations	$< 10^{-12} \text{ rad}/\sqrt{\text{Hz}}$	$f \approx 1 \text{ kHz}$
Position stability	$\lesssim 0.7 \text{ mm}$	Peak motion at low frequency

Several other components need almost as much vibration isolation as the test masses: the mode-cleaner mirrors, beam splitter, steering mirrors, and recycling mirror. These will be suspended similarly to the test masses. Other optical components will be suspended by pendulums isolated with less elaborate stacks, or none at all. Local position sensors and associated force-feedback transducers are used to damp the pendulum motions and for coarse alignment of suspended components.

Figure IV-B-3 shows a standardized mount and control mechanism for a typical suspended optical component. The self-contained sensing and feedback system is designed to provide adequate accuracy and sufficiently low noise for all but the most critical components. By limiting the number of variations on this design to two or three, automation of interferometer control will be simplified, and economies of scale will be realized in the mechanical and electronic components.

7. Other elements of the design

a. **Variable-reflectivity recycling mirror.** The design will include the option of operating without the recycling mirror, for diagnostic purposes. The current concept for the recycling mirror is to build it as a composite of two low-loss mirrors, with piezoelectric spacing adjusters. The reflectivity, and consequently the recycling factor, can then be adjusted by varying the separation between the mirrors.

b. **Antiseismic suspension-point interferometer.** A secondary optical system to reduce seismic noise will be installed either during the initial interferometer construction, or early in the operations phase. This suspension-point interferometer⁶ has arms parallel to those of the primary interferometer; it measures the

⁶ See Volume 1, Appendix C for a description.

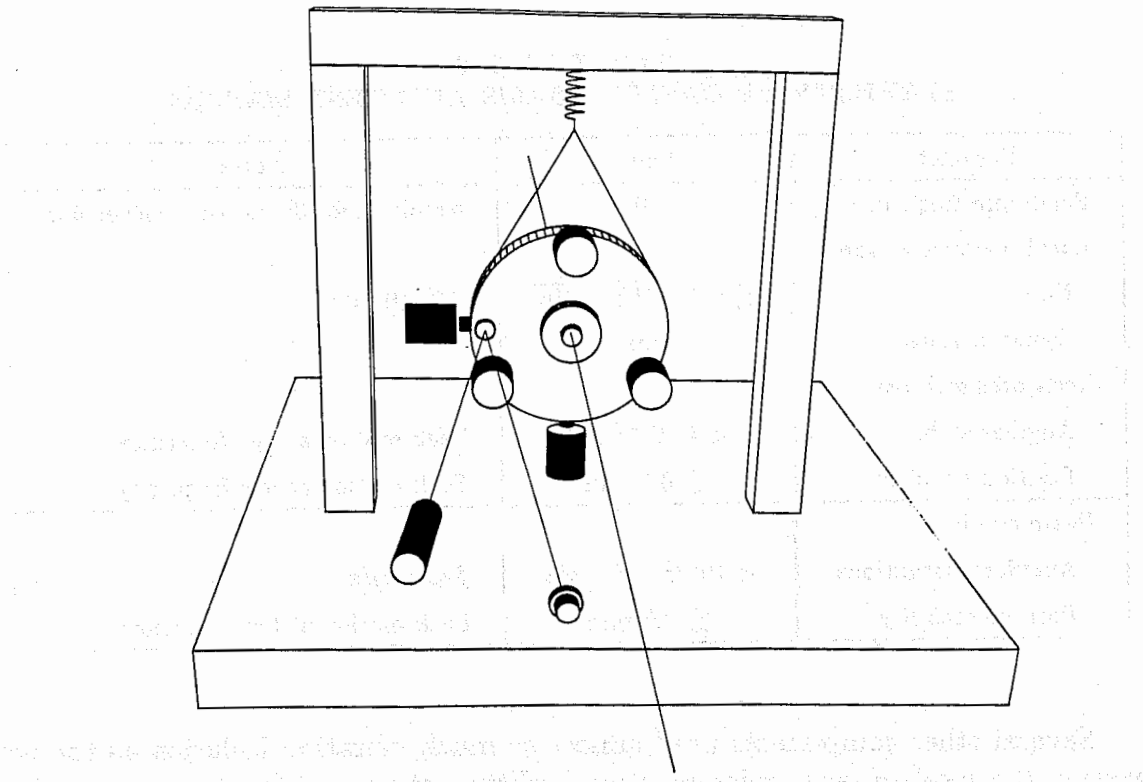


Figure IV-B-3 Alignment, position, and damping control of a typical suspended optical component. A transparent optical component is shown suspended in a holder with five small permanent magnets attached to it. The position of each magnet is sensed optically and controlled with a separate sensing/feedback head, resulting in control of five degrees of freedom (two axes of pendulum motion, vertical position, pitch, and yaw). Also shown is an optical lever consisting of a laser, a mirror at the left edge of the holder, and a position-sensitive photodetector. The optical lever provides enhanced sensitivity for monitoring pitch and yaw motion. Except for small modifications, the same design for sensing and control can be used for almost all of the suspended components in the interferometer.

motion of the bars at the top of the pendulum wires. Its output signal is used to reduce the effect of seismic noise in the main interferometer, either by subtraction from the recorded data stream, or by controlling the longitudinal position of the suspension bars in a closed-loop servo. The overall interferometer design leaves the inclusion of the suspension-point interferometer as an option that can be installed with minimum disruption to operations.

c. Automatic alignment and centering of beams. Although simple controls of the type used in the prototype interferometers should suffice to meet the specifications listed in Table IV-B-6, the highest precision control of the orientation of beams and test masses will be provided by alignment systems based on the main interferometer beams. The complete system, consisting of automatic alignment, centering sensors and controlling transducers, should keep the beams precisely aligned at all times, and stationary relative to the test masses.

d. Detailed design analysis and modeling. During the engineering design of the interferometer, a detailed system-engineering analysis, including the effects of scaling up from 40 m to 4 km, will be carried out. Among the key parameters are: (1) the increased beam sizes that scale with \sqrt{L} , (2) the increased precision required in angular alignment, which scales as $1/\sqrt{L}$, and (3) the increased delay times in some of the servo systems, which scale as L .

and the other two were not. The first was a small, dark, irregularly shaped mass, which had been partially melted by the fire. It was covered with a thin skin of white, crystalline material, which had been partially melted by the fire. The second was a small, dark, irregularly shaped mass, which had been partially melted by the fire. It was covered with a thin skin of white, crystalline material, which had been partially melted by the fire.

The third was a small, dark, irregularly shaped mass, which had been partially melted by the fire.

C. Vacuum System: Mechanical Design

1. General characteristics of the vacuum system

The LIGO vacuum system is designed to meet several key requirements. The beam tubes must:

- Provide a 1-m-diam clear aperture for the optical beams along the 4-km length of each LIGO arm.
- Provide a vacuum good enough that interferometer sensitivity is not degraded by statistical fluctuations in the index of refraction of the residual gas.
- Control the propagation of scattered light.

The chambers in the corner station, end stations, and mid stations must:

- Accommodate a wide variety of interferometer components and configurations.
- Provide access for installation and servicing of interferometer components with minimum disturbance to operating interferometers.
- Assure a clean, low-vibration, high-vacuum environment for interferometer optical components.

The LIGO vacuum system will be constructed entirely of stainless steel. To reduce pumping or bakeout requirements, stainless steel with low hydrogen content has been developed (see Appendix D). We plan to use this type of steel for all internal parts of the vacuum system.

High vacuum throughout the LIGO is achieved and maintained by ion pumps, which are vibration-free and reliable. Condensable gases from interferometer components are pumped by quiet liquid-nitrogen-cooled surfaces.

Gate valves at the ends of the beam-tube modules allow isolation of the major elements of the LIGO vacuum system. Additional gate valves within the stations facilitate installation and servicing of interferometer components and vacuum hardware.

Rough pumping from atmospheric pressure to the range of 10^{-6} torr is done by mechanical-pump/turbomolecular-pump sets, located in the stations at both ends of each beam-tube module. The same rough-pumping sets are used for the beam tubes and the chambers in the stations. Less than 24 hours is required to rough-pump a beam-tube module sufficiently to proceed with leak testing operations. Once the beam tubes are pumped down, they will remain continuously under vacuum. The relatively small chambers in the stations can be rough-pumped to 10^{-6} torr in a few hours; then the noisy pumps can be turned off, permitting unperturbed interferometer operation.

Critical optical surfaces in opened chambers will be protected against particle contamination by local high efficiency particulate air (HEPA) filter showers. Operation of these showers will be integrated with the chamber pumpdown and backfill

procedures—they will be gradually turned off after the start of pumpdown, used to backfill the chambers, and left on at all times when at atmospheric pressure.

Operation of the vacuum-system valves and pumps will be manually initiated under the control of a central operator, with interlocks enabled by automatic system-monitoring equipment.

**TABLE IV-C-1
2-KM BEAM-TUBE MODULE DESIGN PARAMETERS**

Number of modules per LIGO Installation	4
Clear aperture	1 m
Length	2 km
Inside diameter	48 in.
Wall thickness	0.125 in.
Material	Stainless steel, Type 304L
Stiffener spacing	24 in.
Optical baffle spacing	80 in.
Length of finished tube section	40 ft
Weight of finished tube section	3060 lb
Expansion-joint interval	40 ft
Tube-support interval	40 ft
Number of sections per module	160
Vacuum-pump spacing	804 ft
Number of pumps per module	7
Pump-tee length	4 ft

2. Beam tubes

a. **Summary.** The beam tubes at each site are made up of four identical 2-km-long modules. Key design parameters of the modules are provided in Table IV-C-1, and a segment of a beam-tube module is illustrated in Figure IV-C-1. Beam-tube modules are designed to be supported on a continuous mat foundation and covered with a concrete-arch enclosure after completion of field assembly, alignment, leak testing, and bakeout (see Section IV.E.3 for a description of the cover construction technique). Each module is composed of 40-ft-long sections of tubing, each with an integral expansion joint. The sections are joined by vacuum-compatible welds. Seven ion pumps are distributed along each module at equal intervals.

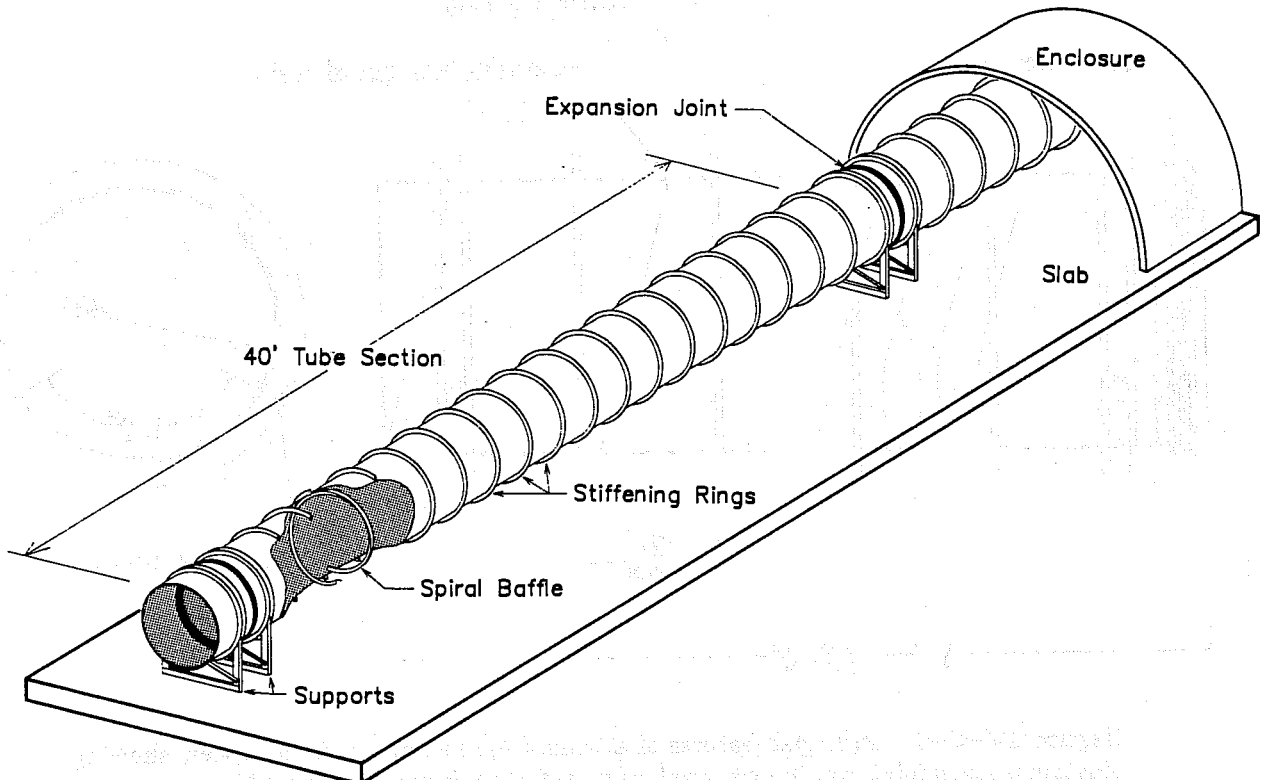


Figure IV-C-1 Segment of a beam-tube module showing stiffening rings and supports.

Each prefabricated 40-ft tube section has an integral expansion joint at one end. A portion of the tube section is shown cut away to reveal one of the spiral baffles fitted inside the tube. The semi-cylindrical beam-tube enclosure (shown cut away) is mounted on the slab after the beam-tube module has been fully assembled and tested.

The 48-in. inside diameter tube sections are manufactured at an off-site commercial mill; the 40-ft lengths are the longest that can be readily transported by conventional highway trucks. The tube is spiral-rolled from 1/8-in.-thick stainless steel, type 304L, with carbon-steel stiffening rings installed on the exterior at 24-in. intervals. An expansion joint is welded into each tube section to accommodate construction handling and thermal stresses. The ion pumps are attached to 4-ft-long pump tees spaced one per 20 sections. A 6428-ft-long beam-tube module requires 160 tube sections and seven pump tees. Together with beam-tube extensions incorporated into the stations, the two beam-tube modules along an arm make up a single 4-km-long vacuum envelope.

b. Design and fabrication of the beam-tube elements.

i. *Tube section design and fabrication.* Figure IV-C-2 shows the principal design features of a 40-ft beam-tube section. The tube is produced in a continuous, automated factory process. Coils of stainless steel sheet, 1/8 in. thick, 4 ft wide, and weighing about 20,000 lbs, are loaded into a machine that simultaneously rolls the sheet into a spiral-formed tube and welds the incoming sheet edge to the outgoing

1/8" wall, stainless steel tube

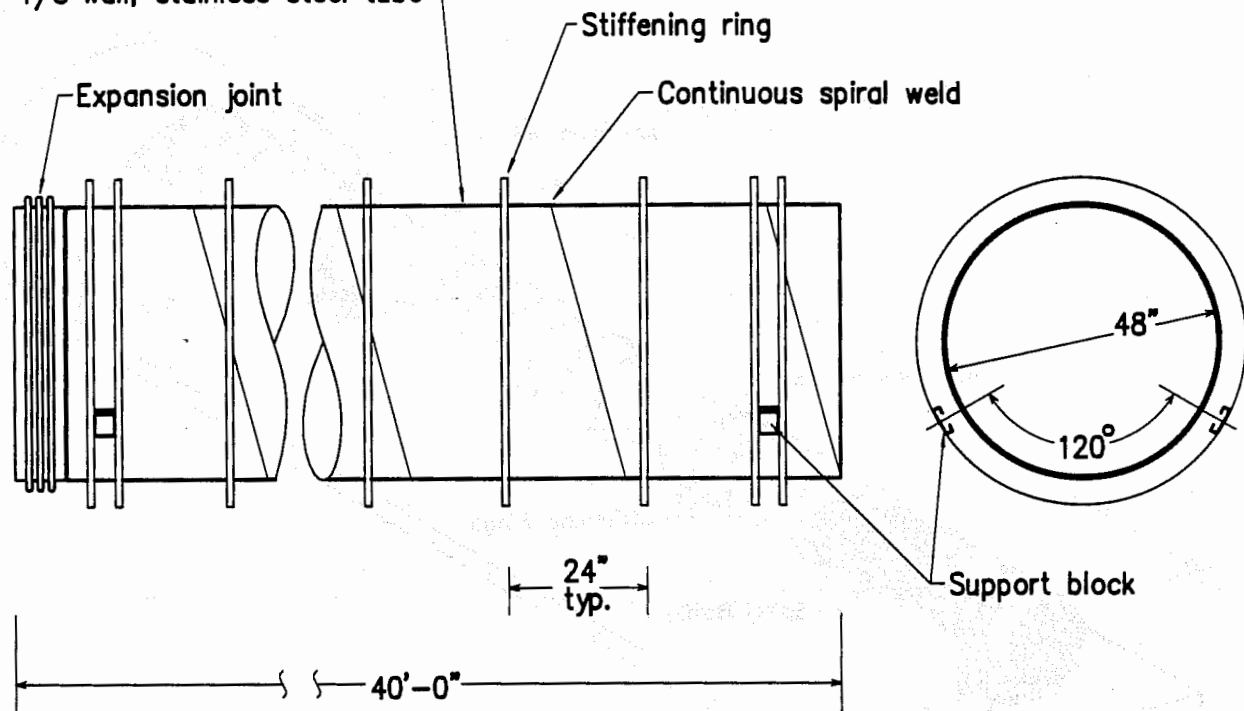


Figure IV-C-2 Principal features of a beam-tube section. *Left:* Side view showing single expansion joint, continuous spiral weld, stiffening rings and support block locations. *Right:* View along cylinder axis. To reduce stress on the thinwall tubing, the tube is held by support blocks mounted between two closely spaced stiffening rings.

tube product¹. The tube is cut to length and stiffening rings² are welded into place. Using a rolling process, each end of the tube section is then expanded for a distance of about 2 in. along the tube axis to a standard circumference to remove diameter variations. The end is faced off to leave a smooth, planar, end surface. The result is a stiffened tube section suitable for subsequent fit-up and butt-welding operations. An expansion joint³ is butt-welded onto one end of the tube, completing the 40-ft tube-section assembly.

¹ The process is well established in the piping industry, with about 50 U.S. companies producing carbon steel and stainless-steel pipe in diameters ranging from 4 to 150 in. and wall thicknesses ranging from 0.052 to 0.62 in. A full-penetration tungsten-inert-gas (TIG) weld is applied by machine from the inside of the tube. The weld joint is continuously monitored ultrasonically for weld quality. The output tube product is cut to length by a plasma torch.

² The stiffening rings, 1/4 in. wide by 2 in. high, are produced by rolling carbon-steel bar stock into a helix, which is then cut into rings with a small overlap. The rings are expanded to fit loosely over the finished tube product, positioned into place, and released to give a tight fit around the tube. An extra stiffening ring is installed near each end of the tube section to accommodate the tube supports.

³ The expansion joint, a conventional formed bellows with 0.020 in. wall thickness and five cycles of 1.25-in. period, is fitted with 1-in.-wide rings of expanded, controlled-circumference tubing stock welded to each end by the bellows manufacturer.

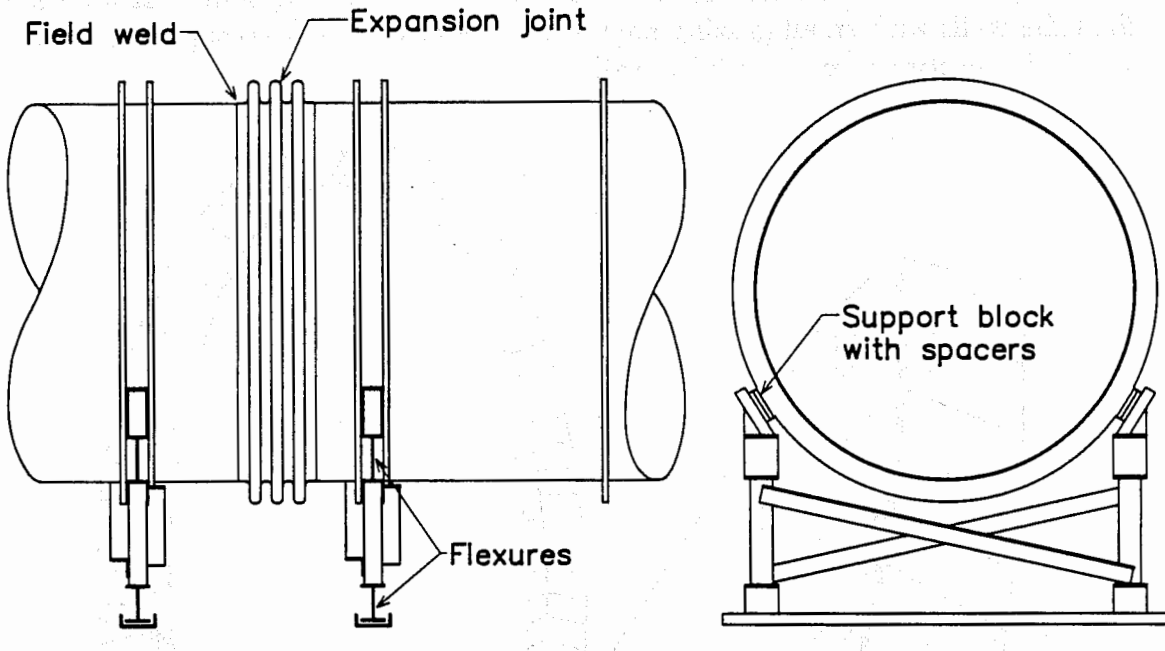


Figure IV-C-3 Sketch showing beam-tube supporting hardware. *Left:* The joint between tube sections. The two sections are butt-welded together in the field. Sections are supported by simple flexible supports that allow thermal expansion without slipping. *Right:* Cross-section of tube and supporting structure. The supports are made of roughly-cut pieces of standard carbon-steel structural members. These are welded together in a jig that defines the spatial relationship between the base-channel and support-block faces; all other dimensions are noncritical. The base-channel piece has two 6-in. slots to allow horizontal adjustment of the tube relative to the base. Vertical adjustment involves inserting spacers between the tube supports and tube sections.

After the tube section is cleaned, temporary covers are clamped onto the ends and the section is pumped down and tested with a residual gas analyzer for leaks and cleanliness. After testing, the tube sections are fitted with shipping covers for transport to one of the LIGO sites.

ii. Tube supports. The tube supports are simple and inexpensive steel structures shown in Figure IV-C-3. Two supports are used for each tube section. The supports are designed to allow adjustment of the beam-tube alignment, with up to 6 in. of adjustment range in both transverse directions.⁴ The supports also accommodate thermal stresses of the tube sections by flexing without stick-slip effects.

iii. Baffles. The beam tubes must control the propagation of scattered light, as discussed in Section II.D. This requirement is partially met by random variations in tube diameter, ellipticity, and alignment of the tube wall. These variations will

⁴ Initial alignment of the beam-tube foundations is expected to be within ± 1 in. vertical, so there is ample adjustment-range margin.

arise naturally during the fabrication, field assembly, and alignment of the beam-tube modules.⁵ In addition, baffles with a "V" cross section are installed in the beam tubes at 80-inch intervals. The baffles reflect scattered light that approaches the tube walls with small grazing angles into rays that suffer strong attenuation by multiple reflections from the tube walls.⁶

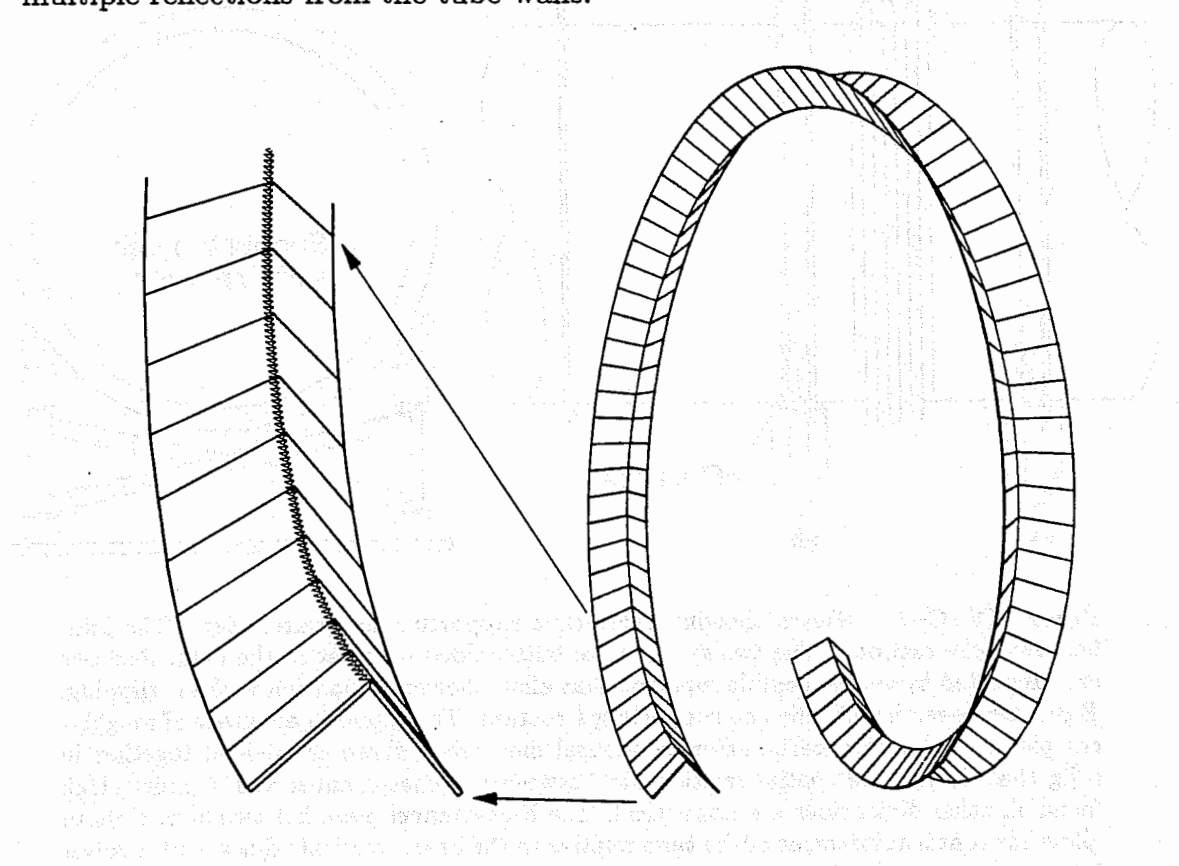


Figure IV-C-4 Spiral baffles. The baffles reflect stray light approaching the tube wall with small grazing angles into steeper angles, leading to absorption by the tube through multiple reflections. The serrated inner edge (exaggerated for clarity) randomizes the phase of paraxial diffracted stray light (see Volume 1, Appendix F). The shape and placement of the baffles is not critical (typical sheet metal tolerances are satisfactory). The baffles are installed by inserting them into the tube in a compressed state and are held in place by friction on the tube walls after being released.

The baffles, illustrated in Figure IV-C-4, are cut from a continuous helix⁷ and installed in the beam tube during field assembly.

⁵ Centimeter-scale variations are required; it is actually important to avoid building and aligning the beam tubes as precisely as, e.g., an accelerator beam tube.

⁶ For a more detailed discussion, see Volume 1, Appendix F.

⁷ Fabrication of the baffles employs a machine-rolled spiral-forming process similar to that used for the tube sections. Coils of 7-in.-wide stainless-steel (processed for low hydrogen content) sheet stock are loaded into the roll-forming machine. As the stock is peeled off the coil, it is first folded 90 deg. along its center line; then the serrations are cut into the folded edge; finally, the folded,

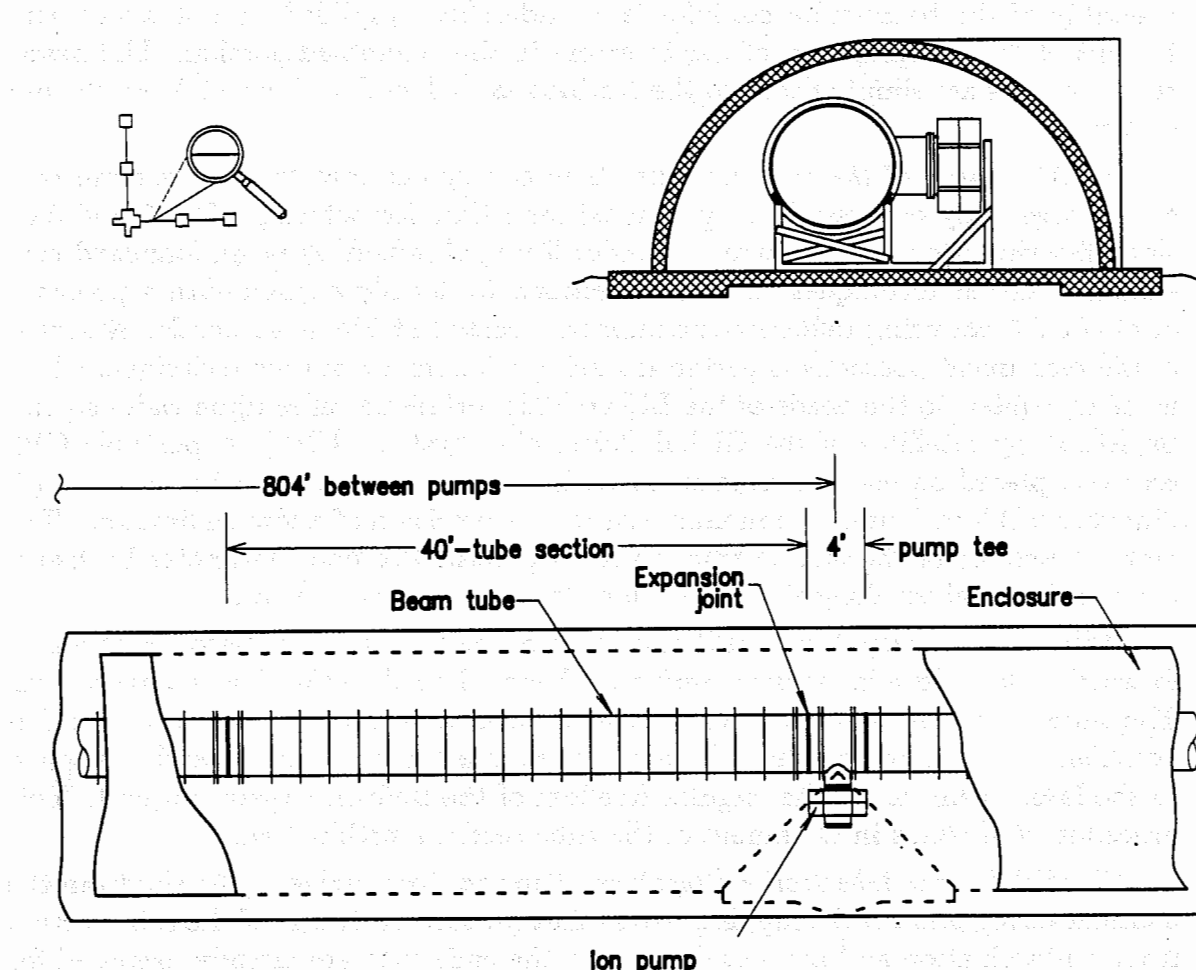


Figure IV-C-5 Attachment of ion pumps to the beam tubes. *Upper:* Section view showing an ion pump connected to the beam tube. *Lower:* Plan view showing pump attached to 4-ft-long tee. There are seven ion pumps installed on each 2-km-long beam-tube module.

iv. Pump stations. A vacuum pumping station is installed between each group of 20 tube sections of a beam-tube module. It uses a $2500 \text{ L} \cdot \text{s}^{-1}$ ion pump, separately supported, which is installed during field assembly of the beam-tube module. The installation⁸ is illustrated in Figure IV-C-5.

c. Field assembly of the beam-tube modules. The design and field

serrated stock is rolled to produce a continuous helical output of about 50-in. outside diameter. The output product is cut into rings with about 1 ft of overlap to allow for separation of the overlapped area during insertion into the beam tube. Crude sheet-metal processing techniques are adequate to meet the tolerances on shape, fit, surface roughness, and edge definition.

⁸ The pump tee, is fabricated in a similar manner to the 40-ft tube sections. A short, flanged nozzle of 18-in.-diam is added to one side to attach the ion pump. A 2.5-in.-diam flanged nozzle is included for attachment of diagnostic instrumentation. The pump tee is installed into the beam tube in the same manner as a tube section.

assembly of the beam-tube modules is considerably simplified by not attempting to control the accumulation of length errors in the assembled portion. The beam-tube modules are simply fitted to the stations at each end with special-length tube sections.

i. Alignment of the tube sections. The continuous mat foundations are constructed as early as possible to give maximum time for settling. The foundation slabs describe a plane with errors of order 3 cm, obtained by using standard construction survey techniques. The tube sections are locally aligned with a precision of about 0.5 cm using reference monuments, located at 250 m intervals. A survey of the monument positions is performed using a kinematic survey technique, which is ideally suited to the needs of the LIGO. This technique relies upon radio signals broadcast by satellites of the Global Positioning System (GPS). A portable GPS receiver, placed on each monument in turn, is used to determine the relative (3-dimensional) locations of the monuments with a precision of a few millimeters. The vertical contour of the slab is traced with a precision of one centimeter by transporting the receiver along the foundation slab between monuments.

With these survey data,⁹ field alignment of the tube sections becomes straightforward. A laser leveling transit provides a beam aligned to the clear-aperture axis. The tube section is supported on a movable jack at each end. The mating end is positioned for welding to the tube already installed and the other end is aligned to the laser beam, using the angular freedom of the built-in expansion joint. This procedure will result in alignment of the tube sections within 1 cm.

ii. Welding the tube sections together. Tube sections arrive at the site from the manufacturing plant with shipping covers that protect the inside of the tube section from contamination and prevent damage to the ends that are already prepared for welding.

Portable enclosures¹⁰ are sealed around the new tube section to protect the inside of the tube from wind-carried debris. The shipping covers are removed, an expandable backing ring¹¹ is inserted into the mating joint, and the new tube section is fitted to the built-up tube. An automatic welding machine¹² is then installed and a TIG weld is made. After the weld is completed, the expandable

⁹ The receiver data are recorded on floppy disk. The field assembly crew will work from instructions generated from these data that specify tube-section alignment relative to the nearest reference monuments.

¹⁰ The portable enclosures have flexible ends wrapped around the adjacent tube walls to obtain an environmental seal.

¹¹ The pneumatically-actuated expandable backing ring, grooved under the weld joint, is inserted inside the tube to obtain accurate alignment of the joint and to contain the backside inert purge gas for the weld.

¹² The welding machine is guided by a flexible track installed around the tube for accurate tracing of the joint contour. The expandable backing ring and track-guided automatic TIG welder are commercially available.

backing ring is withdrawn through the newly attached tube section. The baffles are installed (see next subsection), and a protective cover with an alignment target is attached to the free end of the tube. The portable enclosures are detached from the tube and moved out of the way.

The reusable shipping covers are returned to the tube manufacturing plant for use on new tube sections.

iii. Installing the baffles. Six baffles are inserted into each tube section, one at a time, by spreading the overlapped ends (thus contracting the diameter of the baffle) with a simple tool on the end of a boom. Once a baffle is located into position, the tool is released and withdrawn, permitting the baffle to spring into place. No additional attachment to the tube wall is required. Baffle spacing is not critical (the tolerance on baffle position is ± 1 m).

iv. Installing the supports. The tube supports are positioned on the foundation slab beneath the pair of stiffening rings provided for this purpose (refer to Figure IV-C-3), and fastened to the slab. Support blocks welded to the stiffening rings are bolted to the support via spacers selected to match the tube height.¹³

d. Design tradeoffs.

i. Material. The possible material choices for the LIGO beam tube are stainless steel, carbon steel, and aluminum. Stainless steel is strong and stiff, has good welding characteristics, resists corrosion, and is traditionally used in high-vacuum systems.

Carbon steel, although about 1/6 the cost of stainless steel per unit weight, is generally not used in vacuum systems at pressures below 10^{-6} torr. It is more subject to corrosion than stainless steel, which may lead to excessive outgassing rates. Compared to stainless steel, it has a much higher diffusion rate for hydrogen.¹⁴ The additional pumping speed required to cope with a higher permeation rate would negate any cost advantage. We conclude that using carbon steel for the LIGO beam tubes is too risky.

Aluminum is lightweight but less stiff than stainless steel, requiring either thicker walls or more stiffening rings. At today's prices, an aluminum beam-tube

¹³ The tube section is now supported, aligned, and secured to the slab foundation. Subsequent vertical adjustments (if required by, for example, settlement of the foundation slab) are made by changing the spacers. Horizontal (transverse to the tube axis) adjustment is accomplished by loosening the fasteners that secure the tube support to the slab and sliding the tube support on the slab.

¹⁴ Although room-temperature diffusion-rate data are not available, extrapolation of high-temperature data to room temperature suggests that the diffusion rate of hydrogen in carbon steel may be six orders of magnitude larger than for stainless steel. Our estimate for the permeation rate of hydrogen, generated on the exterior surface due to corrosion from water vapor and permeating through the bulk material to the high vacuum side, is that it might exceed 10^{-12} torr \cdot L \cdot s $^{-1}$ cm $^{-2}$.

section would cost about 7% less than the proposed stainless-steel sections. On the other hand, most fittings and flanges for high-vacuum systems are made from stainless steel, and joining aluminum and stainless steel is technically difficult. The additional cost of attaching ion pumps, instrumentation fittings, and valves would offset some or all of the potential cost savings. Aluminum is free of dissolved hydrogen, so that no high-temperature bakeout is needed. The low-hydrogen-content stainless steel proposed for the LIGO beam tubes also requires no high-temperature bakeout. We conclude that there is no advantage to considering aluminum for the beam tubes, and have chosen traditionally favored stainless steel.

ii. Tube-wall thickness. Tube-wall thickness is chosen to balance the cost of stainless steel with the cost of stiffening rings. Although the ASME Boiler and Pressure Vessel Code¹⁵ excludes vacuum vessels from its scope, this standard is commonly used as a guide for design of vacuum tubing and chambers, and was used to determine the wall thickness of the beam tube. The code permits the option of increasing equivalent wall stiffness by the use of external stiffening rings.

Without stiffening rings, the wall thickness of the beam tubes would need to be nearly 1/2 in. By adding inexpensive, external carbon-steel stiffening rings, the thickness of the relatively expensive stainless-steel walls is significantly reduced. Optimization minimizes the sum of the cost of the bulk stainless-steel sheet material and the cost of fabricating and installing the stiffening rings. This, in turn, depends upon the price of steel. Table IV-C-2 displays the recent cost history of stainless steel; the costs include about seven cents per pound for the special low-hydrogen-content processing.

**TABLE IV-C-2
COST OF STAINLESS STEEL**

Date	Steel price, \$/lb
4/87	0.90
7/88	1.30
11/88	1.54
3/89	1.87
5/89	1.49

At the time of this writing, tube cost optimization has a broad minimum for wall thicknesses in the range of 1/8 to 3/16 in. An increase in the price of stainless steel favors thinner walls. We have chosen the lower end of this range (0.125 in.) to minimize sensitivity to prices of stainless steel and to achieve lower weight, which will result in easier handling and installation. This choice will be reviewed during the detailed design of the beam-tube modules.

¹⁵ Section VIII, Pressure Vessels; Division 1.

iii. *Alternate fabrication methods.* We have been investigating corrugated metal pipe (CMP) as an alternative to smooth-wall tubing with stiffening rings. CMP is commercially available as a spiral-formed product for drainage culverts, caissons, and other applications. In the LIGO beam-tube application, spiral-formed stainless-steel corrugated pipe would eliminate stiffening rings, eliminate the need for expansion joints in the tube, reduce wall thickness, and significantly increase attenuation of scattered light.

The required tube wall thickness, using a corrugation profile of 1 in. peak to peak by 5 in. period, is 0.067 in. The major risk involved with this approach lies in the weld integrity. We have initiated an analytical and testing program to characterize the nature of the stresses affecting weld integrity.

3. Vacuum chambers

The vacuum chambers in the corner station, end stations and mid stations provide the operating environment for the interferometer components. To accommodate interferometer evolution (and the anticipated Phase-B and Phase-C expansions of the vacuum system) with minimum disruption, we have adopted a modular approach that provides flexibility in size and geometrical arrangement of the vacuum chambers.

a. Corner station.

i. *Site 1 chamber layout.* The vacuum system for Site 1 is arranged to accommodate two interferometers during the initial (Phase A) operation of the LIGO, with provisions to add modular vacuum chambers for a total of six interferometers at some future time (see Volume 1, Section IV, for a discussion of the anticipated evolution of LIGO operational capabilities). The Phase-A vacuum-system chamber layout for the corner station at Site 1 is shown schematically in Figure IV-C-6. An array of vacuum chambers is connected to enlarged (6-ft-diam) extensions of the beam tubes that provide space for pointing and alignment beams and will accommodate future expansion of the vacuum system. Gate valves are provided where the beam tubes connect to the vacuum equipment in the corner station, to permit isolation of the major elements of the LIGO vacuum system for servicing, modification, or emergencies. The ability to isolate the beam tubes after initial pumpdown allows them to remain under continuous vacuum.

The chamber array is made up of four basic types of chambers: two types of test-mass chambers, the diagonal chambers, and the horizontal-axis modules. The Type 1 and Type 2 *test-mass chambers*, which house the interferometer test masses and cavity mirrors, are located on the beam-tube extensions. In the Type 1 test-mass chambers, the test-mass assemblies are lowered into position through a horizontal gate valve. In the Type 2 test-mass chambers, which are used only at the extreme ends of the beam tubes, the test-mass assemblies are installed in their final operating locations, isolated from the beam tubes by vertical gate valves. The *diagonal chambers* contain the interferometer beam splitters. One diagonal chamber, located at the intersection of the beam tubes, is connected through large

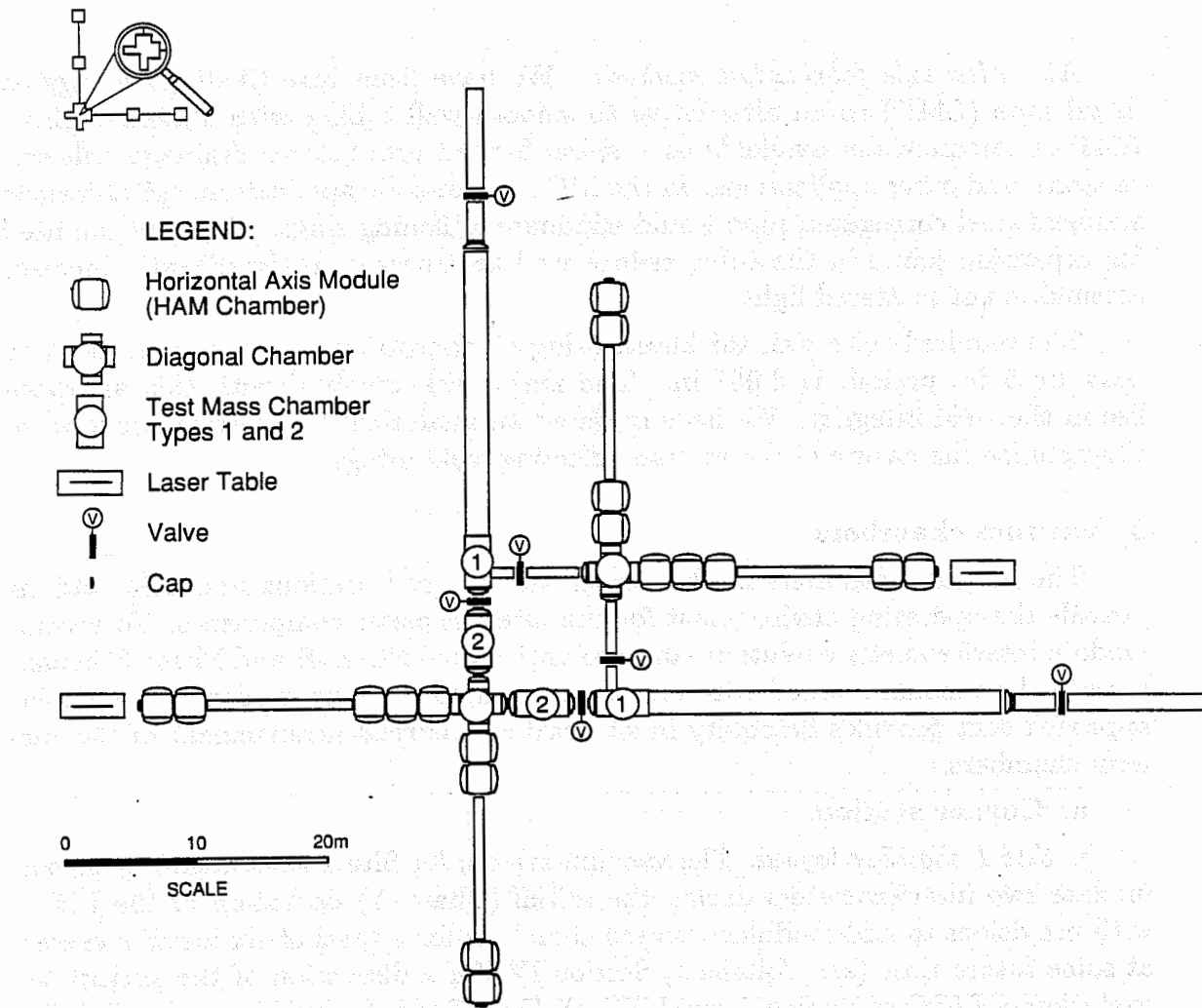


Figure IV-C-6 Layout of the corner-station vacuum chambers for Site 1, Phase A.

The beam tubes (entering top and right) can be isolated from the corner-station vacuum chambers by gate valves. An array of modular vacuum chambers and associated gate valves permit the two interferometers to be operated independently. The horizontal-axis module (HAM) chambers, diagonal chamber, and Type 2 test-mass chambers at the vertex (the intersection of the beam tubes) house the input/output optics, beam splitter, and corner-station test masses for the first interferometer. The chambers are interconnected to form a single vacuum envelope, which may be isolated from the rest of the vacuum system by vertical gate valves between the Type 2 and Type 1 test-mass chambers. Components of the second interferometer are housed in the remaining HAM chambers, diagonal chamber, and Type 1 test-mass chambers. The beam splitter and input/output optics for this interferometer are isolated by the gate valves between the diagonal chamber and the Type 1 test-mass chambers. The Type 1 test-mass chambers (illustrated in Figure IV-C-7) include a lifting mechanism and horizontal isolation valve that permit access without disturbing the vacuum in the rest of the system.

apertures to the adjacent Type 2 test-mass chambers. Beams for this interferometer pass directly between the beam splitter and the test masses. The beams for the

second interferometer pass through the other diagonal chamber to a Type 1 test-mass chamber. The *horizontal-axis modules* (HAMs) contain input and output optics for each interferometer. The HAMs are separated into groups, connected by beam tubes for the mode-cleaning cavities.

When the appropriate pair of gate valves is closed, all of the components for one of the interferometers are accessible for service or replacement except those in the Type 1 test-mass chambers. A test-mass assembly in a Type 1 test-mass chamber can be serviced by lifting it from the beam tube and closing the horizontal gate valve in the chamber. Thus, any component in either interferometer can be accessed without interfering with the vacuum environment of the other.

The set of HAMs and the diagonal chamber associated with an interferometer function like a single vacuum vessel. Because the HAMs are interchangeable, this part of the vacuum system can grow or shrink as necessary to accommodate the evolutionary development of the interferometer optics chains.

We now describe the design concept and features of each of these chambers in more detail.

(a) Test-mass chamber, Type 1. The Type 1 test-mass chamber assembly is shown in Figure IV-C-7. The vacuum envelope includes an *optics unit* with a 6-ft inside diameter which serves as an expanded extension of the beam tube. The expanded diameter accommodates auxiliary optical beams for position and alignment monitoring. The test-mass assembly can be lowered into the optics unit from above through a horizontal aperture in the *air-lock unit*, which is welded to the top of the optics unit. The 5-ft-diam air-lock aperture accommodates test masses up to 50 cm in diameter (up to 1 ton in mass). The laser beams traveling between the diagonal chamber and the test-mass chamber pass through a port (not shown) in the side of the optics unit, opposite the service-access port.

The air-lock unit contains a horizontally driven air-lock cover and actuator. The cover and actuator are simpler than in a standard gate valve, as they are designed to seal against atmospheric pressure in one direction only. Above the air-lock cover, a pair of support beams that carry the weight of the interferometer apparatus penetrates the side walls of the air-lock unit, sealed by soft bellows. A $2500 \text{ L} \cdot \text{s}^{-1}$ ion pump is mounted on the air-lock unit. Other features provided by the air-lock unit include vacuum instrumentation ports, a roughing-pump port, and electrical feedthroughs.

The chamber is covered by a removable *dome*.

The interferometer test mass, reaction mass, beam-deflection mirror, and other interferometer components are suspended from a space-frame structure attached to the top of the vibration-isolation stack, described in Section IV.B.¹⁶ The stack is kinematically mounted on three locating blocks attached to the internal support

¹⁶ The elastomer between the layers of steel in the stack is encapsulated in canisters to protect the vacuum environment from contamination.

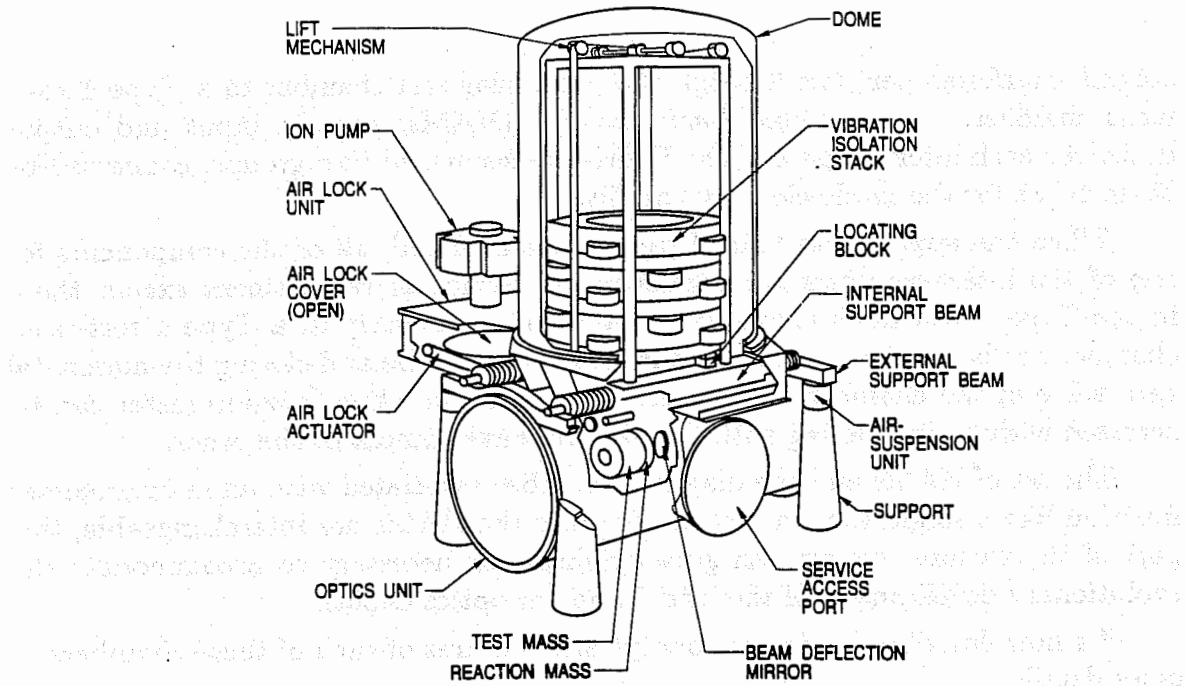
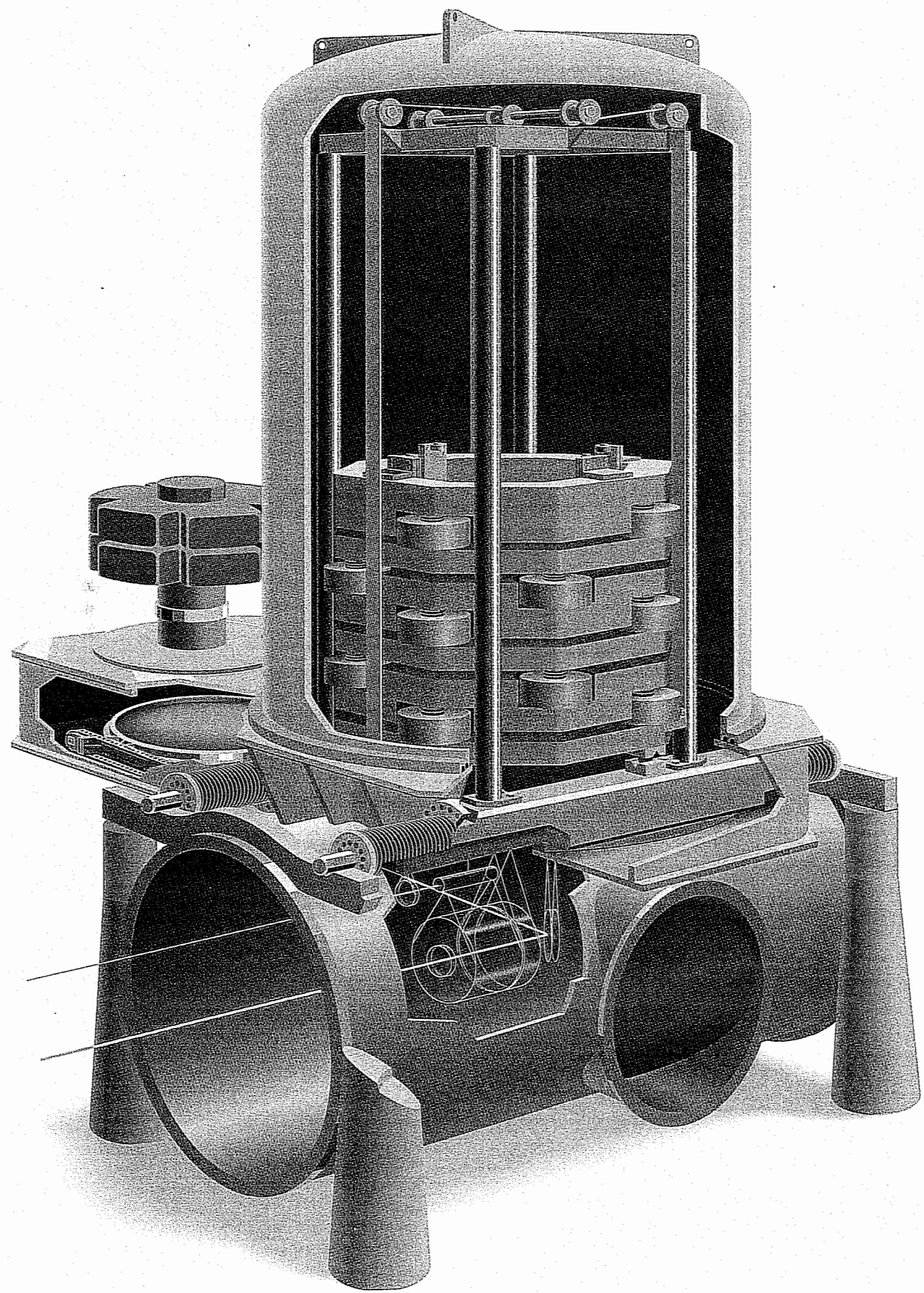


Figure IV-C-7 Representation of Type 1 test-mass chamber (*facing page*), with key components indicated (*above*). Principal elements of the chamber are: (1) the *optics unit* (lower portion) aligned with the beam tube and continuously under vacuum, (2) the *air-lock unit* (welded to the top of the optics unit) containing a horizontally-driven air-lock cover, and (3) the removable *dome*. The vibration-isolation stack and suspended interferometer components are supported by a set of beams resting on four air-suspension units outside of the chamber. Four symmetrically-arranged, soft bellows (*orange*) seal the penetrations through the chamber at the air-lock unit and isolate the interferometer components from external vibration. The interferometer components are serviced by using the lift mechanism (*top*) to raise the vibration-isolation stack and test-mass assembly above the plane of the air-lock cover. Once the air lock is closed the dome can be removed for access to the components leaving the optics unit under vacuum. The *service-access port* (in the side of the optics unit) permits backup access to the system. The optical beams pass to and from the diagonal chamber through a port (not shown) on the opposite side of the service-access port.

beams. This ensures that the stack is positioned accurately when lowered into place. The internal support beams penetrate the vacuum envelope, sealed by soft bellows, and rest on the external support beams, which in turn rest on four air-suspension units.¹⁷ The flexible bellows are symmetrically arranged to provide compensation of atmospheric pressure, so that the support beams do not experience a change in forces when the chamber is evacuated.

This method of supporting interferometer components affords considerable me-

¹⁷ The air-suspension units are mounted on support piers, which carry the weight of the interferometer components, vibration-isolation stack, and support beams. Separate structural supports are provided for the vacuum envelope (not shown in Figures IV-C-7, IV-C-8, IV-C-9, or IV-C-10).



Rendering by J. Nils Lindstrom © 1989 Caltech

chanical isolation from both the chamber wall (which unavoidably acts as a microphone, sensitive to ambient acoustic noise), and the building floor and foundations (which transmit seismic vibrations).

In operation, the optics unit of the test-mass chamber assembly is continuously kept under high vacuum, permitting optical beams from other interferometers to pass through freely. To service or replace an interferometer component, the vibration-isolation stack and suspended interferometer components are raised by the lift mechanism until the lowest component clears the plane of the air-lock cover. The air lock is then sealed, and the volume enclosed by the dome and air-lock unit is air-released. The dome is then removed, and work on any part of the installed apparatus may proceed. When the work is completed, the dome is replaced and the upper section of the test-mass chamber assembly is rough-pumped to a pressure suitable for turning on the ion pump. After the outgassing load (mainly water vapor) drops to a suitable level and the absence of contaminating outgassing products is verified, the air lock is opened. The interferometer apparatus is then lowered into the optics unit, and normal operation is resumed.



The test-mass chamber assembly is mounted on a base which is bolted directly to the floor of the building. The base is a massive rectangular steel plate which is bolted to a massive concrete foundation. The base is designed to provide a stable platform for the chamber assembly, and to absorb any seismic vibrations transmitted through the building floor. The base is also designed to provide a stable platform for the chamber assembly, and to absorb any seismic vibrations transmitted through the building floor.

The test-mass chamber assembly is mounted on a base which is bolted directly to the floor of the building. The base is a massive rectangular steel plate which is bolted to a massive concrete foundation. The base is designed to provide a stable platform for the chamber assembly, and to absorb any seismic vibrations transmitted through the building floor.

(b) Test-mass chamber, Type 2. The Type 2 test-mass chamber is illustrated in Figure IV-C-8. It shares many of the design features of the Type 1 test-mass chamber, but is not as complex. The vacuum envelope is a vertical-axis cylinder, 8 ft in diameter and 15 ft in overall height. The upper portion contains a vibration-isolation stack and internal support beams with soft bellows seals, identical in design to those in the Type 1 test-mass chamber. Similar external support beams and air-suspension units are also provided. The lower section, which contains the interferometer test mass and associated components, has four ports, each 5 ft in diameter, for access to the installed components. Two of these ports, aligned along the direction of the optical beam, are coupled through removable adapters to the adjacent diagonal chamber and to a 4-ft-diam gate valve joined to the beam-tube extension. The other two ports are provided with simple covers. A $2500 \text{ L} \cdot \text{s}^{-1}$ ion pump is installed on the lower section.

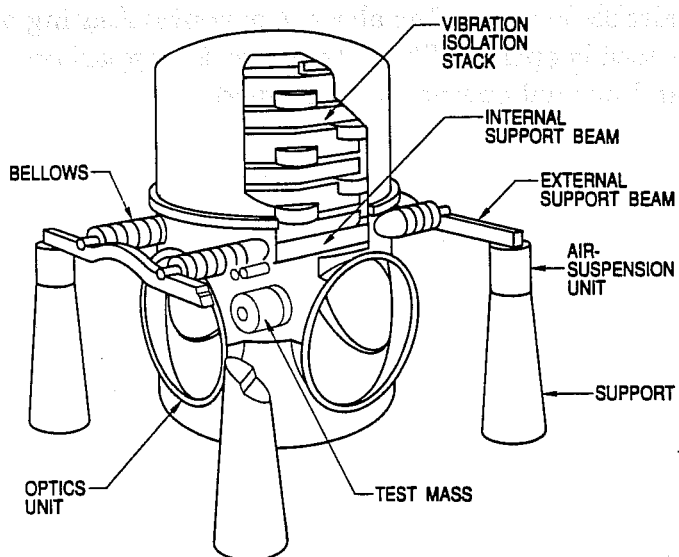
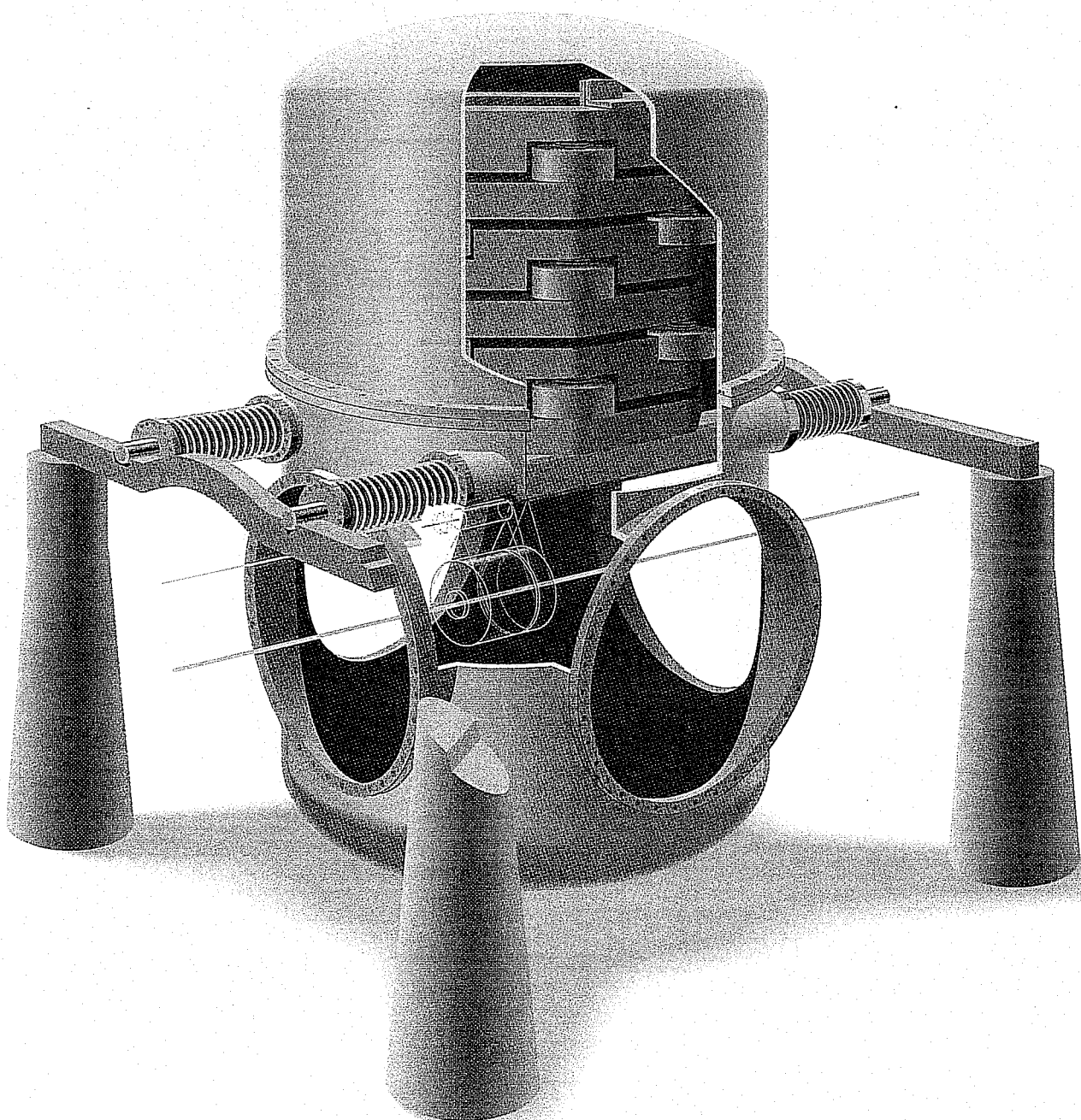
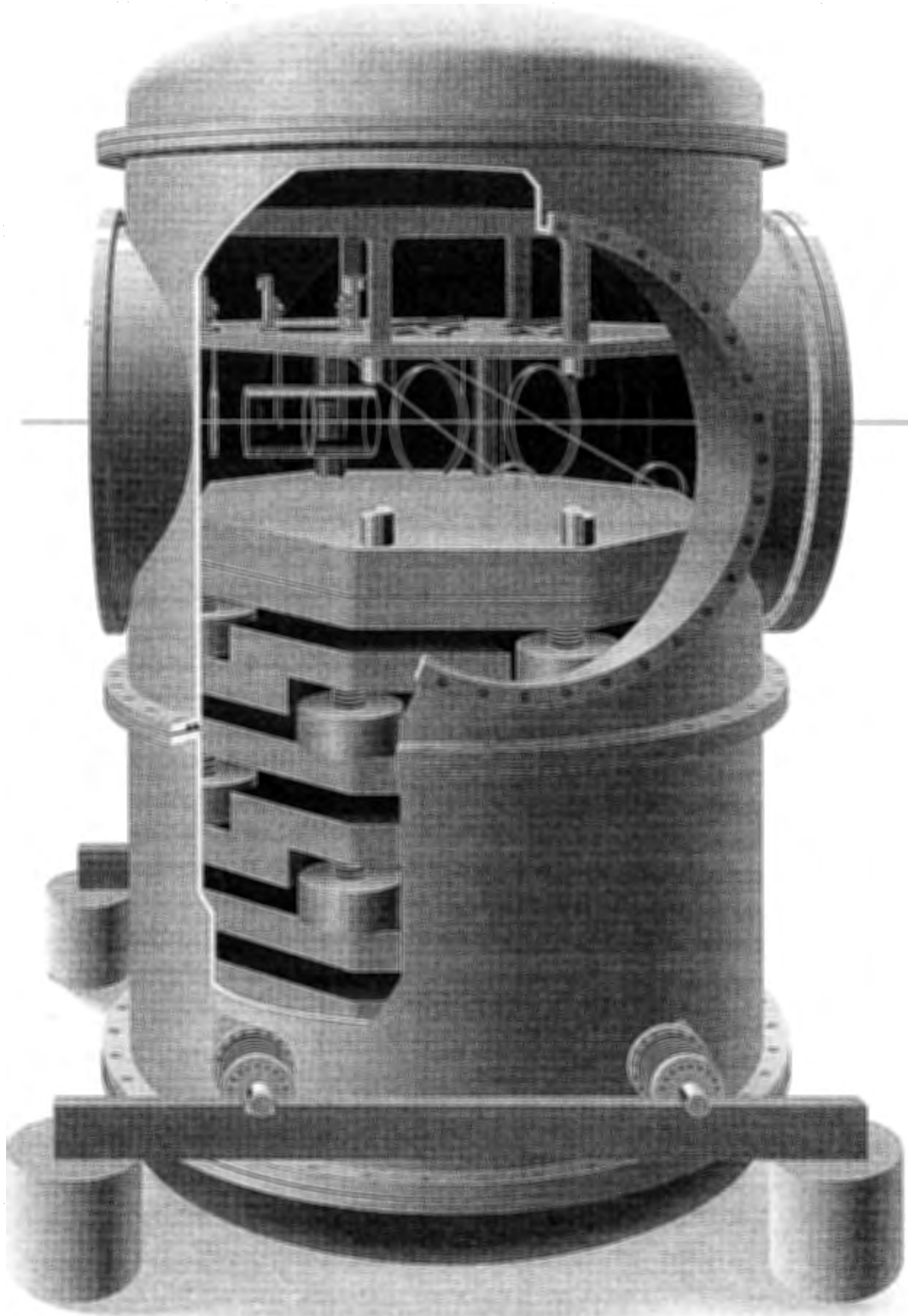


Figure IV-C-8 Drawing of Type 2 test-mass chamber (*facing page*), with key components indicated (*above*). This chamber is used in locations where there are no optical beams from other interferometers. The test-mass assemblies, vibration-isolation stacks, and support beams are nearly identical to those in the Type 1 chamber. The chamber is isolated from the rest of the system by a vertical gate valve in the adjoining beam tube (see Figure IV-C-6). Components are serviced in place through large access ports on all four sides or by removal of the upper section. An ion pump (not shown, but similar to that installed on the air-lock unit of the Type 1 test-mass chamber) is attached to the lower part of the vacuum vessel.

Crane access to the interferometer test-mass assembly and vibration-isolation stack is provided by removal of the upper section. The upper section can be replaced by a taller section (such as the dome used for the Type 1 test-mass chamber) if a larger vibration-isolation stack is necessary.



Rendering by J. Nils Lindstrom © 1989 Caltech



Rendering by J. Nils Lindstrom © 1989 Caltech

(c) Diagonal chamber. The diagonal chamber is shown in Figure IV-C-9. The vacuum envelope is a vertical-axis cylindrical chamber of approximately the same size as the Type 1 test-mass chamber, with horizontal separation planes near the midpoint and at the top. The vertical section between the separation planes includes four ports, each 5 ft in diameter, for connection to the adjacent chambers. In addition to passing optical beams, these ports also provide access for minor adjustments and for installation of small interferometer components. The connections between these ports and the adjacent vacuum-system components are made by 2-ft-long flexible bellows couplers, which are removed when access is required.

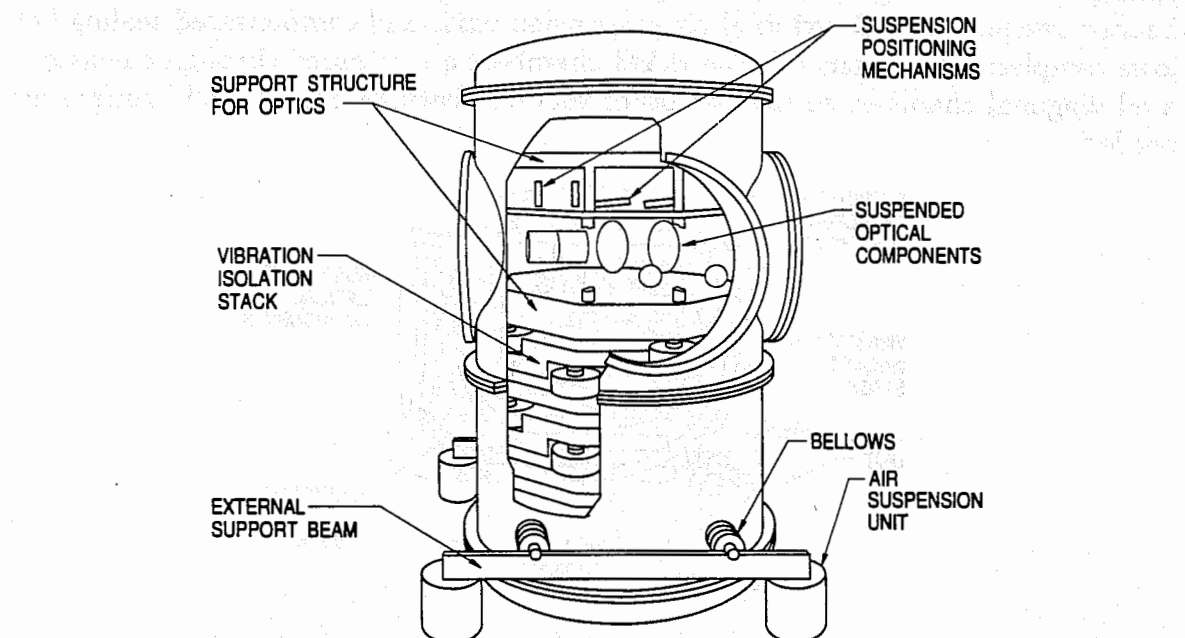


Figure IV-C-9 Illustration (facing page) and labeled sketch (above) of a diagonal chamber. The cut away section reveals the optical components suspended from a space-frame structure attached to an optical table, that rests on the vibration-isolation stack. The load from the vibration-isolation stack is transferred to the floor by support beams. The support of interferometer optical components is simpler than in the test-mass chambers, because the stack and support beams are below the level of the optical beam.

An optical table rests on the vibration-isolation stack whose design, including internal and external supports, is identical to that in the test-mass chamber.

The diagonal chamber includes two ion pumps (not shown) that provide high-vacuum pumping for the complete vacuum envelope (including the HAMs) connected to it. Ports are provided for vacuum instrumentation, a roughing pump, and electrical feedthroughs.

(d) HAM chamber. The horizontal-axis module (HAM), shown in Figure IV-C-10, is the simplest of the four basic vacuum chambers. The vacuum envelope is a horizontal-axis cylinder, 7 ft in diameter and 6 ft wide, flange to flange, oriented with the cylinder axis horizontal and perpendicular to the optical-beam axis. Removable end caps allow convenient access to the interferometer components inside. The chamber has two flanged ports, each 5 ft in diameter, on opposite sides along the laser-beam axis. One of the ports includes an integral expansion joint, making installation and sealing straightforward. The chamber contains a square vibration-isolated optical table, 6 ft on a side. The design of the vibration-isolation stack is scaled down from the design for the test-mass chambers, but employs the same concept of alternating stainless-steel plates and encapsulated elastomer. A support-beam arrangement with external air-suspension units and compensated sealing bellows completes the assembly. The HAM chambers are pumped through the associated diagonal chamber, so that no other vacuum features except feedthroughs are needed.

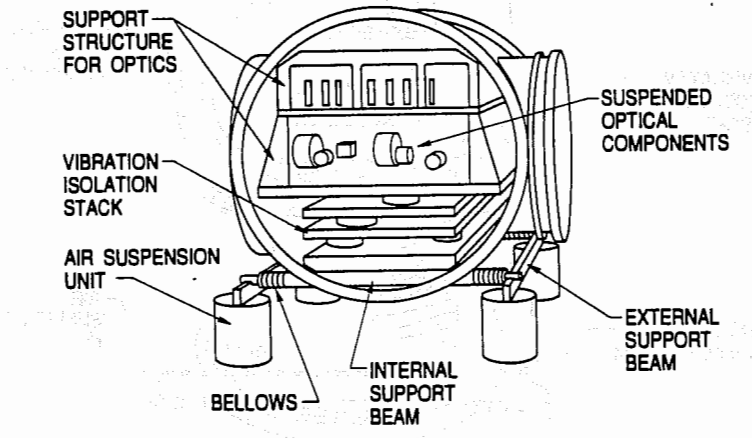
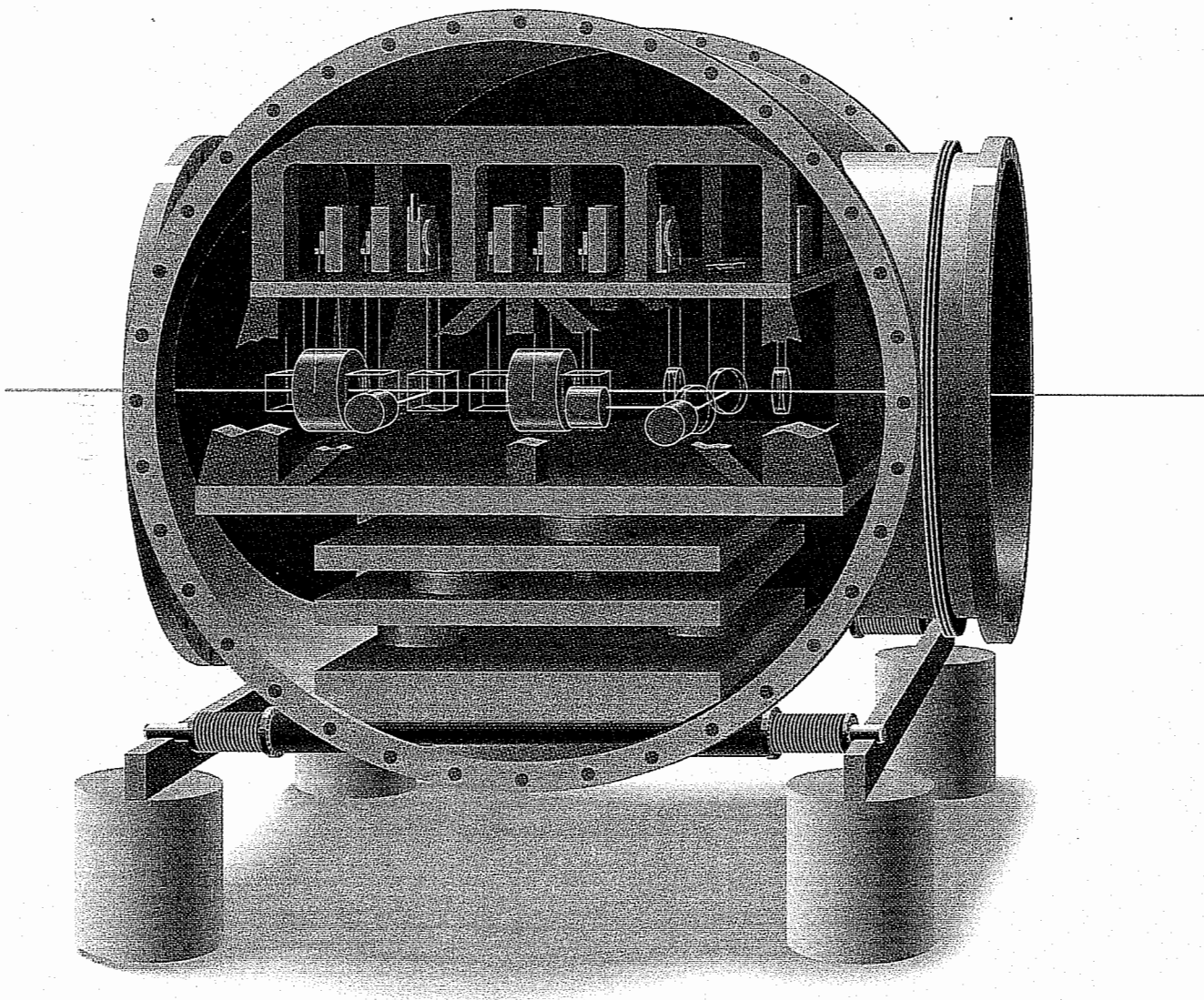
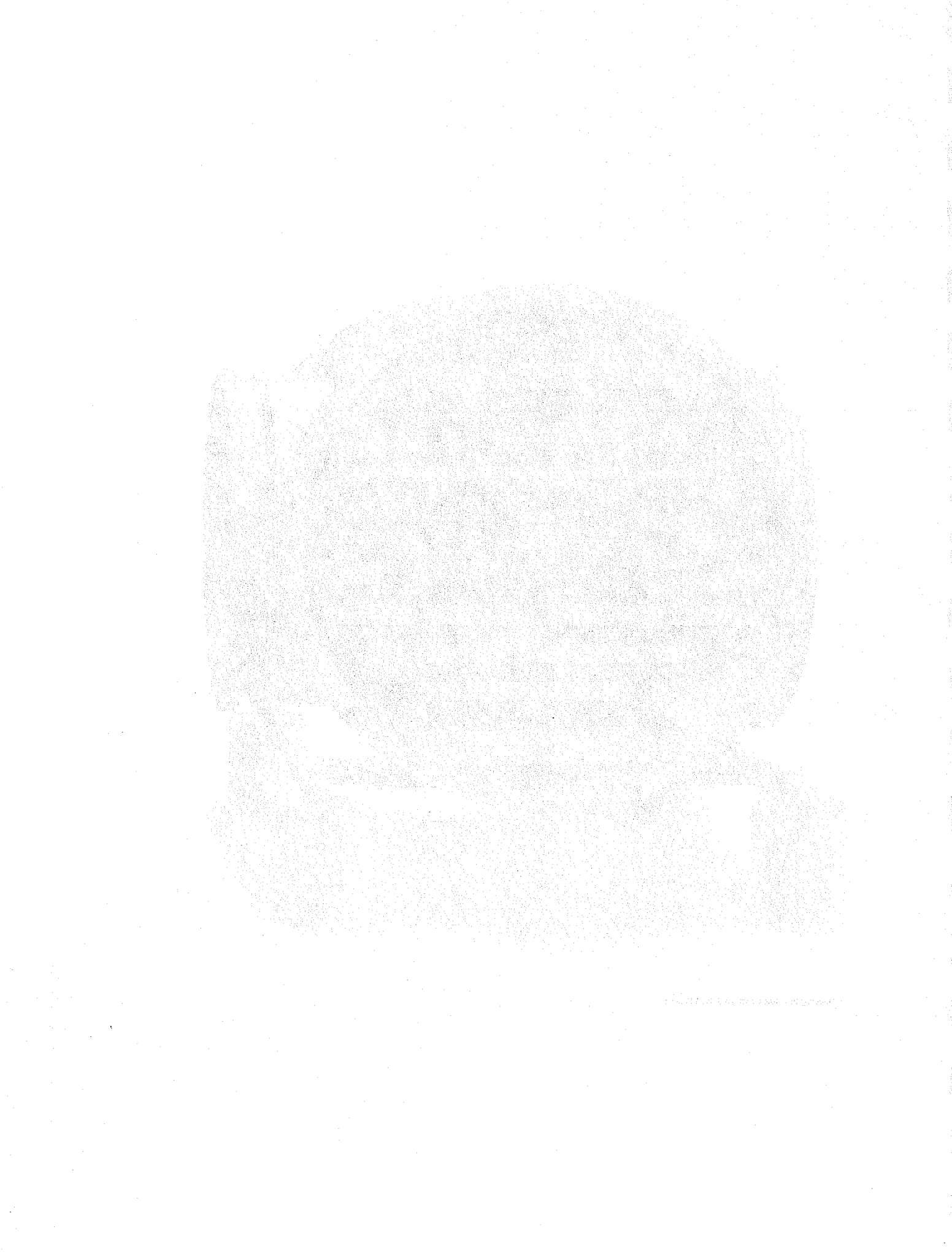


Figure IV-C-10 Representation (*facing page*) and labeled diagram (*above*) of a horizontal-axis module (HAM). One cap is removed showing suspended optical components and the vibration-isolation stack. The principal features of the HAM chamber design are easy access to the optical components, simplicity, and modularity—HAMs can be joined together to allow for a large range of interferometer configurations.



Rendering by J. Nils Lindstrom © 1989 Caltech



The complete family of four modular vacuum chambers (and their elevation features) is illustrated in Figure IV-C-11.

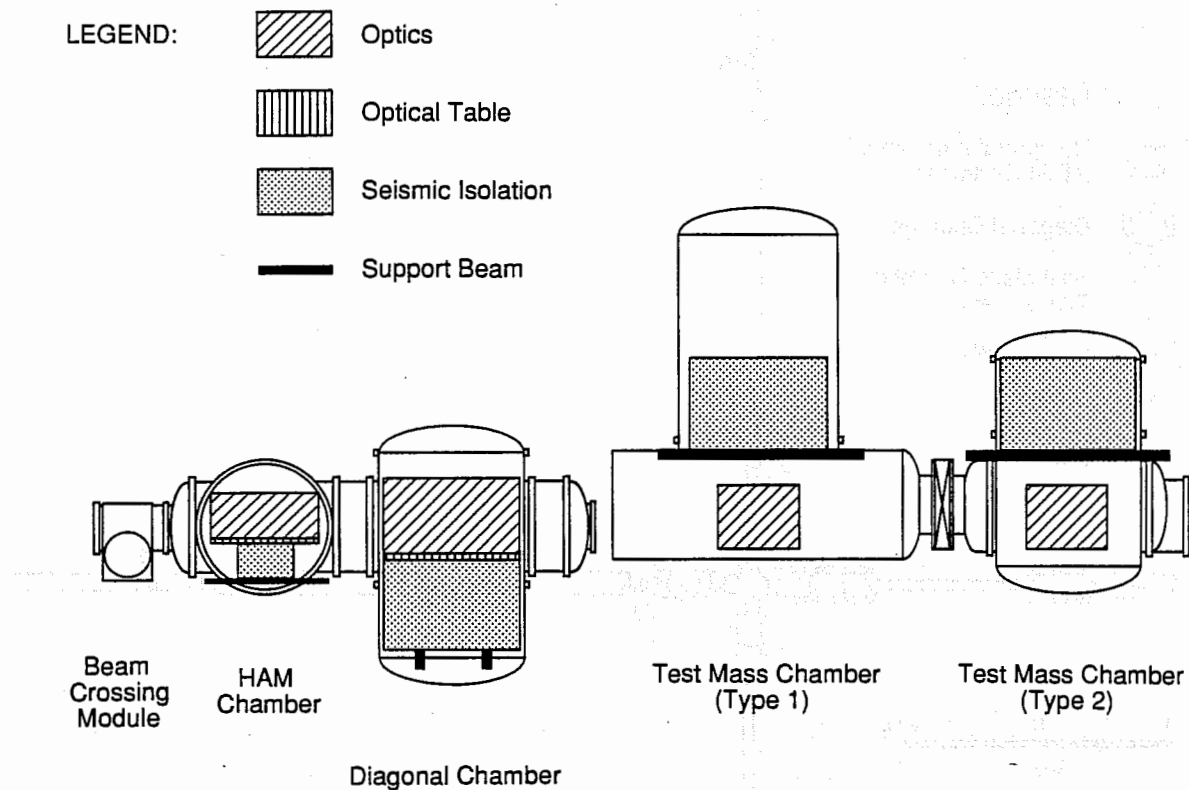


Figure IV-C-11 The family of four modular vacuum chambers, shown in elevation section to illustrate the relative vertical placement of the chambers. The *beam crossing modules* will be used in future expansions of the LIGO vacuum system (see Appendix A).

ii. Site 2 corner-station chamber layout. The vacuum system for Site 2 accommodates one interferometer during the initial (Phase A) operation of the LIGO, with provisions to add modular vacuum chambers for a total of three interferometers. The Phase-A vacuum-chamber layout for the corner station at Site 2 is shown schematically in Figure IV-C-12. The layout is nearly identical to that for Site 1, but without the vacuum chambers for the second interferometer. Type 2 test-mass chambers, a diagonal chamber, and HAM chambers are provided at the intersection of the beam-tube clear apertures in the same manner as at Site 1. The enlarged-diameter beam tube extensions at Site 2 are of the same length as those at Site 1, so that the design of pointing and alignment servos and optics are identical for interferometers at both sites.

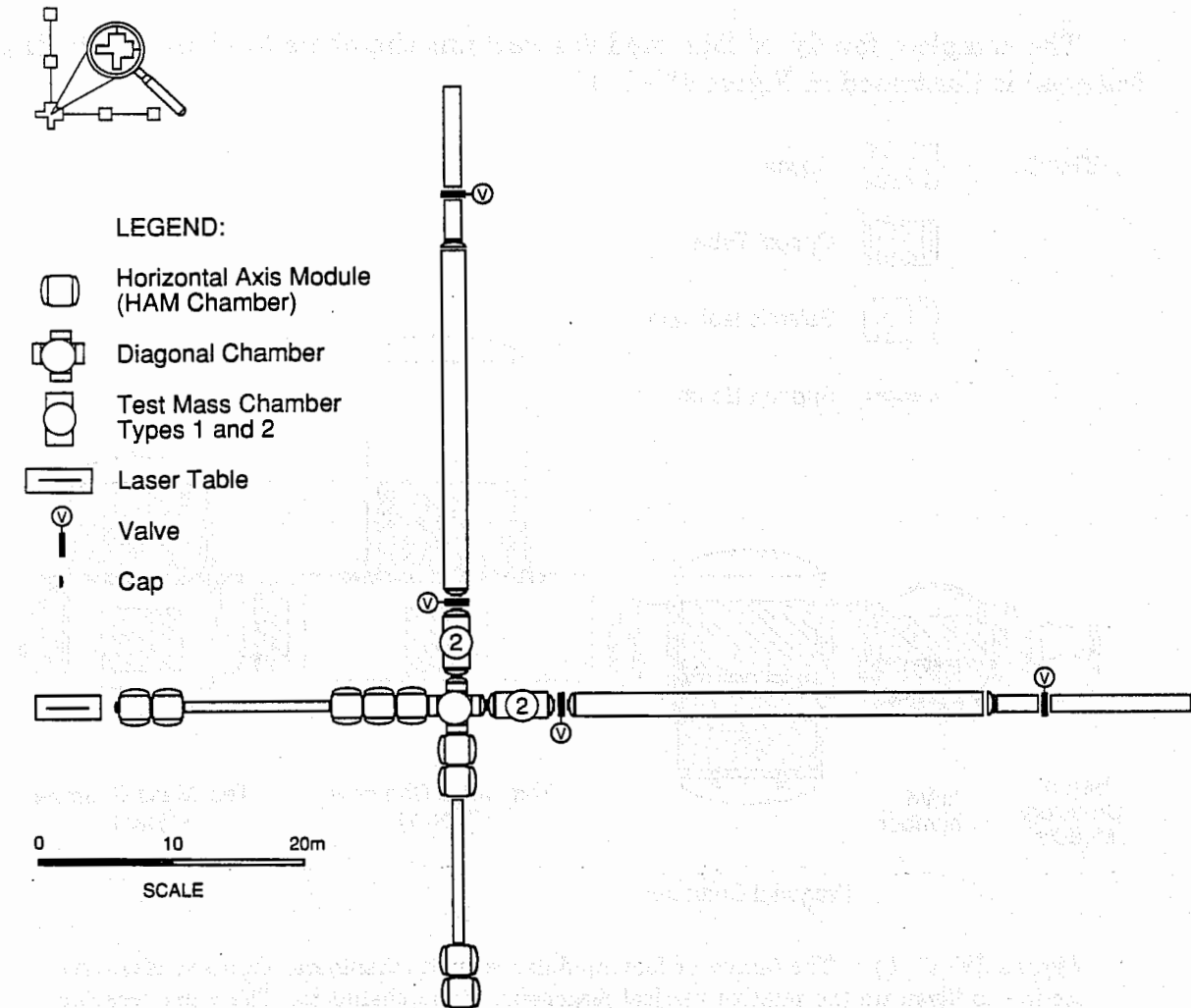


Figure IV-C-12 Layout of corner-station vacuum chambers for Site 2, Phase A. The configuration is identical to that at Site 1 (see Figure IV-C-6) without the Type 1 test-mass chambers and adjoining diagonal and HAM chambers associated with the second interferometer at Site 1.

iii. Illustrative optical configurations. Figures IV-C-13 and IV-C-14 illustrate the layout of optical components in the diagonal and HAM chambers for two interferometer configurations. Figure IV-C-13 shows the layout for the broad-band-recycling configuration that is planned for the initial LIGO interferometers, shown schematically in Figure IV-B-1. Figure IV-C-14 shows the layout for a resonant recycling interferometer which might be installed in the LIGO at some future time (this configuration and its applications are discussed in Volume 1, Appendix C). These figures demonstrate the flexibility and efficiency of the proposed modular vacuum-system arrangement. Growth in complexity of the interferometers tends to require additional linear space along the optical-beam directions between the laser

and the beam splitter (input optics), or between the beam splitter and photodetector (output optics); such additional space can be accommodated by installing additional HAM chambers as needed.

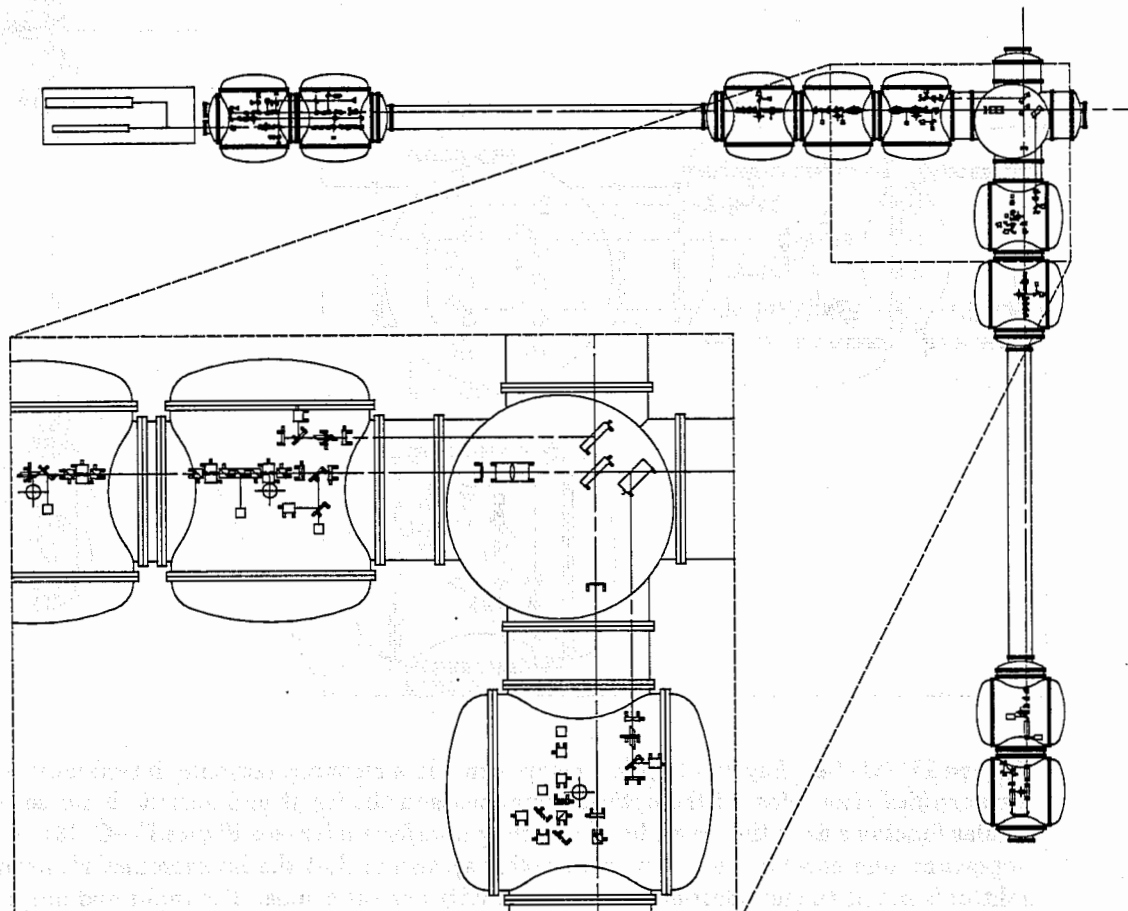


Figure IV-C-13 Layout of input and output optics for a broad-band recycling interferometer, illustrating the optical components located in the diagonal chamber and HAM chambers. Most of the components shown are separately suspended and controlled as illustrated in Figure IV-B-3. The spacing of the components is determined by the beam diameter and the clearances needed for mounts and servo controls (not shown). *Unmagnified view:* The laser and reference cavity are on the optical table at the far left; the HAM chambers adjacent to them contain components to stabilize and filter the laser beam. The two HAM chambers at the bottom contain optics to filter and detect the main interferometer output beam. The long tubes between HAM chambers hold input and output mode-cleaner cavities. *Magnified view:* The light filtered and stabilized by the conditioning optics chain at the left is incident on the recycling mirror in the diagonal chamber. The light propagates to the beam splitter and is then transmitted or reflected to the cavity input mirrors in the two test-mass chambers. The light returned from the cavities is recombined at the beam splitter and directed toward the output optics chain (downwards in the figure).

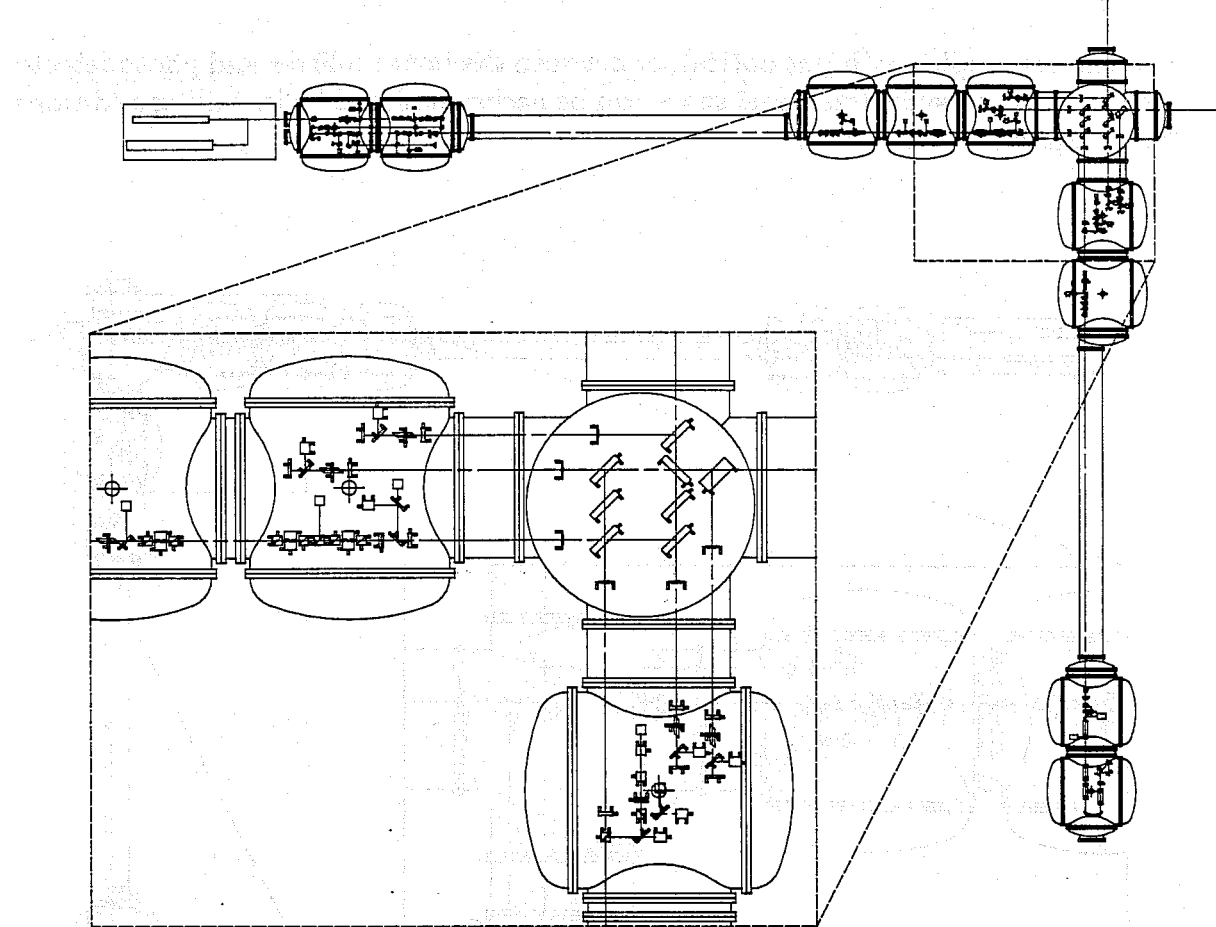
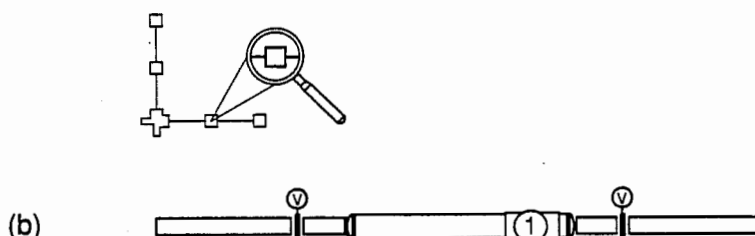
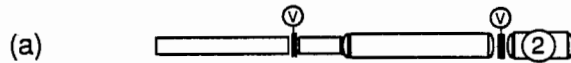
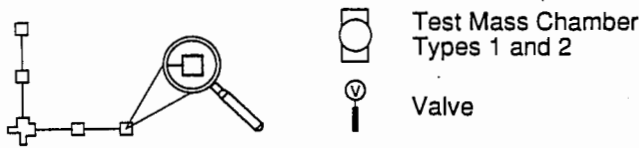


Figure IV-C-14 Layout of optical components in a resonant recycling interferometer.

Unmagnified view: Most of the optical components in the input and output chains serve similar functions as in the broad-band recycling interferometer (see Figure IV-C-13). An important difference in this resonant-recycling system is that the interferometer's beam splitter is not at the intersection of the main-cavity optical beams. The input and output optics chains are offset from the positions in the broad-band recycling interferometer. The offset is made by shifting the locations of the mode-cleaner tubes and associated outer HAM chambers, using appropriate adapters. *Magnified view:* The beam splitter (lower left in the diagonal chamber) is at the intersection of the input and output light beams (lines coming from the left and going downwards). The cavity coupling mirror is at the intersection of the beams that couple to the main cavities (extending to the right and upwards).

b. End stations, mid stations. The end stations and mid stations at both sites (Figure IV-C-15) are relatively simple, containing only test-mass chambers and associated vertical gate valves, pumps, and beam-tube isolation valves. The end stations each house one Type 2 test-mass chamber. An end cap is isolated from the test-mass chamber by an expansion joint and anchored to the building foundation, thereby minimizing perturbations of the test-mass chamber from atmospheric pressure fluctuations.

LEGEND:



0 10 20m

SCALE

Figure IV-C-15 Phase-A vacuum-system layout in (a) the end stations and (b) the mid stations. Site 1 includes two end stations and two mid stations; Site 2 has two end stations and no mid stations. Each mid station houses a Type 1 test-mass chamber (see Figure IV-C-7) and each end station has a Type 2 test-mass chamber (see Figure IV-C-8). Vertical gate valves are placed in the beam tubes near their entry to the station enclosures. Inside the station a short beam-tube extension connects to a larger-diameter filler tube, to be replaced by additional test-mass chambers as part of the upgrades to Phases B and C.

The layout for the mid stations at Site 1 is essentially identical to that of the end stations except that (1) the beam tube extends from both ends of the mid station and (2) a Type 1 test-mass chamber is used to permit access to the test-mass assembly without interfering with the operation of the full-length interferometer.

At Site 2, where no mid station is planned, a gate valve, a roughing-pump set and an ion pump are incorporated at the midpoint of each arm. These simple features permit use of the same 2-km beam-tube module design at both sites.

D. Vacuum System: Vacuum Design

1. Vacuum design requirements

The LIGO vacuum-system design requirements are discussed in Section II-E. Table IV-D-1 repeats the pressure data from that section, shows the conversion to column density, and specifies the maximum leak rate.

TABLE IV-D-1

LIGO VACUUM SYSTEM REQUIREMENTS AND GOALS

GAS SPECIES	INITIAL REQUIREMENT	GOAL
	Allowable column density ¹ (molecules · cm ⁻²)	
H ₂	1.3×10^{16}	1.4×10^{13}
H ₂ O	1.3×10^{15}	1.4×10^{12}
N ₂	7.5×10^{14}	7.9×10^{11}
CO	5.8×10^{14}	6.1×10^{11}
CO ₂	2.7×10^{14}	2.9×10^{11}
	Equivalent partial pressure (torr @ 300 K)	
H ₂	1×10^{-6}	1×10^{-9}
H ₂ O	1×10^{-7}	1×10^{-10}
N ₂	6×10^{-8}	6×10^{-11}
CO	5×10^{-8}	5×10^{-11}
CO ₂	2×10^{-8}	2×10^{-11}
	Maximum pressure in chambers (torr @ 300 K)	
	1×10^{-6}	
	Maximum leak rate (atm · cm ³ · s ⁻¹ of He)	
Each beam-tube module or chamber	1×10^{-10}	
Entire LIGO		1×10^{-9}

¹Column density is defined as the number of molecules contained in the optical path per unit cross-sectional area expressed in molecules · cm⁻². For convenience, the table also gives the specification in terms of the equivalent averaged partial pressure for the 4-km beam tubes.

The vacuum requirements are most demanding in the phase-sensitive paths of the interferometer: the beam tubes, the diagonal chamber, the test-mass chambers, and the interconnecting vacuum tubes. The allowable residual gas pressures given in Table IV-D-1 are set to constrain statistical fluctuations in the refractive index

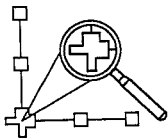
of the residual gas column between the test masses. The less stringent requirement on chamber pressure is set so that residual gas does not degrade the mechanical performance of the test-mass suspensions.

2. Vacuum-system pumping configuration

High vacuum throughout the LIGO is achieved and maintained using ion pumps. All LIGO vacuum pumps and valves are contained in the stations, except for those ion pumps distributed along the beam tubes. Turbomolecular pumps, backed by mechanical pumps, are used for all rough-pumping operations. Quiet liquid-nitrogen-cooled surfaces assist in pumping the high condensable gas-load transients in the stations.

a. **Corner-station configurations.** The vacuum-pump configuration for the corner station at Site 1 is illustrated schematically in Figure IV-D-1; Site 2 is similarly arranged. The roughing-pump sets are located where the beam-tube modules enter the station enclosure. A 24-in.-diam roughing manifold threads its way through the corner station to each Type 1 test-mass chamber and each diagonal chamber. These chambers have ion pumps that are turned on after a few hours of rough-pumping. Coaxial liquid-nitrogen-cooled pumps adjacent to the beam tubes trap the condensable gas load of a newly pumped down test-mass chamber or diagonal chamber complex.

Figure IV-D-1 (facing page) Pumping configuration for the Phase-A corner-station vacuum system at Site 1. The pumping system and associated manifold and valves are overlaid on an image of Figure IV-C-6. A 24-in.-diam rough-pumping manifold runs adjacent to the arms, terminating at two roughing-pump sets. The same roughing pumps evacuate the main beam tubes and the chambers. Each chamber (except the HAM chambers) is connected to the manifold through a valve. After initial rough pumping the chambers are isolated from the roughing manifold by the valves and the vacuum is maintained by vibration-free ion pumps attached to all chambers but the HAMs. The HAM chambers are pumped through the adjoining diagonal chamber. A pair of coaxial liquid-nitrogen-cooled pumps (one on each arm, top and right) provides high pumping speed for water vapor. The Site 2 pumping configuration is similar.



LEGEND:



Coaxial LN2 Pump



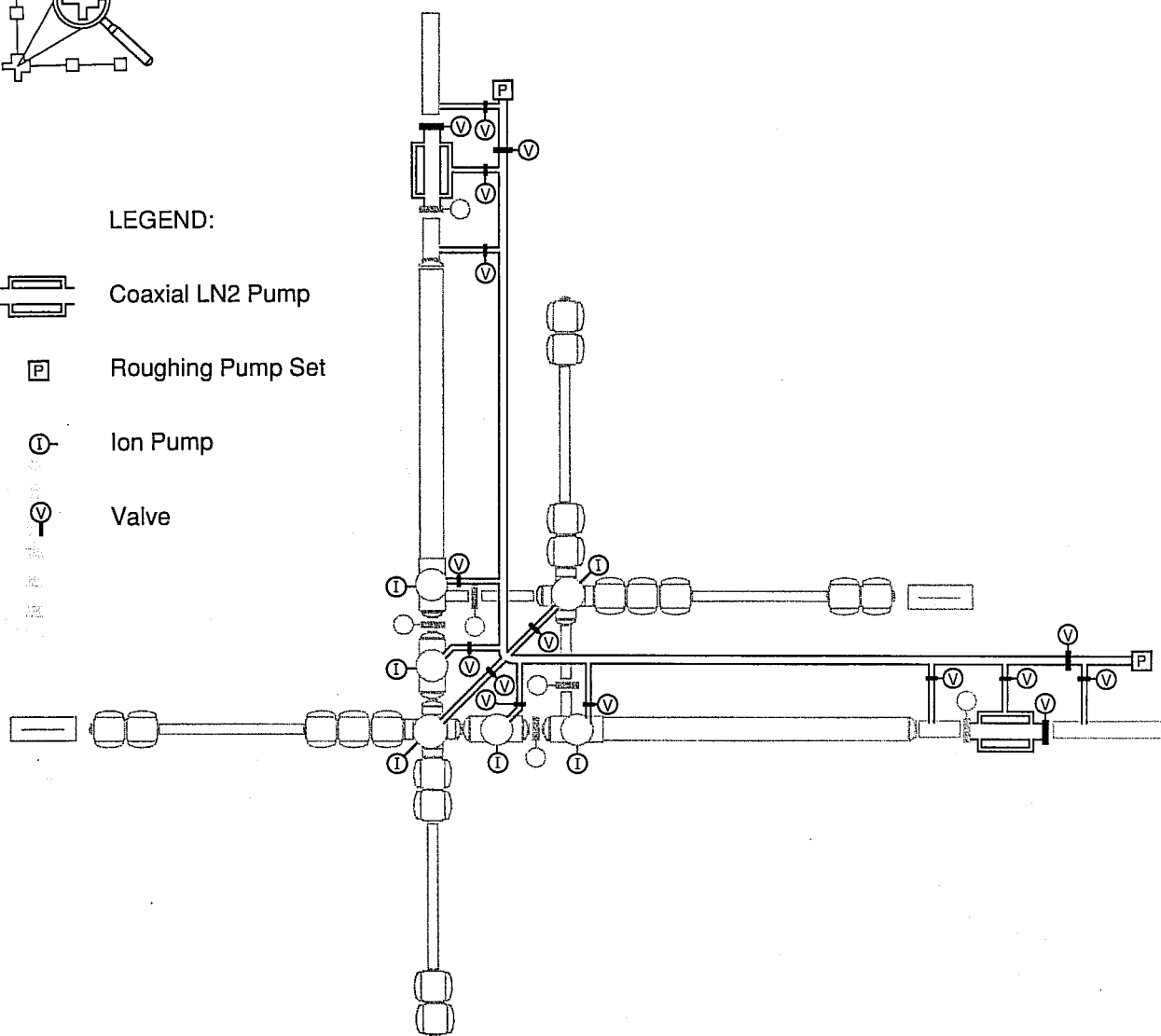
Roughing Pump Set

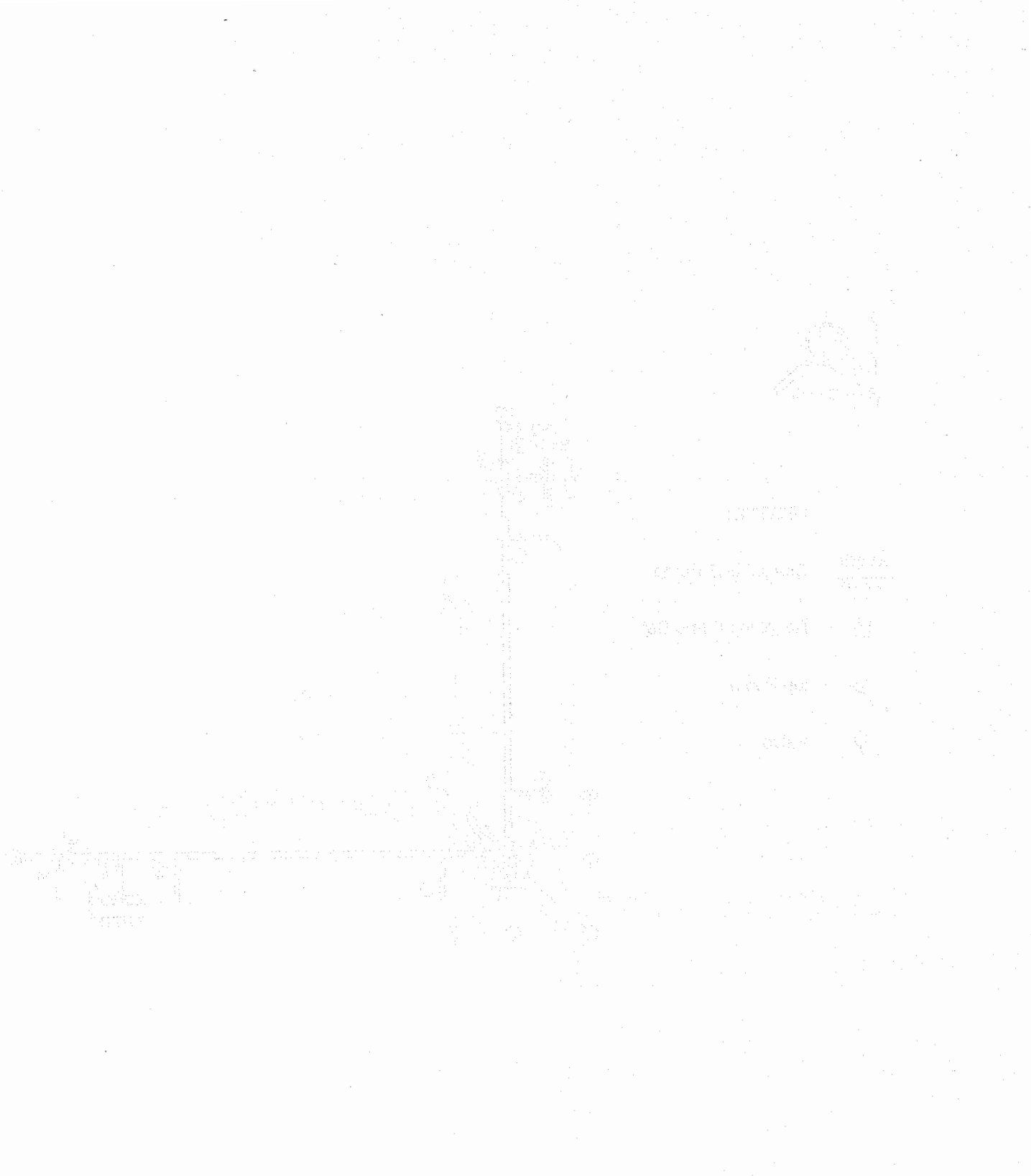


Ion Pump



Valve





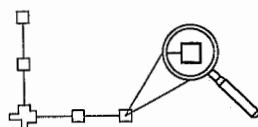
LEGEND:

 Coaxial LN2 Pump

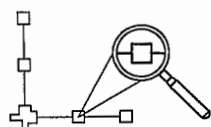
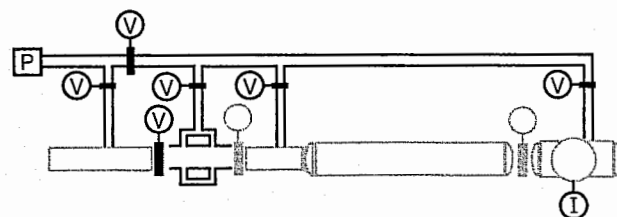
 Roughing Pump Set

 Ion Pump

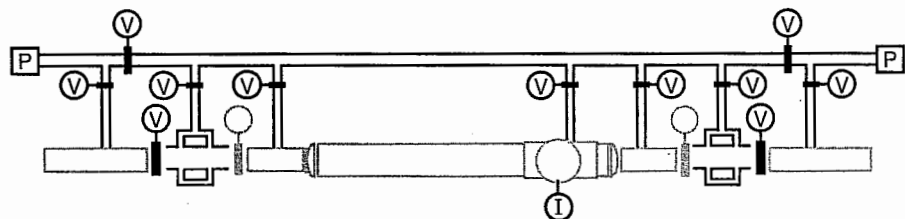
 Valve



(a)



(b)



b. Mid stations and end stations. The vacuum-pumping configurations for the end stations and mid stations are shown in Figure IV-D-2. The configuration and operating strategy follow those employed in the corner station. Rough-pumping sets are mounted on the ends of the beam-tube modules, and ion pumps are installed on each test-mass chamber. Liquid-nitrogen pumps trap the transient condensible gas loads within the stations.

Figure IV-D-2 (facing page) Pumping configuration for Phase A vacuum systems in the (a) end stations (both sites) and (b) mid stations (Site 1 only) overlaid on an image of Figure IV-C-15. The pumping strategy is similar to that employed in the corner station (see Figure IV-D-1). Each station has a 24-in. pumping manifold that connects the chambers to roughing-pump sets located near the adjacent beam tubes. Each chamber includes an ion pump for steady-state pumping, and coaxial liquid-nitrogen-cooled pumps trap the condensible gases within the stations.

c. Beam tubes. Each beam-tube module has seven $2500 \text{ L} \cdot \text{s}^{-1}$ ion pumps (with getters) distributed at equal intervals along its length, as shown schematically in Figure IV-D-3. The ion pumps are installed directly on the beam tube without isolation valves. The pressure will vary along the tube axis, changing from a minimum at the pump locations to a maximum midway between. The pump size and distribution interval have been chosen to tolerate the failure of a pump or the development of a small leak; in such circumstances, the beam-tube module pumping will gradually degrade rather than catastrophically fail.

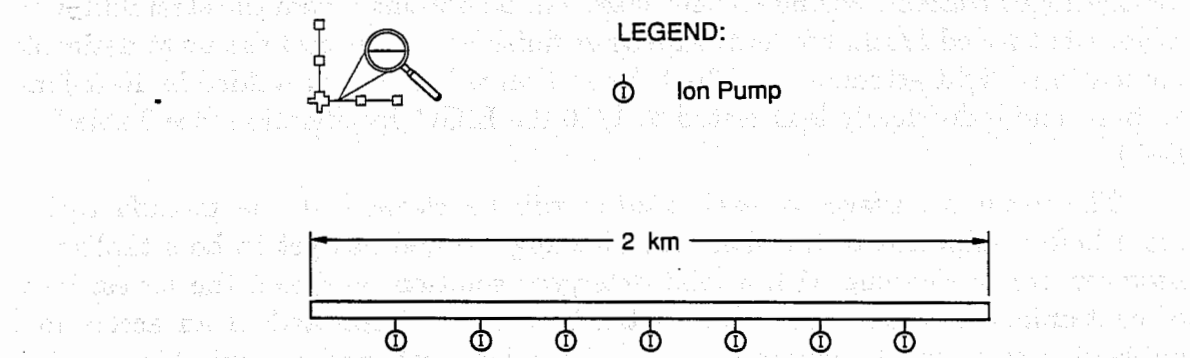


Figure IV-D-3 Distribution of seven ion pumps along a beam-tube module.

d. Roughing-pump sets. Each roughing-pump set consists of a $100 \text{ L} \cdot \text{s}^{-1}$ mechanical pump, a $500 \text{ L} \cdot \text{s}^{-1}$ Roots pump ("blower"), and a $2200 \text{ L} \cdot \text{s}^{-1}$ turbomolecular pump, which effectively prevents backstreaming of hydrocarbons into the vacuum system. The turbomolecular pump is mounted through a short plenum and valve directly on top of the beam tube. Pumping speed at the ends of the beam tubes, in molecular flow, is about $1000 \text{ L} \cdot \text{s}^{-1}$. Pumping speed in molecular flow at the chambers, through the long roughing manifolds, is estimated to be $400 \text{ L} \cdot \text{s}^{-1}$. The roughing-pump sets are provided with valves to accommodate leak detectors for the beam tubes.

e. Chamber pumping. As described in Section IV.C.3, each Type 1 test-mass chamber has a $2500 \text{ L} \cdot \text{s}^{-1}$ ion pump installed on the air-lock unit, above the air-lock cover. With currently estimated gas loads, the ion pump can be turned on, and the roughing pumps shut down, after 4 hours of rough-pumping, resulting in a pressure of less than 10^{-6} torr. After the pressure is low enough, the air lock may be opened.

Each diagonal chamber has two $2500 \text{ L} \cdot \text{s}^{-1}$ ion pumps, and the two Type 2 test-mass chambers connected to the diagonal chamber at the vertex of the beam tubes have one $2500 \text{ L} \cdot \text{s}^{-1}$ ion pump each. The operating strategy is similar to that of the Type 1 test-mass chamber. The diagonal-chamber pumps also evacuate the HAM chambers.

f. Condensable-gas pumping. Each liquid-nitrogen pump¹ in the corner station consists of a dewar, nominally 8 ft in diameter and 12 ft long, with a hold-time of about 3 months. The pumping surface is a section 12-ft long and 48 in. in diameter, aligned with the beam tube. The dewar can be isolated between two 48-in.-diam gate valves for regeneration. A length of 48-in.-diam tube connects the dewar vacuum vessel to the 6-ft-diam extension of the beam tube within the corner station. For gases such as water vapor that condense efficiently at liquid-nitrogen temperature, only 4% of the incident flux propagates into the beam tube. Smaller (4-ft-long) liquid-nitrogen pumps are used in end stations and mid stations.

3. Beam tube vacuum design concept

The beam-tube modules will be built from 304L stainless steel,² processed for low hydrogen content. Stainless-steel sheet will be obtained from the steel mill with a No. 1 hot-rolled finish, the least expensive finish available, and the most desirable for scattered light attenuation. The tube section will be spiral welded in 40-ft-long sections and individually leak tested to 1/10 the LIGO specification (see Table IV-D-1).

The vacuum surfaces of each section will be cleaned at the manufacturing plant before shipment to the site. The cleaning method has yet to be established; however, steam cleaning with a mild detergent solution produced the lowest level of contaminants among the methods tried by us, and resulted in an acceptable outgassing rate (see Appendix D). It is also a low cost method, suitable for high volume cleaning.

Beam tube parameters relevant to vacuum properties are summarized in Table IV-D-2.

¹ The liquid-nitrogen pumps, together with the local ion pumps, provide a water vapor pumping speed of about $26,000 \text{ L} \cdot \text{s}^{-1}$ at the Type 1 test-mass chambers. The speed at the diagonal chamber connected to the Type 1 test-mass chambers is about $14,000 \text{ L} \cdot \text{s}^{-1}$, and the speed at the diagonal chamber at the beam tube intersection is about $32,000 \text{ L} \cdot \text{s}^{-1}$.

² The L grade of 304 is selected to avoid carbon precipitation in the welds, which could eventually lead to leaks.

TABLE IV-D-2
BEAM-TUBE MODULE PARAMETERS

Beam-tube module diameter	48 in.	
Beam-tube module length	2 km	
Beam-tube module volume	2.3×10^6 L	
Beam-tube surface area exposed to vacuum	7.7×10^7 cm ²	
Outgassing rate for hydrogen (t ₀ = 1 hr)	$1 \times 10^{-12} (t_0/t)^{1/2}$	torr·L·s ⁻¹ ·cm ⁻²
Outgassing rate for water vapor (t ₀ = 1 hr)	$1.4 \times 10^{-7} (t_0/t)$	torr·L·s ⁻¹ ·cm ⁻²
Outgassing rate for water vapor (after mild bake)	1×10^{-14}	torr·L·s ⁻¹ ·cm ⁻²
Roughing-pump set, maximum speed in viscous flow	500 L·s ⁻¹	
Roughing-pump set, speed in molecular flow	1000 L·s ⁻¹	
Ion pump speed, nominal	2500 L·s ⁻¹	
Number of ion pumps per beam-tube module	7	
Distance between ion pumps	250 m	
Partial pressure, hydrogen (t = 1000 hr)	4×10^{-10}	torr
Partial pressure, water (unbaked, t = 1 yr)	9×10^{-8}	torr
Partial pressure, water (baked)	1×10^{-10}	torr

a. **Gas load.** Operating pressure in a vacuum vessel is determined by the ratio of gas load to pumping speed. The LIGO beam tubes have no internal components other than the stainless-steel baffles, and the gas load consists solely of material evaporating from or diffusing out of the tube walls and baffle surfaces. The initial gas load from unbaked, stainless-steel chamber walls is almost all water vapor. The conventional procedure to obtain high vacuum is to perform a mild bakeout (100–150 °C) of the system. This almost completely eliminates water vapor, so that the dominant residual gas is hydrogen, which slowly diffuses out of the bulk metal.

The initial hydrogen content of standard commercial stainless steel is in the range of 1 to 4 ppm by weight. The corresponding outgassing rates are 1.5×10^{-10} to 6×10^{-10} torr·L·s⁻¹·cm⁻² after 1 h under vacuum. These rates will decrease as the square root of time under vacuum [IV-D-1]. Reducing the hydrogen outgassing rate to an acceptable level would require bakeout-temperatures in excess of 500 °C. Such high temperatures, even over short segments of the tube, generate considerable mechanical stresses on the tube welds and supports, and would present a major risk. The alternative of increasing pump speed would introduce unacceptable costs.

The low-hydrogen steel we tested has a measured outgassing rate as low as 3×10^{-15} torr·L·s⁻¹·cm⁻². Four chamber samples were fabricated from this steel and subjected to long-term outgassing tests. Details of the experimental setup and measurements are described in Appendix D. As shown in Figure IV-D-4, the samples show considerable scatter; however a rate of 1×10^{-12} torr·L·s⁻¹·cm⁻²

after 1 h under vacuum is a reasonable value to use for design purposes. For the LIGO beam tubes, with the pumps provided, this results in a hydrogen partial pressure of 4×10^{-10} torr after 1000 h under vacuum. This pressure is below the goal level of Table IV-D-1, and will continue to decrease with time.

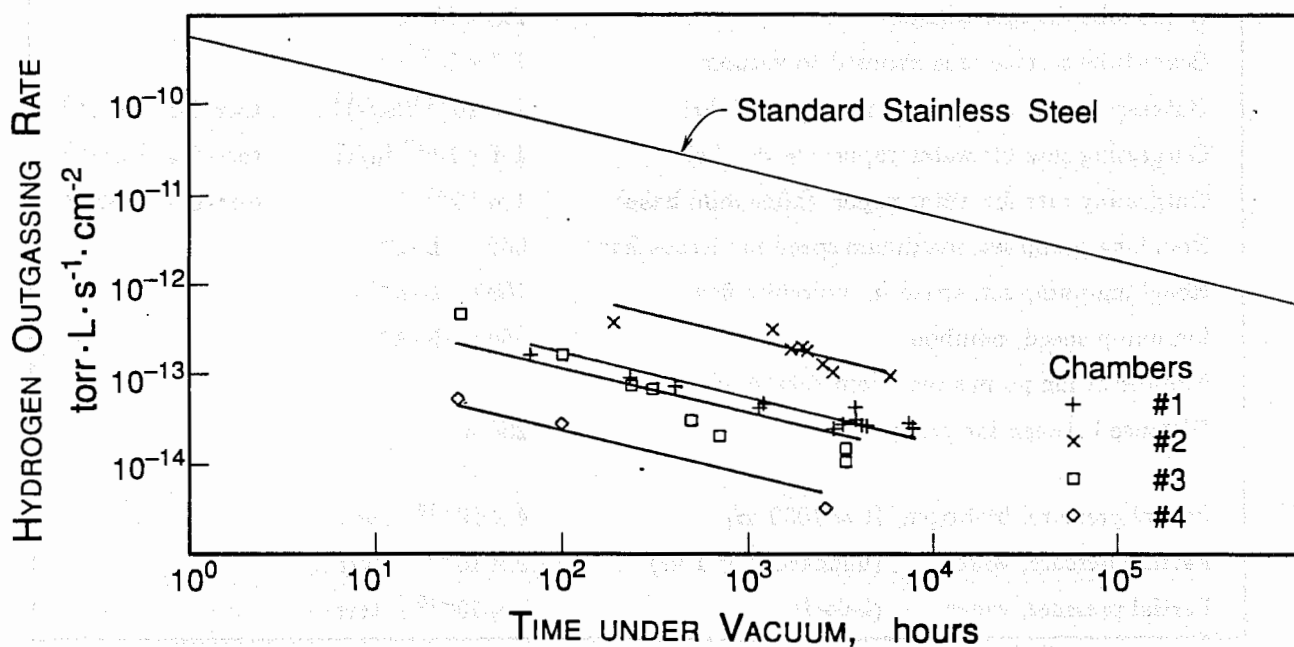


Figure IV-D-4 Hydrogen outgassing rate as a function of time under vacuum for four test vacuum chambers manufactured from low-hydrogen steel (obtained from J&L Specialty Products Corp.). These chambers were subjected to different cleaning procedures: (1) uncleaned, (2) hot water/detergent washed, (3) steam cleaned with detergent, and (4) cold water/detergent washed. The predicted outgassing rate for standard stainless steel is shown for comparison.

Hydrogen outgassing from welds must also be considered; any filler material will be degassed prior to welding, and an inert gas environment for the welding operations should exclude hydrogen from hot surfaces. Because the zone affected by welding constitutes less than 1% of the surface area of the finished tube, these precautions to control the outgassing of welds should be adequate.

Water outgassing from a stainless-steel vacuum vessel has a nominal rate of 1.4×10^{-7} torr · L · s⁻¹cm⁻² after 1 h under vacuum [IV-D-2], and decreases with time under vacuum. All four test chambers have outgassing rates lower than this, by a factor ranging from 2 to 5. The calculated partial pressure of water vapor in the LIGO beam tubes, corresponding to the model in [IV-D-2], meets the initial requirement in Table IV-D-1 after 8000 h under vacuum. As discussed in the next section, a mild bakeout to reduce water vapor outgassing is planned during this period. Reaching the partial-pressure goal of 10^{-10} torr requires reducing the water-vapor outgassing rate to 10^{-14} torr · L · s⁻¹cm⁻², a level that is routinely obtained by mild baking.

b. Implementation. After field assembly of a beam-tube module is completed, it will be pumped down; this will take less than 24 h, using the roughing-pump sets in the stations. After pump down, the module will be leak tested. A residual gas analyzer will be used in preliminary tests to establish the total air leak. A helium probe will be used to locate leaks.³ Leaks in the beam-tube module will be found and repaired until the leak rate drops below 3×10^{-11} torr · L · s⁻¹ of air (10^{-10} atm · cm⁻³ · s⁻¹ of He) which is sufficient to ensure that weld quality is adequate for long term operation.

After leaks have been located and repaired, the partial pressure for air will be leak-rate limited and will be less than 2×10^{-14} torr. Partial pressures for nitrogen, hydrogen and water vapor will be confirmed against the calculated values. Bakeout of the tube to reduce water vapor outgassing will then proceed.

The installation of conventional, permanently-installed bakeout heaters and insulation along the entire LIGO beam tubes at both sites cannot be accommodated in our present budget. In addition, if heaters and insulation were to be installed, they would interfere with subsequent diagnostic leak checking. It is planned, instead, to use manually-installed portable insulated heater jackets which are moved from one tube section to the next. During the final pump down of a beam-tube module, heater jackets are installed on 200 ft of beam tube at a time, and heated to 200 °C for 24 h. During this time the equivalent of $\sim 7 \times 10^7$ hours of room-temperature water-vapor outgassing will be achieved. (This should result in an outgassing rate of 2×10^{-15} torr · L · s⁻¹ · cm⁻².) During this sequential bakeout operation, a purge flow of gaseous nitrogen is introduced at one end to prevent the water vapor released by baking from re-contaminating the previously baked surfaces. A flow speed of 40 cm/s at a pressure of 1 torr reduces the diffusion probability for water vapor to below 10^{-10} at 1 meter upstream from the point of release. The purge gas⁴ thus "sweeps" the water vapor released by baking toward the pumped (and still unbaked) end of the tube.

The procedure outlined above is untried so far, and will be demonstrated on a model before implementing it in the LIGO. The unbaked LIGO beam-tubes will meet the needs of the initial interferometers; nevertheless, we consider it advisable to perform the sectional bakeout described above before startup of interferometer operations in order to expel undetected contaminants from the beam tubes and to advance our readiness for higher sensitivity interferometers. After the initial bakeout, we will operate the interferometers until it appears likely that sensitivity will be limited by gas pressure. At that stage, additional bakeouts will be performed, if necessary.

³ A helium pulse will take about 5 minutes to travel one km and reach 50% of its final value.

⁴ A special requirement on the purge gas is that its partial pressure of water be of the order of 10^{-10} torr or less.

4. Chamber vacuum design concept

In this section, we present an analysis of the pumpdown transient behavior for selected chamber configurations.

The vacuum chambers will be made from the same low-hydrogen stainless steel used for the beam tubes,⁵ and with the specified ion pumps should pump down to $\sim 1 \times 10^{-9}$ torr of hydrogen. The chambers and internal supporting members (vibration-isolation stacks, optical tables) can be vacuum baked as necessary.^{6, 7} These steps will result in a gas load from the chamber that is small compared to the water outgassing from installed interferometer components. Good vacuum engineering of the interferometers will be necessary to achieve acceptable vacuum levels in reasonable times.

A pump-down-transient analysis of the chamber configurations has been done by numerically tracing gas fluxes. Table IV-D-3 summarizes the highlights of this analysis for two representative chamber configurations: (1) a vertex chamber assembly,⁸ and (2) a mid-station Type 1 test-mass chamber. The table gives a "snapshot" of the water-vapor partial pressures at various points in the LIGO vacuum system at two times (4 h and 24 h) after the start of a pump down from atmospheric pressure.

The table shows that the pump-down transients for these cases present no problem for the initial interferometers (expressed as a fraction of the column density requirement; see Table IV-D-1). With the assumptions for the interferometer gas loads given in Table IV-D-3, it would take 18 days to achieve the column density goal desired for interferometers of advanced design. Should this delay become a problem in the future it will be solved by choosing interferometer components more compatible with high vacuum practice than that assumed in the model and possibly installing larger pumps at the chambers.

References

- IV-D-1 R. Calder and G. Lewin, "Reduction of Stainless Steel Outgassing in Ultra-High Vacuum," *Brit. J. Appl. Phys.*, **18**, 1459 (1967).
- IV-D-2 B. B. Dayton, "Outgassing Rate of Contaminated Metal Surfaces," *1961 Transactions of the Eighth National Vacuum Symposium*, **1**, 42 (Pergamon Press 1962).
- IV-D-3 R. S. Barton and R. P. Govier, "The Effect of Cleaning Technique on the Outgassing Rate of 18/9/1 Stainless Steel," *Vacuum*, **20**, 1 (1970).

⁵ Standard stainless steel, baked at high temperature by the chamber manufacturer in order to reduce the hydrogen outgassing rate to $< 1 \times 10^{-12}$ torr \cdot L \cdot s⁻¹ \cdot cm⁻² after 1 h under vacuum, is a practical alternative for the chambers.

⁶ The vacuum seals in the chambers, gate valves, and air locks will be elastomer "O" rings (which limit the maximum bakeout temperature to about 200 °C).

⁷ This processing results, for subsequent pump downs from atmospheric pressure, in a water vapor outgassing rate of 1×10^{-10} torr \cdot L \cdot s⁻¹ \cdot cm⁻² after 10 h under vacuum [IV-D-3].

⁸ A vertex chamber assembly consists of the diagonal chamber, HAM chambers, and two Type 2 test-mass chambers located at the intersection of the arms.

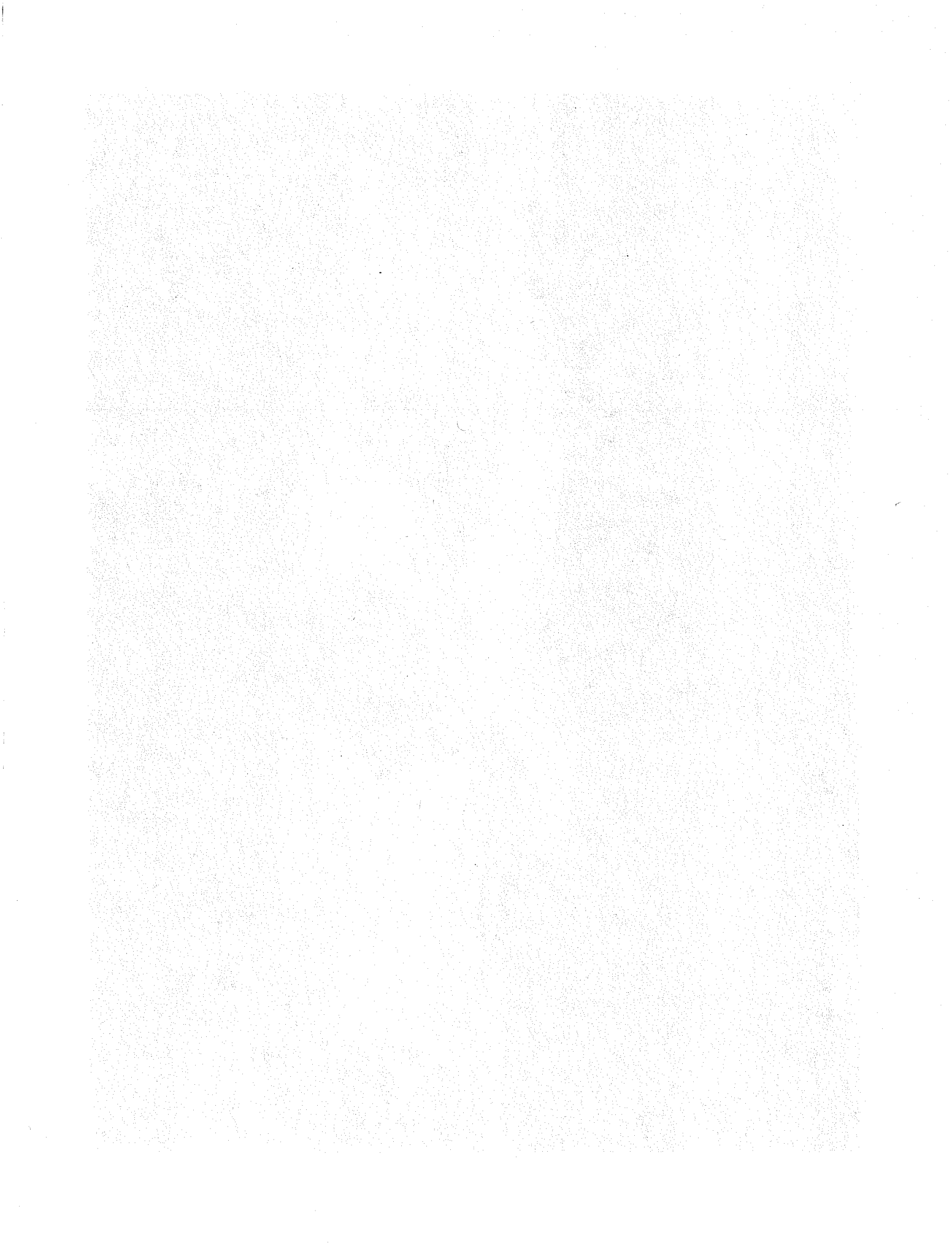
TABLE IV-D-3
CHAMBER PUMPDOWN TRANSIENTS¹

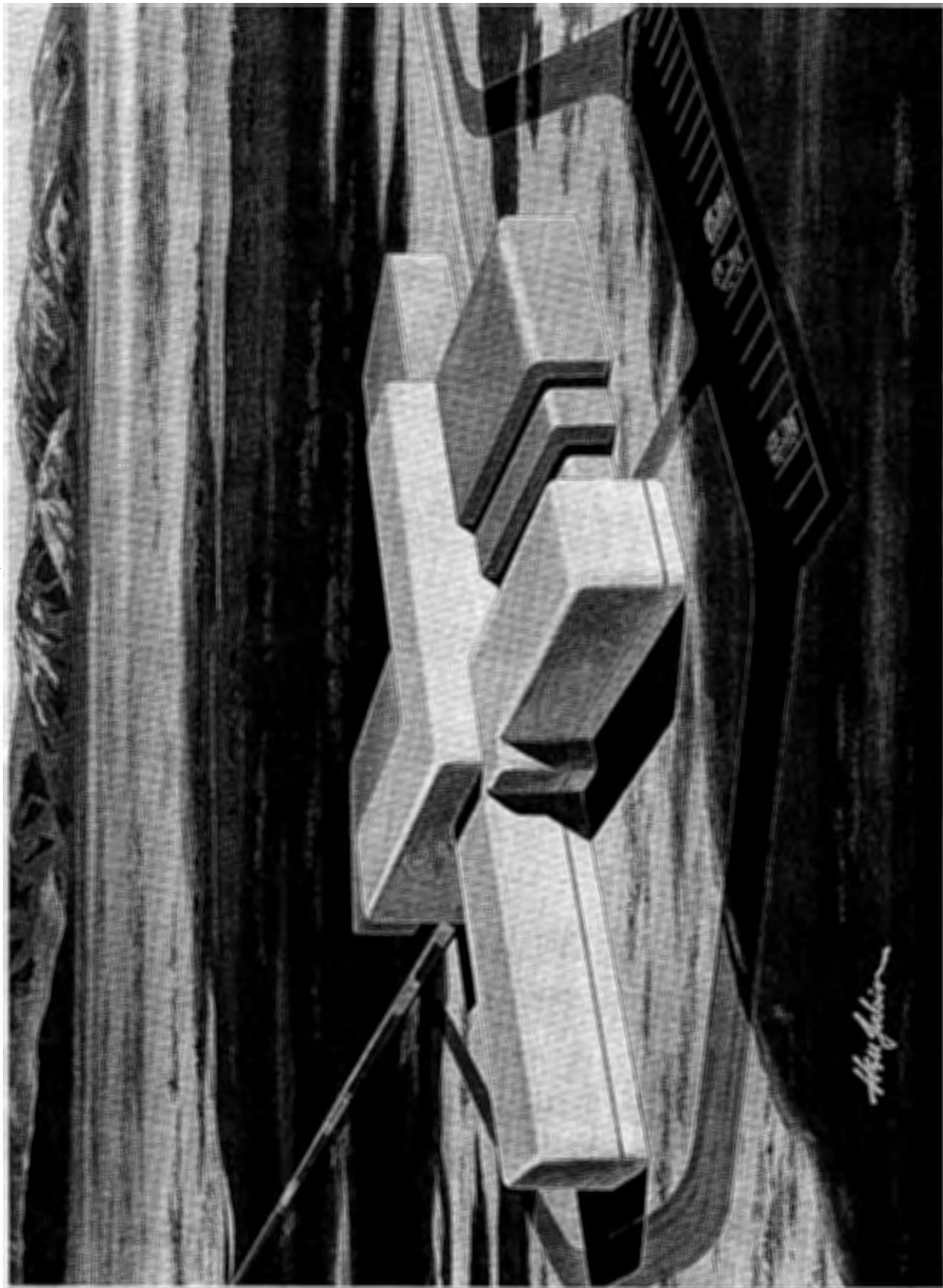
	t=4 h	t=24 h	
CASE A: CORNER STATION VERTEX CHAMBER ASSEMBLY			
Gas load, interferometer components ²	5.3×10^{-2}	8.8×10^{-3}	torr · L · s ⁻¹
Pressure at beam splitter (ion pump OFF) ³	1.4×10^{-4}		torr
Pressure at beam splitter (ion pump ON)	5.5×10^{-6}	9.2×10^{-7}	torr
Pressure at beam splitter (gate valve OPEN)		2.8×10^{-7}	torr
Pressure at LN ₂ trap inlet		2.0×10^{-8}	torr
Pressure at beam tube inlet		9.0×10^{-10}	torr
Pressure at 250 m		5.7×10^{-10}	torr
Pressure at 2 km		2.6×10^{-11}	torr
Column density		2.5×10^{13}	molecules · cm ⁻²
Fraction of allowable column density:			
<i>initial requirement</i>		0.019	
<i>goal</i>		18	
CASE B: MID STATION TEST MASS CHAMBER			
Gas load, interferometer components ²	4.3×10^{-3}	7.1×10^{-4}	torr · L · s ⁻¹
Pressure at test mass (ion pump OFF) ³	1.2×10^{-5}		torr
Pressure at test mass (ion pump ON)	1.9×10^{-6}	3.6×10^{-7}	torr
Pressure at test mass (air lock OPEN)		9.6×10^{-9}	torr
Pressure at LN ₂ trap inlet		2.3×10^{-9}	torr
Pressure at beam tube inlet		9.5×10^{-10}	torr
Pressure at 250 m		6.1×10^{-10}	torr
Pressure at 2 km		2.8×10^{-11}	torr
Column density		3.9×10^{12}	molecules · cm ⁻²
Fraction of allowable column density:			
<i>initial requirement</i>		0.003	
<i>goal</i>		2.8	

¹Table entries assume that the roughing-pump set runs for 4 h, at which time the local ion pump(s) is turned on and the roughing valve is closed. Twenty hours later, the gate valves to the beam tubes are opened. The analyses assume that the water vapor gas load varies as $1/t$, and that the chamber being pumped down is the only source of gas flux in the system. The final results are expressed as column density along the full 4-km system length.

²The gas load from the empty vacuum vessels is typically at least an order of magnitude smaller than the gas load from the interferometer components.

³All pressure values are calculated for a temperature of 300 K.

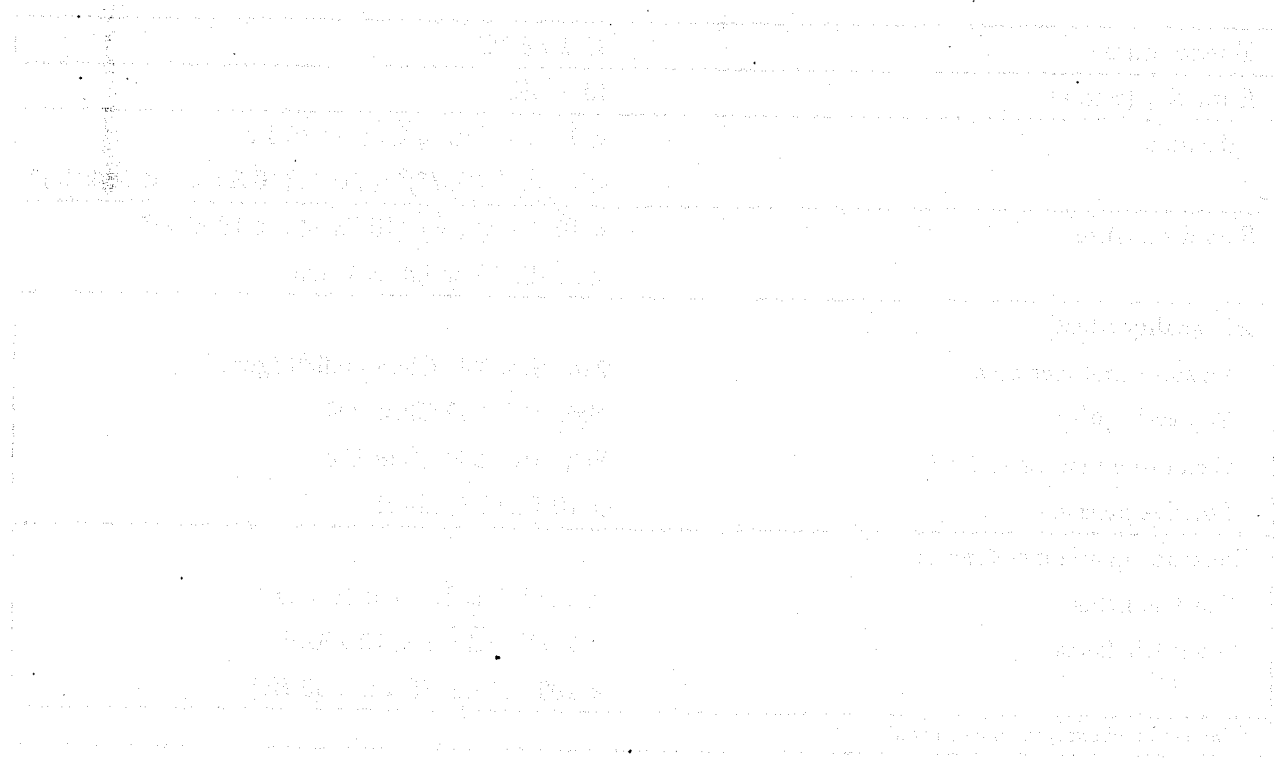




and a sufficient amount of space around the station to provide for the placement of instruments and equipment. The station should be located so that it can be easily observed from the air and the ground. The station should be located so that it can be easily observed from the air and the ground. The station should be located so that it can be easily observed from the air and the ground. The station should be located so that it can be easily observed from the air and the ground.

Figure IV-E-1 illustrates a corner-station enclosure. The figure shows a rectangular enclosure with a corner entrance. The entrance is located at the bottom-left corner of the rectangle. The enclosure has a door and a window. The door is located on the left side of the entrance. The window is located on the right side of the entrance. The entrance is labeled "CORNER STATION".

Figure IV-E-1 (facing page) Illustration of corner-station enclosure.



E. Enclosure Design

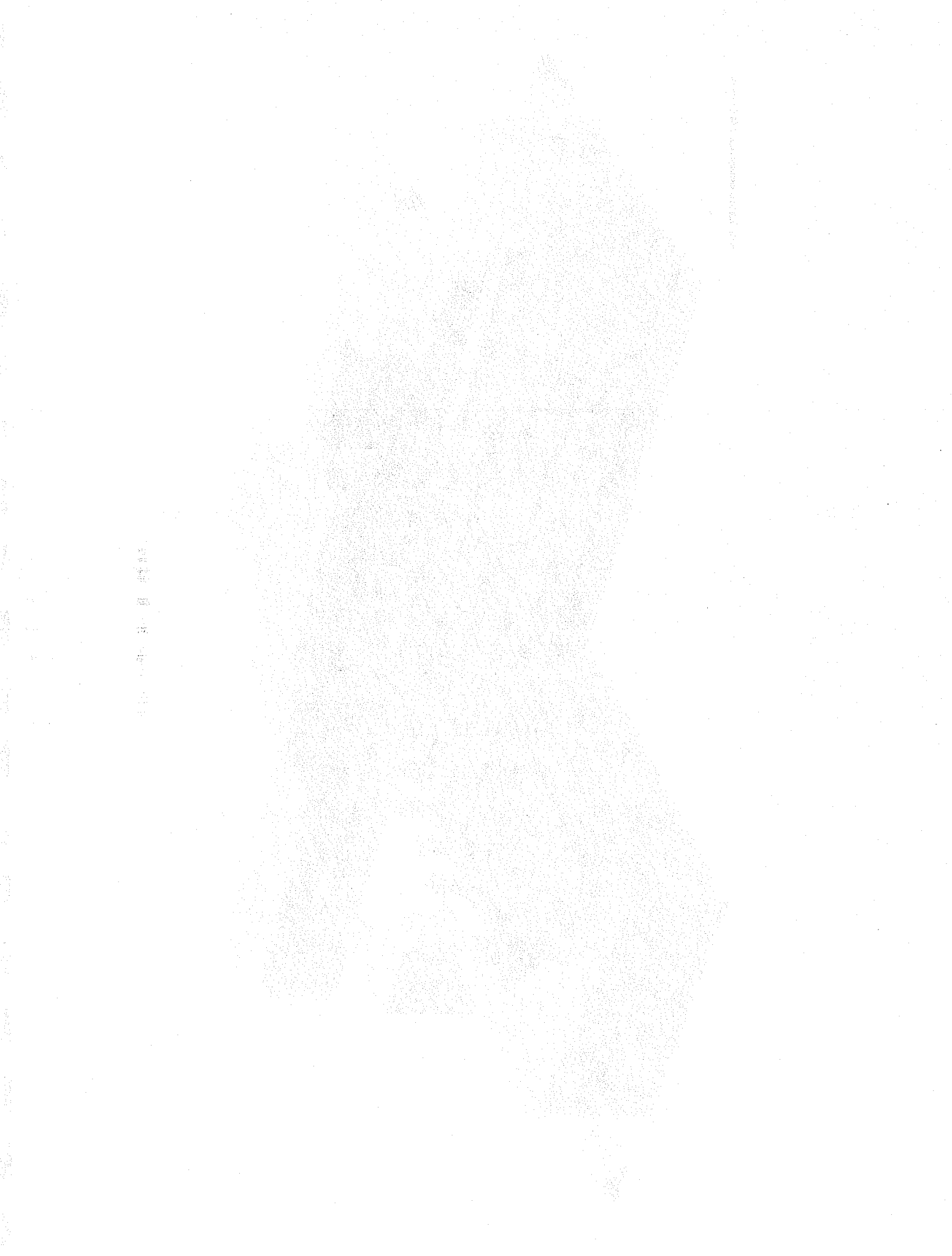
The enclosures for the stations and the beam tubes provide the operating environment for the LIGO vacuum system, equipment, and operations personnel. The buildings must provide a quiet, low-vibration environment for the interferometer components, and must provide a clean environment to minimize contamination of the vacuum system and optical components. The buildings will be sealed and pressurized to preclude entry of dust, pollen, vermin, and other sources of contamination. The most critical systems regarding acoustic and vibrational noise are those that run continuously, such as air-conditioning and laser-cooling equipment. The required ambient conditions in the vicinity of interferometer components are summarized in Table IV-E-1.

Figure IV-E-2 (facing page) Cut-away drawing of Site 1 corner-station enclosure. The vacuum chamber configuration is the mature Phase-C LIGO facility. The beam tubes and their enclosures emerge from the corner station at the far left and far right of the figure.

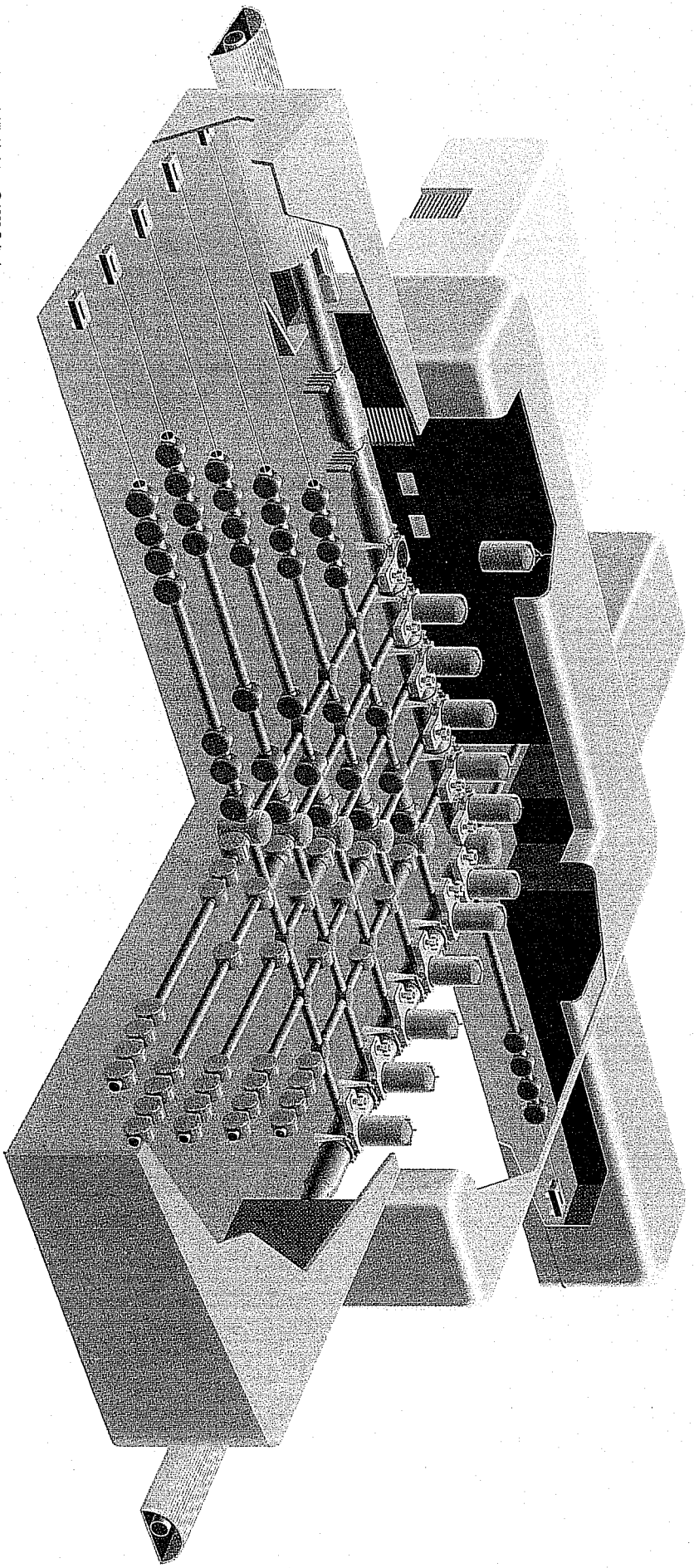
**TABLE IV-E-1
AMBIENT CONDITIONS
FOR INTERFEROMETER COMPONENTS**

Temperature	$23 \pm 1.5^\circ\text{C}$
Humidity (relative)	$40 \pm 5\%$
Vibration	$< 2 \times 10^{-9} \text{ m}/\sqrt{\text{Hz}} (f < 10 \text{ Hz})$ $< 2 \times 10^{-7} (\text{Hz}/f)^2 \text{ m}/\sqrt{\text{Hz}} (10 \text{ Hz} < f < 10 \text{ kHz})^*$
Sound pressure	$< 10^{-4} \text{ Pa}/\sqrt{\text{Hz}} (10 \text{ Hz} < f < 10 \text{ kHz})^*$ $< 45 \text{ dB (A-weighted) rms}$
Air quality (dust)	
Vacuum chamber area	Fed. Std. 209 Class 50,000 (goal)
Exposed optics	Fed. Std. 209 Class 200
Clean room (work surface)	Fed. Std. 209 Class 100
Positive pressure	$> 10 \text{ Pa (0.1 mbar)}$
Electromagnetic interference	
Electric fields	$< 1 \text{ mV}/\text{m}\sqrt{\text{Hz}} (f < 10 \text{ kHz})^*$
Magnetic fields	$< 2 \text{ nT}/\sqrt{\text{Hz}} (f < 10 \text{ kHz})^*$ $< 100 \text{ nT rms (f = n} \times 60 \text{ Hz)}$

*Narrow-band exceptions permitted



Rendering by J. Nils Lindstrom © 1998 Caltech



1. Corner-station enclosure

The corner-station enclosure is illustrated in Figure IV-E-1. Its Phase-A floor plan at Site 1 is shown in Figure IV-E-3, and that for Site 2 in Figure IV-E-4. The floor plans are similar except that the area provided for vacuum chambers at Site 2 is somewhat smaller because it will accommodate fewer interferometers. The layout of the planned Phase-C expansion of the vacuum system is shown in Appendix A, and a representation of the Site-1, Phase-C, corner station is shown in Figure IV-E-2.

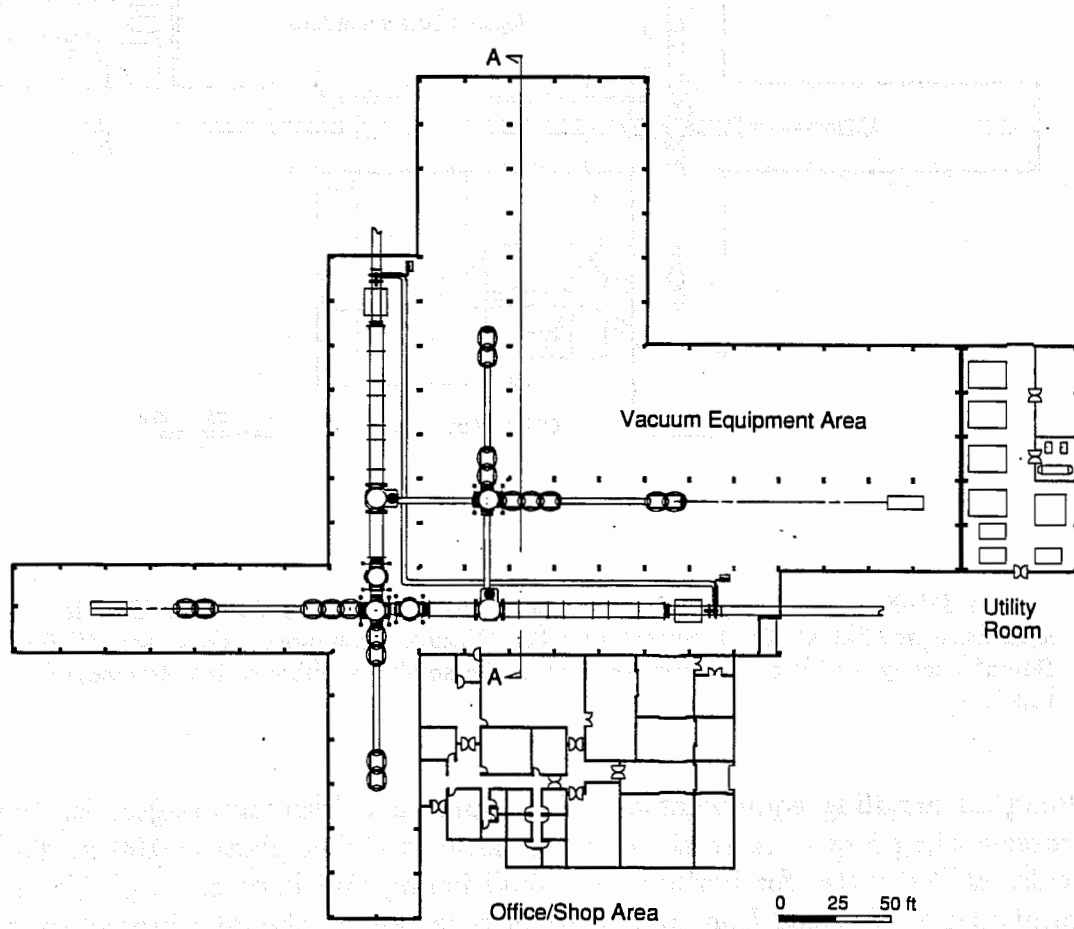


Figure IV-E-3 Floor plan for the Site 1 corner station in Phase A. Upgrades for Phases B and C will introduce more chambers and tubes into the "vacuum equipment area," but will not enlarge the building (see Appendix A, Figure A-4 for comparison). Section (A-A) is shown in Figure IV-E-5.

The buildings house vacuum equipment, lasers, and optical and electronic components necessary to operate the interferometers. A utility room contains the

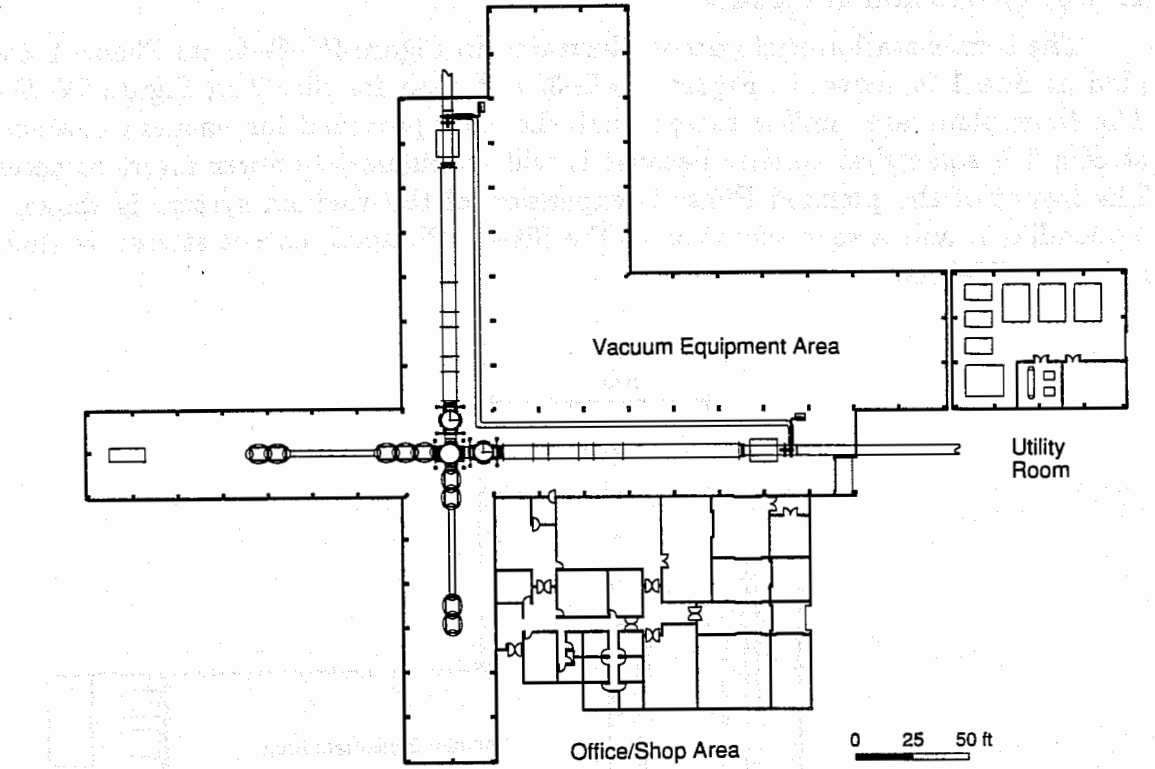


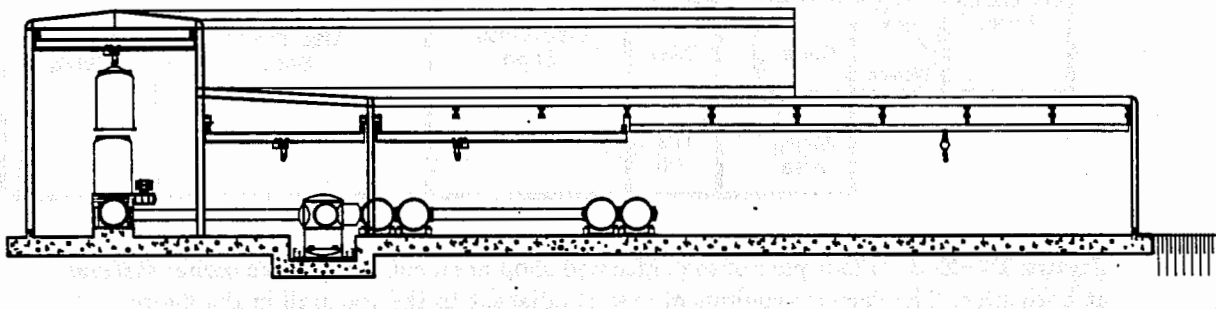
Figure IV-E-4 Floor plan for the Site 2 corner station in Phase A. This layout is identical to that at Site 1, except that the "Vacuum Equipment Area" and "Utility Room" occupy less area, commensurate with the smaller number of interferometers at this site.

building air-handling equipment and the pumps and heat exchangers for the local laser-cooling loops. A small, remotely-located chiller plant (~100 m distant) provides chilled water for building air conditioning and laser cooling. To reduce transmission of vibration from machinery or personnel to the interferometers, separate foundations are provided for the vacuum-equipment and laser area, the utility room, and the office and shop area.

a. Vacuum-chamber and laser area. The vacuum-chamber and laser area enclosure (labeled "Vacuum Equipment Area" in Figures IV-E-3 and IV-E-4) is a single-story structure of varying height with an area of about 60,000 ft² at Site 1, and about 48,000 ft² at Site 2. The building is of steel-frame construction with both interior and exterior walls to provide added resistance to dust penetration from the outside. The roof and exterior walls are metal double-skinned, insulated-foam-core panels with double-lock standing seam. The inside walls are covered by

prefomed panels with baked-enamel finish for sealing and cleanliness control. A dropped ceiling, finished with mylar-covered acoustic tiles, is provided to control acoustic reflections and to trap dust which may leak through the roof. The building interior, including the volume between the inner and outer walls, is pressurized slightly over atmospheric pressure as a further measure of dust protection. The buildings have no windows, eliminating a potential source of dust contamination, improving thermal control, and providing security.

Interior ceiling height is 50 ft in the region over the test mass chambers and 30 ft elsewhere. A section view of this area is shown in Figure IV-E-5. Eight underhung bridge cranes provide complete coverage of the vacuum equipment. The crane system consists of two 10-ton cranes over the test-mass chambers, and six 5-ton cranes for the remaining area. The cranes come with swing-out sections and interlocking crossovers to transfer equipment between the crane runways. All cranes include speed controls and soft-start devices.



SECTION A-A

Figure IV-E-5 Section view of the Site 1 corner station, showing variation in interior ceiling height to accommodate Type 1 test-mass chambers and overhead cranes. The view corresponds to the Section (A-A) indicated in Figure IV-E-3.

The building is constructed on a reinforced-concrete mat foundation, finished with rubber flooring.

b. Utility room. Heating, ventilation, and air conditioning (HVAC), including humidity and dust control, are provided by air-handling equipment in the utility room and by a small chiller plant, which is remotely located. Cooling for the lasers is provided individually by closed-loop deionized-water cooling systems with heat exchangers coupled to the chilled-water lines; the laser-cooling systems are also located in the utility room.

c. Office and shop areas. The office and shop area layout, common to both sites, is shown in Figure IV-E-6. This area contains office space for resident and visiting personnel, rooms for monitoring and control equipment for the facility and interferometers, and space for testing and service operations. The general layout is planned to reduce the introduction of contaminants by having personnel and equipment move from outside to inside through increasingly clean regions.

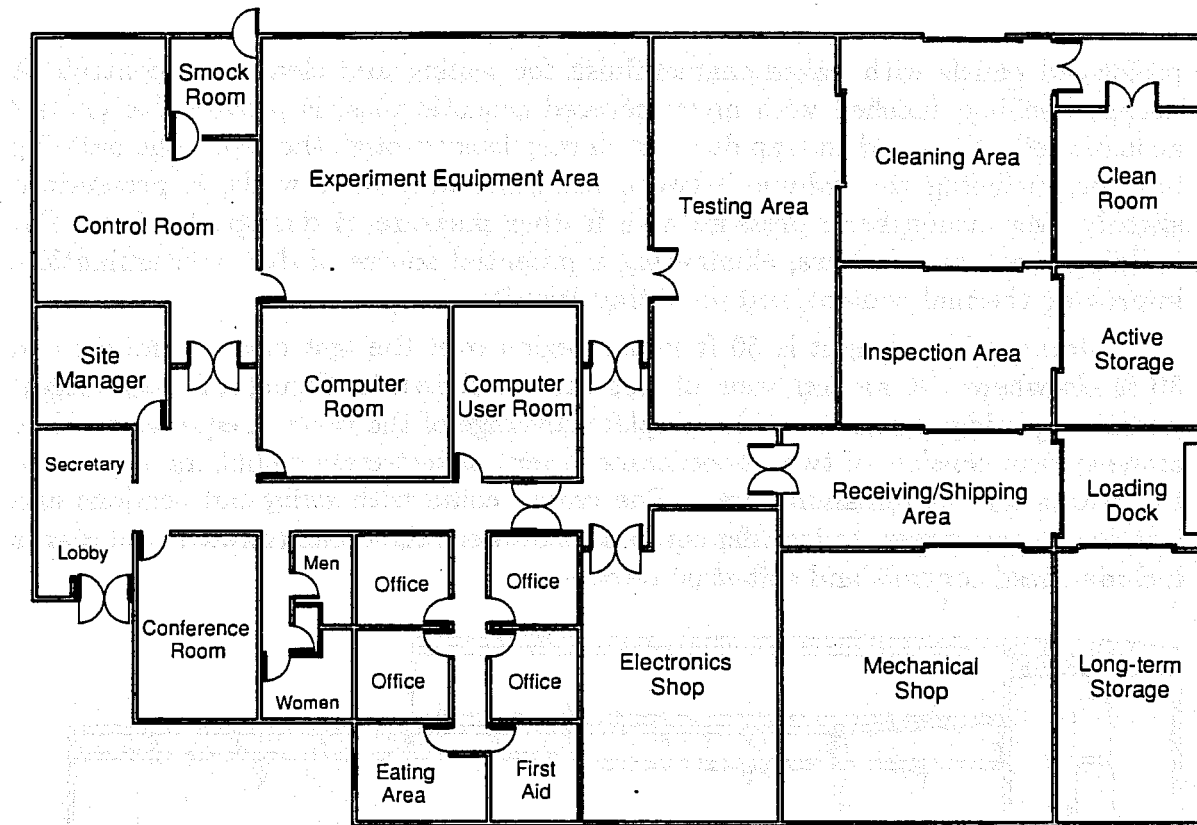
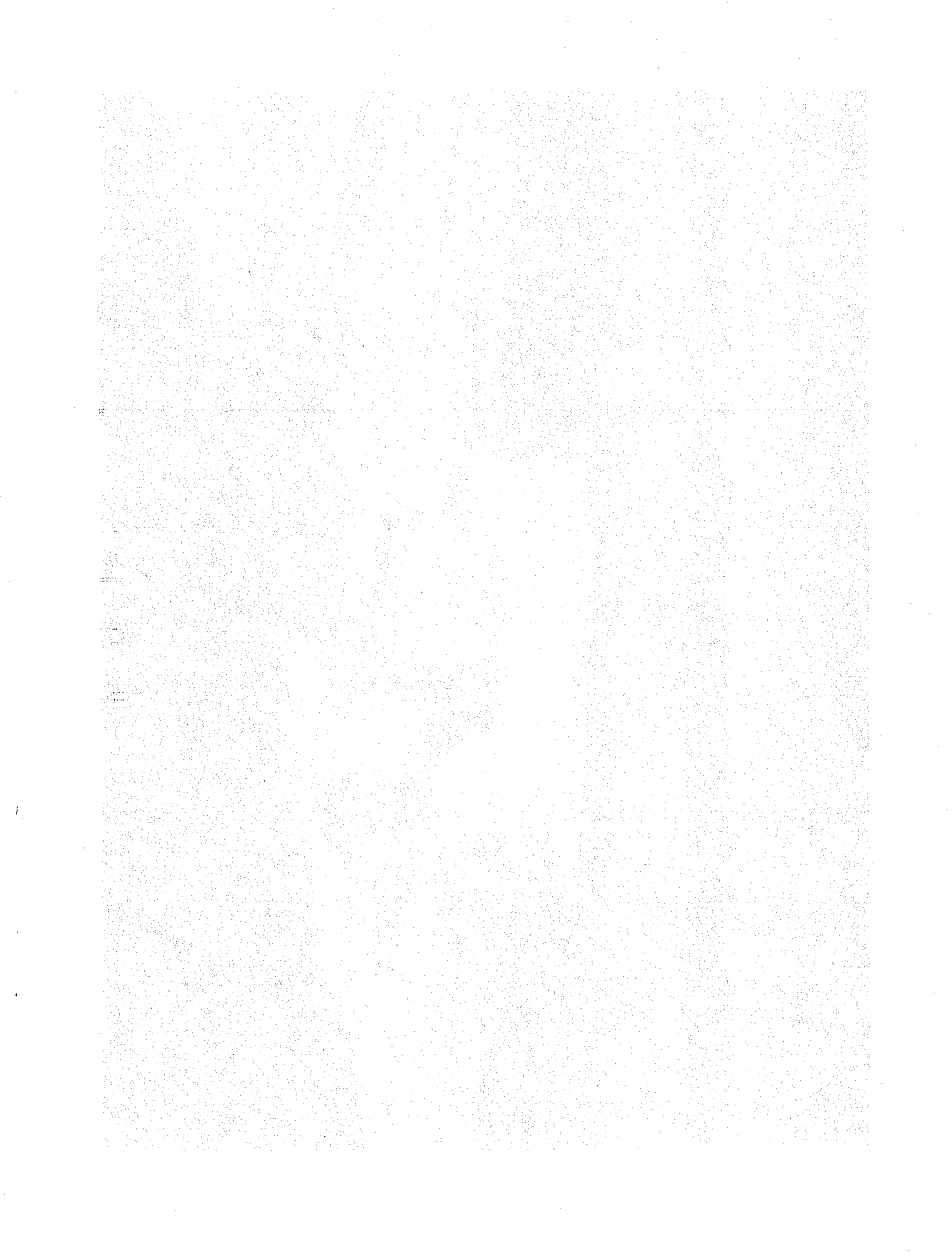
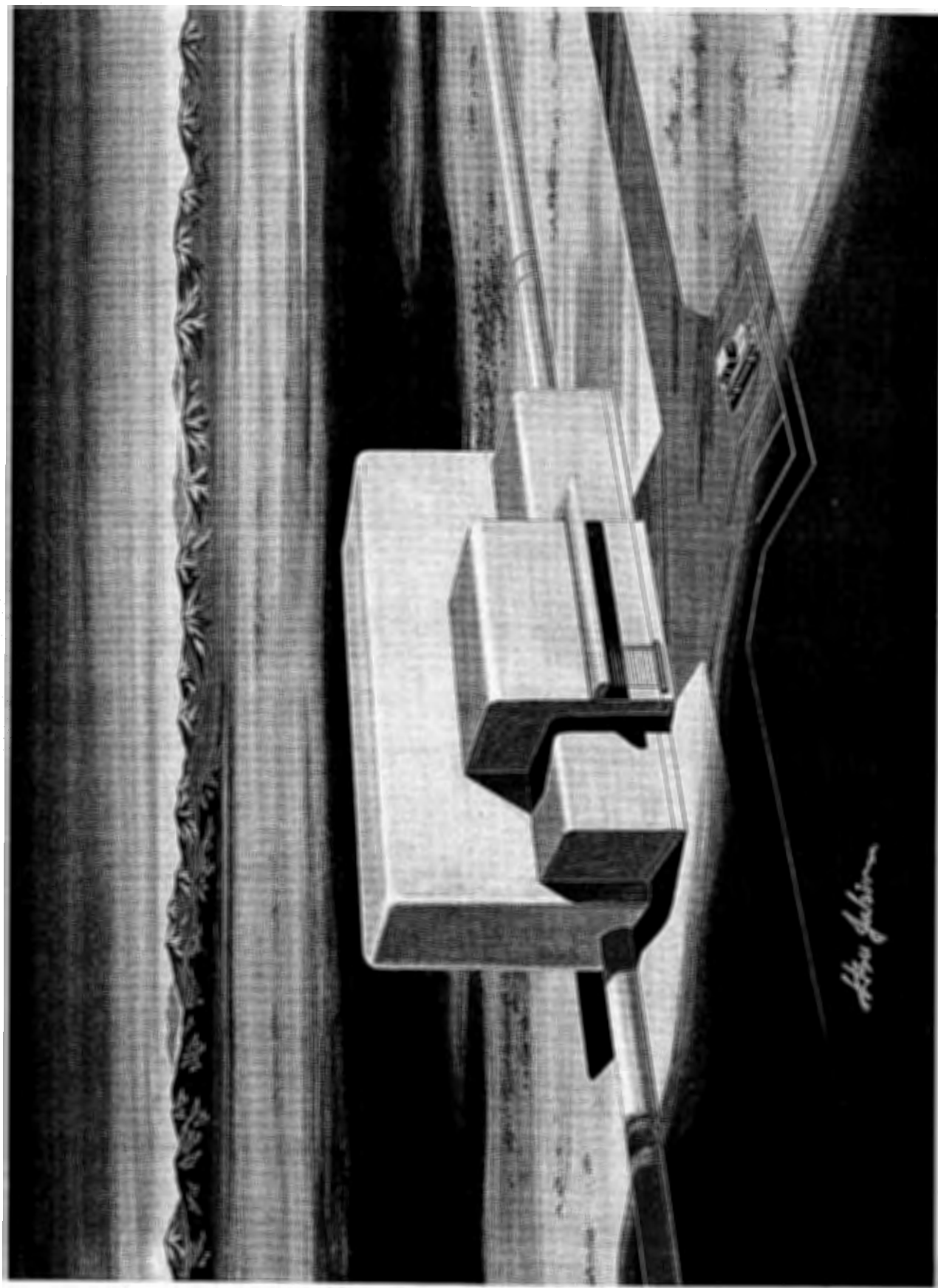


Figure IV-E-6 Floor plan of the office and shop area, common to the corner stations at both sites. The vacuum-equipment area is adjacent to the top wall in the figure.

The control room is the operational center of the facility. Manned 24 h/day, all systems-status and performance parameters are monitored and controlled from this location. Laser power and cooling will be activated from the control room. Vacuum-system pumps and valves will be controlled by the operator, although activation of the large roughing pumps and valves in the remote end stations and mid stations will require positive intervention by another person, local to the equipment. The tape drives for the data logging system are housed in the control room. Interferometer status and alarms will be monitored from here, and the operator will be able to perform some interferometer adjustments. Access to the laser area and vacuum chambers, including the end stations and mid stations, will be controlled by the operator. Physical security of the facility will be monitored by a system of low-light-level television cameras displayed in the control room.

The experimental equipment area will contain electronic equipment for centralized control of—and data acquisition from—the interferometers. This is the primary area for personnel who are working on the development or maintenance of interferometers when they are not installing or removing components in the vacuum chambers. All adjustments of the interferometers can be performed from this area. The experimental equipment area also contains the electronic equipment





John Johnson

for acquiring and processing data from auxiliary-physical-parameter measurements and facility-housekeeping measurements.

A testing area is provided for setup and checkout of interferometer components before installing them into the vacuum system. This room will contain a small laser, vacuum chambers for performance testing, and a vacuum bakeout chamber.

Equipment that arrives at the LIGO installation will be processed in a manner which ensures the integrity of the clean environments. Packages that arrive at the loading dock will be cleaned externally before being moved into the receiving/shipping area. There, they are unpacked from the outer shipping container and moved to the inspection area, where the inner packaging is removed and the contents are verified. Equipment destined for the vacuum equipment area is moved through the cleaning area for removal of dust or contamination. The doors connecting these areas will be opened one at a time, to prevent outside dust or particulate contamination attached to packaging from reaching the clean vacuum-chamber and laser areas. The processing areas and connecting doorways are large enough to handle optics assemblies, vibration-isolation stack components, and vacuum chambers.

A clean room is provided for working on interferometer optics and lasers. It is designed with vertical laminar air flow to provide a Class 1000 room environment; laminar-flow clean benches provide Class 100 working surfaces. Entry is through an air-shower anteroom, large enough to accommodate both the long argon-ion lasers and large test-mass assemblies.

Mechanical and electronics shops are provided for maintenance and repair of interferometer and facility equipment. The electronics shop contains electronic repair instruments and calibration equipment for vacuum instrumentation, auxiliary-physical-parameter instrumentation, computers, and interferometer electronics. The mechanical shop contains small machining and welding equipment for maintenance or modification of interferometer components and vacuum chambers.

Figure IV-E-7 (facing page) Artist's illustration of a right-arm mid-station enclosure. The beam-tube enclosure is shown entering the mid-station enclosure on the left and exiting on the right. The roof line is higher over the vacuum-equipment area and loading zones to allow clearance for test-mass chambers and overhead cranes. The enclosure designs for the left-arm mid station is a mirror image of the figure. The enclosure designs for the end stations are similar to the mid stations.

2. Mid stations and end stations

The enclosures for mid stations and end stations are all of identical design (see Figure IV-E-7), differing only in vacuum equipment layout. The floor plans for the right-arm end stations, and the mid stations at Site 1, are shown in Figure IV-E-8 and Figure IV-E-9 respectively. The design concept follows that of the corner station. The vacuum-equipment area is of double wall construction with covered floors, dropped acoustic tile ceiling, and an overhead bridge crane. The

area contains test-mass chambers, roughing pumps, liquid-nitrogen pumps, and valves. It is sized for the planned Phase-C expansion of the vacuum equipment, which involves adding Type 1 test-mass chambers to each building (see Appendix A).

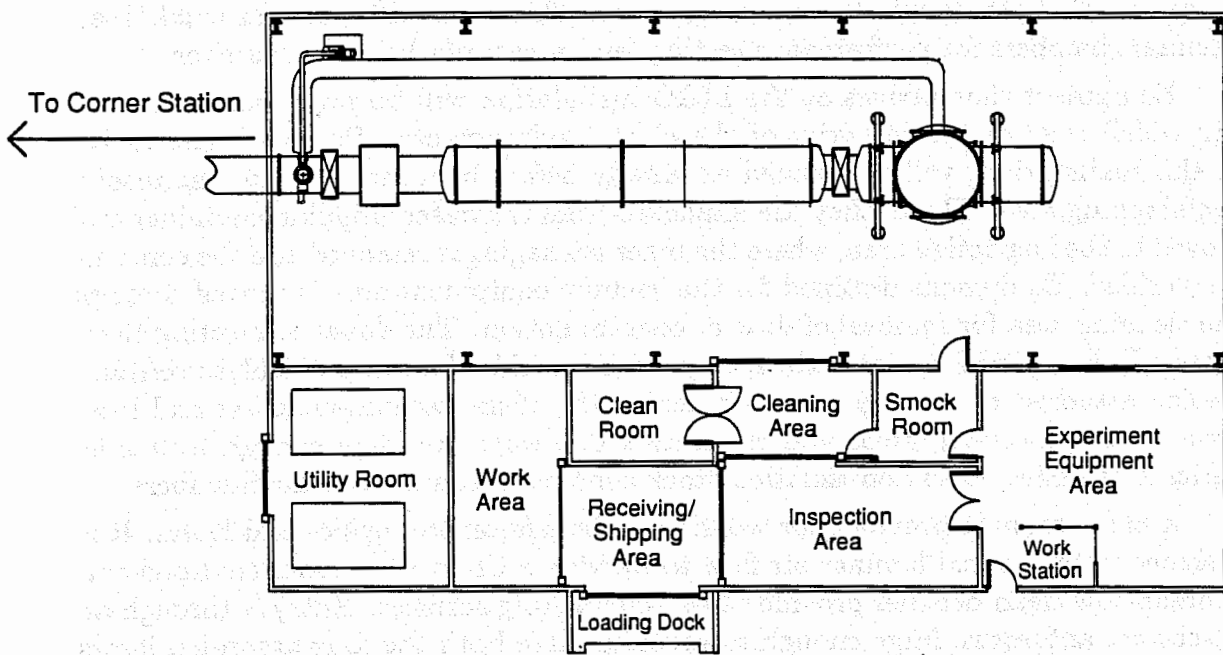


Figure IV-E-8 Floor plan of the right-arm end stations, common to both sites. The left-arm end stations have similar (mirror-imaged) floor plans.

The adjacent service area serves a function similar to the office and shop areas of the corner station. An attached utility room (with separate foundation for vibration control) contains HVAC equipment. A small chiller is remotely located.

Access to the service area and the vacuum-chamber area is controlled and monitored by the facility operator in the corner station.

3. Tube enclosure

The tube enclosure protects the LIGO beam-tube walls from vibration induced by wind. It also provides a degree of protection against vandalism or stray bullets from hunters. An underground tunnel has been ruled out for cost reasons.

A concrete-arch cover design was chosen which, when integrated with the continuous mat foundation,¹ provides a rigid, stable structure enclosing the beam tubes. An elevation section view of the covered tube is shown in Figure IV-E-10. The

¹ The tube cover is built in place in 80-ft sections after field assembly and testing of the beam tubes is completed. An inflated air bag will be used as a form for the arch structure. A section of half-round corrugated-steel pipe is placed over the beam tube to support the air bag. The inflated

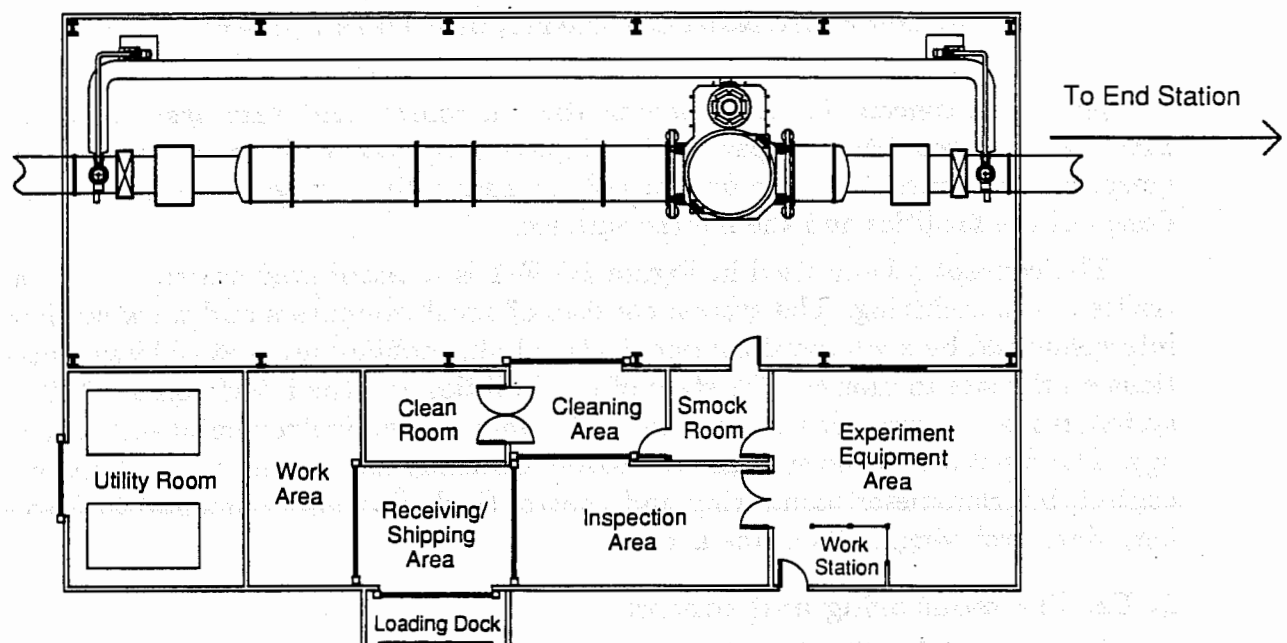


Figure IV-E-9 Floor plan of the right-arm mid station at Site 1. The left-arm mid station has a similar (mirror-imaged) floor plan. There are no mid stations at Site 2.

cover size is chosen to provide adequate room for access to repair leaks, adjust the alignment of the beam tubes, or conduct beam-tube bakeouts. The cover also protects electrical power distribution and communications lines.

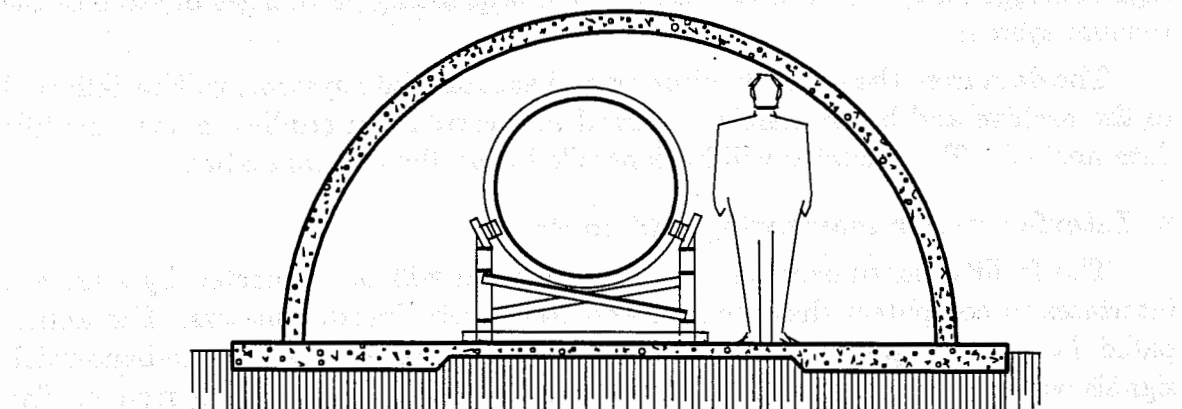


Figure IV-E-10 Elevation section view of the covered beam tube.

air bag is restrained from above by flexible steel straps attached to the foundation slab. Preformed reinforcing bars are laid into place over the air bag form and wired together. High strength, low-slump "shotcrete" is then sprayed in place. In 2 to 4 hrs, the concrete gains sufficient strength to support itself. The air bag is deflated and moved with the half-round steel pipe to the next section.

F. Instrumentation, Control, and Data System

An initial concept for the instrumentation, control and data system for the LIGO is presented, based in part on the experience gained with prototype interferometers. The concept will be further refined during the course of the engineering design of the facilities and the interferometers.

The concept schematized in Figure IV-F-1 is a distributed system with centralized data archiving. The system consists of small computers and work stations interconnected by a standard communication link, enabling users at different locations on the site to monitor the state of the facilities and the interferometers. The system is readily implemented with current computer and instrumentation technology. The functions of the system are broadly classified into facility monitoring and control, interferometer monitoring and control (including environmental monitoring), data archiving, and on-line analysis.

1. Facility monitoring and control

One part of the distributed system will be dedicated to plant monitoring and control. The system acquires and displays the physical variables of the facilities (such as temperatures, power flow, and laser cooling) and state variables (such as building occupancy and fire monitors). It also provides control functions for safe operation of the facilities, such as interlocks on laser power.

Another dedicated system will monitor and control the vacuum system. This system will monitor data such as residual gas pressures, the spectra of residual gas analyzers, ion-pump currents, and the states of valves, mechanical pumps, and liquid nitrogen traps. It will also control the sequencing of changes of state of the vacuum system.

The data from the plant-monitoring and vacuum-data systems will be delivered to the archive and be accessible for trend and correlation studies in the scientific data analysis. The facilities will be controlled from the central station.

2. Interferometer monitoring and control

The facility instrumentation and data system will be connected by standard interfaces to computers that monitor and control the interferometers. The anticipated data rate is approximately 50 kbytes/s/interferometer. The large-bandwidth signals will have a direct data-bus connection to the facility-archiving system. The diagnostic instruments used in interferometer testing and development (such as dynamic signal analyzers, RF spectrum analyzers, and digital oscilloscopes) are controlled by the standard ethernet and IEEE-488 bus network.

Dedicated processors, tightly linked to the interferometers, will be used to control the suspension, automated alignment, and fringe-acquisition systems of the interferometers. The data rates associated with these functions are too high to be included (unprocessed) in the general facility control and monitoring system.

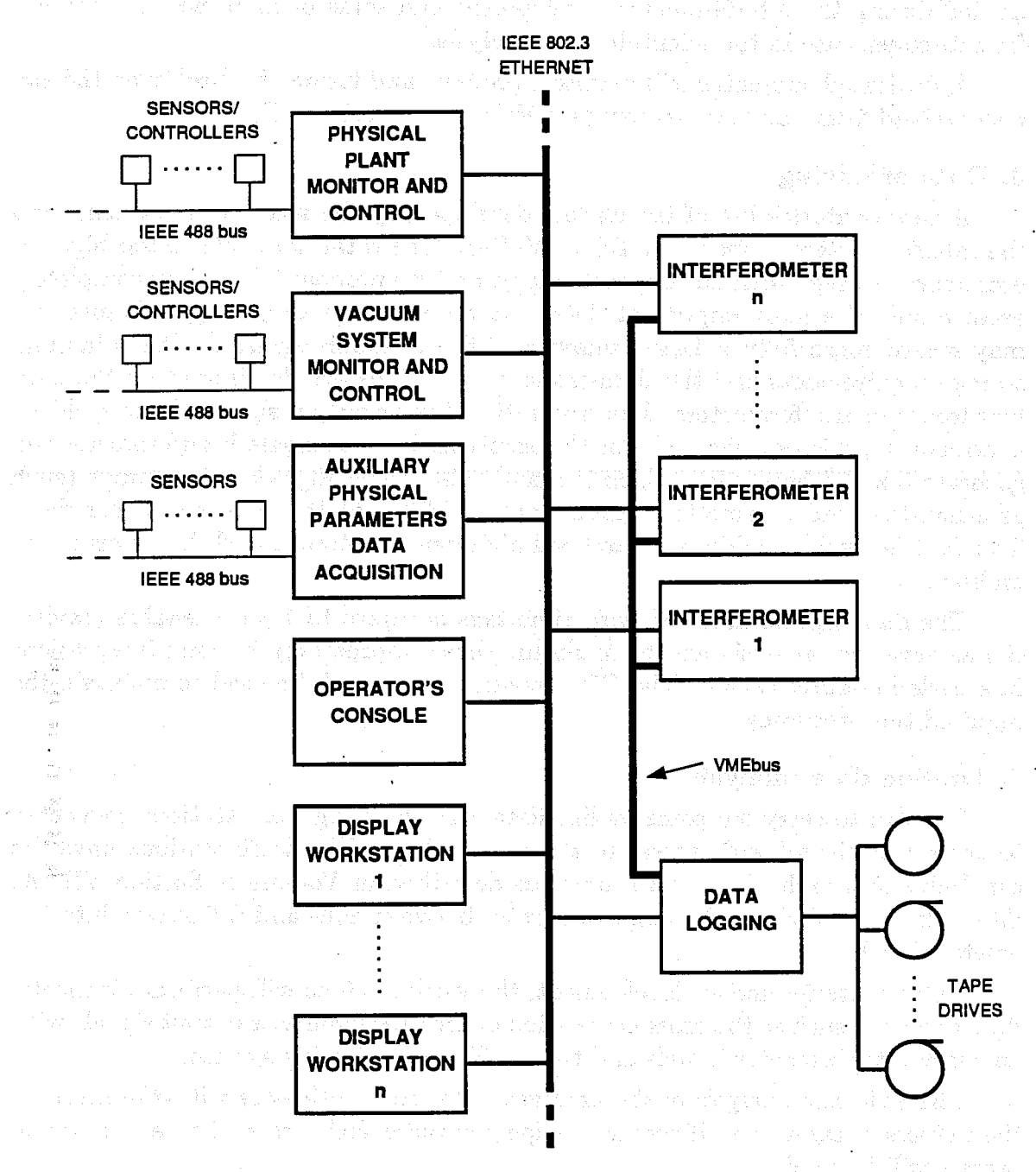


Figure IV-F-1 Diagram of the instrumentation, control, and data system for a LIGO site. A distributed architecture is used for all facility monitoring and control functions serviced by a standard (Ethernet) network. The interferometers are locally controlled by dedicated processors (not shown). The high bandwidth output data from the interferometers are transmitted to the facility archiving system by a dedicated (VME) data bus. The archiving system combines the interferometer output with facility and auxiliary monitoring signals. Display workstations throughout the facility can access data from anywhere in the system.

The interferometers develop a large number of signals involved with the control of lasers, beam positioning, mass positioning, and damping. These signals are

needed during the interferometer development and some of them will be archived for subsequent use in the scientific data analysis.

A dedicated computer will monitor, process, and format for archiving the signals derived from auxiliary sensors (see Volume 1, Section VII).

3. Data archiving

A representative list of the signals developed by the monitoring systems and the interferometers is shown in Table IV-F-1. The total data rate is too high for economical storage with current technology, and we propose initially to completely archive only the most important data. As data storage technology advances we may record more fully a larger number of the available signals. The minimum storage requirements and the data-management plans are dominated by the data flow from the interferometers. The gravitational-wave output signal will be archived continuously; this sets the scale for the archiving load. A single interferometer will generate 5×10^9 bytes/day, which is manageable using high-density storage (such as 8-mm-tape video cassettes, which would be filled at the rate of two per day). The facilities will provide both archival high-density storage and disk storage for on-line analysis.

The data will be archived with time tags accurate to $1 \mu\text{s}$ to enable gravitational-waveform analysis and to maintain phase information for long integrations in a periodic-source search. The GPS satellite system will be used to maintain the required time accuracy.

4. On-line data analysis

We plan to carry out some on-line data analysis using work stations connected to the ethernet and with access to the disk archive. The work stations have the capability to search¹ for burst sources as described in Volume 1, Section VII. At Site 1 they would check the amplitude ratio between half- and full-length interferometer signals.

During interferometer development, the work stations will perform diagnostic data analyses, such as the cross-correlation of the interferometer output signals with ancillary interferometer signals and the auxiliary monitoring system.

The full-scale analysis of the archived data from both sites will take place on the university campuses. If required, supercomputer facilities available in national centers will be used.

¹ One method is to use a dedicated work station for burst-template filtering and threshold detection. The machine would be directly coupled to the interferometer with access to the high-data-rate gravitational-wave output. When a threshold is exceeded, a signal is sent to other processors on the ethernet to request data that have been stored in short-term ring buffers. In this way signals that embrace the time of the threshold crossing and are relevant to the data analysis will be archived, without placing huge demands on data storage capacity.

TABLE IV-F-1
REPRESENTATIVE LIST OF SIGNALS¹

SIGNAL	DESCRIPTION	NUMBER	BAND-WIDTH (kHz)	DATA RATE (kbytes/s)
Interferometer Signals				
Interferometer output	Gravitational-wave signal	1	10	40
Symmetric port	Intensity monitor	1	10	(40)
Main cavity lock		2	10	(80)
Beam splitter lock		1	10	(40)
Recycling mirror lock		1	10	(40)
Main frequency lock		1	10	(40)
Trim frequency lock		1	10	(40)
Side arm lock		2	10	(80)
Alignment Signals				
Main cavity angle	2 angles/mirror	8	1	(32)
Beam position	2 axes/mirror	8	1	(32)
Recycling mirror	2 angles, 2 positions	4	1	(16)
Mode cleaner	2 angles, 2 positions	4	1	(16)
Suspension Signals				
Main cavity mirror	5 degrees of freedom	20	0.1	(8)
Deflection mirror	5 degrees of freedom	10	0.1	(4)
Beam splitter	5 degrees of freedom	5	0.1	(2)
Recycling mirror	5 degrees of freedom	5	0.1	(2)
Mode cleaner	5 degrees of freedom	10	0.1	(4)
Auxiliary Monitor Signals				
Low freq. seismic	1/building	3	0.03	0.4
High freq. seismic	3/test-mass chamber	15	0.3	18
Acoustic pressure	1/test-mass chamber	5	2	(40)
Line power	1/building	3	0.1	1.2
Low freq. mag. field	3 axis magnetometer/building	9	0.03	1.1
High freq. mag. field	3 loops/test-mass chamber	15	0.01	0.6
RF interference	1/building	3	0.1	1.2
Cosmic ray showers	1/building	3	0.01	0.12
Housekeeping	Temperatures, voltages, states, etc.	100	0.001	0.4

¹ The table is included to illustrate the scale of the data flow. The signals with data rates in parentheses are not continuously archived. The data rates (kbytes/s) are based on a sampling rate of twice the bandwidth, and a sampling resolution of two bytes.

G. Electrical Power

The estimated electrical power consumption for the LIGO installations is presented here. Because the power consumption for the fully evolved (Phase-C) LIGO is only modestly larger than that for Phase A, the Phase-C estimates have been used for planning the installed power capacity. The average annual power consumption during Phase A is used for the purposes of estimating operating costs.

The estimates for capacity required and power consumption are summarized in Table IV-G-1 for Site 1. A total installed capacity of 2 MW is planned at each site.

**TABLE IV-G-1
SITE 1 POWER CONSUMPTION**

	Capacity ¹ (kW)	Average ² (kW)
1. Lighting	143	45
2. HVAC	640 ³	450 ³
3. Vacuum pumps:		
Beam tube roughing	200 ^{4,5}	
Chamber roughing	33 ⁴	1
Ion pumps (first year of operation)	6	
Ion pumps (fully operational)		1
4. Electronic equipment	200 ⁶	100
5. Shop and service equipment	60	28
6. Chamber bakeout heaters	80 ⁴	
7. Lasers (including cooling)	320 ^{4,6}	160
8. Reserve	631	
TOTAL	2000	785

¹Short term peak transients excluded.

²Average power consumption after startup of operations.

³Site dependent.

⁴Will not operate simultaneously; only line 7 is included in total.

⁵ 3.8×10^5 kW-h total.

⁶Phase-C maximum estimates.

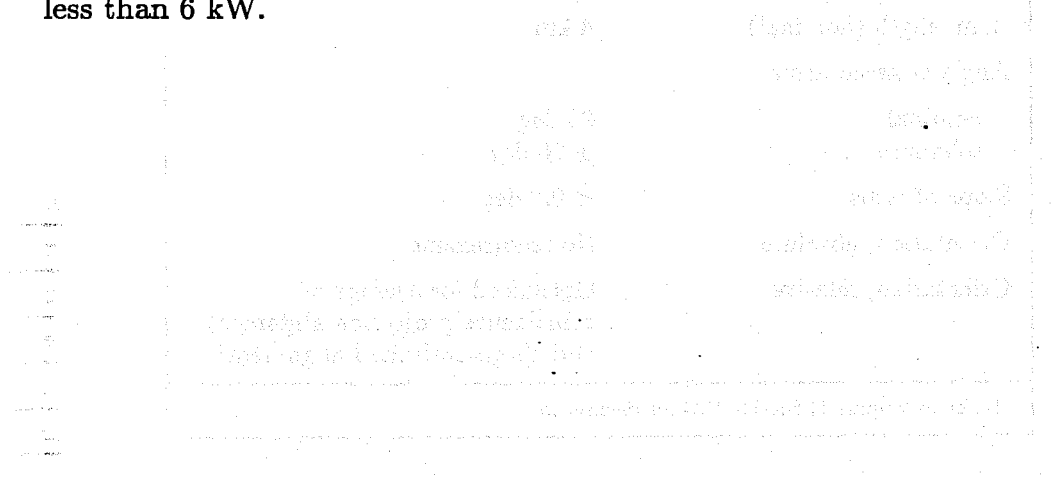
The minimum lighting necessary for personnel and equipment is provided in the large vacuum-chamber and laser areas, supplemented by high-intensity, local lighting for work areas. Incandescent lighting will be used in these areas, for reduced radio-frequency interference.

Power requirements for HVAC equipment may be traded off against capital costs and are site dependent. Standard HVAC design practices, including the use

of "economizers" and chilled-water plenums, have been assumed for the power and cost estimates.¹

Vacuum-roughing pumps are operated at a low-duty cycle and contribute negligibly to the average power consumption. The beam tubes are pumped down only once, during startup operations. During beam-tube rough-pumping, none of the lasers will be operating; during chamber rough-pumping, at least one laser (associated with the interferometer(s) being evacuated) can be shut down temporarily. The power required for the roughing pumps may thus be "borrowed" from the laser power capacity, and need not be added into facility-power capacity requirements. Similar reasoning is used for the chamber bakeout heaters, which are operated only occasionally.²

Because of the low operating pressure of the LIGO, ion-pump power consumption is negligible. The maximum occurs during the first year of operation and is less than 6 kW.



The total power required for the facility is 1000 kW. This is the sum of the power required for the lasers, beam tubes, chambers, chilled water, air conditioning, electrical equipment, and other facilities. The power required for the lasers is 100 kW. The power required for the beam tubes is 100 kW. The power required for the chambers is 100 kW. The power required for the chilled water is 100 kW. The power required for the air conditioning is 100 kW. The power required for the electrical equipment is 100 kW. The power required for other facilities is 100 kW.

It is impractical to use dissipated heat from the lasers to heat the corner building because of the low temperature (35°C max.) of the coolant returned from the laser tubes.

¹ Power for beam-tube bakeout will be provided by rented portable generators.

V. SITES

A. Site Requirements

The scientific demands of the LIGO place a number of conditions on the selection of sites. These are summarized in Table V-1.

TABLE V-1
SITE SPECIFICATIONS

Number of sites	2
Distance between sites	
minimum	2500 km
maximum	4500 km
Arm length (nominal)	4 km
Angle between arms	
nominal	90 deg
tolerance	± 15 deg
Slope of arms	< 0.2 deg
Orientation, absolute	No requirement
Orientation, relative	Optimized for average of coincidence projection alignment and Virgo-optimized alignment ¹

¹Refer to Volume 1, Section V.C for discussion.

The site requirements are met most economically by flat places that are large enough to accommodate the interferometer arms. The sites should be far enough from urban development to ensure that they are seismically and acoustically quiet, but still within convenient distance of housing for resident and visiting staff. Electrical power and road or rail access should be sufficiently close to allow economical construction. Soils and drainage characteristics must be suitable for LIGO construction, and environmental impact concerns must be addressable.

B. Site Investigation Process

An early survey of potential sites was conducted by Stone & Webster Engineering Corporation in 1983. The survey attempted to find flat areas in the continental U.S. owned or controlled by the Federal Government or state governments, and covered over 100 sites. One conclusion of this and other surveys is that the number of suitable sites drops off sharply if the arm lengths exceed 4–5 km. A subsequent JPL study conducted in 1984 identified more potential sites, and additional siting

possibilities were brought to our attention by various interested parties. To illuminate some of the issues involved in site selection, we briefly summarize our findings for eight sample site candidates (Tables V-2 and V-3).¹ One site from Group I and one from Group II could form a site pair that meets the specifications in Table V-1.

TABLE V-2
EXAMPLES OF SITE CANDIDATES

GROUP 1 ("Western" Sites)	
EAFB	Edwards Air Force Base, California
INEL	Idaho National Engineering Laboratory, Idaho
OVRO	Owens Valley Radio Observatory, California
SV	Skull Valley, Utah
GROUP II ("Eastern" Sites)	
COL	Columbia Township, Maine
FD	Fort Dix, New Jersey
LP	Livingston Parish, Louisiana
NRAO	NRAO Greenbank, West Virginia

Site investigations require a succession of increasingly costly studies, summarized in Table V-3. Some studies have already been performed at certain sites, or will be carried out under our present grant. Most require access to the land, and therefore require landowners' approval. The intent is not to fill out the matrix of Table V-3, but to collect sufficient information to permit us to make a reasonable judgment of the suitability of sites. Final site selection will not begin before this proposal is approved by NSF. We will then undertake a site selection process, using procedures approved by NSF, which will weigh scientific merit, availability, construction suitability, and costs for each site. This process is meant to satisfy the highest standards of scientific and technical review, and will be rigorous and thorough in all respects. Upon approval by the NSF to proceed, the required additional characterization studies will be done for the selected sites. The results of the hydrology and geotechnical studies and the topographic survey data will be furnished to the engineering contractors for use in detailed design of the LIGO installations.

¹ These eight sites are listed for illustration; no preference or final selection is implied.

TABLE V-3
LIGO SITE SELECTION TASKS

TASK	EAFB	INEL	OVRO	SV	COL	FD	LP	NRAO
1. Preliminary Layout	X	X	X	X	X	X	X	X
2. Vertical Profile/Earthwork Estimate	X			X		X	X	X
3. Ambient Ground Noise Survey	X					X		X
4. Biological Survey	X							
5. Archeological Survey	I.P.					X		
6. Paleontological Survey	I.P.							
7. Hydrological Survey	X							
8. Preliminary Ground Survey	X					X		
9. Preliminary Geotechnical Survey	X					X		
10. Detailed Geotechnical Survey						X		
11. Topographical Survey								

NOTES:

X denotes task is completed.

I.P. denotes task in process.

Tasks 3-11 require landowners' approval.

Task 3 establishes ambient seismic vibration spectra before construction.

Tasks 4-6 provide data for environmental and cultural impact assessment.

Task 7 determines drainage and flood protection requirements.

Task 8 is a simple staking survey to locate alignment for items 9 & 10.

Tasks 9 & 10 determine excavation, fill compaction and foundation requirements.

Task 11 is aerial photogrammetric contour mapping, to determine earthwork profiles.

C. Site Development

Construction is initiated with surveying and earthwork for the beam-tube and building foundations. Roads that access the LIGO stations are needed both during and after construction.² Provisions for drainage and erosion control, connections to power, water, and sewage utilities, fire protection, site cleanup and landscaping, and fencing for site security and public safety are required. Although the details of these activities vary widely among the candidate sites, site development costs at all sites are dominated by the earthwork required to achieve a level layout of the interferometer arms.

After site preparation and earthwork are complete, the foundations and floor slabs for the stations and the foundation slabs for the beam-tube modules are laid. Reference monuments are installed on the beam-tube-module foundations at 250 m intervals (at the approximate locations of the pump stations). Each end station and mid station has one reference monument, and there are three in the corner station. The reference monuments are used to determine the final alignment of the beam tubes (see Section IV.C.2.c.i).

² Roadways and parking areas will be paved over a suitable base after the main construction activities are completed, so that delicate equipment can be transported with minimum disturbance.

² Roadways and parking areas will be paved over a suitable base after the main construction activities are completed, so that delicate equipment can be transported with minimum disturbance.

VI. IMPLEMENTATION PLAN

In this section, the organization of the LIGO work-breakdown structure is described and the schedule for design and construction tasks is presented. The organization and roles of the personnel who are responsible for implementing the LIGO are discussed, and a subcontracting plan is presented. The section ends with a discussion of the process for designing and fabricating the initial interferometers.

A. Work-Breakdown Structure

The work-breakdown structure (WBS) for the design and construction of LIGO facilities and equipment, including initial interferometers, is shown¹ in Figure VI-1. The WBS presents the organization of all construction-implementation activities and is used to generate schedule and cost baselines. It includes

- (1) *Site development*: earthwork; roads; electrical utility connection, on-site substation, and electrical-power distribution among stations; water supply; sewer or septic tank; fire protection; site cleanup, landscaping, and fencing.
- (2) *Enclosures*: corner-station buildings for the vacuum-equipment and laser area, office and shop areas, utility room, and chiller plant; end- and mid-station buildings; electrical distribution within buildings; HVAC equipment, primary-laser-cooling equipment, and cranes; beam-tube enclosures.
- (3) *Vacuum equipment*: all vacuum vessels (including ports and feedthroughs) except the beam-tube modules; interferometer supports, intravacuum optical benches, and vibration-isolation stacks; integral air showers and backfill systems; all pumps and valves, except those along the beam tubes; LN₂ supply and distribution; adapters, caps, compensators and anchors; rough-pumping lines; installation, bakeout, leak check and performance testing.
- (4) *Beam-tube modules*: beam-tube sections and supports, stiffeners, expansion joints, cleaning, leak checking, sealing and shipping; field assembly (including alignment), baffles; beam-tube pumps, pump tees, and instrumentation ports and valves; system cleaning, leak check and bakeout.
- (5) *Support equipment*: lasers, laser-cooling heat exchangers and flow controllers, optics and electronics for laser addition, laser stabilization, and optical tables; vacuum-system monitoring and control equipment; auxiliary-physical-parameter instrumentation and data-acquisition equipment; data-logging and display equipment; intrasite communications equipment; test and diagnostic instrumentation and equipment; office and shop furnishings and equipment; and security monitoring and control equipment.
- (6) *Initial interferometer(s)*: optics, mechanical assemblies, and electronics for input and output light conditioning; beam splitters and main cavity test-mass

¹ The presentation of the WBS in Figure VI-1 is to Level 2, which will serve the purposes of the discussions in this section. Details of the WBS are presented in tabular form in Appendix C.

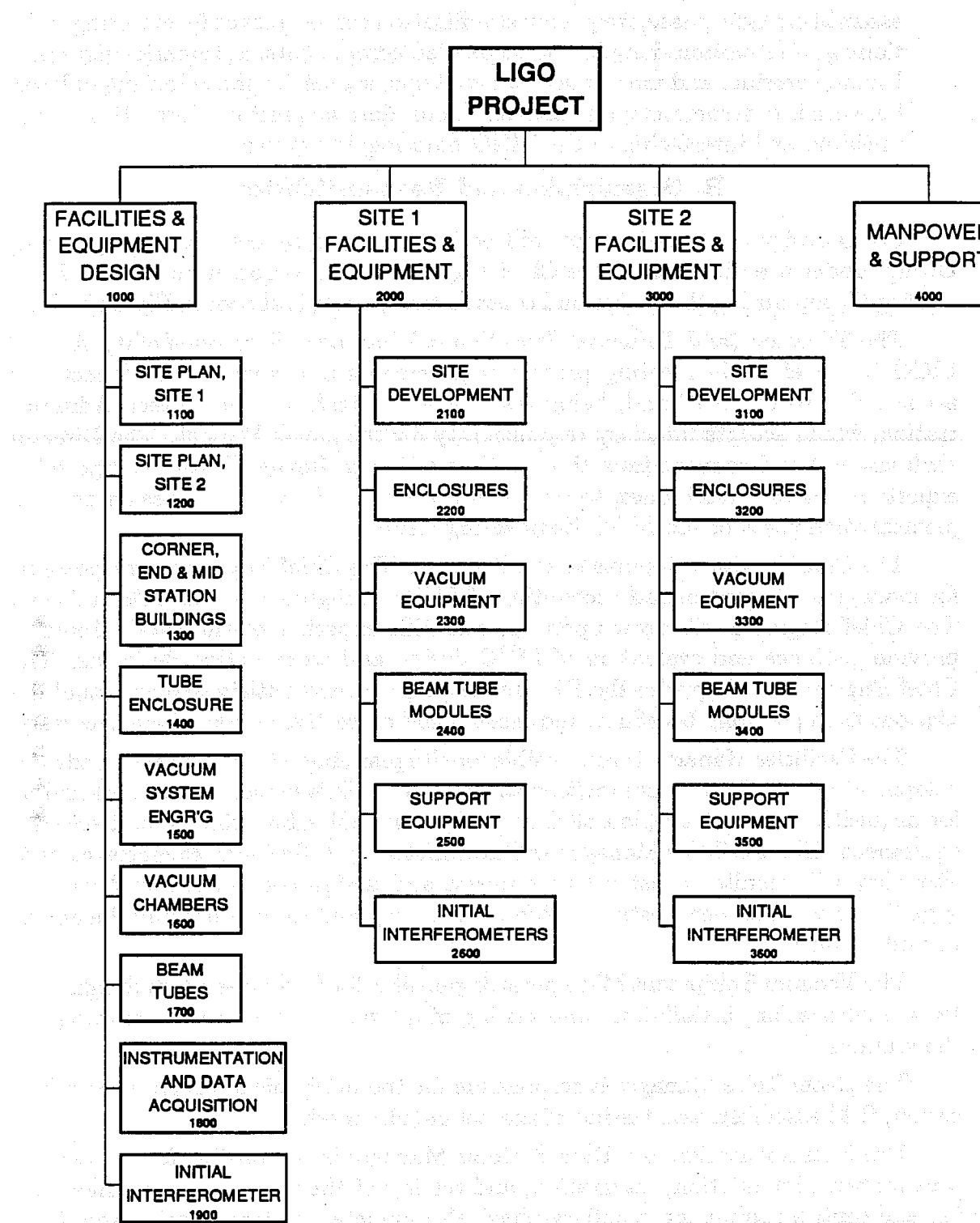


Figure VI-1 Work-breakdown structure (WBS) for the design and construction of the LIGO facilities and equipment.

assemblies; light phase/frequency stabilization servos; servos for pointing, positioning, and motion-damping of suspended components; automatic-alignment, beam-centering, and mode-matching systems; servos for phase locking of lasers between interferometers; and interferometer data acquisition, formatting, compression, and interfacing to the LIGO data-logging system.

B. Organization and Responsibilities

LIGO design and construction will be implemented by the LIGO Engineering Group, under the direction of the Chief Engineer.² The organization of the Engineering Group during the design and construction phases is shown in Figure VI-2.

The Director (and Principal Investigator) has overall responsibility for the LIGO Team effort in meeting project requirements and goals. The Director is accountable to the NSF and, being resident at Caltech, to the Caltech Administration, which accepts fiduciary responsibility for the LIGO Project. The Director shall appoint and convene from time to time a Design Review Board, composed of experts in relevant disciplines, to review and provide advice on the design and implementation plans of the LIGO Engineering Group.

The Chief Engineer reports to the Director. The Chief Engineer is responsible for management, control and accounting of LIGO configuration, schedule and cost. The Chief Engineer will draw upon the scientific expertise of the LIGO Team to provide guidance and evaluation of LIGO design and construction decisions. The Chief Engineer shall apprise the Director of progress and anticipated or actual deviations from planning baselines, and recommend corrective action where necessary.

The Facilities Manager is responsible for site planning, enclosure design, site development and enclosure construction at both sites. This person is also responsible for acquisition and installation of shop equipment, office furnishings, and security equipment. The Facilities Manager will be assisted by a Resident Engineer at each site; they will monitor construction progress and design compliance, and will engage the services of local testing laboratories as required to measure and document as-built quality.

The Vacuum Equipment Manager is responsible for vacuum-system design, and for the fabrication, installation, and testing of all vacuum equipment contained in the stations.

The Beam Tube Manager is responsible for the mechanical design, shop fabrication, field assembly, and testing of the beam-tube modules.

The Instrumentation and Data Systems Manager is responsible for the design, procurement, installation, integration, and testing of the vacuum-system monitoring and control equipment, auxiliary-physical-parameter instrumentation and data-acquisition equipment, intrasite-communication equipment, data logging and dis-

² Support and review functions for all engineering efforts will be provided on a continuing basis by the science groups.

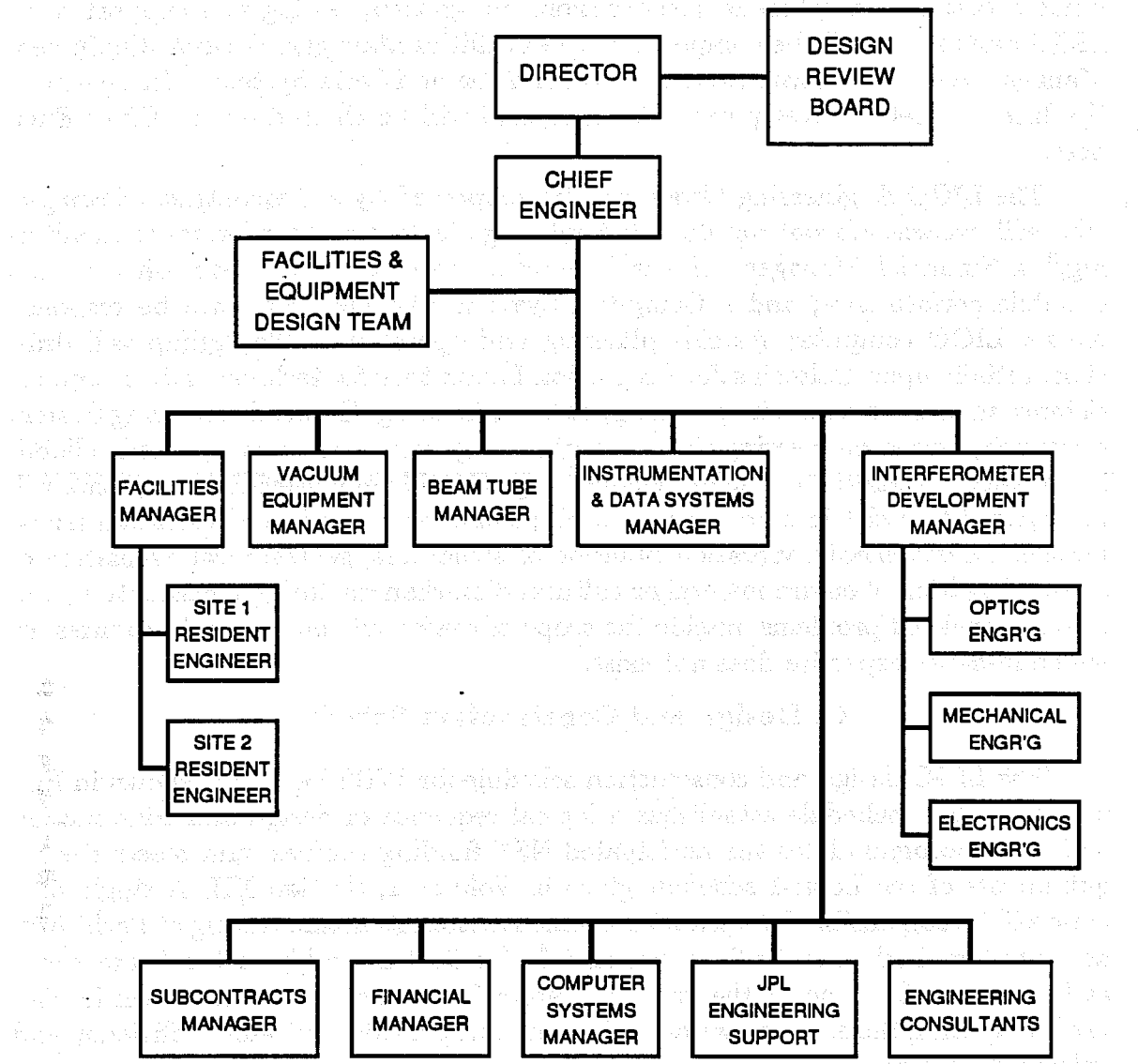


Figure VI-2 Organization chart for the LIGO Engineering Group during design and construction of the facilities.

play equipment, all software engineering and programming, and test and diagnostic equipment.

The Interferometer Development Manager is responsible for design, fabrication, installation, integration, and testing of lasers, optical components, and mechanical assemblies and electronics for the initial LIGO interferometers.

The Instrumentation and Data Systems Manager and the Interferometer Development Manager will interact on a continuing basis with the scientists and the research and development activities.

The Facilities and Equipment Design Team will be responsible for the coor-

dinated design, development, construction, integration, testing and support of all LIGO systems. It will be composed of the Facilities Manager, Vacuum Equipment Manager, Beam Tube Manager, Instrumentation and Data Systems Manager, and the Interferometer Development Manager, and will be chaired by the Chief Engineer.

The LIGO Engineering Group will be supported by a Subcontracts Manager, who will oversee subcontract development, negotiations and performance monitoring;³ a Financial Manager, who will monitor, correlate and report on cost and schedule performance; and a Computer Systems Manager, who will be responsible for LIGO computer systems planning and operations. The group will draw substantially upon Caltech's Jet Propulsion Laboratory for technical advice and assistance in such areas as site planning, soils engineering, Global Positioning System surveying, power engineering, HVAC engineering, structural analysis, and reliability, quality assurance, and safety engineering. Outside engineering consultants will be engaged to assist in certain areas, such as ambient seismic and vibration transmission measurements, vibration isolation of structures, geotechnical evaluation of sites, mitigation of environmental or cultural disturbances during construction, and other specialized problems outside the scope of major subcontractors' activities for which in-house expertise does not exist.

C. Design and Construction Schedule

The LIGO design and construction schedule for WBS Level 2 is shown in Figure VI-3. The schedule establishes a logical sequence of design and construction activities, accommodates the anticipated NSF funding profiles, and meets the requirements of the Level-1 schedule given in Volume 1, Section XII. A single field crew will be responsible for vacuum equipment installation and testing at both sites, and another single crew will be responsible for field assembly of the beam tubes at both sites. Sequencing the vacuum-system field construction as shown in Figure VI-3, using the same crews at both sites, will provide continuity, efficiency and enhanced quality.

The schedule provides long lead times for procurement of low-hydrogen-content steel. Fabrication of beam-tube sections will be matched to the field assembly process, so it will not be necessary to store large quantities of finished, cleaned, tested, and sealed beam-tube sections.

³ The Subcontracts Manager, a procurement professional who is a member of the LIGO engineering staff, technically provides only procurement liaison; fiduciary responsibility for all subcontracting remains with the Caltech Purchasing Department, with review and approval by the Office of General Counsel.

DESIGN/CONSTRUCTION SCHEDULE

	FY90	FY91	FY92	FY93	FY94
	CY90	CY91	CY92	CY93	CY94
PROJECT APPROVAL	△				
FUNDING AVAILABLE					
DESIGN					
SITE 1 CONSTRUCTION					
SITE 2 CONSTRUCTION					
DETAILED DESIGN WORK:					
SITE 1: Site plan, earthwork					
SITE 2: Site plan, earthwork					
Corner buildings					
End, mid station buildings					
Tube enclosures					
Vacuum systems eng'g					
Beam tube modules					
Vacuum chambers					
Vac. sys. monitor/control					
TUBE SECTION FAB. (factory)					
SITE 1 CONSTRUCTION:					
Site preparation					
Buildings, tube slab					
Tube field assembly, test					
Tube cover					
Vac. chamber fab. (factory)					
Vac. chamber install, test					
Support equip. procure, install					
SITE 2 CONSTRUCTION:					
Site preparation					
Buildings, tube slab					
Tube field assembly, test					
Tube cover					
Vac. chamber fab. (factory)					
Vac. chamber install, test					
Support equip. procure, install					
INTERFEROMETERS:					
Conceptual design freeze					
Detailed design, fab., test					
Install and debug (Site 1)					

Figure VI-3 LIGO design and construction schedule.

D. Subcontracting Plan

1. Design phase

a. **Facilities architectural and engineering design.** The LIGO Project will employ the services of one or more architectural, engineering and construction (A&E) firms for detailed design and documentation covering site planning; corner-, end-, and mid-station buildings; and tube enclosures for both sites. The facilities design will be assigned to a single firm, or several firms forming a team, with appropriate expertise. The design-phase product will consist of construction documents (detailed drawings and specifications) suitable for obtaining fixed-price bids for construction. During the construction phase, the A&E firm will maintain control of documentation, generating new documentation as required by design changes, and participate in the review and resolution of nonconformances and claims. It will provide as-built documentation at the completion of construction. Management of the A&E design subcontract for the facilities will be the responsibility of the LIGO Facilities Manager.

b. **Vacuum equipment design (and construction).** A subcontract will be placed with a firm that has large-scale vacuum-system design and fabrication experience to design the LIGO vacuum system, to perform detailed design of all vacuum equipment except for the beam tubes, and to fabricate, install, and test this equipment. Given the novel features of the LIGO vacuum equipment, it is essential that a single subcontractor be responsible for design, fabrication, installation, and testing of an integrated system. Authority to proceed with fabrication, installation, and testing will be given after the design-phase work has been successfully completed and reviewed. Management of the vacuum-equipment subcontract will be the responsibility of the LIGO Vacuum Equipment Manager.

c. **Beam tube design (and construction).** A subcontract will be placed with a firm to provide detailed design engineering, fabrication, installation, and testing services for the beam-tube modules.⁴ The design of the beam tubes has been separated from the rest of the vacuum system because it departs substantially from that of conventional vacuum systems and is more closely related to pipeline construction. This division of design tasks entails no significant risk; the interfaces between the beam-tube modules and the remainder of the vacuum system are few, readily identified and documented. Management and supervision of the beam-tube module subcontract will be the responsibility of the LIGO Beam Tube Manager.

Except for small subcontracts that may be placed for specific design tasks, all other LIGO subsystems will be designed in-house.

2. Construction phase

a. **Facility construction.** Site development, and construction of corner-,

⁴ Although this subcontract may be performed by the same contractor responsible for the vacuum equipment, this is not a requirement.

end-, and mid-station buildings, and tube enclosures for both sites will be subcontracted to a single construction firm. The design-phase A&E subcontractor will provide construction-phase configuration management, documentation maintenance and change control, and implementation advice. Management and supervisory responsibility for facility construction lies with the Facilities Manager, supported by a Resident Engineer at each site who provides on-site monitoring. Quality assurance services will be provided by local testing laboratories, through subcontracts arranged by the Resident Engineers.

b. **Vacuum equipment fabrication.** Installation and testing of vacuum equipment will be performed by the design subcontractor, as discussed above. The construction-phase subcontract will continue to be managed and supervised by the LIGO Vacuum Equipment Manager; on-site installation and testing will be monitored by the Resident Engineers.

c. **Beam tube construction.** Fabrication and field assembly of beam-tube modules will be performed by the beam-tube-design subcontractor. Management and supervision of the beam tube subcontract will be the responsibility of the LIGO Beam Tube Manager, assisted during field assembly by the Resident Engineers.

d. **Other.** A substantial number of small construction-phase subcontracts are anticipated for interferometer optics fabrication and testing, mechanical-assembly fabrication, and electronics fabrication and testing. These will be governed by detailed design drawings and specifications developed within the LIGO team, and will be supervised by the Interferometer Development Manager.

All subcontracts will be competitively solicited, negotiated procurements.

E. Interferometer Design and Fabrication

The initial interferometers will be designed in the future, and a detailed work-breakdown structure for fabrication and installation is therefore not available. The research program described in Volume 1, Section VIII.B will materially affect the final design, now still in a conceptual phase. The Interferometer Development Manager shall have responsibility for the efforts outlined below.

1. Interferometer design, fabrication and testing

The engineering design will begin by dividing the interferometer into a set of functional subsystems. For each subsystem, we will specify technical and performance specifications, a set of tasks that require detailed engineering definition and design, a procedure and schedule for procurement and fabrication, and a description of the test and qualification procedures. The initial interferometers will use common subsystems designs, except for scaling some of the optical and electronic parameters in the half-length interferometer. When practical, components or subsystems will be fabricated through industrial subcontracts. Subsystems will be assembled, inspected and tested⁵ on campus prior to shipment to the sites for integration into

⁵ Although the campus facilities will be capable of assembly and testing of LIGO interferometer

the initial interferometers.

2. Installation and operation of the initial LIGO interferometers

After construction at the first site is completed and the facility is accepted from the contractors, LIGO engineering and scientific personnel will install the initial interferometers. The same group will perform these functions at the second site one year later (supported by a post-construction agreement), and will also train the operations and facilities-maintenance staff.

Once an interferometer is functioning, data runs will be initiated to uncover possible shortcomings in the performance of the interferometer or in the reliability of the supporting facilities. Experience gained during installation of the first interferometer should allow installation of the additional interferometers to proceed with few surprises. The operation of three interferometers in triple coincidence, constituting the initial LIGO detector, will complete the final shakedown of the LIGO facilities and equipment.

subsystems, the first integration of all the subsystems of a LIGO interferometer will take place at the remote sites.

APPENDIX A

EXPANSION TO PHASE-B AND PHASE-C CONFIGURATIONS

Section IV.C describes the configuration for vacuum systems for Phase A, the subject of this proposal; references were also made to design features that accommodate the planned Phase-B and Phase-C expansion¹ by modular addition of vacuum chambers. Chambers for a total of six interferometers can be accommodated at Site 1, and a total of three at Site 2. The corresponding corner-station vacuum-system layouts are shown in Figures A-1 and A-2, respectively. These may be compared directly with the corresponding Figures IV-C-6 and IV-C-12. The end-station and mid-station layouts are shown in Figures A-3(a) and A-3(b), respectively. The corresponding enclosure floor plans, which show the added equipment to scale, are provided in Figures A-4 (Site 1 corner station), A-5 (Site 2 corner station), A-6 (typical end station), and A-7 (typical Site 1 mid station). Building expansions are not required, as discussed in Section III. For a discussion of the goals and planned capabilities of the LIGO for Phases A, B and C, refer to Volume 1, Section IV.

The expansions involve adding Type 1 test-mass chambers symmetrically along each arm of the vacuum system in the corner station and the corresponding end stations or mid stations, and their associated diagonal chambers and horizontal-axis modules (HAMs) to support operation of the additional interferometers. The pumping system need not be expanded or modified. Chambers can be added with only a modest disruption of LIGO operations. For example, at Site 2, diagonal chambers and HAMs can be assembled in place without connecting to the beam-tube extensions and tested without interrupting the operation of the initial interferometer. The vibration and acoustic noise resulting from the construction activity is likely to degrade performance of adjacent operating interferometers, but this can be limited to an approximately 8 h/day shift.

Facility operations must be shut down during installation of test-mass chambers, because it will be necessary to air-release the beam-tube extensions. With adequate advance planning, test-mass chambers can be installed with only 1 or 2 months interruption in operations. The valves that isolate the beam tubes will be closed during installation, and the beam tubes will remain under high vacuum. Full LIGO operation can be restored as soon as the newly installed test-mass chambers are verified for correct operation and the operating vacuum in the chambers and beam-tube extensions is restored.

The laser-beam crossings in the large array of connecting tubes shown in Figures A-1 and A-2 are accommodated by special modules that afford independent vacuum environments for the (up to 6) interferometers. To understand the nature

¹ The reader is reminded that we are not proposing to implement the Phase-B or Phase-C configurations at this time.

of these beam crossings, refer to Figure II-2 in Section II.D; note that beams for pairs of test masses (e.g., 1-2, 3-4, 5-6) are at different heights. Test-mass pairs at the same height belong to full-length and half-length interferometers of the same detector. The height differences are sufficient to allow a vacuum wall to isolate the vacuum envelopes where the beams of different detectors intersect. The intersections shown in Figures A-1 and A-2 are actually small modules composed of intersecting tubes with an interior wall in the horizontal plane. Where interferometer beams cross at the same height, there can be no internal vacuum wall; thus the vacuum envelopes corresponding to pairs of interferometers of the same detector are connected. This arrangement satisfies the requirement of permitting service access to one detector without disturbing another detector.

The cost of expansion from the proposed Phase-A LIGO to a Phase-B configuration, using current estimates, is about \$40M (FY89 dollars). This includes the manufacture, installation, and testing of the vacuum equipment (Site 1: eight Type 1 test-mass chambers plus two diagonal chambers with associated HAM chambers; Site 2: four Type 1 test mass chambers plus a diagonal chamber with associated HAM chambers) and the components and equipment for three additional interferometers. It does not include the cost of LIGO-team work force, expenses or travel associated with the planning and supervision of the expansion or the development, installation, or testing of the interferometers.

Expansion from a Phase-B configuration to a Phase-C configuration would cost a similar amount (\$40M).

Expansion from a Phase-C configuration to a Phase-D configuration would cost a similar amount (\$40M). The cost of expanding the system to a Phase-E configuration would be approximately \$40M. The cost of expanding the system to a Phase-F configuration would be approximately \$40M. The cost of expanding the system to a Phase-G configuration would be approximately \$40M. The cost of expanding the system to a Phase-H configuration would be approximately \$40M. The cost of expanding the system to a Phase-I configuration would be approximately \$40M. The cost of expanding the system to a Phase-J configuration would be approximately \$40M. The cost of expanding the system to a Phase-K configuration would be approximately \$40M. The cost of expanding the system to a Phase-L configuration would be approximately \$40M. The cost of expanding the system to a Phase-M configuration would be approximately \$40M. The cost of expanding the system to a Phase-N configuration would be approximately \$40M. The cost of expanding the system to a Phase-O configuration would be approximately \$40M. The cost of expanding the system to a Phase-P configuration would be approximately \$40M. The cost of expanding the system to a Phase-Q configuration would be approximately \$40M. The cost of expanding the system to a Phase-R configuration would be approximately \$40M. The cost of expanding the system to a Phase-S configuration would be approximately \$40M. The cost of expanding the system to a Phase-T configuration would be approximately \$40M. The cost of expanding the system to a Phase-U configuration would be approximately \$40M. The cost of expanding the system to a Phase-V configuration would be approximately \$40M. The cost of expanding the system to a Phase-W configuration would be approximately \$40M. The cost of expanding the system to a Phase-X configuration would be approximately \$40M. The cost of expanding the system to a Phase-Y configuration would be approximately \$40M. The cost of expanding the system to a Phase-Z configuration would be approximately \$40M.

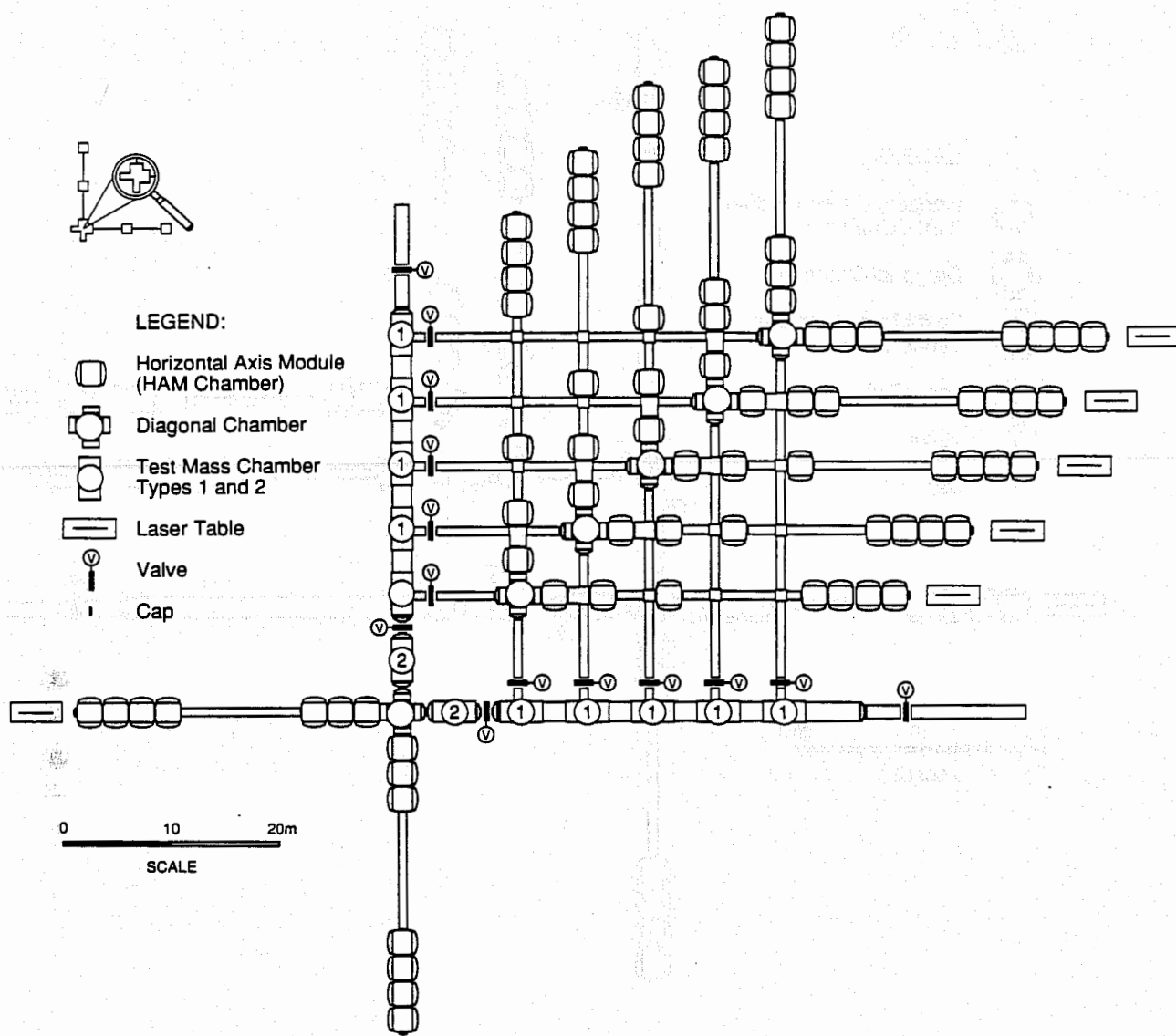


Figure A-1 Layout of corner-station vacuum chambers for Site 1, Phase C, to accommodate six independently operating interferometers. The configuration is an extension of the basic layout described in Figure IV-C-6 and shows how the modular chamber concept of the initial phase A design allows for the expansion of the facility's capabilities. New components, not needed in the initial phase, are the beam-crossing modules placed between the HAM chambers. The phase B configuration would include the chamber complexes for four interferometers.

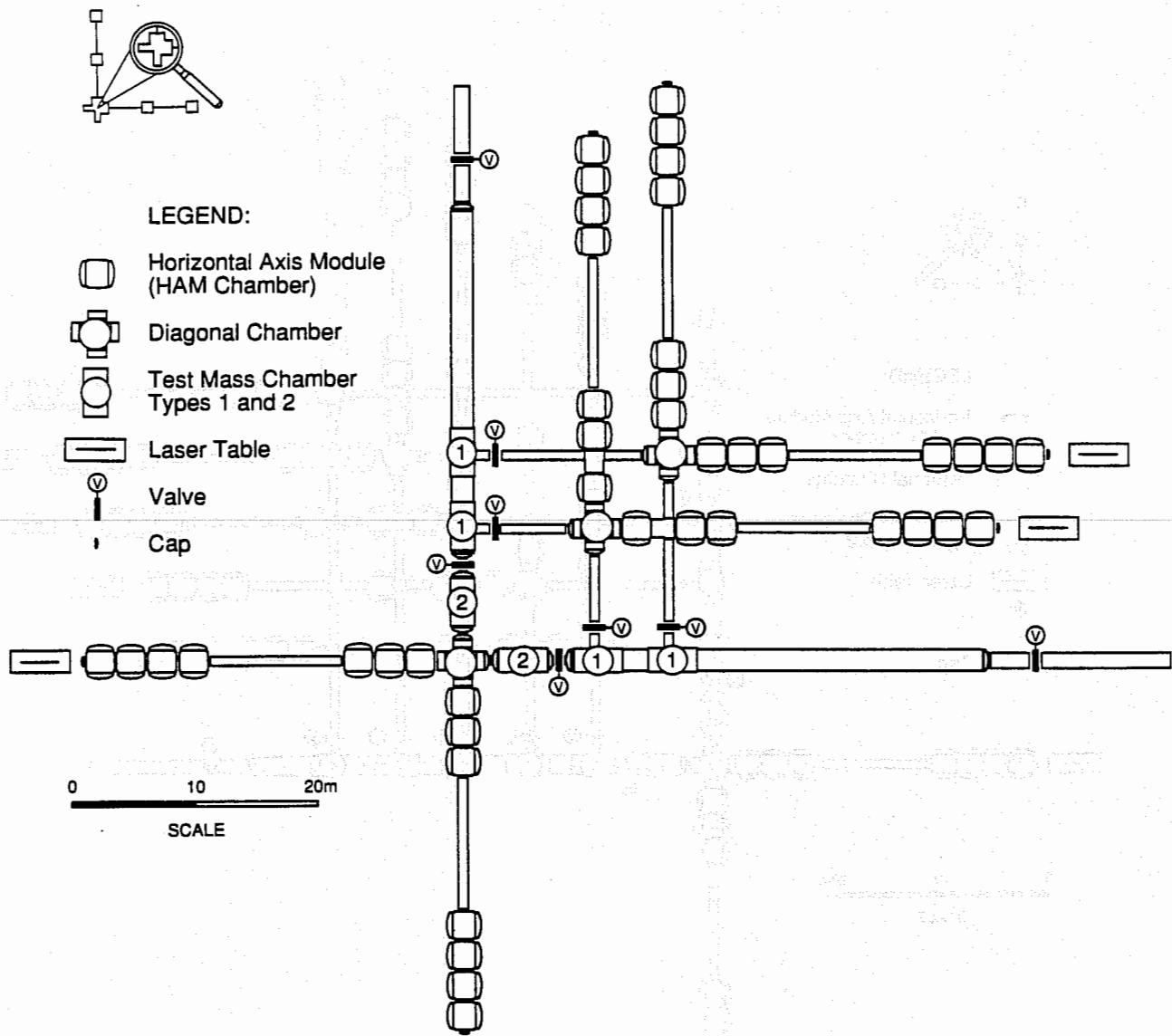


Figure A-2 Layout of corner-station vacuum chambers for Site 2, Phase C, to accommodate three independently operating interferometers. The Phase-B configuration would include the chamber complexes for two interferometers.

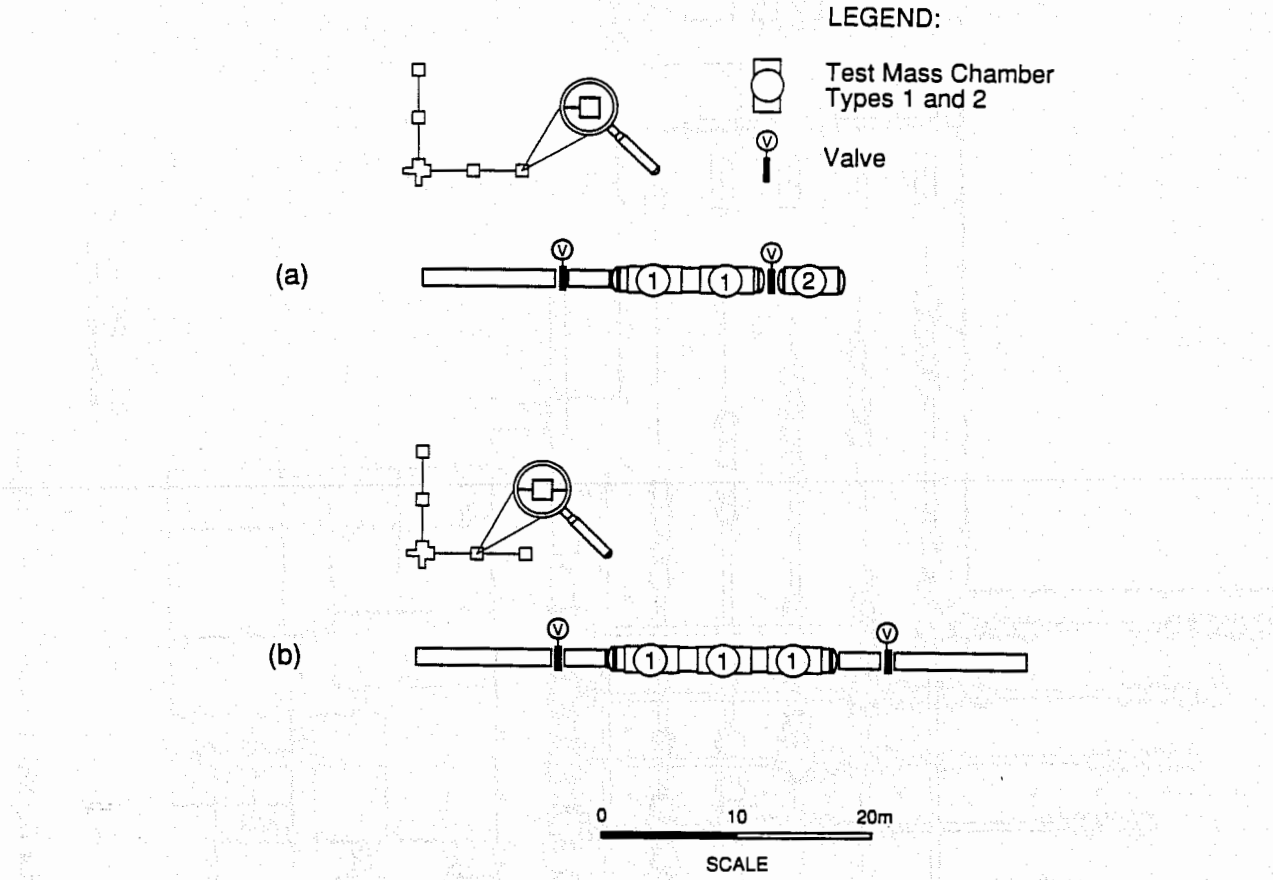


Figure A-3 Phase-C vacuum system layout in (a) the end stations (Site 1 and Site 2) and (b) the mid stations (Site 1 only). Two Type 1 test-mass chambers are added to each station in the positions reserved during the Phase-A construction (see Figure IV-C-15). The Phase-B configuration would include only one additional Type 1 test-mass chamber in each station.

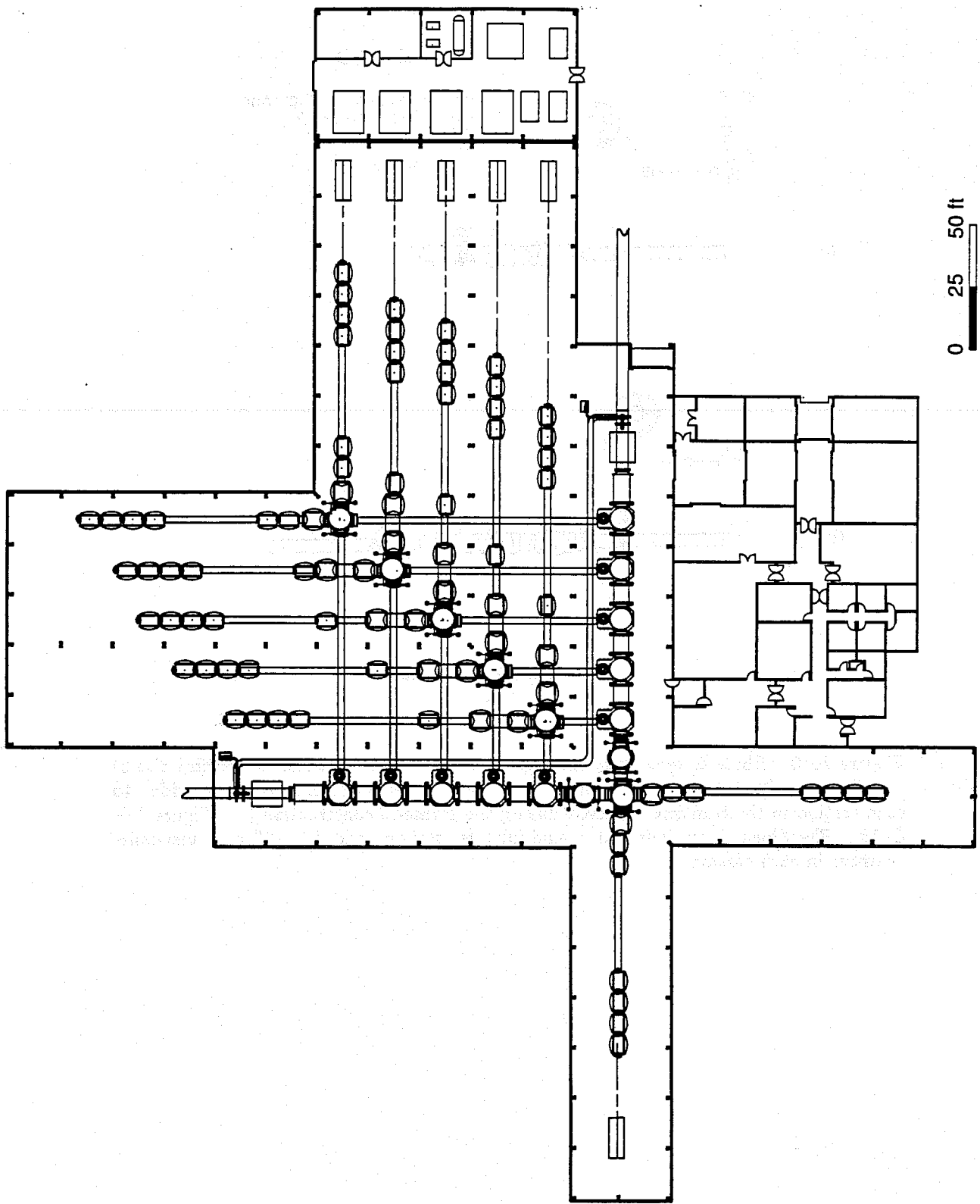


Figure A-4 Floor plan for the Site 1 corner station in Phase C.

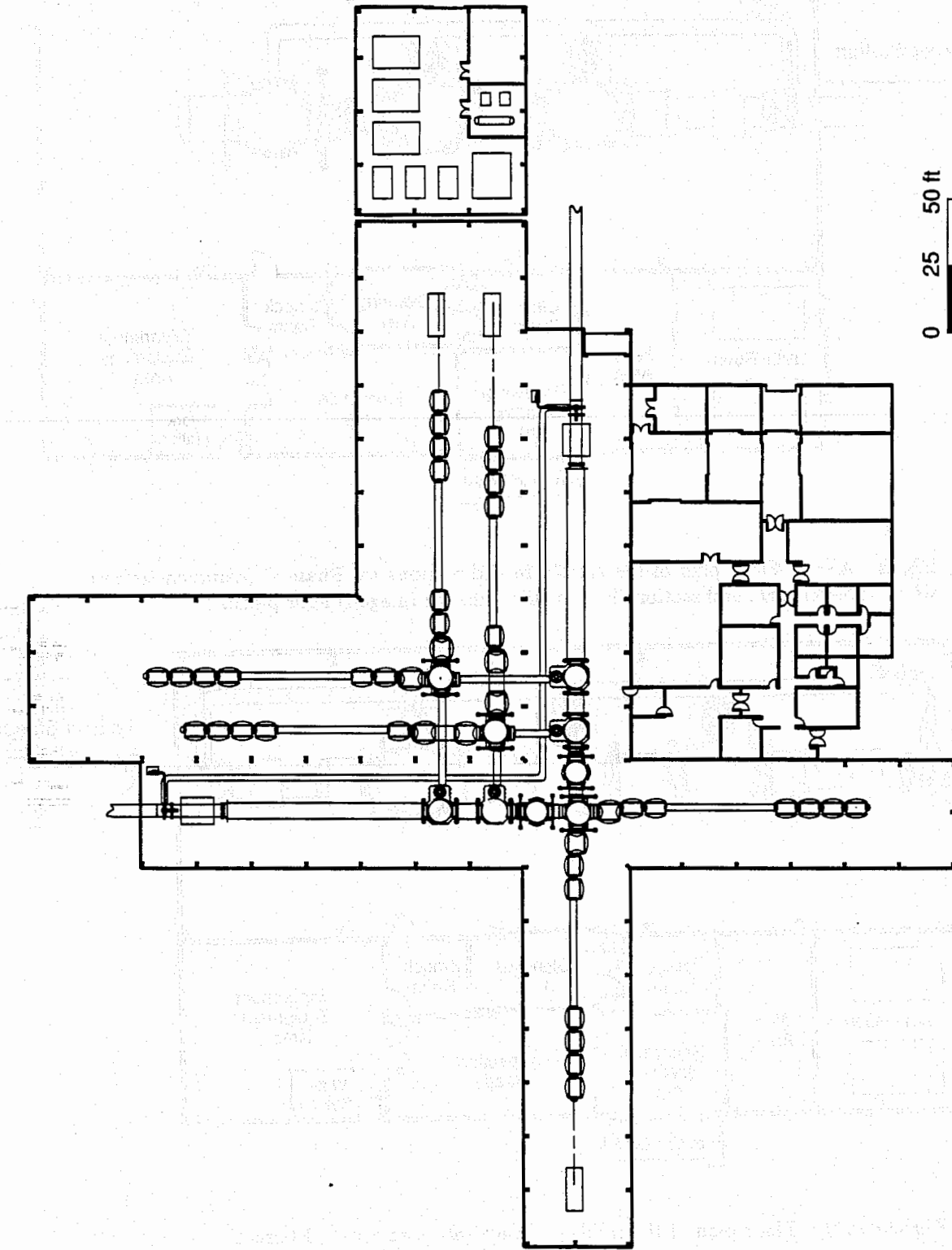


Figure A-5 Floor plan for the Site 2 corner station in Phase C.

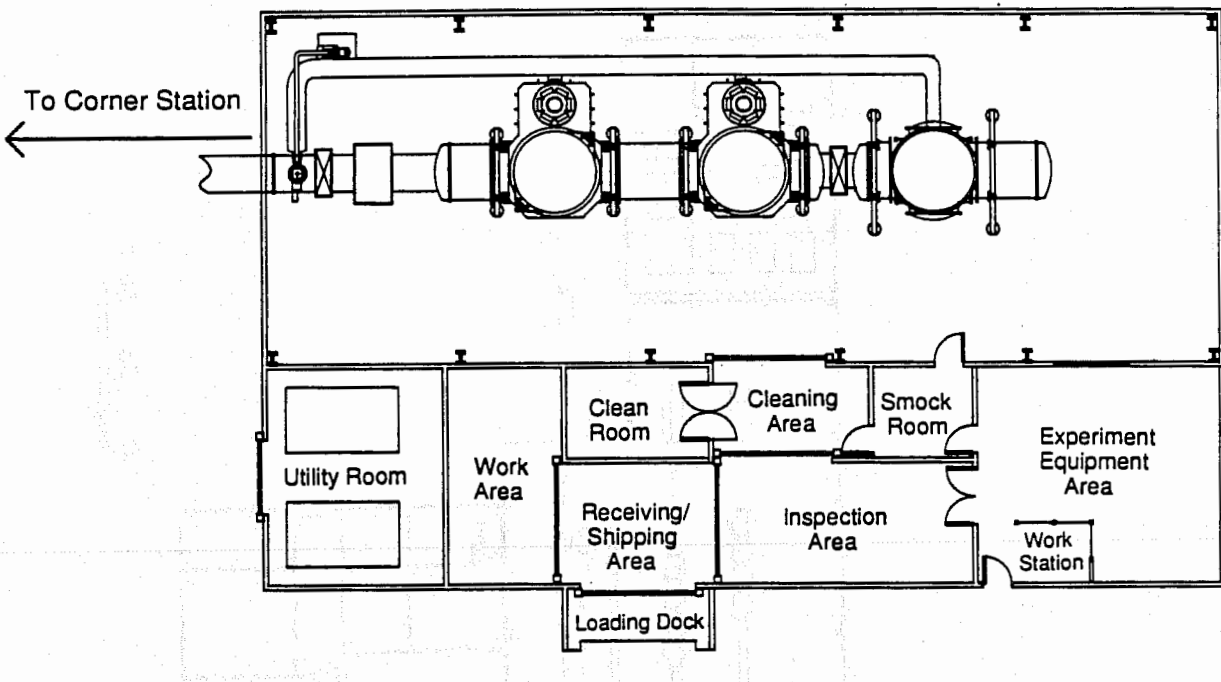


Figure A-6 Floor plan of the right-arm end stations for Phase C (common to both sites). The left-arm end stations have similar (mirror-imaged) floor plans.

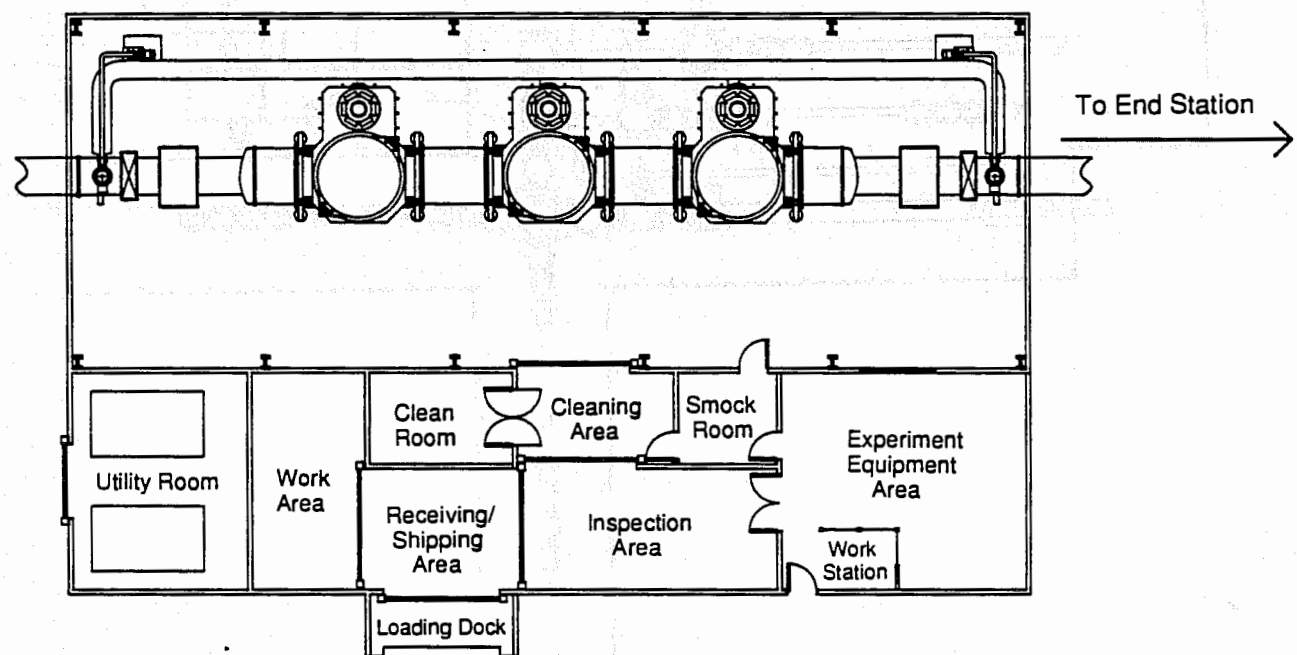


Figure A-7 Floor plan of the right-arm mid station at Site 1, Phase C.